19th - 20th Sept, Harvard, Cambridge, Massachusetts

Conference Proceedings

INTERNATIONAL YOUNG RESEARCHERS' CONFERENCE 2020

The Third Annual Interdisciplinary Conference for High School Students

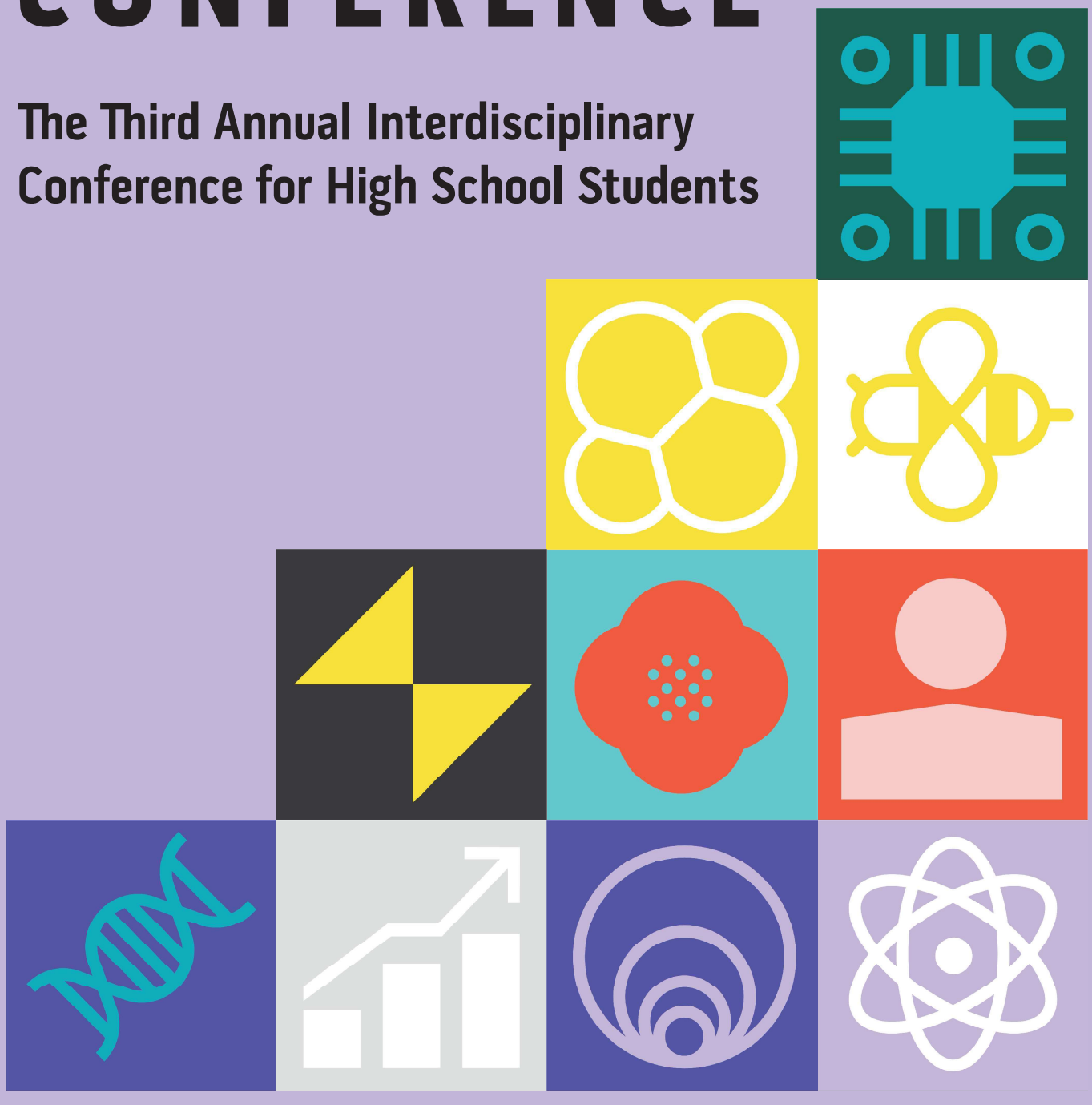

Proceedings of the 3rd International Young Researchers' Conference (IYRC)

September 19th and 20th, 2020

Edited by

Elizabeth Feldeverd

Published 2020

info@the-iyrc.org

Contents

Organizing Committee

Chair

Elizabeth Feldeverd

Committee members

Simon Arango Baquero
James Clay
Drew Mammel
William Hagerty

Organizational support

Francisco Gaddi, Jr.

Reviewers

Michael Amano
JD Andrade
Benjamin Hsu
Kristen Hughes
Tyler Kusunoki
Jonathan Lai
Emma Madden
Sara Metwalli
Hayden Mueller
Naren Najaragan
Robert Oda
Melissa Sarmiento
Taylor Strumwasser
Subodhana Wijeyeratne

The International Young Researchers' Conference would not be possible without the generous support of the Tokyo Academics community.

Letter from the Conference Chair

Dear student researchers, educators, parents, and other distinguished guests,

Welcome to the 3rd International Young Researchers' Conference! It has been a long journey to this year's event, but we are so glad that you could join us to celebrate the amazing work of these young academics.

At the beginning of 2020, we were intending to host the conference at Harvard University with the generous support of the Harvard College Japan Initiative. As the impacts of the novel coronavirus began to unfold in February and March, we soon realized that an in-person conference was no longer an option at the original date. In mid-March, we postponed the conference, hoping to host it on campus in the fall.

By the end of the Spring 2020 semester, COVID-19 had impacted nearly every aspect of education. Standardized tests were cancelled or hastily shifted online, international students were scrambling to make it home amidst flight cancellations, and a staggering one billion students were adapting to remote learning. After much discussion with the committee and other stakeholders, we agreed that hosting a conference, virtual or otherwise, was more important than ever.

This weekend, we are celebrating not only our students' research, but also their resilience and commitment to understanding the world through academic inquiry. Perhaps the most important silver lining of postponing the conference is that, by going virtual, we were able to reach a larger audience of students around the world who may have otherwise been excluded. The number of paper submissions more than doubled from our conference in Fall 2019. Moreover, the academic rigor of student research this year is higher than ever. I am sincerely humbled by what our students have accomplished so early in their academic careers.

Looking ahead, the IYRC organization hopes to expand its scope to empower more students to improve their communities through research and other projects. We hope that you will stay connected with us after the conference ends and support the next generation of researchers.

With gratitude,
Elizabeth Feldeverd
IYRC 2020 Chair

Submission Statistics

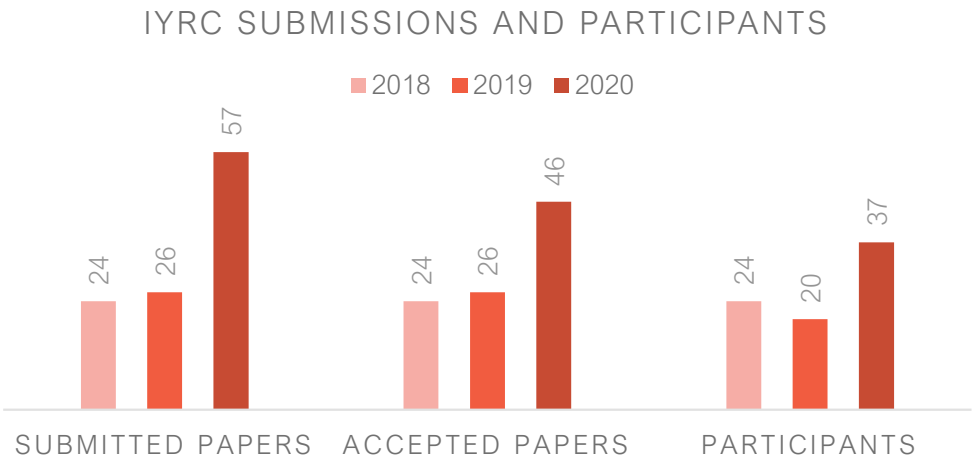

Submissions to this year's conference surged to 57 papers across STEM, social sciences, and humanities. Of the submitted papers, nine were rejected for quality and one was withdrawn. From the accepted authors, 37 students registered for the virtual conference.

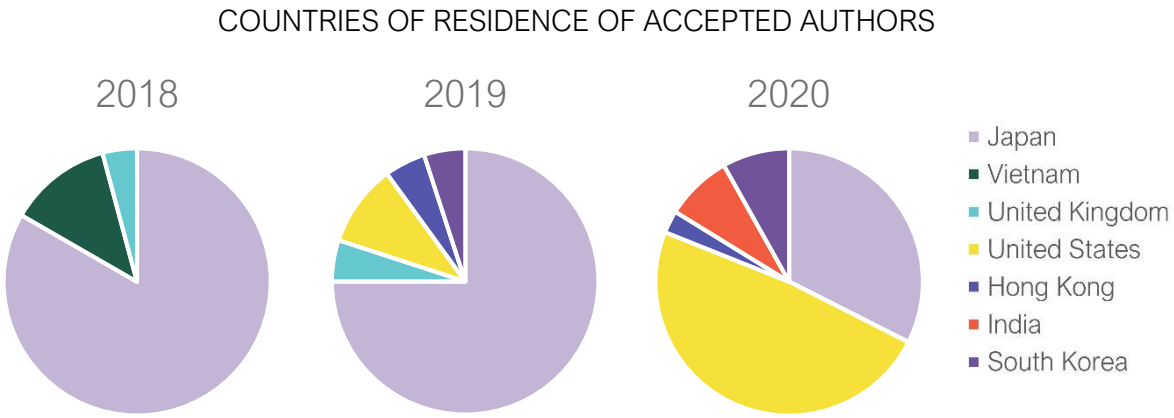

The countries of residence for accepted first authors has shifted dramatically from the conference's inception in 2018. While the number of students from Japan has remained relatively stable, the number of students from the United States has been steadily increasing.

Keynote Speakers

Molly Edwards

Molly Edwards is a PhD candidate at Harvard University in the Department of Organismic & Evolutionary Biology. Her dissertation work focuses on the development and evolution of the uniquely-shaped columbine flower petal, for which she has received a Graduate Research Fellowship from the National Science Foundation. She is a firm believer in the power of outreach and devotes her time outside of the lab to science communication efforts. She is the creator and host of 'Science IRL,' an educational YouTube series whose mission is to cultivate, especially among young people, enthusiasm for and a sense of belonging in science.

Paul M. Lewis

Paul M. Lewis is a Medical Student at Columbia University Vagelos College of Physicians and Surgeons. He holds a Bachelor of Arts degree from Harvard College, where he concentrated in Neurobiology with a secondary in Global Health and Health Policy. He has experience in diverse areas of global and public health, having served as the Director of a program for underprivileged Native American youth, the President of a peer education group to promote holistic wellness, and the Community Education Chair of a drug and alcohol education group. Paul is the Founder of Harvard College VISION Global Health Society and the Global Health and Leadership Conference. Paul is the recipient of the Robert T. Benjamin Prize for his contribution to the health and wellness of Harvard, The Harvard Phillips Brooks House Association Houston Award for exceptional commitment to serving underprivileged communities, and the Harvard Transcript Project Prize for excellence in writing and reflection. He was awarded the Finley Fellowship from Harvard to spend a postgraduate year in Japan to learn about end-of-life care. Afterwards, he worked as a TMS Therapy Clinician at Dignity Brain Health to treat patients with Major Depressive Disorder. At Columbia University, he is currently pursuing his interest in palliative care and neurosurgery.

Harvard College Japan Initiative Panelists

Nabib Ahmed

Nabib Ahmed is a junior at Harvard studying Computer Science and Statistics. He is originally from New York City. However, this semester he will be living on campus in Cambridge. He has been involved with the Harvard College Japan Initiative (HCJI) for two and a half years; he serves on the board, reprising his role as Director of Technology from the previous year, and has helped organize HCJI's digital presence, academic programming, corporate relations, and external affairs. He has visited Japan twice before: once for vacation in Summer 2019 visiting Tokyo, Kyoto, and Osaka, and then again this past winter to visit Tokyo and to Sapporo to lead workshops. He has experience doing research in computer science, statistics, and economics and looks forward to sharing his expertise with students. Some of his hobbies include biking (he's biked in Kyoto), cooking (he's made Japanese omelets and pancakes), and hiking (he's hiked the Nikko mountains)!

Simon Arango

Simon Arango is a rising senior at Harvard studying Neuroscience and East Asian Studies. He has conducted research characterizing the molecular pathways behind emotion and pain for the past four years. He is also an active member of the Harvard College Japan Initiative, working to promote US-Japan relations across business and academia. His combined interest in Neuroscience and East Asia has driven him to pursue research opportunities in Japan, most notably at RIKEN and Hiroshima University. After graduation, Simon hopes to continue engaging with Japanese organizations through a career in the biotechnology industry. During his free time, he enjoys learning about art history, studying foreign languages, and cooking.

Shawn Barrett

Shawn Barrett is a rising senior at Harvard concentrating in Neuroscience with a secondary in East Asian Studies. He conducted neuroscience research both at Harvard throughout his sophomore year and at the University of Tokyo during his sophomore summer. He is taking a leave of absence for the fall 2020 semester and is working in Tokyo as an intern for the Global Recruitment Team at Sony HQ. He is always interested in keeping up with US-Japan relations, and enjoys learning Japanese, deep-sea fishing, and snowboarding.

Jamie Caines

Jamie Caines is a rising senior at Harvard studying Bioengineering, S.B. She has worked on several projects in health technology, most recently to reduce the number of road traffic fatalities in India. She began research after her freshman year of college, working on a novel CT device at a lab affiliated with a hospital. She is passionate about innovation and global collaboration. This year she will divide her time among her studies, a venture capital internship, and completing her engineering thesis. She is always curious about new discoveries and innovation in the sciences and loves meeting new people.

Jacob Heberle

Jacob Heberle is a junior at Harvard studying Government and East Asian Studies. He has worked for several government-related organizations, most recently as a housing policy researcher at the Hawaii Budget and Policy Center, where he helped to write a report for the state government on affordable housing. He is passionate about using data to make effective and equitable public policy recommendations. After graduation, Jacob is interested in working for an international relations think tank and is always excited to meet new people from different backgrounds. In his free time, he likes hiking, listening to podcasts, and cooking.

List of Participants

First Author	School
Nisha Balaji	Dougherty Valley High School
Chiara Blissett	NuVu Studio (Cambridge, MA)
Sena Chang	The American School in Japan
Swathya Chauhan	Delhi Public School, Greater Noida
Meagan Eickelbeck	Byram Hills High School
Karen Fukuda	The American School in Japan
Ananth Goyal	Dougherty Valley High School
William Hagerty	Montgomery Bell Academy
Isabella He	Mission San Jose High School
Chien-Yu Huang	International School of the Sacred Heart
Paras Kumar	M.G.N Public School, Jalandhar, Punjab
Shubham Kumar	Dougherty Valley High School
Kai Kurosu	The American School in Japan
Christopher Lee	Seoul International School
Rachel Lee	Yongsan International School of Seoul
Yongjae Lee	Hong Kong International School
Yongjun Lee	Chadwick International School
Brayden Li-Kato	The Fessenden School
John Lin	Boston Latin School
Max Murakami-Moses	The American School in Japan
Miu Nakajima	The American School in Japan
Takuto Nakamura	The Cambridge School of Weston
Yuta Namba	St. Mary's International School
Marie Nishi	Tokyo Gakugei University International Secondary School
Kanan Nozaki	St. Mary's International School
Caryn Ohki	BYU Independent Study
Artemis Pados	Stanford Online High School (OHS)
Taleen Postian	Byram Hills High School
Kavan Prajapati	Shree Narayana Higher Secondary School
Priyanka Senthil	Davidson Academy
Shravan Kruthick Sridhar	Global Indian International School, Tokyo
Elena Su	Brookline High School
Saachi Subramaniam	South Brunswick High School
Melanie Sun	Mission San Jose High School
Daniela Tejada	Pine Crest School
Zhengbo Xiang	The American School in Japan
Jesang Yim	Kimball Union Academy

Full Conference Schedule

EDT		JST		STUDENT/EVENT	TITLE
SEPTEMBER 19	10:00 AM	SEPTEMBER 19	11:00 PM	OPENING TALK	
	10:15 AM		11:15 PM	KEYNOTE SPEECH – PAUL M. LEWIS	
	10:30 AM		11:30 PM		
	10:45 AM		11:45 PM		
	11:00 AM	SEPTEMBER 20	12:00 AM		
	11:15 AM		12:15 AM		
	11:30 AM		12:30 AM	Melanie Sun	A Review of the Current Education for Children with Attention Deficit and Hyperactivity Disorder and the Effects of COVID-19
	11:45 AM		12:45 AM	Priyanka Senthil	Association Between Cerebral Small Vessel Disease and Risk of Recurrent ICH Among U.S. Minority Survivors
	12:00 PM		1:00 AM	Shubham Kumar	Determining Personalized Head Related Transfer Functions Using Auralization
	12:15 PM		1:15 AM	Jesang Yim	Estimation of Post Milling Particle Size Distribution Using Linear Transformation in Parameter Space
	12:30 PM		1:30 AM	LUNCH	
	12:45 PM		1:45 AM		
	1:00 PM		2:00 AM		
	1:15 PM		2:15 AM		
	1:30 PM		2:30 AM	John Lin	Detecting Differential Transcription Factor Binding Based on DNA Accessibility
	1:45 PM		2:45 AM	Chiara Blissett	The Bio-Actuation Interactive Interface
	2:00 PM		3:00 AM	William Hagerty	Educational Exchange Programs' Impact on Foreign Direct Investment
	2:15 PM		3:15 AM	Elena Su	Mental Health in Adolescents: Analysis of a Nationally Representative Dataset, 2009-2018

EDT		JST		STUDENT/EVENT	TITLE
SEPTEMBER 19	2:30 PM	SEPTEMBER 20	3:30 AM	**Artemis Pados**	The Dynamic Republic
	2:45 PM		3:45 AM	**Daniela Tejada**	The Effects of Demographics on Political Party Affiliation in American High School Students
	3:00 PM		4:00 AM		
	3:15 PM		4:15 AM		
	3:30 PM		4:30 AM	**Isabella He**	Using Technology Enabled Career-Technical Education to Enhance American Education
	3:45 PM		4:45 AM	**Meagan Eickelbeck**	The Use of CpG Oligodeoxynucleotides as an Adjuvant for Immunotherapy to Mediate the T-Helper Cell Response Against Dog Allergies
	4:00 PM		5:00 AM	**Nisha Balaji**	Interpretability for the Automated Diagnosis of Musculoskeletal Radiographs
	4:15 PM		5:15 AM	**Taleen Postian**	Not at the Dinner Table: Utilizing Trait and Ability Emotional Intelligence Scores to Understand Political Opinion
	4:30 PM		5:30 AM	**Ananth Goyal**	A Novel Self-Assessing Compilation Based Searching Algorithm for Analytical Research
	4:45 PM		5:45 AM	**Brayden Li-Kato**	Pandemics, Surgical Masks, and Japanese Collectivism
	5:00 PM		6:00 AM	**Saachi Subramaniam**	Finding Nutritious Alternatives to Ingredients in Recipes Using Machine Learning
	5:15 PM		6:15 AM		
	5:30 PM		6:30 AM		
	5:45 PM		6:45 AM		
	6:00 PM		7:00 AM		
	6:15 PM		7:15 AM		
	6:30 PM		7:30 AM		
	6:45 PM		7:45 AM		
	7:00 PM		8:00 AM		
	7:15 PM		8:15 AM		

EDT		JST		STUDENT/EVENT	TITLE
SEPTEMBER 19	7:30 PM	SEPTEMBER 20	8:30 AM	HCJI WORKSHOP	
	7:45 PM		8:45 AM		
	8:00 PM		9:00 AM		
	8:15 PM		9:15 AM		
	8:30 PM		9:30 AM		
	8:45 PM		9:45 AM		
	9:00 PM		10:00 AM	OPENING TALK	
	9:15 PM		10:15 AM	KEYNOTE SPEECH – MOLLY EDWARDS	
	9:30 PM		10:30 AM		
	9:45 PM		10:45 AM		
	10:00 PM		11:00 AM		
	10:15 PM		11:15 AM		
	10:30 PM		11:30 AM	Rachel Lee	Republic of Korea's Economic Success and the Paris Agreement Goal of Reducing Greenhouse Gas Emissions
	10:45 PM		11:45 AM	Christopher Lee	Methods for Classification of Galaxy Types Using Machine Learning
	11:00 PM		12:00 PM	Yongjun Lee	Meth and Murder: The Violent Success of Duterte's War on Drugs
	11:15 PM		12:15 PM	Chien-Yu Huang	Effects of Breast Cancer Cell-Derived Extracellular Vesicles on Endothelial Cells and Angiogenesis
	11:30 PM		12:30 PM	Yongjae Lee	The Impact of COVID-19 Pandemic on Hong Kong's Domestic Helpers
	11:45 PM		12:45 PM	LUNCH	
SEPT 20	12:00 AM		1:00 PM		
	12:15 AM		1:15 PM		
	12:30 AM		1:30 PM		

EDT		JST		STUDENT/EVENT	TITLE
SEPTEMBER 20	12:45 AM	SEPTEMBER 20	1:45 PM	**Zhengbo Xiang**	PyITA: A Taylor Expansion-Based Data Augmentation Program for ANN Potentials Applied to TiO2
	1:00 AM		2:00 PM	**Caryn Ohki**	Evolution Through Art: Biomimesis in EcoLogicStudio's H.O.R.T.U.S. Series
	1:15 AM		2:15 PM	**Yuta Namba**	Photography as an Elegy: Solitude and Isolation
	1:30 AM		2:30 PM	**Kanan Nozaki**	Identification of Fusarium in Gerbera Using Augmented Ruthenium Red Based Biosensor
	1:45 AM		2:45 PM	**Karen Fukuda**	Education in Context: Examining Attitudes Toward Sexual Assault in Japan and Developing an Educational Tool for High School Students
	2:00 AM		3:00 PM	**Miu Nakajima**	Effects of CYP2D6*10 Mutation on Binding Affinity on Common Antidepressants in Japan
	2:15 AM		3:15 PM	**Max Murakami-Moses**	Analysis of Machine Learning Models Predicting Basketball Shot Success
	2:30 AM		3:30 PM		
	2:45 AM		3:45 PM		
	3:00 AM		4:00 PM	**Takuto Nakamura**	The Impact of Rapid State Policy Response on Cumulative Deaths Caused by COVID-19
	3:15 AM		4:15 PM	**Kai Kurosu**	The Role of Scandal in U.S. and Japanese Politics: Trump, Abe, and Their Political Futures
	3:30 AM		4:30 PM	**Marie Nishi**	Comparative Analysis of Alveolar Bone Resorption Between Male and Female Patients
	3:45 AM		4:45 PM	**Shravan Kruthick Sridhar**	Detection of Fake News Using Machine Learning
	4:00 AM		5:00 PM	**Swathya Chauhan**	The Study of Gravitational Radiation Through the Merging of Binary Neutron Stars
	4:15 AM		5:15 PM	**Kavan Prajapati**	Length of Portion of Euler Line Inside the Triangle
	4:30 AM		5:30 PM	**Paras Kumar**	On Finding the Focal Length of Induced Thermal Lens of Soy Sauce Sample Using Matrix System and Observing the Effect of Variation of Parameters
	4:45 AM		5:45 PM	**Sena Chang**	Considerations for Policymaking in Education: The Determinants of Gender Bias in Adolescents

Contributed papers

Interpretability for the Automated Diagnosis of Musculoskeletal Radiographs

Nisha Balaji
Dougherty Valley High School; San Ramon, United States of America
Email: nishabalaji2003@gmail.com

Abstract – Despite tremendous developments in performance, diagnostic machine learning algorithms are widely regarded as "black boxes." To break down this perception, we propose an investigation of interpretable models: systems that substantiate their conclusions with "justifications." We explore explainable models through the perspective of the diagnosis of musculoskeletal disorders which are among the most prevalent in the world. Two different avenues are pursued for interpretability: saliency imaging techniques to visually localize irregularity region within a radiograph and a clustering of abnormally classified radiographs to isolate different causes of abnormality into separate clusters. As for the model itself, three DenseNet-169 models are fine-tuned to various extents and tested on classification accuracy. The top-bottom (all parameters) fine-tuned model achieves the best AUROC of 0.865, and the saliency maps effectively localize the cause of irregularity within bone X-rays. The clustering algorithm makes substantial associations based on properties such as anatomical region, image orientation, and hardware type. The implications of such developments in interpretability within healthcare range from auditing models to garnering patient and physician trust.

Key Words – computer vision, automated diagnosis, explainable models, saliency imaging

INTRODUCTION

In an era imbued with the advent of technology, instrumentalizing machine learning in the field of medical imaging has become an increasingly prevalent proposition. Within medicine, artificial intelligence has aided in the development of new drugs, managing vast amounts of patient data, clinical prognosis, and even assistance in surgery [2]. One of its most prominent uses is to diagnose abnormal conditions within medical slides (radiographs and magnetic resonance images). Musculoskeletal disorders are extremely widespread, occurring in between 20 to 33% of the world's population. With the exception of cancerous diseases, musculoskeletal conditions are the primary cause of chronic pain [8]. Radiographs are vital to the diagnosis of musculoskeletal abnormalities [17].

In recent years, artificial intelligence diagnostic models have been at par with human radiologists in identifying disorders. In certain cases, such as chest X-ray diagnostics, machine learning models surpass capabilities of human radiologists [11]. Despite such progress, a survey revealed 97% of referring physicians trust human radiologists, in contrast to a mere 33% that trust diagnostic artificial intelligence models [18]. This illustrates the perception of machine learning systems as "black boxes"–its inner workings remain a mystery and its categorizations dubious due to a lack of interpretability.

Without substantial evidence to rationalize their claims, even stunningly accurate models can prove insufficient for real-world use. Machine learning models must be fashioned to explicitly portray the reasoning behind their diagnostic decisions.

In this work, we propose a method to construct interpretable models which "justify" their conclusions. Upon fine-tuning a DenseNet-169 model for musculoskeletal image diagnosis, two relatively distinct methods are utilized to make further deductions about the bone X-rays. Saliency maps are constructed to isolate regions of the image most indicative of irregularity.

In addition, an unsupervised learning algorithm is applied to cluster abnormally classified images based on disorder type. For instance, all anomalies caused by degenerative joint disease would be categorized into a different cluster than those caused by lesions. Such models can be massively contributory to discovering the cause of irregularity: it can be inferred that the abnormality of an image can be attributed to the general cause of abnormality within its cluster. Furthermore, this study provides a comparison of transfer learning DenseNet-169 models and their ability to accurately classify images and construct saliency maps. To summarize, we augment the applicability of artificial intelligence in medical imaging by making predictions more accessible and justified.

RELATED WORKS

The utilization of artificial intelligence for image classification in medicine has advanced tremendously. The conjunction of computer vision and machine learning has a variety of medical applications–for instance, clinical prognosis. A model to determine the effectiveness of neoadjuvant chemotherapy was constructed to replace an invasive procedure [7]. Machine learning also has a

widespread use in diagnostics. In a study conducted in 2015, an Elastic Net classifier was utilized to categorize brain tumor slides as either glioblastoma multiforme or lower grade gliomas [1].

In both forenamed studies, algorithms are created to assign image slides to a binary classification; however, both models do not provide insight as to how the algorithm arrived at a particular decision–the constraint that the following study contends with. A mere designation to a category is inadequate to completely assess the contents of an image. Medical classification models should be designed to provide explanations for their findings.

An interpretable model has already been constructed to identify articles within photographs from the ImageNet database. The model accomplishes this feat through subtle changes in convolutional neural network architecture [19]. The modified convolutional neural network places an emphasis on filters activated by singular parts within distinct object categories.

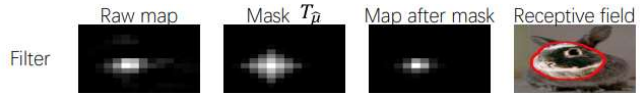

FIGURE 1: The visualizations aid in communicating which parts of the image are most influential in model classification [19].

There is an abundance of applications for interpretability in medicine [15]. Interpretability can be used as metric for auditing models. In addition, interpretable models can provide quality assurance and instill trust into their users.

PURPOSE

1. Fine-tune a pre-trained DenseNet-169 model to classify musculoskeletal radiographs as either "normal" or "abnormal."
2. Accentuate regions of the image slides most influential in the model's diagnosis by using saliency mapping.
3. Cluster resemblant "abnormal" images together and thereby isolate similar causes of abnormality together.

METHODS

I. Dataset

The MURA dataset is utilized for the purposes of this study [13]. The dataset includes 40,561 X-rays of seven anatomic regions organized by study and labeled as either "0" or "1" for "normal" and "abnormal" respectively. There are 36,808 images in the training set and 3,197 images in the validation set. The anatomic regions are elbow, finger, forearm, hand, humerus, shoulder, and wrist.

II. Logistic Regression

As a baseline comparison model, a logistic regression is implemented [10]. Prior to model training, images are processed with a different procedure than that of the convolutional neural network: after center cropping images into 224 by 224 pixels, local binary patterns are extracted from the image. Local binary patterns are image texture descriptors that improve feature detection in certain types of models, such as logistic regressions [12].

In addition, a dimensional reduction with principal components analysis (PCA) is performed on flattened local binary pattern arrays. After PCA, 500 principal components remain. The logistic regression model is trained on these components.

III. Convolutional Neural Network

Prior to training the neural network, the radiographs are processed. First, images are center cropped to 312 by 312 images and then resized into 224 by 224 images. The center-cropping is performed to remove the variance in image dimensions. Images are resized to 224 by 224 pixels since the Dense-Net 169 model only accepts images of that size. In addition, due to the redundancy of color within radiographs, images are converted to three-channel grayscale. In addition, normalization of the pixel values is implemented to systemize pixel values into a standardized range. This processing aids in making the data accessible to fine-tuning the convolutional neural network.

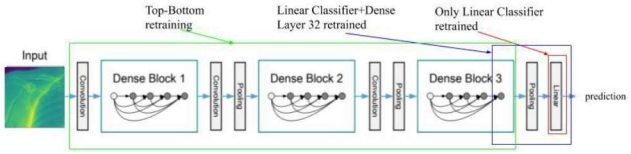

FIGURE 2: The regions within the labeled rectangles represent the parts of the model that are fine-tuned for each of the three model variations.

The DenseNet-169 model is a 169-layer convolutional neural network pretrained for the ImageNet dataset [7, 4]. Three variations of the fine-tuning algorithm are implemented for purposes of comparison:

1. Only the parameters of the linear classifier in the last layer is retrained

2. Both the parameters of the last dense layer (Dense Layer 32) in the third dense block and the last linear classifier is retrained

3. Every parameter of the model, top to bottom, is retrained (top-bottom model)

Binary cross entropy loss function is utilized in addition to stochastic gradient descent with learning rate 0.001 and momentum 0.9. The model calculates and returns the probability that a specified radiograph belongs in the "abnormal" class. If this probability exceeds 0.5, the image is classified as "abnormal." Otherwise it is placed into the "normal" category.

In regard to model training, an early-stopping algorithm is implemented. If the validation accuracy of the model does not improve for four consecutive epochs, the model halts training. Early-stopping and transfer learning are instrumentalized to decrease training time: the model trained in approximately 40 minutes. The model was trained on Google Colab Pro GPUs, and on the training to validation split of 36,808 to 3,197, respectively.

IV. Saliency Imaging

Saliency imaging isolates regions of abnormality within radiographs. The distribution of pixels in the saliency map allows for evaluators to visualize the model's interpretation of the original image.

Saliency mapping is applied to radiographs classified as "abnormal." Upon classification, the gradients of the score for each pixel in the input image are extracted. These weights are represented as superpixels in the saliency map. Brighter super-pixels associate with more important regions [10].

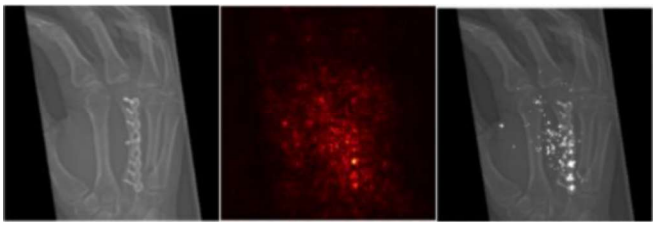

FIGURE 3: The original image's model visualization is shown in the heatmap. This is further processed by selectively choosing the brightest superpixels to appear in the final saliency map.

The saliency maps are then blended into the original radiograph for ease of visualizing. To prevent congested final images, superpixels in the bottom 25th percentile of brightness are discarded. When transferred to the final blended image, saliency map pixels are brightened even more to distinctly appear within the background radiograph.

V. Clustering

A K-means clustering algorithm is performed on images classified as abnormal by the top-bottom model. The abnormally classified images are taken from both the training and validation set to augment the size of the clustering dataset. The model only considers images *classified* as abnormal for consistence with real-world settings where "gold standard" data labels are nonexistent, and the model's classification is the basis for evaluation.

The algorithm clusters features extracted from the top-bottom model prior to the linear classifier layer. Principal components analysis algorithm (PCA) is performed to reduce the dimensionality of the features. After the PCA, a K-means clustering algorithm is executed on the components, with K=4. This specific K-value is chosen since the MURA dataset contains four general categories of abnormalities: fractures, hardware, degenerative joint disease, miscellaneous (typically lesions and subluxations).

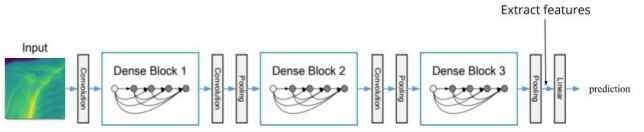

FIGURE 4: Clustering is performed on features extracted from the top-bottom fine-tuned model directly prior to the final linear layer.

In addition to a general clustering of all abnormally classified images (the general set), the clustering algorithm was also implemented within specific anatomic regions.

RESULTS

I. Classification Performance

TABLE 1: Metrics for the top-bottom model in classification performance

F1-Score	ROC-AUC	Recall	Precision
0.775	0.865	0.871	0.698

The performance metrics for the top-bottom model are included in Table 1. The model also attains a validation set accuracy of 80.638%. The proportion of false positives is higher than that of false negatives.

Sensitivity is defined as a medical metric for ability to identify disorder (abnormality), and specificity is the ability to identify lack of disorder (normality) [16]. The sensitivity of the model is 0.871 while it attains a specificity of 0.766.

TABLE 2: Comparison of ROC-AUC scores for all three fine-tuned models

Linear	Dense32 + Linear	Top-Bottom
0.806	0.783	0.865

As shown in Table 2, the three fine-tuned models had varying performances, with the top-bottom fine-tuned model attaining the best ROC-AUC score of 0.865. The fine-tuned models that are exclusively retrained at the last layers typically suggested probabilities that tended toward the threshold of 0.5, while the top-bottom trained model calculated more extreme probabilities nearing either 1 or 0. The logistic regression performed the poorest with a ROC-AUC score of 0.576.

II. Saliency Imaging

Saliency mapping tends to provide reasonable justifications for abnormality cause. In the specific case of localizing hardware abnormalities, the saliency maps are especially successful. Typically, superpixels are concentrated at the site of irregularity. As the distance from the region of abnormality increases, the density of the superpixels decreases.

However, in certain cases the saliency maps provide more ambiguous results for cause of abnormality. In these instances, gray space or irrelevant anatomical regions are accented. In others, a dispersed set of superpixels appear without a notable area of concentration.

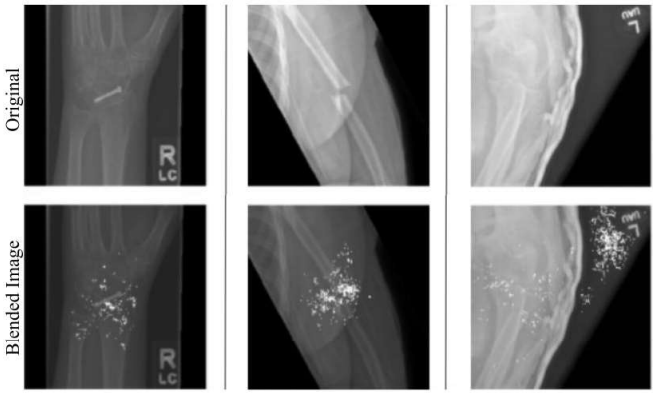

FIGURE 5: In Column A, the original image contains hardware in the wrist region which the blended saliency map accurately isolates. In Column B, the original image contains a fracture in the humerus which is also isolated by the saliency map. In Column C, the saliency map highlights arbitrary gray space in the radiograph, which is irrelevant to the task of abnormality detection.

The top-bottom model localizes abnormality cause most accurately. Isolating black space or irrelevant regions of the image are more common in the less comprehensively retrained models.

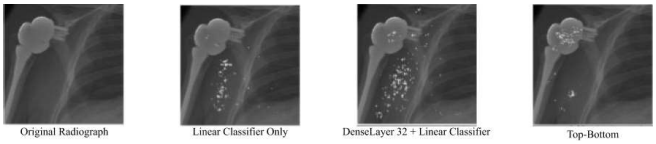

FIGURE 6: The top-bottom model effectively isolates the hardware abnormality. The other fine-tuned models highlight irrelevant portions of the image.

III. Clustering

The clustering algorithm does not separate radiographs based on the four primary abnormalities within MURA (as forenamed: fractures, hardware, degenerative joint disease, and a miscellaneous category with substantial amounts of lesions and subluxations). It tends to differentiate based on some properties irrelevant to diagnosis such as radiograph orientation and anatomical region of the radiograph. One diagnosis-based property that the clusters appear to make associations are the hardware abnormalities.

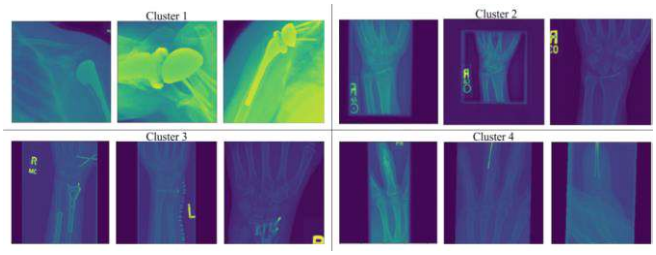

FIGURE 7: Upon categorizing a general set of abnormally classified images, notable patterns found include in Cluster 1) an extensive amount of shoulder socket hardware appears, in Cluster 2) wrist images without hardware abnormalities appear, in Cluster 3) a disproportionate number of wrist images with hardware plates appear, in Cluster 4) an example of clustering based on anatomical location is shown as a large majority of finger region images are observed in this cluster. The above images are samples of radiographs that appeared frequently in the specified clusters

As noted in Figure 7, the clustering of the general set of abnormally classified images appears to make substantial correlations based on hardware type and anatomical position. It is also notable that a disproportionate quantity of shoulder-socket hardware appears within the same cluster.

In the case of clustering within specific anatomical regions, there was an absence of abnormality-oriented clustering. Instead the algorithm's clustering entirely tends to center more around positional properties such as orientation and anatomical region. For example, in exclusive clustering of the forearm region, a separation of horizontally-oriented forearms versus vertically-oriented forearms appear.

DISCUSSION

The top-bottom model's performance exemplifies the benefits of implementing transfer learning. Pre-trained models can be fine-tuned with short training durations, in addition to attaining acceptable accuracy. The superior results of the top-bottom model in both classification accuracy and saliency imaging demonstrates that models that are more extensively fine-tuned perform better.

Saliency mapping provides insight into the decision-making process of the convolutional neural network. By accurately localizing abnormalities, the machine learning model justifies its reasoning, and its predictions can be accepted as well-informed. However, in cases where the saliency maps provide accents of irrelevant regions of the radiograph, the trustworthiness of the classification is questionable. Such discrepancies must be rectified. Architectural changes and the integration of local rule-extraction methods [4] in the convolutional neural network can combat such deviations.

The clustering model seems effective at distinguishing abnormalities caused by hardware presence. It can be inferred that such an association occurs specifically for hardware abnormalities than other types of abnormalities since hardware is especially semblant in radiographs. To

extend such differentiations to other types of abnormalities, changes to the architecture of the convolutional neural network can be explored, like with saliency mapping. Since the algorithm clustered based upon features extracted from the fine-tuned model, the algorithm's differentiations based upon orientation and anatomical region divulges the neural network extracts a substantial number of features based on these non-abnormality detection properties. To control for differences in anatomical region, the neural network can be trained separately for each anatomical region. By doing so, features that are more oriented toward abnormality detection rather than positional properties may be extracted. This would be far more useful than model visualizations of orientation-based properties, as such characteristics of radiographs do not require specialized medical training to find.

Interpretability holds monumental implications in real-world settings [15]. In the context of regulation, interpretability can serve as a qualitative metric for model evaluations. Auditing models on the basis of their internal mechanisms can establish quality assurance. In addition, interpretable models garner trust within physicians and patients. An increased confidence in diagnostic models can augment their use within clinics, thereby streamlining workflow and improving patient outcomes while remaining feasible and affordable [3].

CONSIDERATIONS FOR FUTURE INVESTIGATIONS

To improve existing performance in saliency imaging and clustering, architectural changes to the convolutional neural network can be explored. An integration of local rule-based explanations, which utilize genetic algorithms and derivation counterfactual rules, can also prove beneficial [4]. Influence functions, statistical tools used to evaluate the influence of removing an observation, are also relevant to the study of interpretable models [6].

Linguistic explanations for diagnostic choices can offer further clarity into the model's decision-making process [15]. Another possible course of exploration would be composition of example and counterexample groups for specified images. These groups can serve as comparisons to the original input radiograph [15].

CONCLUSION

This work proposes a method to construct interpretable models for diagnosing abnormality in musculoskeletal radiographs. We implement transfer learning with the DenseNet-169 model to detect irregularities within medical slides. Interpretability is then explored through two distinct lenses: saliency imaging and clustering. Saliency imaging provides reasonable visual justifications for the final model classification. K-means clustering succeeds in differentiating properties such as anatomical region, radiograph orientation, and hardware type. Furthering the precision of these methods and exploring other venues within interpretability can augment the use of artificial intelligence diagnostics in clinics. Such an integration would inevitably improve patient outcomes, while being fiscally affordable and productivity-wise efficient.

Interpretability holds monumental implications in real-world settings [11]. In the context of regulation, interpretability can serve as a qualitative metric for model evaluations. Auditing models on the basis of their internal mechanisms can establish quality assurance. In addition, interpretable models garner trust within physicians and patients. An increased confidence in diagnostic models can augment their use within clinics, thereby streamlining workflow and improving patient outcomes while remaining feasible and affordable [3].

ACKNOWLEDGEMENTS

The author would like to thank the Summer STEM Institute staff and mentor Allison Tam for their continual guidance during this research.

REFERENCES

[1] Jocelyn Barker, Assaf Hoogi, Adrien Depeursinge, and Daniel Rubin. Automated classification of brain tumor type in whole-slide digital pathology images using local representative tiles. Medical Image Analysis, 30,12 2015.

[2] Sam Daley. Surgical robots, new medicines and better care: 32 examples of ai in healthcare., July 2019.

[3] GE Healthcare. Three benefits to deploying artificial intelligence in radiology workflows, August 2019.

[4] Riccardo Guidotti, Anna Monreale, Salvatore Ruggieri, Dino Pedreschi, Franco Turini, and Fosca Giannotti. Local rule-based explanations of blackbox decision systems. CoRR, abs/1805.10820, 2018.

[5] Gao Huang, Zhuang Liu, Laurens van der Maaten, and Kilian Q. Weinberger. Densely connected convolutional networks, 2016.

[6] Pang Wei Koh and Percy Liang. Understanding black-box predictions via influence functions, 2017.

[7] Subramani Mani, Yukun Chen, Lori R. Arlinghaus, Xia Li, A. Bapsi Chakravarthy, Sandeep R. Bhava, E. Brian Welch, Mia A. Levy, and Thomas E. Yankeelov. Early pre-diction response of breast tumors to neoadjuvant chemotherapy using quantitative mri and machine learning. AMIA ... Annual Symposium proceedings. AMIA Symposium,2011, 868–877., 2011.

[8] World Health Organization. Musculoskeletal conditions, November 2019.

[9] Adam Paszke, Sam Gross, Soumith Chintala, Gregory Chanan, Edward Yang, Zachary De-Vito, Zeming Lin,

Alban Desmaison, Luca Antiga, and Adam Lerer. Automatic differentiation in pytorch. 2017.

[10] F. Pedregosa, G. Varoquaux, A. Gramfort, V. Michel, B. Thirion, O. Grisel, M. Blondel, P. Prettenhofer, R. Weiss, V. Dubourg, J. Vanderplas, A. Pas-sos, D. Cournapeau, M. Burcher, M. Perrot, and E. Duchesnay. Scikit-learn: Machine learning in Python. Journal of Machine Learning Research,12:2825–2830, 2011.11

[11] Jasmine Pennic. Ai vs. humans: Ai solution beats Stanford radiologists in chest x-ray di-agnostics competition. 2019.

[12] Matti Pietik¨ainen. Local binary patterns. 2010.

[13] Pranav Rajpurkar, Jeremy Irvin, Aarti Bagul, Daisy Yi Ding, Tony Duan, Hershel Mehta, Brandon Yang, Kaylie Zhu, Dillon Laird, Robyn L. Ball, Curtis Langlotz, Katie S. Shpanskaya, Matthew P. Lungren, and Andrew Y. Ng. MURA dataset: To-wards radiologist-level abnormality detection in musculoskeletal radiographs. CoRR, abs /1712.06957, 2017.

[14] Aditya Rastogi. Visualizing neural networks using saliency maps in pytorch. 2020.

[15] Mauricio Reyes, Raphael Meier, S`ergio Pereira, Carlos A. Silva, Fried-Michael Dahlweid, Hendrik von Tengg-Kobligk, Ronald M. Summers, and Roland Wiest. On the interpretability of artificial intelligence in radiology: Challenges and opportunities. Radiology Artificial intelligence, May 2020.

[16] Robert Trevethan. Sensitivity, specificity, and predictive values: Foundations, pliabilities, and pitfalls in research and practice. 2017.

[17] Alexandra Villa-Forte. Tests for musculoskeletal disorders, March 2020.

[18] Yao Xie, Melody Chen, David Kao, Ge Gao, and Xiang “Anthony” Chen. Chexplain. Proceedings of the 2020 CHI Conference on Human Factors in Computing Systems, Apr2020.

[19] Quanshi Zhang, Ying Nian Wu, and Song-Chun Zhu. Interpretable convolutional neural networks. In 2018 IEEE Conference on Com-puter Vision and Pattern Recognition, CVPR2018, Salt Lake City, UT, USA, June 18-22,2018, pages 8827–8836. IEEE Computer So-ciety, 2018

The Bio-Actuation Interactive Interface

The 'Undefined' Installation

Chiara Brielle Blissett
NuVu Studio; Cambridge, United States
Email: chiara_blissett@yahoo.com

Abstract – In cities, masses of individuals cooperate to travel within pre-established ranges of motion; the vessel, or city, is unresponsive to each existence. Individuals muted by the city's bustle inevitably seek a sense of presence, an amplification to rejoice in their uniqueness. Permanently fixed frameworks and outlined trajectories construct urban environments, through apparent, unambiguous forms and stationary walls. All physical barriers are obstacles that create predefined, stationary routes that humans are forced to adapt to, muffling the ability for humans to be present and perceive the world through the full scope of their senses.

Curated to break down barriers among everyday objects and biology, the *Bio-Actuation Interactive Interface* allows humans to 'communicate' with bacteria and watch the space around them morph. The bacteria showcased are genetically engineered to secrete color, the output of a chemical reaction. The interface enhances the user's state of mind as the color that the bacteria secretes is programmed for specific times of the day, evoking certain feelings, responses, and emotions, formulating a positive image for biotechnology.

How can humans delineate the space around them? How does this affect the mental health of large populations?

Key Words – Bio-actuation, biomimicry, agitation, urban reimagination/revamp

INTRODUCTION

The *Bio-Actuation Interactive Interface* is a tangible re-imagination of urbanism for all to engage with, reshape, and burgeon the capacity at which their senses can be engaged by diminishing the overwhelming effects of urban environments. Actuated by human presence, the installation responds to motion and physical interaction, unveiling how the body can construct the environment surrounding them, in contrast to the physical boundaries of the vessel, or city restricting a person's movement and ability to engage with their surroundings.

Organic landscapes are created by the entities inhabiting them and are reformed and reconstructed by mutual interactions based around the needs of living organisms in their ecosystem. Natural landscapes also embody subjective decisions as microcosms in each natural ecosystem or macrocosm. In natural environments, the presence of each individual is amplified as each step leaves a unique impression, the space recognizing individual existence.

DESIGN INTENTIONS

I. Educate the public about technology in design

Biotechnology – How can biology power the future (combat climate change)? Why is bio-design important today?

'Communicate' with bacteria – How can people engage with bacteria, something that is often stigmatized? Will an interactive (bio-powered) installation create a positive image for biotechnology and bacteria seen everywhere?

II. Enliven public spaces

Engage multiple senses – How can the senses be stimulated? How can bio-interactivity be optimized to its capacity? How can urban spaces/environments be reimagined and improved?

Improve the user's state of mind - How can installations improve peoples' moods on the global scale? How can installations evoke positive feelings and emotions that can be translated into the workplace? Could an installation help individuals to improve their quality of work, productivity, and overall success?

THE FUTURE OF BIOTECHNOLOGY

Typically, installations do not embrace biology and the miraculous ways it can intersect with technology. Stigma leads children to believe that bacteria are disgusting and are insignificant, although the planet will undoubtedly rely on them in the immediate future. [1]

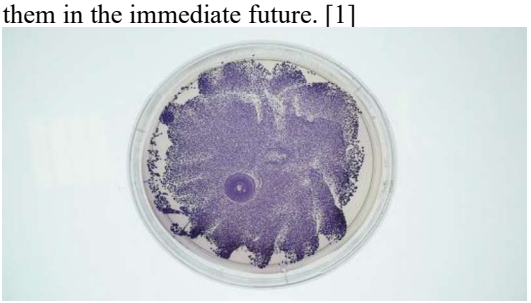

FIGURE 1: *E. Chromi.* – Bacterial sensors (bio-bricks) are inserted into *E. Coli* to produce pigment. [2]

E. Chromi., a precedent for the *Bio-Actuation Interactive Interface*, utilizes standardized sequences of DNA in a format called bio-bricks. Genetically engineered bacteria design their own bio-bricks using genes copied from existing organisms, which are then inserted into *E. Coli* that can secrete colors visible to the naked eye. Bacterial biosensors (bio-bricks) can tell a person the concentration of the pollutant with a detection bio-brick. The detector is linked to two other bio-bricks, the sensitivity tuner and the color generator. The sensitivity tuner determines how drastic the environmental change is and communicates a color and a level of transparency or intensity to the color generator. In the future, *E. Chromi* will be used for personal in-home disease monitoring in the form of a yogurt. The bacteria in the yogurt react to the culture in your gut and secrete colors in one's stool to tell the user if their gut culture is healthy.

THE IMPORTANCE OF SENSORIAL ENGAGEMENT

The Impact of Sensory-Based Movement Activities on Students in General Education (2016) is a study that delves into the movement of students throughout the school day and the effects it has on academics and "time on task." The investigation examined impacts of sensory-based movement activities on academic learning and analyzed the teacher's and student's perceptions of the activities. [3] Similarly, other studies examining sensorial engagement and its correlation with boring cityscapes suggests that dull environments increase sadness, addiction, and disease-related stress. Streetscapes and buildings ignore the need for sensory engagement, not allowing for comfort, happiness, or optimal functionality for future human populations. [4] Many studies show that breaks (for periods of sensory engagement) are essential in helping employees de-stress and re-charge for the rest of the workday. Regular breaks can also help improve overall job satisfaction and productivity levels. [5] Walking past an interactive installation in the city while taking a break for lunch is a great way to get some fresh air and engage the senses, even for a quick moment.

The physical and social environments of urban life can contribute both positively and negatively to mental health and wellbeing. Cities are associated with higher rates of mental health problems compared to rural areas: an almost 40% higher risk of depression, over 20% more anxiety, and double the risk of schizophrenia. Additionally, cities correlate to more loneliness, isolation, and stress. Good mental health can improve people's enjoyment, coping skills, relationships, educational achievement, employment and physical health problems.

People who live in the city experience increased levels of stimuli: population density, noise, smells, sights, disarray, pollution, and intensity of other inputs. Every aspect of urban environments is deliberately designed to assert meanings and messages, such as advertisements that evoke behavioral responses and attitudes. These stimuli trigger action and thought and become more potent as an inability to 'cope' sets in, often overloading the mind and resulting in burnout. Overload increases the body's baseline levels of arousal, stress, and preparedness, but also drives people to seek relief in quiet, private spaces. Over time this urge may evolve into social isolation associated with depression and anxiety, and also forms the basis of the ecological hypothesis of schizophrenia. [6]

COLORS AND PSYCHOLOGICAL CORRELATION

The colors in a person's surroundings can affect a person's health – physically or mentally. Various colors propagate varying impacts. Blues and greens form a calming ambiance, whereas oranges and yellows heighten productivity and the ability to focus. In color theory, every hue on the spectrum from white to black has an influence on how a person thinks, acts, and responds to the world around them.

TABLE 1 : PSYCHOLOGICAL EFFECT OF COLORS [7]

Color	*Psychological Effect(s)*
Yellow	• Brightens mood, increases energy levels, uplifting, lively, joyful
Orange	• Exciting, burst of energy
Pink	• Calms nerves, relieves feelings of anger, aggression, and neglect, love, playfulness, kindness
Green	• Reduces anxiety, feelings of prosperity, restorative, mind-clearing, encourages composure
Light purple	• Sparks creativity, calming feeling, light and airy
Blue	• Calming feeling, centered, relaxed, serene, lowers blood pressure, clears the mind, steadies breathing

Research shows that the colors generally found in hospitals and healthcare sites are white and green as these tones promote healing, facility competence, and motivation for both staff and patients. At the same time, spaces for children are usually colorful, bright, and full of patterns to boost morale.

Mental health units developed by the London-based charity Hospital Rooms bring color to wards and healthcare facilities to provide welcoming and inclusive atmospheres for patients in rehabilitation experiencing personality disorders, self-harm, depression, and other mental health issues. The rooms, founded by Tim Shaw and Niamh White, introduce colorful interiors and exteriors, resulting in an overwhelmingly positive response. [8]

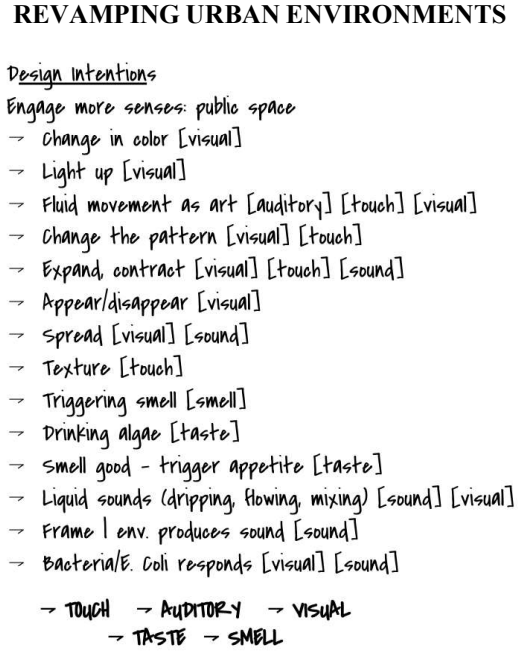

FIGURE 2: Chiara Blissett – conceptual ideation and sensorial design intentions. [9]

Drawing upon sensorial engagement research and color psychology, I generated lists of captivating, abstract reimaginations of urban expanses and the forms they could take. All of these reimaginations engaged multiple types of physical perception. From these lists, my sketches emanated, each expressing a wall that one could interact with and manipulate. Urban spaces should have the embedded capacity to involve the five senses and improve city-dwellers' psychological states, as they could significantly improve human mental health. This could translate to their educational or work-related engagement and success, and reduce the likelihood of burnout.

The final design includes a modular partition system composed of aggregated tiles, each of which is cast from translucent silicone. Each silicone piece appears to resemble a flower embedded with hollow channels and paths. These span to the tips of the 'petals,' which stem from the center. A biopsy punch was used to create a hole in the center of the hollow channel, connecting a syringe. The syringe houses genetically engineered bacteria that secrete color in response to a chemical reaction or a change in their environment. Programmed sensors on the tips of the 'petals' detect the motion of a person passing by, causing the syringes to pump the bacteria into the actuators.

When the movement of the algae occurs, the bioluminescent algae are agitated, evoking a reaction of oxygen within the complex molecule luciferin. This reaction releases the extra energy in the form of cold light. What makes the installation more interesting is that the algae will subsequently dispense a specific color, depending on the time of the day.

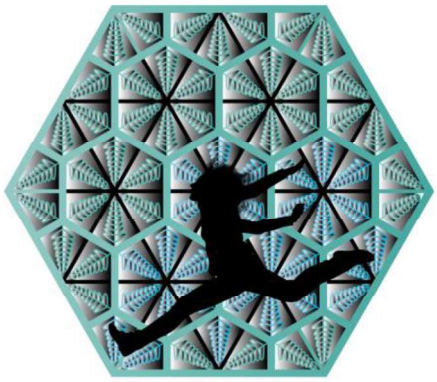

FIGURE 3: Chiara Blissett – A digital rendition of the final wall installation. [10]

The chart below illustrates the range of environments that bacteria are in that cause them to secrete particular pigments at particular times. The intensity and transparency of the hue are reliant on how drastic the changes are in the environment from its previous state identified by the detection bio-brick. The detector passes this information to the sensitivity tuner, which determines how deep the pigment will be. The tuner then translates the pigment hue to the color generator, which then secrets a color visible to the naked eye, hopefully evoking positive user responses.

TABLE 2 : Genetic Program Inputs, Outputs, and Correlative Time [11,12]

Input	*Output*	*Time of Day*
↓ Light	Yellow	Early morning
↑ Heat	Orange	Late morning
↑ Light	Pink	Early afternoon/ lunchtime
↓ Heat	Green	Late afternoon
↓ Acidity	Light Purple	Early evening
↑ Acidity	Blue	Late evening

DISCUSSION

How can we reimagine urban environments in a way that doesn't physically restrict us?

Chiara: *"Attempting to reimagine the urban spaces we live in today is challenging – the world we inhabit is composed of an inconceivable number of factors, many of which are not submissive. Revamping cities is not necessarily a matter of coming up with solutions to specific problems. Often times, the best designs arise from the miraculous, out-of-this-world ideas that are not produced for any particular reason except to expand the boundaries of what is tangibly possible. But*

that doesn't mean the product can't serve a purpose. The purpose should be discovered throughout the process – the abstraction should be the mainstay of each creation. Try to reimagine urban spaces as you know them; the results may be enthralling!"

How can society engage with biology and the static objects around them?

Chiara: "Today you can find numerous ways that scientists and designers are intersecting biology and everyday objects. Attempting to redesign objects to be powered by biology is difficult, but don't be discouraged! Find everyday objects that you want to revamp and find ways that biology could be embedded within, no matter how insane. For example, imagine devices and electronics you use every day being powered by the energy that bacteria produce, instead of requiring electricity – the possibilities are endless!"

AKNOWLEDGEMENTS

I would like to commemorate Katia Zolotovsky, Ryan Ferguson, and Luis Carbajal for assisting with conceptual ideation and technical design, as well as my family and the NuVu crew for their support.

REFERENCES

[1] Lee, Sang Yup. "Biotechnology: What It Is and How It's about to Change Our Lives." *World Economic Forum*, Korea Advanced Institute of Science and Technology, 2016, www.weforum.org/agenda/2016/12/what-is- -how-will-it-change-our-lives/.

[2] Ginsberg, Alexandra Daisy. "E. Chromi: Living Colour from Bacteria." *The--Dots*, 2009, the-dots.com/projects/e-chromi-living-colour-from-bacteria-210505.

[3] Anderson, Julie, "The Impact of Sensory-Based Movement Activities on Students in General Education" (2016). School of Occupational Therapy Doctoral Theses. 2. http://soundideas.pugetsound.edu/drot_theses/2

[4] Ellard, Colin. "Why Boring Streets Make Pedestrians Stressed and Unhappy – Colin Ellard: Aeon Essays." *Aeon*, Aeon, 10 Mar. 2020, aeon.co/essays/why-boring-streets-make-pedestrians-stressed-and-unhappy.

[5] Kohll, Alan. "New Study Shows Correlation Between Employee Engagement And The Long-Lost Lunch Break." *Forbes*, Forbes Magazine, 30 May 2018, www.forbes.com/sites/alankohll/2018/05/29/new-study-shows-correlation-between-employee-engagement-and-the-long-lost-lunch-break/#448b757e4efc.

[6] "How the City Affects Mental Health." *Centre for Urban Design and Mental Health*, Weebly, www.urbandesignmentalhealth.com/how-the-city-affects-mental-health.html.

[7] Yildirim, K., et al. "Effects of Indoor Color on Mood and Cognitive Performance." *Building and Environment*, Pergamon, 4 Oct. 2006, www.sciencedirect.com/science/article/abs/pii/S0360132306002289.

[8] Palin, Emma Jane. "Can Colour Improve Your Mental Health?" *Virgin*, 14 Mar. 2019, www.virgin.com/entrepreneur/can-colour-improve-your-mental-health.

[9] Blissett, Chiara Brielle. "Sensorial Design Intentions." *NuVu Studio*, 2020, cambridge.nuvustudio.com/studios/open-innovation-v1/chiara#tab-documentation-url.

[10] Blissett, Chiara Brielle. "Bio-Actuation Interactive Interface." *NuVu Studio*, 2020, cambridge.nuvustudio.com/studios/open-innovation-v1/chiara#tab-documentation-url.

[11] Blissett, Chiara Brielle. "Genetic Program Inputs, Outputs, and Correlative Time." USA, 2020.

[12] Akers, Adam, et al. "Visual Color Perception in Green Exercise: Positive Effects on Mood and Perceived Exertion." *Visual Color Perception in Green Exercise: Positive Effects on Mood and Perceived Exertion | Environmental Science & Technology*, American Chemical Society, 2012, pubs.acs.org/doi/abs/10.1021/es301685g#.

The Possible Determinants and Influences of Gender Bias in Adolescents

Sena Chang
The American School in Japan; Tokyo, Japan
Email: 24changs@asij.ac.jp, senachang77@gmail.com

Abstract – Given the current climate of social discrimination, it has become pertinent to understand why certain groups form biases against their "outgroups". In this study, the extent to which adolescents (12-19) have gender bias was measured using two contextual factors: 1) relation to family and 2) relation to the country at large. Using a sample of 41 adolescents from 20 cultural backgrounds, the IAT Test was used to measure gender bias alongside three of Hofstede's dimensions of national culture, which were used as a measure of one's culture. Employing a mixed-methods approach framed within a Simmelian perspective on group affiliations, it was found that a higher assessment of individualism and masculinity in one's country significantly increased one's tendency to stereotype. In regard to family-level characteristics, the presence of a working mother was identified to lower the severity of gender stereotypes. This study contributes to an understanding of the predictors of gender bias in adolescents and can be utilized by policymakers combating the climate of gender discrimination and educators fostering children during their process of identity formation.

Key Words – in-group, out-group, individualism, masculinity, Georg Simmel

INTRODUCTION

It has been widely recognized that the societal standards concerning women and their role in the workplace have changed drastically throughout the last few decades. From the ratification of the 19th Amendment in the U.S. in the early 20th century to a global female labor force participation rate (LFPR) of 48.47 percent [1], the systemic barriers separating men from women seem to have diminished greatly. However, the legacies of such disparity between the two sexes remain to this day on a global scale, with men entering Science, Technology, Engineering, and Mathematics (STEM) fields at a hugely disproportionate rate when compared to women overall [2]. Another case of remaining conformity to traditional gender roles can be observed in Japan, which— despite being a highly developed country— ranks 110th out of 144 countries in terms of gender inequality [3].

However, the focus should not be on the particular instances of gender inequality that can be observed today, but the agents of socialization and culturalization that together form a basis for those situations to flourish. This is where the work of Georg Simmel holds relevance. As argued by Simmel, the unique characteristics held by one are shaped by the multiple group affiliations one holds [4]. Explaining the influence of these diverse relationships on an individual's frame of mind, Simmel writes,

"The number of different social groups in which the individual participates, is one of the earmarks of culture. The modern person belongs first of all to his parental family, then to his family of procreation and thereby also to the family of his wife. Beyond this he belongs to his occupational group, which often involves him in several interest-groups."

In this statement, Simmel explains that the interplay of multiple group affiliations— ties to one's family, peer groups, and the society at large— come to ultimately form a cohesive way of thinking. The lasting relevance of Simmel in fields of sociological research is demonstrated by the work of many researchers [5] as they use his theory of culture as a foundational basis to their studies. Amongst these various social factors proposed by Simmel, the study maintains that group affiliations with both the family and the country as a collective are most influential in shaping one's societal perspective and thence, the extent to which one forms gender biases.

As aforementioned, the focus is on the social and cultural contexts that shape one's gender biases. For this reason, the research is centered on the age group of 12 to 19 year-olds, otherwise labeled as adolescents. Adolescents are a demographic uniquely different from that of children or adults as they tend to have more diverse social circles [6] and have "biographical availability" [7] which allows for them to engage in higher-risk activities. Additionally, adolescence is a critical time for the emotional and physical development of the brain and its functions as youngsters transition from child to adult. For instance, the brain's limbic and prefrontal regions have been observed to significantly develop throughout adolescence [8] [9] alongside the formation of one's identity and lifelong values. Such a period of rapid development and identity formation may also be the time when particular stereotypes and norms are formed and solidified. Thus, examining this demographic of 12 to 19 year-olds may be an indispensable part of uncovering the social factors that influence one's gender bias. Below is a

review of the conceptual toolkit utilized to study the above topics.

Theory

Based upon Georg Simmel's theories of the impact of membership in multiple group settings and the literature introduced above, the study deduces that country-level cultures such as the extent to which a country is collectivist and family-related characteristics such as a parent's educational background are most influential in shaping an adolescent's tendency to form gender biases. Gender bias, in the context of the study, is defined as the inclination to associate certain roles to each gender. For instance, one may hold a high level of gender bias if they firmly believe that women should be restricted from participating in the workforce. Conversely, one may also hold strong gender bias if they associate males with domestic activities and females with work-related activities, though this is a less common form of bias. The country-level cultures that were thought to most impact one's gender bias were selected using Geert Hofstede's Six Dimensions of Culture [10] and were chosen as 1) Collectivism vs. Individualism, 2) Uncertainty Avoidance, and 3) Masculinity. As for family-related characteristics, parents' educational attainment level and their employment status were deemed most important in shaping one's tendency to form gender stereotypes. Through the research of these two levels of culture— country-level and family-level— the key influences that give rise to gender bias in adolescents may be learned.

The Present Research

There were several major limitations to the studies reviewed and mentioned above. Firstly, the majority of the studies either focused on the formation of stereotypes across one or two cultures. This poses a threat to the generalizability of these studies' findings, as systematic differences across many cultures may warrant great disparity when applying their findings in other cultural contexts. In contrast, the present research sampled 41 participants collectively sharing 23 different nationalities. This diversified sampling perhaps adds to the population validity of this study as the sample represented a range of cultures that were rated contrastingly on Hofstede's scale of cultural dimensions. The examination of the development of gender stereotypes on such a globalized scale may ensure less setting threat to the validity of the research. Additionally, the structure of the research ensures reduced demand characteristics and social desirability bias with regards to measuring the extent of one's gender bias. The specific implicit-association test used measured one's response time autonomously and took into account whether the examinee had had prior experience with the test. Thus, the chances of the results of the test being manipulated to the participants may decrease, minimizing threats to internal validity. The present study is framed within the Simmelian perspective regarding group affiliations introduced above and focuses on these primary hypotheses:

H_1: Adolescents' stereotypes on traditional gender roles is likely to be more severe if their cultural background is more collectivist, masculine, and has higher uncertainty avoidance.

H_2: Adolescents' tendency to form gender bias is likely to be less severe if their mother is working or has attained academic degrees.

H_3: Adolescent females will be more likely to be influenced by country-level cultures and family-level characteristics than adolescent males. However, this will hold little influence on females' tendency to form gender stereotypes compared to males.

METHOD

Design

Using a mixed-methods approach coupled with an independent measures design, the study quantified variables of interest and ran multiple regression analyses to assess the extent to which the independent variables influence one's gender stereotyping. More specifically, ordered probit regression was used over ordinary linear regression as the dependent variable, level of gender bias, is an ordered categorical variable. Thus, it was more fitting for the study to use this type of regression analysis. By employing these statistical methods, age, gender, ethnicity, and parents' educational and work background were able to be controlled. Qualitative data were used from conglomerated interviews and were utilized to contextualize the results of the data. Though following an independent measures design, the method of random allocation was not employed in the study as it would be highly inefficient and futile, especially when considering the scope of the research.

Participants

This study draws data on 41 adolescents aged 12-19 from various academic institutions and communities on a globalized scale. Of these, the majority of adolescents sampled were in middle adolescence (15-17) (n = 23). The sample comprised of adolescents of various ethnicities; those of Hispanic/Latino (n = 3), East Asian (n = 10), South Asian (n = 13), Black or African American (n = 1), Pacific Islander (n = 1), and Caucasian/White (n = 19) descent were represented in the sample. The sample consisted of three age groups: early adolescents (10-14 years; M = 13.36 years, SD = 0.67; n = 11 [8 females]), middle adolescents (15-17 years; M = 16.56 years, SD = 0.66; n = 23 [19 females]), and late adolescents (18-20 years; M = 18.29 years, SD= 0.49; n= 7 [4 females]).

In regard to the results of the Harvard IAT test all participants took unproctored, nearly half received a result of "Moderate automatic association for male with career and female with

family" (n = 17), one value below the extreme of "Strong automatic association or male with career and female for family". The sample comprised of participants with a range of gender biases; scores of 1 (n = 1), 2 (n = 2), 3 (n = 2), 4, (n = 6), 5 (n = 10), 6 (n = 17), and 7 (n = 3) were represented.

Materials

In the study, a questionnaire comprising Harvard University's Implicit Association Test (IAT) for Gender-Career [11] and 8 demographic items relating to the participant's ethnic and family background and cultural identity was used. Additionally, the Country Comparison Tool from Hofstede Insights [12] was used to assess each country's rating on the cultural dimensions of interest. All three dimensions of interest— Individualism versus Collectivism (IDV), Masculinity versus Femininity (MAS), and Uncertainty Avoidance (UAI)— were assessed on a scale of 1-100, with 1 indicating almost no presence of the dimension in that specific country, and 100 indicating a

TABLE 1: Descriptive Statistics

Variable	n	Percentage	Mean	SD	Min. Value	Max. Value
Gender						
Male	10	24.39				
Female	31	75.61				
Age (years)						
10-14	11	26.83	13.36	0.67	12	14
15-17	23	56.10	16.56	0.66	15	17
18-20	7	17.07	18.29	0.49	18	19
Ethnicity						
Hispanic/Latino	3	6.38				
American Indian or Alaska Native	0	0.00				
East Asian	10	21.28				
South Asian	13	27.66				
Black or African American	1	2.13				
Pacific Islander	1	2.13				
White	19	40.13				
Cultural Identity						
North America	18	43.90				
South America	2	4.88				
Africa	0	0.00				
Asia	14	34.15				
Australia/Oceania	3	7.31				
Europe	4	9.76				

widespread presence. Harvard's IAT Test was used to measure the strength of associations between both sexes (men and women) and concepts (work and family). The online test consists of a 10-question survey asking to associate certain words with the male or female sex, followed by a section on demographics asking common questions about the participant's background. Next, participants are asked to sort items such as "Wedding", "Ben", "Corporation", and "Michelle" into one of the following categories: Male, Female, Career, and Family. Using specific keys on their keyboard, subjects were asked to categorize the items as quickly as possible. It is assumed that one will make a response more easily, and therefore, more quickly, when related items have the same key. For example, one may hold more traditional gender stereotypes when they are quicker to respond when [Female + Family] and [Male + Career] are paired together than when [Female + Career] and [Male + Career] are paired.

Results were then analyzed using the statistical software STATA. The use of such software ensured that variables such as age and ethnicity were controlled for and did not have a biasing effect on other variables. Furthermore, multiple regression analyses were run to simultaneously take into consideration a multitude of variables. This way, the extent to which each variable influenced another was able to be examined.

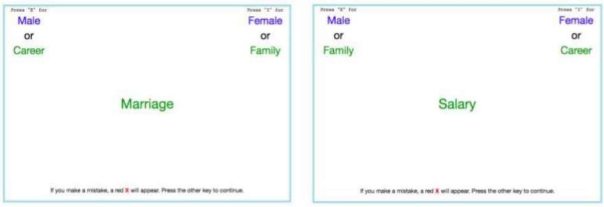

FIGURE 1 : Displays of two of the seven different iterations of the IAT Test that participants must complete. Participants are asked to press the "E" key to sort the given word to the left categories, and the "I" key to sort into the right categories.

Procedure

Most, if not all participants were recruited via email or text through each researcher's personal social connections developed in both casual and professional settings. There were great imbalances in terms of the age and sex of the participants, but it was observed that these differences did not affect the extent to which one forms gender stereotypes (p = 0.844 (age), r = 0.197 (sex)), nor did it influence any other variables tested. Participants were administered an online questionnaire that included an external link to a test measuring their tendency to associate men and women with either career or family. All 41 adolescents received and completed the test in the environment of their choice, with no proctoring of the examinee. In addition, a few of these adolescents were interviewed by phone to gain further contextual information with regards to their results on the IAT and the relationships found in the regression analyses.

RESULTS

From the multiple regression analyses ran, it can first be assumed by looking at Model 1 that level of uncertainty avoidance, one of three country-level cultural characteristics examined, does not influence one's tendency to form gender stereotypes ($p = 0.212$). However, a country's level of individualism and masculinity seem to have a great influence ($p = 0.034$, $p = 0.057$) on participants' scores on the IAT. These results partially reject Hypothesis 1, which assumes that one's gender bias is likely to be more severe if their cultural background is more collectivist, masculine, and has higher uncertainty avoidance. Likewise, the regression model shown in the first column shows that gender bias consistently decreases with an increase in individualism and increases with the level of masculinity, while holding little relation to uncertainty avoidance ($p = 0.212$). These two culture-related variables and their strong relation to the tendency to form stereotypes seems to be a continuing trend throughout the regression analyses, as elaborated on in later sections.

Model 2 isolates family-level characteristics such as one's parents' educational attainment from country-level characteristics that were examined before and investigates the effect these family-level characteristics directly have on gender bias. Contrary on Hypothesis 2, the level of educational attainment of the mother was positively related to the formation of traditional gender stereotypes, though not in any way that was statistically significant (p = 0.431) (college degree); p = 0.997) (Masters & Ph.D.)) When examining a father's educational attainment level in relation to the formation of traditional gender stereotypes, it was observed that the higher the degree obtained, the greater gender bias one tends to have. However, the p-values of these observations (p = 0.323 (college degree), p = 0.135 (Masters & Ph.D.)) suggest a weak relationship between these variables. As hypothesized, adolescents with low gender bias tend to be in a household where their mother is one of the breadwinners (p = 0.137), and the presence of a working father is linked to a greater level of gender bias (p = 0.508). Even so, these values were overall not statistically significant, which may indicate that these variables themselves do not directly affect one's tendency to form gender stereotypes.

Thirdly, it was analyzed if the effects of country-level characteristics (e.g. Individualism vs. Collectivism) and family-related variables (parents' work status, educational attainment) remained robust when those two social contexts were considered simultaneously. In this regression model, both individualism ($p = 0.000$) and masculinity ($p = 0.001$) held statistically significant relationships to one's level of gender bias. Once more, it was found that a higher score of individualism is linked to less gender bias and that a higher score of masculinity is associated with greater gender bias. In regard to the family-related characteristics that were analyzed, adolescents had more gender bias when in a household with a mother that had completed tertiary education and above. To specify, a mother's attainment of a college degree (*Coef.* = 1.640) had a greater impact on the formation of gender stereotypes than if they had obtained a attainment of an academic degree had a positive relation to the tendency to stereotype. Notably, adolescents whose fathers had completed a master's or Ph.D. degree were most likely to have gender bias (p = 0.031).

TABLE 2: Ordered Probit Regression on Gender Bias

	(1)	(2)	(3)	(4)
Individualism	-.0150*		-.0324***	-.0309***
	(.0071)		(.0090)	(.0095)
Uncertainty Avoidance	-.0108		-.0129	-.0010
	(.0087)		(.0097)	(.0101)
Masculinity	.0383**		.0843***	.0853**
	(.0201)		(.0255)	(.0271)
Mother's educational attainment (Ref. ≤ high school diploma)				
College degree		.4310	1.640*	1.524*
		(.5478)	(.6580)	(.6854)
Masters or Ph.D.		.0023	.0487	.0204
		(.6323)	(.6737)	(.6975)
Father's educational attainment (Ref. ≤ high school diploma)				
College degree		.5267	.3701	.5299
		(.5334)	(.5806)	(.6565)
Masters or Ph.D.		.8879	1.393*	1.512*
		(.5933)	(.6473)	(.6674)
Mother's working status (Ref. not working)				
Working		-.6199	-.8783*	-1.024*
		(.4167)	(.4431)	(.4794)
Father's working status (Ref. not working)				
Working		.4421	.6022	.5299
		(.6685)	(.7232)	(.7706)
Sex				.5593
				(.4331)
Race (Ref. White)				
Asian				.2723
				(.4275)
Other				.1853
				(.6273)
Age				.0220
				(.1120)
Pseudo R2	0.0554	0.0647	0.2082	0.2253
Observations	41	41	41	41
Cut1	-1.513	-1.319	.9020	1.997
	(1.304)	(.8149)	(1.774)	(2.828)
Cut2	-.8679	-.7867	1.627	2.749
	(1.268)	(.7595)	(1.755)	(2.821)
Cut3	-.5499	-.4603	2.033	3.187
	(1.265)	(.7538)	(1.768)	(2.830)
Cut4	.0251	.1690	2.807	3.986
	(1.272)	(.7395)	(1.791)	(2.847)
Cut5	.7231	.9000	3.773	4.971
	(1.273)	(.7530)	(1.822)	(2.868)
Cut6	2.308	2.491	5.850	7.124
	(1.309)	(.8124)	(1.939)	(2.997)

*p<.05. **p<.01. ***p<.001.

Note. Values are given as Std. Err. (Coef.).

The tendency to stereotype decreased, however, when participants lived in a household with a working mother and increased with the presence of a working father. These findings further support the first two hypotheses introduced in the above section. To conclude, variables that had statistically significant relationships with gender bias in the

last two regression models remained significant, only to a greater extent.

Model 4 was used to examine whether these results would remain robust when controlling for demographic variables such as ethnicity and sex. This model revealed that the significance of certain variables did indeed remain consistent with the above findings. A greater level of individualism suggested a lower tendency to gender stereotype (p = 0.001), and a greater level of masculinity in countries was linked to more gender bias in adolescents (p = 0.002), providing further empirical evidence for Hypothesis 1. As for the family-level characteristics hypothesized to heavily influence the development of one's stereotypes, the trends observed in the last few models remained, with a parent's obtainment of a college degree or higher increasing gender bias the most. In regard to the employment status of the parents and their influence, the presence of a working mother held statistically significant relationships to a lower tendency to stereotype (p = 0.033), and the presence of a working father held rather weak relationships (p = 0.444). However, this may be due to the huge variety of jobs that these parents hold. Concerning the demographic variables that were controlled, females tended to have greater gender bias (p = 0.197), and those who identified as Asian held more bias when compared to Caucasian and Other (Hispanic/Latino, African American, etc.) (p = 0.524). Higher age was also very loosely related to more gender bias (p = 0.844). However, the p-values of these control variables suggest that they hold little influence in shaping one's gender stereotypes. It can be concluded that significant relationships between masculinity, individualism, and mother's working status and parents' educational attainment remain, even with control of demographic variables.

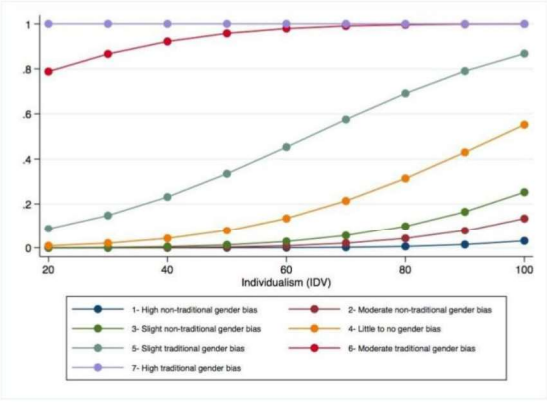

FIGURE 2: Cumulated Predicted Probabilities (Individualism Dimension)

As another form of analysis cumulated predicted probabilities for each of Hofstede's dimensions of interest were run. As displayed in Figure 3, the probability of forming traditional gender stereotypes (i.e. men should be the sole breadwinner) increases as a country is more individualistic. Notably, the probability of adolescents that hold slight traditional gender bias seems to increase by four-fold in a country with individualist scores in the 90s when compared to a country with scores in the 40s. The large fluctuations in the probability of forming traditional gender biases suggest a strong relationship between the level of individualism a culture has and the tendency to form gender bias.

The cumulated predicted probability model examining the masculinity dimension shows that the probability of one having non-traditional gender biases (ie. All women should participate in the workforce) decreases as the level of masculinity increases. This relationship between lower masculinity and less gender bias provides further support for Hypothesis 1, along with findings from Figure 2.

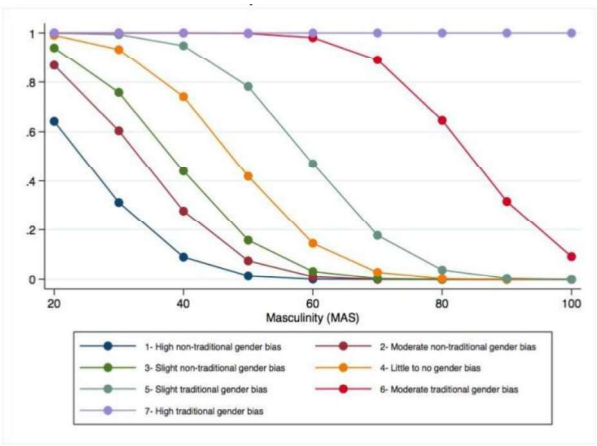

FIGURE 3: Cumulated Predicted Probabilities (Masculinity Dimension)

Interviews

In order to gain further insight into the country-level characteristics and the family-level characteristics that influence one's tendency to form gender bias, several interviews were conducted with adolescents of varying cultural and family backgrounds. One persistent trend in a couple of the interviews was the overlapping of two dimensions in one's daily life. For example, one respondent expressed that the classroom environment she was in leaned towards a collectivist culture, whilst her family environment emphasized individuality. This reveals yet another level of culture that were not addressed in the study, which is namely the school-level characteristics that may shape one's gender bias. This trend also leads us to consider other cultural levels which may influence adolescents' gender bias such as the types of media they are exposed to and the overall culture of the neighborhood they are raised in. When one respondent was asked about the differences that coexist in their household, they answered, "I don't really see much differences in terms of cultures, but there are definitely differences in religion in my household." This shows yet another facet of one's background that was not addressed in the study— religion. From several interviews, it was derived

that one's religious views could also be relevant in determining how collectivist and masculine one's background may be, along with several other factors that were noted above.

DISCUSSION

This research examined the predictors and influences of gender stereotyping in adolescents 12-19 years of age. The absence of these biases could generally be associated with a lower assessment on the masculinity dimension ($p < .002$) and a higher assessment on the individualist dimension ($p < .001$) in addition to the presence of a mother participating in the workforce ($p < .05$). These findings align with research previously conducted on the cultural factors that shape biases and stereotypes of out-groups [13] [14] [15]. These studies have attributed the avoidance of heterogeneity in collectivist cultures as a key reason that explains less-positive views regarding one's out-group. Therefore, it can be said that those in collectivist countries tend to strive for social inclusion, and in the process, conform to traditional gender norms that have been rooted in their respective countries for centuries. In summary, the results provide empirical evidence that two of three country-level characteristics examined— individualism and masculinity— play a significant role in shaping one's tendency to form gender stereotypes. However, it should be noted that the sample in the study was not representative of the population. Therefore, several threats to validity exist.

In regard to family-level characteristics, a higher level of educational attainment was shown to be a significant factor in decreasing one's gender bias, which dovetail previous research [16] [17]. An irregular finding was that demographic variables were overall not that influential in determining one's tendency to stereotype, which may have been due to the study's small sample size. This contrasts research previously conducted on adolescents [18] [19] which demonstrate that implicit bias and stereotyping increase as one ages.

Addressing Gender Bias

Considering that adolescence is a time of identity formation in which particular stereotypes and values are formed and solidified, the present study's results hold great relevance to policymakers in education and teachers alike. The results may lend insight into certain classroom structures and cultures that may effectively lower a child's tendency to develop extreme gender biases in the future. For instance, classrooms could adopt more individualistic classroom cultures with elements of cooperation and modesty, in contrast to a more masculine culture. As the findings derived from the study show, adolescents have already internalized traditional gender roles from a young age, and they remain in later adolescence as well. Therefore, the changes in policy and culture that should follow must directly intervene with one's own way of differentiating between the two genders to truly combat the current climate of inequality around the globe.

AKNOWLEDGEMENTS

A special thanks to Mr. Seungwon Lee of Columbia University for being my mentor; to Claire, Meera, Jack, and Anna for partaking in this project with me.

REFERENCES

[1] *Labor force participation rate, female (% of female population ages 15+) (modeled ILO estimate) | Data*. Data.worldbank.org. (2020). Retrieved 11 August 2020, from https://data.worldbank.org/indicator/SL.TLF.CACT.FE.ZS.

[2] *Data - OECD*. Oecd.org. (2020). Retrieved 10 August 2020, from https://www.oecd.org/gender/data/why-dont-more-girls-choose-stem-careers.htm.

[3] *Japan needs women to remain the world's third-largest economy*. World Economic Forum. (2020). Retrieved 11 August 2020, from https://www.weforum.org/agenda/2018/11/japan-needs-women-to-remain-the-worlds-third-largest-economy/.

[4] Simmel, G. (2014). *Conflict and the web of group affiliations* (pp. 135-139). Free Press.

[5] Thiel, A., & Seiberth, K. (2017). Migrant background, culture and ethnicity: sociological terms without explanatory value?!. *European Journal For Sport And Society*, *14*(3), 183-185. https://doi.org/10.1080/16138171.2017.1360553

[6] Rytina, S., & Morgan, D. (1982). The Arithmetic of Social Relations: The Interplay of Category and Network. *American Journal Of Sociology*, *88*(1), 88-113. https://doi.org/10.1086/227635

[7] McAdam, D. (1986). Recruitment to High-Risk Activism: The Case of Freedom Summer. *American Journal Of Sociology*, *92*(1), 64-90. https://doi.org/10.1086/228463

[8] Romeo, R. (2013). The Teenage Brain. *Current Directions In Psychological Science*, *22*(2), 140-145. https://doi.org/10.1177/0963721413475445

[9] Hartley, C., & Somerville, L. (2015). The neuroscience of adolescent decision-making. *Current Opinion In Behavioral Sciences*, *5*, 108-115. https://doi.org/10.1016/j.cobeha.2015.09.004

[10] Hofstede, G. (2009). Geert Hofstede cultural dimensions.

[11] Greenwald, A., & Farnham, S. (2000). Using the Implicit Association Test to measure self-esteem and self-concept. *Journal Of Personality And Social Psychology*, *79*(6), 1022-1038. https://doi.org/10.1037/0022-3514.79.6.1022

[12] *Country Comparison - Hofstede Insights*. Hofstede Insights. (2020). Retrieved 8 August 2020, from https://www.hofstede-insights.com/country-comparison/.

[13] Bastian, B., & Haslam, N. (2006). Psychological essentialism and stereotype endorsement. *Journal Of Experimental Social Psychology*, *42*(2), 228-235. https://doi.org/10.1016/j.jesp.2005.03.003
[14] Robert B., C., Richard J., B., Avril, T., Marcus Randall, W., Stephen, F., & Lloyd Reynolds, S. (1976). Basking in reflected glory: Three (football) field studies. *Journal Of Personality And Social Psychology*, *34*(3), 366-375. https://doi.org/10.1037/0022-3514.34.3.366
[15] Tajfel, H., Billig, M. G., Bundy, R. P., & Flament, C. (1971). Social categorization and intergroup behaviour. *European journal of social psychology*, *1*(2), 149-178.
[16] Garrido, N. (2017). *Does Education Reduce Sexism?*. Editorialexpress.com. Retrieved 12 August 2020, from https://editorialexpress.com/cgi-bin/conference/download.cgi?db_name=espe2017&paper_id=168.
[17] Saito, Y. (2014). Nier.go.jp. Retrieved 11 August 2020, from https://www.nier.go.jp/English/educationjapan/pdf/201403GEE.pdf.
[18] Pauker, K., Ambady, N., & Apfelbaum, E. (2010). Race Salience and Essentialist Thinking in Racial Stereotype Development. *Child Development*, *81*(6), 1799-1813. https://doi.org/10.1111/j.1467-8624.2010.01511.x
[19] Gonsalkorale, K., Sherman, J., & Klauer, K. (2009). Aging and prejudice: Diminished regulation of automatic race bias among older adults. *Journal Of Experimental Social Psychology*, *45*(2), 410-414. https://doi.org/10.1016/j.jesp.2008.11.004

The Study of Gravitational Radiation Through the Merging of Binary Neutron Stars

Swathya Singh Chauhan
Delhi Public School Greater Noida; Greater Noida, India
Email: swathya2604@gmail.com

Abstract – The study of gravitational waves/radiation was initially limited to only one way of detection and generally involved the study of black hole mergers. In 2017, the unanimous detection of GW170817 by LIGO and Virgo, and GRB 170817A by NASA's Fermi Space telescope led to an interest in studying binary neutron star mergers as it presented confirmation for past predictions by the Theory of General Relativity and also had new implications related to the Hubble's Constant, the resolution of stochastic backgrounds, the formation of the heavier elements in the universe and a lot more. There is also a possibility of the discovery of a new class of black holes as the nature of the post-merger remnant is unknown. This was the first discovery of its kind to have an electromagnetic component and this has led to the growth of multi-messenger astronomy, promoting further collaborations for these detections. LIGO and Virgo held another operation run later and one more binary neutron star merger candidate has been identified. Further detections and analyses are awaited.

Key Words – Relativity, LIGO, Binary neutron stars, Mergers, Multi-messenger discoveries

INTRODUCTION

Gravitational Waves, i.e., ripples through the fabric of space-time were first predicted by Einstein's Theory of General Relativity in 1916. [1] Einstein's mathematics showed that massive accelerating objects would disrupt space-time in a way such that 'waves' of space-time would propagate from the source, travelling at the speed of light in all directions. They carry information about their dramatic origins and about the nature of gravity itself. [2]

A lot of research and debate has been done on their nature and existence and they can be mathematically understood better through a simpler metric that was derived from Einstein's original equations by Asher Peres. He studied the plane wave-like line element for gravitational waves and obtained a metric defined through the proper time:

$ds^2 = -dx^2 - dy^2 - dz^2 + dt^2 - 2f(x, y, u)(dt - dz)^2$

where $u = t - z$ and f is a function of x, y and u. [3]

As further debate and research led to more and more conclusions on their existence, the hunt to detect gravitational waves started. Finally, nearly 100 years later, a gravitational wave signal was detected by both of the twin U.S.-based Laser Interferometer Gravitational-Wave Observatory detectors at Livingston, Louisiana and Hanford, Washington in 2015 from a black hole merger. [4] Since then, LIGO and other detectors like the Virgo interferometer at Italy have been working carefully to detect even more signals to learn more about the universe. Up until 2017, there had been no electromagnetic counterpart to the gravitational wave detections and as a result, these fields weren't really unified. However, an accidental detection of a strange signal led to a discovery that would change everything as it became the most talked-about discovery of the decade. A binary neutron star merger had been detected and it gave off both, gravitational as well as electromagnetic radiation.

DISCOVERY

On August 17, 2017, 8:41 pm EDT, a gravitational signal named GW170817 was detected by the LIGO detector at Hanford, Washington during the O2 Operation Run. It was originally identified as a single detector event at Hanford by a low-latency binary-coalescence search because the saturation at LIGO-Livingston detector prevented this from being reported as a simultaneous event. The low latency transfer of data from the Italy-based Virgo detector was also delayed. However, a visual inspection later revealed a clear chirp coming from a single source (Figure 1). A Gamma-ray burst (GRB 170817A) was also detected by NASA's Fermi space telescope around the same time. This was considered unlikely to be a mere coincidence and multiple follow up observations were launched around the world. [5]

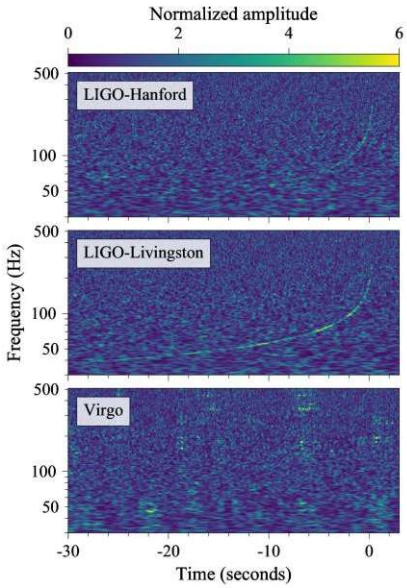

FIGURE 1: Time-Frequency plots with the upward-sweeping chirp for GW170817 from LIGO-Hanford, LIGO-Livingston and Virgo. The glitch in Livingston data has been removed. Chirp is not visible in Virgo due to low sensitivity and source location. [5]

The sources were predicted to be neutron stars, i.e., extremely dense remnants from the collapse of massive stars. This was because they were not as massive as the previously detected black holes; their masses were estimated to be somewhere between 1.1 to 1.6 solar masses, which lies close to the mass range for neutron stars. Scientists gave this mass estimation after analysing the recorded chirp. According to the theory of general relativity, the gravitational waves emitted by inspiraling compact objects during a quasi-circular orbit are characterized by a chirp like time evolution in their frequency that depends on a combination of the component masses and on the mass ratio and spins of the components. The equation used is:

$$M = \frac{c^3}{G}\left(\left(\frac{5}{96}\right)^3 \pi^{-8} (f_{GW})^{-11} (f'_{GW})^3\right)^{\frac{1}{5}}$$

where $M = \frac{(m1m2)^{\frac{3}{5}}}{(m1+m2)^{\frac{1}{5}}}$ is the chirp mass and $f'_{GW} = \frac{df_{GW}}{dt}$ is the rate of change of frequency. [5][6]

The chirp mass was measured to be $1.188^{+0.004}_{-0.002}$ $M\odot$, and the chirp, in this case, lasted 100 seconds and was seen through the entire frequency range of LIGO. This was unusual as binary black hole mergers produce chirps lasting a fraction of a second and are detected only by LIGO's sensitive frequency band. This meant that their masses were significantly lower than that of black holes. The LIGO data also gave their location to be quite close to Earth; around 130 million light-years. Collected data indicated that they had been spiralling in towards in the past and as they spiralled faster and came closer together, they stretched and distorted the surrounding space-time, releasing energy as gravitational waves, and then finally smashed into each other. [5]

This was the first time a cosmic event was detected in both gravitational waves and electromagnetic radiation. Due to the multiple detectors, we were able to quickly pinpoint the location of the event in the sky and launch multiple follow up observations. It was later confirmed that the signal was the result of the merger of two neutron stars in the lens-shaped galaxy NGC 4993, which was 140 million light-years away. [5] The results of these observations and further analysis had major scientific implications and confirmed several predictions made by the Theory of General Relativity by Albert Einstein.

IMPLICATIONS

I. Confirmations about the speed of gravitational waves in agreement to the Theory of General Relativity

GRB 170817A was observed 1.7 seconds after GW 170817. This leads to strong constraints being forced on the nature of gravity and gravitational waves when you combine this observed delay in evidence with knowledge of the source luminosity distance. Placing these bounds required a very deep understanding of waveform modelling and the uncertainties associated with it. The Shapiro time delay effect (also called gravitational time delay effect) is one of the classic tests of general relativity and in it, radar signals experience space-time dilation and there is a time delay because of the increase in path size. The observations were in agreement with this and after doing the required adjustments, the speed of gravitational waves was finally found to be equivalent to the speed of light to very high precision. This verifies the assumption in the Theory of General Relativity that gravitational waves travel at the speed of light in a vacuum (c). Various other tests were also conducted and they were all in good agreement with the Theory of General Relativity. [5][7]

II. Estimating the Hubble's Constant and expansion of the universe

Direct measurement of the luminosity distance of the source can be obtained from the gravitational wave signal and after calculating the redshift, we can infer cosmological parameters without relying on the cosmological distance ladder, which is not always accurate. The Hubble's Constant is calculated to be $H_o = 70^{+12}_{-8}\ km\ s^{-1}\ Mpc^{-1}$ when you use the association with the galaxy NGC 4993. This is the most probable value (minimum 68.3% probability) when compared with Plank Hubble's Constant, which is $H_o = 67.90^{+0.55}_{-0.55}\ km\ s^{-1}\ Mpc^{-1}$. This was consistent with the estimated value of Hubble's Constant through EM studies. Now, this provides confirmation and the calculations about the expansion of the universe can be more accurate. We can also assume the cosmological constants to be known and then calculate the luminosity distance of the source using the

redshift and the above association. This would lead to improved measurement of the inclination angle of the source and would also help in figuring out the gamma-ray burst opening angle. [5][8]

III. Resolving stochastic background from unresolved Binary Neutron Star mergers

To create a background, we need the rate of merger and through this discovery, we have a very reliable source for calculating the rate in Binary Neutron Stars. Within LIGO's O2 Operation Run, GW170817 was the only discovery to have a false alarm rate below 0.01 year and by using this as a foolproof source, we can infer the local coalescence rate density (R) of Binary Neutron Star (BNS) systems. For GW 170817, we assume the mass distribution of the components to be flat between 1 and 2 solar masses, and their dimensionless spins to be below 0.4. $R = 1540^{+3200}_{-1220}\ Gpc^{-3}\ yr^{-1}$ when we impose the upper limit of $12600\ Gpc^{-3}\ yr^{-1}$ which was found as a result of LIGO's O1 Operation Run earlier. Through this inferred rate, countless unresolved BNS mergers can be localised and compared in magnitude to existing Binary Black Hole (BBH) mergers. This can be used to create a combined as well as separate stochastic background for BNS and BBH mergers which will help detect gravitational waves in the future for further research. [9]

IV. Study of the post-merger remnants as a possible new class of black holes

The object resulting from the merger is 2.7 solar masses and it's a kilonova, i.e., the remaining material from the merger is being blown out into space and it can reach up to 1000 times the brightness of a classical nova. The kilonova AT2017gfo is the first kilonova for which detailed optical spectra has been recorded. [10] Binary neutron star mergers may result in a short or long-lived neutron star remnant that could emit gravitational waves following the merger and there are 4 predictions about its nature:
1) It could form a black hole directly,
2) It could form a hypermassive neutron star that would collapse into a black hole within a second,
3) It could form a supramassive neutron star that would collapse into a black hole on timescales larger than 1 second or,
4) It could form a stable neutron star. [11][12]

The result depends upon the final mass as well as the chemical properties of the neutron stars. This post-merger remnant is predicted to be a hypermassive neutron star that has collapsed into a low-mass black hole by now. [13] This would mean the discovery of a new class of black holes by LIGO. However, other options cannot be ruled out yet and this can only be confirmed once the gravitational waves from this remnant are detected and analysed. Several attempts were made at detecting these in vain but continued observations over the next several years may confirm or refute this prediction. [11]

V. Origin of the heavier elements in the universe

Because we were able to pinpoint a specific location in the sky due to LIGO and Virgo's observations, Electromagnetic (EM) follow-up observations were possible and they revealed that a large fraction, roughly half, of the universe's heavier elements were created by neutron star mergers. The key method used to figure this out was by looking at the optical spectrum of the event as the light of the kilonova AT2017gfo comes from the material released by the neutron stars as they merged. It was observed that the material contains abundant heavy elements and this provides a plausible explanation for their origins. Now, it's widely accepted that all elements starting from Niobium (Atomic number 41) to Uranium (Atomic number 92) excluding Technitium (Atomic number 43) and Promethium (Atomic number 61) have been created in large quantities during and as a result of binary neutron star mergers. [14]

FUTURE RESEARCH AND CONCLUSION

LIGO and Virgo started their O3 operations run in April 2019 with more sensitivity than the last time and on 25 April 2019, the LIGO Livingston Observatory picked up what appeared to be gravitational ripples from another collision of two neutron stars. This has been named GW190425 and it serves as confirmatory evidence for the implications of the previous discovery. [15] LIGO suspended its O3 run earlier in March 2020 instead of April 2020 due to the COVID-19 Pandemic. [16] Multiple candidates have been identified as possible Binary Neutron Star, Binary Black Hole and Neutron Star-Black Hole mergers, but further analyses of the data sets are required before any confirmed detections. [17]

When dealing with gravitational wave detections, it has been observed that the low sensitivity of the instruments being used is often a hindrance to accurate detections, leading to a lot of time being lost while working with incomplete data. To counter this, a more interferometers could be built and upgraded from time to time, thereby increasing their sensitivity and detection range. Another suggested solution to the common problem of high false alarm rates in observations could be to build a space-based detector as that would largely prevent any noisy disturbances from Earth. The list of possible improvements or upgrades is endless and so are the possibilities of what we might uncover because of them in the future.

The most remarkable aspect about this infamous discovery is that it wouldn't have been possible without the cooperation of several astronomers and physicists spread across the globe. The communication was swift and collaboration was easily facilitated. This demonstrates the strength of multi-messenger astronomy in projects of such crucial importance dealing with gravitational waves. Now,

data sets and possible gravitational wave detections by the LIGO-Virgo Collaborations are being made public as soon as possible as Open Public Alerts to facilitate gravitational-wave transient event detections. The era of multi-messenger astronomy is here with a bang, especially so for gravitational radiation research [17], and the author believes that in the future, physical barriers would be almost non-existent as the entire planet would transform into a giant observatory, uniting in the quest to uncover the secrets of the mysterious cosmos.

ACKNOWLEDGEMENTS

The author would like to thank Professor Arvind Borde for introducing her to the Theory of General Relativity and his valuable guidance during the initial stages of this paper during the summer of 2019. She would also like to express heartfelt gratitude for the extensive feedback sent by the reviewers for the IYRC, as their suggestions and critique played a crucial role in shaping and polishing the paper into its final version.

REFERENCES

[1] Einstein, A. (n.d.). Volume 6: The Berlin Years: Writings, 1914-1917 (English translation supplement) pages 146 - 199. Retrieved from https://einsteinpapers.press.princeton.edu/vol6-trans/158

[2] What are Gravitational Waves? (n.d.). Retrieved from https://www.ligo.caltech.edu/page/what-are-gw

[3] Peres, A. (1959). Some Gravitational Waves. Physical Review Letters, 3(12), 571-572. https://doi.org/10.1103/PhysRevLett.3.571

[4] Abbott, B. P., et al (2016). Observation of Gravitational Waves from a Binary Black Hole Merger. Physical Review Letters, 116(6), 061102. https://doi.org/10.1103/PhysRevLett.116.061102

[5] Abbott, B. P., et al (2017). GW170817: Observation of Gravitational Waves from a Binary Neutron Star Inspiral. Physical Review Letters, 119(16), 161101. https://doi.org/10.1103/PhysRevLett.119.161101

[6] Abbott, B. P., et al (2016). The basic physics of the binary black hole merger GW150914. Annalen Der Physik, 529(1-2), 1600209. https://doi.org/10.1002/andp.201600209

[7] Abbott, B. P., et al (2019). Tests of General Relativity with GW170817. Physical Review Letters, 123(1). https://doi.org/10.1103/PhysRevLett.123.011102

[8] Abbott, B. P., et al (2017). A gravitational-wave standard siren measurement of the Hubble constant. Nature 551, 85–88. https://doi.org/10.1038/nature24471

[9] Abbott, B. P., et al (2018). GW170817: Implications for the Stochastic Gravitational-Wave Background from Compact Binary Coalescences. Physical Review Letters, 120(9). https://doi.org/10.1103/PhysRevLett.120.091101

[10] Abbott, B. P., et al (2019). Properties of the Binary Neutron Star Merger GW170817. Physical Review X, 9(1). https://doi.org/10.1103/PhysRevX.9.011001

[11] Another long hard look for a remnant of GW170817. (n.d.). Retrieved from https://www.ligo.org/science/Publication-GW170817PostMergerLong/index.php

[12] Abbott, B. P., et al (2017). Search for Post-merger Gravitational Waves from the Remnant of the Binary Neutron Star Merger GW170817. The Astrophysical Journal, 851(1). https://doi.org/10.3847/2041-8213/aa9a35

[13] Abbott, B. P., et al (2020). Model comparison from LIGO–Virgo data on GW170817's binary components and consequences for the merger remnant. Classical and Quantum Gravity, 37(4), 045006. https://doi.org/10.1088/1361-6382/ab5f7c

[14] Watson, D., et al (2019). Identification of strontium in the merger of two neutron stars. Nature, 574(7779), 497-500. https://doi.org/10.1038/s41586-019-1676-3

[15] Abbott, B. P., et al (2020). GW190425: Observation of a Compact Binary Coalescence with Total Mass $\sim 3.4\ M\odot$, The Astrophysical Journal, 892(1). https://doi.org/10.3847/2041-8213/ab75f5

[16] Observatory Status. (n.d.). Retrieved from https://www.ligo.caltech.edu/page/observatory-status

[17] Abbott, B. P., et al (2017). Multi-messenger Observations of a Binary Neutron Star Merger. The Astrophysical Journal, 848(2). https://doi.org/10.3847/2041-8213/aa91c9

The Use of CpG Oligodeoxynucleotides as an Adjuvant for Immunotherapy to Mediate the T-Helper Cell Response Against Dog Allergies

Meagan Eickelbeck and Sanny Chan
Byram Hills High School; Armonk, United Sates
Email: meaganjbeck@gmail.com

Abstract - Dog allergies are a nationwide concern, with 15 million Americans suffering from this allergy. Currently, the treatment against allergies, allergen immunotherapy (AIT), lacks efficacy in treating most allergies and has yet to focus on improving AIT for dog allergies. This study is the first to determine whether or not adding a bacterial adjuvant, CpG ODNs, to AIT will prevent an allergic response to dog allergens. *In vitro* observation of cell responses to dog allergens, combined with and without CpG ODNs, was assessed. When evaluating the effectiveness of adding the CpG ODN, the type of T-helper cell response was determined through flow cytometry. Results indicated a decrease in Th2 cells, with no increase in Th1 cells. Overall, this demonstrates that the use of CpG ODNs has the potential to amend the immune response. Ultimately, the goal of this research extends beyond treating dog allergies. Ideally, researchers hope to fully understand the method of using bacterial adjuvants against allergies so the treatment can be widespread across different types of allergies.

Key Words – T-helper 2 cells, CpG ODNS, AIT

INTRODUCTION

More than 50 million Americans suffer from allergies; three in ten are allergic to dogs (Grayson, 2018). There are currently seven known dog allergens, classified as Can f 1-7, that are considered a major risk factor for developing allergic rhinitis and asthma (Chan & Leung, 2018) As allergies are growing at a rapid rate, at 6.4% increase per year (cdc.gov, 2017), the need for an effective treatment is critical.

Allergies present themselves when a foreign antigen is displayed to immune cells. Allergens are recognized by CD4 T helper (Th) cells, specifically, CD4 Th2 cells that stimulate the production of immunoglobulin E (IgE) antibodies from B cells through chemical signals, such as interleukins (IL) (Reece et al., 2018). The type of interleukin secreted determines the nature of the T cell response. Interleukin associated with the Th2 response encourages the production of IgE, ultimately leading to an allergic response. Allergic responses cause symptoms that can range from watery eyes, sneezing, rashes, to anaphylaxis (Grayson, 2018). To cure these allergic responses there is currently only one treatment method, allergen immunotherapy (AIT) (Cox, 2018). AIT works to counteract the Th2 allergic response by promoting the production of immunoglobulin antibodies and interleukins associated with the Th1 response, which normally occurs in response to intracellular parasites (Janeway, 1999). AIT involves the gradually increasing introduction of allergenic substance that an individual is allergic to. The goal is to modify the immune system away from an allergic Th2 response upon exposure. However, AIT faces barriers, such as a lack of effectiveness when using the crude allergen extract; therefore, future research must focus on new solutions to overcome this obstacle (Chan & Leung, 2018). One possible solution is the addition of an adjuvant, a substance that modulates immune responses to an antigen.

Adjuvants have been shown to amplify the effect of immunotherapy by modulating the immune response (Shi, 2019). By recruiting specific populations of immune cells, adjuvants play a role in stimulating a Th1 response (Shi, 2019). One promising adjuvant is the cytosine-guanine oligodeoxynucleotide (CpG ODN). CpG ODN is a short single-stranded segment of bacterial DNA that contains unmethylated CpG dinucleotides (invivogen.com). CpG ODNs are agonists of Toll-like receptor (TLR) 9, which is important because TLRs play a key role in the induction of Th1 immune responses (Farrokhi et al., 2017). The use of CpG ODNs in immunotherapy has the potential to be curative in the treatment of allergic diseases (Farrokhi et al., 2017). Thus, the focus of this study is to improve immunotherapy for dog allergies with the use of the CpG ODN adjuvant. This study is the first of its kind to use dog allergens and the CpG ODN adjuvant together. In the end, this treatment may have the potential to alter the immune pathway, ultimately stopping allergic reactions and reducing the risk of anaphylaxis, a potentially deadly condition.

I. The Immune System and Th1/Th2 Cell Response

Th2 cells play an important role in the humoral immune response by releasing interleukins to signal the production of antibodies, specifically the allergic antibody, IgE (Umetsu & DeKruyff, 1997). When produced, IgE binds to mast cells, producing an allergic response (Galli & Tsai, 2012). Th2 cells represent a harmful adaptive response to antigens by amplifying and prolonging allergic inflammation, as well as

late-phase reactions, which are associated with airway hyperreactivity that can lead to asthma and allergic rhinitis (Umetsu & DeKruyff, 1997). By contrast, Th1 cells inhibit the development of allergic reactions because the chemicals secreted, IFN-γ and IL-12, do not promote IgE synthesis (Umetsu & DeKruyff, 1997).

It has been found that the Th1 cell response cascade inhibits the proliferation of Th2 cytokines, thus inhibiting allergic responses (reviewed in D'Elios et al., 2011). The Th1 cell response includes the secretion of IL-12 and IL-18, which signal for IFN-γ and inhibit the secretion of IgE (Yoshimoto et al., 1997). However, Th2 cells cannot signal for the synthesis of IgE when Th1 cytokines are proliferating because these chemicals secrete signals for different antibody production (Oriss et al., 1997). Therefore, the ideal immune response is the Th1 cell response. It is possible to induce a Th1 reactions over a Th2 reaction with the use of adjuvants, one being CpG ODNs. CpG ODNs have been shown to suppress the Th2 response and induce a Th1 response; therefore, CpG ODNs are currently studied as a tool to induce Th1 cell responses.

II. CpG ODNs Help Induce Th1 Cell Response

Preclinical models of asthma have demonstrated that CpG-ODNs are potent inhibitors of atopic (allergic) responses, suppressing Th2 cytokines and reducing airway eosinophilia and levels of IgE (reviewed in Fonseca & Kline, 2009). Airway eosinophilia was significantly reduced ($p < 0.01$) in mice treated with CpG ODN immunotherapy compared to mice treated with regular AIT (Jain et al., 2003). CpG ODNs are currently being developed as a vaccine adjuvant to prevent or treat allergies (reviewed in Hanagata, 2017). Thus, the introduction of an adjuvant provides a promising alternative to improve immunotherapy.

CpG ODNs bind to cells that express toll-like receptor 9 (TLR9) inducing a response that is biased toward Th1 immunity (Shirota & Klinman, 2014). In 2018, Lehto et al. (2018) found that mice who were allergic to timothy grass allergen and received CpG ODN immunotherapy reacted with a Th1 cell type response, resulting in a significant decrease in allergen-specific IgE levels ($p < 0.05$). This finding indicates that the CpG ODN sequences worked to decrease and weaken the allergic symptoms. The results are promising, suggesting that this technique, AIT with CpG ODNs, could be applied with different allergens.

Another study by Srivastava et al. (2015) analyzed the use of CpG ODNs with AIT against peanut allergies in a murine mouse model. Only 30% of the mice that received the CpG ODN with the peanut allergen had an allergic response, whereas 100% of the mice receiving the allergen alone had an allergic reaction. Additionally, a significant decrease in IgE was observed ($p < 0.001$), indicating a shift to a Th1 response. Further, Marshall et al. (2001) conducted a study with similar results, examining the properties of CpG ODNs linked with Amb a 1, a ragweed allergen, *in vitro*. This study found a marked reduction of allergen-induced IL-4 ($P < 0.05$) and IL-5 ($P < 0.05$) production while also showing an increase of IFN-γ ($P < 0.005$). Together, the data indicates a shift away from the Th2 response, since IFN-γ is connected to the Th1 response. Thus, the linkage of Amb a 1 to CpG ODNs appears to alter the immune response through the downregulation of the Th2 cytokine response by promoting the secretion of IFN-γ. Other studies, such as Kitagaki et al. 2002, have analyzed the relationship between interleukins and the Th2/Th1 response.

Since interleukins are the signaling molecules that determine whether a response is Th1 or Th2, they are an important factor in the immune pathway. Kitagaki et al. (2002) found CpG ODN-induced suppression of established Th2 responses in mice through the inhibition of antigen-induced IL-5 and the production of IL-12. When CpG ODNs were administered with immunotherapy, the production of IL-5 was significantly inhibited ($p = 0.01$). In other words, the therapy stimulated the production of interleukins associated with the Th1 response resulting in Th2 response being inhibited.

Overall, the results from multiple studies provide promising results for the use of CpG ODN sequences in immunotherapy to prevent allergies. The use of CpG ODNs has been shown to decrease the Th2 allergic response with ragweed (Lehto et al., 2018) and peanut allergens (Srivastava et al., 2015), but has never been tested with dog allergens. Therefore, this study will be the first of its kind to focus on how CpG ODNs are able to affect the immune pathway of cell cultures from patients sensitized to dog allergens. The goal of this study is to inhibit allergic response by inducing a Th1 cell response.

1. Obtain lymphocytes and culture the cells with commercially bought dog allergens
2. Break the cells cultures into four treatment groups, one being the experimental, which is IL-2 with an active form of CpG ODNs
3. Analyze cell proliferation of Th2 and Th1 cells, using in the different cell cultures by flow cytometry and FlowJo software

H_0: Lymphocytes that receive the CpG oligodeoxynucleotide adjuvant immunotherapy will not experience a decrease in the Th2 immune reaction.

H_1: CpG oligodeoxynucleotide adjuvant immunotherapy will significantly decrease the Th2 immune reaction within the dog sensitized lymphocyte cultures.

METHODS

I. Samples

Twelve human blood samples were obtained as cryopreserved buffy coat with peripheral blood mononuclear cells (PBMC's) from the biobank under IRB approval, six were sensitized to dogs and six were non-allergic. The blood samples were separated and organized in 96 well plates. For each sample there two negative controls, a positive control, and an experimental group. One negative control contained

the sample and dog allergen only. The other negative control contained the cells, Can f 1-7, IL-2, and inactive CpG ODNs. The experimental group contained the sample with the IL-2, active CpG ODN, and allergen. Finally, the positive control group contained the sample and IL-2 only.

II. CpG Oligodeoxynucleotide

The CpG ODN were purchased from InvivoGen. The purchased adjuvant was ODN-2395 - TLR ligand; this was a class C synthetic CpG ODN.

III. PBMC Separation

Diluted blood with PBS in equal amounts and layered on top of Ficoll-Paque PLUS density gradient media (#GE17-1440-03, Millipore Sigma) and centrifuge. Obtained the buffy coat layer by using a transfer pipet, mixed with PBS to rinse, centrifuge. Freezing media containing 10% DMSO with 90% fetal bovine serum (FBS) and frozen to -80°C.

IV. Preparation of Cell Cultures

Rinse frozen buffy coats PBS and resuspended in X-vivo 20 (Lonza) + 20% FBS at 1x10^6 per ml. Spin 10' at 400g full brake. Aspirate off liquid and resuspend pellet in 10 ml PBS, take out 10ul for counting. Calculate cells/well for 96 well plate 3x10^5 cells per well needed. Separate out depending on conditions. Pellet cells and add to 200ul of X-vivo with a final 4ul of Acetone Precipitate Dog Extract (Stallergenes Greer) with CpG ODN 2395 or CpG ODN 2395 Control (InvivoGen) as indicated and incubated at 37°C for 1h. Add 0.3ul IL-2 (100U/ml) to ensure T cell surivial. For 96 well plate there will be ~300ul of media/cells. CpG at 0.6ul (2uM final concentration InvivoGen ODN 2395). Re-suspend cells to 1x10^6/ml in X-vivo 20+20% FBS media and plate at 5x10^5 per well and add PBS in empty wells around cells and leave for 5-7 days. During incubation media was not replenished and viability was assessed during flow cytometry using LIVE/DEAD fixable aqua.

V. Intracellular Staining of Cells

BD biosciences Fix and Perm Fixation and Permeabilization kit GAS003. LIVE/DEAD Fixable Dead Fixable Stain Dye BD biosciences L34957. Take ~1x10^6 cells out per FACs tube and spin down 12000 RPM for 5min. Add 1ml PBS(or in dye free (D10 or R10) media). Decant off and keep at room temp 20 min. Spin 12000 rpm for 5 min, leave the residual ~300ul. Add antibody as recommended by manufacturer in dark hood and mix. Incubate Room temp 20' in dark. Wash with 1ml PBS and spin 12000 rpm for 5 min. Add 210 ul of Cytofix/cytoperm for 20 min. Wash x2 1ml each with Perm buffer and spin 12000 rpm for 5min, leave residual fluid. Add intracellular antibody as recommended and incubate 30min at room temp in dark. Spin and resuspend in 1%PFA. Prepare Comp tubes.

VI. Flow Cytometry

For evaluation of surface receptors, LIVE/DEAD Fixable Aqua stain (#L34957, ThermoFisher) was used to determine living cells followed by antibodies directed against surface markers CD4 (#317417), CD8 (#344741), CD19 (#302205), and CD21 (#354911, BioLegend). Cells were incubated with antibodies at room temperature for 20 min and then washed with PBS. For intracellular staining cells were permeabilized with True-Nuclear™ Transcription Factor Buffer Set (BioLegend) per protocol followed by incubation with antibodies against T-bet and Fox-P3 for 1h at 37°C and fixed. Figure 1 shows a detailed list of all antibodies. Samples were acquired using a Fortessa flow cytometer (BD Bioscience) and analyzed using FlowJo software.

Laser	EM Filter	Marker	Color / Format	Host / Target	Isotype	Catalog *	Amout used per 1E6 cells (ul)	Voltages	
FSS								400	A,H,W
SSC								250	A,H,W
637	670/30	GATA-3	APC	Mouse anti-Human	IgG2b κ	653805	5	610	
637	780/60	CD4	APC-Cy7	Mouse anti-Human	IgG2b κ	317417	5	450	
488	530/30	CD19	FITC	Mouse anti-Human	IgG1 κ	302205	5	450	
405	525/50	Live/ Dead Aqua	BV510	All Species		#L34957	1	500	
405	610/20	CD8	BV 605	Mouse anti-Human	IgG1 κ	344741	5	400	
561	586/15	FoxP3	PE	Mouse anti-Human	IgG1 κ	320007	5	550	
561	610/20	T-bet	PE-Tx Red (PE-Dazzle 594)	Mouse anti-Human	IgG1 κ	644827	5	485	
561	670/30	CD25	PE-Cy5	Mouse anti-Human	IgG1 κ	302607	5	560	
561	780/60	CD21	PE-Cy7	Mouse anti-Human	IgG1 κ	354911	5	600	

Figure 1. ***Antibody list for flow cytometry.*** These are all the antibodies used for flow cytometry including the EM filter, marker, color, heat/target, isotope, catalog, amount used, and voltage.

VII. Statistics

Data analysis was performed in Excel (Microsoft) to define the mean and standard deviation. A t-test was used to find significance between groups. Alpha was set at 0.05.

RESULTS

I. Cell Cultures

Before evaluating the types of cells that proliferated in each sample, pictures of each cell culture were taken (Figure 2). The pictures depicted high cell proliferation, however, the pictures did not reveal what type of T cells were present.

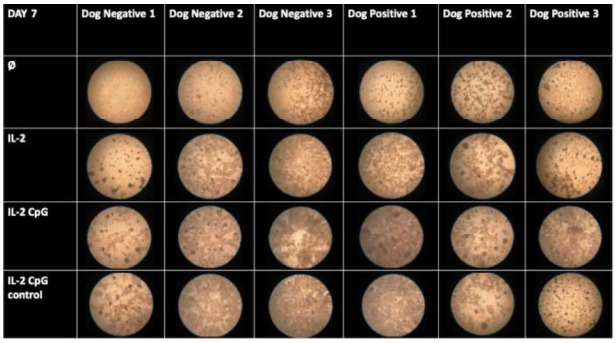

Figure 2. ***Pictures of cell cultures.*** This picture shows the cell cultures of half the dog allergic and non-allergic samples. These pictures were taken seven days after incubation. The dark spots indicate cell proliferation.

II. T Helper Cell Characterization

T helper cells were stained and run through flow cytometry in order to identify the type of T cells that proliferated. The family of T helper cells was derived based upon the transcription factors present; cells that are GATA-3+ are Th2 cells, and cells that are T-Bet + are Th1 cells. The percent of Th1 and Th2 cells were compared between the dog allergic treatments and non-allergic treatments. Using flow cytometry percent of cells that were GATA-3+ or T-Bet + were determined (Figure 3).

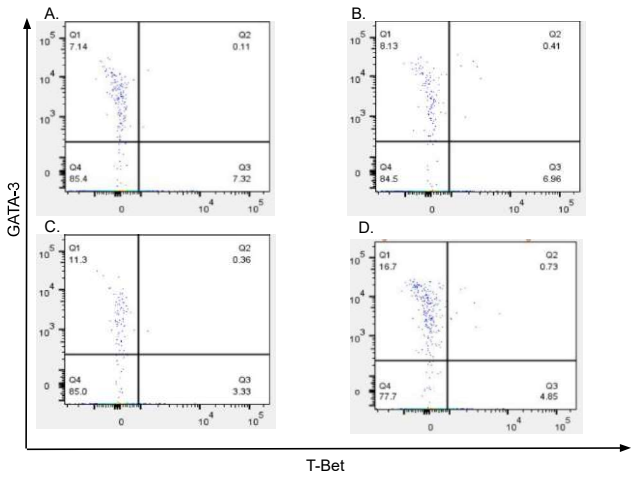

Figure 3. ***Flow cytometry results of an dog allergic sample.*** A. The graph shows the T-cells for the control group. B. The T-cell results for the group that only received IL-2 and the allergen. C. The T-cells that resulted from IL-2 CpG treatment. D. The T-cells that resulted from the CpG control group. Note that this data represents only one sample and demonstrates where the following data originates from.

III. Observing the T Helper Cell Responses to Major Dog Allergens Can f 1-7

After flow cytometry, the percentage of cells that were GATA-3+ (indicating the presence of Th2 cells) was averaged. Standard deviation was then calculated for each average. Results showed a decrease in Th2 cells with the allergic group that received the IL-2 CpG treatment compared to the non-allergic IL-2 CpG group at a significant value ($p = 0.04954$). In the dog negative control group, 26.99% of the cells were GATA-3+, in the IL-2 CpG dog negative group 29.72% of the cells were GATA-3+, compared to 25.91% of dog positive control cells. These values were compared to the dog positive IL-2 CpG group that had 5.90% of their cells GATA-3 positive (Figure 4).

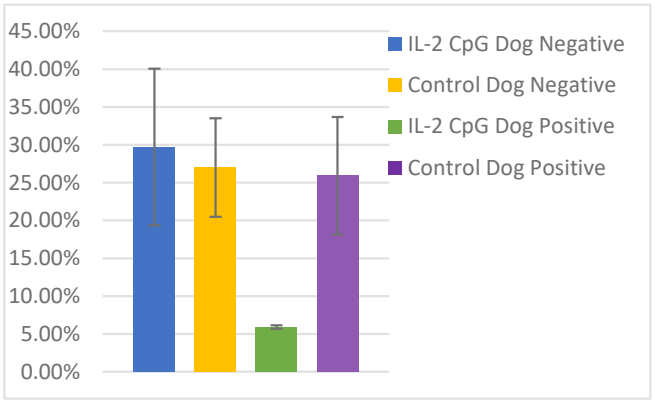

Figure 4. ***The percent of cells that are GATA-3+ and T-Bet-.*** This graph shows the averages of GATA-3+ or Th2 cells for each treatment group and also includes standard deviation error bars. The averages were taken from the six samples in each treatment group.

The percent of T helper cells that are T-Bet+ represent the Th1 cell population. Averages were taken from each allergic and non-allergic treatment group. Standard deviation was derived from these averages. The overall level of T-Bet + cells were higher in the allergic and non-allergic control, but there was not a significant increase ($p = 0.211$, $p = 0.391$) among any of these values (Figure 5).

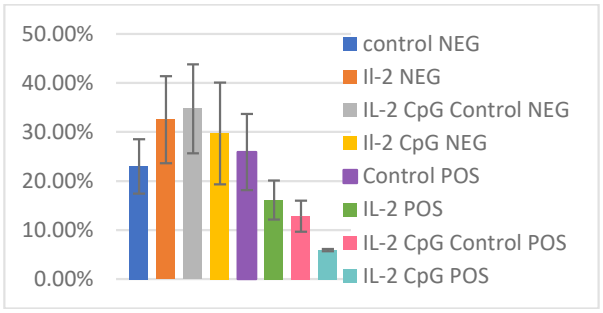

Figure 5. ***The Percent of Cells that are GATA-3 - and T-Bet+.*** These cells were identified by flow cytometry based on if the T-Bet transcription factor was present. Each sample average and standard deviation are depicted in the graph above. Significance was calculated, however, no significance was observed.

DISCUSSION

This study aimed to determine whether or not adding CpG oligodeoxynucleotides to AIT would alter the T helper cell response from a Th2 response to a Th1 response of a dog allergic individual. Results revealed there was a decrease of Th2 cells produced by the group that was dog allergic and received the active CpG treatment and this finding was statistically significant ($p = 0.04954$). This is important since Th2 cells are associated with an allergic response. However, to fully evaluate the effectiveness of the use of CpG ODNs,

the Th1 cell population was also observed. Using transcription factor T-Bet and flow cytometry, the percent of proliferated cells that were Th1 type was found. The important group to observe was the dog allergic experimental treatment group, which was compared against all the control groups. Ultimately, we did not detect a noticeable increase in Th1 cells. This is an interesting finding. Due to the properties of the CpG ODN, as the population of Th2 cells decreased, the Th1 cell population should have increased. This was not the case. Future research should repeat this study with the goal of advancing the field of immunology.

This study has the following limitations. Ideally, our goal was to have fresh lymphocytes, however, the cells were obtained from the biobank were frozen. Once samples were thawed and cells were counted, there was a limited number of living cells due to poor cryopreservation. This low cell count potentially affected the results. Additionally, this study used a commercial mixture of dog allergenic proteins, which included Can f 1-7. Ideally, future studies should look to make their own protein so that they are using one specific allergen and the exact amount of the allergen they are using is known. Going forward, this study should be replicated with samples that have higher cell counts by using a fresh sample compared to a frozen one and using fresh lab made recombinant allergens.

In the future, immunotherapy research must continue. If our method can be used successfully with dog allergens, it is likely that it can become more widespread and be utilized with even more allergies or other diseases, such as cancer (Hanagata, 2017), and even in making normal childhood vaccinations more effective with the addition of CpG adjuvants. Therefore, it is important to repeat this study for more reliable results and to use this study's methods as a model for future studies that work at targeting the body's T helper cells.

Much research has shown the benefits of living and working with dogs, from the joys of companionship to the life-saving attributes of service dogs. However, millions of Americans are faced with the obstacle of debilitating dog allergies, potentially preventing them from interacting with various breeds of dogs. Currently, allergy treatments are limited, and allergen immunotherapy has yet to show clear effectiveness and efficacy against dog allergens. The use of a bacteria adjuvant with immunotherapy has shown promising results in altering the immune response against other allergens. Therefore, this study was the first of its kind to evaluate the use of CpG ODNs against dog allergies. Results of this study, although not statistically significant, showed a decrease in Th2 cells, with no increase in Th1 cells. Be that as it may, this study suggests a trend that promotes the use of CpG ODNs as a method to alter the immune response to dog allergens. In the future, there are several factors that should be addressed. Research should aim to use a single recombinant allergen and further investigate dosing of CpG. In addition, the amount of allergen used in each treatment should also be evaluated, with the ultimate overall goal to complete the study *in vivo*. Finally, researchers should turn to other emerging methods such as the use of nano-allergens. Nano-allergens are modified nanoparticles that are able to detect the number of epitopes on an allergen to recognize the severity of that allergen. This could be an important method to explore, as it has the potential to bring the field of treating allergies to a new level of personalized medicine.

In the end, results from this paper, along with past findings concerning the use of CpG ODNs as an adjuvant for immunotherapy (Lehto et al., 2018; Srivastava et al., 2015; Marshall et al., 2001) lay the groundwork for future research to uncover a more efficient method for treating allergies. As allergies are on the rise, it is important that a reliable treatment is developed, as the threat of dog allergies is ever present. Even when a dog leaves a public area, evidence of their allergens remain for several hours and even days. In addition, AIT can cost over a thousand dollars a year. Our study suggests further exploration into effective adjuvant therapy, with the hope of developing methods that could spread across more than one allergy. Ultimately, the goal of all allergy researchers is to provide a successful treatment for the millions of people who are limited in the interactions they can have with man's best friend.

REFERENCES

Chan, S., & Leung, D. (2018). Dog and Cat Allergies: Current State of Diagnostic Approaches and Challenges. Retrieved from http://doi.org10.4168/aair.2018.10.2.97

CpG ODNs - TLR9 Agonists. (n.d.). Retrieved from https://www.invivogen.com/tlr9-agonist

Data Finder - Health, United States - Products. (n.d.). (2017). Retrieved from https://www.cdc.gov/nchs/hus/contents2017.htm?search=Allergy

Cox, Linda (2018). Immunotherapy. (Retrieved from https://acaai.org/allergies/allergy-treatment/allergy-immunotherapy

D'Elios, M., Benagiano, M., Della Bella, C., & Amedei, A. (2011). T-cell response to bacterial agents. *The Journal of Infection in Developing Countries*, *5*(09), 640-645. https://doi.org/https://doi.org/10.3855/jidc.019.

Farrokhi, S., Abbasirad, N., Movahed, A., Khazaei, H. A., Pishjoo, M., & Rezaei, N. (2017). TLR9-based immunotherapy for the treatment of allergic diseases. *Immunotherapy,9*(4), 339-346. doi:10.2217/imt-2016-0104.

Fonseca, D. E., & Kline, J. N. (2009). Use of CpG oligodeoxynucleotide in treatment of asthma and allergic disease. *Advanced Drug Delivery Reviews,61*(3), 256-262. doi:10.1016/j.addr.2008.12.007

Galli, S. J., & Tsai, M. (2012). IgE and mast cells in allergic disease. *Nature medicine*, *18*(5), 693–704. doi:10.1038/nm.2755

Grayson, Mitchell (2018). Allergies and Allergic

Reactions. Retrieved from https://www.aafa.org/allergy-facts/Allergy

Hanagata, N. (2017). CpG oligodeoxynucleotide nanomedicines for the prophylaxis or treatment of cancers, infectious diseases, and allergies. *International Journal Of Nanomedicine*, *Volume 12*, 515-531. doi:10.2147/ijn.s114477

Jain, V. V., Businga, T. R., Kitagaki, K., George, C. Kitagaki, K., Jain, V. V., Businga, T. R., Hussain, I., & Kline, J. N. (2002). Immunomodulatory Effects of CpG Oligodeoxynucleotides on Established Th2 Responses. *Clinical and Vaccine Immunology,9*(6), 1260-1269. doi:10.1128/cdli.9.6.1260-1269.2002

Lehto, M., Wolff, H., Leino, R., Alenius, H., & Savolainen, J. (2018). A novel glycocluster molecule prevents timothy-induced allergic airway inflammation in mice. *Allergy*, *73*(8), 1700-1706. doi: 10.1111/all.13419

Marshall, J. D., Abtahi, S., Eiden, J. J., Tuck, S., Milley, R., Haycock, F., . . . Nest, G. V. (2001). Immunostimulatory sequence DNA linked to the Amb a 1 allergen promotes TH1 cytokine expression while downregulating TH2 cytokine expression in PBMCs from human patients with ragweed allergy. Journal of Allergy and Clinical Immunology, 108(2), 191-197. doi:10.1067/mai.2001.116984

Ozdemir, C., Kucuksezer, U. C., Akdis, M., & Akdis, C. A. (2011). Specific immunotherapy and turning off the T cell: How does it work? *Annals of Allergy, Asthma & Immunology,107*(5), 381-392. doi:10.1016/j.anai.2011.05.017

Oriss, McCarthy, Morel, & Campana. (1997, April 15). Crossregulation between T helper cell (Th)1 and Th2: Inhibition of Th2 proliferation by IFN-gamma involves interference with IL-1. Retrieved from http://www.jimmunol.org/content/158/8/3666.long.

Reece, J. B., Urry, L. A., Cain, M. L., Wasserman, S. A., Minorsky, P. V., Jackson, R., . . . Walde, S. J. (2018). *Campbell biology*. Don Mills, Ontario: Pearson Canada.

Shi S, Zhu H, Xia X, Liang Z, Ma X, Sun B. (2019). Vaccine adjuvant : Understanding the structure and mechanisms of adjuvanticity. *Vaccine.* doi:10.1016/j.vaccine.2019.04.055.

Education in Context: Examining Attitudes Toward Sexual Assault in Japan and Developing an Educational Tool for High School Students

Karen Fukuda
The American School in Japan; Tokyo, Japan
Email: karenfukuda16@gmail.com

Abstract – In Japan, the reluctancy to talk about sexual assault has lead to a culture where harmful attitudes toward the crime create a toxic environment for survivors of sexual violence. These attitudes are only reinforced by the lack of a standardized curriculum for sexual violence education. Without education, misconceptions of the crime are able to persist. This paper discusses the reasons behind this silence in Japan, and how to use the understanding of the silence to effectively educate students about sexual violence in Japan's context. Through examining a variety of academic and non-academic resources, I discovered that the main barrier to better outcomes for survivors is the reluctance to discuss what is considered a private discussion in public. With this understanding I created a sexual violence educational tool that addresses the pressing issues in Japan's culture surrounding sexual violence. Normalizing the discussion around sexual assault is a vital step in creating a better environment for survivors in Japan.

Key Words – sexual violence, Japan, education

INTRODUCTION

The United Nations have cited 17 Sustainable Development Goals to achieve by 2030. Of them, Goal 5 aims to "achieve gender equality and empower all women and girls." Aside from being a "fundamental human right," empowering women and girls will enhance the lives of over half the global population, thus creating a more progressive, sustainable world ("Gender Equality: Why it Matters"). Currently across the world, girls and women continue to face many forms of gender inequality, one of them being gender-based violence. One form of gender-based violence is sexual violence, which is a term that "refers to crimes like sexual assault, rape, and sexual abuse" ("Types of Sexual Violence," 2020). Sexual violence is any sort of non-consensual sexual contact, and can happen to all genders of all ages ("Sexual Abuse," 2020). The attitudes surrounding sexual violence are a facet of gender inequality because they encompasses a society's perception of gender roles. Therefore, examining the above can give insight into the culture that surrounds sexual assault and the way survivors are treated within their community.

Within Japan, historical practices of depicting women as objects and as inferior beings has led to a society where it is taboo to speak out about sexual assault. As Jake Adelstein, a crime journalist (1993-2005) for the Yomiuri Newspaper, says, "Japan is a very sexual society." At convenient stores, it is common to see sexual magazines on display in view of anyone who enters the store, including children. According to Motoko Rich, the Tokyo bureau chief of the New York Times, "there is a sense in the culture that it is OK for a man to view women as objects" (Woods, 2018, 18:47). However, "to talk about date rape, or sexual assault… you don't see open discussions about that," says Adelstein (Woods, 2018, 4:55). This creates a destructive cycle, one where distorted images of gender enforce distorted perceptions of gender roles, but there are no open discussions in place to fix these skewed perceptions. The acceptance of these perceptions of genders, especially of women, feed the toxic culture surrounding sexual assault, including misconceptions about consent, the psychological consequences of sexual assault, and even the very definition of sexual assault. Although it is common for many women, especially high school girls, to be sexually assaulted on the train, not many come forward (Woods, 2018, 42:45). One reason for the under reporting is because many are unaware that these actions count as sexual assault. However, Hiroko Goto, a law professor at Chiba University, says another reason is because survivors of sexual assault are often told to "forget about it," or act as if nothing happened. "Victims are always told it's their own fault" (Woods, 2018, 6:10).

In this paper I examine the attitudes toward sexual assault and survivors in Japan. Using this cultural context, I developed a peer to peer educational tool that addresses unique issues in Japan pertaining to sexual assault.

EXAMINING JAPAN'S ATTITUDE TOWARD SEXUAL ASSAULT THROUGH THE LAW

Japan's penal code pertaining to sexual offenses was created in 1907. In this original penal code, the crime of rape was limited to cases where the victim was a female. Additionally, the crimes of rape and other indecent acts were only prosecutable upon a formal complaint by the victim (Kitagawa, 2018). The section of the code that required a "formal complaint by the victim" illustrated the law's disregard for

the aftermath of the crime - the confusion, the feelings of guilt, shame, and more - that makes it very difficult for survivors of sexual assault to report the crime ("Sexual Abuse," 2020).

This original code lasted for 110 years before the first major revision in 2017. The revision redefined the crime of rape to include all people as victims (Article 177, Japan Penal Code. Accessed through http://www.japaneselawtranslation.go.jp/?re=02). Additionally, the revision enabled crimes to be prosecuted without a victim complaint (Article 180, Japan Penal Code. See link above). The 2017 revision therefore marked a marginally improved attitude toward sexual assault in Japan, one which only partially acknowledged the complexity of the crime. However, the current Japanese law still defines the crime of rape narrowly. Unless force, violence, or intimidation can be proven, the crime is not considered rape. Lack of consent is simply not enough to convict the perpetrator (Article 177, Japan Penal Code. See link above).

By defining rape as a crime where the victim is unable to resist due to force, violence, or threat, it reinforces the dominant narrative that rape is a violent act that takes place among strangers, when in fact the reality is that the perpetrators of these acts are often someone that the victim knows.

Furthermore, the law excludes psychological factors that can contribute to an inability to resist. Studies show that "many victims simply freeze when they are attacked," regardless of whether there is force or violence involved (Woods, 2018, 11:37). The law not only "[echoes] socially dominant values and conventions," but also establishes "dominant narratives," and excludes incidents that do not conform to those narratives (Burns, 2005, p.5). The law makes it the victim's responsibility to say no, when in fact consent should never be assumed unless there is a yes. This fails to meet international standards for sexual violence protection by the law (Amnesty International, 2011). The failure of Japan's law to revise this critical clause is evidence that there is little discussion, as well as incentive, to reflect the complexity of sexual violence, as well as little progress towards providing justice for a majority of survivors.

Although many factors contribute to harmful attitudes toward sexual assault and gender, what it boils down to is the lack of education and discussion around the matter. Sexual assault education programs can increase rape knowledge, as well as change attitudes toward the crime (Anderson & Whiston, 2003). Specifically, long term educational programs can be particularly effective in altering "rape attitudes and rape-related attitudes" (Anderson & Whiston, 2003). Instead of burying the topic in to shame, we must speak out about it in order to clarify rape myths, clouded views of consent, and the tendency to blame the victim.

EDUCATION IN JAPAN

Unfortunately in Japan, the skewed perceptions of gender roles and sexual assault are only enforced further by a lack of organized education. Like many other countries, the Japanese government issues a standardized curriculum outline for various subjects for all grades through high school. However, there is no standardized guideline for sex-ed in Japan, resulting in the inconsistent content of these classes. Without strict guidelines, teachers are free to skip over content they deem unimportant, or even worse, are unaware of ("New Learning Guidelines and Sex Education: Focusing on Junior High," 2020). This poses a problem, as there is a risk for individual views of sexual assault and gender to be passed down without check. As for the few books that have been published for school guideline use, the Japanese Association for Sex Education (JASE) states that they are outdated, some even published back in 1990. Even the more recent published guidelines are deemed as *fujūbunn*, or insufficient, by JASE and in need of revision.

It is vital for sex-ed and sexual assault education to be taught together because young students must be aware of sexual violence. In a world where 1 in 6 women and 1 in 33 men are victims of rape or attempted rape ("Victims of Sexual Violence," 2020), it is essential that students are taught how to react to or respond to an uncomfortable or dangerous situation. Furthermore, the lack of discussion around sexual assault is what allows destructive narratives to persist, which forces survivors into further shame and fear.

Although it is a school's primary job to teach this, many independent companies have compiled their own educational resources in an attempt to provide better education on the matter. However, as most of these resources do not fully address the pressing issues in Japan's culture surrounding sexual assault, they do not directly combat misconceptions of gender and sexual assault in Japan. Therefore I aimed to create a sexual violence educational tool that addresses the topic in the context of Japan.

EDUCATION IN CONTEXT: EXPLORING ATTITUDES TOWARD SEXUAL VIOLENCE IN JAPAN

Prior to creating this educational tool, I examined a variety of academic and non-academic resources, including journal articles, documentaries, news articles, legal documents and existing educational platforms. Through my literature review, I discovered the main barrier to better outcomes for survivors is the reluctance to discuss what is considered a private discussion in public. Two main reasons I have uncovered for this silence are the traditional gender roles and the lack of a standardized sexual assault and sex-ed curriculum for students in Japan.

In Japan, historically and presently, public expressions of dissent with the norm are uncommon, if not taboo. Women are especially aware of this outgroup. Specifically, when women voice their opinion, it can be seen as "unfeminine" in Japan (Woods, 2018, 19:35). Because sexual violence education involves teaching being assertive about personal boundaries, these gender roles make it difficult for women to hold an open discussion about sexual violence without being criticized for breaking the traditional expectation of womanly behavior.

A quote from politician Sugita Mio in "Japan's Secret Shame" illustrates this expectation for women quite well:

"If you're working as a woman in society, you'll be approached by people you don't like. Being able to properly turn down those advances is one of your skills" (Woods, 2018, 34:07).

Her words demonstrate the deep and complex reasons behind the silence in Japan. She, like many others, focuses on why the woman was not able to avoid an inappropriate "advance," rather than focusing on the wrong of those "advances." The origin of these beliefs is at least in part from the media, where women are viewed and pressured to be compliant (Woods, 2018, 18:50).

It should be noted that while these views reflect the struggles of a specific scenario, wherein the victim is a woman and the perpetrator is a man, they do not capture the distinct and equally substantial struggles of men, LGBTQ+ persons, persons with disabilities, elderly persons, and other frequently ignored survivors.

Ultimately, these factors that create a culture of silence around sexual violence reinforce harmful attitudes about the crime, specifically, victim blaming and clouded views of consent. With this in mind, I aimed to create an educational tool that addresses these two main issues within the context of Japanese culture.

DEVELOPING AN EDUCATIONAL TOOL

I created an educational tool that can be used as a guideline for teaching about sexual assault in Japan. My educational tool is in a PDF format, and the PDFs are posted on a website to ensure easy access to them. Because attitudes toward sexual assault differ in various communities and cultures, I chose a format that would allow for a standardized, yet flexible and personalized education.

FORMAT

I first identified the lack of a standardized curriculum for teaching sexual assault in Japan to high school students, and created my tool to bridge that gap ("New Learning Guidelines and Sex Education: Focusing on Junior High," 2020). Students who want to learn or teach the topic of sexual assault can access the PDFs which include evidence based information. I wanted my tool to be a reliable, standardized, and convenient tool that people in Japan, mainly high school students, can easily use to educate themselves and others in their community.

Additionally, my tool will allow flexibility in the learning process. The first way my tool allows flexibility is the setting and group size of learning. Because sexual violence is a sensitive, serious, and personal topic to discuss, those who wish to learn about it on their own may do so by accessing the PDF on their own, thus allowing for personalization and confidentiality. For those who wish to learn in a group setting, they can decide on the composition of the group. Being able to choose who to discuss this topic with puts the power in the hands of the learners, thus eliminating possible feelings of powerlessness that otherwise might be felt in a larger traditional classroom setting. Feeling in control of the ongoing discussion is especially important when the receiving audience includes survivors of sexual violence. In these situations, it is essential that the way the information is being taught ensures feelings of trust and safety (Konradi, 1993). The second way my tool allows flexibility is in the teaching style. In addition to aiding the traditional adult teacher to student format, my tool will allow for peer to peer education. Research has shown that youth are more likely to change their attitudes about topics such as sexual violence if the relayer of the information is somebody who they feel faces similar pressures and concerns (Sloane & Zimmer, 1993).

Especially in Japan where many are reluctant to discuss sexual violence, we must be creative in our approach. Therefore, the PDFs, which lay out what topics to cover in sexual assault education, will serve as a standardized yet flexible and personal educational tool that can be customized to individual communities' needs in Japan. Additionally, I plan to translate the PDFs to make both an English and Japanese version. Much of the progressive information and research on sexual assault is in English. Therefore by making my tool bilingual, my hope is to bridge the gap between these two communities.

CONTENT

The PDFs include basic information about sexual violence, common myths about the crime, the psychological aftermath of the crime, as well as tips for safety planning.

This general education about sexual violence will increase knowledge about the crime, and therefore will increase empathy for survivors. The law illustrates the damage that an incomplete or inaccurate understanding of the crime can have. If there is education about the complexity of the crime, people will be more likely to change their attitudes toward the crime, and create a better, less hostile environment for survivors in Japan (Anderson & Whiston, 2005).

I also included an explanation and analysis of different aspects that contribute to the overall attitudes surrounding sexual violence in Japan. This includes examination of the penal code pertaining to sexual violence, as well as harmful attitudes about sexual violence that are especially pervasive in Japan, including victim blaming and clouded views of consent. I included this because it is important for one to first understand the attitudes toward sexual violence in Japan in order to understand why there is such little conversation about the topic. From there, it is possible to educate people about the dangers of this silence, and how to speak up with cultural sensitivity.

Additionally, throughout the PDFs I explain the "why" and "how" behind the topics that are included. In Japan, where most are reluctant to speak about sexual assault, it is important to explain *why* these topics need to be discussed first in order to get the conversation going. The "how" should be explained in order to give the teachers tips on how to deliver the content with cultural sensitivity. Whoever is teach-

ing the subject should keep in mind that if listeners are suddenly confronted with a topic they are uncomfortable with, they are likely to be less receptive to the information that is being presented to them (Konradi, 1993). Therefore, I included the "how" sections in my tool to create a guideline for how to discuss these topics within the cultural context of Japan. An example is given below from one section of my PDFs.

EXAMPLE

As an example, from my research I knew that a topic like consent needed to be taught in a way that was approachable to Japanese students. It had to be presented in a way that people in Japan would be receptive to learning about. Therefore, I included a section called "How to talk about consent in Japan" where I give an alternative way to approach the topic by implicitly referencing consent through one of four themes: communication skills, decision making, personal space and interpersonal relationships. This method of teaching certain aspects of consent without explicitly mentioning the term is used in many schools in the U.S.(Willis, Jozkowski, & Read, 2018). Talking about these four themes is a way to establish respect for others' personal decisions, and is also a way to teach young people to be assertive about their personal boundaries. Although an implicit reference to consent is not nearly as effective as an explicit discussion of consent, it is a starting point (Willis, Jozkowski, & Read, 2018). After all, an implicit reference to consent is an improvement from the current lack of conversation about consent .

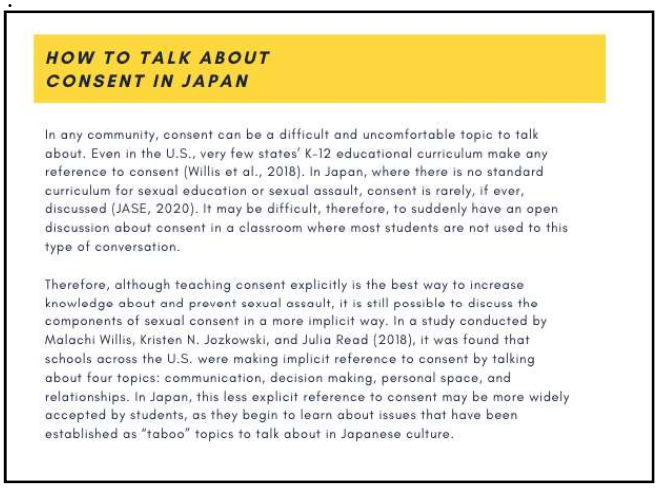

FIGURE 1: Example heading that provides context to the consent education portion of my tool. (Enlarged examples from my tool can be viewed at this link: https://docs.google.com/presentation/d/1N8h6Z5tBr4g6f9Fk22CsB8Jk0WKLTa03b0iCzuXb-vg/edit?usp=sharing)

FUTURE PERSPECTIVES

My plan is to first test this tool within my community at my school in a peer to peer education style. Ideally, I would work with small groups and have multiple sessions with these same groups. I will constantly be gathering feedback on the receptiveness of my peers, as well as how my peers' attitudes toward the crime change over time. I also plan on training fellow peers on how to teach this material. After gathering feedback from my school, my hope is to expand to include students in other Japanese schools.

Although an uncomfortable topic, sexual violence education must be implemented in schools to teach young people how to protect themselves, as well as how to support others who are survivors of sexual violence. Only by normalizing the discussion around sexual violence can we hope for a better environment for survivors in Japan.

AKNOWLEDGEMENTS

I would like to thank Elizabeth Feldeverd for all of your support and encouragement over this long process! Additionally I would like to thank Subo Wijeyeratne for introducing me to a new perspective of Japanese history.

REFERENCES

U.N. (n.d.). Gender Equality: Why it Matters. Retrieved from https://www.un.org/sustainabledevelopment/gender-equality/

RAINN. (2020-a). Types of Sexual Violence. Retrieved from https://www.rainn.org/types-sexual-violence

TELL. (2020). Sexual Abuse. Retrieved from https://telljp.com/lifeline/tell-chat/homepage/resources/sexual-harassment/

Woods, B. (Producer), & Jenkin, E. (Director & Producer). (2018). Japan's Secret Shame [Motion picture]. United Kingdom: BBC Two.

Kitagawa, K. (2018). "Penal Code Amendment Pertaining to Sexual Offenses." Retrieved from https://www.waseda.jp/folaw/icl/news-en/2018/02/06/6110/

Burns, C. (2005). *Sexual Violence and the Law in Japan*. Milton, United Kingdom: RoutledgeCurzon.

Amnesty International. (2011). Rape and Sexual Violence: Human Rights Law and Standards in the International Criminal Court. Retrieved from https://www.amnesty.org/download/Documents/32000/ior530012011en.pdf

Anderson, L.A., & Whiston, S.C. (2005). Sexual Assault Education Programs: A Meta-Analytic Examination of Their Effectiveness. *Psychology of Women Quarterly, 29(4),* 374-388. https://doi.org/10.1111/j.1471-6402.2005.00237.x

JASE. (2020). “New Learning Guidelines and Sex Education: Focusing on Junior High.” Retrieved from https://www.jase.faje.or.jp/

RAINN. (2020-b). Victims of Sexual Violence. Retreived from https://www.rainn.org/statistics/victims-sexual-violence

Konradi, A. (1993). Teaching About Sexual Assault: Problematic Silences and Solutions. *Teaching Sociology*, *21*, 13-25. http://www.jstor.org/stable/1318847

Sloane B.C., & Zimmer, C.G. (1993). The Power of Peer Health Education. *Journal of American College Health*, *41(6)*, 241-245. http://dx.doi.org/10.1080/07448481.1993.9936334

Willis, M., Jozkowski, K. N., & Read, J. (2018). “Sexual consent in K–12 sex education: an analysis of current health education standards in the United States.” *Sex Education, 19(2),* 226-236. https://doi.org/10.1080/14681811.2018.1510769

A Self-Assessing Compilation Based Search Approach for Analytical Research and Data Retrieval

Ananth Goyal
Dougherty Valley High School; San Ramon, USA
Email: ananthgoyal@gmail.com

Abstract - Whenever meta-analytic research is conducted, sifting through the sheer amount of sources made available through individual databases and search engines can be time-consuming and often degrades the specificity to which sources are analyzed. This study sought to predict the feasibility of a research oriented searching algorithm across all subjects and a searching technique to counter flaws in dealing with large datasets by automating three key components of meta-analysis (a query-based search associated with the intended research topic, selecting given sources and determining their relevance to the original query, and extracting applicable information including excerpts and citations) A prototype algorithm was tested using 5 key historical queries, and results were broken down into the total number of relevant sources retrieved, the algorithm's efficiency, the total time it takes complete one cycle, and the quality of the extracted sources. On average, the program collected a total of 126 reputable sources per search with an average efficiency of 19.55 sources per second suggesting that an algorithm built across all subject areas can make strides in future research methods.

Key Words – Databases, Web Mining, Searching Algorithms

INTRODUCTION

A searching algorithm is any computational algorithm finding a specified attribute within a collection of data or dataset array (data repositories, data archives, etc.)[1]. The term 'search engine' is used in the context of this study, because it considers relevance and association with a query rather than direct equivalence between two data components found on the web [2]. The most widely used search engine is Google [3], which conducts about 92% of all searches worldwide, and is by far the most accurate and powerful search engine [4][5]. Although Google, and its subdivision Google Scholar are holistically superior to other search systems, their broad scope frequently compromises the quality of results with a preference for high speed and lower runtimes [6], still requiring the user to assess each result making it impractical for focused needs. Additionally, most reliable information that is provided by research-oriented search engines, such as Google Scholar require payment and have biases [7], when sources of equivalent, credible, and impartial material in the public domain are available.

This paper demonstrates a newly proposed algorithmic concept for countering these predicaments and for predicting whether its mechanism can be extended to all searching systems, specifically when conducting research or organizing large quantities of data. The algorithm can be broken down into two proposed novel categories:

Multitudinous Database Search (MDS) focuses on using a number of topic-related databases and their built-in searching mechanisms to increase the amount of sources by which information is being extracted, ensuring that the scope of the search is optimal for the focus of the query.

Source Analysis and Extraction Algorithm (SAEA) sifts through several results determining whether or not a specific source should be used and what specific components of those sources should be extracted (quotes, excerpts, citations, images, data, etc.)

The rest of the paper is structured as follows: The second section *Prior Work* discusses current algorithms referenced in this paper. Section three *Methods* elaborates on the proposed algorithm and its mechanics. All results and data collected from experimental testing will be compared to Google Scholar and are found in the *Results* section followed by *Conclusions*.

PRIOR WORK

This section discusses extant searching techniques/methods germane to the proposed algorithm.

I. On-Site Searching Methods

Most searching systems within a site or database primarily operate by using the frequency of keywords to determine the relevance of that source or webpage to the query. All the words in a given search query are of equal importance and relevance [8], making it imperative for the user to refrain from including any conjunctions and filler words to the query that would produce a coherent sentence— diverting the focus of the search; to streamline the number of

results—thereby improving—the accuracy of the results, searching with only keywords and topics is suggested. Repeated searching within every sub-page is avoided by pre-indexing information on page content and their associated topics within a dataset, making the process for displaying relevant links efficient [9][10].

The use of Proximity Searching (PS) is one particular approach to increase the accuracy of on-site search results. PS focuses on the nature of certain keywords, rather than their frequency [11]. Through using predetermined object relationships, results will contain goal information even when it is not directly related to the query [12]. Although Google search is not an on-site searching system, it uses a PS-based algorithm to retrieve tangentially related results when not explicitly specified in the query [13]. For example the word "thriller", in Google's indexing database is in close proximity to Michael Jackson who is renowned for performing a song with the same name.

II. Google PageRank

First Pioneered by Google, PageRank (PR) was designed to be a method of ranking search results by popularity and link information [14]. The PR value of a webpage, node, or link is the page's calculated ranking when compared with other results given a search query [15][16]. The primary aim of this organizational technique is to allow the user to obtain results that are mostly referenced in other sites, since more source references implies greater relevance and significance for the search query [17]. The PR formula is shown below:

$$PR(u) = (1-d) + d\sum_{i=1}^{n}\left(\frac{PR(i)}{L(i)}\right)$$

The letter *'u'* represents any given page prior to calculating its PR value while *'L'* denotes the number of outbound links referenced. The letter *'i'* represents a referenced web page used to calculate the target PR of page *u.* A key aspect of the PR algorithm is the damping factor (denoted as *'d')* which is the constant reduction in probability for the user to click on any further links after having already analyzed the information found in prior ones [18][19]. For example, if page 'A' has a higher PR score than others, then it will rank first on the PR result page; however, since the following links are lower in reference popularity the user may refrain from opening new links after only a few, making it critical to employ a damping factor.

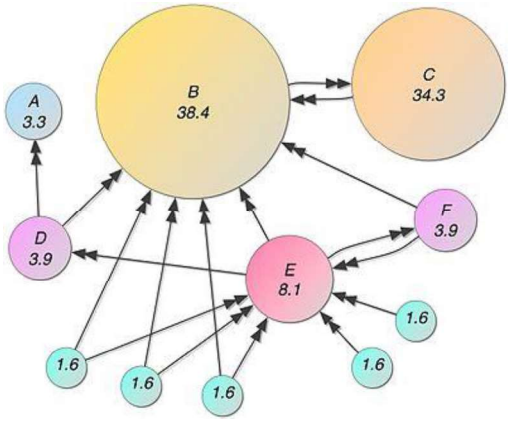

Fig. 1: Depicts variability in PR scores from factors including page importance, relevance, outbound links, and damping factor [20]. In this scenario, page 'B' has the highest PR score (38.4), likely making it the first link to appear after a Google search.

The inherent nature for researchers and students to avoid lower ranked PR links is inevitable, thus the proposed solution (explained in "Methods") addresses this problem by automating data extraction from all relevant sources listed.

METHODS

Each database used in this study was a public domain historical primary source bank, each with different interfaces and mechanics, requiring slightly altered web-crawling methods to optimize performance. *MDS* was applied using Proximity Searching techniques from the integrated search system of the databases to generate a result page of all links related to content grouped by relevance and popularity (PR). Then, *SAEA* was used to analyze and accumulate the relevant data from every source to be displayed on the final page, which consisted of the primary source document (speech, article, image, map, etc.) and citation, all organized by their respective relevance scores.

The historical databases used in this study were DocsTeach National Archive , Yale Avalon Project (YA), EyeWitness to History (EW), The Ancient Encyclopedia (AE), and the John Carter Brown Library (JCB). To produce the best results and comply with the variability of searching mechanics, a separate class has to be built and implemented for each database. Each class consists of two key methods, one designed for *MDS* and one built for *SAEA.* The retrieved information was all compiled and displayed on a local web file.

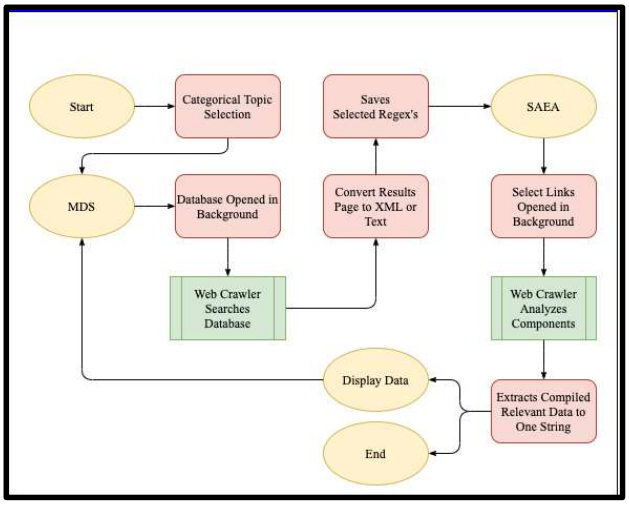

Fig. 2: Depicts the whole algorithmic process from search to display including the most notable components.

I. Multitudinal Database Searching (MDS) System

MDS is influenced by on-site searching and its subdivision Proximity Search, as it replicates a single search in a database across several, maximizing the amount of information that could potentially be available to the user. Prior to the submission of the search query, the user focuses the scope of their research by selecting categorical topics that conform to their desired results. This reduces the number of databases the MDS system would have to reference, reducing the time for which the algorithm will operate. After the query is submitted, the web-crawler uses the built-in search mechanisms of the databases by parsing the query into a search format, which is then inputted into the search parameter of the URLs. Some databases use Google's "Custom Search" algorithm to index and retrieve their information [21], in that case, MDS is applied through that mechanism.

The links to each of the articles and sources retrieved from each database are saved into a dataset. The links are separated from the remaining XML or text components by continuously approximating their location using index search function to target the particular regex/regular expression (used to describe a component of a string [22]) for however many links present in the file page of the results. This process occurs simultaneously for every database until every set of resulting URLs are stored into a data set.

II. Source Analysis Extraction Algorithm (SAEA)

For keyword relevance, each stored link is opened and evaluated to filter out any non-applicable components of articles. All relevant information, including the citation which is found by regex approximation, is then stored into a string to be displayed after all the information from the entire database has been collected. SAEA is developed to bypass the PR system for each database/Google result page, as it analyzes more than the first 1-3 resultant pages. Unlike Google/Scholar, instead of simply listing out links with a brief description, SAEA opens the links and compiles what the user intends to extract themselves, automating the entire search process altogether.

The method by which SAEA extracts a component from a source is entirely dependent upon the database being used and the type of data being processed. Different methods and subroutines are developed to properly extract the information, depending on the type of source. If the user selects image files as their target type, then the retrieval method is standard; isolate the image tags found in the XML script. However, if a particular type of information other than an image is being targeted, then a specialized algorithm will be developed for identifying it. These include identifying textual patterns in headings, paragraphs, descriptions, etc., looking at the particular formatting of the text, such as a citation, or identifying where in the source/file the target information will be, if it is repetitive or has a significant pattern. These methods are independently developed for each circumstance.

In order to predict the total number of sources compiled through SAEA at any instant in time, timestamp information from each database containing completion data is used to model and predict *S (number of sources)* as a function of *t* (*time*) using a variant *Interpolation Polynomial Formula* (IPF) which outputs a differentiable function that runs through the set of given data points [23]. Data points collected are represented as *(time, # of sources)*; the total number of databases used is represented by '*n*' as each point being used in IPF is the completion cycle for a single database. The letter *'y'* denotes the output of the data-point, which in this case is the number of sources retrieved from this database. The formula is shown below [24]:

$$S(t) = \sum_{i=1}^{n} (y_i) \left[\prod_{k=1}^{n} \left(\frac{t - t_k}{t_i - t_k} \right) \right]$$

IPF is used to model the results collected from every search query; however, by taking the derivative of the IPF polynomial, a new function is constructed to predict the efficiency or speed of the program at any given moment in time. The efficiency function defined as E(t), estimates the instantaneous speed represented as a data-point of (x~seconds, y~sources per second), revealing patterns of more and less effective algorithmic segments. Manual and automated compilation can be compared at specific moments time or as an average of the number of sources retrieved.

The average number of retrieved sources is calculated by using the Average Value Theorem (AVT) which calculates a function's average value over a certain interval [25]. In this case, AVT is used to find the average number of sources retrieved using the S(t) function produced from IPF.

$$A(t) = \frac{1}{t_f - t_i} \int_{t_i}^{t_f} S(t)$$

This method is used to measure an atypical mean, as it factors in the possible inclusion of more databases, allowing the resulting data to predict future implications of source retrieval. It is calculated by using two time components, the initial and final bounds of its compilation process which usually range from 3 to 10.

RESULTS

I. Numerical Results of MDS/SAEA

The numerical data for the proposed algorithm is divided into 3 categories provided a search query—the number of sources retrieved from each database, the time to complete each cycle, and the modeled source and efficiency function.

The results were collected by using a built-in method that records the timestamp information of every database, which includes the number of sources retrieved and the amount of time it took to do so. Table 1 displays the data collected from each group across the various databases when given a sample historical search term from different periods. The first number under each database represents the time it takes to complete a cycle and the number below denotes the number of sources retrieved in that cycle ('S').

Search Query	EW	YA	AE	JCB	Total (SAEA)
Christopher Columbus	2.88 sec 33 S	3.78 sec 46 S	4.75 sec 8 S	5.21 sec 54 S	5.21 sec 141 S
Slave Trade	5.84 sec 27 S	4.36 sec 56 S	5.35 sec 13 S	3.37 sec 43 S	5.84 sec 139 S
WWI	7.34 sec 32 S	5.74 sec 45 S	n/a	4.18 sec 36 S	7.34 sec 113 S
WWII	7.28 sec 31 S	6.35 sec 37 S	n/a	4.72 sec 41 S	7.28 sec 109 S

Table 1: The collected time stamp information for varying search queries across the test databases (n/a means the search term is not from the target time range of the database)

Search Query	Source and Efficiency Function of Time
Christopher Columbus	$S(t) = 14.516t^3 - 188.549t^2 + 821.01t - 1114.36$ $E(t) = 43.548t^2 - 377.098t + 821.01$
Slave Trade	$S(t) = 37.1105t^3 - 507.342t^2 + 2306.13t - 3387.15$ $E(t) = 111.3315t^2 - 1014.684t + 2306.13$
WWI	$S(t) = -2.79942t^2 + 56.6164t - 151.744$ $E(t) = -5.59884t + 56.6164$
WW2	$S(t) = 4.15389t^2 - 23.2841t + 58.3592$ $E(t) = 8.30778t - 23.2841$

Table 2: The IPF generated functions that model the functional progress of SAEA for varying search queries across the test databases with respect to time.

The following graph is an example of an IPF generated function for the total number of sources and the efficiency / speed function at an instant of time. The dotted lines represent the data's restricted domain, since that is the region of time in which the given functions operate. Use of IPF enables us to model the performance of the algorithm's functional progress for better comparisons and future modifications.

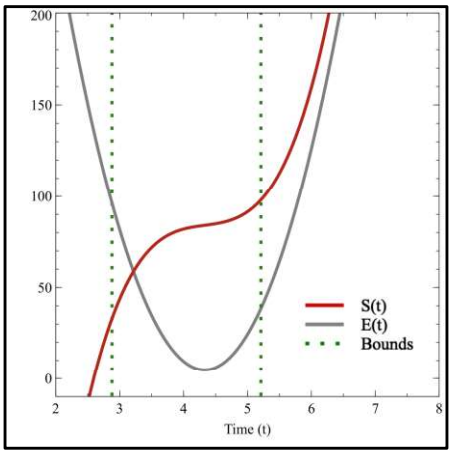

Fig. 3: SAEA Graph for Query: "Christopher Columbus"

II. Comparative Results of Google Scholar

Results were compared to test results from searches on Google Scholar (GS). GS is designed so it can deliver thousands to millions of results in less than a second. Identical search queries from the previous tests were used on

GS. Although direct results cannot be properly used for comparison, further analysis and predictive modeling make it possible.

Search Query	Retrieval Time (sec)	Total Number of Sources
Christopher Columbus	0.06	222,000
Slave Trade	0.05	1,460,000
WWI	0.03	4,610,000
WW2	0.05	4,780,000

Table 3: The directly retrieved data after each search on GS. Note: Retrieval time and the number of sources pulled are not indicators of overall effectiveness, primarily just speed.

The direct retrieval and index speed of GS is significantly superior; however, the necessity for the user to open each link and the lack of automation in source analysis is what SAEA addresses and is what is being compared. GS is not a compilation-based search engine and does not self-analyze its results, which are both done by the user. Compilation times are simulated to check its efficacy properly with MDS/SAEA, compilation times will be simulated. The manual compilation time is how long it will take a researcher to extract the intended information from all the selected sources, in this case from each link to the historical primary source material. Only the first page of results (10 sources) should be used, as a PR system indicates the user is unlikely to go any further. Since the secondary purpose of the proposed algorithm is to be cost-effective (free of charge), the cost of all sources available on the first result page (10 sources) will be totaled.

Search Query	Number of Sources Used	Manual Compilation Time (secs)	Total Cost of Sources Used (USD)
Christopher Columbus	10	414	$44.64
Slave Trade	10	378	$56.59
WWI	10	438	$103.99
WW2	10	412	$66.95

Table 3: Calculated data after each search on GS for MDS/SAEA comparisons.

Results of these methods were contrasted by taking the compilation times average and dividing by the total number of sources used/retrieved. This introduces a new efficiency function, which can be graphically modeled between the time bounds as the derivative/slope of the secant line. On average, it was found after testing that: manual extraction of target information using GS takes about 0.026 sources per second. Comparatively, automatic extraction using the proposed algorithm runs approximately 19.55 sources per second. The purpose of this algorithm is not to replace Google Scholar because, overall, GS has far more capabilities and substantially higher retrieval rates; however, MDS/SAEA would do best when searching for specific components in a paper (images, methods, results), primary source material, citations, excerpts, or any situation where the researcher is frequently searching for a particular component, over the entire source. GS may be viewed as a database itself and integrated into MDS as if the information extracted came from a single source. This will theoretically extend the reach from which source components can be obtained, and in effect increase the pace and degree to which research is conducted.

III. Examples of Retrieved Material

A few examples of primary source material extracted from documents, files, and websites through MDS/SAEA when searched for the term “Slave Trade” are shown below:

“During my stay on the coast of Africa, I was an eye-witness of the following transaction: a black trader invited a Negro, who resided a little way up the country, to come and see him. After the entertainment was over, the trader proposed to his guest, to treat him with a sight of one of the ships lying in the river. The unsuspicious countryman readily consented, and accompanied the trader in a canoe to the side of the ship, which he viewed with pleasure and astonishment. While he was thus employed, some black traders on board, who appeared to be in secret, leaped into the canoe, seized the unfortunate man, and dragging him into the ship, immediately sold him [26].”

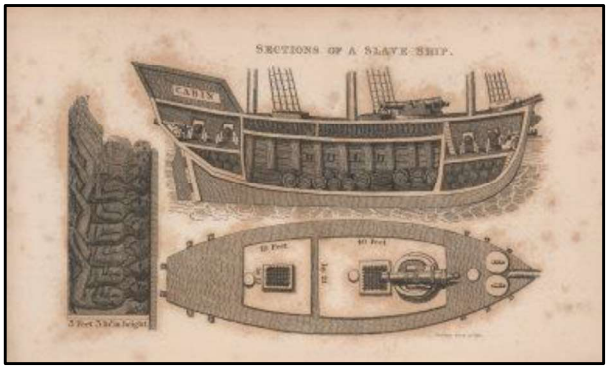

Fig. 7: Diagram of a slave ship showing the hold where the slaves were kept. Extracted from JCB. Search Query: “Slave Trade”; Method: MDS/SAEA; File Name: [“Sections of Slave Ship”]; Publication: [Boston][1831] Creator: [Walsh, Robert][1772-1852] [27]

CONCLUSION

In this paper, a new method to enhance analytical research using multiple databases was presented. Upon checking and observing the discrepancies between source quality and efficiency from varying combinations of databases and search queries, it is evident that this method will enhance current research techniques in all subject areas. This research was performed using historical documents only; however, the basic dynamics and functionalities of the algorithmic method would virtually remain identical regardless of the intended subject matter. First, *MDS* is used to find all associated sources and then *SAEA* is used to filter out any irrelevant findings and extract the appropriate components. The final results show the method can retrieve an average of 126 related source results within 4 to 8 seconds, all with an average efficiency of 19.55 at any given moment in time.

ACKNOWLEDGEMENTS

The completion of this research report and entire project holistically would not have been possible without the support from Mr. Sudhir Kamath, Mr. Rober Gedron, Professor Jeffery Ullman, and Mrs. Katie MacDougall and I greatly appreciate them for all their contributions.

REFERENCES

[1] A. C. Dalal, "Searching and Sorting Algorithms." [Online]. Available: http://www.cs.carleton.edu/faculty/adalal/teaching/f04/117/notes/searchSort.pdf

[2] S. Brin and L. Page, "The anatomy of a large-scale hypertextual Web search engine," Computer Networks and ISDN Systems, vol. 30, no. 1-7, pp. 107–117, 1998.

[3] Patterson, Mark R., Google and Search Engine Market Power (April 27, 2012). Fordham Law Legal Studies Research Paper No. 2047047.

[4] Search Engine Market Share Worldwide," Dec-2019. [Online]. Available: https://gs.statcounter.com/search-engine-market-share.

[5] Ioannis Lianos, Evgenia Motchenkova, MARKET DOMINANCE AND SEARCH QUALITY IN THE SEARCH ENGINE MARKET, Journal of Competition Law & Economics, Volume 9, Issue 2, June 2013, Pages 419–455, https://doi.org/10.1093/joclec/nhs037

[6] Brutlag, J. (2009). Speed matters for Google web search.

[7] Diaz A. (2008) Through the Google Goggles: Sociopolitical Bias in Search Engine Design. In: Spink A., Zimmer M. (eds) Web Search. Information Science and Knowledge Management, vol 14. Springer, Berlin, Heidelberg

[8] "LibGuides: Research Process: Proximity Searching," Proximity Searching - Research Process - LibGuides at Northcentral University, 24-Feb-2020.

[9] R. Shaw, "Understand How On-Site Search Works," Inc.com, 07-Apr-2000. [Online]. Available: https://www.inc.com/articles/2000/04/18342.html.

[10] Marti Hearst, Ame Elliott, Jennifer English, Rashmi Sinha, Kirsten Swearingen, Ka-Ping Yee Communications of the ACM Vol. 45, No. 9 (September 2002), Pages 42-49

[11] "Proximity Operators," 13-Jan-2009. [Online]. Available: https://library.alliant.edu/screens/proximity.pdf.

[12] Goldman, R. and Shivakumar, N. and Venkatasubramanian, S. and Garcia-Molina, H. (1998) Proximity search in databases.

[13] D. M. Russell, "Advanced Search Operators," 23-Aug-2019. [Online]. Available:https://journalismcourses.org/courses/DATA0819/Eng/Google_Advanced_Search_Operators.pdf.

[14] I. Rogers, "The Google Pagerank Algorithm and How It Works." [Online].Available:https://www.cs.princeton.edu/~chazelle/courses/BIB/pagerank.htm.

[15] L. Page, "The PageRank Citation Ranking: Bringing Order to the Web," Stanford InfoLab, Jan. 1998.

[16] Amy N. Langville & Carl D. Meyer (2004) Deeper Inside PageRank, Internet Mathematics, 1:3, 335-380, DOI: 10.1080/15427951.2004.10129091

[17] E. Roberts, "The Google PageRank Algorithm," 09-Nov-2016. [Online].Available:https://web.stanford.edu/class/cs54n/handouts/24-GooglePageRankAlgorithm.pdf.

[18] "The Damping Factor," The Damping (or dampening) Factor, 2004. [Online]. Available: http://www.pagerank.dk/Pagerank-formula/Damping-factor.htm.

[19] Boldi, P., Santini, M., & Vigna, S. (2005, May). PageRank as a function of the damping factor. In Proceedings of the 14th international conference on World Wide Web (pp. 557-566).

[20] Simple example of PageRank. Damping 85%. Area of circles equals PageRank. 2007

[21] Mysen, C. C., Verma, N., & Chen, J. (2011). U.S. Patent No. 8,082,242. Washington, DC: U.S. Patent and Trademark Office..

[22] J. Goyvaerts, Regular Expressions: The Complete Tutorial. Princeton, 2007.

[23] V. Dahiya, "Analysis of Lagrange Interpolation Formula," - International Journal of Innovative Science, Engineering & Technology, vol. 1, no. 10, Dec. 2014.

[24] Archer, Branden and Weisstein, Eric W. "Lagrange Interpolating Polynomial." From MathWorld--A Wolfram Web Resource. http://mathworld.wolfram.com/LagrangeInterpolatingPolynomial.html

[25] P. Dawkins, "Average Function Value," Calculus I - Average Function Value, 30-May-2018. [Online]. Available: http://tutorial.math.lamar.edu/Classes/CalcI/AvgFcnValue.aspx. [Accessed: 07-Mar-2020].

[26] Falconbridge, Alexander, An Account of the Slave Trade on the Coast of Africa (1788); Curtin, Phillip D. Atlantic Slave Trade (1969); Matheson, William Law, Great Britain and the Slave Trade, 1839-1865 (1967).

[27] Robert Walsh, Notices of Brazil in 1828 and 1829 (London, 1830), vol. 2, p. 479; also in ibid., Boston and New York, 1831, vol. 2, facing title page.

Educational Exchange Programs' Impact on Foreign Direct Investment

William Hagerty, Matin Khadem
Montgomery Bell Academy; Nashville, Tennessee, United States of America
hagertywilliam03@gmail.com

Abstract – Job creation, specifically through foreign direct investment, is extremely important for states in providing jobs for their citizens. This study determines ways to increase foreign direct investment, this study analyzes the impact foreign exchange students participating in educational exchange programs has on the number of jobs created by foreign companies. After running multivariate regression analysis methods with several independent control variables, it was found that there is a significant, quantifiable correlation between the number of exchange students participating in the J-1 Visa program and the amount of jobs created in each state.

Key Words – foreign direct investment, exchange programs, jobs creation, educational exchange

INTRODUCTION

In the United States, policy-makers at both the federal and state level are constantly looking for ways to increase the number of jobs available to its citizens. States are often competing with one another to become the most attractive to potential companies looking to expand their operations. Typically, these companies are foreign, and are looking to open new manufacturing plants/sales offices in the United States to expand their market. To be more competitive, states need to use every institution available to persuade foreign companies to expand and create jobs for local citizens. Many states are already competing in a number of areas, for example by lowering tax burdens and becoming right to work states, yet considerably less attention has been given to the largest institutions in America, schools and universities, until recently [1]. The extent to which educational institutions can be harnessed to entice foreign companies to invest in America, has only received limited attention in research. As such there remains uncertainty around the impact schools and universities have on job creation by foreign companies, which makes it more difficult for policy-makers to conduct adequate cost-benefit analyses. This difficulty can explain why many states have been reluctant to tap into any job-creating potential of schools and universities. This study attempts to contribute to the nascent literature by considering the extent to which increasing the scope of international exchange programs can contribute to the expansion of foreign-owned companies in a given state and/or region. To investigate this pertinent topic and bring it to the data, the paper addresses the following question: to what extent does the number of international exchange students participating in educational exchange programs impact the number of jobs created by foreign companies?

LITERATURE REVIEW

The federal nature of the system of governance in the United States grants decision makers at the state level wide discretion over policies which have a direct impact on the number of exchange students. These measures include partnering with educational institutions and companies and encouraging more program sponsors for the J-1 Visa program. It is natural therefore that policy makers seeking to find efficient and innovative ways to support the local economy and attract both foreign talent and investment would be vitally interested in understanding the precise relationship between the flow of exchange students and job creation by foreign firms.

In the case of international students who are enrolled in full-time higher education, a number of studies such as [2][3] have drawn a link between international student mobility and socio-economic outcomes, with higher student mobility being found to be an important channel for high-skilled immigration who generally are considered to have high social capital which in turn can act as an aid for stimulating exchange in ideas and technology across countries, thereby encouraging FDI [4]. However it is unclear the extent to which these arguments are directly applicable to exchange students due to the temporary nature of their stay.

Furthermore, a recent study by [5] analyzed the effects of international students on inbound FDI into the UK and US and found a significant and positive impact, with educational networks being emphasized as a key factor in explaining the causal mechanism for more foreign students stimulating inbound FDI. It has been hypothesized that such networks among international students act as important means through which information regarding economic opportunities in the host country is relayed back home. In a similar vein, [6] analyze the link between German migration and FDI, with their results offering broad support for the importance of cultural linkages in stimulating investment from abroad.

Applying these findings to the American setting and the present analysis, the large proportion of foreign high-school and university exchange students arriving on the J-1 visa each year is likely to form an important educational

network which acts as a catalyst for inward FDI. Moreover, [6] argue that such linkages provide incentives for migrants and firms to locate in specific areas, emphasizing that not only are effects of interest at the national level but also that individual states will want to reflect on how best to capitalize on any FDI-stimulating effects of state-initiated educational exchange programs to gain a competitive advantage.

DATA

The two main independent variables of interest in this study are the number of international exchange students participating in educational exchange programs in the United States at college and high school level. For both measures, we use the number of international college students on educational exchanges in each individual state arriving under the J-1 Visa in 2018. This data comes from the United States State Department online database. The dependent variable in our analysis is the number of jobs created by foreign companies in each respective state. These values were provided by SelectUSA, the U.S. government program that measures and promotes foreign direct investment in the United States. Figure 1 shows a scatterplot of the dependent variable against the total number of international exchange students in 2018. The R^2 value is 0.85, indicating a strong positive correlation.

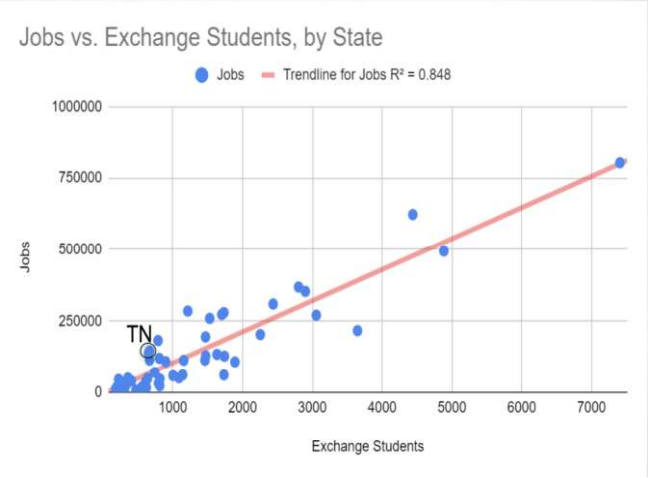

FIGURE 1: Jobs versus exchange students by state.

ANALYSIS

While Figure 1 depicts an extremely high correlation between the number of international exchange students and jobs created by foreign companies, the model does not control for other confounding factors. This means that Figure 1 can not confidently depict a significant relationship between the number of exchange students and job creation. In an attempt to address this problem, multivariate regression models were developed using key independent control variables confirmed by the Tennessee Department of Economic and Community Development to directly impact foreign direct investment. These variables are shown in Table 1 below.

TABLE 1: Control variables for regression analysis.

Control Variable	Source	Comment
Population	United States Census Bureau	Population of each respective state
Purchasing Power of the Dollar	Bureau of Economic Analysis	Power of the USD in each respective state
Tax Burden	ALEC-Laffer State Economic Competitiveness Index	Measured per $1000 income; compilied variable
Average Occupational Wage	Bureau of Labor Statistics	Average occupational wage for each state
Corporate Tax Rate	Tax Foundation	Corporate tax rate in each respective state
Right to Work State	Workplace Fairness Organization	Right-to-work laws of each respective state
Northeast	United States State Department	Dummy Variable; Midwestern states being control
South	United States State Department	Dummy Variable; Midwestern states being control
West	United States State Department	Dummy Variable; Midwestern states being control

Through multivariate regression analysis methods, we are able to predict how the number of jobs created by foreign companies is impacted by the number of exchange students by taking into account the contribution of the various control variables depicted in Table 1. Figure 2 shows the regression equation used to create the multivariate regression model. In this equation, α refers to the constant in the regression. The β_1 and β_2 represent the coefficients of interest of the college exchange student and high school exchange student variables. The $\mathbf{X_i}$ represents the vector containing the independent control variables, and the $\boldsymbol{\delta}$ represents each control variable's respective coefficients. Finally, ε_i represents the residual, or what our model cannot explain.

$$\text{ForeignJobs}_i = \alpha + \beta_1 College_i + \beta_2 Secondary_i + \boldsymbol{X_i\delta} + \varepsilon_i$$

FIGURE 2: Equation for the multivariate regression model.

Through this equation, and by using data from the variables depicted in table 1, we were able to create our multivariate regression model, as shown in Table 2.

TABLE 2: Multivariate regression model.

Regression Analysis:

Regression Statistics	
Multiple R	0.973310665
R Square	0.9473336507
Adjusted R Square	0.9320881285
Standard Error	42582.39664
Observations	50

ANOVA

	df	*SS*	*MS*	*F*
Regression	11	1239405866651	112673260605	62.13848499
Residual	38	68903899149	1813260504	
Total	49	1308309765800		

	Coefficients	*Standard Error*	*t Stat*	*P-value*
Intercept	223933.8695	344053.7852	0.6508687862	0.5190477497
College	42.03226243	13.60181892	3.090194236	0.00373240024
Secondary	47.28195513	22.99170537	2.05647882	0.04665055875
Population	0.01338773163	0.002381602918	5.621311399	0.000001882929
Purchasing Power of Dollar	-150719.3268	201306.9701	-0.7487039656	0.4586451074
Tax Burden	-213.9546662	625.2852843	-0.3421712802	0.734107331
Average Occupational Wage Rate	-0.5677741162	2.543546047	-0.2232214812	0.8245587772
Right to Work State	-17721.24947	23621.83242	-0.7502063834	0.4577505414
Corporate Tax Rates	-2489.684114	2529.951657	-0.9840836708	0.3312989228
West	-44096.64454	23557.5951	-1.871865288	0.0689372285
Northeast	5154.512704	27124.78239	0.1900296427	0.8502974093
South	16614.90866	20956.46102	0.7928298889	0.4327992988

As depicted in these tables, the p-value was below 5% for both college international exchange students and high school international exchange students, indicating that there is a *significant* correlation between the number of international exchange students participating in educational exchange programs and job creation by foreign companies. The respective coefficients can be interpreted as the number of jobs created by foreign companies for each one unit increase in a given independent variable. Therefore, the multivariate models suggest that every additional college exchange student is associated with the creation of 42 new jobs and every additional high-school exchange student is associated with the creation of 47 new jobs. These coefficients were then used to predict the number of jobs created by foreign companies, and were plotted against the actual number of jobs created by foreign companies in Figure 3.

FIGURE 3: Predicted versus actual foreign jobs by state.

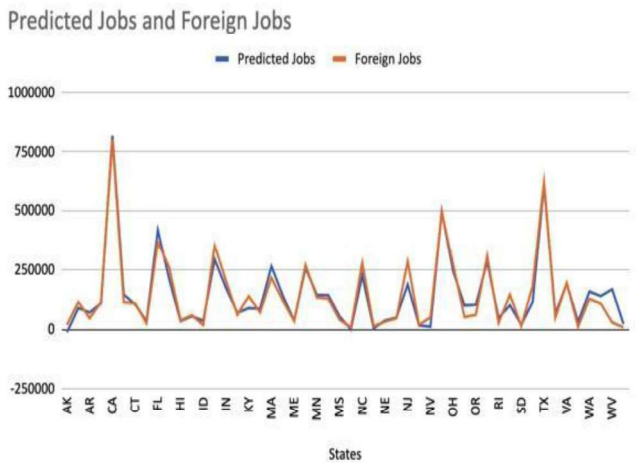

Figure 3 shows that the model we have constructed has very high predictive power, explaining approximately 94% of the variation in foreign job creation across states. This is important because it reinforces the notion that educational programs have a palpable effect on job creation through tangible coefficients that depict the exact numerical impact international exchange students actually have on job creation by foreign companies

DISCUSSION AND LIMITATIONS

However, there are a few limitations to the multivariate regression analysis used in this study. First of all, the coefficient values for both college exchange students and high school exchange students are fairly large. The coefficient is admittedly likely to be biased upwards due to omitted variables. However we argue that the values may not be as implausible as they first seem because the effect one exchange student has on the number of jobs created by foreign companies is amplified through educational network effects, as outlined in the literature review section. Furthermore, despite our attempts to control for possible endogeneity through the use of a rich set of control variables, the multivariate regression analysis cannot confidently determine the direction of causality. Ideally, if we had data from more time periods, we could run a fixed effects model. This would have been preferable and would have been more informative about the causal relationship as we could have controlled for fixed effects; however, we were unable to model in this fashion due to the fact that the data for the College/University and Secondary Student J-1 Visa subcategories was only made available very recently because of the recent creation of these respective subcategories. We therefore leave this task to future research. Also, based on the regression analysis, it is not entirely clear what mechanism is driving the relationship between exchange students and job creation. This can be addressed in future studies through more detailed surveys of both college and high school international exchange students to understand the nature of the network effect and to gauge exactly how big of an impact this trend could have on job creation by foreign companies. Despite these setbacks, the multivariate analysis methods used in this study still depict a strong, significant correlation between the number of international exchange students and jobs created by foreign companies.

CONCLUSION

In conclusion, it was found that the correlation between the number of college and high school international exchange students and the number of jobs created by foreign companies is extremely high and determined to be significant. It was also found that the coefficient values attributed to both high school and college exchange students are proven to be reliable in predicting job creation by foreign companies. While this study determines a strong correlation but not necessarily a causal relationship between foreign job creation and exchange students, the study can serve as a great segway for deeper research and analysis to determine causality between foreign direct investment and exchange programs. In conclusion, states across the U.S. should actively partner with educational institutions and companies to increase the number of exchange programs in order to make the United States even more attractive for foreign companies.

ACKNOWLEDGEMENTS

Tennessee Department of Economic and Community Development, University of Tennessee, University of Memphis, Japanese Consulate Office.

REFERENCES

[1]Maister, Philippa. (2015) “A Learning Curve: How Foreign Students Can Provide an FDI Boost.” FDi Intelligence www.fdiintelligence.com/article/61121

[2] Kahanec, Martin, and Renáta Králiková (2011). *Pulls of International Student Mobility*. IZA Institute of Labor Economics, IZA DP No. 6233

[3] Ritzen, J. M. M. and G. Marconi. (2011). “Internationalization in European Higher Education”, International Journal of Innovation Science, 3(2): 83 – 100.

[4] Bonin, Holger, et al. (2008). “Geographic Mobility in the European Union: Optimising its Economic and Social Benefits”, IZA Research Report No. 19, Bonn: Institute for the Study of Labor.

[5] Marina, Murat (2017). "International Students and Investments Abroad," Global Economy Journal, De Gruyter, vol. 17(1), pages 1-33

[6] Buch, Claudia M., et al. (2006) “Where Enterprises Lead, People Follow? Links between Migration and FDI in Germany.” *European Economic Review*, vol. 50, no. 8

Using Technology Enabled Career-Technical Education to Enhance American Education

Isabella He
Mission San Jose High School; Fremont, United States
Email: ihe210699@gmail.com

Abstract – Recent data has determined that American teenagers have been performing at stagnant levels for decades. Comparative analyses of education systems around the world determine that the absence of educational improvements are due to a lack of demand to learn. This study determines that career-focused education and personalized learning are two major factors that contribute to the academic successes of top education systems. Career-technical education (CTE) has shown to improve student engagement in secondary and post-secondary education. Furthermore, research supports that career-technical education is most effective in middle school, an optimal time for career exploration with less of an emphasis on core academic courses than high school. Barriers to CTE implementation in middle school include a lack of career counseling and funding. This paper explores an approach that allows CTE to reach more students in the American education system by using technology-enhanced learning to alleviate such barriers. Personalized e-learning allows for student choice, maximizing learning effectiveness and improving motivation to learn. This study concludes the merits of such an approach to enhance the American education system.

Key Words – Career-technical education, technology-enhanced learning, secondary education, personalized learning, academic engagement

INTRODUCTION

I. Background

Around 100 years ago, American education took an almost unprecedented leap forward by making high school secondary education compulsory, driving much of America's economic boom for the last 100 years [1]. However, as the U.S. News reports in 2018, "At no level – early childhood, K-12, higher ed – are we [American education] even in the top 10 internationally... It is scary and it does not bode well for the future" [1]. Innovative leaps forward in American education have not been taken in recent decades, as the Program for International Student Assessment announced in 2019 that American teenagers have been performing at stagnant levels since 2000 [2, 3]. With education being essential to acquiring knowledge, maintaining society, stimulating the economy, and developing human virtue [4], such evidence of lack of improvements in the American education system in decades prompts a need for change.

II. Comparative Analysis

One of the best ways to improve a system is to learn from mistakes and successes of education systems from all over the world. However, as the United States is a heterogeneous society of many students with diverse backgrounds, comparisons to other countries with homogenous societies will have limitations. Limitations that could impact the comparability between countries include language barriers and cultural differences among the United States' large immigrant population [5]. This study acknowledges these limitations while focusing on data-backed objective comparisons to propose approaches for improvements to the American education system.

Comparative analyses between American and other international education systems demonstrate a lack of efficiency in areas of American education. Stephen P. Heyneman summarizes data of over 60 countries from the OECD's study called the "Programme for International Student Assessment" (PISA), which shows that American schools devote around 3 and 5 more hours/week to core academic subjects than Northern European countries, yet students from those countries have higher PISA achievement scores than American students [5]. Heyneman concludes that such inefficiency in American education compared to other countries results from a lack of a 'demand to learn.' Heyneman defines 'demand to learn' as a "culturally-shaped attitude or disposition that places the value of education higher or lower on a scale of socially desirable activities" [5]. Adopting the best practices across the globe to increase student motivation and demand to learn is essential. Conducting a deeper comparative analysis between education systems further unveils the causes for this lack of demand to learn and outputs several markers for improvement of the American education system. This paper chooses to analyze education systems in Singapore and Northern Europe for their similar standards of living to the United States and their high international rankings.

Ranking as best in the world according to OECD in 2015 and as first for primary and secondary levels in PISA scores from OECD's 2019 data, Singapore's students are achieving undeniably high academic results [6]. Analyzing

the top reasons for Singapore's success reveals that a curriculum focused on practical knowledge, real-world skills, and personalized learning pathways are large contributors to Singapore's high rankings on PISA studies [7].

Singapore dedicates a top reason for their education system's success to a curriculum focused on problem-solving and real-world applications [7]. Singapore's curriculum equips students for practical knowledge in specific real-world subjects and careers, which surveys and studies have shown American education lacking in. In a survey conducted by The New York Times, students reported that the American secondary education system should better prepare students for real life. Bella Perrotta from Kent Roosevelt High School states, "I am frustrated about what I'm supposed to learn in school. Most of the time, I feel like what I'm learning will not help me in life" [8]. Skye Williams from Florida summarizes the issues to address in American education in her statement: "I think that the American education system can be improved by allowing students to choose the classes that they wish to take or classes that are beneficial for their future" [8]. Results from a poll of ninth and tenth graders in California found more than 90% of respondents stated that they would be more motivated to learn and more engaged in their education if skills and knowledge relevant to future careers were a focus in their classes [9].

Singapore's education system provides students with options for different learning pathways, depending on their preferences and learning profiles. After course exploration in primary and secondary school, students choose between two vocational pathways from Polytechnics and Junior Colleges that can both lead to University [10]. These personalized pathways originated from the belief that every student learns differently with different career interests and at different paces. Implementing elements of Singapore's personalized learning pathways in American education can enhance students' learning experiences, as such a model of learning has produced high academic performance and demand to learn.

Beyond Singapore, Northern European education systems also demonstrate success from personalized pathways. Compared to American teenagers, Northern European teenagers are 10+ percent more likely to graduate from secondary school. John H. Bishop from Cornell University lists the number one key for Northern European success as "Parents/students decide which program of study to enter." [11]. Mike Anderson analyzes the benefits of personalization and student choice in education, finding that student choice through personalization can provide a solution to Heyneman's top reason for inefficiency in American education: a lack of demand to learn. Personalization allows students to be active participants in their education and learn in the zone of proximal development in subjects they're motivated to pursue, leading to high student engagement [12]. Additional research demonstrates that student choice and personalized learning will lead to improved academic performance on tests such as the PISA achievement test, concluding that, "students who were given a choice in their learning and whose instruction met their learning needs showed significant improvement on standardized tests" [13].

Nations such as Singapore and those in Northern Europe address student motivation to learn through curriculums focused on career-relevant, practical knowledge and personalized vocational learning pathways.

III. Purpose Statement

Based on the comparative analysis on Singapore and Northern Europe's successes, this paper will explore approaches to increase student engagement and demand to learn in American education through career-relevant, practical learning, technology-enhanced learning, and personalization of learning pathways.

VALUE OF CAREER-TECHNICAL EDUCATION

Engagement with school declined approximately 20% between elementary school and middle school from nearly 80% to 60%, with a further decline to only 44% engagement in high school [14]. In comparison, students in secondary education with greater exposure to career planning and career exploration were found more likely to be engaged in their education [15]. Career-technical education (CTE) is the pathway to career-relevant planning and exploration to increase demand to learn in American education and fulfill students' requests for classes that prepare them for real-world careers. CTE is the practice of teaching specific career skills to students, including business, finance, information technology, law, arts, training, and more [16].

As evidence of the benefits of practical-centric learning and career-technical education, data from 2019 shows that 95% of CTE students graduate high school. This is compared to the national average graduation rate of only 85% [17]. Increasing high school graduation rates enables more students to follow a path to success while strengthening the American economy [18]. With better graduation rates also comes higher student satisfaction with education, as "80% of all CTE students say they're satisfied with their education and the career prospects that come with it," which is almost twice as many students in proportion as the 45% of students satisfied with traditional education [19]. The impact of CTE courses also extends beyond secondary education to the workforce and the long-term benefits of successful education. As labor force data of public high school graduates from 2013 in Figure 1 depicts, a 12% lower unemployment rate is demonstrated from those with 3.00 or more CTE credits compared to those with 0.00-0.99 CTE credits.

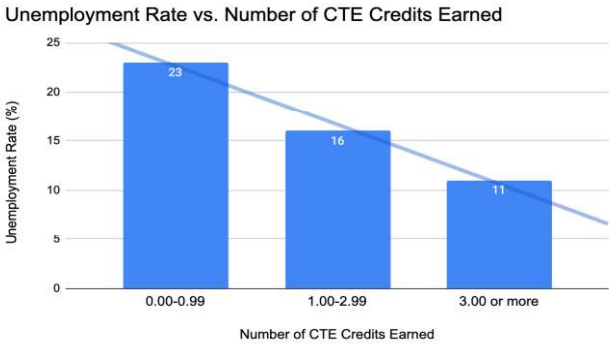

FIGURE 1: Labor force data from public high school graduates from 2013 by percentage unemployment rate vs. the number of CTE credits earned. Raw Data Source: U.S. Department of Education, Institute of Education Sciences, National Center for Education Statistics, High School Longitudinal Study of 2009 (HSLS:2009), Base-year, 2013 Update, Second Follow-up, and High School Transcript File.

Maximizing CTE's impact addresses the concerns raised by research studies and surveys depicting low student motivation and a lack of real-world preparation in American education [8, 9].

DATA: CASE STUDY WITH CTE

This study uses data from Michigan's Department of Education and the 100,000+ students that participate in Michigan's CTE programs each year to further analyze the benefits of CTE with a real-world case study [20]. The data in Table 1 showcases that students enrolled in CTE programs demonstrate performance that exceeds state targets in technical skills, school completion, graduation rate, and placement rate. This data further validates the potential of CTE programs to improve secondary education.

TABLE 1: Performance indicators from students in Michigan's CTE program. Raw Data Source: Michigan Department of Education, "MI CTE Reports." Cteis.Com, 2020, reports.cteis.com/.

Performance Indicator	Performance	Relation to State Target
Technical Skills	63.53%	Exceeds Target
School Completion	98.44%	Exceeds Target
Graduation Rate	96.61%	Exceeds Target
Placement Rate	96.36%	Exceeds Target

However, enrollment in CTE in America is still minimal and currently declining, with less than 3 CTE credits earned by students in their 4 years of high school education, as Figure 2 illustrates. This paper therefore explores an approach to maximizing CTE's demonstrated benefits.

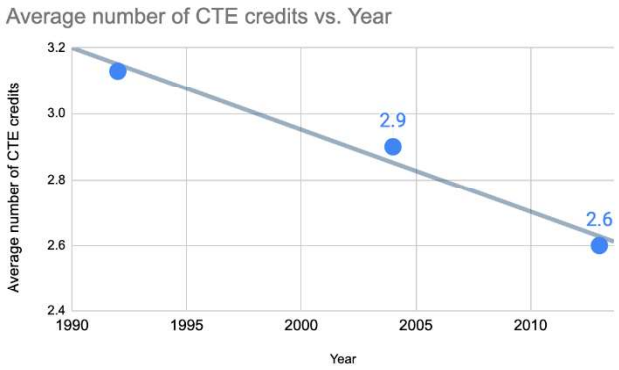

FIGURE 2: Average number of career and technical education (CTE) credits by year earned. Raw Data Source: U.S. Department of Education, Institute of Education Sciences, National Center for Education Statistics, National Education Longitudinal Study of 1988, 2002, 2009, 2013 (NELS:88)

APPROACH: CTE IN MIDDLE SCHOOL

While CTE in high school has demonstrated benefits in graduation rates, student motivation, and employment rates, research has shown that students benefit most from career exploration in middle school — learning about potential careers, building self-awareness, and developing a plan for reaching future goals [21]. Career-technical education is the most effective to middle-school students, whose brains are receptive to training employability skills: critical thinking, adaptability, problem-solving, oral and written communications, collaboration, creativity, responsibility, professionalism, ethics, and technology use [21, 22]. As these employability skills are reported to be critical to the workforce as well as postsecondary success, middle school is a pivotal time for college and career readiness [23]. Expanding CTE courses in middle schools allows students to explore career options and determine their subjects of interest before high school. CTE in middle school can effectively prevent dropouts and increase student motivation, serving "as a key dropout prevention strategy, mitigating many of the challenges students face as they transition into high school, such as disengagement or lack of preparation" [24]. Implementing career-technical education to middle schools across the United States increases students' demand to learn from an early age to carry on to later stages of education in high school and postsecondary engagements.

Emphasis on core academic courses, especially in high school when these core academic courses are considered essential for college preparation, has limited accessibility to CTE [23]. Misconceptions about CTE courses and college-preparatory options have made the implementation or expansion of CTE difficult for many schools. Research conducted in Mississippi school districts concerning the

perception of CTE by students and educators indicates 55% of the 403 Mississippi residents interviewed believed that students enrolled in CTE courses could not receive college-preparatory diplomas [25]. Although CTE courses have demonstrated excellent results in terms of college preparation and high school graduation, and aid students in applying their core academic knowledge to real-world skills [18], the disconnect between CTE courses in high school and college-preparatory education prevents CTE from reaching its potential.

Analysis of the average number of credits earned by curricular areas (core academics vs. CTE) demonstrates that while credits earned in core academic courses have been increasing, credits earned in CTE courses are declining (see Figure 3.) The disconnect between college preparation and CTE and the emphasis on core academic courses has limited career-technical education's impact on the education system and its students.

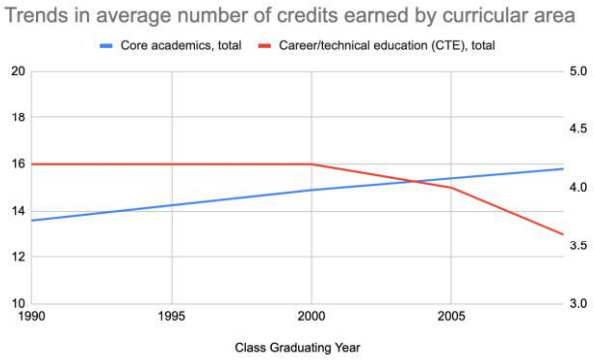

FIGURE 3: Average number of credits earned by 1990, 2000, 2005, and 2009 public high school graduates during high school, by curricular area (total core academics compared to CTE). Raw Data Source: U.S. Department of Education, Institute of Education Sciences, National Center for Education Statistics, High School Transcript Study (HSTS), 1990, 2000, 2005, and 2009.

Implementing CTE in middle school diminishes the barrier from the emphasis of core academic courses since the courses students take in high school impact their college admissions, whereas middle school has a lower workload and academic pressure in comparison. Having CTE courses in middle school is the best time to build a foundation for students' communication, time-management, problem-solving, critical thinking, and work-related skills critical for success in later secondary education and post-secondary careers [23].

APPROACH: CTE WITH TECHNOLOGY-ENHANCED LEARNING

There are 2 major barriers to implementing CTE in secondary schools: a lack of school counselors, and a lack of funding [23]. Research studies validate an approach using technology-enhanced learning to lower these barriers.

I. Career Counseling

Counselors and other career development professionals are instrumental in assisting students with self-exploration, future planning, career exploration, and work-based learning in classrooms [23]. Career guidance is critical as students who participate in such guidance demonstrate better grades, greater knowledge of jobs, higher self-esteem, and more engagement in career and academic planning [23]. However, a lack of awareness or access to market data and other relevant information on career pathways by many career counselors limits student exposure to career pathways to their own direct experience [24].

Although the current use of online tools and other technologies cannot replace school counselors, scalable technologies such as Career Cruising, the DISCOVER program, and the CHOICES program can decrease counselors' burdens while guiding students' decisions about their future course-taking and potential careers [21, 23]. Career Cruising, an online future planning and exploration program, is already being put to use in Wisconsin's school districts for self-exploration, creating online portfolios, discovering potential interests, skills, interests, abilities, and jobs [23]. A study conducted with a similar interactive program, DISCOVER, which has vocational self-assessments and an abundance of occupational information, found that middle-school students who worked with DISCOVER for one hour a day over a two-week period revealed significant gains in career maturity [21]. Additional programs such as MAPP, the Life Values Self-Assessment Test (LVAT), and CareerOneStop can all aid in career counseling through online self-assessments and information on planning for future-readiness. Many such programs are certified with validity studies on their accuracy and also provide free guidance to counter issues with funding for career counseling [26]. The occupational information and scalable career-interest assessments provided in these programs alleviate the barriers of lack of access, awareness, and training to market data or career pathways from school counselors.

II. Funding for CTE

Educational funding is a major factor of student success as it enables acquisition of required materials, services, and administrative support. Financial challenges to implementing CTE in middle school prevent it from maximizing its impact. Although the Carl D. Perkins Career and Technical Education Act supports career exploration in middle school, Perkins funding for states is decreasing with current funds at about $150 million less than the Fiscal Year 2010 levels, indicating a lack of adequate funding for new and developed CTE programs.

Alleviating budgetary limitations to CTE is possible through education technology by reducing reliance on manual resources, being flexible and scalable, and by improving course management efficiency. Curriculum

redesigns with technology-enhanced learning in the U.S. evidenced average savings of 31% with reduced course delivery costs [27]. Cost savings from the technology redesign did not sacrifice quality — student outcomes improved, with 72% of projects delivered by students showcasing higher quality [27]. Advance CTE presents the use of technology as one of five core strategies for expanding CTE, with online and virtual courses to be leveraged to reach economies of scale across vast geographic regions [28]. Quality-controlled virtual courses can reduce material, classroom, and staff costs to bring CTE to students across the United States.

APPROACH: PERSONALIZED E-LEARNING

By enabling career exploration in middle school, students will be more informed on their subject and career interests to make decisions on personalized learning pathways in high school. As research into student choice, as well as successes in Singapore and Northern Europe reveal, personalized learning is a key strategy for improving students' demand to learn and their academic results. Case studies on using technology to create personalized learning plans have found average increases of 30% in student achievement and test scores [29].

Virtual learning environments provided by technologies such as Brightspace create personalized learning plans and content (videos, e-portfolios, documents) to suit the individual learner's needs. By presenting students with their own engagement data, Brightspace increased 81% of its learners' study times [27].

Furthermore, with the possibilities of technology ever-growing, personalized adaptive learning through machine learning can boost academic engagement and results by synthesizing large amounts of data to produce fully student-centered learning [30]. Using technology to bring personalized learning combined with career exploration throughout secondary education addresses the lack of demand to learn in American education and improves students' satisfaction with their learning.

LIMITATIONS

New research points to possible limitations of the long-term benefits of CTE, finding that employment advantages provided by vocational training are limited to the start of the career and diminish with age [31]. Rapidly changing economics and required skill sets demonstrate the necessity for more research into improving CTE programs to be more adaptable and thus provide life-long employment advantages.

A limitation of this study is its narrowed focus on exposure to CTE in secondary education without accounting for variations in quality of CTE across programs. Additional research into the characteristics of high-quality CTE programs is necessary to understand the other possible benefits of CTE and recommend the best practices across different programs. Furthermore, this study did not differentiate between the effectiveness of different methods of student access to CTE: public schools, private schools, shared-time CTE schools, and full-time CTE schools. More longitudinal data studies and analyses of student performance and workforce data will broaden the scope of studies on the American education system in relation to CTE.

CONCLUSION

The findings from this research paper reveal the merits of an approach to elevating the American education system through technology-enabled career-technical education in secondary education. The comparative analyses between international and American education systems demonstrated the validity of improving demand to learn through education on career-relevant, practical knowledge, and personalized learning. CTE has proven benefits for graduation rates, student satisfaction of learning, the workforce, and the American economy. An optimal approach is to implement CTE throughout secondary education, including and emphasizing its implementation in middle school. In addition to evidence that middle school is the best and most impactful time for career-relevant exploration, implementing CTE in middle school alleviates the barriers that come with the emphasis on core academic courses in high school.

Technology-enabled learning can further reduce the barriers that prevent CTE in middle school from maximizing its impact: a lack of resources for career counseling and funding for schools. Computer-assisted career guidance resources such as Career Cruising, DISCOVER, and CHOICES improve counseling scalability and have proven benefits for career exploration as well as students' career maturity. Additionally, technology-enhanced learning provides counselors with self-assessment tools such as MAPP and the Life Values Self-Assessment Test to make accurate interest and career assessments accessible to students. Flexible and scalable in nature, technology-enhanced learning can address concerns with funding by reducing reliance on manual resources and improving course management efficiency. Results from curriculum redesigns with technology-enhanced learning have demonstrated that technology can reduce costs while improving the quality of education.

Personalized learning through technology has vast opportunities and many potential benefits. By increasing student choice and thereby improving student engagement, personalized learning makes education more efficient and effective. Acknowledging the possibilities of machine learning to further individualize education leaves additional research into this area a worthy topic for improving education.

Further research can study the possible effects of career-technical education and personalization on students' mental health. By enabling students to discover career goals and study subjects they are interested in, personalized CTE

education broadens the scope of learning and allows students to adjust their learning to their strengths.

While making changes to an established system comes with risks, the stand-still state of current American education poses greater risks to the future generation and the American economy.

ACKNOWLEDGEMENTS

The author would like to thank Ms. Katy Kuei for her support, guidance, and encouragement in writing this paper.

REFERENCES

[1] Levy, Gabrielle. "Rethinking Education in America." *US News & World Report*, U.S. News & World Report, 2018, www.usnews.com/news/the-report/articles/2018-07-27/americas-schools-arent-working-for-americas-kids

[2] OECD. PISA 2018 Results Combined Executive Summaries. 2018, www.oecd.org/pisa/Combined_Executive_Summaries_PISA_2018.pdf.

[3] "'It Just Isn't Working': PISA Test Scores Cast Doubt on U.S. Education Efforts." *The New York Times*, 3 Dec. 2019, www.nytimes.com/2019/12/03/us/us-students-international-test-scores.html.

[4] Bhardwaj, Ajay, and Sr Assistant. "Importance of Education in Human Life: A Holistic Approach." *International Journal of Science and Consciousness (IJSC): A Bio-Psycho-Spiritual Approach Published by the Research Foundation for Science & Consciousness*, vol. 2, no. 2, 2016, pp. 2455–2038, 2016, ijsc.net/docs/issue4/importance-of-education-in-human-life.pdf.

[5] Lemke, et al. "The Future of Higher Education." *Committee on Education Beyond High School*, vol. 16, no. 1, 1947, pp. 74–89, www.tc.columbia.edu/cice/pdf/30413_16_1_Stephen_Heyneman.pdf. 2013.

[6] "World Best Education Systems." *Educate Every Child on the Planet: The World Top 20 Project*, July 2020, worldtop20.org/worldbesteducationsystem.

[7] "6 Reasons Why Singapore's School System Is the Best Worldwide." *SmileTutor*, 5 Dec. 2019, smiletutor.sg/6-reasons-why-singapores-school-system-is-the-best-worldwide/.

[8] "What Students Are Saying About How to Improve American Education." *The New York Times*, 19 Dec. 2019, www.nytimes.com/2019/12/19/learning/what-students-are-saying-about-how-to-improve-american-education.html.

[9] "Report Findings Based on a Survey Among California Ninth and Tenth Graders." Peter D. Hart Research Associates Inc. April. 2006, www.connectedcalifornia.org/downloads/irvine_poll.pdf

[10] "Why Singapore's School System Is So Successful? | Education in Singapore." *In-Singapore.Education*, 2020, in-singapore.education/why-singapores-school-system-is-so-successful/#:~:text=The%20results%20of%20international%20education,in%20the%20world%20in%202015

[11] Bishop, John H. Which Secondary Education Systems Work Best? The United States or Northern Europe. Cornell University, 2010, digitalcommons.ilr.cornell.edu/cgi/viewcontent.cgi?article=1104&context=workingpapers.

[12] Anderson, Mike. "Chapter 1. The Key Benefits of Choice." The Key Benefits of Choice, 2016, www.ascd.org/publications/books/116015/chapters/The-Key-Benefits-of-Choice.aspx.

[13] "Impact of Student Choice and Personalized Learning," Hanover Research, 2014, https://www.gssaweb.org/wp-content/uploads/2015/04/Impact-of-Student-Choice-and-Personalized-Learning-1.pdf

[14] Busteed, Brandon. "The School Cliff: Student Engagement Drops With Each School Year." Gallup.Com, Gallup, 7 Jan. 2013, news.gallup.com/opinion/gallup/170525/school-cliff-studentengagement-drops-school-year.aspx.

[15] Perry, Justin. "School engagement as a mediator of academic performance among urban youth: The role of career preparation, parental career support, and teacher support." Counseling Psychologist, 38, 269-295, 2010.

[16] Bri Stauffer. "What Is Career & Technical Education (CTE)?" *Aeseducation.Com*, 2020, www.aeseducation.com/blog/career-technical-education-cte.

[17] Career and Technical Education & Student Achievement. Advance CTE, 2018, cte.careertech.org/sites/default/files/CTE_Student_Achievement_2018.pdf.

[18] ACTE. Career and Technical Education's Role in American Competitiveness, 2018.

[19] High, Most, and Schoolers Feel. Learning from Student Voice. http://youthtruthsurvey.org/wp-content/uploads/2016/01/YouthTruth-Learning-From-Student-Voice-College-and-Career-Readiness-2016.pdf

[20] "Career and Technical Education." Mischooldata.Org, 2017, www.mischooldata.org/DistrictSchoolProfiles2/CareerAndTechnicalEducation/CareerAndTechnicalEducation.aspx. Accessed 28 July 2020.

[21] Hughes, Katherine, and Melinda Karp. School-Based Career Development: A Synthesis of the Literature. 2004, https://files.eric.ed.gov/fulltext/ED498580.pdf

[22] ACTE. "What is "Career Ready"?" 2010.

[23] ACTE. Career Exploration: In Middle School. 2018, www.acteonline.org/wp-content/uploads/2018/02/ACTE_CC_Paper_FINAL.pdf.

[24] Godbey, Samantha, and Howard Gordon. Middle Grades Review Career Exploration at the Middle School Level: Barriers and Opportunities Career Exploration at the Middle School Level: Barriers and Opportunities. Vol. 5, no. 2, 2019, files.eric.ed.gov/fulltext/EJ1230750.pdf.

[25] Jordan, Julie, et al. *CTE in Mississippi Confronting the CTE Stigma Perceptions of CTE Among Mississippi Public and Educators*. 2016, http://ijsc.net/docs/issue4/importance-of-education-in-human-life.pdf

[26] "MAPP," Assessment.com, 2020, www.assessment.com/AboutMAPP/ValidityAndReliability.

[27] Davies, Sarah, et al. *Rebooting Learning for the Digital Age: What next for Technology- Enhanced Higher Education?*

[28] Advance CTE. CTE On The Frontier: Rural Strategy Guide. cte.careertech.org/sites/default/files/files/resources/CTE_RuralStrategyGuideFINAL.pdf.

[29] Grinager, Heather. How Education Technology Leads to Improved Student Achievement. 2006, www.ncsl.org/portals/1/documents/educ/item013161.pdf.

[30] Jacopo Mauri. "4 Benefits Of AI In Personalized Learning." *ELearning Industry*, eLearning Industry, 10 Dec. 2019, elearningindustry.com/benefits-of-artifcial-intelligence-in-personalized-learning.

[31] Hanushek, Eric A., et al. "General Education, Vocational Education, and Labor-Market Outcomes over the Lifecycle." Journal of Human Resources, vol. 52, no. 1, 8 Mar. 2016, pp. 48–87, 10.3368/jhr.52.1.0415-

Effects of Breast Cancer Cell-Derived Extracellular Vesicles on Endothelial Cells and Angiogenesis

Chien-Yu Huang
International School of the Sacred Heart; Tokyo, Japan
Email: 21chihiro21@students.issh.ac.jp

Abstract - The severity of breast cancer is greatly increased once cancer cells undergo metastasis and spread throughout the body. Interactions between our body's endothelial cells (EC) and extracellular vesicles (EV) excreted from breast cancer cells are thought to induce metastasis— endothelial cells are responsible for angiogenesis, the formation of new blood vessels, and create new pathways for cancer cells to spread. In this investigation, the effects of breast cancer cell derived EV on EC are observed through changes in the angiogenic ability of EC. Angiogenic ability before and after successful EV to EC incorporation was observed in in vitro environments. Results displayed that EV influenced EC activity to enhance cancer metastasis. With added EV, EC angiogenesis ability intensified to form larger networks of tubes formation in in vitro environments. Therefore, breast cancer cell EV play a role in the escalation of cancer metastasis via angiogenesis and EC — the prevention or restriction of breast cancer would lie heavily in further understanding of EV.

Key Words - Extracellular vesicles (EV), endothelial cells (EC), angiogenesis, metastasis, tube formation

INTRODUCTION

I. Research Question

What effects do breast cancer cell-derived extracellular vesicle have on human endothelial cells and, consequently, angiogenesis?

II. Background Context

Breast cancer is the accumulation of abnormal, cancerous cells in the breast area and is the most common. cancer for women worldwide [1]. 1 in 8 women in the United States will develop breast cancer at least once in her lifetime and in 2018 alone, approximately 2.1 million new cases of breast cancer were diagnosed [2]. The survival rate of breast cancer patients is heavily dependent on the level of metastasis, the spread of cancer cells to different parts of the body [3].

Metastasis can occur when cancerous tumor cells disseminate either through the blood vessels or the lymphatic vessels. Angiogenesis, the creation of new blood vessels, therefore plays a significant role in metastasis and tumor growth in different parts of the body as angiogenesis creates new pathways for cancer to spread. This investigation delves into the effects that breast cancer cells (BCC), their DNA dense extracellular vesicles (EV) in particular, have on the body's angiogenic ability and metastasis. These effects are investigated by incorporating BCC EVs with our body's endothelial cells (EC), which are vital in the production of new blood vessels and angiogenesis [5], and observing the effects on of angiogenic ability.

LITERATURE REVIEW

I. Breast Cancer and Metastasis

Metastasis occurs when cancerous cells spread to different parts of the body, away from its origin [6], and is the most important factor in determining the survival rate of the breast cancer patient. When the breast cancer cells have not metastasized, women have a high 5-year survival rate of 99% [7]. However, once breast cancer cells undergo metastasis and spread to various parts of the body, the 5 year survival rate significantly drops to 27% [7]. Metastatic breast cancer cells are difficult to treat by conventional methods such as surgery or radiotherapy since the cancer cells have already spread away from the origin and are much harder to pinpoint and treat [8]. The prevention of breast cancer cells from reaching this stage of metastasis would therefore increase mortality rate of breast cancer patients.

II. *Role of Angiogenesis in Metastasis*

Angiogenesis is a critical process required for metastasis. Angiogenesis is the formation of new blood vessels from pre-existing blood vessels [9] and, under non-cancerous conditions, is a typical body process during one's growth and wound healing. However, in cancerous conditions, angiogenesis is an essential step in the development of new metastatic pathways in which the BCC can enter the bloodstream and spread [10].

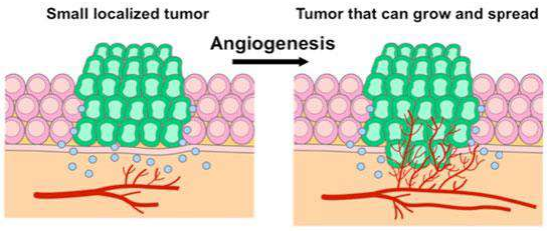

FIGURE 1: Role of Angiogenesis in the Spread of BCC [11]

New blood vessels created via angiogenesis provide new routes by which tumor and cancer cells exit the original tumor site and enter the circulation — triggering metastasis (Fig. 1) [10]. Instead of the tumor simply growing larger in size to reach pre-existing blood vessels, BCC could *possibly* influence angiogenesis to create new blood vessels to reach the tumor itself — this investigation will study the degree to which BCC will be able to influence angiogenesis and therefore, metastasis.

III. Endothelial Cells and Angiogenesis

Endothelial cells (EC) form the single cell layer that lines all blood vessels and the proliferation in EC numbers are accompanied with the rise of mature blood vessels— making EC vital for angiogenesis [12]. EC assist in angiogenesis by forming capillary-like structures, and extending and remodeling pre-existing blood vessels [13]. ECs are nearly always found near the tumor microenvironment [14] and can directly impact the rate of angiogenesis. Therefore, changes in EC activity after BCC incorporation compared to EC activity without incorporation will strongly indicate that BCC will also influence angiogenic ability.

IV. Breast Cancer Cell-Derived Extracellular Vesicles and Endothelial Cells

BCC can influence our body's endothelial cells through interactions between the BCC's extracellular vesicles (EV) and the body's endothelial cells (EC). EVs are membranous structures excreted from cells and often act as a biological cargo for lipids, proteins, and (most importantly) RNAs and DNAs [15]. EVs excreted by BCC allow for intercellular communication between cancerous cells and our body's cells through the exchange of genetic material [16]. Several past studies exemplify how strands of DNA and RNA in the EV could be selectively packaged *and* functional in their target cells [17]. In theory then, incorporating EVs derived from breast cancer cells with endothelial cells should cause an exchange of genetic material between EV and the body's EC.

PURPOSE OF STUDY

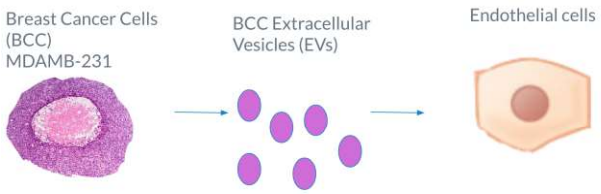

FIGURE 2: Flow Chart Exemplifying Effects of BCC to EC

I. Objective

The objective of this investigation is to examine the effects of BCC on EC through intercellular interactions through the genetic material found in BCC derived EV. As seen in Figure 2, BCC will excrete EV (filled with genetic material) and in turn affect EC and its behaviors in angiogenesis and metastasis. Investigating intercellular interactions between BCC derived EV and EC would deepen our understanding in the role of BCC EV in angiogenesis, which could be applied to clinical procedures in the prevention of metastasis.

II. Phenotype investigated

The phenotype investigated are changes in angiogenic ability. Results will compare differences between the control (only EC) versus the variable (EC with EV incorporated in them). Angiogenic ability is investigated through an endothelial cell tube formation assay. Both the control and the variable are placed in *in vitro* conditions which mimic the body's microenvironment (matrigel and nutrients) to allow the endothelial cells to create tube formations in the gel. These tube formations represent blood vessel formations in the body. Differences between tubes formed by the control and the variable exemplify differences in angiogenic ability due to EV incorporation.

HYPOTHESIS

I. Hypothesis for Angiogenic Ability

After EV incorporation, the EC+EV (EC with added EV) samples should have increased tube formations in the *in vitro* conditions compared to samples only containing EC. Tubes formed by EC+EV samples should be longer in length and form more extensive networks. As these tube formations represent blood vessels, the degree of impact that BCC EVs would have on our body's EC and angiogenesis will be determined.

METHODOLOGY: INCORPORATION OF EV TO EC

I. Justification

This investigation requires the comparison between EC and EC+EV. The EC used is store bought Human Umbilical Vein Endothelial Cells (HUVEC). However, the EV are derived from breast cancer cells straight from the hospital. From the range of different types of BCC, MDA-MB-231 is used. MDA-MB-231 is a triple negative cancer, and metastases easily, making this BCC a suitable sample in this investigation. To obtain only EV from BCC, a thorough separation procedure is needed. The standard method for EV extraction [18] was slightly adjusted for this investigation but the underlying principles stayed the same.

II. Experimental Procedure

BCC solution was obtained directly from the hospital. The BCC solution was poured into 6 micro-centrifuge tubes and centrifuged under 1000rpm, 4°C for 5 minutes. The BCC solution was centrifuged again under 2100rpm, 4°C for 20 minutes. After ensuring the micro-centrifuge tubes were not damaged, the BCC solutions were centrifuged in a super centrifuge under 37000 rpm for 70 minutes. The supernatants were carefully removed from the micro-centrifuge tubes using a mechanical pipette. The EVs found in the precipitate were stained with PKH26. PBS was added to fill up the micro-centrifuge tubes so nearly the entire tube was filled. Again, the PBS and EV mixture was centrifuged in a super centrifuge under 37000rpm for 70 minutes. The PBS and EV mixture was removed and the EV concentration obtained using a spectrophotometer [19]. The EV concentration for this investigation was 0.087 µg/mL.
To create samples, 60mL of HUVEC [20] was added into 10 cell culture dishes. Five of the cell culture dishes were labeled as "EC" while the remaining were labeled as "EC+EV" using tape and marker. 69mL of EV solution was added to the cell culture dishes labels "EC+EV" (*Refer to Calculation: Volume for Assay Samples to find how volume of 69mL was determined)*. The cell culture dishes labeled "EC+EV" were mixed by slowly rotating the dishes. All 10 dishes were left in an incubator at 36°C for 24 hours.

METHODOLOGY: ANGIOGENIC ASSAY

I. Justification

To observe the formation of new blood vessels, the samples will be placed in *in vitro* conditions to mimic the body's microenvironment. The tube formation assay is a widely used *in vitro* assay which model the ability of EC to perform angiogenesis [21], and will be used in this investigation. The samples placed *in vitro* will form tubes which represent blood vessel formation in the body. The sample cells will be placed in Matrigel Growth Factor Reduced, a gel used to commonly used to culture cells. The preparation of the matrigel and the tube formation assay was followed accordingly to the procedure provided [22] with adjustments to include the sample of EC+EV.

II. Experimental Procedure

2mL of matrigel was thawed in ice (matrigel is typically stored in -20°C conditions). After several minutes, 200µL of matrigel was added into 10 new cell culture dishes using a mechanical pipette. The matrigel filled culture dishes were incubated at 37°C for 30 minutes. While the dishes were incubating, the EC and EC+EV samples were collected from the incubator. As the EC and EC+EV were stuck to the bottom of the dishes, any solution in the samples was removed. PBS solution was pumped in and out of the cell culture dishes several times to clean the dish. 200µL of trypsin was added to each dish and incubated at 37°C for 2 minutes. 800µL of UCB mix was then added into each dish. 10 new eppendorfs were prepared. 5 of these eppendorfs were labels as "EC" while the remaining were labels as "EC+EV". 20µL of EC or EC+EV solution were moved into their respective eppendorfs. The remaining sample solutions were moved to 10 new centrifuge tubes, also with 5 tubes labels as "EC" and the remaining as "EC+EV". 4mL of UCB was added to each centrifuge tube and centrifuged under 1000rpm for 5 minutes. The supernatant was removed to 10 new cell pellets and labeled accordingly.

The 20µL of solution removed above was placed as a single drop on a hemocytometer. A slide cover was carefully placed on top of the single drop. The hemocytometer was placed under a microscope under x20 magnification.

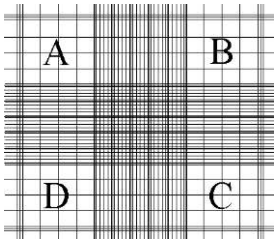

FIGURE 3: Hemocytometer Cell Count [20]

Cells visible in fields A, B, C, and D were counted. The hemocytometer was moved and fields counted again — therefore, a total of 8 fields was counted for each sample. This cell count procedure was repeated for all samples of "EC" and "EC+EV". Cell count was calculated using the formula: *cell count = (sum of cells counted)/number of boxes* $\times 10^4$. Final cell counts are recorded in *Calculations: Cell Count* below.

After cell counts were recorded, the 10 matrigel-filled dishes were removed from the incubator. Based on the data from *Calculations: In Vitro Volumes*, 360µL of "EC" solution was moved from the cell pellets into 5 matrigel-filled dishes. 1.14mL IMDM solution was also added to these 5 dishes and were labels as "EC". 1mL of "EC+EV" solution

and 0.5mL of IMDM solution was added into the 5 remaining matrigel filled dishes, and were accordingly labelled as "EC+EV". Photographs were taken under x20 magnification microscope for all 10 samples in 3 hour intervals (starting from 0 hours). Between each photograph, the 10 samples were incubated in 37°C environments.

CALCULATIONS

I. Volume for Angiogenesis Assay Samples

For 100% (or near complete) incorporation of EV to EC, there should be 0.2 nanogram of EV per $1x10^4$ EC. The volumes of EV will be adjusted to fit this ratio of EV to EC.

1. Each dish holds $3x10^5$ of EC (known)
2. EV Volume per $3x10^4$ of EC= 0.2/0.087=2.3mL
3. EV Volume/well= 2.3 × 30= 69mL

II. Cell Count

"EC"

Cell count = (sum of cells counted)/number of boxes x 10^4 = (34+29+50+61+48+49+41+59)/8 x 10^4 = 5×10^5cells/mL

"EC+EV"

Cell count = (17+22+15+17+14+23+16+20)/8 x 10^4 = 1.8×10^5cells/mL

III. In Vitro Volumes

As the number of cells in "EC" and "EC+EV" are different (as shown by the different cell counts), the volumes were adjusted so that "EC" samples have only $1.8x10^5$cells/mL.

Volume = $(1.8 \times 10^5)/(5 \times 10^5)$= 0.36mL = 360µL of "EC" per well.

EVALUATION OF ERRORS

As the volume for EV was adjusted for the best possible EC incoporation, nearly all EC should have incorporated with EV. However, as shown by the photos taken after incorporation, not all of the EC had EV incorporated in them. This could have been caused by slight differences in the volume of EV and EC (which could change the incorporation of cells by the hundreds). Luckily, although not all EC contained an EV, many of the EC did have EV incorporated in them, which is shown in *Incorporation Success*. The incorporation of EV could have been repeated to increase the number of successful incorporations; however, it would have been extremely expensive and time consuming to obtain more BCC samples from the hospital. Therefore, since there were still many EV which incorporated with EC, the investigation was continued.

Also, it must be considered that this investigation is conducted *in vitro.* While tube formation assays are widely regarded as reliable replicates of the body's microenvironment [23], the results obtained would be limited to an experimental scope of a petri dish which might not accurately represent how EV and EC interact in the body. Therefore, the results obtained are only predictions of the *likely* relationship between EC and EV in the body.

RESULTS

I. Incorporation Success

Before analyzing any results from the angiogenesis assay, the incorporation of EV with EC must show successful results. To determine this, a comparison of photos between EC and EC+EV must be compared to check whether or not the EV were incorporated in the EC. In methodology: Incorporation of EV to EC, the EV were stained with PKH26 and this stain was used to track EV. PKH26 is a fluorescent dye which stains the membranes by intercalating (inserting between DNA) with the EV's lipid bilayer [24]. The excitation maximum of PKH26 is 551 nm and emission maximum is 567nm. Under a red fluorescent light, the EV stained with PKH26 shine red and act as markers to indicate whether or not EV are found in the EC. PKH27 was used as it does not deteriorate even after several hours of EV incorporation. EC+EV were taken under both red fluorescent light (showing PKH26 stained EV) and white light (showing only EC), and these photos were combined to display where the PKH26 stained EV were located in the normal white light photo. The two photos were merged to observe whether or not the red EVs would be found in ECs in the white light photo.

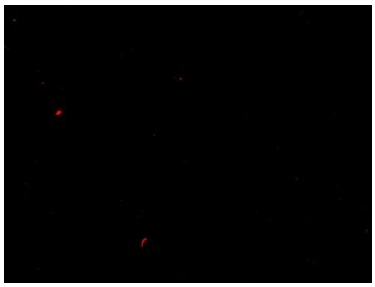

FIGURE 4: EC+EV under Red Fluorescent Light

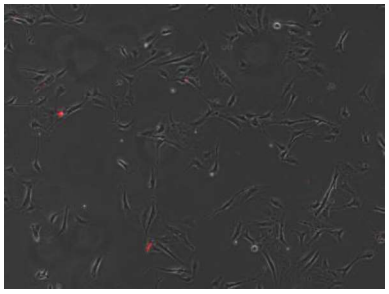

FIGURE 5: EC+EV Combined Photo with Red Fluorescent Light + White Light Photo

The red spots in Figure 4 justify the existence of PKH26 stained EV. After combined with the white light photo, Figure 5 exemplifies how the PKH26 stained EV are

physically spotted in the EC — thus showing that the incorporation of EV with EC was a success.

II. Tube Formation Photos

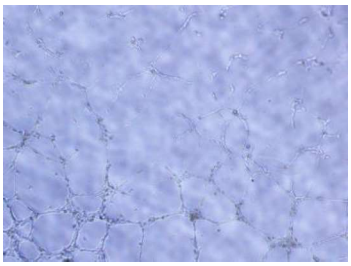

FIGURE 6: EC Tube Formation After 6 Hours

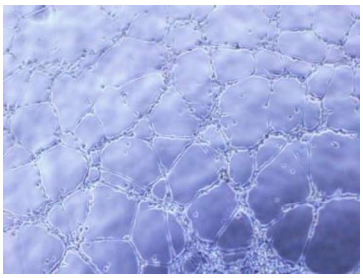

FIGURE 7: EC+EV Tube Formation After 6 Hours

Comparison between photos taken for both EC and EC+EV after 6 hours visibly show how tubes formed after EV incorporation created thicker and longer tubes with extensive networks. As these tube formations *in vitro* exemplify blood vessel formation in the body, the EV must have had an exchange of genetic material with EC to influence ECs to create thicker and longer blood vessels in our body. These blood vessels would therefore heighten the likelihood of metastasis as there are simply more pathways for the BCC to circulate throughout the body — supporting the hypothesis.

III. Tube Formation Length

Besides simple observation of tube formation, the average length of the tubes formed were calculated using ImageJ software [25].

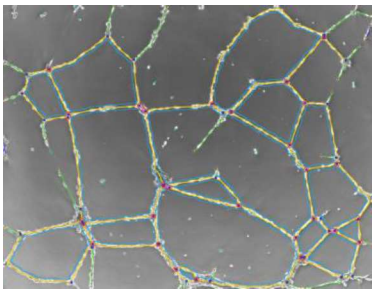

FIGURE 8: Example ImageJ Analysis of Tube Formation [25]

Using the photos taken during the 6 hour time frame, the computer software ImageJ performs an analysis on the skeleton of the tube formations, measuring the exact length of the tubes formed to the micrometer (shown in Figure 8). Using ImageJ and the photos of both "EC" and "EC+EV" after 0, 3, and 6 hours, the tube lengths shown below were calculated.

TABLE 1: Total Tube Lengths from ImageJ Scan

	EC (μm)	EC+EV (μm)
0 Hours	10526	16782
	11127	18790
	14248	14988
	16312	13459
	9569	15485
3 Hours	11969	13273
	9243	16625
	15742	14986
	15474	16789
	15496	15989
6 Hours	11183	16697
	11735	15691
	13176	15691
	11966	15502
	9822	13243

TABLE 2: Mean and Standard Deviations for Each Sample

	Mean (μm)	STDEV (μm)
EC (0 Hours)	12356.4	2822.07
EC+EV (0 Hours)	15900.8	2005.77
EC (3 Hours)	13584.8	2886.92
EC+EV (3 Hours)	15532.4	1447.82
EC (6 Hours)	13176.0	1221.51
EC+EV (6 Hours)	15364.8	1275.58

Comparisons between the mean for each hour show that the tubes formed after EV concentration was higher: a difference of 3,544.4 μm at 0 hours, 1,947.6 μm at 3 hours, and 2,188.8 μm at 6 hours. Using the standard deviations and means from the ImageJ measurements, the following graphs were made for each time interval.

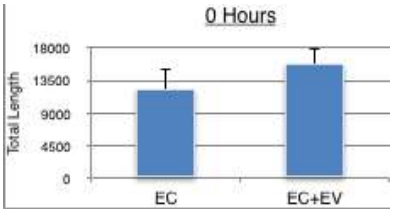

FIGURE 9: EC+EV Tube Total At 0 Hours

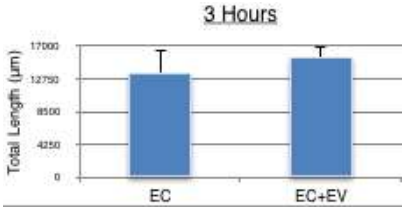

FIGURE 10: EC+EV Tube Total At 3 Hours

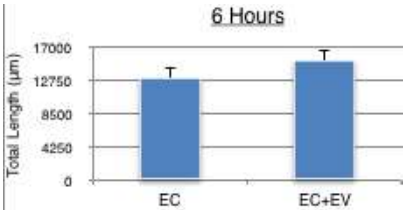

FIGURE 11: EC+EV Tube Total At 6 Hours

The graphs exemplify how the average tube length of the tubes formed were consistently higher for samples with added EV compared to control samples. Unfortunately, the error bars in both 0 hours and 3 hours were extremely large, indicating that there were no significant differences between the EC and EC+EV samples. However, the graph depicting tube formations after 6 hours show a smaller error bar — this graph will be used as the "model" tube formation result. After given enough time for tube formation to occur, the EC and EC+EV showed an obvious difference in tube length with little error compared to previous hours. Based on previous research on EV and EC (found in *Literature Review)* and the relative accuracy of past *in vitro* tube formations in mimicking angiogenic ability, it can be deduced that the presence of EV led to an increase in tube length. The recordings after 0 and 3 hours exemplify how total tube length at initial hours was not particularly influenced by EV incorporation when the error bars were taken into account. However, at 6 hours, the EV incorporation led to an increase in total tube length with relatively low error bars — indicating that EV incorporation alters tube formation behavior in *in vitro* environments and could possibly also alter angiogenic ability in the body. More tests and trials would need to be made to affirm the results of this investigation. The importance of EV in the role of angiogenesis, as shown by this investigation, would be vital in understanding how to control and prevent metastasis in cancerous cells.

CONCLUSION

In this investigation, the effects of BCC derived EV on angiogenesis was investigated through changes in EC activity, as EC play a vital role in the development of angiogenesis and in turn, influence metastasis. Comparisons between control samples of EC and variable samples of EC incorporated with EV exemplified that the BCC derived EV enhanced angiogenesis by creating lengthier and more complex tube formations in *in vitro* settings after 6 hours. These tubes mimic new blood vessel formation in the body, and an increase in tube length and formation after EV incorporation show that BCC derived EV are responsible in promoting angiogenesis and possibly metastasis of BCC. The results in this investigation show potential in further research on BCC-EV and endothelial cells — as shown in this investigation, the correlation between the two could prove to be essential in the limitation of metastasis in the future.

REFERENCES

[1] Worldwide cancer data. (2019, July 17). Retrieved July 27, 2020, from https://www.wcrf.org/dietandcancer/cancer-trends/worldwide-cancer-data

[2]Breast Cancer Facts. (2019, September 27). Retrieved July 29, 2020, from https://www.nationalbreastcancer.org/breast-cancer-facts

[3] What is Metastasis? (2019, December 05). Retrieved July 31, 2020, from https://www.cancer.net/navigating-cancer-care/cancer-basics/what-metastasis

[4] Alberts, B. (1970, January 01). Blood Vessels and Endothelial Cells. Retrieved July 23, 2020, from https://www.ncbi.nlm.nih.gov/books/NBK26848/

[5] S., B. (n.d.). Endothelial Cells: Function & Explanation. Retrieved August 9, 2020, from https://study.com/academy/lesson/endothelial-cells-function-lesson-quiz.html

[6] What is Metastasis? (2019, December 05). Retrieved July 27, 2020, from https://www.cancer.net/navigating-cancer-care/cancer-basics/what-metastasis

[7] Breast Cancer - Statistics. (2020, August 13). Retrieved July 29, 2020, from https://www.cancer.net/cancer-types/breast-cancer/statistics

[8]Qian, C., Mei, Y., & Zhang, J. (2017, April 3). Cancer metastasis: Issues and challenges. Retrieved August 2, 2020, from https://www.ncbi.nlm.nih.gov/pmc/articles/PMC5379757/

[9] Adair, T. (1970, January 01). Overview of Angiogenesis. Retrieved August 2, 2020, from https://www.ncbi.nlm.nih.gov/books/NBK53238/

[10] BR;, Z. (1998). Angiogenesis and tumor metastasis. Retrieved July 27, 2020, from https://pubmed.ncbi.nlm.nih.gov/9509272/

[11] Research Hallmarks: Circa Today -Angiogenesis. (n.d.). Retrieved August 3, 2020, from https://cisncancer.org/research/what_we_know/advances/angiogenesis.html

[12] Naito, H., Iba, T., & Takakura, N. (2020, January 30). Mechanisms of new blood-vessel formation and proliferative heterogeneity of endothelial cells. Retrieved July 27, 2020, from https://academic.oup.com/intimm/article/32/5/295/5717666

[13]Endothelial Cell Tube Formation Assay for the In Vitro Study of Angiogenesis. (2014, April 1). Retrieved August 3, 2020, from https://www.ncbi.nlm.nih.gov/pmc/

[14] J;, S. (2020). Endothelial Cells in the Tumor Microenvironment. Retrieved August 2, 2020, from https://pubmed.ncbi.nlm.nih.gov/32040856/

[15] Harding, C., BT. Pan, K., H. Valadi, K., K. Al-Nedawi, B., J. Ratajczak, K., Raposo, G., . . . Y. Wang, V. (1983, January 01). Imaging extracellular vesicles: Current and emerging methods. Retrieved August 9, 2020, from https://jbiomedsci.biomedcentral.com/articles/10.1186/s12929-018-0494-5

[16] Niel, G., D'Angelo, G., & Raposo, G. (2018, January 17). Shedding light on the cell biology of extracellular vesicles. Retrieved August 4, 2020, from https://www.nature.com/articles/nrm.2017.125

[17] Zaborowski, M., Balaj, L., Breakefield, X., & Lai, C. (2015, June 26). Extracellular Vesicles: Composition, Biological Relevance, and Methods of Study. Retrieved August 26, 2020, from https://academic.oup.com/bioscience/article/65/8/783/240409

[18] Carnino, J. M., Lee, H., & Jin, Y. (2019, October 30). Isolation and characterization of extracellular vesicles from Broncho-alveolar lavage fluid: a review and comparison of different methods. Respiratory Research. https://respiratory-research.biomedcentral.com/articles/10.1186/s12931-019-1210-z

[19] Carnino, J. M., Lee, H., & Jin, Y. (2019, October 30). Isolation and characterization of extracellular vesicles from Broncho-alveolar lavage fluid: a review and comparison of different methods. Respiratory Research. https://respiratory-research.biomedcentral.com/articles/10.1186/s12931-019-1210-z

[20] T.F.S. (2011, October 16). Endothelial Cell Tube Formation Assay. Thermo Fish. https://www.thermofisher.com/nl/en/home/references/protocols/cell-and-tissue-analysis/cell-profilteration-assay-protocols/angiogenesis-protocols/endothelial-cell-tube-formation-assay.html

[21] Endothelial Cells. (n.d.). Retrieved July 30, 2020, from https://www.promocell.com/app/uploads/product-information/manual/C-12200.pdf

[22] Haemocytometers procedure. (n.d.). Retrieved July 29, 2020, from https://home.cc.umanitoba.ca/~adam/lab/Haemocytometer.htm

[23] [Islam, S. (2010, May 13). Assay Procedure. Corning. https://www.corning.com/catalog/cls/documents/protocols/protocol_DL_030_Endothelial_Cell_Tube_Formation_Assay.pdf]

[24] Dominkuš, P. (2018, June 1). PKH26 labeling of extracellular vesicles: Characterization and cellular internalization of contaminating PKH26 nanoparticles. ScienceDirect. https://www.sciencedirect.com/science/article/pii/S0005273618300932

[25] Carpentier, G. (2012, October 20). Angiogenesis Analyzer for ImageJ. Retrieved July 31, 2020, from http://image.bio.methods.free.fr/ImageJ/?Angiogenesis-Analyzer-for-ImageJ

On Finding The Focal Length Of Induced Thermal Lens Of Soy Sauce Sample Using Matrix System And Observing The Effect Of Variation Of Parameters

Paras Kumar
M.G.N Public School, Punjab, India
Email: kumarparas218@gmail.com

Abstract- The paper presents the problem in which a Gaussian beam is passed through an absorbing medium which results in heating of the medium which leads to the formation of the thermal lens due to radiative and non-radiative relaxation processes. In this paper, we also discuss the method to find the focal length of the induced thermal lens and by varying parameters such as concentration, focal length, power of the beam. We were able to infer the trend. At last, we were able to spot the effect of gravity in our experimental result during the experiment of the knife-edge method.

INTRODUCTION

Thermal Lens Spectroscopy (TLS) has many industrial and scientific applications; it was first observed by Gordon et. Al[6] and Leite et. Al[5]. TLS is used in measuring concentrations, finding traces of elements in gases and absolute absorption coefficients. Over the decades, scientists have improved the accuracy of finding quantum yields, diffusivity and thermal conductivity of solid media. In our experiment, a laser beam with a Gaussian profile is passed through a thin layer of soy sauce (about $200\mu m$), forming a thermal lens. We chose soy sauce for our experiment as it is a readily-available and affordable liquid capable of producing a thermal lens. It is a fluid that has intense optical absorption in the visual range of the EM spectrum. And it's constituent's solutes have the same linear absorption coefficients. A Gaussian beam from a modulated CW or pulsed laser is focused onto a liquid or solid medium containing fluorophores. After the absorption of the excited beam, the fluorophores at ground energy state are excited to higher energy states, from which they decay by radiative and non-radiative processes. The latter process relies on the transference of heat to the host, thus leading to a time-dependent transverse spatial profile of the temperature $\Delta T(r, t)$ in the sample. The temperature gradient $\Delta T(r, t)$ creates a refractive index gradient($^{dn}/_{dt}$) normal to the beam axis. The resulting gradient $^{dn}/_{dt}$ produces a lens-like object, which is known as a thermal lens (TL), explained by the following equation:

$$n\,(T + \Delta T) = n_0 + \frac{dn}{dT}\Delta T$$

Briefly, we can say that when light traverse an absorbing medium, the absorbed electromagnetic energy of the beam is partially converted into heat by a non-radiative relaxation process which leads to the heating of medium. This can be explained by the following two aspects: heat equation and diffraction theory. The heat equation predicts the rise in temperature of the medium and the diffraction theory suggests due to rise in temperature of the medium wave in front of a probe beam entering the soy sauce sample undergoes specific modification.

THEORY OF GAUSSIAN BEAM

The Gaussian beam is a beam of monochromatic electromagnetic radiation whose amplitude envelopes in the transverse plane and is given by a Gaussian function. This also implies Gaussian intensity (irradiance) profile, given by:

$$I(r) = I_0 e^{-r^2/\omega^2}$$

Where I_0 is the intensity at $r = 0$ and ω_0 is the radial distance at which intensity has decreased to 1/e of its peak value. A lot of information can be concluded about a beam from its wavelength and q parameter. Before introducing the q parameter, we will introduce the beam parameters. The curvature is infinite at z=0. And the beam waist at distance z from the propagation axis can be written as:

$$\omega(z)^2 = \omega_0 \left[1 + \left(\frac{\lambda z}{2\pi\omega_0^2}\right)^2\right]$$

Gaussian beams go through modifications when passed through a cavity or a medium, which will be explained later.

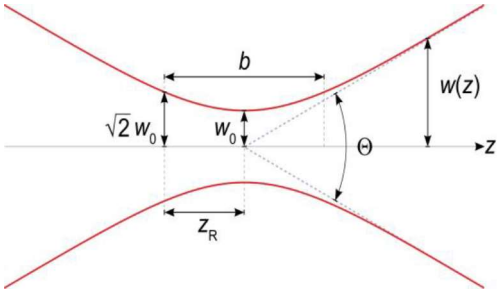

FIGURE 1: The shape of a Gaussian beam

FIGURE 2: Monochromatic Gaussian beam ($\lambda = 532nm$)

The shape of a Gaussian beam of a given wavelength λ is governed solely by the beam waist ω_0(as shown in fig1). The confocal parameter or Rayleigh distance is the distance at which the intensity of the beam is maximum and also at that distance the beam width is 1.414 times the beam waist. We used a gaussian beam with a wavelength of 532nm (as shown in fig2.). We were able to calculate the beam waist of the Gaussian beam by using the knife-edge method, and we were able to plot a Gaussian curve shown in fig3.

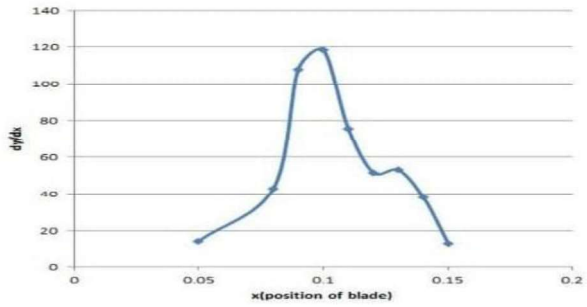

FIGURE 3: Plot of Gaussian beam calculated using knife edge method($\lambda = 532nm$)

EXPERIMENT

When a Gaussian laser beam is passed through a thin sample (about 200$\mu m$to 0.1 mm) of soy sauce; we can observe the thermal lensing effect. We infer a set of concentric rings on the screen.

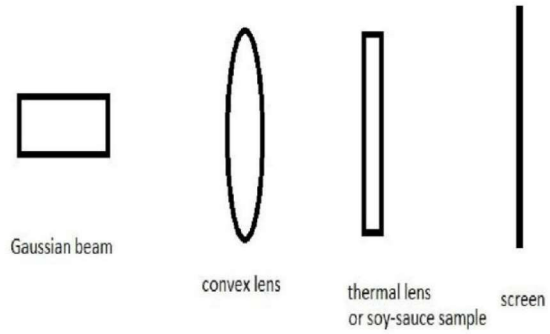

Figure 4: Block diagram of experimental setup

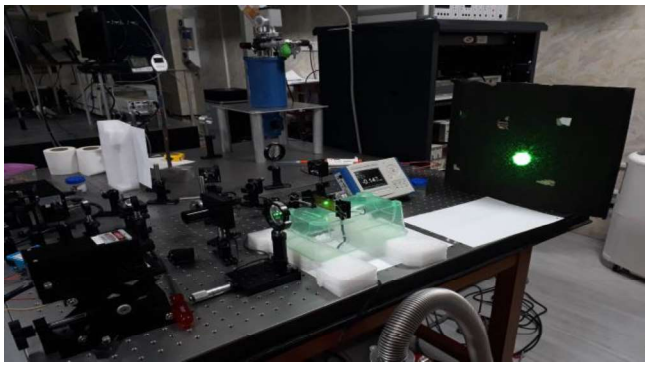

FIGURE 5: Experimental setup.

First of all, we will prepare a sample of soy sauce (100%). Take a few drops of soy sauce on the slide and then gently place the other slide on it and both sides carefully attached using a clip as shown in fig 6. The area with no bubbles was best suited for the experiment. We arranged the equipment (as shown in fig4). Fig5 shows the actual arrangement in our lab. Now the Gaussian beam is passed through the collimator (f = 10cm) to converge the beam and then it is passed through the soy sauce sample .After some time, we could see the thermal lensing effect as concentric rings are formed(as shown in fig7).We can observe that it took some time for these rings to form, which shows in this process Thermal lenses are formed because thermal processes are slower in comparison to nonlinear electric effects. On page1 we have shown why the thermal lens is formed, to surmise it: thermal lens is formed when light passes an absorbing medium such as soy-sauce, it absorbs electromagnetic energy and converts the energy into heat by non-radiative relaxation processes which lead to heating of the medium and further leads to change in the refractive index of the medium. The formation of concentric rings can be explained by diffraction theory and spatial self-phase modulation. We can also explain the formation of the thermal lens by heat exchange theory but the math involved is complicated for e.g. Whinery solution gives us the mathematical expression for the change in heat when a beam is passed through a sample

FIGURE 6: Soy sauce sample.

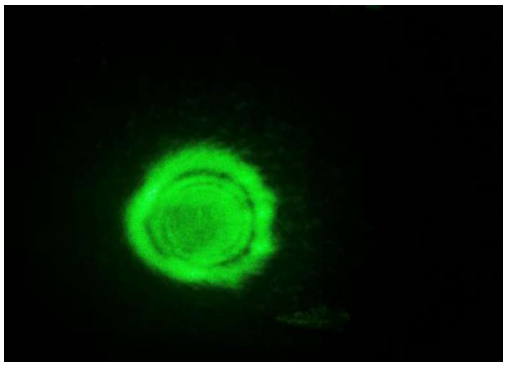

FIGURE 7: Concentric rings formed on screen (N=7).

DIFFRACTION THEORY

According to paper by Gordon [6] in 1965 focal length of induced thermal lens can be written in terms of some physical factors.

$$f = \frac{\pi k \omega_0^2}{2.303 P_e (\frac{dn}{dt}) A}$$

Where A is the area, k is the thermal coefficient, dn/dt is thermo optic coefficient, and P is the power. Now according to him if the Thermo optic coefficient is greater than 0 it will behave as a concave lens, elsewise it behaves as a convex lens. In our experiment, we can see that the soy-sauce sample behaves as a convex lens.

The diffraction theory proposes that change in temperature arises due to the phase delay in the wavefront of the beam. Born and E. Wolf [4] in their book 'Principles of optics' describes it as a perturbation due to an additional phase lag to phase beam of a spherical wave. We can see in fig8 the difference between the wavefront before and after hitting the medium. wavefront emerges from the soy-sauce sample having an additional phase lag.

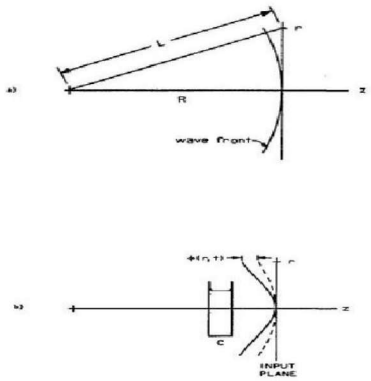

FIGURE 8: a) wave from before entering the soy sauce sample b) wave front with additional phase lag exiting the soy sauce sample for a) and b) the optical path length can be written as:

$$\varphi = nl$$
$$\varphi(r,t) = ln(r,t) - n(0,t)$$

we know,

$$n(r,t) = n_0 - \frac{dn}{dT}\Delta T(r,t)$$

solving this we get,

$$\frac{2\pi}{\lambda}\phi(r,t) = \frac{2\pi}{\lambda}\frac{dn}{dt}l\Delta T(0,t) - \Delta T(r,t)$$

This equation shows us that due to change in phase, there is a change in temperature which leads to change in the refractive index of the medium [2].

CALCULATION OF FOCAL LENGTH

First of all, we need to introduce the q parameter to understand ABCD LAW and how we can calculate the focal length of the induced thermal lens using the matrix method. The q parameter or gaussian complex curvature parameter can be derived from the basic gaussian equations, but we won't derive the equation here. we can express q in a relation as following

$$\frac{1}{q} = \frac{1}{R} - \iota\frac{\lambda}{\pi\omega_0^2}$$

where R is curvature of beam.

When the beam enters the soy sauce sample the q at the entrance(q_1) and at the exit of sample(q_2) are related by the following equation:

$$q_2 = \frac{Aq_1 + B}{Cq_1 + D}$$

OR

$$\frac{1}{q_2} = \frac{C + {}^{D}/_{q_1}}{A + {}^{B}/_{q_1}}$$

where A, B, C, D are the elements of the ABCD matrix which are unique for every optical system and can be determined experimentally.

Matrix for a lens can be written as

$$\begin{pmatrix} A & B \\ C & D \end{pmatrix} = \begin{pmatrix} 1 & 0 \\ -1/f & 1 \end{pmatrix}$$

Matrix for free space can be written as

$$\begin{pmatrix} A & B \\ C & D \end{pmatrix} = \begin{pmatrix} 1 & l \\ 0 & 1 \end{pmatrix}$$

Where l is the distance and f is focal length of the lens.
3.For an optical system the effective matrix can be written by the multiplication of individual matrices.

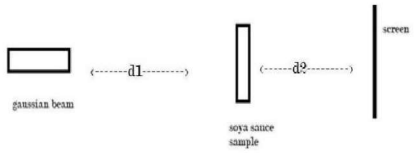

FIGURE 8: Simple block diagram of optical system for e.g., the effective ABCD matrix for optical system described in fig is

$$\begin{pmatrix} A & B \\ C & D \end{pmatrix} = \begin{pmatrix} 1 & \mathrm{d}_2 \\ 0 & 1 \end{pmatrix} \begin{pmatrix} 1 & 0 \\ -1/f & 1 \end{pmatrix} \begin{pmatrix} 1 & \mathrm{d}_1 \\ 0 & 1 \end{pmatrix}$$

We will be using this system to calculate the focal length of the soy sauce sample. A convex lens is removed in this experiment to ease the calculation. As we can see that the distance between beam and screen will be affecting the focal length, but we will discuss this in the next section. Solving the equation, we can find an expression for focal length (the proof of the expression is available in the appendix.)

$$f_{th} = \frac{d_1\omega_2^2 - d_2\omega_1^2}{\omega_2^2 - \omega_1^2}$$

In this experimentω_1 is the waist of the beam at the left of the thermal lens, which we can calculate using the knife-edge method. on plugging the values $d_1 = 10.5cm$, $d_2 = 20.45cm\omega_1 = 0.23mm$ and $\omega_2 = 0.31mm$, we get the focal length of the induced thermal lens equal to -1.68cm, which means it behaves like a diverging lens.

VARIATION OF PARAMETERS

I. Number of rings

During the experiment, we noticed that if we vary the power of the beam, we observe a linear change in the no.of rings also, we were able to plot the data on a line graph, a straight line graph was obtained.

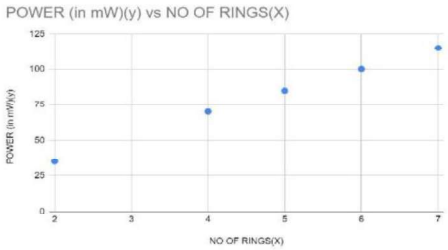

FIGURE 9: We can see no. of rings increases linearly with power ($^{P}/_{N} \approx 17$)

II. Effect of concentration

According to beer lambert law, intensity of beam after passing through the sample can be written as:

$$\frac{I_0}{I} = 10^{bcl}$$

where b is the coefficient of absorption, c is the concentration and l is the thickness of the sample. we know that

,

$$P = \frac{I\pi\omega^2}{2}$$

using this in equation 3 we get

$$f = \frac{2k}{IA({}^{dn}/_{dt})}$$

which means it is inversely related to I, using beer lambert law we can generalise the equation and rest of the terms A, dn/dt, b, l and k are physical constants and have their usual meanings. so, we can say that $f = m10^{ac}$ where m and a are

constant. from here we can expect the relation between concentration and focal length. Similarly, we were able to plot the graph between P and concentration, by modifying the equation (9) and were verified with experimental results as shown below.

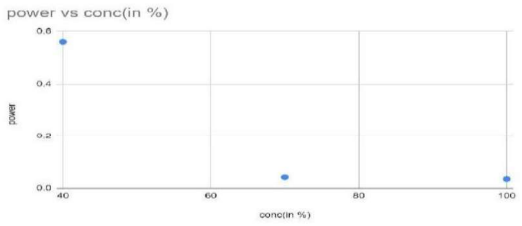

FIGURE 11

III. Varying the focal length of lens

In this experiment, we used a diverging lens and noticed the change in focal length of soy sauce sample with a change in focal length of the diverging lens. The focal length was calculated using the matrix method. we obtain the following plot.

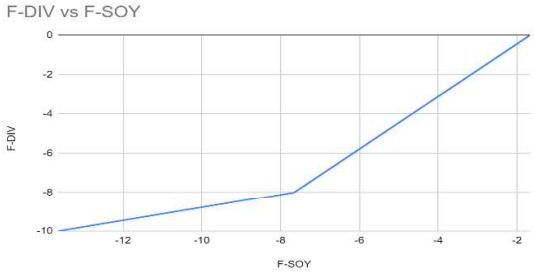

IV. Effect of gravity

This is the most important aspect. As mentioned earlier thermal optical phenomena are slow as compared to other non-linear effects. This means we need to expose the sample for a specific duration of time. Now due to gravity, the sample will naturally flow down changing the concentration of the exposed area, which leads to change in calculations. We were not able to formulate maths behind the effect of gravity, but it is visible from our experiment (as seen in the figure below) that the bump in the Gaussian curve arises due to change in concentration. This curve was drawn during the calculation of ω_2 for calculating the focal length using matrix-method.

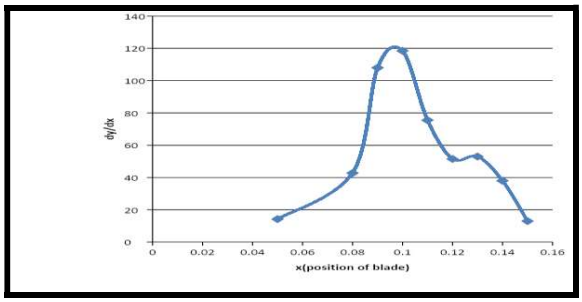

V. The distance x

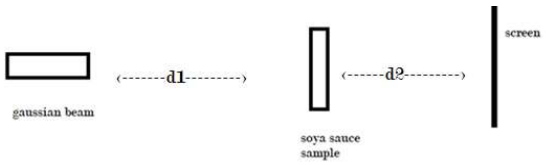

We know $d_1 + d_2 = d$ and let us assume $d_1 = x$
Putting $d_2 = d - x$ in eq (11)
We get,

$$f = x * \frac{\omega_2^2 + \omega_1^2}{\omega_2^2 - \omega_1^2} - d * \frac{\omega_1^2}{\omega_2^2 - \omega_1^2}$$

We conducted experiment in which we varied the value of x and plotted the following graph

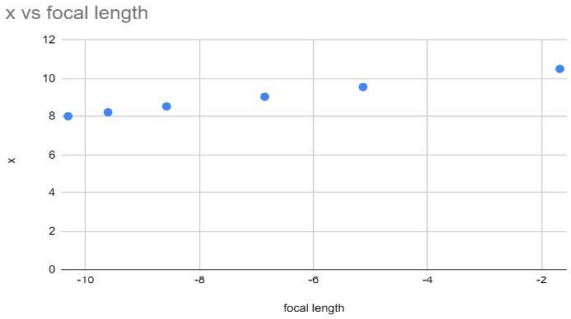

CONCLUSION

In this paper, we proposed the idea of the non-linear effect, which was proposed by Gordon in 1965, using the diffraction theory, we were able to understand the reason behind the change in the refractive index. We also used the matrix method to calculate the focal length of the thermal lens then lastly we varied various parameters to observe their effect on the focal length of the soy-sauce sample for e,g.. gravity, concentration etc.

ACKNOWLEDGMENT

The authors are thankful to Indian institute of science and research Kolkata, Dr BipulPal, National institute of technology Jalandhar and Aryano Ray.

APPENDIX

In eq (8) if,

$$R \rightarrow -\infty$$

(because at focus the wave front is flat)

$$\frac{1}{q} = -\iota\frac{\lambda}{\pi\omega_0^2}$$

modifying eq (9) we get,

$$Cq_1q_2 + Dq_2 = Aq_1 + B$$

q_1q_2 will be real, so comparing real and imaginary terms we can say

$$\omega_1^2 = \frac{A}{D}\omega_2^2$$

now modifying eq (10) we get

$$\begin{pmatrix} A & B \\ C & D \end{pmatrix} = \begin{pmatrix} 1 - {}^{d_1}/_f & d_1 + d_2 - {}^{d_1 d_2}/_f \\ -1/f & 1 - {}^{d_2}/_f \end{pmatrix}$$

Comparing the two we can say

$$\omega_1^2 = \frac{1 - {}^{d_1}/_f}{1 - {}^{d_2}/_f}\omega_2^2$$

and modifying this we get our final answer which we have used to calculate the focal length

$$f_{th} = \frac{d_1\omega_2^2 - d_2\omega_1^2}{\omega_2^2 - \omega_1^2}$$

BIBLIOGRAPHY

1.Turchiello, Rozane de F., Luiz AA Pereira, and Sergio L. G´omez. Low-cost nonlinear optics experiment for undergraduate instructional laboratory and lecture demonstration." American Journal of Physics 85.7 (2017): 522528

2.Sheldon, S. J., L. V. Knight, and J. M. Thorne." Laserinduced thermal lens effect: a new theoretical model." Applied optics21.9 (1982): 1663-1669.

3.Snook, Richard D., and Roger D. Lowe. " Thermal lens spectrometry. A review." Analyst 120.8 (1995): 20512068.

4.E. Hecht, Optics, 4th ed. (Addison Wesley, San Francisco, 2002)

5.THE THERMAL LENS EFFECT AS A POWER-LIMITING DEVICE R. C. C. Leite 1967

6.LongTransient Effects in Lasers with Inserted Liquid Samples Gordon 1965

7. C. Hu and J. R. Whinnery, Appl. Opt. 12,72 (1973)

Determining Personalized Head Related Transfer Functions using Auralization

Shubham Kumar
Dougherty Valley High School; San Ramon, United States
Email: dh.skumar@students.srvusd.net

Abstract - This project aims to explore the basis of an enhanced way to deliver spatial audio in an observer's horizon using acoustic modeling in place of low-pass filtering, interaural time differences, and simple attenuation functions. The approach described in this paper determines two interpolating functions, used as head related transfer functions ("HRTFs") which provide the illusion of spatial audio. The HRTF is obtained by solving the wave and Helmholtz partial differential equations. The parameters for the aforementioned equations can be adjusted to account for any source and observer orientation in any anechoic space. In addition, the shape of the observer's head can be modeled to create a personalized HRTF, tailored to the specific observer instead of a standard one. The model was able to successfully attenuate different frequency intervals and phase shift the audio signal for each channel to provide sufficient binaural cues to localize sound. Results from this implementation, although obtained through computationally intensive processes, could potentially be extended to virtual reality-based systems which would, in theory, provide for a more realistic audio experience, at a much lower cost.

Key Words – Acoustics, Psychoacoustics, Spatial Audio, Sound Localization, HRTFs.

INTRODUCTION

As virtual reality systems have matured past their infancy stages and serve as a viable medium to deliver immersive experiences, there has been an increase in research and development of such systems. Although much of the recent progress has been focused on enhancing the visual aspect, there is indeed an emphasis on refining the audio experience by using spatial audio and high-fidelity acoustics to provide for more realistic user experience [1, 2]. HRTFs are used in these systems to modify audio and recreate the acoustic filtering of sound as it propagates. When paired with headphones or any binaural audio delivery system, these functions can be used to simulate spatial audio by processing the audio that is delivered to each channel.

Since HRTFs are dependent on the geometry of a person's head, torso, and pinnae, they vary significantly among individuals. Because of the impracticality of determining customized HRTFs with existing experimental approaches, most virtual reality systems use generic or standard HRTFs. Since the aforementioned variations are left unaddressed with generic HRTFs, the user can experience unconvincing spatial audio and localization errors [3, 4]. This motivates the use of more accessible methods to determine HRTFs. The method described in this paper utilizes a numerical, simulation-based approach to deliver spatial audio in an observer's horizon.

BACKGROUND

Neuroscientists have been able to pinpoint the binaural and monaural cues that enable the human brain to accurately localize sound (determining a sound source's azimuth and elevation angles relative to the observer).

I. Horizon Localization

Specifically, they found that the brain determines interaural time differences ("ITDs") and interaural intensity differences ("IIDs") [5], as illustrated in Figure 1, to establish the azimuth of a sound source relative to the observer. ITDs describe the variation in sound arrival time for each ear and exist as a result of the difference in distance between the observer and source. IIDs describe the variation in amplitude and exist as a result of a sound wave attenuating after reaching a boundary such as an observer's head or traversing long distances.

II. Elevation Localization

The elevation of sound relative to the observer is determined by more complex monaural cues, specifically, spectral notches [6], which are closely related to head related impulse responses ("HRIRs"). These responses are dependent on several attributes including head diffraction, reflections from various body parts, and other refractions/diffractions due to the pinna. This phenomenon will not be covered in the scope of this paper, as the focus is to deliver spatial audio in the observer's two-dimensional horizon. However, a three-dimensional rendering of the

user's head could in theory be used in the simulation domain, effectively allowing for the HRTF to accept elevation data as a parameter. This would require including the third spatial dimension, namely elevation, into the models, which may influence the overall performance and introduce new sources of complexity to the process.

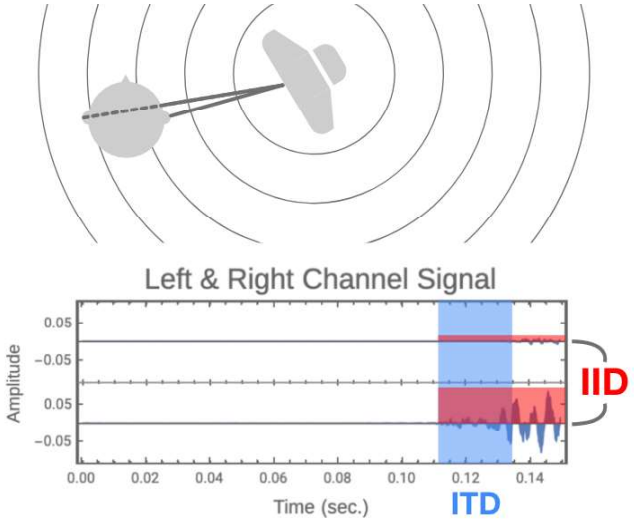

FIGURE 1: Certain arrangements of a sound source and observer yield subtle differences in the sound wave arrival time and amplitude for each ear. The signal for the left ear is described by the audio plot above and the signal for the right ear is described by the audio plot below. The areas shaded in blue and red on the graph highlight the ITD and IID respectively. Notice the delayed start and lower amplitude for the left ear signal relative to the right ear signal.

However, it's worth noting that these cues may not be completely unique for every source and observer arrangement, yielding the same signal produced for both ears despite the orientation being different. This results in a phenomenon known as the cone of confusion [7]. One can easily circumvent this problem by simply moving their head and take note of changes that may occur in the signal for each ear.

RELATED WORK

Since the brain relies on relatively simple parameters to localize sound, there has been significant progress over recent years to create standard HRTFs for spatial audio [8]. These HRTFs alter an audio signal to provide the illusion of spatial sound by processing two parameters, namely, the frequency of sound and the spatial location of the source relative to the observer.

However, many of the studies required investment in expensive resources including state-of-the-art anechoic chambers, high-quality speakers, and microphones to collect readings experimentally. Typically, these speakers are arranged spherically around a subject who has a pair of microphones inserted into their ear canals. These microphones collect readings of various tones which are then analyzed to design an HRTF. The measurement process takes up to one hour and the computational processes can take days. Additionally, this approach uses standard dummy heads to generalize the geometry of a human head, which yields a "one size fits all" HRTF. Hence, it fails to address the details that typically vary depending on the shape of an individual's head and ears. Although one investigation has shown that one can adapt to a new hearing profile, it doesn't make for the most realistic experience [9] since it takes time to adjust and often fails to capture the variances in perception from person to person. As a result, localization errors are produced and the generated audio is no longer capable of providing sufficient cues to enable the listener to correctly localize sound.

The process of creating personalized HRTFs for every single individual experimentally is infeasible. It would require the use of expensive acoustic equipment and computational resources which are generally inaccessible to the average consumer. Hence, the proposed method utilizes acoustic modeling to simulate the traditional measurement-based process. Ideally, the only equipment required would be a modern smartphone camera to recreate a three-dimensional rendering of a user's head. LIDAR mapping is another option that could be used, especially since there is an increasing number of handheld devices that integrate it into their optical systems. By simulating the experiment with a deterministic system, the costs and infrastructure associated with creating a custom HRTF would effectively be bypassed.

ACOUSTIC MODELING

Pressure changes in a medium, caused by wave propagation, are typically described using the wave equation in the time domain and the Helmholtz equation in the frequency domain. These differential equations enable us to probe pressure data at any spatial location and at any point in time or at any frequency in order to obtain attenuation coefficients. Typically HRTFs accept a spatial location and frequency as parameters, but examining wave propagation in the time domain helps visualize some of the behaviors that aren't immediately clear when visualized in the frequency domain. Moreover, the data visualizations in the time domain helped fine-tune some of the parameters that helped eradicate inconsistencies observed in the simulations and results.

I. Approach Overview

By initializing a sound source to emit the original audio signal or a relevant frequency and the head of an observer in the anechoic region as depicted in Figure 2, the pressure at the location of each ear can be probed to define the attenuation coefficients. Additionally, the phase shift can also be determined through a similar process, either through the model or a simple delay, based on the difference in distance from both ears. However, the latter is less computationally intensive.

II. *Defining Equations*

Variable symbols, definitions, and units are used as described in Table 1.

TABLE 1: Nomenclature as used in the following equations and expressions.

Symbol	Definition	Units
X	Position vector	$[m]$
t	Time	$[s]$
ρ	Density of a medium	$[kg/m^3]$
c	Speed of sound in a medium	$[m/s]$
p	Sound pressure	$[Pa]$
Ω	Simulation domain	$[m]$
ω	Sound wave angular frequency	$[rad/s]$
$Z_{\square}$	Specific Impedance	$[Pa * s/m]$
Z_b	Boundary Impedance	$[Pa * s/m]$
F	Dipole Source	$[1/s^2]$
Q	Monopole Source	$[1/s^2]$

The partial differential equations ("PDEs") used to model sound propagation and pressure distribution inside the space are the wave equation and the time-independent variant of the wave equation, the Helmholtz equation [10, 11]. The equations are defined as follows:

Neumann boundary conditions were used to dictate how sound waves interacted with walls and the observer's head. The head used an impedance boundary condition and the walls used an absorption boundary condition; each defined as follows respectively:

$$\nabla \cdot \left(-\frac{1}{\rho}(\nabla p(X) + F)\right) - \frac{\omega^2}{\rho c^2} p(X) = Q$$

$$\frac{1}{\rho c^2}\frac{\partial^2 p(t, X)}{\partial t^2} + \nabla \cdot \left(-\frac{1}{\rho}(\nabla p(t, X) + F)\right) = Q$$

$$\vec{n} \cdot \left(\frac{1}{\rho}\nabla p(X)\right) = -\frac{i\omega}{\rho c} p(X) - \frac{R(r)}{\rho} p(X)$$

$$\vec{n} \cdot \left(\frac{1}{\rho}\nabla p(X)\right) = -i\omega \frac{p(X)}{Z_b}$$

III. *Solving the PDEs*

The PDEs were solved using discretization using the finite element method for easy implementation on digital computers. The results returned were in the form of interpolating functions. The Helmholtz PDE was also parametric, with the parameter being frequency.

IV. *Visualizing and Interpreting Results*

By plotting the interpolating functions, many of the expected behaviors become apparent, as shown in Figure 2 (time domain) and Figure 3 (frequency domain). Sound propagation in the time domain occurs as anticipated and effects such as head shadowing are visible in the pressure distribution in the frequency domain. By solving the PDEs with discretization, the data is no longer continuous and hence yields certain anomalies in the data; however, these anomalies aren't too noticeable when it is applied to the audio.

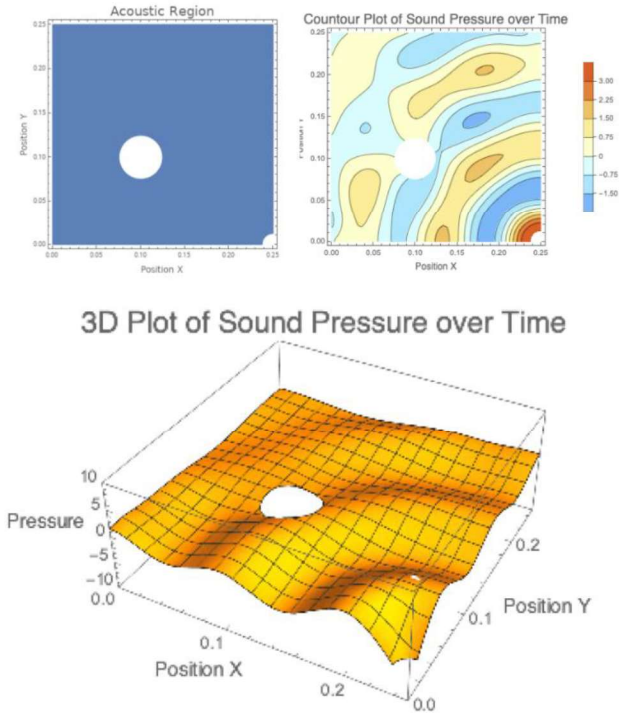

FIGURE 2: Graphs are identified one through three starting at the top left clockwise. Graph one shows the anechoic region with the large white circle representing the observer's head and the small white quarter circle at the bottom right representing the sound source, defined by a Neumann radiation boundary. A circle was used to model the head and ears instead of a more representative shape because of the lack of depth-sensing instruments. However, the models could indeed be adjusted to accept a more accurate geometric representation. Graph two and three display the pressure distribution at a single point in time as a contour and three-dimensional plot respectively; generated using the wave equation in the time domain.

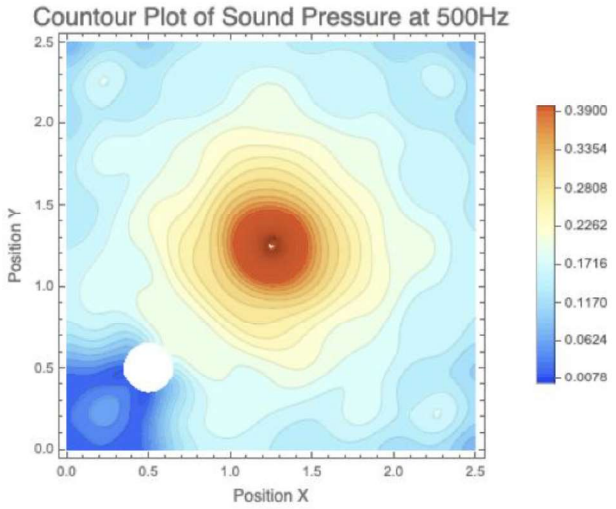

FIGURE 3: This contour plot depicts the pressure distribution in the anechoic region with a monopole sound source emitting a frequency of 500Hz and the head of an observer; generated by solving the Helmholtz equation in the frequency domain. Head shadowing is evident from the low pressure behind the head and the contour matches the predicted distribution.

AUDIO PROCESSING

Having determined an HRTF that accepts a frequency and a spatial location as parameters, the next step would be applying the functions to an audio input. The most effective way to do so is by using a Fast Fourier Transform and an Inverse Fast Fourier Transform pair along with a window function to fill in any discontinuities that appear while processing.

I. Fourier Transform

Decomposing the original audio into a sum of sinusoids using a Discrete Fourier Transform gives access to frequency intervals which can be attenuated using the parametric function obtained by solving the Helmholtz equation. Additionally, applying the Fourier Transform allows for informative visualizations using the spectrogram. The spectrogram helps visualize the changes in the amplitude for each frequency interval and the quality of the generated audio.

II. Attenuating Frequency Intervals

The spatial location of each ear is passed into the parametric function in addition to a frequency parameter. To expedite processing time, frequencies were inputted at intervals of 500Hz yielding a total of ten interpolating functions. While this didn't produce the most accurate results, it was the most computationally reasonable process. Obtaining an interpolating function from the parametric was a rather time-consuming operation.

Each interpolating function returns an attenuation coefficient for its specific frequency interval and is convolved with corresponding frequencies in the original audio data. Once each frequency interval has been attenuated successfully, the generated audio is recreated using an Inverse Fast Fourier Transform.

III. Hann Smoothing Window

Through this process, several artifacts are introduced into the generated audio and there is substantial data loss. To alleviate this problem, a Hanning (Hann) window was used to smooth discontinuities in the audio, preserve frequency resolution and reduce spectral leakage. Upon close examination of the spectrogram plots of the audio before and after applying the function, it is revealed that each frequency interval has been attenuated as expected, shown in Figure 4.

Other window functions including Blackman, Gaussian, and Poisson were used to experiment with different audio files. However, the Hann window was able to generalize to all tested audio inputs the best and outperformed the others in terms of quality.

RESULTS

As seen in Figure 4, attenuation appeared to have been performed as expected. When compared to spectrograms of experimentally determined HRTFs, such as MIT KEMAR, Figure 5, the results were similar, but there are a few notable shortcomings. The most prominent was the low-quality audio output after processing.

One reason could be the significant data loss even after applying a Hann window. While some discontinuities were eradicated, the overall audio still experienced a noticeable loss in quality. Additionally, the introduction of artifacts in certain frequency intervals still persisted. The investigation presented in this paper was conducted in its entirety using the Wolfram Language in Mathematica [12], which is known for being a high-level language and may have been the cause of quality loss. The aforementioned issues would likely be resolved if the entire process was translated to a lower level language with proprietary algorithm implementations. Not only would this make the entire process run at a reduced time complexity, but it would also enable more flexible experimentation since there would be no restriction to exclusively use the built-in functions offered by the Wolfram Function Repository.

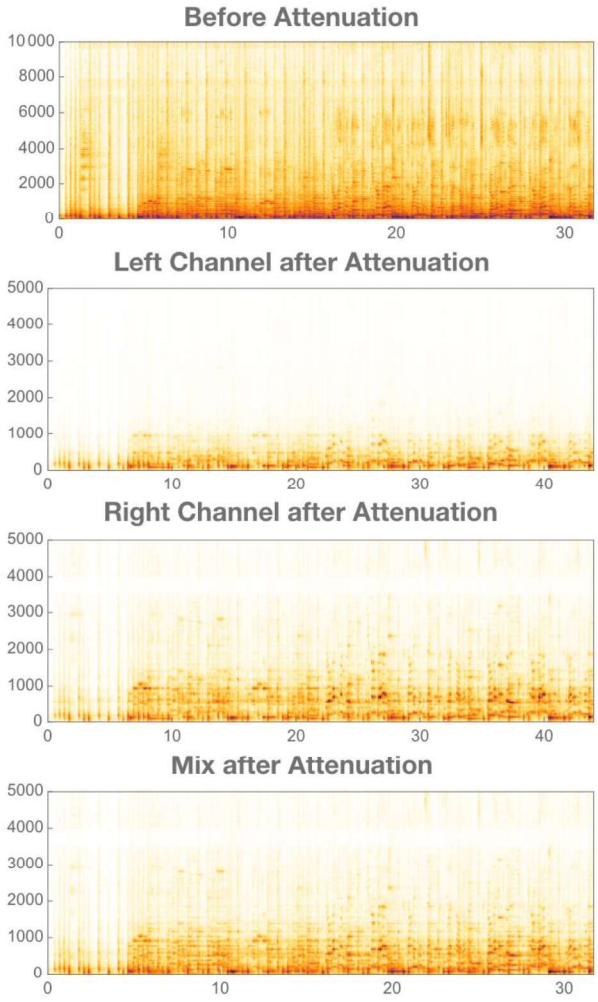

FIGURE 4: Spectrograms are identified one through four starting at the top. Spectrogram one depicts the original audio with data for nearly all audible frequencies. Spectrograms two and three show frequency data for both the left and right channels. Since the top end of the spectrogram became lighter, it is suggested that the higher frequencies are attenuated at a higher magnitude in comparison to the lower frequencies, as predicted. Moreover, the left channel experienced a more significant loss in higher frequencies in comparison to the right channel due to the orientation of the sound source and observer. The sound had to propagate through the observer's head to reach the left ear, hence preserving only the lower frequency sound. Spectrogram four z the final mix after combining both channels. Notice the change in scale along the frequency axis for the first spectrogram and the rest; The generated audio has no data for frequencies above 5000Hz. This is most likely attributed to a loss in quality after processing since experimentally measured HRTFs possessed data for those frequencies.

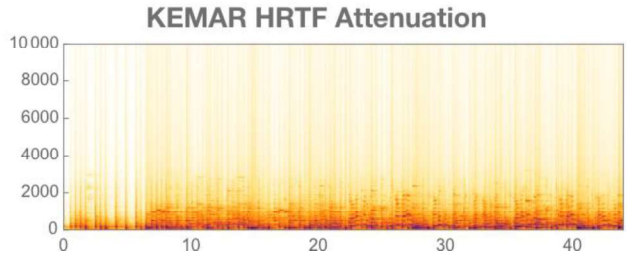

FIGURE 5: Spectrogram result after applying the KEMAR HRTF to the same audio input. Frequency data was possessed, although at lower amplitudes for up to 10000Hz, resulting in a fuller sounding result. Applying an audio normalization to the audio generated in this paper yields a similar amplitude distribution, however there is a noticeable loss in frequency.

Frequency interval ranges could have also been decreased to provide for a more immersive experience but would have come at the expense of processing time. This tweak would have required solving for more than the ten interpolating functions from the parametric function obtained from the Helmholtz equation. Hence, it wasn't feasible with the Wolfram Language. However, as mentioned earlier, lower language implementation may alleviate this problem. Note that all code from this project is stored in Github [13] and the preliminary work is documented in the Wolfram Community [14].

FUTURE WORK

This project, although far from perfect, serves as a strong underlying foundation for future improvement. The proposed method produced reassuring results and provided a clear path for future work. As suggested in the results, one of the next steps would include transcribing the Wolfram Language code into a slightly lower level language like Python that would still offer built-in methods and frameworks which would streamline the development process, while still allowing for flexibility in experimentation and customizability.

Additionally, introducing the third spatial dimension into the model and comparing the monaural spectral cues it produces with experimentally measured cues could be interesting. Another possible extension would be to create three-dimensional renderings of an actual head using LIDAR or another form of depth-sensing to truly produce a custom HRTF. Most importantly, however, there is a need for a concrete metric to quantify the performance and quality of results. As of now, the comparison consisted of looking at the phase shift for each channel and the amplitude differences. If the project is implemented to simulate a three-dimensional space, the current form of analyzing results won't be as effective since it would be difficult to closely examine the monaural cues through a spectrogram.

It may also be informative to investigate some of the behaviors of the model in an environment with obstacles and different types of boundaries. This may help gauge the accuracy and performance of the model. Another possible extension could include utilizing an accelerometer on the user's headset to determine their position relative to other objects in the simulated room and make changes to the audio in real-time. These ideas are indeed far-fetched, but may be possible to implement if the quality of the audio is improved and the third spatial dimension is incorporated into the existing model.

ACKNOWLEDGEMENTS

I would like to express my gratitude for Wolfram Research and their undeniably helpful staff who've managed to provide effective mentorship throughout the entire development of this project, especially amidst these uncertain times. The Wolfram summer program enabled me to put forward my best effort and ultimately produce some of my highest quality work. I would also like to thank my family and close friends for their continued support and commitment to keep me motivated.

REFERENCES

[1] D. R. Begault. 3-D Sound for Virtual Reality and Multi media. Academic Press, 2000.

[2] R. D. Shilling and B. Shinn-Cunningham. Virtual auditory displays. Technical report, DTIC Document, 2000.

[3] P. Larsson, A. Väljamäe, D. Västfjäll, A. Tajadura-Jiménez, and M. Kleiner. Auditory-induced presence in mixed reality environments and related technology. In The Engineering of Mixed Reality Systems, pages 143–163. Springer, 2010

[4] E. M. Wenzel, M. Arruda, D. J. Kistler, and F. L. Wightman. Localization using nonindividualized head-related transfer functions. The Journal of the Acoustical Society of America, 94:111, 1993.

[5] Jeffress, L. A. (1948). A place theory of sound localization. *Journal of Comparative and Physiological Psychology*, 41(1), 35-39. doi:10.1037/h0061495

[6] Butler, R. A., & Humanski, R. A. (1992). Localization of sound in the vertical plane with and without high-frequency spectral cues. *Perception & Psychophysics, 51*(2), 182-186. doi:10.3758/bf03212242

[7] Carlile, S. (2011). Psychoacoustics. In Hermann, T., Hunt, A., Neuhoff, G., editors, The Sonification Handbook, chapter 3, pages 41-61. Logos Publishing House, Berlin, Germany.

[8] Kapralos, B., Jenkin, M. & Milios, E. (2003). Auditory Perception and Spatial (3D) Auditory Systems, chapter 3, pages 70-76.

[9] Hofman, P. M., Riswick, J. G., & Opstal, A. J. (1998). Relearning sound localization with new ears. *Nature Neuroscience*, 1(5), 417-421. doi:10.1038/1633

[10] Wolfram Research, Inc, Acoustics in the Time Domain. (n.d.). Retrieved July 14, 2020, from https://reference.wolfram.com/language/PDEModels/tutorial/Acoustics/AcousticsTimeDomain.html

[11] Wolfram Research, Inc, Acoustics in the Frequency Domain. (n.d.). Retrieved July 14, 2020, from https://reference.wolfram.com/language/PDEModels/tutorial/Acoustics/AcousticsFrequencyDomain.html

[12] Wolfram Research, Inc., Mathematica, Version 12.1, Champaign, IL (2020).

[13] Kumar, S. (2020). Wolfram Spatial Audio. *Zenodo*. https://doi.org/10.5281/zenodo.3987494

[14] Kumar, S. (2020). *[WSC20] Simulate Audio with Different Arrangements of Speakers*. Online Technical Discussion Groups Wolfram Community. https://community.wolfram.com/groups/-/m/t/2034599.

The Role of Scandal in U.S. and Japanese Politics: Trump, Abe, and Their Political Futures

Kai Kurosu
The American School in Japan; Tokyo, Japan
Email: 21kurosuk@asij.ac.jp

Abstract - Continuing the research I began in my previous paper *The Acquisition of Formal and Informal Political Power in the United States and Japan* (presented at the Young Researchers Conference in 2018) in this paper I will examine the role of scandal in the politics of the United States and Japan, as well as the extent to which scandals lead to the decline or consolidation of formal and informal political power. In these last two years since the presentation of my first paper, the United States and Japan have both experienced dramatic changes and important events in politics. Using the research compiled in the previous paper as background information on U.S. and Japanese political culture, this new and updated paper will analyze shifts in American and Japanese politics and will predict whether or not Trump and Abe's scandals will have a significant effect on the future of their respective political careers.

Key Words – Political Scandal, Political Culture, Donald Trump, Shinzo Abe, Elections

INTRODUCTION

At the time of writing, the U.S. presidential election is nearly seven months away, and voters will be forced to make an important decision: whether or not to allow President Donald J. Trump a second term. Trump's rise to power in 2016 was unusual, as he held no prior experience holding political office. He was also well known for his long career in the real estate business, and for the numerous scandals he was said to be involved in. Trump's victory in 2016 illustrated his ability to overcome those major hurdles for his campaign, and also illustrated the willingness of American voters to overlook those issues. However, Trump has been faced with numerous new scandals after entering the White House, including the "Russia collusion" investigation, multiple reports of extramarital affairs, and a controversial call with a foreign leader that led to his impeachment. As Trump begins to campaign for a second term, there is no doubt that these scandals will play some kind of role in the 2020 election.

In Japan, numerous scandals have haunted the Abe administration. Unlike Trump's scandals, these cases have not attracted widespread attention from the rest of the world, nor have they led to any widespread protests or demonstrations. Attempts by the opposition to remove Abe from office (through a vote of no confidence) have also been soundly defeated, although the scandals have led to sporadic declines in Abe's approval ratings. Over the years Abe has been able to consolidate power despite the divisions and different factions within the Liberal Democratic Party and has also been able to lead the party to impressive victories in parliamentary elections. His ruling coalition currently holds 314 out of the 465 seats in Japan's House of Representatives. With this strong support behind him, Abe has become the longest-serving Japanese prime minister since the end of the Second World War.

This piece will argue that the scandals of both Trump and Abe will not have a major impact on their long-term informal political influence and will likely have a minimal impact on the outcome of elections (the consolidation of formal political power). My examination of recent U.S. and Japanese politics suggests that although scandals are important in terms of temporarily shaping public opinion and can sometimes lead to specific election outcomes, it is generally not the most important factor that citizens and voters consider.

For the purposes of this paper, 'scandal' is defined as acts of legal or moral misconduct by those who hold significant societal power, as well as the public criticism and outrage that comes as a result of this behavior. This paper will analyze several political scandals and will place a particular focus on the public backlash that came as a result of these cases. As previously defined in my 2018 paper, 'formal political power' is the legitimate acquisition of positions of political office through legal appointments and elections, while 'informal political power' refers to unofficial political influence over powerful public officials or the public itself. Informal power can thus be observed in lobbying data, public approval numbers, social media trends, and any other metric that represents one's popularity and influence in society or among the politically powerful.

THE HISTORY OF POLITICAL SCANDAL IN THE UNITED STATES AND JAPAN

Before diving into the question of how scandal will affect future political events in the U.S. and Japan and how this ties into the systems of formal and informal power mentioned in the previous paper, one must examine the history of scandal in the United States and Japan, and how this has affected culture, society, and elections in the past.

United States In the United States, scandal has always been present at the highest levels of government, including the presidency. Thomas Jefferson was known for having extramarital affairs, Warren G. Harding's presidency is still plagued by the Teapot Dome scandal, and more recently even popular presidents such as Ronald Reagan and Bill Clinton have faced widespread public criticism for scandals that they played a role in. Additionally, members of Congress have been involved in numerous scandals over the years (such as the Jack Abramoff scandal). This section will examine the Watergate scandal during Richard Nixon's presidency, the Iran-Contra scandal during Ronald Regan's presidency, and the extramarital affair scandal of Bill Clinton's presidency as a framework to analyze the effect that Trump's scandals will have on his political future.

Watergate is perhaps the most consequential political scandal in the history of the United States. Although scandals have always played an important role in American politics, the extensive investigation and widespread media coverage was something that the nation had never seen before. The case involved a break-in into the Watergate complex in Washington D.C. in July 1972, where the Democratic National Committee office was located. Those arrested had ties to Richard Nixon's reelection campaign and had been caught stealing documents and wiretapping phones. Nixon immediately denied his involvement in the break-in and took sweeping action to cover up any potential link between those involved and his administration. After an extensive investigation by intelligence agencies and the Congress that spanned nearly two years, Nixon resigned in 1974.

Nixon remains the only U.S. president to ever resign the office, and this came after two years of extensive investigation and overwhelming pressure from congressional leaders and political insiders, which indicated to Nixon that his chances of impeachment and removal from office were inevitable. The Watergate case illustrated that evidence of a link between a politician (in this case the president of the United States) and suspicion of criminal conduct (or other wrongdoing of equal stature) is not necessarily enough for someone to immediately lose the formal political power he or she has consolidated over the years. Nixon was reelected the same year as the Watergate break-in with an electoral landslide, defeating Democrat George McGovern with 520 electoral votes compared to McGovern's 17 electoral votes, and secured a popular victory of nearly 20 million votes. [1] However, Nixon later made serious mistakes in his own handling of the scandal. For example, it was revealed that he had arranged "hush money" for the five burglars caught breaking into the DNC office. He had also ordered the CIA to obstruct the FBI's investigation into the break-in, and had fired Archibald Cox, the independent special prosecutor tasked with investigating the break-in. These abuses of presidential power and Nixon's obstruction of justice were investigated over a long period by Congress and the public, who now had easy access to this information through 24-hour news coverage. [2] This led to Nixon's eventual demise, and it is often said that the cover-up was what brought Nixon down, not the break-in. Nixon not only suffered a serious loss of his formal political power (by resigning from his position as president), but also a loss of the informal political influence that he had consolidated over the years. President Gerald Ford's pardoning of Nixon is generally considered to be a major factor in Ford's loss to Jimmy Carter in the 1976 presidential election and compounded on the distrust of government and Nixon's allies, which had come as a result of Watergate. [3] Although public sentiment on Nixon's tenure has shifted somewhat in recent years (notably, Nixon has been praised in recent years for his efforts regarding environmental protection), at the time the scandal received enough public outrage to cause a demise in Nixon's formal and informal political power, and the loss of Nixon's informal political power over the public (a decline in public trust) even led to the loss of Ford's formal political power.

Watergate, however, seems to be an outlier and a stark contrast to the way political scandals have played out in more recent years, such as in the case of Iran-Contra. Iran-Contra was a major scandal that plagued Ronald Reagan's administration. Reagan's administration had operated an arms trade with Iran, which had recently gone through an Islamic revolution in 1979 and had been holding American hostages. Using the funds secured by this arms deal, the administration would be able to fund the Contras in Nicaragua, an anti-communist group that had been fighting a guerrilla conflict with the leftist Sandinista government. The press first reported on the scandal, and after further investigation by Attorney General Edwin Meese, it was revealed that much of the money secured from the arms deal ($18 million of the $30 million total) was not officially accounted for. Reagan was forced to retract earlier statements in which he denied any negotiations with Iran or terrorists, and it was revealed that Reagan's national security advisor John Poindexter was aware that the diverted funds had been sent to the Contras. Investigations by Congress concluded that Reagan's lack of oversight had enabled the diversion of funds, and included televised testimonies of key players in the scandal, including President Reagan. Reagan's vice president George H.W. Bush was elected president in 1988 and pardoned many who were implicated in the scandal. [4] Reagan did, to an extent, lose the trust of the public during this scandal. However, it can be said that Reagan managed to maintain both formal political power and informal political influence. In terms of formal political power, there were no serious attempts to impeach Reagan, and his own vice president was able to carry the 1988 election in a 426-111 electoral landslide. [5] In terms of informal political power, Reagan continues to be revered to this day by the American center-right as a hero of modern American conservatism.

Bill Clinton's extramarital affair with White House intern Monica Lewinsky consumed the second term of his presidency. Kenneth Starr was an independent special prosecutor appointed to investigate the Whitewater controversy, a scandal that involved Bill and Hillary Clinton and a series of real estate transactions they had made with James and Susan McDougal. Several inquiries were opened

into the Whitewater case, but none had gathered enough evidence to charge the Clintons with criminal conduct. [6] However, when Kenneth Starr took over the investigation in 1994, the investigation would change direction and look into a completely different issue: Bill Clinton's extramarital affair with a White House intern, Monica Lewinsky. Bill Clinton had faced allegations of sexual misconduct prior to his election as president and the investigation into these allegations, combined with the Starr investigation into the Whitewater scandal, led to the stunning reveal in 1998 that Clinton had been having an affair with Lewinsky. The case went to federal court, and after denying the claims for months, Clinton eventually testified before the court's grand jury, admitting responsibility and apologizing to the American public. He was impeached in January of 1999 for perjury and obstruction of justice but was acquitted of both charges in a Senate trial the following month. Clinton did lose some formal and informal political power as a result of his scandals. He became the second president in American history to be impeached by the House of Representatives, and his scandals contributed to a long-lasting public image of Clinton and his family as inauthentic, untrustworthy, and unethical. However, Clinton was *not* removed from office, and the Democratic Party even gained seats in the 1998 midterms. [7] The focus by Republicans on impeachment is generally considered to be a cause of the Democratic gains in these elections. [8] Clinton also left office as one of the most popular presidents in modern American history, maintaining a strong hold on his influence over the public. [9]

Japan Japanese politics was completely reformed at the end of the Second World War when the occupying American forces reformed Japan's government and wrote a new constitution for the country. Since then, several political scandals have captivated the nation and led to the demise of some powerful political figures. While there haven't been quite as many large-scale political scandals as the United States (where virtually every administration has faced at least one), these scandals have shaped the political culture and history of Japan and can provide hints as to how political scandals will shape the future.

The Lockheed scandal (ロッキード事件) occurred in 1976 and is often considered to be the most high-profile political scandal in Japanese history. The case involved bribes between the Lockheed Corporation (now Lockheed-Martin) and top Japanese politicians and business officials, including Prime Minister Kakuei Tanaka. Lockheed's former chief operating officer and vice president A. Carl Kotchian admitted to this on February 6, 1976, to the U.S. Senate Foreign Relations Committee, and revealed that the bribes involved a promise that All-Nippon Airways (a major Japanese civilian airline) would purchase Lockheed's Tri-Star jet. When these reports reached Japan, it was revealed that leaders of the Liberal Democratic Party had been involved. Among them was Kakuei Tanaka, the former prime minister, who was eventually arrested and imprisoned. Although the LDP suffered a setback in that year's elections, it held onto its parliamentary majority. [10] [11] Today, Tanka remains one of Japan's most popular prime ministers. Although the LDP's formal political power took a major loss, Tanaka continued to hold on to informal political power. The prime ministers who followed Tanaka were known to be close allies of him, and the Japanese public continues to admire the uneducated and poor country boy who eventually became prime minister. [12] [13]

The Recruit Scandal (リクルート事件) was exposed in 1988 and involved some of Japan's top political leaders. Recruit was a Japanese real estate company that engaged in insider trading with Japanese media executives, bureaucrats, and politicians. Between 1984 and 1986 it offered unlisted shares in real estate subsidiaries to this group, and those who purchased the unlisted shares were able to sell them at high prices after Recruit went public in 1987. Those implicated in the scandal included Prime Minister Noboru Takeshita, Chief Cabinet Secretary Keizo Obuchi, and former Prime Minister Yasuhiro Nakasone, as well as numerous other high-profile politicians. At the time, Japan had very few anti-insider trading laws and regulations, and thus very few of these politicians were ever charged with crimes. Formal power and informal power were both lost to an extent; the LDP suffered setbacks in elections and lost some public support. [14] [15] [16] However, the LDP managed to hold on to their formal political power (as the ruling party) until 1993, and although their credibility was hurt temporarily, they remained a powerful and popular force in Japanese politics.

TRUMP, ABE, AND SCANDAL: WHAT HAS HAPPENED SO FAR

Trump In the two years since I presented my previous paper *The Acquisition of Formal and Informal Political Power in the United States and Japan*, the political scene of the United States has changed dramatically. The midterm elections were a stunning blow to the Trump administration and the Republican Party, as the Democrats were able to gain a majority in the House of Representatives. The new Democratic majority supported the Russian election meddling and Trump-Russia collusion investigation, and this culminated in the publishing of Robert Mueller's official report in April 2019. Although Mueller did not charge Trump with any official crimes, he also did not rule out the possibility that Trump had committed crimes. Despite calls for further investigation by Congressional Democrats, the investigation ended there and did not lead to impeachment proceedings or an indictment of the president. Some key Trump campaign officials, such as former National Security Advisor Michael Flynn, former Trump campaign CEO Paul Manafort, and longtime Trump advisor Roger Stone have been arrested and indicted for criminal conduct. However, Trump claimed that the Mueller report had vindicated him, and his approval ratings remained static. [17] In September of 2019, an anonymous whistleblower reported that Trump had pressured (with the threat of halting military aid) Ukrainian president Volodymyr Zelensky on a phone call to

investigate former Vice President Joseph R. Biden Jr., a political rival who had announced his candidacy for the Democratic presidential nomination in 2020. This allegation led to heavy criticism from Congressional Democrats, who argued that Trump had invited a foreign power to interfere in the 2020 presidential election, and that he had abused the powers of the presidency to advance his personal political interests. House Democrats, now in the majority, quickly began an investigation into the matter, calling witnesses to committee hearings and introducing articles of impeachment. Despite arguments from Congressional Republicans that the process was rigged and that Trump had genuine concerns about Biden's alleged corruption in Ukraine, the witnesses confirmed that Trump had solicited a "quid pro quo" with Zelensky, asking for an investigation into Biden in exchange for military aid and an official White House meeting between the two leaders. Democrats introduced two articles of impeachment: abuse of power and obstruction of Congress. The two articles passed Congress on December 18, 2019, with no Republican support for both articles. This made Trump the third president in U.S. history to be impeached by the full House of Representatives. His defense team in the Senate trial included high-profile lawyers such as Alan Dershowitz and Kenneth Starr. The Republican-controlled Senate refused to call witnesses to the trial, and both articles were rejected on party lines (48-52 and 47-53), with the exception of Sen. Mitt Romney (R-UT) who voted yes on article I, the abuse of power. [18]

There is no evidence that these scandals had an immediate impact on Trump's approval among the American public, which shows he has been able to maintain his hold on informal political power. His approval ratings instead improved, indicating that impeachment does not seem to be a major concern among American voters. Additionally, while several reports of extramarital affairs and other claims of inappropriate behavior have dominated press coverage of the Trump administration, there haven't been major drops in his approval and disapproval ratings, as his approval rating has remained near 40 percent and his disapproval rating at around 50 percent. [19] The 2020 presidential election will be the true test of whether or not these scandals can contribute to the demise of his formal political power, but because he has been able to so firmly maintain his grip on informal political power, it seems unlikely that this will have a major effect on the outcome of the election.

Abe The Abe Administration, which has become the longest-lasting Japanese administration since the end of the war, has seen its fair share of scandal as well. In February of 2017, it was revealed that the Japanese Finance Ministry sold heavily discounted land in Osaka prefecture to Moritomo Gakuen, a private school that was known for promoting right-wing nationalist education. Prime Minister Abe's wife Akie Abe was listed as an honorary principal of Moritomo Gakuen, and this led to allegations of government favoritism. The ministry maintained that this was not a reason for the sale, but documents detailing the transactions between the ministry and the school were destroyed. Allegations of Abe's favoritism and overstep of power arose again in May of the same year. A new veterinary department at the Okayama University of Science had been requesting approval from the Japanese Education Ministry for nearly 50 years and had finally received government approval. This department was to be run by school operator Kake Gakuen, and the allegations that Abe was personally involved came about after it was revealed that Abe and the head of Kake Gakuen were longtime friends. [20]

These scandals led to the worst drops in approval ratings for Abe. In February, after the Moritomo story broke out, Abe's approval ratings fell 8.3 percent (41 percent approval), and a poll conducted in July of 2017 indicated that Abe's approval ratings had fallen to 26 percent. [21]

The most recent scandal to hit the Abe administration is the Sakura Wo Miru Kai (桜を見る会) Scandal, which broke in November of 2019. The scandal centered on the annual cherry blossom-viewing event that Japanese prime ministers hold in the spring. The allegations against Abe were that he had misdirected public funds and prioritized his own supporters (in his Koenkai organization) from his home constituency to participate in the event. His office in his home constituency had offered special exclusive packages to his Koenkai supporters, which included transportation to Tokyo and a stay at a luxurious hotel. Opposition parties took advantage of this opportunity to criticize the administration and slow its legislative agenda. Abe and his senior aides said documents detailing guest lists had been shredded, and that it could not provide specific information about guests out of concern for their privacy. The opposition pointed out what they claimed was a pattern of hiding and covering up wrongdoing, as well as an abuse of the prime minister's office for Abe's personal affairs. Although this led to an immediate six-point drop in approval ratings, his approval rating had improved since the Moritomo-Kake scandals and was still at a relatively strong 42 percent after the scandal broke. [22] [23] While Abe has sporadically suffered serious threats to his informal political influence over the public, his public image seems to recover, and he has been able to hold on to formal political power through elections.

More recently, Abe's administration and the LDP have been put under more intense scrutiny for the conduct of top party officials and members of parliament (some who served in Abe's cabinet) who have been investigated for various criminal activities, as well as a controversial new bill that would give the prime minister new powers over prosecutors. However, Abe's history of overcoming scandals suggests that it is unlikely that these new problems will destroy his political future.

CONCLUSION: WHAT WILL HAPPEN NOW?

Although these scandals have revealed the weaknesses of both leaders, they have also shown their strengths. Trump's major appeal among his core base of

supporters is his 'authenticity', a concept that extends to his proclivity towards scandalous behavior. Thus, although some of Trump's behaviors have led to public outrage, this outrage is also what precisely excites Trump's core base. Although Abe has faced serious accusations of abusing the powers of his office, his ability to prevail over these problems and succeed in elections has revealed his ability to hold on to power by stressing the LDP's historical mandate to power (a mandate based on providing economic stability), rather than social issues which place more of a focus on the personal conduct of politicians.

Trump and Abe both lead powerful democracies and economies, and will continue to face critical decisions that will have long-lasting effects. Terrorism, the threat of climate change, and the spread of the novel coronavirus (COVID-19) all illustrate the need for leaders who can unite and gather broad support from the people. Political scandals will most likely not have wide-scale or long-lasting impacts on the political futures of these two leaders, in terms of both formal and informal power. However, there is no doubt that both leaders will both face higher levels of public scrutiny and accountability as the world moves towards a more dangerous era.

REFERENCES

[1] "Presidential Election of 1972." *270toWin.Com*, www.270towin.com/1972_Election/.

[2] History.com Editors. "Watergate Scandal." *History.com*, A&E Television Networks, 29 Oct. 2009, www.history.com/topics/1970s/watergate#section_3.

[3] Miles, David. "Political Experience and Anti-Big Government: The Making and Breaking of Themes in Gerald Ford's 1976 Presidential Campaign." *Michigan Historical Review*, vol. 23, no. 1, 1997, pp. 105–122. *JSTOR*, www.jstor.org/stable/20173633. Accessed 7 June 2020.

[4] History.com Editors. "Iran-Contra Affair." *History.com*, A&E Television Networks, 10 Aug. 2017, www.history.com/topics/1980s/iran-contra-affair.

[5]"1988 Presidential Election Interactive Map." *270toWin.Com*, www.270towin.com/1988_Election/interactive_map.

[6] Beers, Brian. "What Was the Whitewater Scandal?" *Investopedia*, Investopedia, 11 Mar. 2020, www.investopedia.com/ask/answers/08/whitewater-scandal.asp

[7] "Statistics of the Congressional Election of November 3, 1998" (PDF). U.S. House of Reps, Office of the Clerk. Retrieved 10 April 2017.

[8] Abramowitz, Alan I. "It's Monica, Stupid: The Impeachment Controversy and the 1998 Midterm Election." *Legislative Studies Quarterly*, vol. 26, no. 2, 2001, pp. 211–226. *JSTOR*, www.jstor.org/stable/440200. Accessed 8 June 2020.

[9] Organization, The Gallup. *Bush Presidency Closes With 34% Approval, 61% Disapproval*, web.archive.org/web/20090119053947/www.gallup.com/poll/113770/Bush-Presidency-Closes-34-Approval-61-Disapproval.aspx.

[10] Blaker, Michael. "Japan 1976: The Year of Lockheed." *Asian Survey*, vol. 17, no. 1, 1977, pp. 81–90. *JSTOR*, www.jstor.org/stable/2643443. Accessed 13 Mar. 2020.

[11] Tokumoto, Eiichiro. "Lockheed Scandal 40 Years on: The Downfall of Prime Minister Kakuei Tanaka." *Asia Times*, 17 Feb. 2020, asiatimes.com/2016/12/lockheed-scandal-40-years-downfall-prime-minister-kakuei-tanaka/.

[12] Johnson, Chalmers. "Tanaka Kakuei, Structural Corruption, and the Advent of Machine Politics in Japan." *Journal of Japanese Studies*, vol. 12, no. 1, 1986, pp. 1–28. *JSTOR*, www.jstor.org/stable/132445. Accessed 7 June 2020.

[13] "大ブーム「田中角栄」は何がスゴかったのか？: 国内政治." 東洋経済オンライン, 3 Nov. 2016, toyokeizai.net/articles/-/141468.

[14] Nester, William. "Japan's Recruit Scandal: Government and Business for Sale." *Third World Quarterly*, vol. 12, no. 2, 1990, pp. 91–109. *JSTOR*, www.jstor.org/stable/3992261. Accessed 13 Mar. 2020.

[15] Yates, Ronald E. "FOR JAPAN, SCANDAL IS A REAL EDUCATION." *Chicagotribune.com*, Chicago Tribune, 3 Sept. 2018, www.chicagotribune.com/news/ct-xpm-1989-02-06-8903030410-story.html.

[16] Taro, Yayama. "The Recruit Scandal: Learning from the Causes of Corruption." *Journal of Japanese Studies*, vol. 16, no. 1, 1990, pp. 93–114. *JSTOR*, www.jstor.org/stable/132495. Accessed 7 June 2020.

[17] Sheffield, Matthew. "Trump's Approval Rating Little Changed after Mueller Report." *TheHill*, 24 Apr. 2019, thehill.com/hilltv/what-americas-thinking/440367-trump-approval-rating-little-changed-after-mueller-report.

[18] O'Key, Sean, and Zachary B. Wolf. "How Each Member of the House of Representatives Voted on Impeachment." *CNN*, Cable News Network, 18 Dec. 2019, edition.cnn.com/interactive/2019/12/politics/house-impeachment-vote/.

[19] Jacobs, Emily. "Trump Approval Rating Hits a High Post-Impeachment." *New York Post*, New York Post, 20 Feb. 2020, nypost.com/2020/02/19/trump-approval-rating-hits-a-high-post-impeachment/.

[20] Author, No. "The Kake and Moritomo Scandals and the Bureaucracy." *The Japan Times*, The Japan, 20 Oct. 2017, www.japantimes.co.jp/opinion/2017/10/20/editorials/kake-moritomo-scandals-bureaucracy/#.XmuDvJMzbs0.

[21] "Cabinet Approval Rating at 26%, Lowest since Abe Returned to Power in 2012: Poll." *The Mainichi*, The Mainichi, 24 July 2017, mainichi.jp/english/articles/20170724/p2a/00m/0na/010000c.

[22] Author, No. "Abe Nips Tokyo Cherry-Blossom Party in the Bud as Critics Cry Cronyism." *The Japan Times*, 13 Nov. 2019, www.japantimes.co.jp/news/2019/11/13/national/politics-diplomacy/shinzo-abe-cherry-blossom-event-criticism-cancel/#.Xt2XTZ4zZmA.

[23] Herskovitz, Jon. "Japan Cherry Blossom Scandal Starts to Drag Down Abe Support." *Bloomberg.com*, Bloomberg, 2 Dec. 2019, www.bloomberg.com/news/articles/2019-12-02/japan-s-cherry-blossom-scandal-starts-to-drag-down-abe-s-support.

Methods for Classification of Galaxy Types using Machine Learning

Christopher Lee
Seoul International School; Gyeonggido, South Korea
Email: chrisjlee2002@gmail.com

Abstract - Lately there has been a great sharing of astronomical data, especially the images from large telescopes such as the Hubble Space Telescope. Although all galaxies were formed by gravitational pull acting on stars, each resulted in a quite different shape. Galaxy Zoo contest in Kaggle.com offered an ideal dataset to apply machine learning to the galaxy classification problem. The dataset's labeling process was unique in that they were statistical, directly reflecting the people's judgement. Although the labels of the galaxy images went into subcategories as well, this research focused on the first level classification between the spiral and the elliptical galaxies. The training data they offered were numerous enough that over 10,000 images of each class could be split into training and testing data, to measure the accuracy of the classifier. Variations of LeNet were chosen, to squeeze more performance from it. The resulting accuracies were within about 95-97% in agreement to the labels, which were only 80% confident of the classification themselves.

Key Words - Galaxy Classification, Machine Learning, Galaxy Zoo, Kaggle

INTRODUCTION

The galaxy's morphology is an important piece of knowledge that would lead to a better understanding of the physics of galaxies, and the universe. Lately, there has been a great sharing of astronomical data, especially the images from large telescopes such as the Hubble Space Telescope [1] as shown in Figure 1. The images of the galaxies could be classified by an expert, or by volunteers on websites such as Galaxy Zoo [2]-[3]. Galaxy Zoo is an astronomy project that people contribute to by classifying a huge number of different galaxies. However, even with this crowdsourcing, galaxy classification is an overwhelming task due to its scale: for example, the Hubble Telescope captured more than 256,000 galaxies in a single image, according to MIT Technology Review May 2020.

Kaggle is the largest data science/machine learning community website. It includes projects and competitions with different data sets. "Machine learning is a field of computer science that uses algorithms and techniques to give the computer system the ability to learn, i.e., improving performance on a specific classification, with data, without being directly programmed to do certain steps" [4]. These algorithms work by building a model from a training data set of input and output pairs. Without being explicitly programmed, machine learning tries to produce an algorithm that matches the input output pairs in the training dataset as closely as possible. When the algorithm is presented with an input it has never seen, it will produce an output that is called "prediction." The goal is to have these "predictions" match the observed reality as closely as possible.

Different industries and agencies use machine learning for various purposes. For example, financial services such as credit card companies use machine learning for fraud prevention. Online merchants such as Amazon or Netflix use it to recommend books or movies that customers would actually enjoy.

Machine learning can also be used for image classification. The goal of this study is to present automated morphological classification of galaxies using machine learning algorithms and image analysis. This research uses machine learning to match categorizations of the galaxies done by humans, so that future images can be accurately classified with computers alone.

A pre-existing convolutional neural network (i.e. LeNet [5]) is used with a varying number of layers. Further tweaking made it possible to enhance the performance to the point of matching the human classification result.

Incidentally, the data that Kaggle provides does not definitely state the types of galaxies. Instead, it statistically scores the types of galaxies through the results of surveys.

FIGURE 1: Procedure of morphology classification of galaxies using the Hubble Telescope, Galaxy Zoo, and Kaggle [1]-[2]

CLASSIFICATION METHODOLOGY

I. Experimental Procedure

Mathematica version 11.3 and MacBook Pro (2.5 GHz Intel Core i7, 16 GB 2133 MHz LPDDR3) are used for machine learning programming. The hypothesis is that if machine learning is used to classify galaxy images into two categories, its accuracy should match human classifications with an error range of 5%.

Experimental procedure is shown in Figure 2. Galaxy Zoo data from Kaggle is used. This data contains 61,578 jpeg images. These images are labeled into several layers of galaxy classifications, and sub-classifications, and then sub-sub-classifications as shown in Figure 3. This research focuses on level 1 classification into the first (elliptical) or the second (spiral) types of galaxies. They are named Class 11 and Class 12 respectively throughout this report. There is also a third class, "Others," (Class 13) but this is not considered because the probabilities are negligible. The sum of the probabilities of all these three classes will always add up to 1.

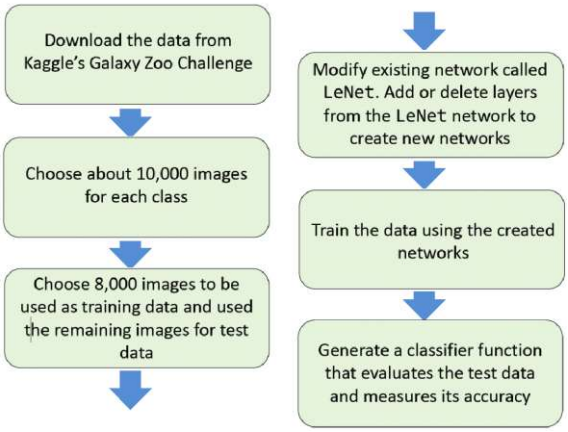

FIGURE 2: Experimental procedure of automated classification

These galaxy images are not classified nominally. They are only given the probability of belonging to that class according to many human classifiers who performed the task in the past. Only the top ranked (in terms of probability) 10,000 images of each class are chosen out of a total of 61,578 images. The chosen 10,000 images in each category have probabilities higher than 76.2% in Class 11, and higher than 87.2% in Class 12. These disparate probabilities stem from selecting a matching number of 10,000 images from each category. Class 12 images are labeled with higher confidence. Those images are stored in their respective folders. These two groups of high-probability images serve as labeled, nominal data. 8,000 (80%) images from each group are randomly selected for training data and the rest are used as testing data in the first phase.

A pre-existing network called LeNet is used as the basis to form the basic layers. The encoders and decoders, which are the inputs and outputs of the chain respectively, are altered based on the dimensions and the color space of the astronomical images. More layers and nodes are added or deleted to the LeNet in each cycle in search of higher accuracy. The training is done with the NetTrain command. Accuracy is measured using the ClassifierMeasurements command.

II. Galaxies Classification

As shown in Figure 3, Galaxy images are provided by the Hubble Space Telescope. The images were acquired during the "Galaxy Zoo: Hubble" project [2].

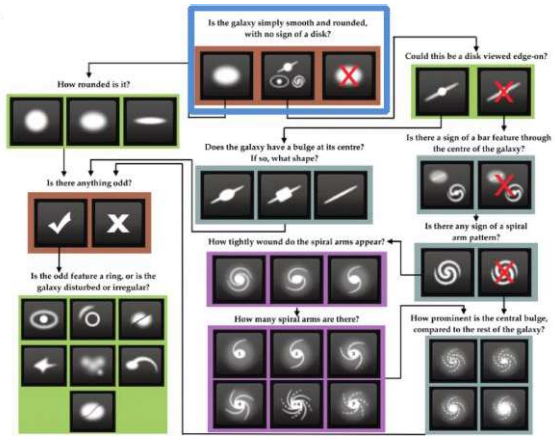

FIGURE 3: Classification of Galaxies [6]

Galaxy classification using Machine Learning was a success. A network called LeNet [5], which is initially used for handwritten character recognition, was utilized in this galaxy classification task. Several readily available networks were tried. Although some premade networks, such as VGG-16, produced very poor results while taking days to compute, LeNet in particular produced excellent results, achieving a 90% accuracy range.

III. Overview of the Whole Dataset

Figure 4 shows the distribution of the Class 11 probabilities out of 61,578 images. As shown in the histogram, the area of the data is more on the left side than on the right, which means that most of the classifiers thought that there were more images that belong to Class 12 than Class 11.

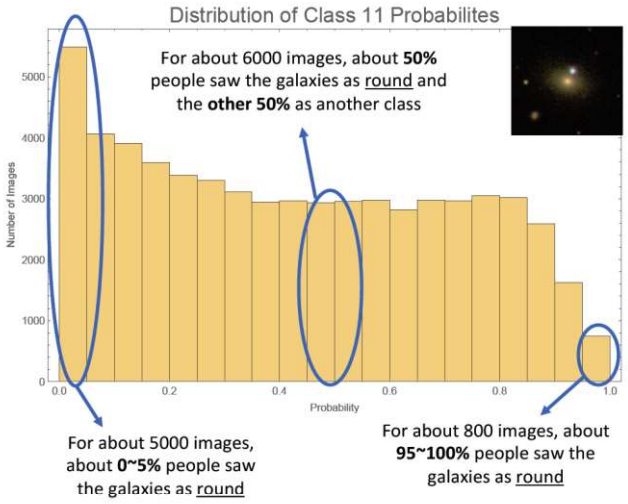

FIGURE 4: Distribution of Class11 Probabilities

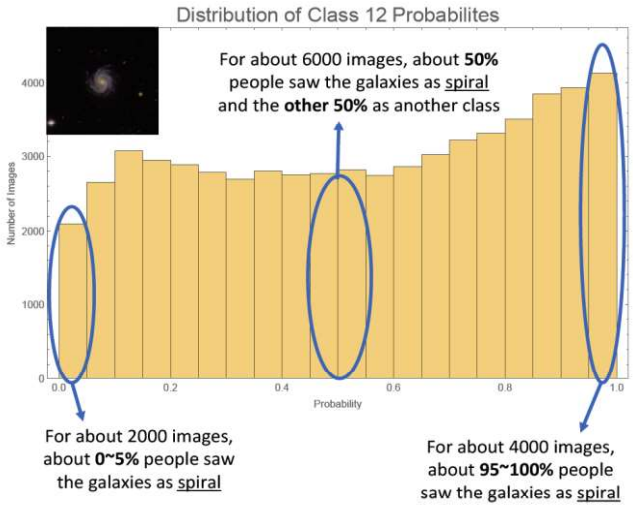

FIGURE 5. Distribution of Class12 Probabilities

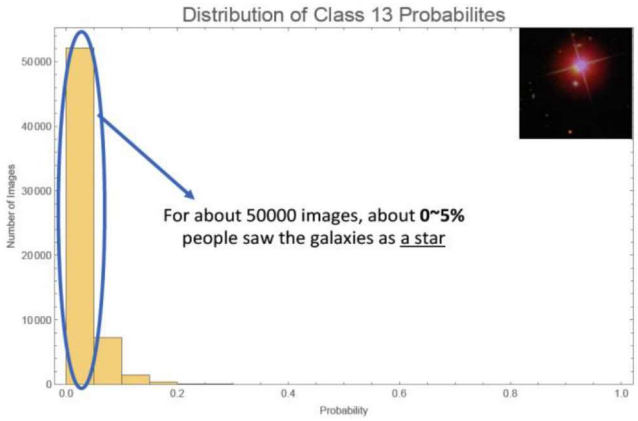

FIGURE 6: Distribution of Class13 Probabilities

In contrast, Figure 5 shows the distribution of the probabilities of Class 12 images in the whole dataset. As shown in the histogram, the area of the data is more tilted towards the right side than the left, which signifies that the classifiers thought that most of the images fit into Class 12 than others. The histograms in Figure 4 are not exact mirror images to Figure 5 because some of the images were classified as Class 13, which makes the count imprecise.

Figure 6 shows the distribution of the probabilities of Class 13 images in the whole dataset, which are non-galaxy images. However, as seen in the histogram, people who saw these pictures thought that they were mostly galaxies, and not stars. So since the probabilities of Class 13 images are negligible, this class can be ignored.

RESULTS AND DISCUSSION

I. Classification Results

Figure 7 indicates the structure of the chain with 20 layers. Each box in the diagram indicates a layer in the actual chain; they are connected together and going in one direction. This chain has the greatest number of layers out of all the chains that have been tested, and took the longest to compute. The classification also had an accuracy of about 97%, which is one of the highest results obtained in this research. Overall, counterintuitively, the more layers there are, the less time it takes to classify the images. After that, the computation time dramatically shoots up. This strange phenomenon needs to be further investigated.

In addition, the more layers there are, the more accurate the classification becomes. The optimal number of layers to have in a chain is around 14 layers, after which the accuracy plateaus while the computing time increases dramatically.

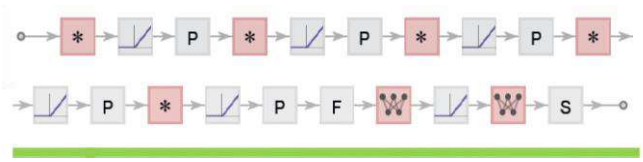

FIGURE 7: Structure of the chain with 20 layers

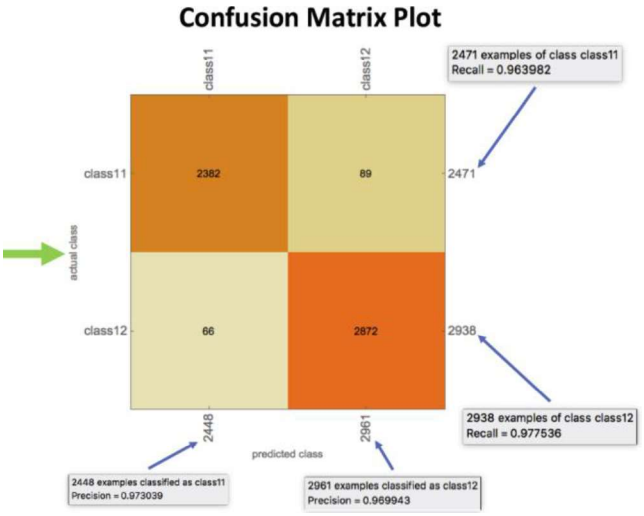

FIGURE 8: Confusion matrix showing the performance of machine learning

Figure 8 shows the result of the machine learning performance on the aforementioned data. 2,382 images of Class 11 were classified as Class 11, while 89 images were misclassified as Class 12. 2,872 images of Class 12 were classified as Class 12, while 66 images of Class 12 were misclassified as Class 11. This means that 96% of the images were classified correctly while 4% were classified incorrectly for Class 11. On the other hand, 98% of the images were classified correctly and 2% were classified incorrectly for Class 12. The overall classification resulted in a 97% accuracy for both classes, which is excellent.

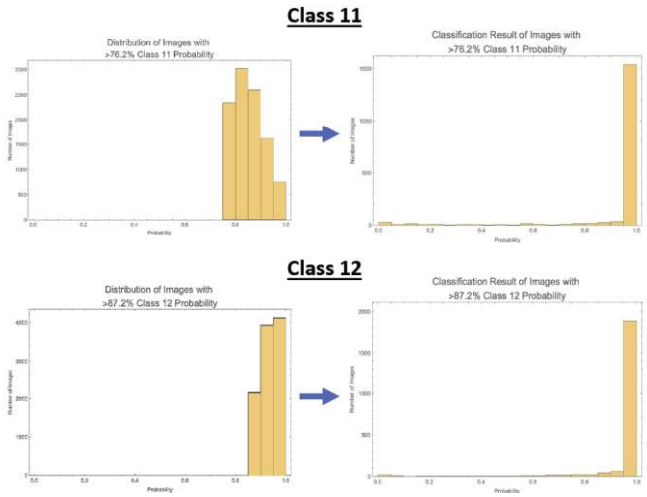

FIGURE 9: Distribution result of class 11 and 12 Probabilities

The confusion matrix plot shown in Figure 8 is binary, which means that it either classifies the images as Class 11 or Class 12 without any regards to the confidence of the prediction.

The middle 50% line is the threshold for the classification. For the top histogram in Figure 9, any bar that is on the right side of the middle line would be classified as Class 11 while the left side would be classified as Class 12. The classes are reversed for the pair of histograms at the bottom.

Histograms in Figure 9 show what is happening behind the scenes. The left top histogram is the input of the classifier, while the right top histogram is the result of the classification. Although the right histogram seems to have pushed all bars against the right wall, a low height bar can be observed near the floor, reading all the way to the left wall. This means that some images were classified as Class 12. The fact that some were misclassified was clear from the confusion matrix. This histogram shows just how many of them displayed a degree of Class 12-ness.

A similar story repeats for Class 12 histograms shown at the bottom of Figure 9. While appearing to have become more radicalized Class 12, there was an undercurrent of misclassification into Class 11 by varying degrees all the way to the left wall, which indicates near 100% Class 11-ness.

II. Network Optimization

Top in Figure 10 illustrates the effect of the number of layers of a chain on the accuracy of the classification of the galaxy images. As shown on the line graph, the line seems to increase then plateau. Although the accuracy continues to improve (with a slight dip at 17 layers, which is a mystery), it reaches a diminishing return around 14 layers.

At the bottom of Figure 10, the line graph shows the effect of the number of layers of a chain on the computation time. The graph seems to go on an exponential decay, as the amount of time it takes seems to decrease as the number of layers in a chain increases. This is a complete mystery. More layers should result in a longer computation time. But this is what was observed.

Then the line suddenly shoots up after 17 layers. The abruptness with which the computation time increases is also counterintuitive. This mystery in computation time must be investigated further. However, if this phenomenon is real, then this indicates that there might be a sweet spot where the highest accuracy can be attained without proportional expense in computation time.

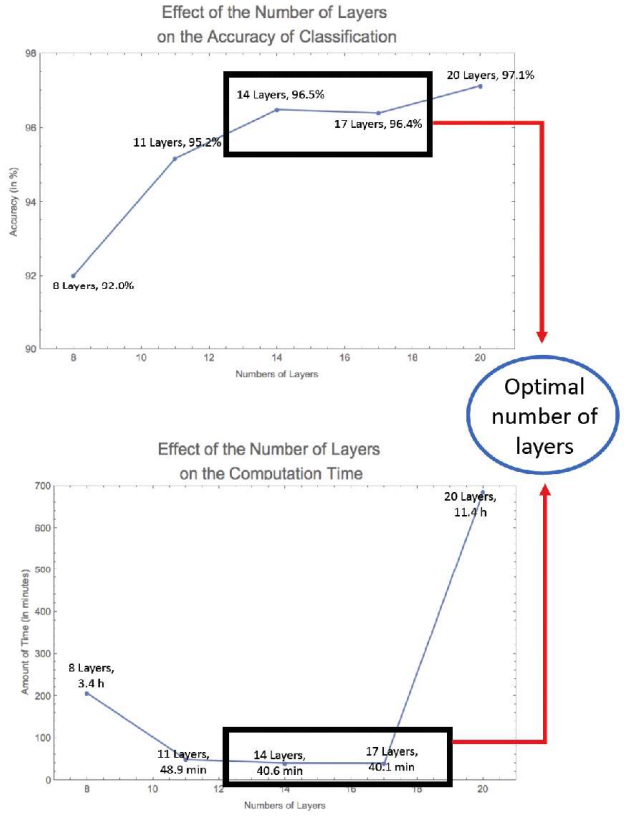

FIGURE 10: Effect of the number of layers on the performance (i.e., accuracy and computation time) of automated classification using machine learning method

CONCLUSION

Automated morphological classification of galaxies using machine learning algorithms and image analysis was examined. Machine learning was used to match the human categorization accuracy of the galaxy images. Results showed that the accuracy was high and the classification was successful, which was about 97%. The optimal number of LeNet layers for maximum performance per computation time was between 14 and 17. Future research is needed to resolve the strange phenomenon of "less computing time for more layers" observed during research. This machine learning based image classification is only the beginning: more applications shall come into effect as the performance continues to increase.

REFERENCES

"Hubble Space Telescope," Wikipedia, 9 October 2018. [Online]. Available: http://en.wikipedia.org/wiki/Hubble_Space_Telescope.

T. Zooniverse, "GALAXY ZOO: HUBBLE," Galaxy Zoo, 10 April 2010. [Online]. Available: https://blog.zooniverse.org/2010/04/23/galaxy-zoo-hubble/.

M. Banerji et.al., "Galaxy Zoo: reproducing galaxy morphologies via machine learning," Mon. No. R. Astron. Soc., vol.406, pp.342-353, 2010.

"Machine Learning," Wikipedia, [Online]. Available: https://en.wikipedia.org/wiki/Machine_learning.

W. N. N. Repository, "LeNet Trained on MNIST Data," Wolfram, 30 January 2017. [Online]. Available: https://resources.wolframcloud.com/NeuralNetRepository/resources/LeNet-Trained-on-MNIST-Data.

K.W. Wilett et.al., "Galaxy Zoo 2: detailed morphological classifications for 304,122 galaxies from the Sloan Digital Sky Survey," Mon. No. R. Astron. Soc., vol.435, pp.2835-2860 , 2013.

Republic of Korea's Economic Success and The Paris Agreement Goal of Reducing Greenhouse Gas Emissions

Rachel Jimin Lee
Yongsan International School of Seoul; Seoul, Republic of Korea
Email: Rachel.jimin.lee@gmail.com

Abstract – South Korea is one of the most polluted countries in the world — in 2016, Korea had 76 days with bad air quality and only 45 days with good air quality. This is an issue of immense significance: medical studies conclude that polluted air can cause serious health problems such as stroke, heart disease, lung cancer, and other ailments. Particulate matter floating in the air smaller than 10 micrometers profoundly threatens children and asthmatics and can be easily absorbed into the bloodstream of adults. The Republic of Korea or ROK is a signatory to the Paris Agreement, which aims to reduce greenhouse gas emissions below the current Business As Usual (BAU) emissions by 37% by 2030. The ROK Ministry of Environment currently oversees Korea's pollution monitoring and regulations; however, attaining the Paris Agreement goals may be difficult considering the nature of Korea's export-oriented economy. The ROK is the 5th largest exporter of goods in the world — the resulting success and trade surplus have significantly increased per capita income and improved the standards of living. An atmospheric test using measuring equipment provided by NASA found that half of the air pollution in Korea originates from industry, power generation, buildings, and transportation vehicles. The fact that the majority of South Korea's air pollution comes from within makes proactive solutions possible. This paper will investigate the path forward, examining how industrial contributors to air pollution in Korea can work with NGO actors, environmental experts, and government officials to achieve the ambitious Paris Agreement goals.

Key Words – South Korea Air Pollution, Particulate Matter Harm, Paris Agreement signatories – South Korea, ROK trade surplus correlation with increased air pollution

INTRODUCTION

From immensely popular K-everything to the country's rapid growth in the 20th century, South Korea has crawled its way to the spotlight in recent years. And yet, despite how prosperous the nation may be, it faces an immense problem: air pollution. In 2018, 17,000 people died in South Korea because of air pollution, according to the "State of Global Air 2019" report published by the Health Effects Institute (Nam, 2019). It's not uncommon for South Korean citizens to spend the majority of their days in masks. School events and sports practices get canceled due to poor air quality. Residents of South Korea regard this issue as a major aspect of their lives.

The issue of air pollution naturally draws concern. After all, air pollution is identified as the cause of one-third of deaths from stroke, lung cancer, and heart disease (World Health Organization, 2019). In 2017, South Korea was designated as one of the most polluted countries in the world, with estimated costs to the country of $9 billion annually. According to the website AirView, three of the most polluted cities in the world are in South Korea, one of which is the nation's capital: Seoul (Harris and Buseong, 2017).

The fundamental cause of health problems in both humans and animals attributed to air pollution is from particulate matter smaller than 10 micrometers, or PM10. These microscopic substances pose great risks because they can easily infiltrate into the bloodstream or to the lungs, penetrating deep into the respiratory and circulatory systems. This may cause damage to the lungs, heart, and brain (WHO, 2019).

Particulate matter represents a harsher threat when children and asthmatics are impacted. After studying the hospitalization and health records of children, medical experts identified detrimental health effects from the air pollution measured in South Korea's population centers, and concluded it's a problem that must be addressed with more care and attention. (Lee, Kim, Song, Hong, Cho, et al, 2002).

When considering these detrimental health effects, the fact that air pollution has grown to be an almost all-consuming factor in South Korean life is undoubtedly concerning. With increasing concern towards this issue, the Korean government has indeed taken steps to remedy it. Not only has the government signed on to the Paris Agreement, but South Korea has also attempted to cut down on air pollution by decreasing coal-fired plants and increasing public bike stations (Babe, 2018). Despite such efforts, the government has displayed some tensions in relation to China's role in Korean air pollution. These tensions must be well navigated in order for South Korea's air pollution to show drastic improvement; the truth behind China's supposed major role in South Korea's air pollution is a topic that demands discussion. When considering South Korea's

rapidly expanding economy, China's role in the equation may be less than what is expected.

AIR POLLUTION IN SOUTH KOREA

South Korea is one of the most polluted countries in the world. Noelle Selin, Associate Professor of Engineering Systems and Atmospheric Chemistry at the Massachusetts Institute of Technology, states that a carbon footprint is the "amount of carbon dioxide (CO2) emissions associated with all the activities of a person or other entity (e.g., building, corporation, country, etc.)." (Selin, 2010). In 2018, Norwegian researchers found Seoul to have the worst carbon footprint out of 13,000 world cities, with inhabitants producing 276.1 metric tons of carbon dioxide a year (Babe, 2018).

Such poor air quality is a major topic of concern for South Korea's population — in a 2017 national survey, South Koreans identified fine dust and air pollution as their No.1 stressor in life (Haas, 2018). In fact, Koreans are more worried about getting sick from pollution than they are about nuclear weapons proliferation in North Korea (Haas, 2018). A 2018 study by the Ministry of Environment found 97% of Korean adults felt physical or psychological pain due to dust. 60% thought the problem was "serious" while another 30 per cent thought it was "extremely serious" (Lee, D., 2019). This concern is not unfounded. In 2016, Korea had 243 days with moderate air quality, 76 days with bad air quality, and only 45 days with good air quality (Haas, 2018). On an average day in Seoul, many citizens can be seen with masks donned to prevent harmful particles from entering their bloodstream. Mothers will chide their children to remember to bring their mask on their way to school. And at school, students will remind each other again of how the air quality is on that day. As such, concern for air pollution is a very real factor in Korean life.

LONG-TERM IMPACT ON HEALTH

The majority of concern about air pollution comes from its effect on health. Some aspects of the long-term effects of air pollution on health remain unknown. Still, evidence suggests that there is a direct connection between air pollution with higher rates of cancer, stroke, heart disease, and respiratory diseases (Nunez, 2019). One of the most compelling cases of evidence for this can be seen in the respondents to the 9/11 tragedy. These responders who attempted to rescue victims and retrieve remains at the World Trade Center in 2001-2002 (policemen, firemen, rescue paramedics and the drivers of busses and trucks) still suffer from poor health and are developing cancer 18 years later (Herbst, 2019).

According to Dr. Michael Crane, medical director of the World Trade Center Health Program at the Icahn School of Medicine at Mount Sinai in Manhattan, some 40,000 of these workers have developed health conditions, including 10,000 responders and volunteers diagnosed with various cancers associated with exposure to toxins (Herbst, 2019). Nearly 18 years after the terrorist attacks, more than 2,000 people have died of an illness related to this incident (Goldberg and Tracy, 2018).

It is expected that by the 20th anniversary of 9/11, more people will have died from 9/11-related illnesses than the 2,700 who died at the Twin Towers that day (Goldberg and Tracy, 2018).

EFFECTS OF AIR POLLUTION ON CHILDREN AND ANIMALS

As air pollution grows as a worrying issue in many countries, another topic of concern has emerged: its impact on the health of children. A published report found that 543,000 children younger than five die annually from respiratory disease caused by air pollution (World Health Organization, 2019). Not only that, but maternal exposure to air pollution during pregnancy is related to adverse birth outcomes such as early fetal loss, preterm delivery, lower birth weight, and more (Schwartz, 2004). Thus, air pollution is a health threat to society as a whole rather than a single age group.

Animals also reflect the harmful effects of air pollution. In truth, animals may actually be more vulnerable to this issue than humans (Pal, M., Yirgalem, M., Anberber, M., Giro, B., Dasguta, R. 2015). Because animals are not as well equipped to protect themselves from air pollution as humans are, they are naturally much more vulnerable to this presence of particulate matter (Pal, M., Yirgalem, M., Anberber, M., Giro, B., Dasguta, R. 2015). The harmful gases inhaled with contaminated air are believed to affect animals in the same manner as humans, leading to organ damage in the long run (Pal, M., Yirgalem, M., Anberber, M., Giro, B., Dasguta, R. 2015). This is a problem that affects farm animals and pets alike, causing disease such as acute bronchiolitis, emphysema, and heart failure (Pal, M., Yirgalem, M., Anberber, M., Giro, B., Dasguta, R. 2015).

REGULATIONS

In 2015, the government of South Korea (ROK) signed the Paris Agreement, joining many other nations. The Paris Agreement aims to reduce greenhouse gas emissions by 37% below BAU emissions by 2030. Because compliance with the Paris Agreement ensures that roughly a million lives would be saved annually by 2050 purely as a result of reductions in air pollution, it has revealed itself to be one of the most critical aspects of South Korean regulation concerning air pollution (World Health Organization, How Air, 2019).

South Korea did not get off to a good start after signing the Paris Agreement – in the very next year, 2016, the non-governmental agency Climate Tracker found that the ROK increased emissions per capita and labeled the country's efforts as "inadequate" (Mattheson, 2016). The figure below shows the grey circles, which are the 2020 targets, with actual

emissions much higher than the progress goal designated by the Paris Agreement.

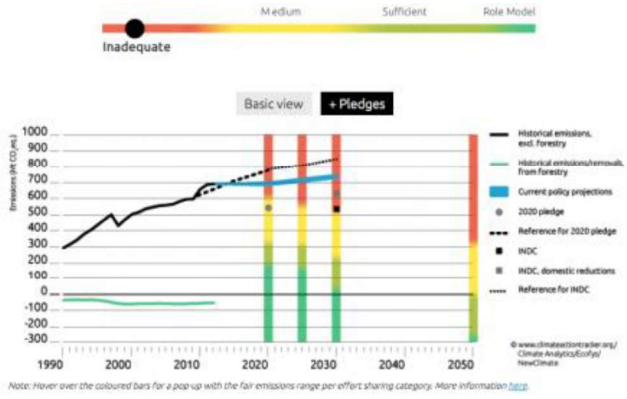

Figure 1. South Korea increased emissions in 2016 after signing the Paris Agreement (Mattheson, 2016)

The Ministry of Environment oversees South Korea's regulations concerning pollution monitoring and prevention, working with the National Legislature to enact policies that are designed to protect the environment. However, the Ministry will have a practical challenge hitting the quantitative targets of the Paris Agreement for the following reason: South Korea generates approximately 52% of its air pollution domestically, with the other half drifting over from the second-largest economy in the world - The People's Republic of China - from the West across the China Sea and from its neighbor on the Korean peninsula the Democratic People's Republic of Korea, most often referred to as North Korea (Da-sol, 2017).

According to the landmark atmospheric tests of air quality using measuring equipment provided by NASA, domestic air pollution in the RoK originates from industry, power generation, buildings and transportation vehicles (Hu, 2017). The single largest contributor to air pollution is coal-fired power plants. South Korea is home to 54 coal-fired power plants, which account for 30 percent of the country's power generation (Chung, 2019).

One of the coal-fired power plants in South Chungcheong Province is a major source of nitrogen compounds and sulfur dioxide that cause chain chemical reactions in the air, generating more fine dust and ozone (Lee, S. 2017). Therefore, the role that these power plants play in polluting the nation cannot be denied (Lee, S. 2017).

In July 2016, South Korea's Trade Minister announced that the country would aim to close down the 10 coal-fired plants by 2025, while also replacing turbines at several power plants to increase efficiency and reduce emissions (Lee, S.2017). The government also stated that existing coal-fired power plants will be more tightly regulated through tougher emissions standards (Lee, K. 2017).

To adhere to the standards presented by this agreement, the South Korean government has made a variety of attempts, including the installment of bike-sharing stations, enactment of fines on specific diesel-fueled vehicles and the discontinuation of government parking lots (Babe, 2018).

However, many of these measures have had little success. In 2019, seven major cities in South Korea suffered record high concentrations of harmful PM 2.5 particles, leading to popular backlash over current regulation (McCurry, 2019). Following this crisis, the national assembly passed a series of bills in March to provide authorities access to emergency funds for measures to mitigate these high concentrations, such as the installation of air purifiers in classrooms (McCurry, 2019). It is unclear how effective this new regulation will turn out to be.

The success of these regulations remains unclear as of the writing of this report. In all, the South Korean government can be said to take a moderately active role in placing regulations to reduce air pollution. However, based on the research we conducted for this paper, we do not believe that the implemented regulations are drastic enough to create significant changes in the number of days of poor atmospheric air quality. The government may need to take a more aggressive role in attempting to cut carbon if the nation's citizens are to see more days with blue skies than gray.

THE RELATIONSHIP WITH CHINA

China is commonly identified as the greatest cause of Korea's air pollution. However, a NASA study concluded that in reality, less than half of Korea's poor air quality can be attributed to China. The study determined that approximately 48% of pollution originated outside of the country, from the following regions - 22% from China's Shandong Province, 9% from North Korea, 7% from Beijing, 5% from Shanghai, and a combined 5% for the three regions of China's Liaoning Province, Japan and the West Sea (Sa-sol, 2017).

Experts also believe that the public blames China unfairly. "The government is sitting idly by while passing the buck to China," said Kim Shin-do, a professor of environmental engineering at the University of Seoul (Harris and Beseoung, 2017). Professor Kim's assessment of China's share of the pollution blame is 20% (Harris and Beseoung, 2017).

The results are expected to silence those who blamed China the most for Korea's bad air quality. Some people even filed a compensation suit against the Chinese government earlier this year (Kim S., 2019). South Korea must acknowledge its own prominence in the harsh air pollution of the nation, rather than assigning blame solely to its neighbors (Hu, 2017). So far, the nation seems to be taking some action to do so. The National Assembly took action in February and March of 2019, passing several bills that paved the way for a 3 trillion won (US$2.65 billion) emergency fund to tackle the problem and designated fine dust as a social disaster. A second law, the Special Act on the Reduction and Management of Fine Dust, granted the government the ability

to limit the use of vehicles, coal-fired power stations and building sites (Lee, D. 2019).

As in many democratic countries with multiple political parties, when a national crisis occurs, the issue becomes politicized. South Korean President Moon Jae-in (Democratic Party) proposed a joint project with China to use artificial rain to clean the air in his country, but the Chinese Foreign Ministry Mr. Lu responded "I wonder if the South Korean side has any basis that its smog is from China," noting that fine dust readings have been higher in Seoul than in Beijing recently. "All countries realize that the cause is very complicated" (South Korea Proposes, 2019).

The politics of the issue are growing complex. The floor leader of the conservative Liberty Korea Party, Na Kyung-won, announced a necessity for Mr. Moon to address the current levels of air pollution as a national disaster (Kim, 2019). For President Moon, the dirty air appears to be eroding his approval rating, which dropped to 44% in March 2019 from a peak of 81% in June 2017, according to data from Gallup Korea (Lee, D. 2019).

In all, the role of China in Korea's air pollution problem remains complex. While the particles blowing in from China are undeniably real, the truth remains that there is much that can be done within South Korea to mitigate its own carbon emissions. The common "man in the street" in Seoul wants to hold China responsible, as scientists have attributed roughly 50% of harmful particulate matter pollution drifting over from multiple regions of China. However, it will not be easy to craft a mutually agreeable solution with the Communist power (Choi and Chao, 2019).

The South Korean government and public must stop framing China as the sole source of blame. Rather, the nation must focus on its own internal affairs to reduce emissions. After such steps have been taken, diplomacy with China about joint-mitigation of carbon emissions may prove to be easier.

IS COAL TO BLAME FOR THE FINE DUST PARTICLE?

52% of air pollution generated domestically was created by the coal-fueled power industry, diesel cars/buses, heating homes, apartments, and office buildings, as well as diversified industrial manufacturing. According to the comprehensive report measuring CO2 emissions for all countries, South Korea ranked 9th in Fossil CO2 emissions. The top 10 nations on the list contributed 67% of the planet's CO2 gases (Crippa, et al 2017).

Nevertheless, there are many other countries in the world — especially in Europe — that produce smog and pollution because coal is the primary source of their power generation plants, and a significant percentage of workers rely on coal production and/or economically rely on its supply chain.

This is why the location of the last meeting of the UN Climate talks, Katowice, Poland, was significant: it is in the heart of the Silesia Coal region. There is significant tension between the advocates of the environment and those who want to protect the jobs that coal creates. The result of the December 2018 negotiations in Poland was a document that became known as the Paris Rulebook (Evans and Timberley, 2018).

WHAT IS IN THE PARIS RULEBOOK?

Nearly 200 countries signed the Declaration at the end of the Katowice conference, pledging to follow a 156-page rulebook for implementing the landmark Paris Agreement on climate change (Cuddy, 2018). The landmark Paris Agreement 2015 deal aims to limit global temperature rises to "well below" two degrees Celsius (Cuddy, 2018). The UN says the new Rulebook guidelines "promote trust among nations that all countries are playing their part in addressing the challenge of climate change" (Cuddy, 2018). A consensus was finally reached when ministers managed to break a deadlock between Brazil and other countries over the accounting rules for the monitoring of carbon credits, deferring much of the discussion to next year (Cuddy, 2018).

Specifically: The 256-page common rulebook, known as the Katowice Climate Change Package, is split into thematic sections. It details how countries should monitor and report their greenhouse gas emissions and the efforts they're taking to reduce them, and how they will update their emissions plans (Cuddy, 2018). Poor countries also secured assurances on getting financial support to help them cut emissions, adapt to changes, and pay for damages (Cuddy, 2018).

Guidelines in the package also explain how to conduct the "Global Stocktake" of how effective climate action has been by 2023 as well as the process for creating new goals on finance from 2025 onwardsto aid developing countries (Cuddy, 2018).

KOREA'S SUCCESS AS A NET EXPORTER OF GOODS LEADS TO INCREASED WEALTH

After the Cold War, South Korea initiated a government-backed export policy which led to great success. Since 2008, Korea has only had two quarters with a trade deficit. The trade surplus hit a high of $12BN in 2016 (Trading Economics Reference site, 2019).

The trade surplus has declined since then, but over the last 10 years, one metric of wealth, GDP per Capita, has risen sharply. In 2009, GDP per Capita was $20,843 — in 2018, it was $31,335, an increase of 50% (Trading Economics Reference site, 2019). Koreans now are ranked 28th in the world as measured by GDP per Capita wealth (Trading Economics Reference site, 2019). The data proves that Koreans' success in exporting their goods increased the economic well-being of the average citizen, who has more money to heat up their apartments and travel by buses or cars. Rising wealth per person leads to the ability to pay for the natural resources that create carbon dioxide — this is the core problem that conflicts with achieving the Paris Agreement targets.

CAR SALES IN SOUTH KOREA, 2008-2018

In 2008, Koreans bought 1.2 million cars and light trucks (Dement, 2019). Sales rose steadily and hit a peak of 1.8 million in 2015 (Dement, 2019). In the last three years, sales have fallen by less than 1%, with 1.78 million cars and light trucks sold in 2018 (Dement, 2019). Despite this recent fall in sales, it is reasonable to conclude that this drastic increase of cars on Korea's streets would have contributed to the air pollution the nation struggles with today (Dement, 2019). As the Korean car industry continues to grow, its environmental impact must be carefully examined.

Year	Units Sold in South Korea
2018	1.784.614
2017	1.761.404
2016	1.795.215
2015	1.800.984
2014	1.629.763
2013	1.511.931
2012	1.516.300
2011	1.553.062
2010	1.541.433
2009	1.439.546
2008	1.200.283

Data from (Dement 2019)

CARBON CREDITS

Several emissions-trading schemes (ETSs) have been established to reduce CO2 emissions, such as the EU ETS, California-Quebec ETS, and New Zealand ETS, among others (Choi and Qi, 2019). The ETS provides a way to reduce pollutant emissions using market measures, which is more scientific and effective than compulsory administrative measures (Choi and Qi, 2019). The main compliance tools under the carbon ETS involve directly decreasing CO2 emissions and purchasing emission allowances, and thus, power plants must be well-versed in these two measures' costs and benefits (Choi and Qi, 2019).

Korea's coal-fueled power plants have the potential to play a key role in reducing carbon emissions, as they account for 43% of the nation's electricity generation and approximately 25% of its total carbon emissions (Choi and Qi, 2019). The energy and electricity-generation sectors collectively account for 43.6% of the ETS market's total quota, and thus, the Korean ETS' effectiveness should be based on that of the coal-fueled power industry (Choi and Qi, 2019).

Korea is the 11th largest economy worldwide and consumed approximately 2.2% of the world's total primary energy in 2017, making it the eighth-largest global energy consumer. Moreover, Korea accounted for 2.3% of global coal consumption in 2017, or sixth worldwide (Choi and Qi, 2019). To shoulder more of its various responsibilities — from curtailing global carbon emissions to relieving burdens on the domestic environment — the Korean government established its "low carbon-green growth" national carbon reduction policy in 2009, then passed a law mandating decreased national CO2 emissions by 37% below BAU levels by 2030 (Choi and Qi, 2019).

The Korean government should strengthen its regulations to more effectively implement a green economy. Policymakers could impose a carbon tax; substantially decrease the carbon emissions-free quota; and provide more incentives, especially to the energy-intensive, resource-saving, coal-fueled power plants.

CONCLUSION

This paper highlighted a conundrum that South Korea faces. The success of the government-backed economic programs, which emphasized investments in manufacturing export goods, was successful in creating a positive balance of trade, which accrued to the average worker as measured by significant increases in the per capita GDP. Companies that are selling goods at a profit want to produce more, which leads to an increase in industry-related air pollution. Workers with higher wages can afford to keep the heat on in their residences, which leads to an increase in CO2 emissions. And a stronger economy means more cars and trucks on the road, which also leads to an increase in air pollution.

In 2019, only four years after the signing of the Paris Agreement, South Korea experienced a "national emergency" because of persistent air pollution. The National Legislature took action in the Spring, but it's too early to judge the policy effectively. It is hard for observers who have studied the issue of South Korea to be optimistic at this time that the country can reduce its CO2 emissions by 37% in 11 years.

In a decade in which climate change is receiving more attention than ever, days with gray skies and complacent mask-wearing cannot become the norm. Students stuck inside and unable to play for fear of harmful particles in the air should not be normalized. Rather, one should feel safe on any day, when performing the most fundamentally human act of breathing. Students should be able to walk under a bright blue sky in a clean atmosphere without worrying about the air quality, worrying instead about friends or tests or what to eat for dinner. This is the future South Korea must envision.

REFERENCES

[1] Babe, A. (2018). High Flying Ideas? Betting on Technology, the South Korean Capital Deploys Drones to Fight Smog. US News and World Reports, Retrieved from https://www.usnews.com/news/world/articles/2018-08-08/seoul-turns-to-tech nologyto-battle-air-pollution

[2] Choi, Y. and Qi, C. (2019). Is South Korea's Emission Trading Scheme Effective? An Analysis Based on the Marginal Abatement Cost of Coal-Fueled Power Plants, Journal of Inha University, Incheon, Korea

[3] Chung, J. (2019, June 18). South Korea fires up on renewables, to close more coal plants, Reuters, retrieved at https://www.reuters.com/article/us-southkorea-

energyrenewable-an alysis/south-korea-fires-up-on-renewables-to-close-more-coal-plantsidUSKCN1TJ0JK
[4] Cuddy, A. (2019). What is the COP24 climate change rulebook and why do we need it? Euronews answers, EuroNews, retrieved from https://www.euronews.com/2018/12/1 6/what-is-the-climate-change-rulebookadopted-at-cop24-and-why-do-we-need-it-euronews-answer
[5] Crippa, M., Oreggioni, G., Guizzardi, D., Muntean, M., Schaff, E., Lo Vulo, E., … Vignati, E. (2017, October 30). Fossil CO2 and GHG emissions of all world countries, 2019 report. Retrieved from https://edgar.jrc.ec.europa.eu/overview.php?v=booklet2019
[6] Da-sol, K. (2017, July 19). Half of fine dust from Korean sources: study, The Korea Herald, retrieved from http://www.koreaherald.com/view.php?ud=20170719000994
[7] Demant, Bart, CarSalesBase.com Blog, 2019, retrieved at http://carsalesbase.com/totalmarket-sales-country/south-korea-car-sales-data/
[8] Evans, S and Timberley, J. (2018, December 18). COP24: Key outcomes agreed at the UN climate talks in Katowice, Carbon Brief, retrieved at https://www.carbonbrief.org/cop24-keyoutcomes-agreed-at-the-un-clima te-talks-inkatowice
[9] Ferreira, J. (2019) South Korea Balance of Trade, Trading Economics, Retrieved at https://tradingeconomics.com/south-korea/balance-of-trade
[10] Goldberg, N. and Tracy, T. (2018, September 10). So many deaths from 9/11-related illnesses, victims' fund may run out of money, originally published in The Daily News (New York), retrieved on https://www.seattletimes.com/nation-world/so-manydeaths-from-9- 11-related-illnesses-victims-fund-may-run-out-of-money/
[11] Haas, B. (2018, May 15). South Koreans more worried about air pollution than Kim's nukes, The Guardian, retrieved at https://www.theguardian.com/world/2018/may/16/south-koreans-m ore-worriedabout-air-pollution-than-kims-nukes
[12] Harris, B. and Buseong, K. (2017, March 29). South Korea joins ranks of world's most Polluted countries, Financial Times, retrieved from https://www.ft.com/content/b49a9878-141b11e7-80f4-13e067d5072c
[13] Herbst, D. (2019, July 4). 'People Dropping Like Flies': Meet the 9/11 First Responders Now Fighting for Their Own Lives. Retrieved from https://people.com/politics/911-respond er-deaths-fight-congress-victims-compensation-fund/
[14] Hu, E. (2017). Armed With NASA Data, South Korea Confronts Its Choking Smog, National Public Radio, retrieved at https://www.npr.org/sections/parallels/2017/10/1 0/552264719/armed-with-nasa-datasouth-korea-confronts-its-choking-smog
[15] Kim, J. (2019, April 2). 'Killer dust' pollutes South Korea's relations with China, Nikkei Asian Review, retrieved at https://asia.nikkei.com/Spotlight/Asia Insight/Killer-dust-pollutes-South-Korea-s-relations-with-China
[16] Kim, S. (2017, July 19). 52% of fine dust generated in Korea, Korea Times, retrieved at http://koreatimes.co.kr/www/common/printpreviews.asp?categoryCode=371&newsId x=233295
[17] Kim, T. (2019, March 6). S. Korea proposes rain project with China to clean Seoul air. Retrieved from https://abcnews.go.com/Technology/wireStory/south-korea-proposes-clear-air-project-china-61495218
[18] Lee, D. (2019, March 15). China is to blame for South Korea's air pollution. Really?, South China Morning Post, retrieved from https://www.scmp.com/weekasia/healthenvironment/article/3001741/china-blame-south-koreas-air-pollution-really
[19] Lee, J.T., Kim, H., Song, H., Hong, Y.C., Cho, Y.S., Shin, S.Y., Kim, Y.S. (2002). Air Pollution and Asthma Among Children in Seoul, Korea. Epidemiology, 13(4), 481 484. Retrieved from https://journals.lww.com/epidem/Fulltext/2002/07000/Air_Pollutio n_and_Asthma_Among_Children_ in_Seoul,18.aspx
[20] Mathiesen, K. (2016, November 4). South Korea Leads List of 2016 Climate Villains. Retrieved from https://www.climatechangenews.com/2016/11/04/south_korea_climate_villains/
[21] McCurry, J. (2019, March 13). 'Social disaster': South Korea brings in emergency laws to tackle dust pollution, The Guardian, retrieved at https://www.theguardian.com/environment/2019/mar/13/social-disaster-south-koreabrings-in-emergency-laws-to-tackle-dust-pollution
[22] Nam, S. (2019, April 3). Air pollution causes 17,000 deaths in S. Korea in 2017: study. Retrieved from https://en.yna.co.kr/view/AEN20190404010800315
[23] Nunez, C. (2019). Air pollution, explained, National Geographic, retrieved at https://www.nationalgeographic.com/environment/global-warming/pollution/
[24] Pal, M., Yirgalem, M., Anberber, M., Giro, B., Dasguta, R. (2015). Impact of Environmental Pollution on Animal Health, Journal of Natural History, Vol. 11, No 1, retrieved at https://www.researchgate.net/publication/327871070_Impact_of_environmental_poll ution_on_animal_health
[25] Schwartz, Joel (2004). Air Pollution and Children's Health, American Association of Pediatrics, 2004, retrieved at https://pediatrics.aappublications.org/content/113/Supplement_3 /1037.short
[26] Selin, N. (2010, May 25). Carbon Footprint. Retrieved from https://www.britannica.com/scien ce/carbon-footprint
[27] South Korea proposes artificial rain project to combat Seoul air pollution. (2019, March 6). Retrieved from https://www.telegraph.co.uk/news/2019/03/06/south-korea-proposes -artificial-rain-project-combat-seoul-air/

The Impact of COVID-19 Pandemic on Hong Kong's Domestic Helpers

Yongjae Lee
Hong Kong International School; Hong Kong, Hong Kong
Email: lee.yongjae.0306@gmail.com

Abstract – January 23rd, 2020, the first case of COVID-19 was confirmed in Hong Kong. By March 2020, more than 130,000 citizens were unemployed, which is an increase of over 12,000 from the previous month. This is a 9-year record high for Hong Kong's unemployment rate. The current situation in Hong Kong is putting much pressure on its citizens, but it brings even more pressure to the domestic helpers living in Hong Kong. They are migrant workers looking to be employed by local households to work as live-in maids. These "helpers" make up about 10% of Hong Kong's working population, and are easily the most detrimentally affected by this pandemic—both financially and mentally. However, the Hong Kong government has not done an adequate job alleviating the stress for these domestic workers, which makes it harder for them to survive this pandemic. This paper aims to study the socioeconomic impact of this pandemic on migrant workers in Hong Kong, specifically the domestic helpers. It will also explore some of the key issues that these workers face, and suggest the ways that the local government can alleviate those problems.

Key Words – COVID-19, Hong Kong, Domestic Helpers, Migrant Workers

INTRODUCTION

January 23rd, 2020, the first case of COVID-19 was confirmed in Hong Kong. Hong Kong was one of the first countries to be hit by this global pandemic. By March 2020, more than 130,000 citizens were unemployed, which is an increase of over 12,000 from the previous month. This is a 9-year record high for Hong Kong's unemployment rate, and its financial secretary, Paul Chan, predicts that it will likely increase [6].

The current situation in Hong Kong is putting much pressure on its citizens, but it brings even more pressure to the domestic helpers living in Hong Kong. The 400,000 domestic helpers are composed of 45% Indonesian and 44% Filipino women [23]. They come to Hong Kong looking to be employed by local households to work as live-in maids. These "helpers" make up about 10% of Hong Kong's working population [7], and are easily the most detrimentally affected by this pandemic.

SOCIOECONOMIC BACKGROUND

Helpers are an essential part of the Hong Kong lifestyle, as they fulfill many different roles for their employers. Depending on the household, they take care of the elderly or the children: they take the children to school, feed them, wash their clothes, spend time with them, and more. Although these helpers make up an integral part of Hong Kong's society and culture, they are not allowed to be a permanent resident of Hong Kong. This can bring many disadvantages, especially during a global pandemic. Unsurprisingly, the current situation in Hong Kong has made the lives of most domestic helpers worse—both financially and mentally.

The majority of domestic helpers in Hong Kong come to this city to support the big family they have back home. These helpers are aware that working in Hong Kong is a greater advantage for them, since if they worked in the Philippines, their minimum wage for working as a domestic helper would be around 800 HKD [19]. Whereas, if they were to work in Hong Kong, their minimum wage would be around 4,185 HKD. That is why so many Filipino women choose to work in Hong Kong, and send their money to their families back home. These helpers mostly get into Hong Kong through employment agencies, who can set them up with employers and give them basic training as a helper. These agencies help the women learn how to cook, speak English, do the laundry, and take care of different family members [9].

Domestic helpers are the backbone to the economy of Hong Kong. A study done by ENRICH, a charity promoting the economic empowerment of migrant domestic workers, and Experian, a global information services company, concluded that these migrant helpers had contributed about 12.6 billion USD to Hong Kong's GDP. However, this figure does not include the indirect impact these domestic helpers have had on Hong Kong's economy. The estimated true value of the work these helpers do for their employers amount up to 71.2 billion USD. Furthermore, helpers free up significant time for their employers, who, in turn, contribute up to 20.1 billion USD to Hong Kong's economy during those freed up time [7]. This means that, without these helpers, Hong Kong's economy and GDP would be at a much lesser value.

Domestic helpers have a significant impact on the women of Hong Kong, and their representation in the economy. By taking care of the children and the elderly of the household, the domestic helpers make it possible for many mothers to have their own careers. According to Lucinda

Pike, the director of ENRICH, "the dual income individual families are able to access has significant knock-on effects, and allows them to attain a higher socioeconomic status [15]." Thanks to the helpers, 110,000 mothers were able to rejoin the workforce in 2018, as they had their helper at home, looking after their children [7].

Helpers are also the backbone of the economy back in their home countries. The Philippines and Indonesia are especially reliant on helpers working in Hong Kong, because they, on average, send around 50-60% of their salary back to their home countries and support about 4 to 5 people in their households [8]. In 2018, around 33.7 billion USD were sent from overseas workers to the Philippines, and around 3% of the money was from domestic workers [7]. By sending much of their income back home, helpers are actually raising the GDP of their home countries, as the money they send over will be spent on goods and services in their country. Furthermore, they improve their household's socioeconomic status in their home country: within 4 years of working in Hong Kong, helpers double the income of their households in the Philippines and Indonesia [7]. The employability of the helpers' family members and people they interact closely with increases as well, as helpers learn new skills from their years abroad. These helpers acquire many new skills in Hong Kong: cooking, personal finance, communications, and other life skills. By sharing these newly acquired skills, helpers make their own communities more educated [7]. Clearly, these domestic helpers play important roles in both economic and social development of their communities.

HARDSHIPS HELPERS FACE

Surprisingly, when these domestic helpers first arrive in Hong Kong, many are already in debt. This is because domestic workers bear a large financial cost, around 1,135 USD, to get a job placement in Hong Kong, as they have to pay Filipino agencies for the transfer, and to become a worker in Hong Kong. These employment agencies also force domestic workers to undergo unnecessary training in order to increase their profits. The most surprising fact is that Filipino employment agencies are actually prohibited from charging placement fees [21]. Although most employment agencies charge workers a sizable illegal fee for the placement service, the helpers cannot really do anything about this, as there are plenty of helpers who are willing to go through this illegal process. And because most would-be helpers do not have enough money to pay this fee, the agencies connect them to lending companies. These companies give out loans in the Philippines, and collect the payments from Hong Kong. But the interest rate on these loans can get as high as 60% [18]. Many helpers get paid around 4600 HKD a month, just above the minimum wage of 4310 HKD. This means it takes them around 6 months just to pay this loan off [16]. However, if they were to switch employers in the middle of the 6 months paying period, the helpers would actually need to take out more loans, as they would have to pay more to the agencies for their transfer. Although this is a completely illegal practice, it has been normalized in Hong Kong. The legally permitted placement fee employment agencies in Hong Kong can charge is 10% of their first month's salary. However, the average loan that helpers have to pay back is around 11,321 HKD or 1,459 USD, which is 25 times greater than the legally permitted amount [21].

Even after the job payment the helpers also have to worry about unexpected expenses, as they remit around 2,119 HKD, or 46% of their monthly salary, to support around 3.6 individuals, which not only include their immediate family members but also their extended family members, such as uncle and aunts. Often, these remittances are used to invest in projects that the domestic helper's family has started, such as a small company or a shop [16]. Although the helpers remit much of their salary back home to fund these projects, their families also rely on these helpers to pay for worst case scenarios, whether it be a natural disaster or family emergency. Therefore, many helpers are forced to take out loans to help out their families [16]. These women are often the primary breadwinner of the family, and they are pressured to send money back to their home country, even when they do not have enough money for themselves [16].

Unfortunately, around 36% of these helpers lack understanding in personal finance, so they routinely finance their investments through loans rather than their savings, which swallows these domestic helpers into further debt [7]. Around 46% reported in a survey that they had outstanding loans from a lender in Hong Kong, and pay around 60% of their salary in loan installments each month. 80% of these loans were taken out from money lending companies, which, on average, give out loans at 12 month duration of 25% per annum [16].

THE IMPACT OF COVID19 ON HELPERS

With the COVID-19 pandemic, the situation for helpers has gotten much worse—especially their habit of loaning from predatory loan sharks. Because of COVID-19, Hong Kong's domestic workers were pushed into debt traps: as many families of the helpers had no income while being under lockdown in their home countries, most helpers were forced to borrow more money so that their families could stay afloat. This means that they are actually loaning much more than they can afford to, and after this pandemic, they would have to keep working to pay off the debts that they have incurred. However, the money lending companies are not taking their situations into account, and are demanding their money back: one helper even stated, "They send me more and more messages each day, I hope they understand the situation [4]."

With the start of the pandemic and quarantine, many helpers were immediately faced with hardships. The pandemic offered around 60% of Hong Kong workers to work from home as a result of the pandemic [10]. This means that the helpers are pressured to do more work, as they have more chores to tend to the family members who are now spending more time at home. A survey found that around half

of the helpers in Hong Kong actually had increased workload since the pandemic has started [22]. Not only do the helpers have more work to do, but they also do not get to rest. Normally, during the weekends and holidays, the helpers would go to Admiral or Central and spend time with their friends on makeshift cardboard carpets. They would chat, play games, eat food, and just relax. However, this weekly ritual has been taken away from them due to the pandemic, as residents of Hong Kong could only meet with 2 people, and were strongly recommended to stay inside.

For helpers who are living in the homes of their employers, their rest days do not feel like rest days, as they now have to "rest" in the same house as their employers, making it difficult for them to even relax. It is estimated that around 40% of helpers actually never left their residence since the pandemic has hit [22]. Many of them were strongly urged by their employers not to go outside, which the helpers themselves thought was too dangerous. Unfortunately, being confined to the same space with their employers for so long, with no way to truly relax, has only increased their stress. Sheila Tebia-Bonifacio, the chairwoman of Gabriela Hong Kong, an organisation that supports Filipinos in Hong Kong, has raised concerns about domestic helpers not getting an appropriate living space in their working household. Research done by an NGO found that 3 out of 5 domestic workers in Hong Kong either endure alternative accommodation arrangements or their designated bedroom serves other multiple functions in the household [22]. Tibia-Bonifacio stated that helpers should be allowed to go out of their employers' homes on rest days or risk exhaustion. However, during this pandemic, many were mistreated, as around 20% of helpers did not receive their rest day, and one helper even claimed that she has not had a rest day for 9 weeks [22].

IMPACT OF COVID19 ON EMPLOYMENT STATUS

To make matters worse, some helpers were fired during this pandemic. There are different reasons why the helpers were fired during this pandemic: ranging from arguments over the time helpers were allowed to spend outside the house on their days off, to employers claiming they had lost their jobs or were leaving the city [2], as Hong Kong's unemployment hit a nine-year high in February with 3.7% of the workforce unemployed [6]. Whatever the case, more helpers are getting fired. For example, just between February 9th and March 25th, the Philippine Consul General Raly Tejada reported that the consulate had assisted 70 displaced Filipino workers, 93% of whom were affected due to the relocation of their employers [24].

Getting fired is a horrible ordeal for many helpers, as they only have 2 weeks, according to the law, to either find a new job or go back to their home countries [13]). This 2 week rule, even without the restrictive conditions of a pandemic, is absurd. This is clear as even the immigration department of Hong Kong acknowledged in a letter to Amnesty International that processing an application for a change of employer takes "about 4-6 weeks" once all necessary documents are received. This basically forces many workers to leave the territory until the government approves their paperwork [1]. Even if the helpers apply for a visa extension (costing 160HKD per fortnight), the helpers cannot work while they are waiting. Meanwhile, they have to pay for food and shelter, which would put them in debt. This explains why word of mouth from employer to employer is so important to the helpers: as it is virtually impossible to get a new employer through the government, their next employment can only be found through their current employer. This also is why it is very hard for helpers to file a complaint against their employers, as this would ruin their reputation and relationship with their employer, which in turn makes it extremely difficult for the helpers to find new jobs. And even if the helpers decided to seek justice through a labour tribunal case, it takes at least 2 months to get a case processed, which means that it is extremely difficult for helpers to seek justice [1].

Nevertheless, many helpers were usually not affected by this 2 week rule, as it is required by law for their employers to give a month's notice before terminating any contract, giving them enough time to either look for a plane ticket back home or find new employers [11]. However, because of the pandemic, many helpers were fired due to sudden relocation of their employers: 93% of helpers who were fired between February and March were fired because of the relocation of their employers [24]. This means that it was difficult for the employers to give the legally-mandated one month's notice. Without this buffer period, it's almost impossible for the fired helpers to find new jobs, as they are only allowed to stay in Hong Kong for 2 weeks, which is not enough time to find a new employer or get their visa extensions approved [11]. Their only option is to go back to their home country before the 2 weeks period is over, or they will be fined. But finding a plane ticket back to their home country is harder now than before, even more so if their home country is severely affected by the COVID-19 [9].

On top of these problems, helpers also have to deal with their housing situation while unemployed. They either have an option to stay at a hotel, which is too expensive, or at the housing units offered by their agencies. However, the housing units offered by the agencies are often unethically overpriced. They are 80 HKD per night, which is around 10 USD, while they have to buy all their necessities such as food, clothes, toiletries etc. This actually puts a bigger burden on them as they often have to pull money from their savings [20].

The personal stories of how the lives of domestic helpers changed after getting fired displays how discrimination is taking place in Hong Kong. Under the Disability Discrimination Ordinance, it is unlawful for employers to terminate contracts with their employees on the grounds of any disability, including infectious diseases. But unions stated they had received dozens of complaints from workers who had been fired after falling ill [14]. An example is of an Indonesian woman named Susanti, who arrived in Hong Kong in late February, but fell ill with stomach problems

soon after starting work in March. Susanti's employer took her to a hospital, where she was tested for the coronavirus. Her test came back negative the next day, but Susanti's employer insisted she be quarantined for two weeks with no pay, then terminated her contract three days later. The employer brought Susanti back to the agency, where she loudly insulted her and called her a pig. Susanti then had to fly back to Indonesia on March 25, with only 600 HKD in cash, as it was nearly impossible for her to find a new employer in 2 weeks, with the raging COVID-19 pandemic. This is just one example of dozens of similar cases that are happening in Hong Kong [17]. They were unjustly fired, and not given the right protections and treatment either. Mission For Migrant Workers—the longest standing charity for domestic helpers—found through a survey that 11-14% of helpers had not received masks or sanitizers from employers [22].

Even though many helpers are mistreated by their employers, they are hesitant to actually lodge a complaint with the Equal Opportunities Commission. Even before the pandemic, writing a complaint about their employers resulted in a very bad reputation for the helpers and made it hard for them to get another job in Hong Kong. This is because the helpers rely heavily on word of mouth to get new jobs. So, if their relationship or reputation is ruined with their employer they cannot find a new job, meaning they would have to go back to their home countries. 80% of people surveyed by the Helpers Union in Hong Kong stated that they have faced discrimination during the pandemic, but did not know that they could even file a complaint with the EOC [14]. Furthermore, amidst the pandemic, the EOC has announced that they will ban all their online complaint forms and only allow complaints filed in person [12]. This is because they realized that their online complaint form was just too confusing for both the helpers and the EOC to deal with. However, this is worse for the helpers, as physically going to the EOC to write their complaints is more time-consuming and inconvenient. On top of that, the limited manpower present at these offices during the pandemic has been an issue as well: 21 workers reported encountering difficulties with government services, such as being unable to file grievances due to limited services at the Labour Tribunal and Labour Department [22].

Because of the immense stress that these workers face, a majority of them will feel as if they are at their wit's end. Recently, a helper actually committed suicide due to the financial and mental stress of the pandemic. In an interview, Lucinda Pike, the executive director of ENRICH, told the story of how this helper felt trapped by this pandemic, and thought that the only way to escape was through suicide. The longer these helpers stay trapped in their employers' homes, barely getting any rest, they can start to have unhealthy thoughts. This can worsen as it seems like the whole society and the government are against them, not getting any help from Hong Kong's government and getting minimal help from the governments of their home countries [20]. Pike states that "when there's a crisis, a lot of people who have low income get left behind the most." In the case of Hong Kong, that would be the domestic helpers.

RELIEF EFFORTS

Nevertheless, the Hong Kong government is not doing their best to alleviate the challenges that these helpers are facing. Domestic helpers are ineligible for permanent residency in Hong Kong, even after they have lived here for 7 years, which is the minimum someone has to stay to apply for a permanent residency [3]. This means that the helpers are also ineligible to receive the 10,000 HKD relief package that the permanent residents of Hong Kong can get. Many organizations have asked that domestic workers be included in the distribution of the relief packages, but the government refused. In response, the chairwoman of the International Migrants Alliance said, "the government keeps telling us to share the burden, to stay in the house—although that means more work for us—not to meet our friends, and keep Hong Kong safe … but there are no relief measures that include us." A helper from the Philippines said: "when it comes to relief, we are not even considered as human beings in distress. Is it because in the eyes of the government we are 'not ordinarily residing' in Hong Kong? Will the virus not ordinarily affect us? Why are we being neglected in times of crisis [3]?" This reflects the anger these helpers must feel.

In the absence of governmental assistance, non-profit organizations, like ENRICH and Mission For Migrant Workers (MFMW), have stepped in to alleviate some of the stress that these helpers are feeling. For example, ENRICH has hosted mental awareness seminars through Zoom to help alleviate the anxiety and depression that many helpers are experiencing at the moment. ENRICH has also kept its 1:1 financial counseling sessions going online. Other NGOs in Hong Kong have also distributed masks and other personal protection equipment that have become a necessity for this pandemic. Through their quick actions, these organizations provided some much-needed relief to the helpers.

The Filipino and Indonesian government also provided some relief to these domestic helpers. The two governments have been distributing masks and other personal protective equipment to their citizens in Hong Kong. The Indonesian government has also given out 200 USD relief packages and distributed around 223,320 masks to their helpers as a way to lift some of their financial burdens [24]. The two governments are trying their best to help out the domestic workers, as they play a very vital role in their economies.

LIMITATIONS

Because COVID-19 is an ongoing pandemic, not much academic research has been done on its specific impact, let alone its impact on domestic helpers of Hong Kong. This limits the number of academic sources available. However, using previous research done before the pandemic on domestic helpers and socioeconomic issues that affect them, this paper aimed to analyze the impact of the pandemic and

the helpers' response. This is also why this paper relies heavily on sources from the media, as the stories of the helpers can be useful in providing context to what is happening to the helpers of Hong Kong.

CONCLUSION

To alleviate any unnecessary pain in the most vulnerable population of Hong Kong, the government should be more involved in the issues related to domestic helpers. However, the Hong Kong government has not done an adequate job. For example, the Labour Department, between 2014 and 2015, only secured 10 convictions for overcharging. This included agencies or unlicensed operations, and were fined 1,500 HKD to 45,000 HKD which is only 193 USD to 5,800 USD [21]. Considering there are thousands of unethical agencies in Hong Kong, taking down 10 and barely fining them shows how little the government is doing at the moment. Meanwhile, due to the pandemic, helpers are forced to take out more loans, mainly from unethical agencies. The government should use more of their power to bring down these illegal agencies and money lending companies so that they cannot operate again. This will encourage the domestic workers to choose the few ethical and legal agencies and money lending companies to take out loans. Although the process for lending would take longer, it will ultimately benefit the helpers and the community in the long run, even after the pandemic.

The government can also implement new laws in favor of domestic helpers: it can extend the 2-week time period for helpers to either find a new employer or move back to their home country, and provide shelters for those in between jobs. Extending the grace period to a month or two, and providing public shelters just for this situation, can make all the difference for these domestic workers. Given the longer transition period, the Immigration Department can have time to process these helpers to other employers. It also will allow more time for helpers who have faced discrimination to prepare for Labour Tribunal cases, which will punish those who have been unfair towards their employees, and make sure the same injustice never happens again. With the government funded shelters, they would have less financial stress. It'll also ensure that their shelters are free and clean, as most existing shelters in the city are run by churches and nonprofit groups that lack financial support [3].

The Hong Kong government should also provide private spaces for these helpers to rest on their days off, while socially distancing and abiding by the appropriate laws. To ensure that the helpers abide by the social distancing rules, the Hong Kong government can regulate the admitting process. This can be done as it is currently done in shopping malls, where hundreds of people wearing masks are together in confined places. The helpers would enter these facilities with their temperature checked, and then they would be divided in groups. The Hong Kong government can also benefit from this, as they can test the helpers with higher temperatures for COVID-19.

The NGOs should also continue doing their absolute best to help the lives of these domestic helpers. With the mental health awareness seminars and 1:1 financial counseling sessions, ENRICH not only boosts the morale of the helpers, but also encourages the workers to gain a new skill set. Other NGOs, such as MFMW, have distributed personal protection products to helpers. However, the most effective way to achieve progress is for the general public to have a different mindset towards the helpers. As Eman Villaneuva, a domestic worker and spokesperson for the Asian Migrants Coordinating Body, stated, "If you want to protect your family, you should include your domestic worker.... By leaving one unprotected, you are putting all your family at risk" [5].

REFERENCES

[1] Amnesty International. Amnesty International Publications , 2014, pp. 1–9 , *Hong Kong, Submission to the Legislative Council's Panel on Constitutional Affairs on the Third Report by HKSAR under the ICESCR*.

[2] Carvalho, Raquel. "Coronavirus Fuels Rise in Hong Kong Domestic Worker Sackings." *South China Morning Post*, 1 Mar. 2020.

[3] Carvalho, Raquel. "Hong Kong Domestic Workers Seek Inclusion in Coronavirus Relief Measures." *South China Morning Post*, 9 Apr. 2020.

[4] Carvalho, Raquel. "How Covid-19 Traps Hong Kong Domestic Workers in Debt." *South China Morning Post*, 2 May 2020.

[5] Carvalho, Raquel. "'It's Chaos': Hong Kong's Domestic Workers Call for Help amid Virus Outbreak." *South China Morning Post*, 4 Feb. 2020.

[6] Cheng, Lilian. "Economic Hit from Covid-19 Worse than during Sars, Says Minister." *South China Morning Post*, 22 Mar. 2020.

[7] ENRICH, and Experian Asia Pacific. Experian , 2019, pp. 1–29 , *THE VALUE OF CARE. Key Contributions of Migrant Domestic Workers to Economic Growth and Family Well-Being in Asia*.

[8] Fair Employment Agency. "Handling Domestic Helper Debt Problems in Hiring and Managing." *Fair Employment Agency*, 1 June 2020.

[9] Fair Employment Agency. "Updates Related to COVID-19 & Domestic Helpers Processing." *Fair Employment Agency*, 20 Aug. 2020.

[10] FastLane Team. "Infographic: Work From Home Hong Kong Survey COVID-19." *FastLane*, 11 May 2020.

[11] HelperChoice. "Domestic Helper Contract Termination" *HelperChoice,* n.d.

[12] Hong Kong. Equal Opportunities Commission. *Refinement of channels for enquiries and complaints with effect from 28 September 2020.* Equal Opportunities Commission, 12 August 2020.

[13] Hong Kong Overseas Filippino Workers, "Understanding The 2-Week Rule for Workers in Hong Kong." Edited by Hong Kong OFW, *Hong Kong OFW*, Hong Kong OFW , 18 Dec. 2018.

[14] Idwfed, IDWFED. "Hong Kong: FADWU Survey on Disability Discrimination Ordinance." *International Domestic Workers Federation*, 22 July 2020, Lai, Greta. "How Covid-19 Will Affect Hong Kong's Migration Dynamics." *South China Morning Post*, 12 Apr. 2020.

[15] Leung, Hillary. "Here's How Much Domestic Workers Add to Hong Kong's Economy." *Time*, Time, 6 Mar. 2019.

[16] Lim, Wooyoung, and Sujata Visaria . "The Borrowing Puzzle: Why Do Filipino Domestic Workers in Hong Kong Borrow Rather than Dissave?a." *The Borrowing Puzzle: Why Do Filipino Domestic Workers in Hong Kong Borrow Rather than Dissave?*, 30 Aug. 2019, pp. 1–30.

[17] Low , Zoe. "Dozens of Helpers Fired in Belief They Caught Covid-19, Unions Say." *South China Morning Post*, 3 Aug. 2020.

[18] Mahee. "What Do You Need to Know About Domestic Helper Loan Sharks?" *HelperChoice Blog*, 7 Oct. 2019.

[19] Philippines. National wages and Productivity Commission. *Daily Minimum Wage Rates.* National wages and Productivity Commission, 22 November 2018.

[20] Pike, Lucinda. Personal interview. 7 July 2020.

[21] PLUDWHK and Hong Kong Federation of Asian Domestic Workers. Between a Rock and a Hard Place: The Charging of Illegal Agency Fees to Filipino Domestic Workers in the Philippines and Hong Kong. 2016.

[22] "Press Release: [MFMW Service Report 2019]." *Mission for Migrant Workers*, MFMW , 25 May 2020.

[23] "[Press Statement] New Study Shows MDWs Woes On Unsuitable Accommodation, Lack Of Privacy And Insufficient Amenities." *Mission for Migrant Workers*, 10 May 2017.

[24] Westbrook, Laura. "Hong Kong's Domestic Helpers Urge Recognition of Role in Covid-19 War." *South China Morning Post*, 28 Mar. 2020.

Meth and Murder:
The Violent Success of Duterte's War on Drugs

Yongjun Lee
Chadwick International School; Seoul, South Korea
Email: ylee2021@chadwickschool.org

Abstract - Since his election in 2016, President of the Philippines Rodrigo Duterte has pursued violent anti-narcotic police operations, resulting in the deaths of more than 27,000 suspected drug users and dealers. Police forces have worked to conceal the bloody consequences by hiring paid killers and deliberately planting false evidence. Duterte publicly promotes his "war on drugs" as a success of his presidency, but his actions have drawn condemnation from international human rights organizations who have accused him of crimes against humanity. However, Duterte's supporters argue that the crackdown is necessary to combat rampant drug-related crime in the Philippines, with 82% of Filipinos satisfied with the war on drugs due to "a perception of less drugs and crime in the country". Political opponents and investigative journalists claim that Duterte's war on drugs constitutes a systematic policy of brutality and repression; supporters see it as an effective anticrime measure. This paper will examine the current state of the Filipino anti-drug effort and outline how the policy's inherent violence may or may not be justified.

Key Words - Philippines, narcotics, Duterte, violence

INTRODUCTION

I. Background

Since his election as the 16th President of the Philippines in 2016, Rodrigo Duterte has maintained, endorsed, and enacted a strict anti-narcotics policy centered around the extrajudicial murder of alleged drug users and dealers. In the last three years, the death toll of Duterte's War on Drugs has climbed to nearly 27,000 according to Human Rights Watch, with the vast majority of killings being committed by police, paramilitary officers, and vigilantes outside the course of regular judicial proceedings. With only three policemen having been convicted of murder since Duterte's election, international observers have concluded that the Philippine National Police (PNP) have been granted near-absolute impunity from prosecution (Gutierrez, 2018). Far from denying the violence, Duterte has embraced it: in one memorable press conference, he equated his policy with the Holocaust, claiming that "Hitler massacred three million Jews (sic). Now, there are three million drug addicts. I'd be happy to slaughter them. If Germany had Hitler, the Philippines would have (me)." In short, his message has always been succinct and clear; he will "order the police to find those people [using drugs] and kill them" ("License to Kill", 2017).

II. Past Policies: Duterte in Davao

Examining Duterte's rise to prominence provides insight into the connection between the President's beliefs and his record of systematic extrajudicial killings. Duterte was elected to his first political position in 1988 as Mayor of Davao - then known as the "Murder City" of the Philippines - "on a pledge to restore law and order" (Rauhala, 2016). As the capital of the southern island of Mindanao, Davao was in a near-constant state of undeclared war between government forces, communist insurgents, drug-trafficking gangs and Muslim separatists; Duterte promised the city's residents that his tough-on-crime approach would bring peace and security to the streets (Marshall, 2016). He quickly established a reputation as a political infighter who was ready to get tough: those who visited the Mayor's Office in Davao were greeted by a gold-plated revolver on his desk "ready to use" (Peel, 2017). This strongman personality echoed itself in Duterte's rhetoric; he famously called criminals in his city "a legitimate target of assassination" (Peel, 2017) and even bragged about shooting three criminals himself during a police operation (Mogato et al., 2016).

As police enforcement in Davao increased, the city underwent a transformation; by the end of Duterte's rule in 2015, the region enjoyed an economic growth rate of 9.4% and Davao itself was named the 5th safest city in the world (Hegina, 2015). This newfound sense of order made Duterte a celebrity among residents, while his official logo - a clenched fist - found itself "emblazoned on souvenir mugs and other Duterte memorabilia" (Mogato et al., 2016).

But Davao was also the place where the brutality of Duterte's approach started to become mainstream. The so-called "Davao Death Squad", a group of armed men "on motorbikes carrying .45 handguns and butcher knives" (Rauhala, 2016) operated extensively under Duterte's oversight. More than 1,400 petty criminals, drug pushers, and even unaccompanied street children died at the hands of the Death Squad between Duterte's election as Mayor in 1988 and his ascendance to the presidency in 2015 (Marshall, 2016). Although Duterte officially denied the existence of this paramilitary arm of the municipal government, he continuously maintained that his anti-crime model was effective *because* of its often violent consequences. During a campaign speech in 2016, he took his personal outlook to the national level, telling Reuters: "if you are afraid to kill criminals, then you have no business being a president" (Mogato et al., 2016).

ELECTION AND LEGISLATION

Duterte used Davao as the foundation of his case for aggressive policing throughout his 2016 presidential campaign. Propelled by expletive-laden language and populist rhetoric, he eventually won the election as a dark horse candidate in a highly contested five-way race with 39% of the total vote (Head, 2016). The 2016 general election also yielded a clear majority for Duterte's PDP-Laban party and its allies - informally known as the "Coalition for Change" - in both houses of the Congress. Duterte's political victory was further cemented by the collapse of the opposing Liberal Party during the 2019 midterm elections, when it failed to elect a single senator to a vacant Senate seat due to a complete lack of internal cohesion (Head, 2016). This provided Duterte with unprecedented legislative power and enabled him to immediately launch the Drug War upon his formal ascension to the presidency in June 2016 (Smeallie, 2019).

I. Endorsement of Violence

Violence has been the centerpiece of Duterte's political platform: the President has consistently endorsed and even glamorized the indiscriminate use of force against small-scale drug pushers and users regularly in his campaign speeches (Hincks, 2016). During his presidential campaign, he promised that "if by chance that God will place me [on the Presidency], watch out because the 1,000 [people allegedly executed while Duterte was mayor of Davao City] will become 100,000. You will see the fish in Manila Bay getting fat" ("License to Kill", 2017). After he became president on June 4, 2016, he later issued a more sinister warning to drug dealers: "I am going to kill you. Don't take this as a joke. I'm not trying to make you laugh. Sons of bitches, I'll really kill you" (O'Connor, 2016). On September 28, 2018, he openly admitted committing the "sin of extrajudicial killings", thereby publicly implicating himself in the extrajudicial brutality for the first time (Ellis-Petersen, 2018), but continued to justify his legacy, asking "what is my fault?" Duterte's repeated invocation of violence in public distinguishes his behavior on the global stage from most other heads of nominally democratic states.

II. Scope and Scale

Aside from two month-long suspensions in 2017 when the Philippine Drug Enforcement Agency (PDEA) was put in charge, the primary enforcer of Duterte's crackdown has been the Philippine National Police (PNP) (Kine, 2017). The PNP's reporting methods document only a fraction of the killings because they fail to take into account thousands of murders committed by "unidentified individuals" often openly linked to the authorities (Coronel et al., 2019). Although the PNP has reported 5,526 extrajudicial killings committed directly by police officers during altercations with suspects, the exact number of fatalities is therefore difficult to determine due to the high number of "homicides under investigation" ("World Report", 2020). Starting in mid-2018, the PNP stopped disclosing figures in this category, at which point there were more than 23,000 such cases recorded; this brings the total death toll to roughly 27,000 as of mid-2019 when estimates were last put forward by expert studies of the Duterte administration ("They Just Kill", 2019).

METHODOLOGY OF KILLINGS

I. Vigilante Violence

A majority of the extrajudicial murders are conducted by non-police vigilantes and are classified as "homicides under investigation", enabling the PNP to justify their reduced reporting of drug-related killings. Independent investigations by both domestic and international agencies have established that such vigilantes are in fact "paid killers hired by the police or disguised police officers" ("They Just Kill", 2019). According to Human Rights Watch's assessment of police reports and witness statements, "the [armed assailants] would wear civilian clothes, often all black, and have their faces shielded by balaclava-style headgear", while "even if not visible before a shooting, special crime scene investigators would arrive within minutes" ("License to Kill", 2017). This hints that the "unknown armed persons" said to be responsible for the killings are mere agents of the police. Amnesty International was able to corroborate this theory from interviews conducted with former police officers ("They Just Kill", 2019); BBC provided further corroboration through an exclusive interview with contract killers hired by the police to kill alleged drug offenders (Gabuco, 2016). The latter source also revealed that many vigilantes are simply lower economic-status locals initially attracted to the valuable commissions who often later find themselves unable to leave the team once they are involved due to the threat of assassination (Gabuco, 2016).

II. Buy-Bust Narrative

The PNP has attempted to further conceal its role in the extrajudicial killings by providing a so-called "buy-bust" rationale, which claims that plain-clothed police officers launched sting operations targeting local drug dealers (Hincks, 2016). Once the targets were aware that they were interacting with the police, they supposedly attacked them (according to the PNP), forcing the police operatives to retaliate and kill the suspects. The alleged claim of "nanlaban" (fighting back) has been applied nearly unconditionally throughout reports on use of force by the PNP; in 14 of the 17 Bulacan police reports it examined, the Amnesty International report found that police had cited undercover operations with drug dealers followed by self-defence due to "nanlaban" to justify the death of the subject (They Just Kill, 2019).

However, detailed investigations of the "buy-bust" narrative reveals that the accounts of events told by local civilians are completely at odds with the police reports. Widespread outrage resulted when surveillance footage confirmed that seventeen-year-old Kian delos Santos had not been killed while "fighting it out" with the police as described by internal PNP reports; instead, "police officers had dragged him to a cul-de-sac, handed him a handgun and shot him as he had turned to run away" (Smeallie, 2019). Senior officers within the PNP acknowledged that many other deaths were similarly orchestrated as "planned executions" conducted in deliberately created security blind spots (Mogato et al., 2017). Contrary to the usual pre-arranged nature of sting operations, policemen also often barged into the homes of suspects and family members and physically subdued them without prior warning (Coronel et al., 2019).

III. Police Reliability

Even in cases where forensic evidence is not available, the PNP's version of events have markedly lacked credibility in comparison to the testimony of witnesses and family members. One of the most telling characteristics of the police reports is the formulaic nature of their observations, "differing little besides the names, places, and dates" ("License to Kill", 2017) in a "template nanlaban" pattern ("They Just Kill", 2019). This sentiment was also echoed by Dr. Raquel Fortun, a forensic pathologist at the University of the Philippines, who observed multiple gunshot wounds far beyond the level of disabling an assailant during over a dozen independent autopsies of victims. Furthermore, an even more troubling trend is the falsification of evidence by police; several former officers have admitted to routinely planting guns and drug packets at crime scenes to create the impression of armed resistance (Mogato et al., 2017).

POLITICAL SILENCING OF CRITICS

Another distinct feature of Duterte's presidency is his invocation of political force as a means to silence his domestic critics. Duterte's political domination has allowed him to retaliate against vocal opponents without fear of backlash, starting in June 2016 with Leila de Lima, one of the few remaining Liberal Party senators who led an investigation to determine the extent to which the executive branch was responsible for the deaths of Filipino citizens. Lima became the target of a concerted "character assassination" effort by Duterte's Senate allies, in which she was accused of drug trafficking and eventually subjected to a congressional inquiry (Macaraeg, 2019). Lima was arrested in February 2017 and still remains imprisoned, awaiting trial as of April 2020. She continues to denounce Duterte, calling the President "a coward...he hates me, but I never thought he would have me jailed. He made an example out of me." (Santos, 2020).

After de Lima's arrest on questionable charges, Duterte revoked the amnesty of Liberal Party Senator Antonio Trillanes IV, immediately arresting him and forcing him to remain on the Senate premises. Trillanes had previously been pardoned in 2011 by former president Benigno Aquino III for his involvement in a 2007 military rebellion, and the move was widely seen as Duterte's exploitation of a political technicality to eliminate one of his most outspoken critics (Villamor, 2018). In November 2019, the Makati Regional court upheld Duterte's official Proclamation No. 572 to this effect, paving the way for Trillanes' future indictment or even imprisonment (ABS-CBN, 2019).

With de Lima and Trillanes removed, Duterte was then able to turn his attention to Vice President Maria Leonor ("Leni") Robredo, who was elected vice president as a member of the Liberal Party during the separate vice presidential election of 2016. On October 31, 2019, Duterte appointed her co-chairman of the Inter-Agency Committee on Anti-Illegal Drugs (ICAD), effectively putting Robredo in charge of the war on drugs (Valente, 2019). However, after Robredo made public calls to "revamp" Operation Double Barrel and its Oplan Tokhang policy in order to "hold those responsible to account" for "senseless killings", Duterte immediately removed her from the position on November 24, "accusing Robredo of embarrassing the country by trying to draw undue international attention to his War on Drugs" (Lema, 2019). Subsequently, the PNP launched a separate sedition case accusing Robredo, de Lima, Trillanes and their colleagues for attempting to destabilize the nation by "spreading lies against the President" (Damicog, 2020).

INTERNATIONAL RESPONSE

I. Human Rights Defenders

Duterte's "complete disregard for human rights" ("License to Kill", 2017) has been the subject of close scrutiny by global human rights organizations, including Human Rights Watch and Amnesty International. Both organizations conducted independent investigations into Duterte's drug enforcement tactics in 2017 amid the growing violence, and found evidence directly connecting the extrajudicial killings to the President himself. Both organizations found that "Duterte's outspoken endorsement of the campaign implicates him...in command responsibility for crimes against humanity". Both recommended that the United Nations and international governance institutions take immediate measures to prevent more egregious human rights violations in the Philippines ("License to Kill", 2017).

The international scrutiny culminated during the 41st session of the United Nations Human Rights Council on July 5th, 2019, when the "promotion and protection of human rights in the Philippines" was discussed (UNHRC, 2019). During the debate, member nations led by Iceland drafted Resolution 41/20, which "urged the Government of the Philippines...to prevent extrajudicial killings... in accordance with international norms and standards" (UNHRC, 2019). The resolution also "expressed concern" regarding "the

allegations of human rights violations in the Philippines, particularly those involving killings...arbitrary arrest and detention, the intimidation and persecution of or violence against….members of the political opposition" (UNHRC, 2019). In order to combat these violations, the resolution called for the Philippines to comply with an independent investigation by the High Commissioner for Human Rights. Despite fierce resistance from the Philippine delegation led by Evan Garcia, the resolution was adopted by a narrow vote of 18-14 (van Sant, 2019), which immediately triggered retaliatory measures by the Duterte administration whereby state companies and agencies were effectively barred from continuing business with nations who had supported the resolution (Lema, 2019). However, the unilateral boycott was lifted on March 4, 2020 seemingly without any substantial economic impact; whether this constitutes a partial withdrawal of Duterte's ongoing feud with the international community remains to be seen (Santos, 2020).

II. International Court of Justice

Duterte's ruthless pursuit of his drug eradication policies also drew the attention of the International Criminal Court (ICC), and its prosecutor, Fatou Bensouda. On February 8, 2018, Bensouda began a "preliminary examination" into the Duterte administration with regard to crimes against humanity and the President's "fostering [of] an environment of impunity and violence" (Office of the Prosecutor, 2018).

Although Bensouda noted that a preliminary examination was not an "investigation" but rather a "process of examining the information...on whether there is a reasonable basis to proceed", there was significant backlash from the Government of the Philippines regarding the opening of the ICC inquiry (Lema, 2019). In an official statement published by Duterte on March 13, 2018, the Government asserted that the police killings did not constitute crimes against humanity because they were "a direct result of a lawful exercise of a police duty" (Duterte, 2018). The same statement also declared that the Philippines would immediately withdraw from the Rome Statute upon which the ICC was founded, citing "international bias and refusal...to support the Philippines' legitimate efforts at…. independence from foreign influence and control." After the one-year delay period integrated into the Statute, the withdrawal was officially recognized on March 16, 2019, leaving "any future international crimes committed in the Philippines…..outside of the court's jurisdiction" (Singh, 2019).

However, the withdrawal has no effect on the Court's jurisdiction regarding crimes committed during the period in which the Philippines was a member; therefore, Bensouda continued her investigation into crimes committed between July 1, 2016 (the official beginning of Operation Double Barrel) and March 16, 2019. In December 2019, in her annual report of all preliminary examination activities, Bensouda remarked upon Duterte's standard *modus operandi* of "encouraging the killing of petty criminals" while "purportedly fighting crime and drug use". Bensouda concluded that the investigation had "significantly advanced" and has since stated she would "aim to finalize the preliminary examination" by 2020 in lieu of seeking authorization for further investigation. Shortly after the publication of Bensouda's report, Duterte asserted that he would refuse to comply with her inspection, telling reporters that he would "never, never, never answer any question coming from [the ICC]. It's bullshit to me. I am only responsible to the Filipino. Filipinos will judge" (Petty et al., 2019).

ASSESSMENT

I. Possible Justifications

Despite the widespread international condemnation and domestic backlash to Duterte's narcotics crackdown, his supporters insist that a stronger anti-drug policy is necessary to combat the illicit drug trade that has plagued Filipinos for decades. As early as 2004, illegal drug abuse had "reached epidemic proportions and [became] one of the top priorities on the government's agenda" (Hembra, 2004). More specifically, most Filipino dealers were involved in the trade of methamphetamine hydrochloride ("meth"), known as "shabu" in the Philippines; over 96% of all drug rehabilitation patients in the Philippines had been hospitalized due to shabu use (Dangerous Drugs Board, 2019). The Dangerous Drugs Board's 2015 Nationwide Survey on the Nature and Extent of Drug Abuse yielded an approximate total of 1.8 million current users, or 1.8% of the entire population of the Philippines, the highest rate of shabu use per capita in East Asia (Gavilan, 2016).The latter was acknowledged even by the Catholic Bishops' Conference of the Philippines in a July 2015 pastoral letter which described shabu being sold in a "daringly ubiquitous [manner], oftentimes peddled openly in parks, bars, and street corners." (Ranada, 2016). These observations seem to indicate that drastic and proactive policing strategies are needed to combat violent drug-related crimes, hence leading many to justify Duterte's hardhanded policy as a desperate measure in desperate times.

II. Public Approval

The strong condemnation from international critics also sharply contrasts with Filipino public opinion polls that reflect overwhelmingly positive reactions to what citizens perceive as an unprecedented stand against endemic drug-related crime in the Philippines. According to Social Weather Stations (SWS), an independent polling agency recognized as credible and competent by the Roper Center for Public Opinion Research of Cornell University (Ithaca, New York), a survey conducted in June 2019 found 82% satisfied with the War on Drugs, and 12% dissatisfied, resulting in a net rating of +70. Although this is lower than the campaign's "highest satisfaction rating in December 2016 at 'excellent' +77...net

satisfaction with the campaign has always been either 'very good' (+50 to +69) or 'excellent' (+70 and above) in all survey rounds since the beginning of the survey in September 2016" (SWS, 2019). In short, the consistent positive ratings at 70% or higher indicate widespread public support for Duterte's anti-drug policies.

It is also illuminating to investigate the rationale behind the reactions of Fillipinos to the government's approach to law and order. 40% of the participants who were satisfied with the policy answered that this was because "drug suspects had lessened", followed by "drug suspects have been arrested" at 18% and "lessened crime" at 13%. Meanwhile, among the 12% who said they were dissatisfied with the War on Drugs in the June 2019 survey, the primary reason was that "drug suspects are still prevalent" (42%). The issue of "too many killings" ranked second at 31%, while "too many wrongful arrests" ranked fourth at only 9%. Notably, this is not attributable to lack of public awareness regarding the bloody nature of Duterte's crackdown; in a separate December 2019 survey by SWS, 76% of adult Filipinos "said there have been many human rights abuses in the administration's war on illegal drugs" (SWS, 2020). Thus, it is reasonable to conclude that a majority of Filipinos view the extrajudicial killings as a necessary human cost in order to combat the deeply rooted drug-related crimes in the Philippines.

III. Policy Effectiveness

The extent to which Duterte's anti-drug policy produced measurable success has been questioned by both the political opposition and PNP insiders. While de Lima and Trillanes focused on the growing death toll and human rights abuses occurring within the program, Vice President Robredo produced a scathing critique questioning the initiative's effectiveness. In her speech on January 6, 2020, concluding her short-lived term as commander of the crackdown, Robredo called the campaign a "failure" and gave it a score of "1 out of 100…[based on] authorities being able to seize only 1% of the total supply of illegal drugs in the country"; the government seized 1,344kg of shabu from January to October 2019 compared to roughly 156,000kg consumed by users across the nation (Cepeda, 2020). She attributed this to the administration's excessive "focus on street-level enforcement, going after the small-time pushers and users". Her sentiment was quickly echoed by Romeo Caramat, current head of drug enforcement at the PNP; on February 7, he told Reuters that the "shock and awe" approach had failed and that major "drug lords" and manufacturers were not being effectively targeted by police operations, leading to continued "rampant drug supply" (Allard, 2020).

CONCLUSION

This research paper has explored the Philippine Drug War from a practical policy standpoint. On one hand, the enforcers of the crackdown have exercised widespread extrajudicial violence against alleged drug dealers and pushers. Their efforts are directly connected to President Rodrigo Duterte and his allies at the highest levels of government, who have publicly authorized and orchestrated the attacks through funding and incendiary rhetoric. Despite the government's attempts to conceal the extent of the brutality through the usage of hired "vigilantes" and faulty statistics, inquiries by human rights organizations have alerted the global community of possible crimes against humanity committed by the Duterte administration.

However, Duterte's War on Drugs has also been an enormous domestic success. His embrace of overt force and controversial political techniques has allowed him to eliminate key dissidents including Vice President Leni Robredo and Senators Leila de Lima and Antonio Trillanes. Meanwhile, his pursuit of proactive police operations has mostly prevented illegal narcotics from being traded out in the open. In doing so, Duterte has answered one of the key demands of the Filipino people; his methods of curbing the rampant drug trade have been met with remarkably consistent public approval despite ongoing controversy regarding their actual effectiveness. Therefore, those who seek to enforce justice must take into account the unique internal circumstances when analyzing the human cost of Duterte's Drug War.

REFERENCES

Gutierrez, Jason. "3 Philippine Police Officers Are Convicted In a Drug War Killing." *The New York Times*, 29 Nov. 2018.

"License to Kill." *Human Rights Watch*, 13 July 2017.

Rauhala, Emily. "Before Duterte Was the Philippines' President, He Was 'The Death Squad Mayor'." *The Washington Post*, WP Company, 28 Sept. 2016.

Marshall, Andrew R.C., and Manny Mogato. "Philippine Death Squads Very Much in Business as Duterte Set for Presidency." *Reuters*, 26 May 2016.

Peel, Michael. "Drugs and Death in Davao: the Making of Rodrigo Duterte." *Financial Times*, 2 Feb. 2017.

Mogato, Manny et al. "Blood and Benefits: Duterte Imposes His Hometown Formula on the Philippines." *Reuters Investigates,* 28 Dec. 2016.

Hegina, Aries Joseph. "Davao City Improves to 5th in Ranking of World's Safest Cities." *The Philippine Daily Inquirer,* 24 June 2015.

Head, Jonathan. "Philippines Election: Maverick Rodrigo Duterte Wins Presidency." *BBC News*, 10 May 2016.

Smeallie, Allison N. "Punishing the Punisher: The Role of t he International Criminal Court in Ending Duterte's 'War on Drugs'." *Temple International and Comparative Law Journal,* vol. 33, no. 1, pg. 173, 24 May 2019.

Hincks, Joseph. “Philippines: Inside Duterte's Killer Drug War.” *Al Jazeera*, 9 Sept. 2016.

O’Connor, Ema. “The Philippines’ New President Will Give You A Medal If You Kill A Drug Dealer.” *BuzzFeed News,* 5 June 2016.

Ellis-Petersen, Hannah. “Duterte Confesses: 'My Only Sin Is the Extrajudicial Killings'.” *The Guardian*, Guardian News and Media, 28 Sept. 2018.

Kine, Phelim. “Philippines’ Duterte Reactivates Police in ‘Drug War’.” *Human Rights Watch*, 5 Dec. 2017.

Coronel, Sheila et al. “The Uncounted Dead of Duterte's Drug War.” *The Atlantic*, Atlantic Media Company, 19 Aug. 2019.

“World Report 2020: Philippines.” *Human Rights Watch*, 16 Jan. 2020.

Gabuco, Carlo. “Philippines Drugs War: The Woman Who Kills Dealers For A Living.” *BBC News*, 26 Aug. 2016.

Mogato, Manuel, and Clare Baldwin. “Special Report: Police Describe Kill Rewards, Staged Crime Scenes in Duterte's Drug War.” *Reuters*, 18 Apr. 2017.

Macaraeg, Pauline. “Premeditated Murder: The Character Assassination of Leila De Lima.” *Rappler*, 6 Dec. 2019.

Santos, Ana P. “'Those Charges Are Bulls**t': Philippines Jailed De Lima Defiant.” *Al Jazeera*, 21 Jan. 2020.

Villamor, Felipe. “Second Philippine Senator Who Defied Duterte Is Arrested.” *The New York Times*, 25 Sept. 2018.

“Court Resets Hearing on Reinstated Rebellion Rap vs Trillanes.” *ABS-CBN*, 18 Nov. 2019.

Valente, Catherine S. “Duterte Appoints Robredo to Anti-Drug Panel.” *The Manila Times*, The Manila Times Publishing Corp, 5 Nov. 2019.

Lema, Karen. “Sacked from Anti-Drugs Panel, Philippines Vice President Warns Duterte.” Edited by Simon Cameron-Moore, *Reuters*, 25 Nov. 2019.

Damicog, Jeffrey. “Resolution on VP's Sedition Case Expected out Early This Year.” *Manila Bulletin News*, 3 Jan. 2020.

United Nations Human Rights Council (UNHRC). “Promotion and Protection of Human Rights in the Philippines.” *United Nations General Assembly,* A/HRC/41/L.20, 5 July 2019.

Van Sant, Shannon. “U.N. Human Rights Council To Investigate Abuses In Philippines' Antidrug War.” *NPR*, 11 July 2019.

Lema, Karen. “Philippines' Duterte Orders Shunning of Loans, Grants from Backers of U.N. Drug War Probe.” *Reuters*, 20 Sept. 2019.

Santos, Eimor. “PH Resumes Accepting Aid from Countries That Backed UN Drug War Probe.” *CNN Philippines*, 4 Mar. 2020.

Office of the Prosecutor. “Report on Preliminary Examination Activities 2018.” *International Criminal Court*, 5 Dec. 2018.

Duterte, Rodrigo Roa. “FULL TEXT: Duterte's Statement on Int'l Criminal Court Withdrawal.” *Rappler*, 14 Mar. 2018.

Singh, Param-Preet. “Philippines Pullout From ICC Won't Block Justice for 'Drug War'.” *Human Rights Watch*, 18 Mar. 2019.

Petty, Martin, and Neil Jerome Morales. “Jail Me, Hang Me: Philippines' Duterte Says Won't Answer to ICC.” Edited by Alex Richardson, *Reuters*, 20 Dec. 2019.

Hembra, M. “Social, Political and Economic Context of Illegal Drug Abuse in the Philippines.” *National Institute on Drug Abuse*, 2004.

Gavilan, Jodesz. “DDB: Philippines Has 1.8 Million Current Drug Users.” *Rappler*, 19 Sep. 2016.

Ranada, Pia. “A Look at the State of Crime, Drugs in the Philippines.” *Rappler*, 5 Jan. 2016.

Social Weather Stations. “Second Quarter 2019 Social Weather Survey.” *Social Weather Stations*, 22 Sept. 2019.

Social Weather Stations. “Fourth Quarter 2019 Social Weather Survey.” *Social Weather Stations*, 15 Jan. 2020.

Cepeda, Mara. “'1 Over 100': Robredo Calls Duterte's Drug War a 'Failure'.” *Rappler*, 6 Jan. 2020.

Allard, Tom, and Karen Lema. “'Shock and Awe' Has Failed in Philippines Drug War, Enforcement Chief Says.” *Reuters*, Thomson Reuters, 7 Feb. 2020.

Pandemics, Surgical Masks, and Japanese Collectivism

Brayden Li-Kato
The Fessenden School; Newton, MS, United States
Email: brayden.likato06@gmail.com

ABSTRACT - This paper explores the history, effects, and responses to the 1918 influenza pandemic and the 2020 coronavirus pandemic in Japan. It argues that the mask wearing culture in Japan has resulted from collectivism in the country. Masks are not very effective in protecting yourself, but only prevent you from spreading viruses to others, and so this is for the benefit of the community and not something selfish. It draws from various sources, including academic papers, news articles, posters about pandemics, and other sources on collectivist theory. Part ethnography, the paper also draws from personal and family experience living in Japan these past few months.

Keywords - collectivism, ingroup, outgroup, pandemics, Japan, coronavirus, 1918 pandemic, COVID-19

INTRODUCTION

Background

The 1918 pandemic, also known as the Spanish Influenza, was a devastating public health crisis that infected an estimated one third of the Japanese population.[1] Of those who were infected, around 200,000 people are estimated to have died. While 200,000 is a large number, Japan's population was around 60 million people at the time, and therefore the death rate in Japan was lower than in most other countries.[2] To protect against the influenza virus, the Japanese government advised people to wear masks, to gargle, and get inoculated.[3] The pandemic ended in 1920, but people in Japan continued to follow these practices long after. One hundred years later, there is a new reason to wear surgical masks globally: the 2020 COVID-19 pandemic.

Thesis and Methods

This paper focuses on masks and why Japanese people continue to wear them. It demonstrates that wearing masks in public is an aspect of Japanese culture that stems from the country's collectivistic nature. It uses scholarly articles from the 1918 pandemic and news articles from 2020 to describe both crises and draw parallels between them. Partly an ethnography, the paper draws from my experiences living in Japan during the COVID-19 outbreak. Finally, it references scholarly writing about collectivism and individualism in Japan to argue that the practice of wearing masks has persisted after the 1918 pandemic because people care about the greater good more than individual concerns.

OVERVIEW OF THE 1918 PANDEMIC IN JAPAN

The influenza pandemic in Japan had three waves. The first wave was relatively mild, and many brushed it off as a minor influenza. However, the second and third waves were devastating, not only in Japan, but worldwide.[4] It is estimated that one third of the Japanese population was infected at one point. The flu in Japan was observed to affect young, healthy adults disproportionately, similarly other countries. However, records about mortality and morbidity rates in Japan are hard to find because they have not been preserved very well: many were destroyed in the firebombing in Japanese cities, meaning that it is hard to find reliable statistics.[5]

The Japanese government took some measures to prevent the spread of influenza. For example, a gargle was provided at some train stations for free, and people were also told to gargle after going out. Furthermore, police officers and the military were required to wear masks. The main methods used to communicate with the public about the crisis were printed leaflets and posters.[6] These posters reveal the attitude of the government during the pandemic: they posters cautioned Japanese citizens of the dangers of the flu and how they could prevent themselves from catching it. Even though these posters were a good way to spread information, and their tone was often quite urgent, overall the government did not do too much in order to prevent the spread of the pandemic. For example, for reasons that are now lost to historical archives, the Japanese government did not ask businesses to close.[7]

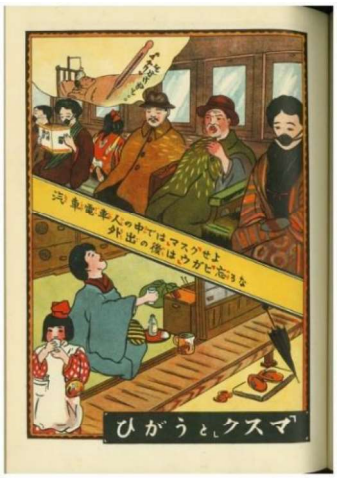

Figure 1: *'Influenza', Ministry of Home Affair, Department of Health. March 1922.*[8]
Top left: "If you don't wear a mask…"
Across the center: "Wear a mask inside the train." And "Don't forget to gargle after going out."
Bottom right: "Masks and gargling"

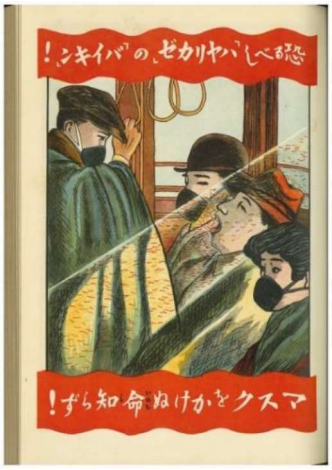

Figure 2: *'Influenza', Ministry of Home Affair, Department of Health. March 1922.*[9]
Across the top: "The contagious wind of bacteria that should be feared!"
Across the bottom: "No mask, no life!"

OVERVIEW OF THE 2020 CORONAVIRUS PANDEMIC IN JAPAN

One hundred years later, there is another major respiratory disease outbreak worldwide. The COVID-19 pandemic of today originated in Wuhan, China and the leading hypothesis is that it came from a food market where it is believed to have jumped from bats to humans.[10] It then spread to other countries, and the first large outbreak outside of China was located in South Korea. It then spread to Italy, where in late March, the country was reporting approximately 6,000 new cases per day.[11] In Japan, the first case was observed on January 16th, 2020, although the person that tested positive swiftly recovered. The man, who had just returned from Wuhan, resides in Kanazawa.[12] The country reported its first death on February 13th, when an elderly woman in her 80s died in Kanagawa prefecture.[13] Any summary of Japan during the coronavirus epidemic would be incomplete without mentioning the Diamond Princess cruise ship, which was quarantined from February 3rd to March 2nd off the coast of Yokohama.[14] Many believe that the government's efforts to stop the spread of the virus on the cruise ship were lackluster, as many passengers caught the disease while the ship was quarantined. This is most likely because people were not effectively contained, and so therefore the virus spread rapidly among those on the cruise ship.[15]

The effects of the pandemic have been felt in all aspects of life in Japan. The country experienced its first major wave of cases in April, followed by a larger second wave that came in July. According to the official Tokyo government COVID website, "The number of Tokyo's confirmed coronavirus cases is approximately 18,000, accounting for around 31 percent of its cumulative total."[16] At the time of writing, August 21st 2020, this information was updates daily.." Japan was supposed to host the 2020 Tokyo Olympics, and many people suspect that Japan purposely downplayed infection numbers by reducing testing to attempt to have the Olympics go on.[17] I lived in Japan during the summer, and many people who live here seem to think this way. This is further corroborated by news articles questioning Japan's low testing rates. The Olympics were ultimately postponed on March 24th, 2020, four months before they were set to start. After the Olympics were postponed, the government finally declared a state of emergency across Japan in mid-April, several weeks after the rest of the world had declared theirs.[18] This included asking some businesses to shut down, such as restaurants, movie theaters or indoor recreational facilities. Similarly to the 1918 pandemic, the government could not mandate that businesses shut down, only request it. However, this is because the Japanese constitution forbids the government from telling people to stay home or from shutting down businesses, so the best they could do was to request that people comply.[19] The government also sent masks to every household and asked that people wear them, but the masks were met with ridicule online, nicknamed "Abenomasks."[20]

Even though there were 100 years between the pandemics, there are some things they have in common. First, the government appeared to have underestimated the severity of the pandemic, but both outbreaks in Japan were relatively mild compared to the rest of the world. The government also tried to get information about the pandemic out to the public, whether that is with posters in 1918 or with digital media today. Masks and gargling were widespread in Japan, and the government encouraged people to build these habits. Also, the government's response was a lukewarm response and both times it refused to enact a lockdown. In terms of the

viruses themselves, both spread extremely quickly and they both diseases that affect the respiratory system.

This begs the question: why has the impact on Japan been so negligible when compared to the rest of the world? Well, for the Spanish Influenza pandemic, we have a few explanations: One reason given is that the first, less severe wave was quite widespread in Japan, and so many people developed a resistance to the H1N1 virus before the second wave.[21] However, this explanation cannot be applied universally, as some prefectures that experienced a weak first wave also had a weaker second wave.[22]

Overall, there is no definite answer to why Japan was not affected as severely as other countries. Preventative measures in Japan have been rather disappointing. Whether due to lack of trying or legal restraints, there seems to be little to nothing stopping the virus from rampaging throughout the country. The Greater Tokyo area is home to almost 40 million people, but we do not see the rampant infection like we do in other major cities around the world. One answer is that Japan has not been testing very vigilantly, and this means that not many cases will be detected and the amount of cases in the official statistics will be lower. Low test rates during the COVID-19 pandemic cast doubt on the government's official numbers. A BBC article written in April explained that "…testing figures are striking both because the number tested is so small and the percentage tested is so high."[23]

OVERVIEW OF MASKS IN JAPAN

Across Asia, masks became popular during the SARS epidemic back in 2003. However, it seems that Japan was spared from SARS, recording a total of 0 deaths. To see where masks in Japan came from, we have to go back much further. The culture of mask-wearing in Japan dates back to before the 1918 pandemic as a luxury item. However, masks only became widespread during and after the 1918 Spanish Influenza, which caused a devastating amount of deaths not only in Japan, but worldwide. One third of the Japanese population was afflicted with H1N1, even though the death rate was relatively low.[24]

COLLECTIVISM AND SURGICAL MASKS

Individualism and collectivism are aspects of a culture which are defined by how much autonomy members must act outside of their group. Social psychologist Geert Hofstede defined individualistic societies as "emphasiz[ing] 'I' consciousness, autonomy, emotional independence, individual initiative, right to privacy, autonomy, pleasure seeking, financial security, need for specific friendship, and universalism."[24] Collectivism usually occurs in countries with more authoritarian, right wing ideals.[25] Collectivistic societies "stress "we" consciousness, collective identity, emotional dependence, group solidarity, sharing, duties and obligations, need for stable and predetermined friendship, group decision, and particularism."[26] In societies, there are "ingroups" and "outgroups" for each person. A person's ingroup is those who they care about greatly. In more individualistic societies, this would be just your direct family. In collectivistic cultures, this might extend to more distant relatives. Meanwhile, the outgroup refers to those who you are not related to, from coworkers to people you pass by in the street.

Japan in general is more collectivistic than western societies. This means that in Japan, people tend to have larger ingroups. The size of somebody's ingroup is closely related to how collectivistic the environment they grew up in was. Having a larger ingroup means that there are more people you have a risk of transmitting diseases to, so therefore people will most likely take more precautions. A larger ingroup means that you will be pressured to take care of members of your ingroup. During a pandemic, larger ingroups may lead people to take more aggressive preventative measures, like wearing a mask in public, not only for themselves, but for each other.

It is important to note that even though Japan is more collectivistic than western societies, it is home to around 130 million people, and not all of them hold the same ideals. A study conducted in Japan analyzing collectivism in all 47 prefectures of the country showed that rural areas tended to be more collectivistic than urban areas.[27] This study is supported by the fact that Japan has seen a recent resurgence in cases, most of which occurred in Tokyo, which is reported to be one of the least collectivistic prefectures in Japan. [28] (Even with the rise of cases in Tokyo, there are still less cases in Japan overall than in most other nations.)

Given how collectivistic Japan is, it is plausible that people in the country wear masks for two reasons: to protect those close to them, and because they value the opinions of their peers more so they feel pressured to wear a mask. In collectivistic cultures, people care more about the greater good and how other people in the community view them so they will wear masks to show that they are caring for others. Furthermore, when you have a larger ingroup, you also have more people you care deeply for and so you will want to wear a mask to make sure none of them will be endangered if you contract the virus.

During the 1918 pandemic, people started wearing masks to protect against the influenza virus. Masks were not widespread in Japan before the pandemic, and were mostly a status symbol.[29] However, after a government public health campaign, people started to wear them to protect themselves and each other, showing a concern for the greater good. People continued to wear masks even after the pandemic was over. Today, people still wear masks when they go outside. As the threat of COVID-19 grew between the months of January - May, masks in Japan were sold out at most establishments, and people have been diligent about wearing them throughout the pandemic. It is common to draw disapproving stares if you are out in public without a mask. For comparison, mask mandates have drawn ire in many other countries, such as the US, where a large number of people still refuse to wear masks.[30] In the US, which is a more individualistic society, the average ingroup tends to be

smaller, leading to the normalization of refusing to wear a mask, which means people will be more empowered to not wear a mask as opposed to Japan.

CONCLUSION

Analyzing the usage of surgical masks in Japan throughout the 1918 and 2020 pandemics shows that masks are an example of the collectivistic nature of Japanese culture. While I have tried my best to ensure that this paper is as accurate as possible, I recognize that I have had limited access to some resources, especially for the 1918 pandemic, because they are only available in archives with access limited to a small number of people. Also, since COVID-19 is a current event, and due to the unpredictability of pandemics, the information presented here is subject to change rather quickly. However, some key facts remain the same: In 1918, people started wearing masks after the government asked the public to do so in an attempt to stop the spread of the deadly influenza virus H1N1 virus. Through 2020, the culture of wearing masks (especially during the winter) had persisted. Surgical masks were sold out for months after COVID-19 became a global issue.

Analyzing the usage of surgical masks in Japan throughout the 1918 and 2020 pandemics shows that masks are an example of the collectivistic nature of Japanese culture. While I have tried my best to ensure that this paper is as accurate as possible, I recognize that I have had limited access to some resources, especially for the 1918 pandemic, because they are only available in archives limited to a small number of people. Also, since COVID-19 is a current event, the unpredictability of pandemics, means that the information presented here is subject to change rather quickly.

In 1918, people started wearing masks after the government asked the public to do so to stop the spread of the deadly influenza virus H1N1 virus. Through 2020, the culture of wearing masks (especially during the winter) had persisted. Surgical masks were sold out for months after COVID-19 became a global issue. People's willingness to wear masks during both of these pandemics in order to protect themselves and those around them shows Japan's collectivistic nature. A larger ingroup means there are more people to care for, and so therefore people will be more careful to not spread the virus to them.

ACKNOWLEDGEMENTS

I would like to thank Michael Amano at Tokyo Academics for translating the posters. I would also like to thank Melissa Sarimento for helping me with this paper and helping me to keep going.

REFERENCES

[1] Palmer, Edwina and Rice, Geoffrey W. 1993. "Pandemic Influenza in Japan, 1918-19: Mortality Patterns and Official Responses." *The Society for Japanese Studies* 19 (2): 394. Accessed June 2020. https://www.jstor.org/stable/132645?seq=1#metadata_info_tab_contents

[2] Ibid, 411.

[3] Ibid, 401.

[4] Ibid, 393.

[5] Ibid, 417.

[6] Ibid, 402.

[7] Ibid.

[8] Posters from the influenza pandemic are available online via the National Institute of Health. Translations were courtesy of Michael Amano at Tokyo Academics. https://www.niph.go.jp/toshokan/koten/Statistics/10008882-p.html

[9] Ibid.

[10] Campbell, Charlie, Yunnan, Yuxi, and Park, Alice. "Inside the Global Quest to Trace the Origins of COVID-19--and Predict Where It Will Go Next," *Time Magazine*. July 23, 2020. Accessed August 20, 2020. https://time.com/5870481/coronavirus-origins/

[11] "Italy." Worldometer. Accessed August 23, 2020. https://www.worldometers.info/coronavirus/country/italy/.

[12] Kyodo, "Japan confirms first case of coronavirus that has infected dozens in China," *Japan Times*. January 16, 2020. Accessed August 25, 2020. https://www.japantimes.co.jp/news/2020/01/16/national/science-health/japan-first-coronavirus-case/

[13] Yotsumoto, Jun. "Japan confirms first death of person infected with coronavirus," NHK World. February 14. Accessed July 30, 2020. https://www3.nhk.or.jp/nhkworld/en/news/backstories/875/.

[14] Princess Cruises. "Princess Cruises: Diamond Princess Updates - Notices & Advisories." www.princess.com, March 16, 2020. https://www.princess.com/news/notices_and_advisories/notices/diamond-princess-update.html.

[15] BBC. "Passengers Leave Diamond Princess Amid Criticism of Japan," February 20, 2020. Accessed August 20, 2020. https://www.bbc.com/news/world-asia-51555420

[16] These statistics are provided by the official Tokyo government COVID website. https://stopcovid19.metro.tokyo.lg.jp/en/ Please note that

these statistics will change over time as the pandemic unfolds.

[17] Goh, ZK and Kano, Shintaro. 2020. "Tokyo 2020 Olympic And Paralympic Games Postponed To 2021." *Olympic Channel.* March 24. Accessed July 30, 2020. https://www.olympicchannel.com/en/stories/news/detail/tokyo-olympic-games-postponed-ioc/.

[18] Kyodo News. "Japan declares nationwide state of emergency amid coronavirus spread." *Japan Times*. April 16, 2020. Accessed August 25, 2020. https://www.japantimes.co.jp/news/2020/04/16/national/japan-nationwide-state-of-emergency/

[19] Sieg, Linda. "'Lockdown', Japan style: Pressure to conform, not penalties for non-compliance." *Reuters*. April 5, 2020. Accessed August 25, 2020. https://www.reuters.com/article/us-health-coronavirus-japan-emergency-ex/lockdown-japan-style-pressure-to-conform-not-penalties-for-non-compliance-idUSKBN21O08J

[20] Kyodo News. "2 firms recall masks from PM Abe's distribution program." *Kyodo News.* April 5, 2020. Accessed July 30, 2020. https://english.kyodonews.net/news/2020/04/084513e72dd4-update1-2-firms-to-recall-products-under-pm-abes-mask-handout-program.html.

[21] Palmer, 412-413.

[22] Ibid.

[23] Wingfield-Hayes, Rupert. "Coronavirus: Japan's low testing rate raises questions," *BBC*. April 30, 2020. Accessed August 25, 2020.

[24] Martin, Alex. "The history behind Japan's love of facemasks," *Japan Times*. July 24, 2020. Accessed August 20, 2020. https://www.japantimes.co.jp/news/2020/07/04/national/science-health/japans-history-wearing-masks-coronavirus/#.Xz82H-hKjD4 https://www.bbc.com/news/world-asia-52466834.

[25] Kim, Uichol. Individualism and Collectivism: A Psychological, Cultural and Ecological Analysis. Copenhagen S, Denmark: NIAS Books, 1995. 4. Accessed August 25, 2020. http://web.b.ebscohost.com.revproxy.brown.edu/ehost/ebookviewer/ebook/ZTAwMHhuYV9fNDYzNDcwX19BTg2?sid=484bb2f3-0b00-4251-aee3-594a28b35d18@sessionmgr103&vid=0&format=EB&lpid=lp_3&rid=0.

[26] Triandis, Harry Charalambos, *Individualism and Collectivism.* Boulder: Westview Press, 1995. Accessed August 25, 2020. https://books.google.com/books?id=dXNgDwAAQBAJ&printsec=frontcover#v=onepage&q&f=false.

[27] Kim, 4.

[28] Yamawaki, Niwako. "Within-Culture Variations of Collectivism in Japan." *Journal Of Cross-Cultural Psychology* 43, no. 8: 1191–1204. Accessed August 21, 2020. doi:10.1177/0022022111428171. https://journals.sagepub.com/doi/10.1177/0022022111428171.

[29] Ibid.

[30] Martin, Alex. "The history behind Japan's love of facemasks," *Japan Times*.

[31] McKelvey, Tara. "Why are Americans so angry about masks?" *BBC.* July 20, 2020. Accessed August 25, 2020. https://www.bbc.com/news/world-us-canada-5347712

Detecting Differential Transcription Factor Binding Based on Single-Cell DNA Accessibility

John Lin
Boston Latin School; Boston, USA
Email: johnzhuanglin@gmail.com
Mentor: Dr. Thouis (Ray) Jones

Abstract — **Common genetic diseases—systemic diseases that are caused by thousands of mutations—affect millions of people around the world. Many of these mutations fall within regulatory regions. While the mutations associated with these diseases are widely known, the link between these mutations and their role in disease pathogenicity has largely gone undiscovered. This study harnesses single cell ATAC-seq data to differentiate bound and unbound sites in regulatory regions, serving as a first step to understanding these diseases. By computing observed and expected cuts for footprint regions, this study finds that regions with lower observed cuts than expected cuts conferred to protection from sequencing enzymes, indicating the presence of a bound transcription factor. In contrast, regions with higher observed cuts than expected indicate the absence of protection from sequencing enzymes, suggesting an absence of a bound transcription factor. In distinguishing between bound and unbound transcription factors, this study paves the way for using single cell ATAC-seq to understand common diseases by identifying the cell types and changes in transcription factor binding caused by mutations**

Key Words – transcription factor, single-cell sequencing, common genetic diseases, DNA accessibility

INTRODUCTION

Common genetic diseases are often caused by thousands of mutations and affect millions of people in the world each year. These diseases, which include heart disease, schizophrenia and Crohn's disease, are difficult to treat because their exact pathogenicity remains unclear. Despite the identification of mutations for these diseases, the link between these mutations and their role in expressing disease phenotypes has been largely undiscovered, particularly in understanding the cell types and biological pathways that are affected by the mutations. An analysis of these mutations, however, found that 80% of these mutations occur in distal regions, containing *cis* regulatory elements that drive gene expression [1]. The exact effects of these mutations on these regulatory regions remain unclear. Specifically, understanding the role of mutations in transcription factor binding is incredibly important as transcription factors play a large role in activating/suppressing gene expression. Despite this, there has been little information on detecting differences in transcription factor binding, serving as the premise for this study.

Sequencing technology has provided a plethora of information about gene regulation in cells. Specifically, Assay for Transposase-Accessible Chromatin sequencing (ATAC-seq) and DNase-seq identify accessible regions which are often regulatory regions. In the case of DNase-seq, this has led to the creation of DNase-I hypersensitive site (DHS) databases, creating a reference library for mapping regulatory regions [2] [3]. ATAC-seq harnesses a sequencing enzyme, Tn5 transposase, to attach adapters onto regions without nucleosomes which characterize accessible regions; these adapters are visualized by the sequencer in order to visualize the accessible regions. Furthermore, the rise of single cell ATAC-seq (scATAC-seq) has provided clearer resolution in identifying the accessible properties within a single cell as well as subpopulations in cells, particularly tissue [4]. This new technology has provided unprecedented ability to visualize accessibility regions in order to not only cluster different cell types but also explain the role of specific transcription factors in biological processes, such as cell differentiation [5].

These sequencing techniques have also been applied in DNA footprinting. ATAC-seq and DNase-seq use sequencing enzymes to cut accessible regions, which are not bound or "protected" by a protein. Footprinting involves observing drops in accessibility caused by the inability for a sequencing enzyme to cut a bound region. This technique has been harnessed to study within the regulatory region, especially in relation to transcription factor binding. Transcription factors typically recognize and bind to particular DNA motifs (short, distinct sequences) in accessible regions in the genome. However, not all accessible motifs have transcription factors to bind to them due to a variety of factors, including the lack of transcription factor expression or the absence of necessary cofactors. Footprinting allows us to visualize which motifs are actually bound by observing slight drops in accessibility caused by transcription factor:motif binding [6].

Despite the wealth of information that footprinting brings, there has been little knowledge about whether this information can be translated to single cell sequencing data. By determining whether footprinting can be detected in scATAC-seq data, this study identifies where these transcription factors may bind and also characterizes

whether they are bound or unbound. In relation to common genetic diseases, mutations in these regions often confer to changes in gene expression [6]. Thus, detecting differences in transcription factor binding, in the context of allele specific binding, for single cells has the potential to be an incredibly powerful tool in understanding these complex common genetic diseases [7].

Building upon this understanding, this study addresses this fundamental challenge in understanding common diseases by providing the link between mutation and disease phenotype through identifying the cell type, biological pathways and nearby genes that are involved in functional changes due to variants linked to disease phenotypes. In doing so, this study opens the doors for drug development that targets and stimulates or suppresses transcription factor binding sites in affected cells to address these common diseases.

METHODS

A. Extraction and Verification of Sequencing Data

Single cell ATAC-seq fragments data for CD8+ T cells was downloaded from Gene Expression Omnibus platform [8]. (Accession Number: GSM4293910). CD8+ T cell data was used specifically due to its relevance to a variety of autoimmune diseases, such as Crohn's disease as well as abundance of high-quality CD8+ ATAC data. DHS index and footprint data were downloaded from their respective papers to serve as a reference to map accessible fragments to footprints and index regions[2] [3]. The ATAC-seq fragments and the DHS index were overlapped in *bedtools* to map accessibility (in the form of these fragments) to footprints, and the number of overlapped cuts along with the location of the overlapped regions were mapped in order to confirm that the cuts came from lymphoid cells [9].

A. Enrichment Determination

In order to determine the most relevant or active transcription factors in the CD8+ T cell ATAC data, the enrichment of these transcription factors was calculated. To do so, a threshold was set at one cut per base (from arcsinh transformed data). If an overlapped region had more than one cut per base, then it was considered "more accessible;" If an overlapped region had less than one cut per base, then it was considered "less accessible." Each of these data sets (more accessible and less accessible) were overlapped with a DHS footprint library in order to match footprints and motifs with an accessible category. For each transcription factor, the frequency of the motif in the more accessible and less accessible categories were calculated separately. The equation for the enrichment or the fraction of the motif that was present in the more accessible category was developed and was calculated such that:

$$E = \frac{freq(more\ accessible)}{freq(more\ accessible) + freq(less\ accessible)}$$

B. Footprint Ranking and Candidate Identification

The enrichment ratio serves as an indicator for how active a certain motif was in the CD8+ T cell type. After calculating the enrichment ratio for each motif, we ranked all the transcription factors by the motif enrichment ratio. The ten most enriched motifs were the candidate footprints.

C. Calculating Sequence Bias and Expected Cuts

After determining the candidate footprints, the number of cuts expected within a region was calculated to serve as a control to detect differential binding. The Tn5 enzyme for ATAC-seq does not cut the fragments in a uniform manner, but instead, demonstrates a bias for cutting at certain sequences [10]. To account for sequence bias when determining the expected number of cuts, a table listing different 8-mers and their respective bias values was obtained [10]. For each candidate footprint, the DHS index element that makes up the general region of the footprint was divided into 8-mers. A query between the 8-mers in the sequence and the sequence bias table was executed, and the sum of the sequence bias values was determined in order to calculate the total bias in the sequence. The same procedure was repeated in the area of the footprint itself. The expected number of cuts within a given footprint region, *e*, was calculated based on the total cuts within the DHS element as well as bias within the footprint itself as well as in the entire region:

$$e = n_{cuts\ in\ total\ region} \cdot \frac{\Sigma(bias\ of\ footprint)}{\Sigma(bias\ of\ region)}$$

D. Determining Differential Binding

In order to investigate whether a transcription factor is bound or not bound, the number of observed cuts within a region was determined by overlapping the ATAC-seq fragments with the DHS footprints and calculating the number of intersections between ATAC-fragments and DHS footprints for each footprint. If the number of observed cuts is greater than or equal to that of expected cuts, the higher number of observed cuts indicates that the region was not protected from the fragmentation of the Tn5 enzyme during ATAC-seq; thus, footprint is unbounded. If the number of observed cuts was less than the number of expected cuts, the footprint is bound because the region faced protection from the Tn5 enzyme, resulting in fewer fragments and indicating the presence of a bound transcription factor.

E. Statistical Analysis

To calculate significance between the observed and the expected values, Anscombe transformation was first applied to normalize the distribution of the values. The transformation turns these values into a unit of standard deviation. Thus, the z-score is calculated by subtracting the

expected value (after transformation) from the observed value for each binding site. The z-score is then converted into a p value. Since many binding site locations (n=159) were tested under a single hypothesis (whether a footprint is bound or not), the p values runs the risk of Type I errors or false positives. To account this, Bonferoni correction was applied: each p value was multiplied by the total number of binding sites.

F. Identifying Potential Binding Sites

Upon calculating the p-value for each footprint binding site, the sites with the most potential for binding were identified for further examination. Sites with the highest binding potential were the footprint sites with significantly lower observed than expected ($p<0.05$) because areas with significantly lower observed than expected suggests the resistance of the footprint to the Tn5 cutting enzyme due to the presence of bound transcription factor.

G. Metaplot Analysis

After identifying the potential binding sites, the profiles for these binding sites were developed to visualize binding within these sites. For a given footprint region, the expected profile was compiled by applying the expected cuts equation for each base in the entire DHS index and mapping out these expected cut numbers in relation to their position on the DHS index element. In addition, the observed profile was developed by mapping where the observed ATAC-fragments fall in the DHS index. Upon calculating the profile, the mean of all the observed and expected profiles were mapped together in order to observe differences between the two categories for the binding sites.

RESULTS

A. Density Plots Identify Enriched Sites in ATAC data

Upon calculating the enrichment ratios, the footprint enrichment data was visualized using density plots to help determine the candidate footprints. As seen in Figure 1, HINFP1/3, the most enriched transcription factor had high frequencies at high log cuts per bases, demonstrating high enrichment. HINFP1/3 is a regulator for DNA methylation and transcription and is over-expressed in CD8+ T-cells [11]. In contrast, ZNF24, the least enriched transcription factor had high frequency at lower log cuts per bases, indicating low enrichment. As for all other transcription factors, the density plots compare the frequency of a footprint to the number of cuts per base. The higher the frequency was at a higher number of log cuts per base, the more enriched a particular footprint was. The plot features "with motif" which maps the relationship for a particular transcription factor and "without motif" which maps the relationship for all other transcription factors as a comparison.

TABLE 1: The ten most enriched transcription factors along with their enrichment ratios

Transcription Factor	Enrichment Ratio
HINFP1/2	0.468354
HINFP1/3	0.457364
ZBTB14	0.408665
KAISO	0.34715
HINFP1/1	0.34569
E2F/4	0.32182
MBD2	0.303204
CENBP	0.292683
AHR	0.275578
GMEB2/3	0.264368

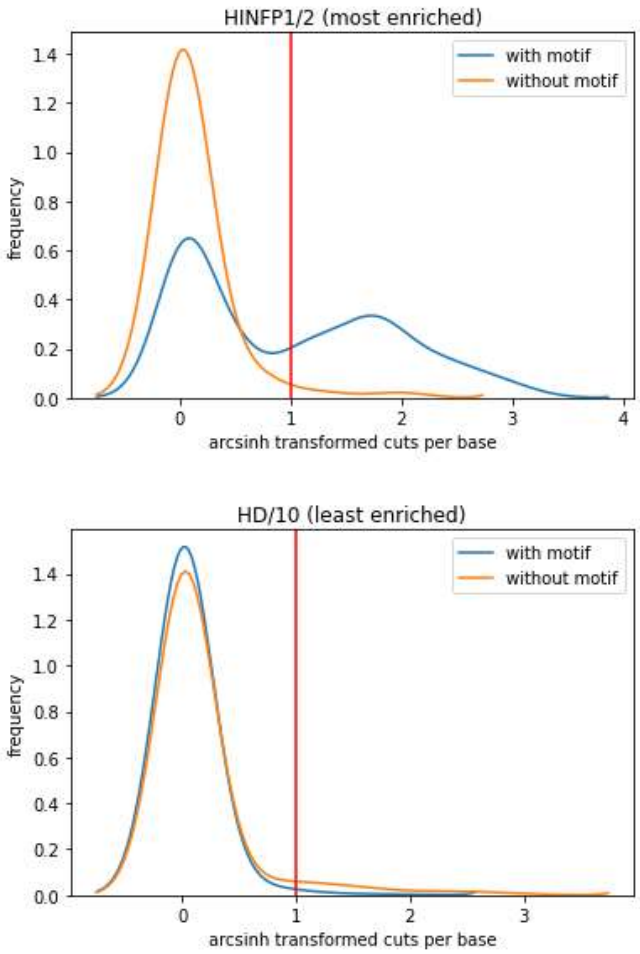

FIGURE 1: Representative density plots of the highest enriched (above) transcription factor (HINFP1/3) and the lowest enriched (below) transcription factor (ZNF24) in CD8+ T cells.

B. ATAC-seq Analysis Maps Potential Binding Sites

For each binding site, the expected and observed cuts were plotted in relation to each other, as shown in Figure 2. The scatter plots serve to identify potential binding locations. These areas are defined by areas with lower observed cuts and higher expected cuts, indicating protection from the sequencing enzyme due to a bound transcription factor. Binding potential was measured using the regularized ratio (see Methods) and visualized with a colormap. The twenty five footprints with the lowest regularized ratios were used to further visualize the binding location and the binding behavior using metaplots. On an additional note, in comparison to HINFP1/2 (most enriched footprint), HD/10 has higher regularized ratios, as seen in Figure 2, possibly due to a lower prevalence of binding sites due to lower expression of the footprint.

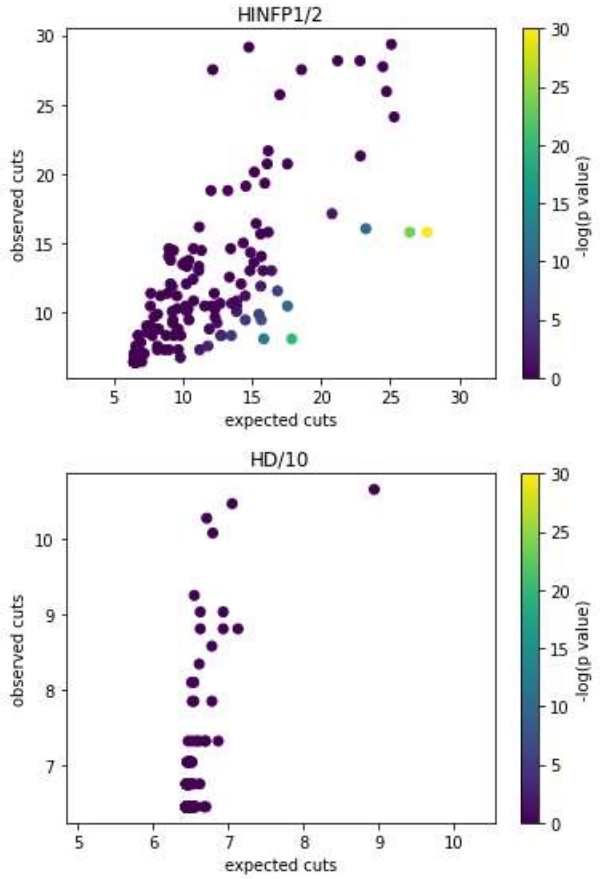

FIGURE 2: Representative scatter plots that map the relationship between observed cuts and expected cuts. Areas with higher binding potential lie in regions with high numbers of expected cuts but low numbers of observed cuts. A color map was developed based on the regularized ratio. More enriched transcription factors (HINFP1/2) have more binding sites with lower regularized ratios compared to less enriched transcription factors (HD/10).

C. Metaplot Analysis Identifies Bound Locations

After identifying potential binding locations, the expected and observed cut profiles for the DHS index were mapped. As seen in Figure 3A and Figure 3C, the lower number of cuts observed in the footprint region than expected due to protection from the cutting enzymes provides evidence for transcription factor binding on that site. In less enriched footprints, such as HD/10, the observed cuts are equal to or greater than the expected cuts, demonstrating that the region was not protected from the sequencing enzyme, providing evidence that the region is unbounded (Figure 3B, Figure 3D).

The expected and observed profiles could be further expanded to the other 24 regions with the highest binding potential in HINFP1/2 as seen in Figure 4. Consistent with the results from Figure 3, there is a large difference between the expected and the observed cuts in the enriched footprints in that the expected cuts are much higher than that of the observed, demonstrating that these regions are likely to be bound. For unenriched footprints, the opposite holds: the observed is equal or higher than the number of expected cuts.

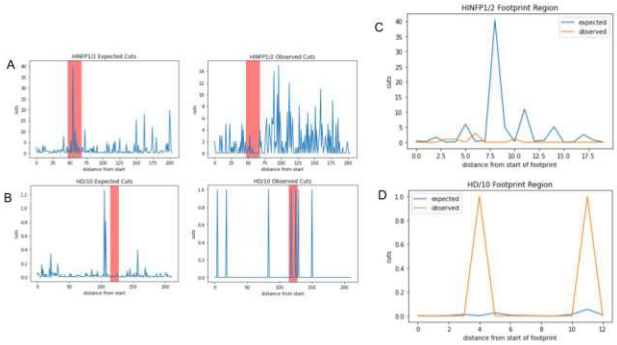

FIGURE 3: Expected and observed cut profiles of a representative HINFP1/2 (A) and HD/10 (B) with the footprint region shaded in red as well as the higher-resolution profile of the footprint itself. Within the enriched footprint (HINFP1/2), the observed cuts seem to be consistently lower than the expected cuts (C). In less enriched footprint (HD/10), the observed cuts are equal or higher than the expected cuts (D).

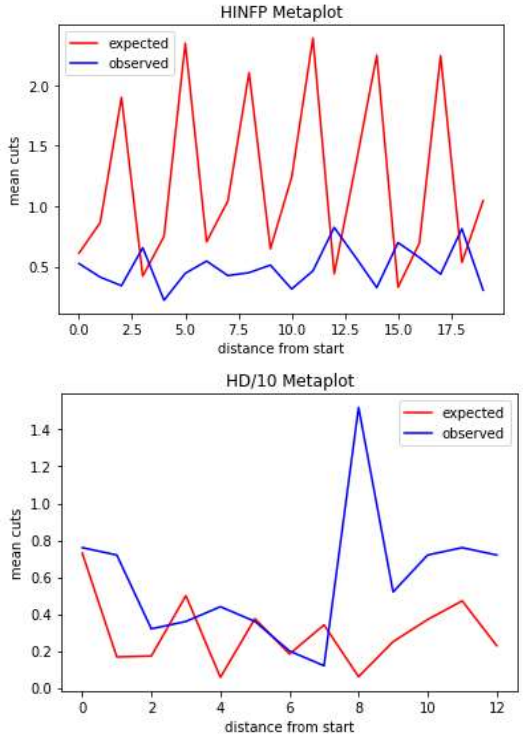

FIGURE 4: Metaplot analysis of the expected and observed cuts of the 25 regions with the most binding potential in HINFP1/2 (left) and HD/10 (right).

DISCUSSION

By comparing the observed cuts and expected cuts in a given footprint region, the results of this study harnesses scATAC-seq to characterize bound and unbound transcription factor sites. Specifically, the paper found that bound sites contained lower observed cuts than expected, resulting from protection by the bound transcription factor within the region. In contrast, unbound sites had an equal number or more observed cuts than expected, indicating that the region showed no protection (allowing the sequencing enzyme to freely fragment the area).

In distinguishing between bound and unbound sites, this study establishes a novel method for studying changes in expression through scATAC-seq. While past studies have identified DNA footprints and accessible sites [2] [3] using DNase-seq, these sequencing techniques lack efficiency to distinguish individual cell types without a large set of materials for input as well as differentiating between sub-populations within a cell type. This study lays the foundation for using scATAC-seq, which allows for identifying specific cell types and subtypes, to study the different transcription factor binding behavior within these specific cell types. In doing so, this study has the potential to influence the study of these common genetic diseases by examining the regulatory context of each cell type and linking mutations to a certain cell type, transcription factor or other regulatory element

Only through identifying these features within the regulatory regions can we fully identify the inner workings behind genetic diseases and develop specific drugs to correct for these mutation-induced differences in the regulatory environment. The potential for single-cell sequencing for understanding common genetic diseases and guiding targeted drug therapies is enormous, and this study serves as a first step for harnessing their potential to understanding and treating these diseases.

FUTURE WORK

This study hopes to expand the data set from CD8+ T cells to a wide variety of other cell types to characterize binding behavior in footprints for other cell types. In expanding the knowledge of transcription factor binding in more cell types, a reference library containing measurements of accessibility and binding for each transcription factor in a particular cell type can be developed. This can serve as a basis for future studies in comparing disease sequences and expression with this library.

It is important to note that DNA footprinting identifies potential sites of interest for binding, but does not confirm and verify binding. While we show that single-cell ATAC data does detect differences in transcription factor binding behavior, further validation is needed to confirm our results. This validation can take the form of ChIP-seq, which is a more direct way of confirming transcription factor binding to validate our results.

Another possibility for this study is to harness and categorize scATAC-seq data from Genome Wide Association Studies (GWAS) for different types of common genetic diseases. Upon categorizing the individual cell types and subtypes, this study will compare the transcription factor binding behavior and accessibility to that of a reference library. From there, differences between the GWAS data and the reference data can be detected, leading to a better understanding of the specific cell types, transcription factors and biological pathways that are relevant in causing diseases. This understanding would be extremely powerful in developing drugs in correcting these differences and alleviating the effects of these diseases.

CONCLUSIONS

This study developed an approach to characterizing the differences in bound and unbound transcription factors by examining ATAC-seq data. This was done in three steps. First, the most enriched footprints were identified in the DHS region by observing the distribution of cuts in relation to a particular footprint. From there, we identified HINFP1/2 as the most enriched footprint and HD/10 as the least enriched footprint. Next, we identified potentially bound sites by computing and comparing the observed and

expected cuts for the candidate footprints. Areas with low observed:expected ratios were selected and used for developing the metaplots. The metaplots compile the profile of the observed and expected to help us better understand the regulatory region specifically. From this compilation, this study identified bound sites as areas with less observed cuts than expected cuts, demonstrating protection from sequencing enzymes caused by transcription factor binding.

ACKNOWLEDGEMENTS

This paper and project would not be possible without the work and support of so many individuals and organizations. I would like to thank my principal investigator, Dr. Eric Lander, and the Lander Lab at the Broad Institute for providing funding and support in making this project possible. I would also like to thank Ms. Ana Lyons who thoroughly reviewed my paper and provided helpful edits. I am thankful for Haydn Bradstreet for providing so much feedback and offering support in reviewing my paper. I am deeply appreciative of the Research Science Institute, the Center for Excellence in Education and the Massachusetts Institute of Technology for providing the opportunity to take part in this incredible project. Lastly, I would like to thank my parents and family for helping and supporting me in nurturing my curiosity as well as my love for science.

REFERENCES

[1] C. P. Fulco, J. Nasser, T. R. Jones, G. Munson, D. T. Bergman, V. Subramanian, S. R. Grossman, R. Anyoha, B. R. Doughty, T. A. Patwardhan, et al. Activity-by-contact model of enhancer–promoter regulation from thousands of crispr perturbations. *Nature genetics*, 51(12):1664–1669, 2019.

[2] J. Vierstra, J. Lazar, R. Sandstrom, J. Halow, K. Lee, D. Bates, M. Diegel, D. Dunn, F. Neri, E. Haugen, et al. Global reference mapping and dynamics of human transcription factor footprints. *bioRxiv*, 2020.

[3] W. Meuleman, A. Muratov, E. Rynes, J. Halow, K. Lee, D. Bates, M. Diegel, D. Dunn,J. Neri, A. Teodosiadis, et al. Index and biological spectrum of accessible dna elementsin the human genome. *BioRxiv*, page 822510, 2019.

[4] C. A. Lareau, F. M. Duarte, J. G. Chew, V. K. Kartha, Z. D. Burkett, A. S. Kohlway, D. Pokholok, M. J. Aryee, F. J. Steemers, R. Lebofsky, et al. Droplet-based combinatorial indexing for massive-scale single-cell chromatin accessibility. *Nature Biotechnology*,37(8):916–924, 2019.

[5] L. S. Ludwig, C. A. Lareau, E. L. Bao, S. K. Nandakumar, C. Muus, J. C. Ulirsch, K. Chowdhary, J. D. Buenrostro, N. Mohandas, X. An, et al. Transcriptional states and chromatin accessibility underlying human erythropoiesis.*Cell reports*, 27(11):3228–3240, 2019.

[6] F. Aguet, A. N. Barbeira, R. Bonazzola, A. Brown, S. E. Castel, B. Jo, S. Kasela, S. Kim-Hellmuth, Y. Liang, M. Oliva, et al. The gtex consortium atlas of genetic regulatory effects across human tissues. *BioRxiv*, page 787903, 2019.

[7] E.-W. Yang, J. H. Bahn, E. Y.-H. Hsiao, B. X. Tan, Y. Sun, T. Fu, B. Zhou, E. L. Van Nostrand, G. A. Pratt, P. Freese, et al. Allele-specific binding of rna-binding proteins reveals functional genetic variants in the rna. *Nature communications*, 10(1):1–15, 2019.

[8] T. Barrett, S. E. Wilhite, P. Ledoux, C. Evangelista, I. F. Kim, M. Tomashevsky, K. A. Marshall, K. H. Phillippy, P. M. Sherman, M. Holko, et al. Ncbi geo: archive for functional genomics data sets—update. *Nucleic acids research*, 41(D1):D991–D995, 2012.

[9] A. R. Quinlan and I. M. Hall. Bedtools: a flexible suite of utilities for comparing genomic features. *Bioinformatics*, 26(6):841–842, 2010.

[10] Z. Li, M. H. Schulz, T. Look, M. Begemann, M. Zenke, and I. G. Costa. Identificationof transcription factor binding sites using atac-seq.Genome biology, 20(1):45, 2019.[11] A. D. Rouillard, G. W. Gundersen, N. F. Fernandez, Z. Wang, C. D. Monteiro, M. G. McDermott, and A. Ma'ayan. The harmonizome: a collection of processed datasets gathered to serve and mine knowledge about genes and proteins. *Database*, 2016, 2016.

Analysis of Machine Learning Models Predicting Basketball Shot Success

Max Murakami-Moses
The American School in Japan; Tokyo, Japan
Email: 22murakamimosesm@asij.ac.jp

Abstract - The most critical aspect of winning a basketball game is shot selection. However, due to the multitude of factors that come into play when deciding if a shot was a good shot selection (a shot that has a high chance of going in is a good shot selection), it is difficult for a human to make a reasonable assumption. Because of this, we used and analyzed a variety of machine learning techniques to predict shot success.

Here, we perform an analysis of the best machine learning models for predicting shot success as well as comparing the performance of these models using different features. Our models (neural network, logistic regression, and gradient boosting) were able to predict shot success between 64.9% - 65.1% accuracy.

Our models performed with about equal accuracy; however, when we altered the features, the accuracy significantly decreased. This highlighted the importance of good quality data as well as the importance of certain features, such as the type of shot, in making a shot.

Keywords - Deep neural network, machine learning, shot selection, and accuracy.

BACKGROUND

Shot selection is vital to winning the game of basketball—good shot selection results in increased points and a better chance at winning. Shot selection is evaluated across many domains, such as the shooter's positions with respect to the basket; positioning of the on-ball defender, rotating defenders, and teammates; minutes remaining on the clock; players skill level; shot type. Though shot selection can be judged based upon observable factors, it is difficult for coaches and players to understand if the shot was good beyond whether or not the ball went in. This is due to the fast pace of the game and the human eye's limited ability to evaluate the multitude of factors that play into a good shot selection.

However, the process of understanding shot selection can be significantly enhanced using machine learning. A model, such as a neural network, can be created and trained to understand what is a good shot selection based upon all of the mentioned factors. This can be of great use for all levels of players as they can learn what shots to pass upon and take, independent of the shot going in. Furthermore, coaches would be able to understand better which players can make the best decisions and give them the ball during crucial moments of the game. Over the last decade, progress in machine learning and access to large amounts of data have allowed data scientists to give sports teams a deeper insight into how to win and how to keep their players healthy. For example, in sports analytics, Machine learning has been applied in the game of soccer. A recent paper in the M edicine and Science in Sports and Exercise outlined how a statistical model was able to predict the likelihood of a hamstring injury [1]. When selecting two players at random, the probability that the player with a higher injury risk would get injured first was 75%. Furthermore, with the model, researchers were able to identify three factors significantly associated with hamstring injury: Seven genetic variants, previous hamstring injuries, and age(with players over 24 being more likely to be injured).

In this paper, we propose building and training a model using a machine learning and data-driven approach to give percentages indicating the shot's success rate. The percentage can be used to analyze whether the player selected a good shot, as a high percentage would signal that it was a good shot and vice-versa. Utilizing a deep neural network, the model could predict if a shot would go in with 65% accuracy.

RELATED WORKS

In an article titled "NBA Shot Prediction and Analysis," Raymond Cen, Harrison Chase, Carlos Pena-Lobel, and Daniel Silberwasser attempted to predict shot success [2]. Their data set included all of the same features of our dataset. However, an important distinction is that they also included the players' FG% from each zone on the court (Figure [1]).

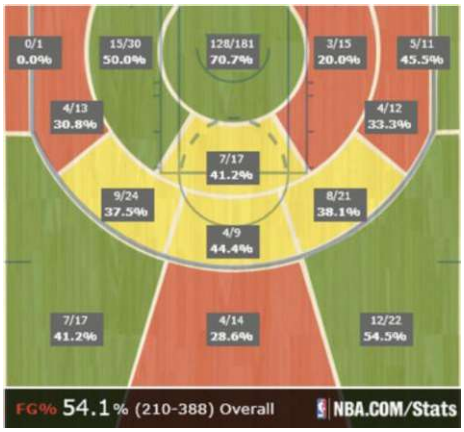

Figure [1]: Image from "NBA Shot Prediction and Analysis."

This gives them a clear advantage in predicting shot success as they have access to the players' FG% in all zones, which allows them to rely on a player's history rather than in-the-moment factors. They utilized a logistic regression model to try to predict shot success. The model was able to achieve 65% accuracy on whether a shot would go in or not. In another paper titled, "Predicting NBA Shots" by Brett Meehan of Stanford University, shot success was able to be predicted between 54%-68% accuracy [3]. Brett used a variety of models, such as Naive Baynes, Random Forest, Boosting, Logistics Regression, and neural network, in an attempt to find the most suitable model for predicting shot success. His dataset came from the NBA via its SportVu tracking system similar to our dataset. However, his dataset differed slightly in features and was significantly larger than our dataset. Though our data set did not include any tracking data, Bretts' data set included features such as the shooters' distance to the basket and the nearest defender. The paper claims to achieve an accuracy of up to 68% using an XGBoosting with a tuning model. However, these results are contradictory to the confusion matrix presented in the same paper (Figure[2]). The max accuracy according to the confusion matrix is 63%, which aligns more closely with results given by other models and in experiments we briefly performed on the same data set.

	Pred p	Pred n	total
Actual p	1040	1875	2915
Actual n	496	2993	3489
total	1536	4868	

Figure [2]: Confusion matrix for Boosting

METHOD

1.Data Set and Features

The data set this paper utilizes was initially provided by the NBA during the 2015-2016 season. However, due to the NBA's decision to restrict public access to their data, we loaded it from pages that hosted the data on their GitHub/Kaggle [4]. The data set consists of 419 NBA players from all 30 of the NBA's teams. Using cutting edge camera technology from SportVu, the NBA carefully recorded the players' movements and actions to provide data for the league, teams private and companies. In total, the dataset contained 84,466 data points. The mean percentage of a made shot per shot(FG%) across the data set was 44.8%. This means the clear accuracy benchmark for our network would be 55.2% percent, as that would be the result of naively predicting a failed shot attempt for all attempts.

2.Data Collecting and Processing

Initially, our dataset contained positional information of the player; however, we did not include it because it did not significantly affect our accuracy. We hypothesize this is due to the data of shot times being inaccurate by a few seconds. Though a few seconds may not seem significant, the positional data of players, even after a second, can dramatically change, m king the data unusable and inaccurate.

Besides positional data, we extracted what we believe to be the 12 most vital data columns in predicting shot success from the original basketball data set.

Four of the columns consisted of categorical data: "ACTION_TYPE" (a column composed of 53 different categorical listings of the type of shot such as dunk, layup, Hookshot, etc.), "PLAYER_NAME," "SHOT_ZONE_AREA," "SHOT_ZONE_BASIC"(a column consisting of 7 individual categorical listings of the location of a shot such as left corner three, in the paint, etc.). We one-hot encoded the categorical data in order to turn the categorical data into numerical data. This allowed for the models to take in only numerical data, which is optimal for performance. The remaining eight columns consisted of numerical data and are described in table 1. Additionally, our data set included a "flag" that noted if the shot was made or not. The main challenge with the data set was a limited amount of features describing an individual's performance. Although there are features that define the player's distance from the basket and XY coordinates on the court, most of the features consisted of high-level features such as "PERIOD" and "EVENT_TIME" which tell us much less about an individual's ability to make a shot. However, as these features could have a small correlation with shot accuracy (later in the game, the player may be more tired and thus may miss more frequently), we decided to include them in our data set (Table [1]).

Table [1]: A table describing each feature used.

ACTION_TYPE	Categorical data labeling the type of shot such as layup, three pointing, and hook shot.
PLAYER_NAME	Categorical data that gives the players full name.
SHOT_ZONE_AREA	Categorical data describing which side of the court the player is on. For example, “Right Side”, “Back Court”, and “Ride Side Center”.
SHOT_ZONE_BASIC	Categorical data describing the area on the court relative to the basket. For example, “Mid-Range”, “Restricted Area”, and “In the Paint”.
EVENTTIME	Time remaining in the quarter.
LOC_X	Numerical data describing the players X coordinate on the court.
LOC_Y	Numerical data describing the players Y coordinate on the court.
MINUTES_REMAINING	Numerical data describing the minutes remaining in a period.
SECONDS_REMAINING	Numerical data describing the seconds remaining in a period.
PERIOD	Numerical data denoting which period, or quarter the game is in (1-4).
SHOT_TIME	The time of highest acceleration before the ball reaches its peak.
SHOT_DISTANCE	Numerical data describing how far the shooter is from the basket when attempting the shot.

Lastly, we randomly split the data set into training data and validation data . 90% of our data was used as training data while the other 10% was used as validation data. This allowed us to properly evaluate our models as there is no inherent bias when testing our models because it has not had the chance to overfit to the validation model.

CLASSIFICATION MODELS

In this paper, we utilized three different machine learning techniques and models to predict shot success. Each model predicted shot success within an accuracy of 64.9%-65.1% accuracy.

1.Deep Neural Network

A deep neural network is a machine learning technique modeled after the human brain and nervous system. The network can recognize individual rel tionships and/or patterns in sets of data in a process that mimics humans, allowing them to make intelligent predictions or classifications. The network consists of connected nodes that are organized into a certain amount of layers. Each node has a weight and threshold associated with it, which is initially set at random before the network is trained. As the network trains, it adjusts the parameters by passing the inputs into the network, calculating a prediction and comparing this prediction with the true known value. The error, or 'loss', between the true known value and the prediction, is back-propagated through the network using tools of calculus to update the parameters in a way that pushes the prediction towards the correct answer.

The final layer of nodes passes through an activation function, which in our network is a sigmoid function. This function takes the output of the network and produces a number between 0 and 1, which corresponds either to a missed shot or a made shot.

See the sigmoid function below (Figure [3]):

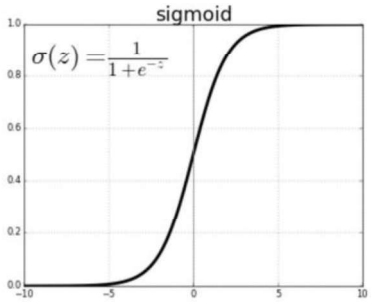

Figure [2]: Sigmoid function and equation.

The sigmoid function is a suitable activation model for a binary classification situation as it restrains the prediction between 0 and 1. Furthermore, it is also a

continuous function as opposed to a Heaviside function. A Heaviside function has an output of a 0 or 1 but has a sudden jump between the two values, making it unusable by a neural network.

The cross-entropy loss gives us the negative log-likelihood of our parameters. Simply put, it is a metric of how likely the true data was to be seen if the current probability predictions we have were true. Minimizing this binary cross-entropy loss (the negative log-likelihood) will ensure that our model assigns a high probability to what truly happened.

See the binary cross-entropy loss equation below:

$$CCE(p,t) = -\sum_{c=1}^{C} t_{o,c} \log\left(p_{o,c}\right)$$

Figure [3]: Cross-entropy loss equation.

2.Gradient Boosting

Gradient Boosting is a machine learning technique that uses an ensemble of weak machine learners and combines them to create a strong learner. The most common learner is the decision tree. In this paper, we used Gradient Boosting from scikit-learn.org [5].

3. Logistic Regression

In Logistic regression, the dependent variable has a binary outcome (1 = success and 0 = failure), which makes it a good fit for this situation. Through a mathematical formula similar to the sigmoid function, it is able to classify data based upon multiple features. Below is a two feature representation of logistical regression, with the blue dots representing a positive classification and the red dots representing a negative classification.

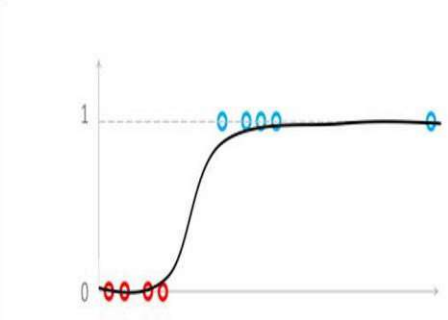

Figure[4]: Illustration of a two feature logistic regression model. The X-axis presents a certain feature while the Y-axis presents if a dot has any correlation with that feature. The blue dots represent a positive result, while the red dots represents a negative result.

Experiments and Results

Our neural network consisted of 2 layers with each layer consisting of 20 nodes each. The activation used for each layer was a relu function; however, the last layer utilized a sigmoid activation function. The network had a learning rate with RMSprop of 0.001, a weight decay of 0.0005 and was tr ined for 10 epochs. Our six-layer neural network predicted shot success with an accuracy of 65%. To our knowledge, no other works have achieved a better accuracy than 65% on this or similar datasets. Given the highly stochastic nature of basketball shot attempts, 65% accuracy can be considered a well-performing model.

Furthermore, our experiments with gradient boosting and logistic regression models produced similar results. Our gradient boosting model was able to achieve 65.1% accuracy. Our logistic regression model was able to hit 64.9% accuracy [Table 2].

Table [2]: Table containing experiment results.

	Accuracy	F1 Score
Neural Network	65%	0.65
Logistic Regression	64.9%	0.72
Gradient Boosting	65.1%	0.71

We also attempted to decipher which factors were the most important to the network to predict shot success. Removing player names from the dataset still allowed the network to have an accuracy of 65% [Table 3]. This shows that the network treated the “PLAYER_NAME” factor as almost obsolete.

However, it is well known that different players vary hugely in their ability to make a shot, and thus it would be intuitive that the player name would be an essential factor. We propose using a larger data set, so the network has more time to understand the player’s history of making - or not-making - shots for the network to truly take into account the player’s name.

Furthermore, removing the “SHOT_DISTANCE” factor resulted in a 64% accuracy [Table 3]. This was because the network could easily compensate for the “SHOT_DISTANCE” with the XY coordinates factor. The most crucial factor for the network was “ACTION_TYPE”. When removing that factor, the network performed at 62% accuracy [Table 3]. This finding suggests that players and coaches should focus on the category of shots they take (ACTION_TYPE) to dramatically increase the shot success.

Table [3]: Table containing accuracy when certain features are removed.

	Accuracy
Original Features and Original Network Shape	65%
Removing "SHOT_DISTANCE" and Original Network Shape	64%
Removing "ACTION_TYPE" and Original Network Shape	62%
Removing "PLAYER_NAME" and Original Network Shape	65%

We have included a link to our code in the references section.

APPLICATION AND CONCLUSION

Overall, our networks were able to predict shot success with an accuracy between 64.9%-65.1%. Also, the neural network allowed us to understand that shot type(dunk, layup, hook shot) was the most significant factor in predicting shot success.

Our networks allow coaches to understand which players are taking the best quality shots. This has real game results as coaches can then give the ball to the player with the best shot selection during crucial moments of the game. This translates to a higher percentage of the shots going in, thus increasing the chances of winning.

For future avenues of further investigation, we suggest for researchers to use data that spans over entire seasons and possibly multiple seasons. The increased data points should hypothetically increase shot success rate prediction accuracy as the models will be able to take into account player names. Furthermore, the increased data points will allow the network to train for longer and further improve its accuracy.

ACKNOWLEDGMENTS

I would like to thank James Borg for mentoring me in this research paper as well as for proof-reading this paper.

REFERENCES

[1]: Larruskain, Jon, et al. "Genetic Variants and Hamstring Injury in Soccer: An Association and Validation Study." Medicine and Science in Sports and Exercise, U.S. National Library of Medicine, 2018, pubmed.ncbi.nlm.nih.gov/28976491/.

[2]: Cen, Raymond, et al. "NBA Shot Prediction and Analysis." NBA Shot Prediction and Analysis by hwchase17, hwchase17.github.io/sportvu/.

[3]: Meehan, Brett. Predicting NBA Shots, 2017, cs229.stanford.edu/proj2017/final-reports/5132133.pdf.

[4]: sealneaward(2018)nba-movement-data [Source Code] https://github.com/sealneaward/nba-movement-data

[5]:"3.2.4.3.5.Sklearn.ensemble.GradientBoostingClassifier ."Scikit ,scikit-learn.org/stable/modules/generated/sklearn.ensemble.GradientBoostingClassifier.html.

Figure [1]: Cen, Raymond, et al. "NBA Shot Prediction and Analysis." NBA Shot Prediction and Analysis by hwchase17, hwchase17.github.io/sportvu/.

Figure [2]: Neuronactivator.com. "What Even Is an Activation Function?" The Neuron Activator - Vaibhavsinh Vaghela, 13 Dec. 2019, www.neuronactivator.com/blog/what-even-is-activation-fu nction.

Figure[3]: Chris. "How to Use Binary & Categorical Crossentropy with Keras?" MachineCurve , 22 Oct. 2019, www.machinecurve.com/index.php/2019/10/22/how-to-use - binary-categorical-crossentropy-with-keras/.

Figure[4]: Narkhede, Sarang. "Understanding Logistic Regression." Medium , Towards Data Science, 26 May 2019, towardsdatascience.com/understanding-logistic-regression9b02c2aec102.

The code used throughout this paper can be found here: https://colab.research.google.com/drive/1Y1jup_Ub2KFUvrnYJCmke89nrmI7wngg?usp=sharing

Effects of CYP2D6*10 Mutation on Binding Affinity on Common Antidepressants in Japan

Miu Nakajima
The American School in Japan; Tokyo, Japan
Email: 21nakajimam@asij.ac.jp

Abstract – In Japan, there is an apparent lack of development and stigma associated with mental health treatment, including the use of antidepressants. Additionally, there is a large portion of the population possessing the allelic variant CYP2D6*10, which is part of the Cytochrome P450 superfamily responsible for metabolizing a wide variety of pharmaceuticals. Through this study, we aim to clarify the effects of genetic variation of CYP2D6 on adverse effects when using different antidepressants. We conducted an *in silico* study of binding affinities of different ligands to two CYP2D6 wild-type models, 4WNW and 2F9Q, and their respective threaded *10 models. Using SwissDock, the 4WNW model showed that the *10 variant had a lower binding affinity as compared to the wild-type. When using the 2F9Q model or X-Score, we had inconsistent results, leading us to question the reliability of these resources. Our results from SwissDock suggest that the *10 variant has a lower binding affinity, and therefore leading to a lower rate of metabolism. This suggests that people with this genetic mutation may be more susceptible to adverse effects when using antidepressants. Furthermore, future experiments regarding the correlation between CYP2D6*10 and drug metabolism should be conducted to advance mental health treatment and personalized medicine in Japan.

Key Words – binding affinity, CYP2D6, Cytochrome P450, mutation

INTRODUCTION

Mental health has, over time, presented itself as a major problem in Japan. Not recognized until the 90's, depression, anxiety, and other mental illnesses are still widely stigmatized and increasingly prevalent in Japanese youth (Nishi et al. 2019). Symptoms oftentimes are difficult to recognize, making it troublesome for the patient and clinicians to notice. Treatment methods include therapy, prescription medicine, or a combination of both. Among many, two major antidepressants sold to treat depressive disorders are fluoxetine and paroxetine (otherwise known as Prozac and Paxil, respectively), which are both selective serotonin reuptake inhibitors (SSRI).

The majority of medicines are metabolized by Cytochrome P450, crucial to the oxidation of xenobiotics and steroids (Guengerich 2007). Within the superfamily, one specific enzyme metabolizing a wide variety of antidepressants and antipsychotics is CYP2D6, primarily expressed in the liver (McConnachie et al. 2004). The CYP2D6 gene has been extensively researched, with many studies showing a strong correlation between allelic variation, drug metabolism and overall efficacy.

Gaedigk et al. (2017) paper gathered CYP2D6 allele-frequency data from various studies and sources to estimate frequencies of phenotypes across major world populations. Subjects categorized in the poor metabolizer status were predicted to make up about 0.4 to 5.4% of the population, intermediate metabolizers (decreased function) between 0.4 and 11%, normal metabolizers between 67 and 90%, and finally ultrarapid metabolizers between 1 and 21% of the population. Certain function and non-functional allelic variants were extracted from the data, as they are only specific to some populations; for example, the CYP2D6*10 decreased-function allele is very high in frequency in East Asia, as 45% of the population is reported to possess the gene (Gaedigk et al. 2017).

Studies conducted show the CYP2D6 wild-type allele and CYP2D6*10 differ in their amino acid sequences; in the *10 variant, the 34th amino acid is changed to a Serine from a Proline, and the 486th position is a Threonine instead of a Serine (Yokota et al. 1993, Dai et al. 2015). The CYP2D6*10 variant is also known to have a decreased metabolism, as discussed above, which suggests an effect on drug efficacy (Del Tredici et al. 2018). Given the association between ethnicity and CYP2D6 genotypes, it would be greatly beneficial to develop phenotype- or allele-specific drugs, utilized differently for various populations.

In a 2018 paper examining frequencies of CYP2D6 alleles, it was observed that 93% of all alleles were single copy alleles, with the majority (62%) functioning normally; of the 7% of structural variants, the majority (68%) had no function. As such, the proportion of structural variants with no or decreased function (72%) were substantially higher than the corresponding proportion of single copy variants (38%), suggesting a strong correlation between structural variants and gene function. Additionally, the proportion of structural variants was higher in Asians (30%) compared to other ethnicities (6-11%), suggesting an overall decrease of CYP2D6 enzyme activity in Asians. There are clear, demonstrated connections between ethnicity and genotype, and an association between structural variants and metabolism type (Del Tredici et al. 2018).

Here, we aim to characterize the interaction between the substrates and the CYP2D6*10 variant. Through

computational methods, we modelled the binding affinity of the three substrates to CYP2D6 wild-type, *10, and Aldehyde Reductase.

METHODS

The 4WNW protein was reported to be the most similar to the CYP2D6*10 enzyme when bound to a ligand (Don et al. 2020). We retrieved the amino acid sequences of both the wild-type CYP2D6 as well as the *10 variant from UniProt in order to model a structure for the latter using SwissModel (Waterhouse et al. 2018). To model the structures for our ligand, we used the application ChemSketch and converted the models to PDB files suitable for Chimera. We then proceeded to remove the remaining substrates and non-integral charges from the retrieved 4WNW crystal structure, leaving just the enzyme itself. Our selected negative control enzyme, Aldehyde Reductase, is not from the Cytochrome P450 superfamily, therefore not metabolizing fluoxetine, paroxetine, venlafaxine or nortriptyline. Glucose is a known substrate of Aldehyde Reductase, but not metabolized by any Cytochrome P450 protein, therefore serving as a positive control for Aldehyde Reductase and a negative control.

In order to prepare the structures for docking, we used the Dock Prep plugin within Chimera; first removing non-complexed ions from the structure (Shapovalov et al. 2011), then determining the residue charges by the Gasteiger method (Wang et al. 2006). We converted the enzyme structures into PDB files in order to make it compatible with SwissDock when submitting the protein-ligand pairs (Grosdidier et al. 2011).

After we received the results, we analyzed the structures in order to determine whether or not the substrates were binding in their correct binding sites. For some of our negative controls, while we did get a full fitness value, we decided to disregard the number as the ligand was not binding in the correct active site. Full fitness value (kcal/mol) refers to the binding affinity of the ligand and the protein; the lower the full fitness value, the better the binding affinity. The Delta G value (Gibbs free energy) also refers to the binding affinity; similarly, the lower the Delta G value, the better the binding affinity.

Additionally, we decided to confirm our data using another CYP2D6 wild-type (PDB code: 2F9Q), as the structure was used in a study conducted in 2008 (Ito et al. 2008). We submitted this structure and the *10 amino acid sequence for threading using SwissModel (Waterhouse et al. 2018). We repeated the preparation process in Chimera and submission to SwissDock.

In order to further validate the SwissDock results, we used X-Score, a program designed to compute binding affinity by Dr. Shaomeng Wang's group at the University of Michigan Medical School (Wang et al. 2002). In order to run the program successfully, we were required to split the PDB files downloaded from SwissDock into the protein and the ligand, a PDB file and a Mol2 file respectively.

RESULTS

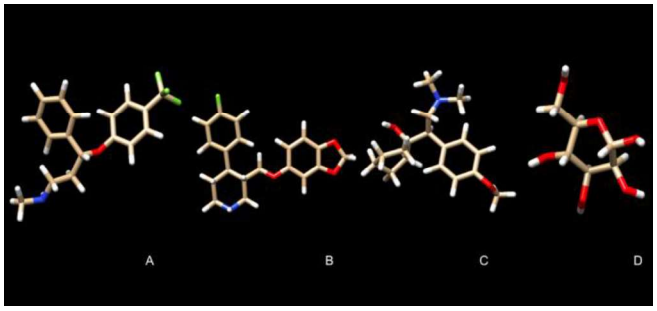

FIGURE 1: comparison of fluoxetine (A), paroxetine (B), venlafaxine (C), and glucose (D) chemical structure.

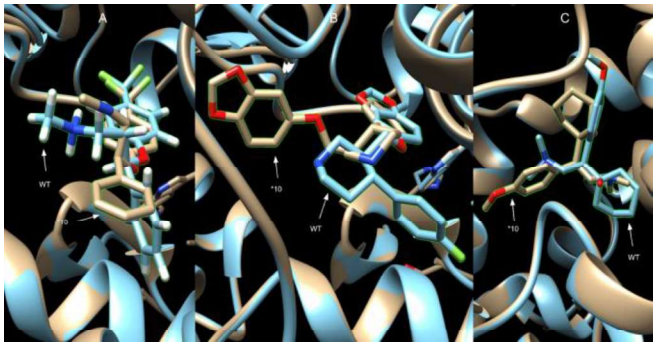

FIGURE 2: Comparison of the WT and *10 binding sites with fluoxetine (A), paroxetine (B), and venlafaxine (C) (blue shows WT, tan shows *10).

After inspection of the amino acid sequences, the mutation in the 486th position of the *10 allele from a Serine to a Threonine is only three amino acids away from the active site. This change seems to have a great effect on the binding affinity, and therefore causes substantially lower metabolism. As shown in Figure 2, CYP2D6 WT and *10 have minimal differences in their structures. One noticeable difference is the orientation of the ligand within the binding site; for example, paroxetine binds completely flipped within the binding pocket. Since there are not many obvious differences between the structures as a whole, this suggests that the orientation of the ligand in the active site immensely affects binding affinity.

TABLE 1: Full fitness (kcal/mol) of each enzyme and substrate. NB indicates SwissDock did not predict binding in the correct binding site.

	CYP2D6 WT (4WNW)	CYP2D6*10 (4WNW)	CYP2D6 WT (2F9Q)	CYP2D6*10 (2F9Q)	Aldehyde Reductase
Fluoxetine	-2104.54	-2006.49	-2277.55	NB	NB
Paroxetine	-2133.69	-2038.27	NB	NB	NB
Venlafaxine	-2106.40	-2005.68	NB	NB	NB
Nortriptyline	-2073.38	-1981.23	NB	NB	NB
Glucose	NB	NB	NB	NB	-1405.39

TABLE 2: Estimated ΔG (kcal/mol) of each enzyme and substrate. NB indicates SwissDock did not predict binding in the correct binding site.

	CYP2D6 WT (4WNW)		CYP2D6*10 (4WNW)		CYP2D6 WT (2F9Q)		CYP2D6*10 (2F9Q)		Aldehyde Reductase	
	Swiss Dock	X-Score	Swiss Dock	X-Score	Swiss Dock	X-Score	Swiss Dock	X-Score	Swiss Dock	X-Score
Fluoxetine	-9.225	-8.10	-9.06	-8.10	-8.01	-8.40	NB	NB	NB	NB
Paroxetine	-9.17	-8.11	-9.13	-8.37	NB	NB	NB	NB	NB	NB
Venlafaxine	-8.63	-7.75	-8.62	-7.87	NB	NB	NB	NB	NB	NB
Nortriptyline	-7.02	-8.32	-8.29	-8.35	NB	NB	NB	NB	NB	NB
Glucose	NB	NB	NB	NB	NB	NB	NB	NB	-6.44	-6.05

As predicted and shown in Table 1, our negative controls showed no binding to either WT nor *10 structures. Our positive control, aldehyde reductase, also bound to glucose. For all substrates except glucose, the wild-type protein was predicted to have substantially lower full fitness compared to the *10 variant when using SwissDock. Out of the four given substrates, paroxetine showed the best binding affinity as compared to the other two for both the WT and *10 CYP2D6 enzyme.

Ito et al. (2008) paper found that the ligand nortriptyline bound to the CYP2D6 wild-type (PDB model 2F9Q) had a ΔG value of -8.89 kcal/mol when modelled, and -9.00 kcal/mol when observed experimentally. It was also predicted that the CYP2D6*10 had a more positive ΔG value as compared to the wild-type protein, suggesting lower binding affinity. In contrast to their findings, none of our ligands bound correctly in the active site to the CYP2D6 wild-type or *10 threaded using the 2F9Q wild-type, with the exception of fluoxetine with the 2F9Q wild-type.

When X-Score was used, the ΔG values of the *10 variant were lower than that of the wild-type, which indicates better binding affinity. These results directly opposed our previous outcomes from SwissDock, as SwissDock had consistently, for all our substrates, predicted the wild-type ΔG value to be lower as compared to *10.

Ultimately, it was difficult to find previous studies with comparable results and data, and to run software that suited our study. Additionally, there was an inconsistency with our data from SwissDock; for example, when looking at the binding affinity of the CYP2D6 WT (PDB code: 2F9Q) with our ligands, only fluoxetine bound to the protein in the correct binding site, though paroxetine, venlafaxine, and nortriptyline are known substrates of CYP2D6.

DISCUSSION

Our results suggest altered docking and lower binding affinity of fluoxetine, paroxetine, venlafaxine, and nortriptyline to CYP2D6*10 when using SwissDock to predict binding affinity by full fitness value. To our surprise, none of the substrates except for fluoxetine bound correctly to the CYP2D6 wild-type 2F9Q model. Moreover, none of our ligands bound with the CYP2D6*10 in the actual active site when the 2F9Q model was used for threading.

From our results, it is probable that possessing the *10 variant causes lower binding affinity, leading to a drop in metabolism. This supports our initial hypothesis gathered from our literature review, as CYP2D6*10 is named as an "intermediate metabolizer". While this negative trend could be seen in the 4WNW wild-type and *10 when using SwissDock, the trend was lost when using X-Score or another model (PDB code: 2F9Q).

Our findings and results were fairly limited due to the lack of availability in software and previous research or resources. Our data was limited to an *in silico* experiment, only using relatively outdated freely available resources (such as X-Score from 2003). There was an apparent lack of possible software that could be used, alongside a frequent need for troubleshooting. Additionally, there was a lack of public available data and studies on the *10 allele and gene-based medication in Japan to use for comparison; we were unable to find reliable data for comparison.

Studies have shown that the *10 allele is most prevalent in East Asians, the gene first being discovered in Japanese subjects. Within a study conducted in 1993, CYP2D6*10 is found to have a lower metabolic rate than a regularly functioning enzyme (Yokota et al. 1993). In the future, we strongly believe the need for an in vivo experiment within a lab to produce accurate results to confirm this study; this would be greatly beneficial towards Japanese health programs and pharmaceutical development. We also suggest, if possible, a population study to view and scrutinize the direct correlation and relationship between allelic variant or genotype and the binding affinity or rate of metabolism. Given the prevalence of the *10 variant within the Japanese population, we hope that this study contributes to the limited body of research on Japanese mental health, and may in the future be applied clinically to lower dosages for Japanese patients as a "regular" dose may put the patient at a higher risk for adverse effects. This further suggests development in personalized medication, especially in Japan, since patients may be more prone to experiencing adverse effects.

AKNOWLEDGEMENTS

The author wishes to thank Elizabeth Feldeverd, for their help and guidance in conducting the experiments and proofreading this paper.

REFERENCES

ACD/ChemSketch, version 2020.1.0, Advanced Chemistry Development, Inc., Toronto, ON, Canada, www.acdlabs.com, 2020.

Bradford, L DiAnne. 'CYP2D6 Allele Frequency in European Caucasians, Asians, Africans and Their Descendants'. *Pharmacogenomics* 3, no. 2 (March 2002): 229–43. https://doi.org/10.1517/14622416.3.2.229.

Dai, Da-Peng, Pei-Wu Geng, Shuang-Hu Wang, Jie Cai, Li-Ming Hu, Jing-Jing Nie, Ji-Hong Hu, Guo-Xin Hu, and Jian-Ping Cai. '*In Vitro* Functional Assessment of 22 Newly Identified CYP2D6 Allelic Variants in the Chinese Population'. *Basic & Clinical Pharmacology & Toxicology* 117, no. 1 (July 2015): 39–43. https://doi.org/10.1111/bcpt.12363.

Del Tredici, Andria L., Alka Malhotra, Matthew Dedek, Frank Espin, Dan Roach, Guang-dan Zhu, Joseph Voland, and Tanya A. Moreno. 'Frequency of CYP2D6 Alleles Including Structural Variants in the United States'. *Frontiers in Pharmacology* 9 (5 April 2018): 305. https://doi.org/10.3389/fphar.2018.00305.

Don, Charleen G., and Martin Smieško. 'In Silico Pharmacogenetics CYP2D6 Study Focused on the Pharmacovigilance of Herbal Antidepressants'. *Frontiers in Pharmacology* 11 (13 May 2020): 683. https://doi.org/10.3389/fphar.2020.00683.

Gaedigk, Andrea, Katrin Sangkuhl, Michelle Whirl-Carrillo, Teri Klein, and J. Steven Leeder. 'Prediction of CYP2D6 Phenotype from Genotype across World Populations'. *Genetics in Medicine* 19, no. 1 (January 2017): 69–76. https://doi.org/10.1038/gim.2016.80.

Gressier, F., C. Verstuyft, P. Hardy, L. Becquemont, and E. Corruble. 'Response to CYP2D6 Substrate Antidepressants Is Predicted by a CYP2D6 Composite Phenotype Based on Genotype and Comedications with CYP2D6 Inhibitors'. *Journal of Neural Transmission* 122, no. 1 (January 2015): 35–42. https://doi.org/10.1007/s00702-014-1273-4.

Grosdidier, A., V. Zoete, and O. Michielin. 'SwissDock, a Protein-Small Molecule Docking Web Service Based on EADock DSS'. *Nucleic Acids Research* 39, no. suppl (1 July 2011): W270–77. https://doi.org/10.1093/nar/gkr366.

Guedes, Isabella A., Felipe S. S. Pereira, and Laurent E. Dardenne. 'Empirical Scoring Functions for Structure-Based Virtual Screening: Applications, Critical Aspects, and Challenges'. *Frontiers in Pharmacology* 9 (24 September 2018): 1089. https://doi.org/10.3389/fphar.2018.01089.

Guengerich, F. Peter. 'Cytochrome P450 and Chemical Toxicology'. *Chemical Research in Toxicology* 21, no. 1 (January 2008): 70–83. https://doi.org/10.1021/tx700079z.

Hawton, Keith, Helen Bergen, Sue Simkin, Jayne Cooper, Keith Waters, David Gunnell, and Navneet Kapur. 'Toxicity of Antidepressants: Rates of Suicide Relative to Prescribing and Non-Fatal Overdose'. *British Journal of Psychiatry* 196, no. 5 (May 2010): 354–58. https://doi.org/10.1192/bjp.bp.109.070219.

Hodgson, Karen, Katherine Tansey, Mojca Zvezdana Dernovšek, Joanna Hauser, Neven Henigsberg, Wolfgang Maier, Ole Mors, et al. 'Genetic Differences in Cytochrome P450 Enzymes and Antidepressant Treatment Response'. *Journal of Psychopharmacology* 28, no. 2 (February

2014): 133–41. https://doi.org/10.1177/0269881113512041.

Ihara, Hiroshi. 'A Cold of the Soul: A Japanese Case of Disease Mongering in Psychiatry'. *International Journal of Risk & Safety in Medicine* 24, no. 2 (2012): 115–20. https://doi.org/10.3233/JRS-2012-0560.

Ito, Yuko, Hiroki Kondo, Peter S. Goldfarb, and David F.V. Lewis. 'Analysis of CYP2D6 Substrate Interactions by Computational Methods'. *Journal of Molecular Graphics and Modelling* 26, no. 6 (February 2008): 947–56. https://doi.org/10.1016/j.jmgm.2007.07.004.

Jain, Tarun, and B. Jayaram. 'An All Atom Energy Based Computational Protocol for Predicting Binding Affinities of Protein-Ligand Complexes'. *FEBS Letters* 579, no. 29 (5 December 2005): 6659–66. https://doi.org/10.1016/j.febslet.2005.10.031.

Mahlich, Jörg, Sunny Tsukazawa, and Frank Wiegand. 'Estimating Prevalence and Healthcare Utilization for Treatment-Resistant Depression in Japan: A Retrospective Claims Database Study'. *Drugs - Real World Outcomes* 5, no. 1 (March 2018): 35–43. https://doi.org/10.1007/s40801-017-0126-5.

Mcconnachie, L. 'Human Liver Cytochrome P450 2D6 Genotype, Full-Length Messenger Ribonucleic Acid, and Activity Assessed with a Novel Cytochrome P450 2D6 Substrate*1'. *Clinical Pharmacology & Therapeutics* 75, no. 4 (April 2004): 282–97. https://doi.org/10.1016/j.clpt.2003.12.003.

Nishi, Daisuke, Hanako Ishikawa, and Norito Kawakami. 'Prevalence of Mental Disorders and Mental Health Service Use in Japan'. *Psychiatry and Clinical Neurosciences*, 29 May 2019, pcn.12894. https://doi.org/10.1111/pcn.12894.

Okubo, Maho, Norie Murayama, Jun Miura, Yasuji Chiba, and Hiroshi Yamazaki. 'Effects of Cytochrome P450 2D6 and 3A5 Genotypes and Possible Coadministered Medicines on the Metabolic Clearance of Antidepressant Mirtazapine in Japanese Patients'. *Biochemical Pharmacology* 93, no. 1 (January 2015): 104–9. https://doi.org/10.1016/j.bcp.2014.11.011.

Rau, T. 'Cyp2d6 Genotype: Impact on Adverse Effects and Nonresponse during Treatment with Antidepressants—a Pilot Study'. *Clinical Pharmacology & Therapeutics* 75, no. 5 (May 2004): 386–93. https://doi.org/10.1016/j.clpt.2003.12.015.

Ronald F B (1995). "Nonsteroidal anti-inflammatory drugs". In Foye, William O., Lemke, Thomas L., Williams, David A (eds.). *Principles of Medicinal Chemistry* (Fourth ed.). Williams & Wilkins. pp. 544–545.

Sadiq, S. Kashif, David W. Wright, Owain A. Kenway, and Peter V. Coveney. 'Accurate Ensemble Molecular Dynamics Binding Free Energy Ranking of Multidrug-Resistant HIV-1 Proteases'. *Journal of Chemical Information and Modeling* 50, no. 5 (24 May 2010): 890–905. https://doi.org/10.1021/ci100007w.

Sansen, Stefaan, Jason K. Yano, Rosamund L. Reynald, Guillaume A. Schoch, Keith J. Griffin, C. David Stout, and Eric F. Johnson. 'Adaptations for the Oxidation of Polycyclic Aromatic Hydrocarbons Exhibited by the Structure of Human P450 1A2'. *Journal of Biological Chemistry* 282, no. 19 (11 May 2007): 14348–55. https://doi.org/10.1074/jbc.M611692200.

Shapovalov, Maxim V., and Roland L. Dunbrack. 'A Smoothed Backbone-Dependent Rotamer Library for Proteins Derived from Adaptive Kernel Density Estimates and Regressions'. *Structure* 19, no. 6 (June 2011): 844–58. https://doi.org/10.1016/j.str.2011.03.019.

Torre, Rafael de la, Samanta Yubero-Lahoz, Ricardo Pardo-Lozano, and Magí Farré. 'MDMA, Methamphetamine, and CYP2D6 Pharmacogenetics: What Is Clinically Relevant?' *Frontiers in Genetics* 3 (2012). https://doi.org/10.3389/fgene.2012.00235.

Wan, Shunzhou, and Peter V. Coveney. 'Rapid and Accurate Ranking of Binding Affinities of Epidermal Growth Factor Receptor Sequences with Selected Lung Cancer Drugs'. *Journal of The Royal Society Interface* 8, no. 61 (7 August 2011): 1114–27. https://doi.org/10.1098/rsif.2010.0609.

Wang, An, C. David Stout, Qinghai Zhang, and Eric F. Johnson. 'Contributions of Ionic Interactions and Protein Dynamics to Cytochrome P450 2D6 (CYP2D6) Substrate and Inhibitor Binding'. *Journal of Biological Chemistry* 290, no. 8 (20 February 2015): 5092–5104. https://doi.org/10.1074/jbc.M114.627661.

Wang J, Wang W, Kollman PA, Case DA. Automatic atom type and bond type perception in molecular mechanical calculations. *J Mol Graph Model*. 2006;25(2):247-260. doi:10.1016/j.jmgm.2005.12.005

Wang, R.; Lai, L.; Wang, S. Further Development and Validation of Empirical Scoring Functions for Structure-Based Binding Affinity Prediction. J. Comput.-Aided Mol. Des. 2002, 16, 11-26.

Waterhouse, Andrew, Martino Bertoni, Stefan Bienert, Gabriel Studer, Gerardo Tauriello, Rafal Gumienny, Florian T Heer, et al. 'SWISS-MODEL: Homology Modelling of Protein Structures and Complexes'. *Nucleic Acids Research* 46, no. W1 (2 July 2018): W296–303. https://doi.org/10.1093/nar/gky427.

Whyte, I.M. 'Relative Toxicity of Venlafaxine and Selective Serotonin Reuptake Inhibitors in Overdose Compared to Tricyclic Antidepressants'. *QJM* 96, no. 5 (1 May 2003): 369–74. https://doi.org/10.1093/qjmed/hcg062.

Zhao, Lizi, and Gisèle Pickering. 'Paracetamol Metabolism and Related Genetic Differences'. *Drug Metabolism Reviews* 43, no. 1 (February 2011): 41–52. https://doi.org/10.3109/03602532.2010.527984.

The Impact of Rapid State Policy Response on Cumulative Deaths Caused by COVID-19

Takuto Nakamura
Cambridge School of Weston; Massachusetts, USA
Email: tnakamura2021@csw.org

Abstract – Amidst the COVID-19 pandemic the majority of US states enacted a statewide stay-at-home order. This paper makes use of state-level heterogeneity in policy responses to conduct a cross-sectional regression analysis of lock-down response on Covid-19 deaths. The results of this paper suggest that states which imposed stay-at-home orders more quickly after reaching a threshold proportion of deaths had significantly fewer deaths 3 weeks after lock-down. We use of a robust set of control variables in order to minimise bias arising from confounding factors. Results show that the predicted increase in the cumulative deaths after 21 days of lockdown for the average state associated with delaying implementation of policy by 1 week is approximately 46%. The result shows that speed is a crucial factor that state governors should consider when enacting a stay-at-home policy.

Key Words – COVID-19, Lockdown speed, Stay-at-home, Ordinary least squares, Cumulative deaths

INTRODUCTION

I. Background

COVID-19 is an infectious disease caused by the SARS-CoV-2 virus that commonly affects the respiratory system and has been classified as a pandemic by the World Health Organisation [1]. In the United States the federal political system grants each state the authority to enact policies at their discretion. This has caused statewide responses to contain the virus to be enacted at different times; policies include stay-at-home orders, face-covering requirements, large gathering bans, and travel restrictions. Measuring the effectiveness of policies is commonly done by tracking cases and deaths. In this paper, we chose to look solely at deaths. Stay-at-home orders have been a popular measure for states to enact. Stay-at-home orders mandate citizens to restrict their movement outside of their residence. Given the prominence of this policy, a number of papers have already analysed 2020 stay-at-home orders.

II. Literature Review

Tian et al. [2] looked at the effect of travel restrictions and other control measures on the prevention of the spread of SARS-CoV-2 in Wuhan, China in the first 50 days of the pandemic. The team used multiple methods of analysis including ordinary least squares (OLS) estimation. Results show that a faster response in intracity transports suspension, entertainment venue closures, and public gathering bans lower the number of COVID-19 cases in the first week. Their model suggested that the national emergency response and travel bans helped limit the confirmed COVID-19 cases by 96% compared to a model where none of these measures were taken into effect.

Fowler et al. [3] researched the effectiveness of stay-at-home orders at a county level in the US. Using data from the COVID Tracking Project, the team graphed the log of confirmed cases of multiple counties and analysed the correlation between the counties that implemented stay-at-home orders and ones that didn't. The team found that, overall, counties that implemented stay-at-home orders saw a reduction in COVID-19 cases compared to counties that did not implement any policy. I used this paper as a basis for our model and analysis.

With the continued lack of containment of COVID-19 cases, we still do not have a clear understanding of measures that are effective in containing COVID-19. By analysing the effect of policies, we can prepare the most effective way of dealing with continuous waves of this current pandemic or a new pandemic in the future. Here, we aim to analyse the correlation between the speed of lockdown and deaths caused by COVID-19.

DATA

Key data used in the analysis comes from the Kaiser Family Foundation[4], a non-profit organisation mainly focusing on medicare and health policies. Population data is from the 2010 and 2019 census [5], income is from the 2016 American community survey [6], and political affiliation is from the 2016 presidential elections [7].

Starting this project our main goal was to look at the effects of policies on the number of deaths that occurred after the policies are enacted. In doing this we first looked at the different policies states implemented during this pandemic. A few common policies were stay-at-home orders, face-covering requirements, gathering bans, and travel restrictions. We chose to look at the stay-at-home policy for our project because this was a policy most states put out and in our hypothesis we thought had the most effect out of the other common policies. From the paper mentioned above, we

TABLE 1: Descriptive Statistics of Key Variables

VARIABLES	Mean	Median	p25	p75	S.D.	#Obs	min	max
death21days	406.0	183	87	537	575.5	41	7	2,854
lockdownspeed	2.341	2	-2	5	6.147	41	-10	21
income	61,141	58,756	54,478	70,315	10,337	41	44,097	83,242
politics	0.561	1	0	1	0.502	41	0	1
population	7.210e+06	5.640e+06	2.976e+06	8.536e+06	7.557e+06	41	623,989	3.951e+07
travelquarantine	0.512	1	0	1	0.506	41	0	1
facecovering	2.439	3	2	3	0.976	41	0	3
urbanpopulation	74.60	75.10	66.30	87.20	14.84	41	38.70	95

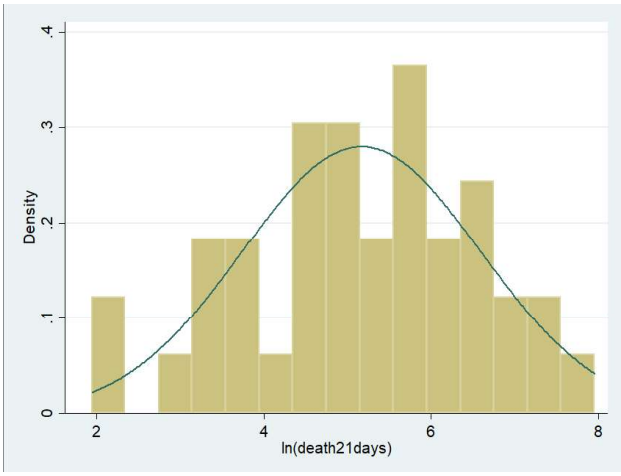

FIGURE 1B: Histogram of logarithm of death21day excluding New York

know that there was a significant effect of having a lockdown at the county level. Our goal is to see if the speed at which this policy is implemented has an effect on the outcome. To measure the speed of lockdown we first thought of choosing a single date as a benchmark to see the difference in timing but this would cause bias in states with earlier COVID-19 cases. Based on existing analyses [8] we came up with taking the number of days between the day at which 1 in 1 million deaths was reported in the state and the day the stay-at-home policy was implemented. This allowed us to get a more reliable benchmark for the speed of lock down because this would adjust for the timing at which each state was introduced with COVID-19 and the differences in population for each state.

In order to evaluate the effect of the stay-at-home order, we looked at the number of deaths that happened after the policy. We chose to solely look at the deaths because of differences in the number of tests in different states, do not allow for a like for like comparison of cases across the states. If early policies were more effective we should see a lower number of deaths in such states.

In order to have a benchmark for the deaths, we follow Fowler et al. [3] in looking at the day in which the lockdown was initiated and taking the number of cumulative deaths 3 weeks (21day) after the enactment of the policy. We believe 21 days is a sufficient period of time to capture most of the deaths prevented due to lockdown based on calculations on the average incubation period and median lag time for fatality.[1] This allows like for like comparison for each state.

In our final data set, we only looked at the mainland state which had a lockdown policy implemented at some point. This was to get a more similar comparison between states. We also excluded New York from our data set because of its anomalous nature. (Figure 1A) This then left us with 41 states in our data set.

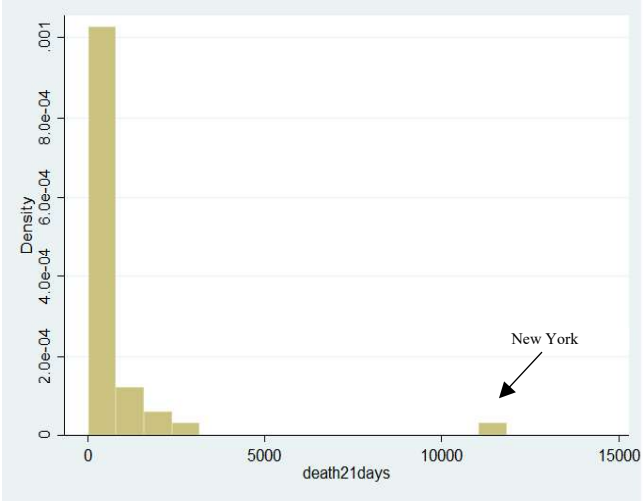

FIGURE 1A: Histogram of death21days

[1]Based on the data from the WHO and the CDC the average incubation period is 5-6 days and the median lag time for fatality is 13 days which, assuming the lockdown has an immediate effect on transmission implies that most of the prevented deaths would have occurred 18-19 days after lockdown. [9][10]

TABLE 2: Variable Descriptions		
Variable	Definition	Purpose
lockdownspeed	The number of days between 1 in 1 million COVID-19 deaths and implementation of a lockdown policy. (Higher values mean slower response time)	Independent Variable
death21days	The number of cumulative COVID-19 deaths 21 days after the implementation of a lockdown.	Dependent Variable
Politics	Republican or democratic state taken from the 2016 presidential election.	Control Variable
Urbanpopulation	% of population classified as urban taken from the 2010 census.	Control Variable
Population	State populations were taken from the 2019 census.	Control Variable
Income	Average state median household income was taken from the 2018 American community survey.	Control Variable
Travel Quarantine	Dummy variable describing the occurrence of a travel quarantine.	Control Variable
Face Covering	Categorical variable describing the different strengths of a face covering policy. Required for General Public (3) Required for Certain Employees (2) Allows Local Officials to Require for General Public (1)	Control Variable

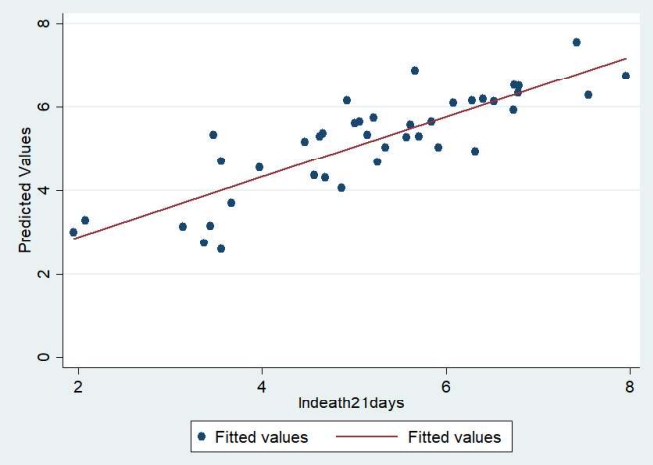

FIGURE 2: Scatter plot of predicted values on the log of number of deaths 21 days after lockdown.

METHODOLOGY

$$\text{lndeath21days}_i = \beta_0 + \beta_1 lockdownspeed_i + \boldsymbol{X_i}\,\boldsymbol{\gamma} + \varepsilon_i$$

The above model is what we sought to estimate with the coefficient of interest being beta 1. The beta 1 coefficient multiplied by 100 is interpreted as the average predicted percentage point difference in the number of cumulative deaths after 21 days in a given state, after controlling for state differences, if the lockdown policy was delayed by 1 day. We considered a quadratic term on our independent variable because of the exponential nature of the spread of viruses. However, in this more flexible specification, we found the coefficient on the square term to be negative and the p-value to be insignificant indicating the linear model to be more appropriate. This is most likely because the early stages of a pandemic are best described in a linear fashion [11].

We estimate the above model using OLS regression. OLS takes the squared difference in the dependent variable and the predicted linear model and minimises the sum of the differences in order to estimate the relationship of the dependent variable on the independent variable. To obtain unbiased and efficient estimates, least squares has a number of assumptions that need to be met. These are discussed below.

In order to demonstrate the normality of residuals, we applied the Shapiro-Wilk test [12] to our residuals. We realised that the dependent variable is log normally distributed through graphical analysis. (Figure 1B)

Hence we used the natural log of the dependent variable in our model. Furthermore, a Shapiro-Wilk test performed on the residuals gives us a p-value of 0.128 which is greater than 0.05, meaning that we fail to reject the null hypothesis of the residuals being normally distributed.

To deal with heteroscedastic terms we used robust standard errors.

To ensure that multicollinearity does not have a significant effect on the standard errors of the estimated coefficients we performed a VIF test, the result of which was

TABLE 3: OLS Results

VARIABLES	(1)	(2)	(3)	(4)
lockdownspeed	0.0519*	0.0730***	0.0807***	0.0660***
	(0.0291)	(0.0238)	(0.0203)	(0.0224)
population		1.01e-07***	3.94e-08	2.60e-08
		(3.11e-08)	(2.51e-08)	(2.59e-08)
politics			0.372	0.620
			(0.389)	(0.410)
income			-3.98e-06	-6.31e-06
			(2.39e-05)	(2.74e-05)
urbanpopulation			0.0613***	0.0647***
			(0.0142)	(0.0151)
travelquarantine				-0.799**
				(0.303)
1.facecovering				-0.251
				(0.418)
2.facecovering				-0.202
				(0.502)
3.facecovering				0.118
				(0.372)
Region Controls?	N	Y	Y	Y
Observations	41	41	41	41
R-squared	0.050	0.435	0.673	0.743

Robust standard errors in parentheses
*** p<0.01, ** p<0.05, * p<0.1

1.92; this low value [13] provides sufficient evidence that we do not have significant multicollinearity in our model.

Strict exogeneity is required in order for the least squares estimator to be unbiased. This can be caused by multiple different factors such as measurement error in the independent variable, simultaneity, and omitted variables. It is reasonable to assume that there is almost no measurement error in the independent variable because we know the exact dates in which the policies were taken into effect. Simultaneity can also be ruled out because our values of the dependent variable were realised 21 days after our independent variable. The most likely source of bias is from omitted variable bias. In our model, we included a range of control variables to minimise omitted variable bias.

In the table above we describe each variable and the purpose it has in our model. (Table 2)

RESULTS

As expected the simple regression model in column 1 (Table 3) shows a positive correlation between speed of lockdown and the cumulative deaths after 21 days but is not statistically significant. However, this result fails to take into account potentially confounding variables. The 2nd column includes population size and region controls which increases the average predicted impact of delayed policy implementation on the cumulative deaths after 21 days of lockdown and the result is now statistically significant at the 1% level. The 3rd column includes additional controls such as urban population, income, and politics demonstrating the robustness of the result: the coefficient on lockdownspeed remains positive and statistically significant. Finally in the 4th column we take into account some of the other policies that were implemented in a similar timeframe to ensure we are not capturing the effect of policies other than lockdown. The magnitude of the coefficient decreased slightly but is still significant at the 1% level.

From our results, we can see that the coefficient does not change greatly in the different variations of the model ranging from 5-8 percentage points and that the p-value of the coefficient implies that there is a statistically significant relationship.

The result from our preferred specification (column 4) suggests that the expected increase in the cumulative deaths after 21 days of lockdown for the average state associated with delaying implementation of policy by 1 week is 46.2%. With the average number of COVID-19 deaths after 21 days of lockdown being 408 deaths, if we imagine a scenario in which the “average” state implements a stay-at-home policy a week later, we would expect to see an increase in deaths from 408 to 596.

DISCUSSION & LIMITATIONS

These results strongly support rapid action from state governments in response to the spread of COVID-19. Additionally as seen in the table urban population and travel quarantine seem to also have a significant effect on the deaths. As expected the urban population has a positive coefficient and travel quarantine has a negative coefficient. This shows that higher urban population % is correlated with an increase in cumulative deaths after 21 days of lockdown and that a travel quarantine is associated with lower deaths.

The R-squared value shows that our preferred specification has high predictive power. Furthermore, this is represented in figure 2 with our predicted deaths strongly correlating with the actual number of deaths.

While we were able to do an analysis on a data set with 41 observations this is rather small from a statistical standpoint and consequently, the power of the statistical tests conducted is low. In future improvements to this analysis, it would be better if we could gather more data. For example, we can work on a county scale, not state-level as done by Fowler et al. [3].

Although we attempted to account for confounding factors, we cannot rule out the possibility of endogeneity and therefore bias as we don't account for every variation between states, such as the age distribution of the state. As such we cannot say with certainty that our results are causal. One possible variable that may affect our data is the availability of beds for COVID-19 patients in each state. This theoretically could have caused a faster response to COVID-19 as the state has a smaller capacity to take in patients and will cause greater deaths after 21days because of the lack of medical preparation the state had. Assuming this is plausible our failure to account for this in our analysis implies our estimate of the impact of the speed of lockdown is an underestimate. Further analysis needs to be conducted.

In our paper, we looked at the stay-at-home policy to be the most effective policy when it came to COVID-19 response. But it is true that there were several other policies that were enacted within days of each other. Although we account for some of these, we cannot say that our findings capture solely the effect of the speed of lockdown but instead captures the effect of lockdown and other bundled policies enacted in the same timeframe.

CONCLUSION

We analysed the effect of the speed of lockdown on the number of deaths after 21 days of lockdown. This shows that the speed of lockdown is a crucial factor that state governors should consider. However, we recommend policymakers take in to account other research of other policies because we do not have a measure to compare different aspects of multiple policies; there is a possibility that there are other factors more impactful than the speed in which the lockdown is enacted. Furthermore, we are not comparing the magnitude of the effect of the speed of lockdown to other significant policy measures like the strength of lockdown, the duration of lockdown, and other policies. We leave this to further research.

AKNOWLEDGEMENTS

The author wishes to thank Matin Khadem for his help and guidance in conducting research and proofreading this paper.

REFERENCES

[1] World Health Organization: WHO. "Coronavirus." World Health Organization, 10 Jan. 2020, www.who.int/health-topics/coronavirus#tab=tab_1.

[2] Tian, Huaiyu, et al. "An Investigation of Transmission Control Measures during the First 50 Days of the COVID-19 Epidemic in China." Science, vol. 368, no. 6491, 2020, pp. 638–42. Crossref, doi:10.1126/science.abb6105.

[3] Fowler, James H., et al. "The Effect of Stay-at-Home Orders on COVID-19 Infections in the United States." SSRN Electronic Journal, 2020. Crossref, doi:10.2139/ssrn.3576826.

[4] "State Data and Policy Actions to Address Coronavirus." KFF, 25 Aug. 2020, www.kff.org/coronavirus-covid-19/issue-brief/state-data-and-policy-actions-to-address-coronavirus.

[5] US Census Bureau. "State Population Totals: 2010-2019." The United States Census Bureau, 30 Dec. 2019, www.census.gov/data/tables/time-series/demo/popest/2010s-state-total.html.

[6] ---. "Data Profiles." US Census Bureau, www.census.gov/acs/www/data/data-tables-and-tools/data-profiles/2016. Accessed 26 Aug. 2020.

[7] "Associated Press Interactive." Associated Press, interactives.ap.org/2016/general-election/?SITE=APQA. Accessed 26 Aug. 2020.

[8] "Coronavirus: The Lost Six Weeks When US Failed to Contain Outbreak." BBC News, 12 May 2020, www.bbc.com/news/av/world-us-canada-52622037.

[9] "Coronavirus disease 2019 (COVID-19) Situation Report – 73" World Health Organization ,2 April 2020, https://www.who.int/docs/default-source/coronaviruse/situation-reports/20200402-sitrep-73-covid-19.pdf

[10] "Case-Fatality Risk Estimates for COVID-19 Calculated by Using a Lag Time for Fatality - Volume 26, Number 6-June 2020 - Emerging Infectious Diseases Journal - CDC." Centers for Disease Control and Prevention, Centers for Disease Control and Prevention, wwwnc.cdc.gov/eid/article/26/6/20-0320_article.

[11] Viboud, Cécile, et al. "A Generalized-Growth Model to Characterize the Early Ascending Phase of Infectious Disease Outbreaks." Epidemics, vol. 15, 2016, pp. 27–37. Crossref, doi:10.1016/j.epidem.2016.01.002.

[12] Shapiro, S. S., and M. B. Wilk. "An Analysis of Variance Test for Normality (Complete Samples)." Biometrika, vol. 52, no. 3/4, 1965, p. 591. Crossref, doi:10.2307/2333709.

[13] Daoud, Jamal I. "Multicollinearity and Regression Analysis." Journal of Physics: Conference Series, vol. 949, 2017, p. 012009. Crossref, doi:10.1088/1742-6596/949/1/012009.

PHOTOGRAPHY AS AN ELEGY: SOLITUDE AND ISOLATION

Yuta Namba
St.Mary's International School; Tokyo, Japan
Email: yutanamba16@gmail.com

Abstract – Photography, like all art, is subjective. Critics view photography to find meaning through the multiple implications they make from the subjects that appear, lighting used, etc. However, photography maintains an objectivity as well in its ability to take a moment out of time itself, a form of elegy. This research paper expands on this idea through examination of two photographs, Eliot Porter's Red Tree Near Cades Cove, Great Smoky Mountains National Park, Tennessee and my Man in Nature. Through Susan Sontag's lens of photography as elegy, I investigate the themes of solitude in nature and isolation from it by analyzing the two photo's subjects, color, and lighting. I end with a call to action for a reexamination of humanity's relationship with nature through the photographic medium in an attempt not only to reconnect with the natural world but also to mitigate the effects of climate change.

Key Words – Photography, Elegy, Eliot Porter, Susan Sontag

INTRODUCTION

Photography. A simple image or "copy" of our world can be created with the effortless press of a button. Nevertheless, what some may see as an elementary process is a grand form of art with the ability to present innovative physical, metaphorical, and metaphysical perspectives [1]. Presenting photography as a true form of art may require a reexamination of the definition of art. To many, art is something pleasing to the eye, something that must send a deep or underlying message to the audience. However, this definition is insufficient and prescriptivist. Instead, art is subjective [2]. It is like water: its form is not predetermined, but rather is shaped by the container that the individual places it in.

Yet seemingly contradicting this subjectivity, an objectivity of photography exists in its "elegiac" nature, as described by Susan Sontag [3]. The same press of a button that captures perspectives simultaneously "freezes" time itself to store the fleeting moment on a chip or on film, essentially "killing" or "removing" the present [3]. This death allows the photographer to reshape and change the meaning of the photograph itself, fundamentally altering the audience's percept. As photographs isolate specific instances of time from linearity, they are "memento mori"; they secure a slice of reality like one would preserve a butterfly for their collection [4].

Viewed as elegy, nature photography above all other forms reveals the fragility of life. Nature photographers work to bring awareness to the solace offered by the natural world as justification for the responsibility humans have to maintain it [5]. The logic of the nature photographer is that if people witness the value and serenity of nature, they will want to preserve it. Unfortunately, their efforts are failing. Climate catastrophe appears inevitable, and the environments once captured in their photos disappear as days pass. In essence, their solitude is replaced with isolation, a separation of man from nature. Yet in taking a picture of this solitude, photographers execute solitude itself, leaving only isolation in its stead. One can never experience the joy the photographer felt when capturing the image; they can only reflect on the impossibility of experiencing it. It is a dead moment. To both reveal the death of solitude shown in Eliot Porter's 1967 *Red Tree Near Cades Cove, Great Smoky Mountains National Park, Tennessee* and to reaffirm the isolation of modernity, I submit my 2020 *Man in Nature* [6, 7].

Most recognizable from his success with the Sierra Club and his pioneering use of Kodachrome film, Porter was one of the most influential photographers to ever hold a camera - especially in the environmentalist world [3]Trained as a scientist, his unique take on nature photography helped to shape narratives around photography's role in preserving nature [5]. His *Red Tree,* as seen in Figure 1, attempts to emphasize the importance of solitude found through nature in its subject, color, and lighting techniques, while my *Man in Nature*, Figure 2, using similar techniques, highlights man's increasing distance from nature and isolation resulting from the use of machines as a substitute for the natural world and the very elegiac nature of photography itself. These two works, through subtle but coherent differences, ultimately express a shift in focus from solitude to isolation.

In this paper, I define solitude as the healing, reflective experience of communing with nature, whereas isolation define as the separation of man from nature and subsequent loneliness and depression resulting from said separation.

FIGURE 1: ELIOT PORTER, *RED TREE NEAR CADES COVE, GREAT SMOKY MOUNTAINS NATIONAL PARK, TENNESSEE.* 1967.

FIGURE 2: Yuta Namba, *Man in Nature.* 2020.

ANALYSIS OF *RED TREE*

Red Tree celebrates solitude in its subject; the image focuses on a sole, red tree against a background of its green cousins. Porter achieves this focus not only through the contrast of foreground and background, but also by centering it. The viewer sees no human, nor any evidence of human interaction or manipulation; instead, they witness only the natural world. The viewer is aware that the photograph has to be taken by someone, but the lack of human interference frames the photographer as "an acute but non-interfering observer" [4]. The trees in the background of this photo are compressed together, with only dead leaves on their thin branches, yet they do not suggest sadness or loneliness. Their distance from the red tree is what allows it to live; were they to invade its space and break the sanctity of this solitude, the red tree would lack the room it needs to grow. Porter's visual claim of solitude highlights the beauty of the red tree, the purity of the deep level of reflection and whole human experience only accessible through solitude in nature.

Porter's use of color in *Red Tree* further showcases the theme of solitude in nature. The red leaves of the central tree contrast sharply with the bluish green of those in the background, yet the red tree is not isolated. It is taking part in the larger cycle of life; its red leaves will soon fade to brown and fall. In this sense, the red Porter has captured is a reminder to the audience of the tree's "mortality" [4]. The trees around it gradually fade into blackness, suggesting the eternal nature of this cycle and celebrating the solitude of this tree. This solitude does not mean that the subject must exist outside of all external influence; that would be impossible in a universe as intimately connected as our own. However, this intricate play of red, green, and black shows how in the natural world one can exist concurrently in the solace of independence and interconnection.

Similarly, Porter uses lighting in innovative ways to emphasize the solitude of *Red Tree*. Even at first viewing, the lighting between the background and foreground heavily contrasts. The background is dark, while the subject in the foreground is lit. This lighting contrast instantly pushes the audience's attention toward the subject, which as noted above, fosters feelings of solitude. The lighting is also symbolic: it is from the natural light source (the sun) that the red tree flourishes. Porter's choice to use natural lighting further distances human interference from the solitude of nature. He could have chosen to use artificial bulbs and flashes, but these would have detracted from the sanctity of the natural experience. To find solace, humans need bring nothing of their own into the natural world; they must simply take in its glory and look at it with "nostalgia" [4].

ANALYSIS OF *MAN IN NATURE*

However, it is exactly this "nostalgia" that is at the root of humanity's seemingly irreparable rift from nature: "Nature has become more a subject for nostalgia and indignation than an object of contemplation" [4]. Humans no longer feel a direct connection with nature and are isolated from it. *Man in Nature* first reveals this isolation through its subject. Instead of the natural symbol of the red tree, *Man in Nature* focuses on a man. Humanity has gone beyond the role of observer and has usurped the center, both pictorially and in a larger metaphorical sense. He has completely isolated himself from nature, killing it away with the artificiality of the man-made devices that surround him. While *Red Tree* approaches the main subject from an upward angle, suggesting the limitless growth of solitude, *Man in Nature* looks down upon the subject, crushing him with the weight of his isolation. This weight is further felt in his collapsed neck; his isolation physically forces him to cower beneath his own creations.

Color in *Man in Nature* further emphasizes this isolation. Whereas the main subject of *Red Tree* glowed a glorious red, the man in this photo is awash in blackness. Like in *Red Tree*, this blackness suggests eternity, but it differs from the celebratory eternal cycle of life. It is the eternity of loneliness, a blackness of the soul. Man has isolated himself from nature and no longer feels its calming effects; the subject and the viewer in turn become "uninvolved consumers" of the artificial world and take no time for peace and reflection [3]. Yes, the monitors on either side of the subject's head project color, but they are the unnatural hues of a computer-generated world, one which illuminates human loneliness.

The very lighting of *Man in Nature* suggests isolation. Instead of the life-giving light source of *Red Tree*, this photo is lit only by computer screens. Beyond them, the viewer sees only darkness. Without his technology, man disappears, but it is this same technology which isolates him. It is not a nourishing light like the sun, and nothing organic exists around the subject to feed him. The artificial light is the eternal moon eclipsing the subject's sun; without its light, he will die. These negative connotations are embodied in the framing of the subject. The subject is literally a negative; the backlighting of the photo traces an outline around him. This negative status is symbolic of the broader role his distanciation from nature has caused in his life, and it connotes sorrow and misery.

CONCLUSION

Although both of these works have created a distinctly contrasting theme, both Red Tree and Man in Nature have separated human from nature. Red Tree represents humans finding solitude not for themselves, but rather in nature. Likewise, Man in Nature represents how humans have completely separated from nature, replacing it with machines. Yet, this theme is not only concurrent in these two photographic works, but is now a part of human nature as well. Though we view our ancient ancestors as part of the natural world, modern humans view themselves as a distinct race. *Red Tree* reminds us of a reality we will never again experience, and *Man in Nature* reflects our present

predicament. This may explain the beauty humanity sees in photography, as its elegiac nature is relatable to our own.

Porter wrote in his first widely-distributed book that "in wildness is the preservation of the world" [8]. As he continued working in nature photography, he saw the degradation of this wildness and "began to appreciate the terrible consequence of this… unnecessary destruction of the natural environment" [8]. Though climate change has accelerated and humans feel less and less attached to nature, photography's elegiac quality reveals to us that we do not need to lose hope yet; we must simply reexamine our relationship with nature. The idea of human and nature is a misnomer: we are a part of the natural world, as is everything else on this Earth.

AKNOWLEDGEMENTS

I would like to thank Hayden Muller for guiding me to achieve this accomplishment of writing this paper. Additionally, I would like to thank the Tokyo Academics staff for giving me the resources for this research paper.

REFERENCES

[1] Walden, Scott. "Photography and Knowledge." *The Journal of Aesthetics and Art Criticism*, vol. 70, no. 1, 2012, pp. 139–149., doi:10.1111/j.1540-6245.2011.01505.x.

[2] Zalta, Edward N. "The Definition of Art." *Stanford Encyclopedia of Philosophy*, Stanford, 2004.

[3] Chianese, Robert Louis. "Arts Lab: Is Nature Photography Too Beautiful?" American Scientist, vol. 102, no. 1, 2014, pp. 64–67., www.jstor.org/stable/43707750. Accessed 5 Aug. 2020.

[4] Sontag, Susan. "On Photography". New York :Farrar, Straus and Giroux, 1977.

[5] Bianco, Jane. "The Macro and the Micro of Eliot Porter's Worlds." Maine Arts Journal, Spring 2020, http://maineartsjournal.com/jane-bianco-the-macro-and-the-micro-of-eliot-porters-worlds/. Accessed 20 August 2020.

[6] Porter, Eliot. *Red Tree Near Cades Cove, Great Smoky Mountains National Park, Tennessee*. 1967. *The Metropolitan Museum of Art*, https://www.metmuseum.org/art/collection/search/262617.

[7] Namba, Yuta. *Man in Nature*. 2020. *Unpublished.*

[8] PBS. "Eliot Porter." 29 January, 1991, https://www.pbs.org/video/colores-eliot-porter/. Accessed 1 Aug. 2020.

Comparative Analysis of Alveolar Bone Resorption Between Male and Female Patient

Marie Nishi
Tokyo Gakugei University International Secondary School; Tokyo, Japan
Email: marie.n10@tguiss.jp

Abstract - **Alveolar bone resorption (ABR) occurs when bone deconstruction takes place in the areas surrounding and supporting a tooth. Traditional diagnostic methods to determine ABR include assessment of clinical parameters and radiographs; however, the current diagnostic techniques lack the capability to predict and assess future ABR occurrence among individuals. Both male and female walk-in patients visiting a local Japanese hospital throughout March 2017 were selected for this study. For fair comparison, all samples were collected focused on the primary molar. Radiographs of the alveolar bone and tooth were taken for diagnostic purposes. From this study, it was established that the alveolar bone matrix is affected by both sex and age. More specifically, box plot analyses show that: alveolar bone matrix is affected by both sex and age; female and male alveolar bone development peaks at the 40s and 50s age group, respectively; female alveolar bone resorption start[s] at the 50s age group, and male alveolar bone resorption starts at the 60s age group.**

Key Words: alveolar bone resorption (ABR); BoneJ; radiographs

INTRODUCTION

I. Background

Alveolar bone/ process is an elevated ridge of the maxima, or mandible where the teeth are housed. [1] There are two components which are alveolar process and alveolar bone proper. Alveolar process is formed to house the developing tooth buds and roots of the teeth. Alveolar bone proper is the portion of bone that lines the tooth socket. There are three different sections in an alveolar bone, which are upper interradicular septum (UIS), middle interradicular septum (MIS) and lower interradicular septum (LIS). Each section has a different densities of alveolar bone matrix.

Alveolar bone resorption (ABR) is the destruction of bone in the areas surrounding and supporting a tooth.[2]Besides, ABR has been associated with oral hygiene and age of the individual, wherein, individuals with poor oral hygiene developing periodontal disease exhibit more ABR while aging individuals slowly and gradually develop ABR. [3]

II. Significance

Alveolar bone health is often neglected, however, the state of the alveolar bone as someone ages may have an impact in one's future health since it could indirectly affect the type and amount of food one will ingest. In this regard, establishing the age-related pattern of alveolar bone matrix could similarly guide dental practitioners in knowing the specific age-related health of the alveolar bone matrix during dental procedures. Moreover, by having establish the age-related AB matrix, dental practitioners may likewise be guided in diagnosing early onset ABR and, subsequently, appropriate therapeutic treatment can be performed immediately.

III. Objective

Currently, traditional diagnostic methods to determine ABR include assessment of clinical parameters and radiographs; [4]however, these conventional techniques are limited since only a historical perspective (not the present and actual appraisal) is used to establish ABR and, more importantly, current diagnostic techniques lack the capability to predict and assess future ABR occurrence among individuals.[5] Gingival crevicular fluid (GCF) is a physiological fluid that is excreted from the gingiva and usually builds up between the dental-gingival space. In the advent of the 21st century, advances in the use of oral fluids (such as the GCF) as possible sources of disease biomarkers are becoming popular since oral fluids contain several mediators often associated with several diseases and disease manifestations, including ABR. However, at present, prospects of using GCF as an indicator of ABR have never been elucidated. In this regard, I hypothesize that certain components found in the GCF have the potential to be used as a biomarker to determine and predict ABR occurrence among individuals.[6] [7]

METHODOLOGY

IV. Patient Selection

Ethical approval was obtained from the local ethics committee prior to the start of this study. Both male and female walk-in patients (n=39) visiting a local Japanese hospital throughout March 2017 were used (Figure 1). A

nonprobability purposive sampling was performed to satisfy the study requirements concerning sex and age. Male and female patients were grouped and at least 3 patients per age group (the 20s, 30s, 40s, 50s, 60s, 70s) were utilized. Age groups were divided by 10 to reflect the patients age that visited during the collection timeframe. Number of patients used for the study is dependent on patient check-in during the designated collection time-frame. All patients were informed that their participation was voluntary, and consent was obtained from each participating patient. Among the selected patients based on age and sex, patients were further subdivided into patients with healthy tissue and patient with periodontal disease. Patients who are smokers, or on an antibiotic regimen, or anti-inflammatory drugs (except for the elderly volunteers) were disqualified from this study.

V. Sample selection

For comparison, all samples collected focused on the primary molar, and probing depth was measured for periodontal tissue examination. Radiographs of the alveolar bone and tooth were taken for diagnostic purposes and results were used for the study. Similarly, GCF was collected using a paper point inserted at 6 different locations of the tooth. Both radiography and GCF collection were performed in all patients following the same timeframe (between 9:00-11:00 AM) prior to any treatment.

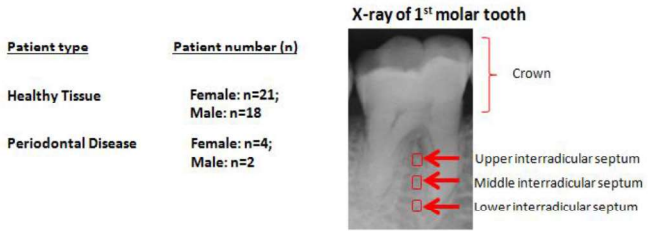

FIGURE 1: Patient selection and sample collection. Upper (UIS), Middle (MIS), and Lower (LIS) interradicular septum are indicated.

VI. Alveolar bone assessment

AB matrix across the age groups, between sexes, and oral condition comparison were determined using the radiograph from each patient and analyzed using BoneJ software (a specialized software used to measure bone matrix).

VII. Biochemical analyses.

Representative cellular stress [oxidative stress: total heme, H_2O_2; nitrosative stress: nitric oxide; ER stress: GADD153][9][10] and cell signaling [substance P[11], calcium[12], NF-□B[13]] [14] components were measured using commercially available kits. [15]

IX. Comparative analysis

Radiographs and GCF samples from subdivided patients with the same sex[16] and age[17][18] were compared to one another in order to establish the possible differences and potential disease markers with therapeutic applications.

RESULTS AND DISCUSSION

Throughout this study, both computational and biochemical approaches were performed in order to establish the age-related differences in the AB matrix. Computational approach (BoneJ) was utilized to establish the differences among UIS, MIS, and LIS between the different age groups. Biochemical approaches (stress and cell signaling) were performed to determine any biochemical patterns that may be associated with variations in AB matrix.

X. Interradicular septum varies between age groups and sex

As seen in Figure 2, the surface plot color and measurement among the interradicular septums (UIS, MIS, LIS) and age (20s-70s) varies. [17] In regards to the interradicular septum (vertical data), the interradicular septum is found between the molar roots and is further subdivided into 3 parts with the UIS being closest to the crown, MIS position underneath the UIS, and LIS located farthest from the crown, but closer to the jaw bone. Among the varying age groups, it is evident that UIS has the lowest AB density, MIS has an intermediate AB density, and LIS has the highest AB density. Overall, this is consistent with how the tooth molar functions. In a chewing scenario, the function of the tooth molar is to grind and breakdown food which in-turn would mean high amounts of physical stress (related to bite force) within the AB matrix. Having a softer UIS would allow for the AB matrix to absorb most of the physical stress related to chewing. Subsequently, the MIS serving as an intermediary between the UIS and LIS may partially function in absorbing physical stress and at the same time hold the tooth molar in place. Ultimately, the LIS may serve as the base thereby provide a solid foundation to hold the tooth molar in place.

In regards to the observed age-related AB matrix variation (horizontal data), it is apparent that the older the patient the AB matrix in the UIS, MIS, and LIS changes. This would suggest that the AB changes as the aging process progresses in both female and male patients. It is possible that at 20s, AB is not fully developed which may explain why there is lower AB density (yellow to yellow green color). Surprisingly, comparing the AB between female and male individuals;the estimated AB matrix (dark green to blue color) is highest during the 30s and 40s among aging female patients, whereas, among aging male patients, estimated AB matrix is highest during the 40s and 50s. This would imply that the AB matrix density is fully developed

at these age groups. Interestingly, after obtaining the highest AB matrix measurement, there seems to be a tendency to dip (50s-60s) and eventually rise again (60s-70s), particularly among the elderly aged group (60s and 70s) which could be due to tooth loss among the elderly population, whereby, loss of tooth among the elderly would in-turn solidify the AB matrix thereby increasing its density Taken together, these results would suggest that: (1) the AB matrix differs between sex and aged groups; and (2) the AB matrix development peaks at the 30s-40s age group for females and 40s-50s age group for males.

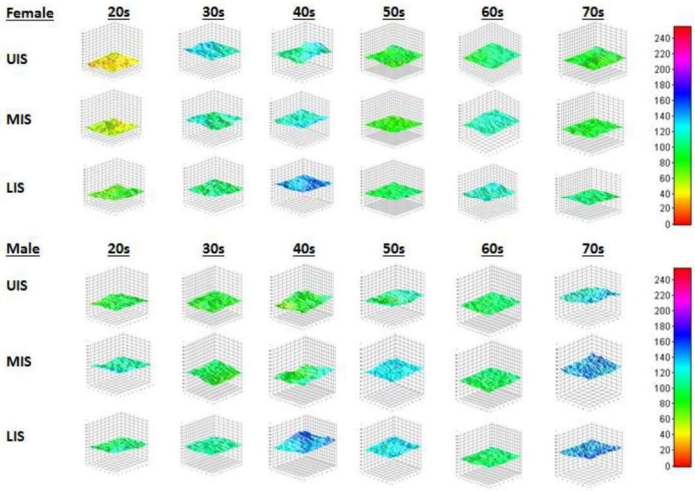

FIGURE 2: Alveolar bone matrix of female and male patients differs. Color legend representing the alveolar bone matrix is indicated on the right. Color gradient going up the legend represents higher alveolar bone density. Color gradient going down represents lower alveolar bone density.

XI. Stress and cell signaling related to bone resorption varies among age and sex

There are various types of cellular stresses occurring in a cell[18], among them: oxidative stress, nitrosative stress, and endoplasmic reticulum stress. Oxidative stress represents an imbalance between pro-oxidant and anti-oxidant activities, nitrosative stress is caused by the reaction of nitric oxide with oxygen or superoxide resulting in the formation of reactive nitrogen species with varying reactivity that could directly affect cellular enzyme activity, and ER stress is considered a cellular response activated when unfolded proteins accumulate within the ER in order to preserve ER function. Cellular stress have been correlated to age-related diseases and considering ABR is age-related it is possible that cellular stress (via oxidative, nitrosative, and/or ER stresses) along the GCF may contribute to ABR induction.

For this study, we established oxidative stress occurrence by measuring both total heme and H_2O_2. Similarly, we established nitrosative stress by measuring the amount of nitric oxide. Finally, we established ER stress by measuring the amount of GADD153. All these biochemical components used for this study are known biomarkers for all 3 cellular stresses, respectively.

Subsequently, cellular stress is known to trigger other physiological cell signals that have been associated with bone resorption, such as: substance P, calcium, and NF-□B. Substance P has been associated with osteoclastic bone cells responsible for breaking down bone tissues, whereas, calcium signaling is known to directly trigger bone resorption. Moreover, NF-□B is known to activate osteoclast-related bone resorption. Thus, all these cell signals are known biomarkers of bone resorption.

In general, among the biochemical components studied (Figure 3), a common bi-modal distribution (40s:60s age group) can be observed in all male patients studied across age groups (*indicated in blue*). In contrast, among female patients studied across age groups (*indicated in red*), multiple sets of bi-modal distribution is observed: 30s:50s; 40s:70s; and 50s:70s age groups. These results would suggest that GCF components and production are consistent in male patients throughout the ageing process, whereas, among female patients, GCF components and production have a tendency to shift as the ageing process progresses.

Admittedly, all data sets are based on theoretical and computational analysis of actual patient diagnosis. Moreover, the collection timeframe is short and collection site was limited to one. As a possible future study, expanding both collection timeframe and site may provide a better overview of the age-related differences in alveolar bone matrix. Additionally, considering all volunteer patients were Japanese, expanding the study to include other nationalities could be another aspect to explore.

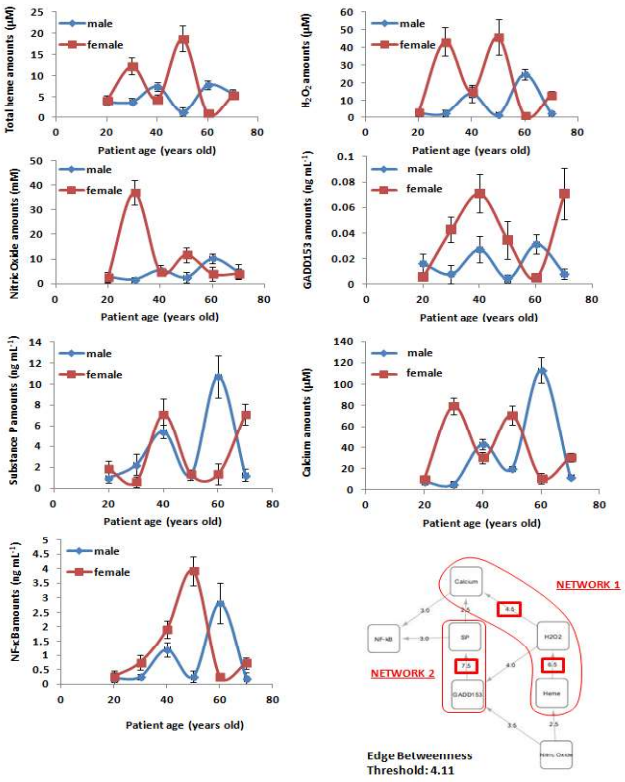

FIGURE 3: GCF cellular stress and stress-related signaling components in female and male patients differ. Stress signaling networks are boxed red .

CONCLUSION AND IMPLICATIONS

In summary, these results suggest that: (1) alveolar bone matrix is affected by both sex and age; (2) female and male alveolar bone development peaks at the 40s and 50s age group, respectively; (3) female alveolar bone resorption start at the 50s age group, and (4) male alveolar bone resorption starts at the 60s age group.

As a possible clinical application, these results demonstrate that certain GCF components could serve as biomarkers for the early diagnosis and treatment of ABR. Moreover, the proposed AB matrix pattern may likewise serve as a reference or guide for dental practitioners when performing procedures or treatment involving AB, such as root canals, implants, and braces.

ACKNOWLEDGMENTS

I would like to express my gratitude to my primary supervisor, Dr. Marni Cueno, who guided me throughout this project. I would also like to thank the Nihon University School of Dentistry for providing radiographs used throughout this study.

REFERENCES

[1] Chu, T.-M. G., Liu, S. S.-Y., & Babler, W. J. (2014). *"Craniofacial Biology, Orthodontics, and Implants."* Basic and Applied Bone Biology, 225–242. doi:10.1016/b978-0-12-416015-6.00011-3

[2] Hienz, Stefan A., et al. "Mechanisms of Bone Resorption in Periodontitis." *Journal of Immunology Research*, edited by Giorgio Mori, vol. 2015, May 2015, p. 615486, doi:10.1155/2015/615486.

[3] Hesby, R. M., Marshall, S. D., Dawson, D. V., Southard, K. A., Casko, J. S., Franciscus, R. G., & Southard, T. E. (2006). *"Transverse skeletal and dentoalveolar changes during growth."* American Journal of Orthodontics and Dentofacial Orthopedics, 130(6), 721–731. doi:10.1016/j.ajodo.2005.03.026.

[4] Jeffcoat, Marjorie K. "Radiographic Methods for the Detection of Progressive Alveolar Bone Loss." *Journal of Periodontology*, vol. 63, no. 4S, 1992, pp. 367–72. *Wiley Online Library*, doi:10.1902/jop.1992.63.4s.367.

[5] Benn, Douglas K. "A Review of the Reliability of Radiographic Measurements in Estimating Alveolar Bone Changes." *Journal of Clinical Periodontology*, vol. 17, no. 1, 1990, pp. 14–21. *Wiley Online Library*, doi:10.1111/j.1600-051X.1990.tb01041.x.

[6] Albandar, Jasim M., et al. "Radiographic Quantification of Alveolar Bone Level Changes." *Journal of Clinical Periodontology*, vol. 13, no. 3, 1986, pp. 195–200. *Wiley Online Library*, doi:10.1111/j.1600-051X.1986.tb01459.x.

[7] Ozan, Oguz, et al. *"The Effect of Removable Partial Dentures on Alveolar Bone Resorption: A Retrospective Study with Cone-Beam Computed Tomography."* *Journal of Prosthodontics*, vol. 22, no. 1, 2013, pp. 42–48. *Wiley Online Library*, doi:10.1111/j.1532-849X.2012.00877.x.

[8] Valko, M., Leibfritz, D., Moncol, J., Cronin, M. T. D., Mazur, M., & Telser, J. (2007). *"Free radicals and antioxidants in normal physiological functions and human disease."* The International Journal of Biochemistry & Cell Biology, 39(1), 44–84. doi:10.1016/j.biocel.2006.07.001

[9] Valko, M., Rhodes, C. J., Moncol, J., Izakovic, M., & Mazur, M. (2006). *"Free radicals, metals and antioxidants in oxidative stress-induced cancer."* Chemico-Biological Interactions, 160(1), 1–40. doi:10.1016/j.cbi.2005.12.009

[10] Schönthal AH. *"Endoplasmic reticulum stress: its role in disease and novel prospects for therapy."* Scientifica (Cairo). 2012;2012:857516. doi:10.6064/2012/857516

[11] Goto, Tetsuya & Yamaza, Takayoshi & Kido, Mizuho & Takana, Teruo. (2001). Substance P Activates

Osteoclast Formation and Osteoclastic Bone Resorption through the Neurokinin1 Receptor. Acta Histochemica Et Cytochemica - ACTA HISTOCHEM CYTOCHEM. 34. 31-38. 10.1267/ahc.34.31.

[12] Clapham, David E. "Calcium Signaling." *Cell*, vol. 131, no. 6, Elsevier, Dec. 2007, pp. 1047–58. *www.cell.com*, doi:10.1016/j.cell.2007.11.028.

[13] Dixit, Vishva, and Tak W. Mak. "NF-KB Signaling: Many Roads Lead To Madrid." *Cell*, vol. 111, no. 5, Elsevier, Nov. 2002, pp. 615–19. *www.cell.com*, doi:10.1016/S0092-8674(02)01166-2.

[14] Fang, F. *"Antimicrobial reactive oxygen and nitrogen species: concepts and controversies."* Nat Rev Microbiol 2, 820–832 (2004). doi:10.1038/nrmicro1004

[15] Streckfus CF, Johnson RB, Nick T, Tsao A, Tucci M. *"Comparison of alveolar bone loss, alveolar bone density and second metacarpal bone density, salivary and gingival crevicular fluid interleukin-6 concentrations in healthy premenopausal and postmenopausal women on estrogen therapy."* J Gerontol A Biol Sci Med Sci. 1997;52(6):M343-M351. doi:10.1093/gerona/52a.6.m343

[16] Sathapana S, Forrest A, Monsour P, Naser-ud-Din S. *"Age-related changes in maxillary and mandibular cortical bone thickness in relation to temporary anchorage device placement."* Aust Dent J. 2013;58(1):67-74. doi:10.1111/adj.12018

[17] Sverdlov, Aaron L., et al. *"Aging of the Nitric Oxide System: Are We as Old as Our NO?"* Journal of the American Heart Association, vol. 3, no. 4, Aug. 2014. *DOI.org (Crossref)*, doi:10.1161/JAHA.114.000973

[18] Barouki, R. (2007). *"Cellular stress".* FEBS Letters, 581(19), 3581–3581. doi:10.1016/j.febslet.2007.07.001

Identification of Fusarium in Gerbera using Augmented Ruthenium Red Based Biosensor

Kanan Nozaki
St. Mary's International School; Tokyo, Japan
Email: kanan77@smis.ac.jp

Abstract - Farmers often encounter significant financial losses due to pathogenic diseases. *Fusarium* is known for damaging plants by secreting polygalacturonase, which causes cell wall degradation. This paper reports the identification of polygalacturonase in *Fusarium* through the fabrication of the ruthenium red-based biosensor. The augmented ruthenium red-based biosensor uses the PGA-RR complex and allows physical experimentation in the actual field. Multiple polygalacturonase enzymes were tested with varying concentrations and the biosensor detected the reflected light from those enzymes using a spectral sensor. Two experiments were conducted: one with the use of chromatography paper and the other without it. The experiments suggested that the biosensors were capable of detecting the enzymes. As the concentration of the enzymes increased, the amount of reflected light at various wavelengths increased. This finding is significant because this new prototype offers possible ways of detecting these pathogenic diseases and, meanwhile, advancing the field of bioengineering and biotechnology.

Key Words – Polygalacturonase, Fusarium, Ruthenium Red, Polygalacturonic Acid, Polygalacturonase Inhibiting Proteins, Reflected Light, PGA-RR complex

INTRODUCTION

I. Gerbera

Gerbera Daisy (*Gerbera jamesonii*) is in the family of Asteraceae and originated from South Africa. It is known for its luminescent colors and is frequently used as ornamental flowers. In 2018, in Japan, the three largest producers and shipping amounts were Shizuoka-ken (59,000 k/flower), Fukuoka-ken (20, 9000 k/flower), and Chiba (8,530 k/flower) (Japan CROPs). Furthermore, Japan's popularity for Gerbera from 2004 to 2018 is in a declining trend with the planted acreage decreasing by 16.2% and the shipping amount by 21.4%. Although the economic impact of Gerbera daisies in Japan is not relatively significant, prefectures such as Shizuoka and Miyagi rely on these flowers for their major flower production. Moreover, flower shops in Japan typically sell these flowers due to their wide range of consumers.

FIGURE 1**:** Image of Gerbera flowers

II. Fusarium

Fusarium is a genus of multiple pathogenic, fungal diseases that are known for damaging seedlings and young shoots, causing leaf spots, leaf blights or leaf rots, sheath rots, and rots of the shoot tip, and also developing oval and dark brown necrotic spots (Srivastava et al. 2018). Its main hosts are over 150 species of fruits, vegetables, and flowers. Although there are nearly 20 species of *Fusarium*, most prefer sub-tropical environmental conditions. Still, there are variances in species regarding optimal humidity and temperature. According to William E. Nganje et al., from 1993 to 2001, *Fusarium* Head Blight had an economic loss of 2.492 billion dollars regarding hard red spring (HRS) wheat, SRW wheat, durum wheat, and barley. This cumulative economic impact continues until today due to the non-existence of effective detection methods. Although numerical evidence of *Fusarium* attacking Gerbera is still unknown, the existence of PGIPs in Gerbera implies the presence of pathogenic diseases such as *Fusarium*.

III. Plant Defense Against Fusarium

Plants, such as Gerbera, secrete polygalacturonase inhibiting proteins (PGIP) to defend against polygalacturonase (PG). To break through the cell wall, *Fusarium* produces PGs that cause cell wall degradation and breakdown of plant tissue. As the PGs slowly break down the cell wall, it also produces oligogalacturonides (OG) fragments, which triggers defense responses of the cell. When the flower detects these

fragments, it secretes PGIPs that inhibits the PGs by slowing down or stopping the spread of PGs.

IV. PGIP Expression in Other Flowers

Gerbera's expression of PGIP's is not well studied; however, researchers have studied other plants that are similar to Gerbera's biological system. *Arabidopsis thaliana* (Arabidopsis) encodes two PGIP's (*AtPGIP1* and *AtPGIP2*). This plant is frequently used in biological experiments because it acts as a model organism with a simple biological structure. Ferrari et al. conducted an experiment where they looked at the responses of two tandemly duplicated PGIP's when *Botrytis cinerea* infection's PG's were released. They discovered that both PGIP's encode functional inhibitors of PG from *Botrytis cinerea* and the overexpression of PGIP's in Arabidopsis slowed the infection and wounding (Ferrari et al. 2003). Sunflowers (*Helianthus annuus* L.), which is also part of the Asteraceae family, contain PGIPs that hinder the progression of PGs. Researchers identified four PGIP genes (*HaPGIP1, HaPGIP2, HaPGIP3,* and *HaPGIP4*) and discovered that sunflower's non-synonymous substitutions are genetically diverse in multiple species: *H. maximiliani*, *H. ciliaris*, *H. paradoxus*, *H. tuberosis*, and *H. petiolaris* (Livaja et al. 2016).

V. PGIP and PG Activity in Gerbera and Fusarium

Although PGIP and PG activity in Gerbera is not well understood, in 2015, Wen Fang discovered PGIP activity in Gerbera against PG's produced by *Botrytis cinerea* (Fang 2015). Fang discovered two distinct PGIPs and six endo-PGs in two Gerbera populations and the quantitative trait locus (QTL). They used gene sequencing and genotyping to identify Gerbera PGs and PGIPs. While the existence of PGIP activity in Gerbera is identified, the amount in which *Fusarium* produces PGs are relatively hard to quantify because of the variation in *Fusarium* species. Nevertheless, the production rate of PGs will not affect our results because the production rate does not directly affect the readings of the biosensor.

VI. Detection of PG activity using assays

Although our research was based on ruthenium red and the PGA-RR complex, the detection of polygalacturonase activity can be accomplished in numerous ways. Qian Li et al. (2015) introduced a method involving dilution of PGs and enzyme reactions with dinitrosalicylic acid (DNS). Although this method provided accuracy, it contained substances that were dangerous in a high school research environment. Another possibility was utilizing a color sensor to detect the presence of rot. However, this was impractical because the biosensor would detect any substance that has that specific absorbance wavelength. Finally, polymerase chain reaction (PCR) is another major detection method for numerous enzymes and substances. It allows researchers to rapidly create millions of copies of the gene to facilitate the observation. For example, the detection of COVID-19 (*Orthocoronavirinae*) utilizes PCR and Kovutunovych et al.'s (2003) research on the identification of *Klebsiella oxytoca* employs PCR to test for the presence of pathogenic DNA. However, our biosensor cannot easily incorporate a fully functioning PCR due to its technical requirements and compact size of the device. The biosensor fabricated in our experiment ensures safety, efficiency, applicability, and effectiveness. The biological idea and technology used in this biosensor are based on Choi et al.'s (2020). The Choi et al.'s research involved the creation of a paper-based biosensor that was able to detect polygalacturonase activity in Allium White rot disease. However, significant improvements are made to meet our research objectives and endeavors.

VII. Reasons to Conduct this Research

Often, farmers fail to detect *Fusarium* and its physical symptoms at an early stage. This causes their crops, flowers, and agricultural products to mold and rot. We hope that our research will allow farmers to detect *Fusarium* earlier and prevent financial and economic losses. Farmers will be able to use these machines without difficulty, and researchers will also gain a more concrete understanding of the relationship between *Fusarium's* PGs and Gerbera's PGIPs. This research puts a strong emphasis on the fabrication and improvement of newly designed biosensors and will possibly open doors for researchers now and in the future.

MATERIALS, METHODS, AND PROCEDURE

I. Reagents

The following reagents were used in this experiment: polygalacturonic acid (PGA) (Nacalai Cat. #: 26243-14), ruthenium red (RR) (Nacalai Cat. #: 30318-14), sodium acetate trihydrate (Nacalai Cat. #:31115-05), and commercially-available polygalacturonase enzyme Pectinex Ultra SP-L (Modernist Pantry Cat. #: 1043-250).

II. Materials for Biosensor and Experiment

The following components were used in the construction of the biosensor: SparkFun Spectral Sensor Breakout - AS7262 Visible, SparkFun 16x2 SerLCD - RGB on Black 3.3V, Plastic Container/Coating, SparkFun Arduino Uno R3, Rechargeable Lithium-Ion Batteries, Lithium-Ion Battery Holder, Switch, SparkFun High Precision Temperature Sensor - TMP117, Heating Pad - 5 x 10cm COM-11288, and Transistor.

III. Construction of PGA-RR Complex and Experiment

The PGA-RR complex requires the combination of polygalacturonic acid and ruthenium red. This substance is ultimately responsible for changing and indicating PG

activity. First, we created a 80 mM sodium acetate buffer. Although the optimum pH of the sodium acetate buffer is 5.5, the buffer that we created had a pH of 8. The change in pH does not directly affect the results but influences the size of the ultimate complex. Results of the chromatography paper, later discussed in the paper, showed that the biosensor worked fine with the pH out of the original range. Next, 120 ug of PGA and 80 ug of RR were combined with the most favorable ratio of 1.5 to 1. However, the amount of PGA-RR complex can vary if the ratio between the two substances and the pH of the sodium acetate buffer are maintained. Then, different enzyme concentrations were created and mixed with the PGA-RR complex. The initial values we attained are data before the heating and the final values we obtained were after being heated at 37 degrees celsius for 20 minutes. With the varying concentrations and reflected light at various wavelengths, a standard curve was created.

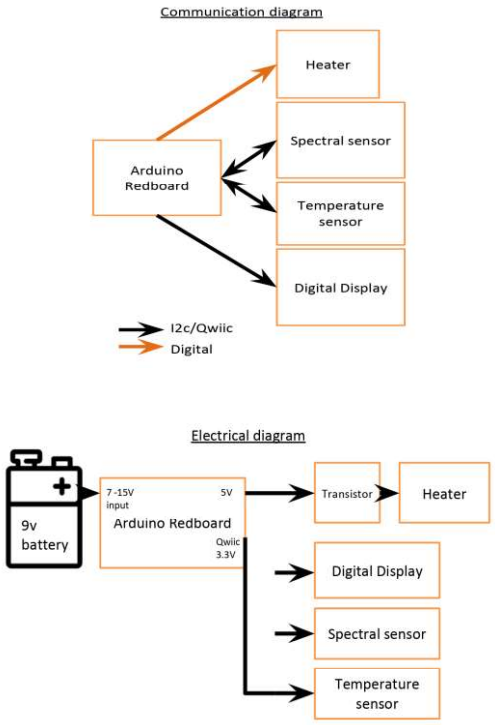

FIGURE 2: Visual diagrams for communication systems between the components and the electrical wiring between the components.

IV. Fabrication of the Biosensor

The overall biosensor mainly consisted of the PGA-RR complex (mentioned above), the heating system, the controller, loading and sensing area, chassis, and the display. To catalyze the chemical reactions, the PGA-RR complex needed to be heated at 37 degrees celsius. We attached *Spark Fun's* 5 x 10 cm Heating Pads, which are capable of producing constant heat similar to our body temperature. To maintain consistency, a temperature sensor was attached beneath it to act as a regulator for the heating pads. When the temperature of the heating pad is higher or lower than 37 degrees Celsius, the sensor sends a signal to the controller to regulate its voltage. Although our biosensor did not incorporate an insulation system to maintain the size and simplicity, an insulation system can be potentially added to keep the spectral sensor and other electronic parts to their optimal temperatures. The Arduino Uno R3 motherboard was placed on the bottom of the biosensor and connected to the display, spectral sensor, temperature sensor, switch, heating pads, and the batteries with wires. Computer programming was done for the biosensor to heat the solution, gather the amount of reflected light, display the results, and repeat this cycle. The loading and sensing area was designed so that the sample can be placed on the biosensor with ease. The chassis was constructed with 3D printing to incorporate simplicity and prevent cost inflation. Finally, the display was designed so that it would present the two wavelengths' (500 nm and 550 nm) reflected light (μW/cm²).

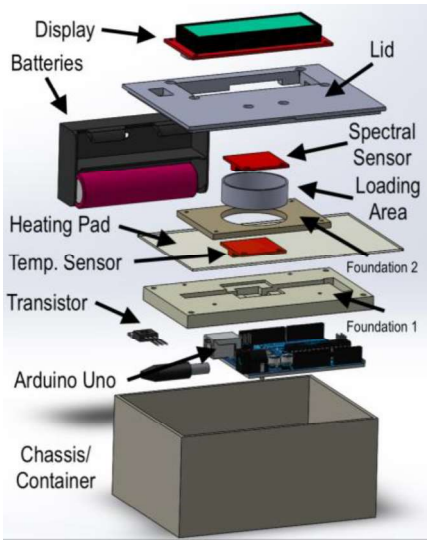

FIGURE 3: The prototype of the newly fabricated biosensor using CAD software. (Exploded View)

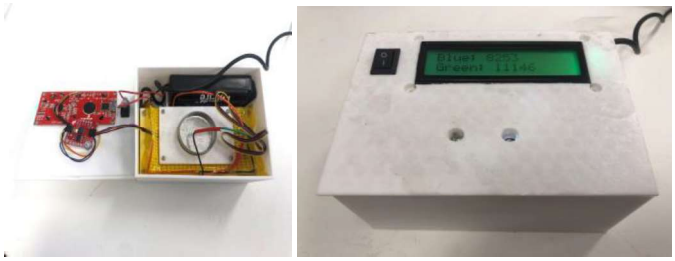

FIGURE 4: The biosensor prototype (Top: Outside view of the biosensor /Bottom Image: Inside view of the biosensor)

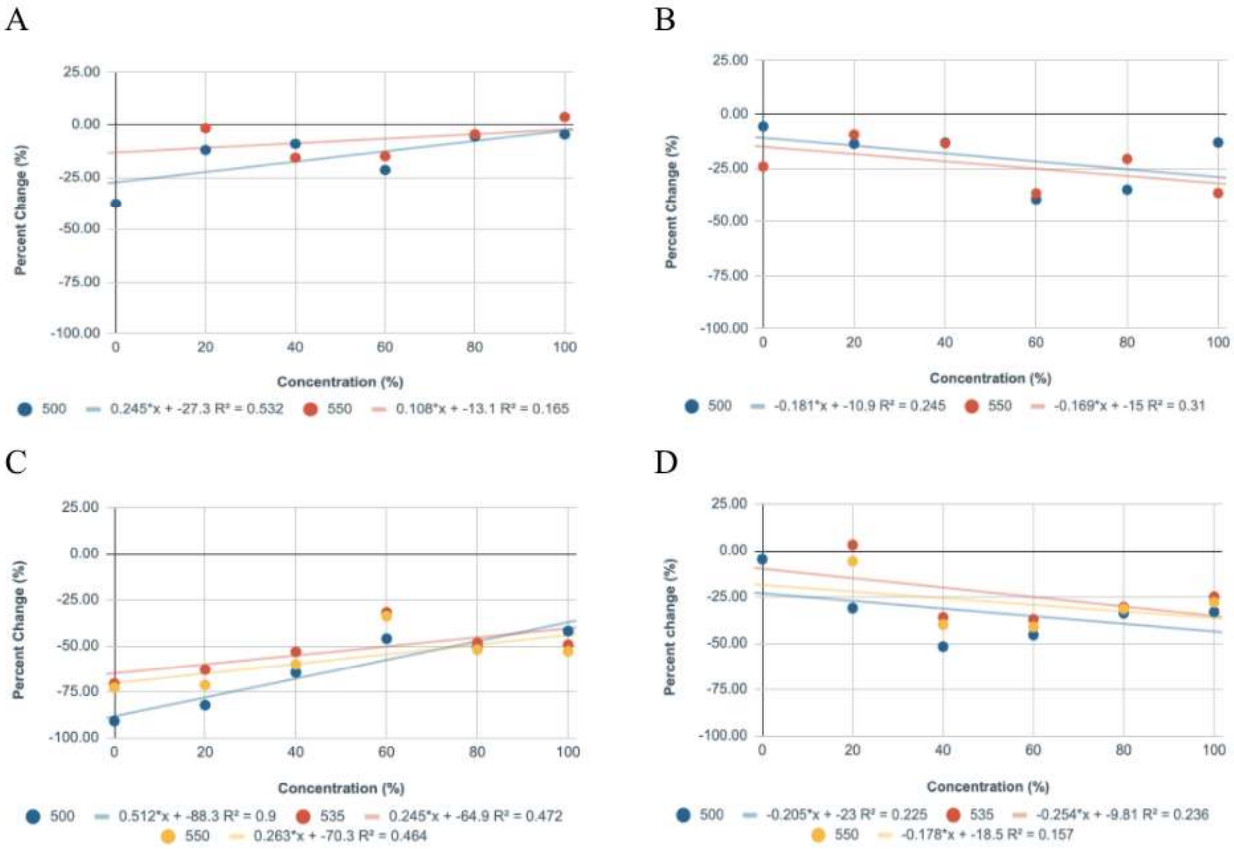

FIGURE 5: Graphs of the relationships/standard curves between the concentration level of polygalacturonase enzyme and the percentage change between the initial and final readings. (Graph A: Biosensor 2.5 uL / Graph B: Biosensor 5 uL / Graph C: Spectrophotometer 2.5 uL / Graph D: Spectrophotometer 5 uL) (Spectrophotometer acted as a control and was compared with the results of the biosensor) (100% Concentration means the solution solely consists of the polygalacturonase enzyme)

RESULTS

Important: (no significant differences between the two prototypes)

- The first prototype is the version where the biosensor lacked an overall chassis and consistent light source. Furthermore, manual programming was required.
- The second prototype is the version where the biosensor includes the overall container and consistent light source. In other terms, it is self-sustaining and no manual programming is required.

a. Analysis of Data of the Biosensor and Spectrophotometer Independently

In the experiment, the biosensor measured the reflected light from the liquid solution and the spectrophotometer measured the absorbance value. The optimum wavelength for PG and PGA-RR complex activity was 535 nm (Choi et al., 2020) but because the spectral sensor we incorporated in our biosensor can only measure 500 or 550 nm, results possibly have varied. In Graph A, it is evident that there is a positive correlation between the concentration and the percent change of reflected light. On the other hand, in Graph B, there is a negative relationship between the concentration and the percent change of reflected light. The positive relationship displayed in Graph A, possibly implies that that 2.5uL of PGA-RR dye was not enough for the biosensor to detect the certain wavelength. This resulted in the percent change, in other words, the amount of color the biosensor detected decreased. In Graph C, a positive relationship can be seen between the concentration and the percent change in absorbance. Furthermore, in Graph D, a negative correlation is evident. It can be theorized that similar to the biosensor's data, the 2.5 uL was probably not enough for the spectrophotometer to detect the absorbance.

b. Analysis of Data Combined

In both analyses, it is apparent that the standard curve's visible trends are consistent in terms of the overall positive and negative relationship between the biosensor and the spectrophotometer. After the heating, the reactions were catalyzed and the samples with greater enzyme concentrations displayed higher percent changes. Moreover, the spectrophotometer captured a greater percent change than the biosensor. In general, the consistency in the trends is highly ideal because the spectrophotometer is capable of detecting this form of activity in more detail due to its augmented sensors compared to the 3D printed and relatively cheap biosensor. As a result, it is reasonable that the spectrophotometer was capable of attaining a greater percent change than the biosensor. However, when contemplating the technology and the materials incorporated in the biosensor and the idea of portability, the augmented biosensor does a great job in achieving these goals with limited resources.

II. Prototype After Complete Fabrication and Design

Overall, the PGA-RR biosensor was fabricated for increased portability and effectiveness. Compared to the first biosensor, this new version can detect PG and PGIP activity in the field and on the spot with necessary materials. Although there is significant room for improvement, the biosensor is capable of conducting the whole process: inserting the plant sample, reacting it with the complex, detecting the reflected light through the spectral sensor, and displaying that data on the LED display. Moreover, the new version includes a concrete structure that holds all the components into one. Regarding results, the biosensor's output is the same as the past prototype (reflected light at wavelengths of 500 nm and 550 nm). However, for the results presented below, chromatography paper was used for improved visual data and results (FIGURE 4). After the reflected light from the solution was gathered, different concentrations of the solution reacted with the chromatography paper. Furthermore, for experimental purposes, we also tested with a wavelength of 650 nm.

a. Visual Data from Chromatography Papers

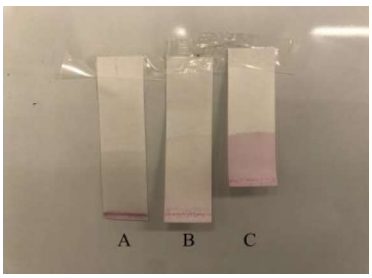

FIGURE 6: Image of different chromatography papers with varying enzyme concentrations and PGA-RR complex. (A: 0% enzyme concentration / B: 20% enzyme concentration / C: 50% enzyme concentration).

In FIGURE 6, it is evident that as the enzyme concentration increases, the color of the solution on the chromatography paper darkens. This darkening of the solution suggests that the biosensor is capable of detecting the increase in enzyme concentration, which means the existence of PG activity can be detected by this new biosensor prototype. Furthermore, because these results can be visually seen too, consumers can have a clear understanding of the existence of PG activity, which directly correlates to the existence of *Fusarium*.

b. Data from Chromatography Papers

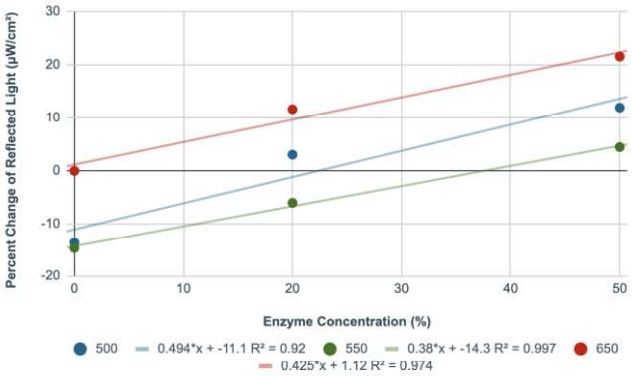

FIGURE 7: Graph of the relationship between the concentration level of polygalacturonase enzyme and the percent change of reflected light from the chromatography paper.

After using chromatography paper to visually see the difference in enzyme concentrations, the new biosensor was used to detect the reflected light from the papers. There is a positive correlation between the three different concentrations with most percent changes starting from the negative side and ending with positive values. The wavelength of 650 nm displayed a strong positive relationship comparable to the 500 and 550 nm. This may be the case because the solution's color itself was similar to the 650 nm's red color. The direct relationship visible in the graph suggests that the biosensor is capable of detecting the existence of PG activity and the breakdown between the complex and PG. These results perfectly match with the visual data from the chromatography paper and the percent change data from the first experiment, strengthening the effectivity of the new prototype.

CONCLUSION AND FUTURE OPTIMIZATION

Optimization of the Biosensor Prototype

With limited time and resources, creating a biosensor that is capable of detecting reflected light through ruthenium red was difficult. Although the final product was able to accomplish the established goals, optimizations and improvements can be made to enhance the biosensor as a

whole. First, better sensors and electronic signals with enhanced capabilities may have provided more accurate results. For example, the constant output from the spectral sensor involved drastic changes in the values, which made it difficult to attain accurate and precise data. In simpler terms, the spectral sensor was too sensitive that it made it difficult to attain constant readings. Second, it was difficult to claim with confidence that the values obtained from the spectral sensor were solely from the PGA-RR complex and the plant sample because the sensing area of the sensor is relatively unknown. In the future, the implementation of a sensor that has a clear indication of the sensing area may enhance the quality of future results.

Optimization of Both Experiments

The experiment itself involved a few errors and inconsistencies; therefore, optimizations can be made. First, an increased number of trials would have created more reliable data. When the number of trials increases, trends in data become more apparent, and numerical uncertainties can be created. Second, the inconsistent lighting environment in the first experiment with the early prototype may have negatively affected the data. Taking into consideration of the spectral sensor's extreme sensitivity and the output of the spectral sensor, consistent lighting is imperative. However, in the experiment, the distance from the emission of light to the sample varied every time. This can be fixed with a set distance from the light source to the sample, consistent light source, and constant lighting environment. Most of these attributes were tackled in the second version of the biosensor but improvements can still be made.

Conclusion and Discussion

This research involved the creation of a ruthenium-red based biosensor that detects fusarium in plant samples such as Gerbera. The biosensor we created mainly focused on portability, applicability, safety, and effectiveness, and taking into consideration the limited resources and time, the biosensor was relatively successful. From the first experiment, it is apparent that as the concentration of the PG enzyme increases, the percentage change between the initial and final readings increased. In the second experiment, as the concentration of PG enzyme increased, the solution darkened and the amount of reflected light at a certain wavelength increased drastically. These results suggest that the biosensor is capable of detecting more *Fusarium* and PG activity if the quantity of the sample is generally larger. Although we did not have the time to test the biosensor on Gerbera that contains *Fusarium* or PG in general, from the results that we have gained, this enhanced biosensor can accomplish this. The field of bioengineering and biotechnology is constantly advancing. Farmers need an efficient way of detecting *Fusarium* in their crops and they can possibly utilize these kinds of biosensors to solve this underlying problem.

ACKNOWLEDGEMENT

I would like to acknowledge and thank Abbi Hamed for the help with the creation and programming of the biosensor.

REFERENCES

[1] Choi, Y.-S., Lee, M. R., Yang, K.-Y., Kim, C. S., & Lee, K.-H. (2020). Paper-based colorimetric sensor for easy and simple detection of polygalacturonase activity aiming for diagnosis of Allium white rot disease. *Analytica Chimica Acta*, *1113*, 1–8. https://doi.org/10.1016/j.aca.2020.04.008

[2] De Lorenzo, G., D'Ovidio, R., & Cervone, F. (2001). THE ROLE OF POLYGALACTURONASE - INHIBITING PROTEINS (P GIPS) IN DEFENSE AGAINST PATHOGENIC FUNGI. *Annual Review of Phytopathology*, *39*(1), 313–335. https://doi.org/10.1146/annurev.phyto.39.1.313

[3] Fang, W. (2015). *Mapping and gene expression of polygalacturonase-inhibiting protein (PGIPs) and endo-polygalacturonase (endo-PG) genes in gerbera in relation to Botrytis cinerea resistance*. Wageningen University.

[4] Ferrari, S., Vairo, D., Ausubel, F. M., Cervone, F., & De Lorenzo, G. (2003). Tandemly Duplicated Arabidopsis Genes That Encode Polygalacturonase-Inhibiting Proteins Are Regulated Coordinately by Different Signal Transduction Pathways in Response to Fungal Infection. *The Plant Cell*, *15*(1), 93–106. https://doi.org/10.1105/tpc.005165

[5] Japan *CROPs Gerbera*. (n.d.). https://japancrops.com/en/crops/gerbera/

[6] Kovtunovych, G., Lytvynenko, T., Negrutska, V., Lar, O., Brisse, S., & Kozyrovska, N. (2003). Identification of Klebsiella oxytoca using a specific PCR assay targeting the polygalacturonase pehX gene. *Research in Microbiology*, *154*(8), 587–592. https://doi.org/10.1016/S0923-2508(03)00148-7

[7] Li, Q., Coffman, A. M., & Ju, L.-K. (2015). Development of reproducible assays for polygalacturonase and pectinase. *Enzyme and Microbial Technology*, *72*, 42–48. https://doi.org/10.1016/j.enzmictec.2015.02.006

[8] Livaja, M., Steinemann, S., & Schön, C.-C. (2016). Sunflower polygalacturonase-inhibiting proteins (HaPGIP) are genetically conserved in cultivated sunflower (Helianthus annuus L.) but diverse in wild species. *Molecular Breeding*, *36*(2), 17. https://doi.org/10.1007/s11032-016-0444-4

[9] Miller, G. L. (1959). Use of DinitrosaIicyIic Acid Reagent for Determination of Reducing Sugar. *ANALYTICAL CHEMISTRY*, 3.

[10] Nganje, W. E., Kaitibie, S., Wilson, W. W., Leistritz, F. L., & Bangsund, D. A. (n.d.). *Economic Impacts of Fusarium Head Blight in Wheat and Barley: 1993-200*. 63.

[11] Srivastava, S., Kadooka, C., & Uchida, J. Y. (2018). Fusarium species as pathogen on orchids. *Microbiological Research*, *207*, 188–195. https://doi.org/10.1016/j.micres.2017.12.002
58(3), 556–564. https://doi.org/10.1111/j.1365-3059.2008.02019.x
[12] Tomassini, A., Sella, L., Raiola, A., D'Ovidio, R., & Favaron, F. (2009). Characterization and expression of Fusarium graminearum endo-polygalacturonases in vitro and during wheat infection. Plant Pathology,

Evolution Through Art: Biomimesis in EcoLogicStudio's *H.O.R.T.U.S.* Series

Caryn Ohki
BYU Independent Study High School; Tokyo, Japan
Email: kalaheolichi@gmail.com

Abstract – In recent years, biomimesis, the practice of using mechanical means to mimic biological functions found in nature, has become increasingly popular in the art world. However, due to the emergent nature of biomimetic art as a field, limited scholarship exists about it. This paper analyzes EcoLogicStudio's *H.O.R.T.U.S.* series in an attempt to expand the current scholarship in the field and to clarify biomimetic art as a whole. First the field of biomimetic art is defined. Next, each individual work in EcoLogicStudio's *H.O.R.T.U.S.* series is demonstrated to be biomimetic, and the biomimetic evolution between the artworks within the series in form, materials, and methods of achieving function is explained. Works like the *H.O.R.T.U.S.* series show the promise of a field that effectively combines multiple disciplines to create highly efficient, self-regulating works which are responsive to urban stimuli. Lastly, I propose that the H.O.R.T.U.S. series is a techno-eco manifesto in a call to action for humanity to consider the role of biomimesis in architectural and technological endeavors.

Keywords – EcoLogicStudio, biomimetic art, biomimesis, bioarchitecture, bioinspiration

INTRODUCTION

The *H.O.R.T.U.S.* series is a set of reinterpreted garden prototypes and artistically-rendered photo-bioreactors, or "apparatus[es] for growing organisms under controlled conditions" [1]. It consists of five works: *H.O.R.T.U.S.* (London, UK 2012); *H.O.R.T.U.S Paris* (Paris, FR 2013); *H.O.R.T.U.S. ZKM* (Karlsruhe, DE 2015); *H.O.R.T.U.S. Astana* (Nur-Sultan, formerly Astana, KZ 2017); and *H.O.R.T.U.S. XL* (Paris, FR 2019 and Tokyo, JP 2019). The *H.O.R.T.U.S.* series was created by Marco Poletto and Claudia Pasquero of EcoLogicStudios. This London-based architectural and urban design firm specializes in environmental design and urban self-sufficiency, integrating bio-inspired form and function [2]. Each individual work in the series presents an interactive, urban renewable energy and agriculture prototype. As architectural engineers, Poletto and Pasquero utilize *H.O.R.T.U.S.* to propose a new consciousness "dictated by human rationality" as mankind approaches alternatives in "bio-artificial intelligence" [3]. I first encountered the *H.O.R.T.U.S.* series with *H.O.R.T.U.S. XL* in Tokyo, Japan, in 2019.

In this paper, I investigate the *H.O.R.T.U.S.* series by EcoLogicStudios and their use and representation of biomimetics and evolution through the collective exhibits. I argue that not only are *H.O.R.T.U.S.*, *Paris*, *Astana*, and *XL* as individual works bio-inspired, but also that the *H.O.R.T.U.S.* series as a whole is biomimetic in that it represents an evolution in materials, form, and function. I begin with a brief definition of biomimesis and biomimetic art. Then, I investigate each individual piece within my definition of biomimetic art. Next, I argue that the *H.O.R.T.U.S.* series as a whole is biomimetic in its embodiment of evolution. Lastly, I submit that the H.O.R.T.U.S. series also represents a call to action for humanity in reminding us of our bio-identity.

BIOMIMESIS

In order to articulate the functions of *H.O.R.T.U.S.*, *Paris*, *ZKM, Astana*, and *XL*, I now define the key terms art, biomimesis, and biomimetic art according to my own definitions. Art is defined as the creation of work to be perceived and admired by an audience. Biomimetics is defined hereafter as the practice of using mechanical means to mimic biological functions found in nature. The word 'biomimetics' comes from the Greek prefix 'bio,' meaning life, and the root word 'mimesis' meaning imitation. The field of biomimetics is emergent and is still considered "in its infancy" [4]. It is unique in its incorporation of multiple disciplines in its attempt to identify and apply the biological functions, structures, and principles of various objects found in nature [5]. In the 3.8 billion years it is estimated that life has existed on Earth, life has evolved to create highly-adapted organisms that efficiently perform their various functions [6]. By mimicking naturally occurring phenomena, practitioners can save time and resources while still accomplishing their goals and "integrat[ing] form, material, and structure into a single process" [7]. Biomimetics has the potential to inspire textiles or designs that are antifouling, self-assembled, respond to their surrounding environments--to name some potential uses. Some examples include buildings (inspired by plants) which absorb light to create energy and moving ceilings which self-adapt their structure depending on atmospheric conditions. Such structures integrate mechanisms which do not require any maintenance [8]. These buildings could potentially save the amount of manpower and cost that come with the upkeep/ wear and

conservation of a building. This extends to the appliance systems required to host its occupants.

While biomimetics can be applied to countless fields, this paper will focus on how it applies to art. Here, biomimetic art is the integration of biological form and function into a work of art. Traditional art often mimics the form of biological life, but biomimetic art introduces the function of it as well. Biomimetic art is not meant to be a literal representation of the form and function of nature. If the function desired for biomimetic purposes derives from the form of the natural entity, the art may take a similar form to its original inspiration.

INDIVIDUAL BIOMIMETIC WORKS

H.O.R.T.U.S., shown in Figure 1, mimics the symbiotic relationship between animals and plants. When humans breathe out CO_2, photosynthetic organisms use it as energy and release oxygen in the process. In the exhibit, spectators contribute their CO_2 by breathing through a tube that directly connects to the pouches of cyanobacteria. The cyanobacteria then photosynthesize and feed the inhabitants of the room with oxygen. The function of each pod is self-contained, creating its own biosphere and mimicking a unicellular organism. However, each individual bio-pod inhabits the same general space.

FIGURE 1: *H.O.R.T.U.S.,* Architectural Association London, London, United Kingdom.

H.O.R.T.U.S. Paris (Figure 2) mimics both the form and function of a tree. Nutrients flow up from the "roots", through the "trunk", and to the "leaves". The "leaves" contain chloroplasts which in turn engage in photosynthesis, producing oxygen and fuel for the organism. *Paris* mimics this by placing nutrient fortified water in receptacles at the base of the "tree", then pumping the liquid reserves through thin tubes into the pods holding cyanobacteria. The cyanobacteria use the nutrients and the CO_2 provided by spectators to photosynthesize and emit oxygen into the room for its occupants. *Paris* is a network of interconnected pipes and pods, representing a multicellular organism.

FIGURE 2: *H.O.R.T.U.S. Paris,* Espace Fondation EDF, Paris, France

H.O.R.T.U.S. ZKM (Figure 3) shares the same tree structure with *Paris*. However, it has evolved to include an overhanging, cloud-like network for algae circulation which acts as a stabilizing structure for the pipes. It mimics the nutrient circulation within a tree's branch system.

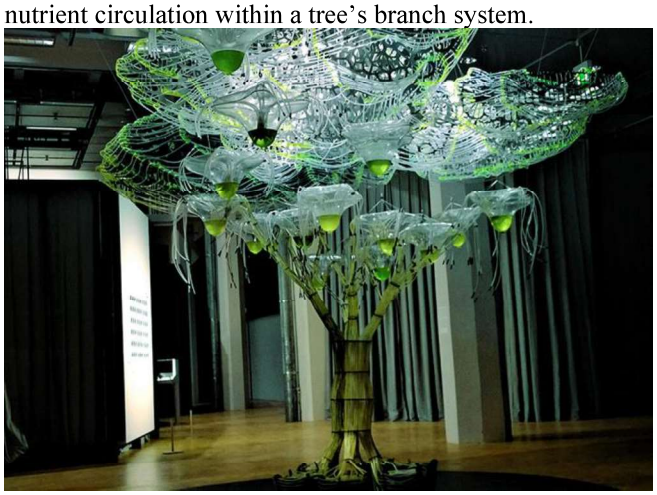

FIGURE 3: *H.O.R.T.U.S. ZKM,* ZKM museum, Karlsruhe, Germany.

The exhibit *H.O.R.T.U.S. Astana* (Figure 4) mimics the phototropism of plants. Plants respond to the surrounding environment by growing towards the direction of sunlight for maximum exposure. In this exhibit, *H.O.R.T.U.S. Astana* was configured using digital computation which allowed the artists to assess the highest energy points in the room. This enabled them to maximize the display's exposure to sunlight. This augmented feature, incorporated with the CO_2 provided by spectators through hand pumps, ensures that the cyanobacteria are able to photosynthesize with utmost efficiency.

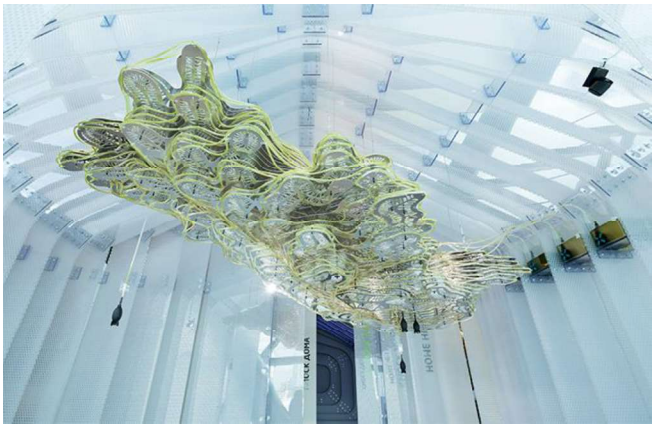

FIGURE 4: *H.O.R.T.U.S. Astana,* Astana EXPO 2017, Nur-Sultan, Kazakhstan.

H.O.R.T.U.S. XL (Figure 5) simulates the growth of substratum in coral morphology [13]. In nature, coral is a host to cyanobacteria colonies which photosynthesize and release oxygen. In *XL*, cyanobacteria are inserted into the structure, providing maximum exposure to sunlight due to the structure's design. The cyanobacteria then photosynthesize, releasing oxygen for surrounding organisms.

FIGURE 5: *H.O.R.T.U.S. XL,* Centre Pompidou, Paris, France.

A BIOMIMETIC SERIES

Having demonstrated the biomimetic qualities of each work, I now argue that the series as a whole is biomimetic. While each individual exhibit itself is inspired and mimics organic mechanisms found in nature, the *H.O.R.T.U.S.* series as an entire whole is biomimetic in its evolution of form, materials, and the methods by which it performs its function. This biomimetic evolution is shown in FIGURE 6.

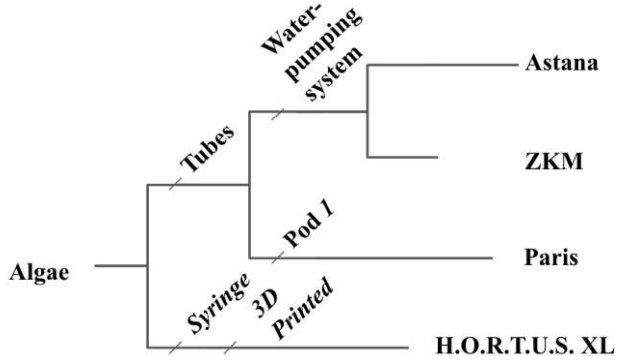

FIGURE 6: Cladogram demonstrating the evolution of the H.O.R.T.U.S.

The first stage of the *H.O.R.T.U.S.* series, *H.O.R.T.U.S.*, is an exhibit showcasing two variations of clear plastic pouches suspended individually from the ceiling. The first variation of plastic bag is similar to an IV bag, while the second is concave and shaped like an upright bellflower. These suspended bio-pods are filled with a mixture of minute algae particles in water--which give it a green or rustic hue. The pouches are hung at different heights throughout the room which allows them to "inhabit" the same space, yet each pod represents its own biosphere. In this sense, the room itself embodies the individual alga coexisting in each of the liquid pouches. Below these hanging clusters, the floor is lined with green carpet. Large rolls of the same carpet are placed throughout the room along which occupants can prop themselves against. This provides an area where visitors can lounge and congregate.

H.O.R.T.U.S. is made up of a wide range of plastic materials for different functions. This includes two types of plastic bags, thin flexible tubes, and plastic strings to suspend individual bags from the ceiling. At first, the use of plastic seems contradictory: plastic is one of the largest contributors to environmental damage. This could be an artistic statement, although the artists' intentions are not known. EcoLogicStudio collected different types of algae from lakes and ponds within Central London, establishing biological diversity within the exhibit [3]. The work also includes a digital interface for the audience to interact with.

H.O.R.T.U.S. allows for visitors to contribute their CO_2 by blowing through the thin plastic tubes and into the plastic bags [photo-bioreactors] containing cyanobacteria. Throughout the week, visitors engage daily with *H.O.R.T.U.S.*. This creates a consistent and fluctuating nutrient dosage for the algae. The cyanobacteria then photosynthesize and produce oxygen, essentially enabling a symbiotic loop with the visitors in the room. The spectators further interact with H.O.R.T.U.S. utilizing Twitter. Information in the form of tweets creates an interactive platform so individuals near and even far away can contribute to feeding the virtual pods via tweets. Its virtual plots are

nurtured by the flow of tweets posted by each visitor both locally and globally, creating new "cyber gardening practices" [15].

In *H.O.R.T.U.S. Paris*, the second stage of the *H.O.R.T.U.S.* series, several bio-pods are hung from a tree-like structure. Flexible tubes are assembled to form the roots and trunk of the tree using black plastic stabilizers to hold them together. Bellflower shaped bio-pods represent both the fruit and the leaves of the tree.

H.O.R.T.U.S. Paris retains the original prototype of hanging algae/water solution in plastic receptacles. Clear, pliable tubing suctions liquid from water tanks on the ground which lead upward and culminate into a large "tree trunk," and further out to the pods. These clear plastic receptacles-- in this instance, upturned bell-shaped pods-- are given the illusion of resting upon the upper "branches."

Materially, Paris uses only one of the two types of plastic bags previously used in *H.O.R.T.U.S.*. Unlike *H.O.R.T.U.S.*, the majority of *H.O.R.T.U.S. Paris* consists of thin, plastic tubes and aluminum which makes up the frame of the overhanging network. Smaller parts include green and black plastic segments to hold the thin tubes together. The exhibit also utilizes a pumping system and four water buckets for the flow of nutrients and algae. The cyanobacteria remain in liquid form. Furthermore, there is no longer a digital interface.

In *H.O.R.T.U.S. Paris*, visitors are still able to blow into the tubes connected to each bag to feed the cyanobacteria inside. However, this time the exhibit has changed in the method by which it achieves its outcome, which is oxygen production. In this case, the structure includes a pumping system at the base. Compared to *H.O.R.T.U.S*, *H.O.R.T.U.S Paris* is a network that integrates the tubing, cyanobacteria, and pods to mimic the shape and also function of a tree. The photo-bioreactor pumps nutrients upward to the rest of the structure, much as a root system does. *H.O.R.T.U.S.* has evolved so that the individual plastic bags [cells] come together to create a structure, and as a garden, it is now easier to distribute nutrients and CO_2 to the cyanobacteria. I submit here that this is an example of reconciling technology with nature's already acquired evolutionary wisdom.

In *H.O.R.T.U.S.* ZKM, the structure retains the tree-like base from Paris, but the form has evolved to include an overhanging structure in the shape of a cloud. The cloud is green in color-- depending on the circulation of algae--and consists of an aluminum base that is covered with a network of tubes. The overhanging cloud-like network of pipes represents the branches of the tree-- circulating nutrients.

The newest component of the *H.O.R.T.U.S.* series is suspended above the tree and the pods in ZKM: an aluminum lattice enveloped in a webbing of the same plastic piping, forming a cloud-like biomass. The plastic piping is held in place with plastic, neon-green stabilizers.

Though the method of achieving function remains the same as Paris, it is executed more efficiently by circulating the flow of algae in the overhanging structure.

The fourth exhibit in the series, *H.O.R.T.U.S. Astana*, reveals a version of the system that is an unspecified shape. Constructed of large flat sheets of laser-cut aluminum, each unique cutout is suspended within close proximity to the next layer. In effect, this creates a 3-dimensional biomass which takes on the appearance of a cloud. It has incorporated the concept of an overhanging cloud-like network from *H.O.R.T.U.S. ZKM*. However, the presentation is cleaner, and the breathing apparatus has been replaced by a black, ovoid hand pump with four fins adorning the bottom. Each pump hangs from a single, transparent tube. This gives the illusion of standing within a cavern or cave. The cyanobacteria are again mobilized through clear transparent tubes that line the edges of each horizontal aluminum plate. The cyanobacteria emit a green hue which highlights the structure's shape.

In contrast with *H.O.R.T.U.S. ZKM*, in *H.O.R.T.U.S. Astana,* the artists have eliminated the use of plastic bags. Instead of thin pipes, they utilize hand pumps hanging from the suspended structure. They have, however, kept the water pumping system. A small pump for fluid circulation, a glass container for the microalgae, and wide-spectrum lights are also integrated [16]. The structure now consists of laser-cut aluminum leaf-like sheets that are stacked to form a cloud. Each layer is lined with clear piping to create a network that carries the flow of cyanobacteria.

H.O.R.T.U.S. Astana was built by first digitally mapping the space to visualize the intensive field of energy[light sources] [16]. The cyanobacteria were then arranged along surfaces, allowing optimal incoming radiation. A network connects the pathways of tubes which carry nutrients and CO_2 to the nodes housing photosynthetic cyanobacteria. In the form of a cloud, the structure is divided into four clusters which operate as an integral unit [16]. The degree of connectedness depends on physical light. Astana again engages with the audience, this time allowing them to contribute via a hand pump.

H.O.R.T.U.S. XL, the final exhibit in the series, shows a significant transformation in form. Now, it takes the shape of a free-standing structure that is opaque and appears to resemble a coral formation. The coral-like structure is porous, 3D-printed, and composed of triangular units that make up larger hexagons for strength and support. It is much lighter but also denser in space and minimalistic compared to the previous exhibits. The 3D-printed structure, which is opaque in color, juxtaposes with the green cyanobacteria.

H.O.R.T.U.S. XL changes from Astana by replacing the plastic tubes, hand pumps, pumping system, and aluminum frame with 3-D printed plastic materials. *H.O.R.T.U.S.* no longer uses pipes or aluminum; rather, it creates a net using only one material built layer by layer. In contrast to *H.O.R.T.U.S. Astana's* liquid cyanobacteria, *H.O.R.T.U.S. XL* uses cyanobacteria in the form of a gel.

H.O.R.T.U.S. XL is a structure that simulates the growth of substratum inspired by collective coral morphologies using a digital algorithm [13]. The piece is algorithmically designed and produced using large-scale, high-resolution 3D printing technology. In order to optimally arrange the photosynthetic organisms along iso-surfaces of increased incoming radiation, the density-value of each "bio-pixel" is also digitally computed [13]. Apart from its technical makeup, the structure itself functions completely differently. Visitors can no longer pump or blow CO_2 into the structure's components. The structure is mostly hands-free, because the gel has already been inserted in each "bio-pixel." The cyanobacteria get CO_2 from the surrounding inhabitants and environment through the porous structure and, because they are in a gel form, have no need to be circulated. Instead, the cyanobacteria are inserted into the triangular units manually.

The structure simulates the growth of substratum inspired by coral morphology which gives it an organic feel, as coral reefs are home to an abundant amount of marine life. This supports the idea of future forms of spatial intelligence that will be able to function and support themselves. Like the coral it was inspired by, *H.O.R.T.U.S. XL* provides a sturdy structure that can be incorporated into various living spaces.

Together, all of these small material changes [microevolution] show a greater change [macroevolution] through the *H.O.R.T.U.S.* series. In contrast to *H.O.R.T.U.S.*, which featured three types of plastic materials and cyanobacteria in liquid form, *H.O.R.T.U.S. XL* has evolved to consist uniformly of one plastic material and a cyanobacteria gel. *H.O.R.T.U.S. XL* eliminates plastic bags, aluminum, pipes, water tanks, hand pumps; plastic tubes, and water pumping systems. The series has evolved so that the work can be built layer-by-layer to create a complex, high-performance structure using limited materials efficiently.

CONCLUSION

In this paper, I have demonstrated that though each individual work in EcoLogicStudio's *H.O.R.T.U.S.* series is biomimetic, the series itself embodies biomimicry in its evolution in form, materials, and function from piece-to-piece and overall. The *H.O.R.T.U.S.* series proposes a future of "new novel material practices"[3], emergence and practice of new fields, and the "collaborative" relationship between the natural biosphere and the artificial urbansphere [16].

Biomimietic art and architecture effectively joins different fields, new practices, and art, showing promising conceptions of future works responsive to urban stimuli. Furthermore, the emerging symbiotic relationship between the artificial and natural worlds could massively influence the future of humanity. The field of biomimetics has great potential for solutions to the global crises of the 21st century: climate change (caused by the emission of greenhouse gases), environmental pollution, sustaining growing populations, and managing earth's natural resources.

The agricultural revolutions of the past occurred through scientific and technological innovation. However, the byproduct of rapid growth is a looming concern. Farming and agriculture have used and continue to use Earth's resources too liberally. Fortunately, with the current awareness of the impact we have on our environment, organizations and individuals are making efforts to steer us from this trajectory and take advantage of this probationary moment to conserve resources and diminish the effects of climate change. Moreover, H.O.R.T.U.S. ultimately is not only a literal demonstration but an art piece, meant to inspire and help us reconsider old ways of thinking while nudging us in a hopeful direction to see the possibilities of these integrated disciplines.

H.O.R.T.U.S. XL features a vertical gardening prototype, conserving space and energy, while *H.O.R.T.U.S. Paris* and *ZKM* are fundamentally-modified hydroponic systems, and novel approaches toward sustainability. The H.O.R.T.U.S. series reminds mankind of its place in this delicate and complex biosphere. Biomimicry is a template for humanity to become more involved with the symbiotic relationship we have with the environment. We're approaching a new space where technology becomes more synthesized with biology, and humans become consolidated into the complex functions of nature.

ACKNOWLEDGEMENTS

I would like to express my deepest gratitude to everybody who has made this paper possible: my mentor Hayden Mueller, Elizabeth Feldeverd, Tyler Kusunoki, and my family.

REFERENCES

[1] “Bioreactors.” Bioreactors - Introduction to Chemical and Biological Engineering, www.engr.colostate.edu/CBE101/topics/bioreactors.html.

[2] “:: About - EcoLogicStudio ::” EcoLogicStudio, www.ecologicstudio.com/v2/about.php?mt=1.

[3] “:: H.O.R.T.U.S. - EcoLogicStudio ::” EcoLogicStudio, www.ecologicstudio.com/v2/project.php?idcat=7&idsubcat=71&idproj=115.

[4] Amato, Ivan. “Heeding the Call of the Wild.” Science, vol. 253, no. 5023, 1991, pp. 966–968. JSTOR, www.jstor.org/stable/2878784. Accessed 13 Feb. 2020.

[5] Reed, Emily J., et al. “Biomimicry as a Route to New Materials: What Kinds of Lessons Are Useful?” Philosophical Transactions: Mathematical, Physical and Engineering Sciences, vol. 367, no. 1893, 2009, pp. 1571–1585. JSTOR, www.jstor.org/stable/40485540. Accessed 13 Feb. 2020.

[6] Ripley, Renee L., and Bharat Bhushan. “Bioarchitecture: Bioinspired Art and Architecture—a Perspective.” Philosophical Transactions: Mathematical, Physical and Engineering Sciences, vol. 374, no. 2073, 2016, pp. 1–36., www.jstor.org/stable/24760325. Accessed 13 Feb. 2020.

[7] Poletto, Marco, and Claudia Pasquero. Systemic Architecture : Operating Manual for the Self-Organizing City, Routledge, 2012. ProQuest Ebook Central, https://ebookcentral.proquest.com/lib/trincoll/detail.action?docID=1016204.

[8] KRIEG, OLIVER DAVID, et al. “HYGROSKIN: METEOROSENSITIVE PAVILION.” Fabricate 2014: Negotiating Design & Making, by Fabio Gramazio et al., DGO - Digital original ed., UCL Press, London, 2017, pp. 272–279. JSTOR, www.jstor.org/stable/j.ctt1tp3c5w.37. Accessed 9 Mar. 2020.

[9] Pasquero, Claudia and Marco Poletto. H.O.R.T.U.S. 2012. London, UK. EcoLogicStudio, http://www.ecologicstudio.com/v2/project.php?idcat=7&idsubcat=71&idproj=115. Accessed December 2019.

[10] Pasquero, Claudia and Marco Poletto. H.O.R.T.U.S. Paris. Paris, France. EcoLogicStudio, http://www.ecologicstudio.com/v2/project.php?idcat=7&idsubcat=71&idproj=127. Accessed December 2019.

[11] Pasquero, Claudia and Marco Poletto. H.O.R.T.U.S. ZKM. 2015. Karlsruhe, Germany. EcoLogicStudio, http://www.ecologicstudio.com/v2/project.php?idcat=7&idsubcat=20&idproj=149. Accessed December 2019.

[12] Pasquero, Claudia and Marco Poletto. H.O.R.T.U.S. Astana. 2017. Nur-Sultan, Kazakhstan. EcoLogicStudio, http://www.ecologicstudio.com/v2/project.php?idcat=7&idsubcat=20&idproj=163. Accessed December 2019.

[13] “:: H.O.R.T.U.S. XL - EcoLogicStudio ::” EcoLogicStudio, www.ecologicstudio.com/v2/project.php?idcat=7&idsubcat=59&idproj=177.

[14] Pasquero, Claudia and Marco Poletto. H.O.R.T.U.S. XL. 2019. Centre Pompadou, Paris. EcoLogicStudio, http://www.ecologicstudio.com/v2/project.php?idcat=7&idsubcat=59&idproj=177. Accessed December 2019.

[15] “:: H.O.R.T.U.S ZKM - EcoLogicStudio ::” EcoLogicStudio, www.ecologicstudio.com/v2/project.php?idcat=7&idsubcat=20&idproj=149.

[16] “:: H.O.R.T.U.S. Astana - EcoLogicStudio ::” EcoLogicStudio, www.ecologicstudio.com/v2/project.php?idcat=7&idsubcat=20&idproj=163.

[17] “:: Alive - EcoLogicStudio ::” EcoLogicStudio, www.ecologicstudio.com/v2/project.php?idcat=7&idsubcat=71&idproj=127.

The Dynamic Republic

Artemis a. Pados
Stanford Online High School (OHS); Stanford, CA, USA
artemispados@gmail.com or apados@ohs.stanford.edu

Abstract – Plato writes through the words of Socrates in "The Republic" that the ideal order and character of a just city-state can be found by examining the soul of a just man. In Book IV, Plato writes that there are three parts to the human soul – "appetite, spirit, and wisdom"- and by analogy, Plato concludes that these categories directly translate to the way in which an ideal state/society should be organized. I argue that there are two significant flaws with Plato's ideal city: (1) The lack of social mobility, which may limit the dreams and ambition of people causing the overall happiness to decline; and (2) the lack of necessary details in determining class assignments (that is, by whom and when), which may lead to considerations of non-optimal power distribution in the city and potential error in placement of its citizens. As a solution, I propose a formal method of regular reevaluation of the classes of the city leading one to reconsider Plato's model as dynamic rather than static as originally presented.

Key Words – Philosophy; Plato; Republic; Soul; City

INTRODUCTION

Plato writes through the words of Socrates in "The Republic" that the ideal order and character of a just city-state can be found by examining the soul of a just man. In Book IV, Plato writes that there are three parts to the human soul – "appetite, spirit, and wisdom"- and by analogy, Plato concludes that these categories directly translate to the way in which an ideal state/society should be organized. He says that based on the part of a person's soul that is dominant, one is placed into one of the following hierarchical categories in the city: A worker (the producing, 'appetitive' class), an auxiliary (soldier/police of the 'emotive' class), or a ruler (the 'rational' most broadly educated class). In this paper, I argue that there are two significant flaws with Plato's ideal city: (1) There is no apparent means of moving in one's life time between the social classes Plato has created, which may limit the dreams and ambition of people causing the overall happiness to decline; and (2) there is ambiguity in how (that is, by whom and when) a person is decided to be in one of the groups, which may lead to considerations of non-optimal power distribution in the city and potential error in placement of the citizens. First, I begin by outlining the guidelines that Plato set forth for an ideal city. Second, I establish the particular problems I see in the Platonic city system and discuss their implications, while also putting forth some of Plato's counter arguments to the problems. Third, I provide some potential solutions to the obstacles that I see and also discuss some elements of Plato's ideas which are visible in our modern democratic states. I conclude that a philosophical discourse on the Republic's ideal state can offer pragmatic, usable information about the current state of political affairs in the world.

DISCUSSION

Plato begins Book IV by saying that the goal of his ideal city is not to make one group of people happy at the expense of another, but to make the city as a whole happy. He says, *"And our answer will be that, even as they are, our guardians may very likely be the happiest of men; but that our aim in founding the State was not the disproportionate happiness of any one class, but the greatest happiness of the whole; we thought that in a State which is ordered with a view to the good of the whole we should be most likely to find justice, and in the ill-ordered State injustice: and, having found them, we might then decide which of the two is the happier. At present, I take it, we are fashioning the happy State, not piecemeal, or with a view of making a few happy citizens, but as a whole; and by-and-by we will proceed to view the opposite kind of State"* (Plato 275). Making the city as a whole happy is a logical goal to set, however, in the end, I see the happiness of individuals being compromised in order to follow the 'ideal system'. I return to further analyze this point later, but I cannot resist noticing a connection between Plato's goals and those stated by past and present communist states. Plato, through the words of Socrates, creates some interesting regulations that he believes will form a perfect society and make the city as a whole content. Firstly, there is to be no money in order to ensure that wealth/poverty creates no disruptions in the peace and happiness of the community. Currency is useful when it is necessary to defend one's country in battle, but according to Plato there will be no need to defend themselves since the state – the Platonic state - will be superior and all others will be willing allies (Plato 277). Secondly, a warning is put forth at the start of the book about the city becoming too large and ungovernable; a cap on the population is said to be necessary (Plato 278-279). Lastly,

Plato decides that it is best if a state is free of laws and the named rulers make decisions as necessary (Plato 280). I view all of the Platonic conditions for a perfect city-state as unprecedented for their time. However, what I see as a most novel concept presented in the book is the tripartite division of an individual's psyche. "Appetite", "spirit", and "reasoning/wisdom" are the three components that are said to make up human soul. The categories directly translate to, and were the inspiration for, the blueprint of the Platonic city – the three categories of the soul become the three categories of people in the city (Brown). The people with dominant trait of "appetite" are those driven by materialistic desire who make up the producing class, the workers. Those full of "spirit" are the courageous who have the ability to control their desire and take the roles of the auxiliaries, the fighters and the police officers. Lastly, the group of "reasoning and wisdom" is the rulers, the philosophers, those capable of logical judgments. A modern, though often regarded as failing, example of Platonic theories is Singapore's social class separation in the 1990s. The Prime Minister of Singapore at the time performed a separation of people similar to Plato's tripartite division. He, however, exercised unprecedented control on human behavior including arranged marriages among the purported intelligent class for the proliferation of the "right species" (Nussbaum).

I have no intention to argue against Plato's partitioning of the citizens in "The Republic" into workers, auxiliaries, and rulers. One can see, however, that there is no obvious way for people to move from group to group in the way Plato has created the 'hierarchy'. There are three groups strictly defined with the rulers/philosophers being at the clear top of the pecking order. Plato does not believe in social mobility. He rejects the idea that humanity is malleable. Humans, according to him are bound by their natures. According to Plato's theory, people have no dreams and ambitions beyond their class. In fact, they do not need dreams and ambitions because the state takes care of them and, in turn, they take care of the state, which leads to general happiness. Consider the case, then, where one or more worker citizens, inspired maybe by political events and city-state infighting and wars, wish to step up to the soldier class to defend their homes and homelands. Plato's system does not seem to offer a way for this change. Consider also a soldier who risked their life fighting state enemies in lands near and far and accumulated such life experiences, best and worst, that make them wise, significantly wiser than their early years. Such a soldier cannot join the ranks of the rulers if they wish. The lack of ability to transition between classes will limit the ambition and aspirations of people, which disagreeing with Plato, I believe people will always have. In this system, a worker will be a worker, a soldier will be a soldier, and a ruler will be a ruler forever. This, in long term, can affect an individual's happiness which may also eventually hinder the overall happiness of the city (a goal of Plato in his quest for perfect justice).

The second issue I find with Plato's model is that it is unclear who decides what category each person belongs to and when in one's lifetime they are placed in their respective group. It seems that there should be designated personnel in charge of identifying people's prevailing characteristics and assigning them to groups in order to have the process be as objective and just as possible. Plato responds to the problem at hand by presenting the idea of having all children taken away from their parents at a young age and having 'specialists' work with them who then decide where the children fit best based on early signs of characteristics associated with people of each group (Bramann). However, there are further concerns with this method. There is ambiguity as to what type of people the specialists are; are they a category of their own – a new, fourth category? Due to the critical importance of this question in the formation of the ideal state, further information and supporting details seem necessary. Lastly, there must be a broad window or time frame for when a child needs to be placed in its appropriate group. There is a risk of misplacement and inaccuracy if people are classified prematurely.

The problems of class mobility and the specialists in Plato's state are not uncorrelated. A solution to one should also treat the other. A consideration is to maintain the three-class partition of Plato and let the class of philosophers/rulers (the wiser of all) be 'the specialists.' The other citizens (workers and soldiers) will be evaluated and consulted by the specialists on a regular schedule. Their just desires will be discussed and accommodated appropriately by the wisemen. The wisemen themselves will meet and consult with each other for evaluation and possible own class reassignment.

There are thinkers that consider Plato's Republic an assault to democracy since it denounces many freedoms that democracies embrace (Nussbaum). Yet, Platonic principles are evident in modern day democracies including the US. Plato's city in today's language and times seems a state run by the educated elite, that is, by those in the judicial, legislative, and executive branches of the government. Today, part of the working class in this country, the United States, believes that this is indeed the current state of political affairs (Williams) despite the fact that our political system is a representative democracy. Division of labor/separation of classes and ruling by the wisemen, the educated elite, are the foundations of the ideal society according to Plato and will lead to justice and happiness (Nussbaum). However, "*history*

has taught us to mistrust what the government [wisemen] *will do when it tries to take control of our lives through superior wisdom*" (Nussbaum). Corruption of government (wisemen, rulers) minimizes access to opportunity and, maintaining the class status quo, is promoted as natural. This leads to a growing, loud discontent with the 'educated elite' who are seen as indifferent, or disinterested, in serving the real needs of the working class. Social classes with minimal opportunity for mobility create class-type envy and hierarchies that may lead to hatred from below and discrimination from above. A prime example that manifests the discontent of the working class toward the educated elite (philosophers/rulers) has been at the voting poll. My "solutions" or, better said, modifications to Plato's system seem to attempt to break the workers-to-rulers barrier and assign a broader definition to 'education' or 'wisdom'. Through life experience and personal reflection and growth, any worker (or soldier) can become equal in wisdom to preassigned rulers and is given the opportunity to join them in their place of governance (after all, an aging soldier cannot be as effective a soldier anymore). In the opposite direction, under my solution-to-be, a ruler can at any time be transitioned to the producing or fighting class which should justly motivate any one of them to pay close attention to the needs and wills of these two classes.

CONCLUSION

In Book IV of "The Republic", Plato put forward the unprecedented concept of an ideal city of just people partitioned in three classes, the working, the fighting, and the ruling. Strong arguments by Plato, in the words of Socrates, explain how this state system can maximize the happiness of the city. In this paper, I raised two concerns: (1) The lack of social mobility and (2) the lack of necessary details in determining class assignments. I proposed as a solution to address these concerns a formal method by which rulers, fighters, and workers convene in regular intervals to discuss and evaluate the will and growth of individuals and, through persuasion rather than coercion, agree in upward and downward class movement. If this solution were implemented successfully, class barriers would not be formed and the individuals would remain free to reach for their evolving dreams and ambitions and pursue their own happiness as they perceive it. In these terms, maybe we should reconsider Plato's model as dynamic rather than static as originally presented. After all, following Plato's own analogy with the individual soul (appetites, emotions, reason), we can argue that just as we grow and change from birth to old age, so should Plato's Πολιτεία[1].

AKNOWLEDGEMENTS

I would like to thank Dr. Heather Walker-Dale, instructor of the History and Philosophy of Science course at Stanford Online Highschool for many intellectually stimulating class discussions. I would also like to thank the anonymous reviewers for their invaluable comments and suggestions.

REFERENCES

Bramann, Jorn K. "Plato: The Failure of Democracy", https://faculty. frostburg.edu/phil/forum/PlatoRep.htm. Accessed Nov. 12, 2019.

Brown, Eric. "Plato's Ethics and Politics in *The Republic*", *The Stanford Encyclopedia of Philosophy*. Fall 2017 Edition. Edward N. Zalta (ed.), https://plato.stanford.edu/entries/plato-ethics-politics /Accessed Nov. 12, 2019.

Plato. "The Republic"– Book IV, May 18 2002, pp. 275-304, http://www. idph.net/conteudos/ebooks/republic.pdf. Accessed Nov. 12, 2019.

Nussbaum, Martha C. "Plato's Republic: The Good Society and the Deformation of Desire", *Library of Congress 1998, Bradley lecture series*. https://www.google.com/books/edition/_/eLCTA QAACAAJ?hl=en&gbpv=1&pg=PA2. Accessed Sept. 5. 2020.

Williams, Joan C., "White Working Class: Overcoming Class Cluelessness in America", *Harvard Business Review Press,* p. 180.

[1] Πολιτεία is the Greek word for city-state.

LENGTH OF PORTION OF EULER LINE INSIDE A TRIANGLE

Prajapati Kavan Gautamkumar
Shree Narayana Higher Secondary School; Ahmedabad, India
Email: prajapatikavan9@gmail.com

Abstract – The Euler line which was discovered in 1763 by Swiss mathematician Leonhard Euler, is a line that goes through the orthocenter, the centroid and the circumcenter of a non-equilateral triangle. Moreover, the distance between the orthocenter and the centroid is always double the distance between the centroid and circumcenter. This paper aims at finding the length of segment of Euler line that lies inside of a non-right scalene triangle if the length of its three sides are given. This paper aims at deriving two approaches to find the length of portion of Euler line that lies inside of a scalene non-right triangle. As a result of the approaches, this papers contributes by providing formulas that can be used for any scalene non-right triangle.

Key Words – Triangle, Euler line, Formula to calculate length

INTRODUCTION

Around 250 years ago, Swiss mathematician and physicist, Leonhard Euler, showed that in any non-equilateral triangle, the orthocenter, circumcenter, and centroid are collinear and the line which passes from these three points is called Euler line of the triangle.

Euler line in different types of triangles
There is no Euler line in an equilateral triangle as the orthocenter, circumcenter, and centroid of the triangle coincide. The Euler line of an isosceles triangle coincides with axis of symmetry of that triangle. In a right triangle, the Euler line coincides with the median to the hypotenuse. For an acute angled triangle, centroid, circumcenter and orthocenter lie in the interior of the triangle. For an obtuse angled triangle, the centroid lies in the interior while the orthocenter and circumcenter lie in the exterior of the triangle.

Application of Euler line
An important application of Euler line is that information about any one of the centroid, orthocenter, and circumcenter can be derived from the information of other two in a triangle.

Motivation for this paper
It was when I was studying Law of Cosines that it occurred to me that if an angle of a triangle can be expressed in terms of three sides of a triangle, then one can also express the length of portion of Euler line inside a triangle in terms of three sides of a triangle.
I did further study and came up with formulas to derive the length of portion of Euler line that lies inside of a non-equilateral triangle using known results.

Scope of this paper
Formulas for finding the length of portion of Euler line that lies inside of different types of triangles are given in the following table.

Type of triangle based on sides	Type of triangle based on angles	Formula for length of portion of Euler line that lies inside of a triangle
Equilateral	Acute	Euler line does not exist
	Right	Right equilateral triangle does not exist
	Obtuse	Obtuse equilateral triangle does not exist
Isosceles	Acute	Length of median to base*
	Right	Length of median to hypotenuse[#]
	Obtuse	Length of median to base*

Scalene	Acute	Will be derived in this paper
	Right	Length of median to hypotenuse#
	Obtuse	Will be derived in this paper

*In isosceles triangle, length of median to base (unequal side of isosceles triangle) is the length of portion of Euler line that lies inside of a triangle.

#Length of median to hypotenus, whose length is half of hypotenus, is the length of portion of Euler line that lies inside of a triangle.

In this paper, we will cover derivation of formulas for following two types of triangle –

I. For acute scalene triangle
II. For obtuse scalene triangle

Notations used in this paper

Let us consider a scalene Δ ABC in which e is the Euler line which intersects two sides of a triangle at points P and Q. AN, BE and CL are altitudes on BC, AC and AB respectively which intersects each other at orthocenter, H. AM is median to BC and CS is median to AB which intersects each other at centroid, G.

Let BC=a, AC=b, AB=c, $\angle A$=A, $\angle B$=B and $\angle C$=C.

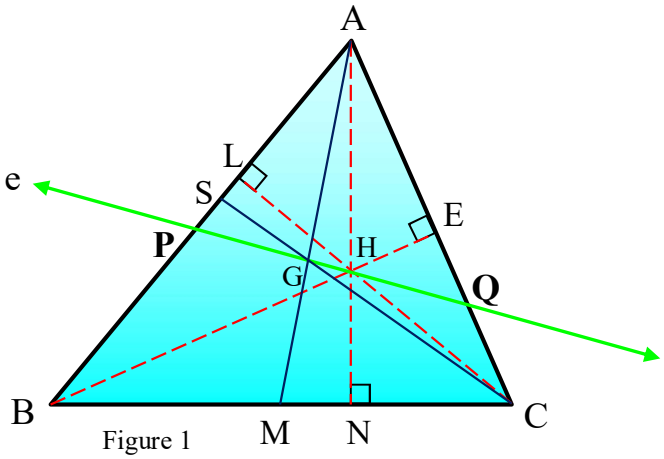

Figure 1

In order to derive the formulas, we will use the following known results:

i. Apollonius's Theorem [1]:

$$AB^2 + AC^2 = 2(AM^2 + BM^2)$$

ii. Centroid Theorem [2]:

$$AG = \frac{2}{3}AM$$

iii. Law of Sines [3]:

$$\frac{a}{\sin A} = \frac{b}{\sin B} = \frac{c}{\sin C}$$

iv. Law of Cosines [4]:

$$c^2 = a^2 + b^2 - 2ab\cos C$$

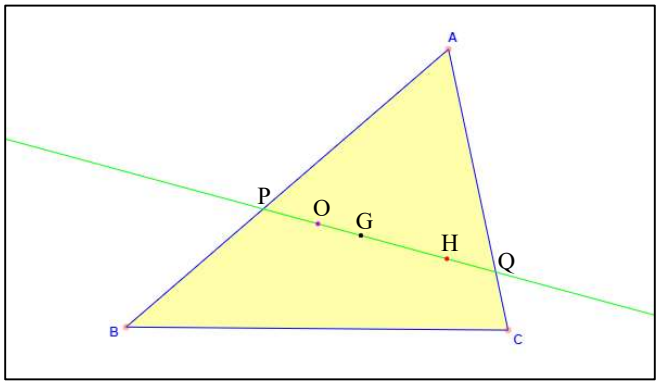

Figure 2: Euler line in acute triangle

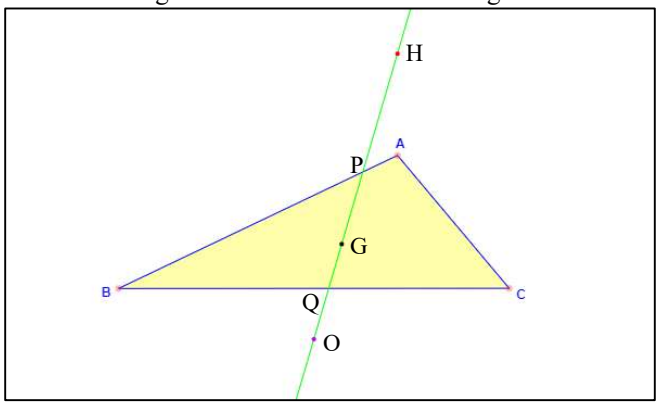

Figure 3: Euler line in obtuse triangle

In figure 2 and 3, $\overleftrightarrow{PQ}$ is the Euler line of triangle, which passes through orthocenter, H, centroid, G, and circumcenter, O.

These points have a unique property, $HG = 2GO$ [6].

I. DERIVATION OF FORMULA FOR ACUTE SCALENE TRIANGLE

Let Δ ABC be acute triangle.

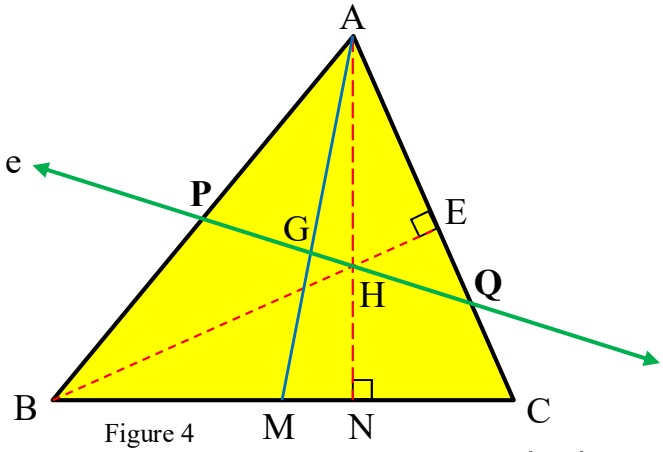

Figure 4

By Law of Cosines,

$$\angle A = cos^{-1}\left(\frac{b^2+c^2-a^2}{2bc}\right)$$
$$\angle B = cos^{-1}\left(\frac{a^2+c^2-b^2}{2ac}\right)$$
$$\angle C = cos^{-1}\left(\frac{a^2+b^2-c^2}{2ab}\right)$$

By Apollonius's Theorem,

$$AM = \frac{1}{2}\sqrt{2c^2+2b^2-a^2} \quad (1)$$

By Centroid Theorem,

$$AG = \frac{2}{3}AM$$
$$\therefore AG = \frac{1}{3}\sqrt{2c^2+2b^2-a^2} \quad (2)$$

For ΔAMC, by Law of Cosines,

$$\angle \mathrm{MAC} = \cos^{-1}\left(\frac{\mathrm{AM}^2+\mathrm{b}^2-\left(\frac{\mathrm{a}}{2}\right)^2}{2\cdot \mathrm{AM}\cdot \mathrm{b}}\right) \quad (3)$$

In eqn. (3), $\angle$MAC is an acute angle.

Also, $\angle NAC = 90° - \angle C$

$$\angle MAN = \angle GAH = \angle MAC - \angle NAC \quad (4)$$
$$\sin B = \frac{AN}{c}$$
$$\therefore AN = AH + HN = c\cdot \sin B \quad (5)$$

For ΔHAE, $\cos\angle HAE = \frac{AE}{AH}$

$$\therefore AH = \frac{AE}{\cos\angle HAE} \quad (5.1)$$

For ΔABE, $\cos A = \frac{AE}{c}$

$$\therefore AE = c\cdot \cos A \quad (5.2)$$

From (5.1) and (5.2),

$$AH = \frac{c\cdot \cos A}{\cos\angle HAE} \quad (5.3)$$

For ΔANC, $\angle NAC = \angle HAE = 90° - \angle C$

$$\therefore \cos\angle HAE = \cos(90° - \angle C)$$
$$\therefore \cos\angle HAE = \sin C$$

Therefore, from (5.3),

$$AH = \frac{c\cdot \cos A}{\sin \mathrm{C}} \quad (5.4)$$

For ΔHBN, $\tan\angle HBN = \frac{HN}{BN}$

$$\therefore HN = BN\cdot \tan\angle HBN \quad (5.5)$$

For ΔBEC, $\angle HBN = 90° - \angle C$

$$\therefore \tan\angle HBN = \cot C$$
$$\therefore \tan\angle HBN = \frac{\cos C}{\sin C}$$

Therefore, from (5.5),

$$HN = BN\cdot \frac{\cos C}{\sin C} \quad (5.6)$$

For ΔABN, $\cos B = \frac{BN}{c}$

$$\therefore BN = c\cdot \cos B$$

Therefore, from (5.6),

$$HN = c\cdot \cos B\cdot \frac{\cos C}{\sin C} \quad (5.7)$$

From (5.4) and (5.7),

$$\frac{AH}{HN} = \frac{\frac{c\cdot\cos A}{\sin C}}{c\cdot \cos B\cdot \frac{\cos C}{\sin C}}$$
$$\therefore \frac{AH}{HN} = \frac{\cos A}{\cos B\cdot \cos C}$$
$$\therefore \frac{AH}{\cos A} = \frac{HN}{\cos B\cdot \cos C} = x$$
$$\therefore AH = \cos A\cdot x \text{ and } HN = \cos B\cdot \cos C\cdot x \quad (5.8)$$
$$AH + HN = x(\cos A + \cos B\cdot \cos C)$$

But $AH + HN = c\cdot \sin B$ From (5)

So, $x(\cos A + \cos B\cdot \cos C) = c\cdot \sin B$

$$\therefore x = \frac{c\cdot \sin B}{\cos A + \cos B\cdot \cos C}$$

But $AH = \cos A\cdot x$ From (5.8)

$$\therefore AH = \frac{c\cdot \sin B\cdot \cos A}{\cos A + \cos B\cdot \cos C} \quad (6)$$

For ΔGAH, by Law of Cosines,

$$GH = \sqrt{AG^2 + AH^2 - 2\cdot \mathrm{AG}\cdot \mathrm{AH}\cdot \cos\angle \mathrm{GAH}} \quad (7)$$

$$\angle AGH = cos^{-1}\left(\frac{AG^2+GH^2-AH^2}{2\cdot AG\cdot GH}\right) \quad (8)$$

For ΔAGQ, $\angle GAQ = \angle MAC$, $\angle AGQ = \angle AGH$

$$\angle AQG = 180° - \angle GAQ - \angle AGQ \quad (9)$$

By Law of Sines,

$$\frac{GQ}{\sin\angle GAQ} = \frac{AG}{\sin\angle AQG}$$
$$\therefore \boldsymbol{GQ} = \frac{AG\cdot \sin\angle GAQ}{\sin\angle AQG} \quad (10)$$

For ΔAGP, $\angle AGP = 180° - \angle AGQ$

$$\angle PAG = \angle A - \angle GAQ \quad (11)$$

$$\angle APG = 180° - \angle AGP - \angle PAG$$
$$= 180° - (180° - AGQ) - (\angle A - \angle GAQ)$$
$$\therefore \angle APG = \angle AGQ + \angle GAQ - \angle A \quad (12)$$

For ΔAGP, by Law of Sines,

$$\frac{PG}{\sin\angle PAG} = \frac{AG}{\sin\angle APG}$$
$$\therefore \boldsymbol{PG} = \frac{AG\cdot \sin\angle PAG}{\sin\angle APG} \quad (13)$$

From (10) and (13),

$$PG + GQ = \frac{AG\cdot \sin\angle PAG}{\sin\angle APG} + \frac{AG\cdot \sin\angle GAQ}{\sin\angle AQG}$$

$$\therefore \text{PQ} = \text{AG} \cdot \left[\frac{\sin(\angle\text{A} - \angle\text{GAQ})}{\sin(\angle\text{AGQ} + \angle\text{GAQ} - \angle\text{A})} + \frac{\sin(\angle\text{GAQ})}{\sin(180° - \angle\text{GAQ} - \angle\text{AGQ})}\right]$$

Let AM=m, GH=d and AH=n. Using eqns. (1) to (13),

$$\boldsymbol{PQ} = \frac{2}{3}\boldsymbol{m} \cdot \left[\frac{\boldsymbol{\sin\left(\angle A - \left\{\cos^{-1}\left(\frac{m^2+b^2-\left(\frac{a}{2}\right)^2}{2 \cdot m \cdot b}\right)\right\}\right)}}{\boldsymbol{\sin\left(\cos^{-1}\left(\frac{\left(\frac{2}{3}m\right)^2+d^2-n^2}{\frac{4}{3}m \cdot d}\right) + \cos^{-1}\left(\frac{m^2+b^2-\left(\frac{a}{2}\right)^2}{2 \cdot m \cdot b}\right) - \angle A\right)}} + \frac{\boldsymbol{\sin\left(\cos^{-1}\left(\frac{m^2+b^2-\left(\frac{a}{2}\right)^2}{2 \cdot m \cdot b}\right)\right)}}{\boldsymbol{\sin\left(\cos^{-1}\left(\frac{m^2+b^2-\left(\frac{a}{2}\right)^2}{2 \cdot m \cdot b}\right) + \cos^{-1}\left(\frac{\left(\frac{2}{3}m\right)^2+d^2-n^2}{\frac{4}{3}m \cdot d}\right)\right)}}\right]$$

This formula is derived with respect to Figure 4.
If three sides of an acute scalene triangle are given, using eqns. (1) to (13) and the final formula, we can find the length of portion of Euler line inside any acute scalene triangle.

Now we will derive formula for obtuse scalene triangle.

II. DERIVATION OF FORMULA FOR OBTUSE SCALENE TRIANGLE

Let Δ ABC be obtuse triangle.

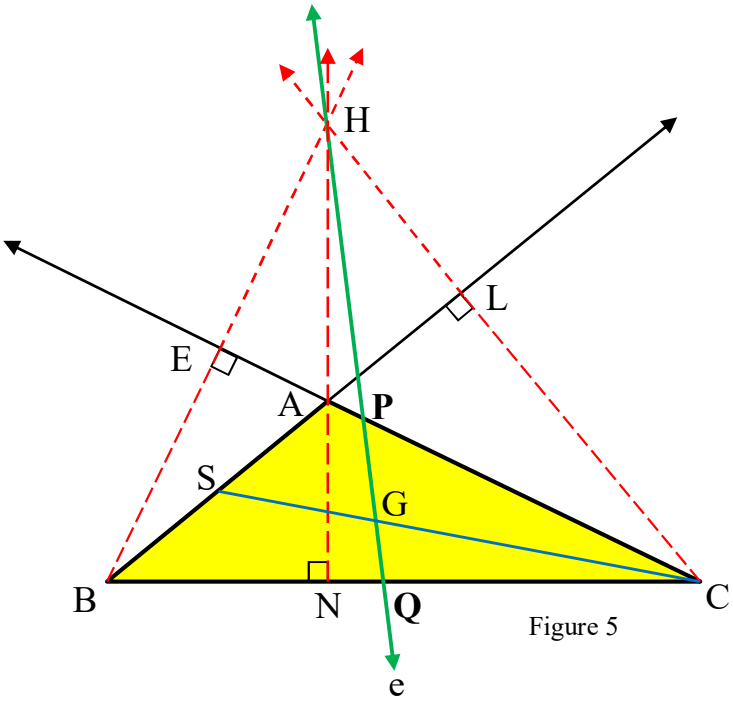

Figure 5

By Law of Cosines,

$$\angle A = \cos^{-1}\left(\frac{b^2 + c^2 - a^2}{2bc}\right)$$
$$\angle B = \cos^{-1}\left(\frac{a^2 + c^2 - b^2}{2ac}\right)$$
$$\angle C = \cos^{-1}\left(\frac{a^2 + b^2 - c^2}{2ab}\right)$$

By Apollonius's Theorem,

$$CS = \frac{1}{2}\sqrt{2b^2 + 2a^2 - c^2} \quad (14)$$

By Centroid Theorem,

$$CG = \frac{2}{3}CS$$
$$\therefore CG = \frac{1}{3}\sqrt{2b^2 + 2a^2 - c^2} \quad (15)$$

For ΔASC, by Law of Cosines,

$$\angle PCG = \angle ACS = \cos^{-1}\left(\frac{b^2 + CS^2 - \left(\frac{c}{2}\right)^2}{2 \cdot b \cdot CS}\right) \quad (16)$$

where $\angle ACS$ is an acute angle.

For ΔALC,

$$\angle ACL = \angle A - 90° \quad (17)$$

$$\angle HCG = \angle ACL + \angle ACS \quad (18)$$

For ΔALC,

$$\cos\angle ACL = \frac{LC}{b}$$

From (17),

$$LC = b \cdot \cos(\angle A - 90°) \quad (19)$$

Again for ΔALC,

$$\sin\angle ACL = \frac{AL}{b}$$

Again from (17),

$$AL = b \cdot \sin(\angle A - 90°) \quad (20)$$

For ΔHAL,

$$\angle HAL = \angle BAN = 90° - \angle B \quad (21)$$

Also,

$$\tan\angle HAL = \frac{HL}{AL}$$
$$\therefore HL = AL \cdot \tan\angle HAL$$

From (20) and (21),

$$HL = b \cdot \sin(\angle A - 90°) \cdot \tan(90° - \angle B) \quad (22)$$

For ΔHGC, $HC = HL + LC$

From (19) and (22),

$$HC = [b \cdot \sin(\angle A - 90°) \cdot \tan(90° - \angle B)] + [b \cdot \cos(\angle A - 90°)] \quad (23)$$

By Law of Cosines,

$$HG = \sqrt{HC^2 + CG^2 - 2 \cdot HC \cdot CG \cdot \cos\angle HCG} \quad (24)$$

By Law of Sines,

$$\frac{\sin\angle HGC}{HC} = \frac{\sin\angle HCG}{HG}$$

$$\therefore \sin\angle HGC = \frac{\mathrm{HC} \cdot \sin\angle HCG}{HG}$$

Since $\angle HGC$ is obtuse,

$$\angle HGC = \angle PGC = 180° - \sin^{-1}\left(\frac{\mathrm{HC} \cdot \sin\angle HCG}{HG}\right)$$

For ΔPGC,

$$\angle GPC = 180° - \angle PCG - \angle PGC \quad (26)$$

By Law of Sines,

$$\frac{PG}{\sin\angle PCG} = \frac{CG}{\sin\angle GPC}$$

$$\therefore \boldsymbol{PG} = \frac{CG \cdot \sin\angle PCG}{\sin\angle GPC} \quad (27)$$

For ΔCQG,

$$\angle CGQ = 180° - \angle PGC \quad (28)$$

$$\angle GCQ = \angle C - \angle PCG \quad (29)$$

$$\angle GQC = 180° - \angle CGQ - \angle GCQ$$
$$= 180° - (180° - \angle PGC) - (\angle C - \angle PCG)$$
$$\therefore \angle GQC = \angle PGC + \angle PCG - \angle C \quad (30)$$

By Law of Sines,

$$\frac{GQ}{\sin\angle GCQ} = \frac{CG}{\sin\angle GQC}$$

$$\therefore \boldsymbol{GQ} = \frac{CG \cdot \sin\angle GCQ}{\sin\angle GQC} \quad (31)$$

From (27) and (31),

$$PG + GQ = \frac{CG \cdot \sin\angle PCG}{\sin\angle GPC} + \frac{CG \cdot \sin\angle GCQ}{\sin\angle GQC}$$

$$\therefore PQ = CG \cdot \left[\frac{\sin\angle PCG}{\sin\angle GPC} + \frac{\sin\angle GCQ}{\sin\angle GQC}\right]$$

$$\therefore PQ = CG \cdot \left[\frac{\sin\angle \mathrm{PCG}}{\sin(180° - \angle \mathrm{PCG} - \angle \mathrm{PGC})} + \frac{\sin(\angle \mathrm{C} - \angle \mathrm{PCG})}{\sin(\angle \mathrm{PGC} + \angle \mathrm{PCG} - \angle \mathrm{C})}\right]$$

Let CS=m, HG=d and $\angle \mathrm{HCG} = \theta$. Using eqns. (14) to (31),

$$\boldsymbol{PQ} = \frac{2}{3}\boldsymbol{m} \cdot \left[\frac{\boldsymbol{\sin\left\{\cos^{-1}\left(\frac{b^2+m^2-\left(\frac{c}{2}\right)^2}{2 \cdot b \cdot m}\right)\right\}}}{\boldsymbol{\sin\left(\sin^{-1}\left(\frac{HC \cdot \sin\theta}{d}\right) - \cos^{-1}\left(\frac{b^2+m^2-\left(\frac{c}{2}\right)^2}{2 \cdot b \cdot m}\right)\right)}} + \frac{\boldsymbol{\sin\left(\angle C - \cos^{-1}\left(\frac{b^2+m^2-\left(\frac{c}{2}\right)^2}{2 \cdot b \cdot m}\right)\right)}}{\boldsymbol{\sin\left(180° - \sin^{-1}\left(\frac{HC \cdot \sin\theta}{d}\right) + \cos^{-1}\left(\frac{b^2+m^2-\left(\frac{c}{2}\right)^2}{2 \cdot b \cdot m}\right) - \angle C\right)}}\right]$$

This formula is derived with respect to Figure 5.

If three sides of an obtuse scalene triangle are given, using eqns. (14) to (31) and the final formula, we can find the length of portion of Euler line inside any obtuse scalene triangle.

RESULTS

If three sides of any non-right scalene triangle are given, then we can find the length of portion of Euler line that lies inside of any acute or obtuse scalene triangle using the two formulas derived in this paper.

Thus, by using these two methods and formulas, we can find the length of portion of Euler line which is in the interior of any acute or obtuse scalene triangle.

APPLICATIONS

Finding the length of portion of Euler line that lies inside of an acute or obtuse scalene triangle is very useful in solving certain complex pure geometry problems. It is also useful in the fields of engineering and construction. It also has applications in the fields of design.

FUTURE CONSIDERATIONS OF THIS PAPER

1. As the formulas are very long, so if possible, I will simplify the formulas.
2. As there are two formulas for two different types of triangles, so if possible, I will make one formula for both- acute and obtuse scalene triangle.

AKNOWLEDGEMENTS

The author wishes to thank U. M. Prajapati and U. H. Pankhania for their great help in this paper. He also wishes to thank his physics and mathematics teachers, A. B. Narang, K. G. Makhija and I. S. Chauhan for their guidance.

REFERENCES

[1] Godfrey, Charles; Siddons, Arthur Warry (1908). Modern Geometry. University Press. p. 20

[2] Ayoub B. (1998). Mathematics Magazine Vol. 71, No. 3 (Jun., 1998), pp. 221-224

[3] Coxeter, H. S. M. and Greitzer, S. L. Geometry Revisited. Washington, DC: Math. Assoc. Amer., pp. 1–3, 1967

[4] Weisstein, Eric W. "Law of Cosines." From MathWorld--A Wolfram Web Resource. http://mathworld.wolfram.com/LawofCosines.html

[5] Loney, S.L. (1912), Plane Trigonometry, Cambridge: University Press.

[6] Durell, C. V. Modern Geometry: The Straight Line and Circle. London: Macmillan, p. 28, 1928.

[7] Euler Line. [online]. Math Open Reference (published 2003). Available at <https://www.mathopenref.com/eulerline.html>.

Not at the dinner table: Utilizing Trait and Ability Emotional Intelligence scores to understand Political Opinion

Taleen Postian
Byram Hills High School; Armonk, United States of America
Email: postiant20@byramhills.net

Recent polls have shown that 70% of Americans are angered by the current political landscape. Given the emotional nature of this problem, emotional intelligence (EI) is relevant to addressing this issue. EI is the ability to perceive, regulate, understand, and use emotions to solve problems. Thus, individuals with high EI scores may be pivotal in creating positive political discourse. Data were drawn from an ongoing study where 149 healthy adults completed EI scales to determine their EI skills and completed surveys to measure their political identity and bias. This study explored correlations among the EI and participants' political identities. Results revealed liberals were shown to have higher Ability EI scores, as opposed to Trait EI scores, while conservatives scored higher in Trait EI scores versus Ability EI. By broadening our understanding of how political preferences relate to EI, our hope is to foster calmer and more constructive communication across American society. Now more than ever, research into the ways Republicans and Democrats emotionally assess social issues is necessary to begin to heal our fractured nation.

Key words - Emotional Intelligence, Politics, Polarization, Democrats, Republicans, Trait EI, Ability EI

INTRODUCTION

Right now, the American people's trust in their own government is at a historic low. In 2019, it was reported that only 17% of Americans trust the government to do what is right, "just about always" (3%) or "most of the time" (14%) [1]. This lack of trust is one reason why 77% of Americans are dissatisfied with the state of politics in their country [2].

The discussion of the presence of emotion in politics has become more popular in recent years [3]. A German sociologist once observed that action in a political community is 'determined by highly robust motives of fear and hope' [4], establishing the emotional base of voting. It has been shown that individual emotional states are affected not only by personal events, but also societal activities, like political events [5]. Concepts similar to that of EI, such as affective intelligence, have been examined in their relationship to current politics [6]. Affective intelligence is a theory based around the different emotional systems that make up decision making strategies. Because of the similarities between affective intelligence theory and EI, this study looked at how political identification could be related to social and emotional skills.

Emotional Intelligence (EI) and wide-ranging success go hand in hand. In an international study of 515 senior executives it was found that EI was a better predictor for success than a high IQ or relevant previous experience [7]. The EI constituent, relationship management, has been suggested to play a vital role in conflict management [8]. Therefore, enhancement of this intelligence construct could be associated with improvements in both personal and social situations. Studies look at the two EI constructs individually to specify which construct of EI is the most useful in different social situations. In addition to the benefits of EI improvement on personal social situations, looking at the political effects of emotionally-fueled decision making like voting can help dissipate polarization in the current political climate.

The goal of this study is to explore the relationship between EI and political perspective. By examining the connection between political identity and the Ability and Trait EI scores, the impact emotions have on important political decisions could be revealed. These political decisions are the building blocks of society, and to have a better understanding of one's own political ideas is beneficial on a personal, social, and societal level.

I. Emotional Intelligence

Emotional intelligence (EI) is a construct that affects social and mental health. EI is correlated to job performance, mental health, leadership skills and overall demeanor [9]; [10]. By contrast, impaired EI has been connected to hopelessness, depression and suicidal ideation [11]; [12].

II. Constructs of EI

There are two main constructs of EI; Trait and Ability. While these two constructs evaluate the same underlying emotional skills, they differ in the method of assessment.

Ability EI is a term used to describe the emotional capabilities of EI and is measured through *performance tasks*. The Mayer Salovey Caruso Emotional Intelligence Test

(MSCEIT) can be used to measure Ability EI through performance tasks. This is in contrast to the way in which Trait EI is measured.

Trait EI evaluates the personal perceptions of individuals' EI abilities and is measured through self-report tests. In other words, when people believe they have high EI, they experience these positive occurrences. While Trait EI assesses the self-perception of emotional capabilities, Ability EI assesses solely these emotional skills.

III. Emotions and Political Behavior

In the past, emotions were neglected in the exploration of political behavior because they were considered difficult to conceptualize [13]. Sociologists preferred to study politics separately and apart from emotion [14], focusing on the relationship between cognitive abilities and political preferences [15]. As emotional abilities' influence over politics gained more recognition, one dominating theory arose, the "approach/avoidance" perspective, viewing emotional reactions to political information as either pleasant and rewarding or unpleasant and harmful [16]. The argument was that these affective reactions guided citizens in their voting patterns. It has been shown that affective displays of oration and presence influence votes on the politician's end of a situation [17]. Specifically, identifying the facial expressions of candidates was shown to strongly affect the opinion of the voter on the candidate [18]. This employing of the EI skill of perception through viewing facial expressions to perceive emotions connects EI abilities to political perception. To have consistency in political preference discussion in this paper, it is understood that partisan sorting has gradually made the Republican and Democratic parties into the parties of conservatives and liberals, respectively [19].

This study will seek to explore how the two theoretical models of EI relate to political preferences. These explorations are of value to the general population because the results influence not only the individual, but their community and country. It is important that people have a better understanding of their own political views through emotional awareness to make better decisions when voting. In the current politically charged climate, EI presents itself as an answer to the idea that the country has become deaf to opposing views. An exploration into the relationship between the different theoretical models of EI and political identity is therefore relevant.

OBJECTIVES

1. To evaluate the relationship between both Trait and Ability EI, and political identity.

HYPOTHESIS

H_0: Extreme political views will not correlate with a bias in the self-perception of EI abilities.

H_1: Political identity will have a significant correlation to both Ability and Trait EI.

METHODS

I. Subjects

A total of 149 healthy participants (age range 18-45 years) were recruited from the general community in Tucson, AZ, as part of a larger study underway by Dr. Killgore. Participants were screened for current Axis I psychopathology, including current affective, anxiety, and psychotic disorders. All participants demonstrated an English reading proficiency at the 8th grade level or higher, underwent a three-hour assessment battery, followed by a computer-generated random assignment to either the active EI Training or Placebo Control Training Program and then returned for a follow-up assessment immediately upon completion of the program. The participants were then separated into two different administration schedules: Distributed Training (n = 230; i.e., participants were given three weeks to complete the modules, with at least two days between each module), Compressed Training (n = 230; i.e., participants completed all training within a one week period with one module per day).

The participants, in addition to completing EI training, completed surveys about their education, job status, income, gender, age, political identity, relationship status, stress levels, resilience, depression, sleep quality, trauma, grit, mindfulness, and emotional intelligence.

II. Scales

This study utilized multiple EI scales when looking for a relationship with political identity. For assessing Ability EI, the Mayer Salovey Caruso Emotional Intelligence Test (MSCEIT) was used. The MSCEIT scale evaluates four defined branches of EI through a performance evaluation. The four branches are the ability to: accurately perceive emotion, use emotions to facilitate thought, understand emotion, and regulate emotion [20].

Scales that evaluated Trait EI comprised the Self Rated Emotional Intelligence Scale (SREIS) and the Trait Emotional Intelligence Questionnaire (TEIQue). The SREIS is a survey that evaluates the same subscales as the MSCEIT but through a self-report method [21]. The TEIQue is structured into four distinct and interrelated dimensions: emotionality, self-control, sociability, and well-being [22].

The Awareness of Social Inference Test (TASIT) was also included for its unique distribution method of

audiovisual nature. TASIT is a clinical assessment of social perception [23].

These surveys were completed on the University of Arizona premises. The data was received via email and analysis was completed through PSPP, a software application for the analysis of sampled data. The data used was quantitative. One-way analysis of variance (ANOVA) analyses were completed with political identity, measured on a 5-point scale from "Strongly Democrat to Strongly Republican" as the common independent variable through each. Frequency and descriptive analyses were completed along with bar graphs, histograms and numerical results.

RESULTS

I. Trait EI

A one-way ANOVA test (Figure 1) for the relationship between the SREIS scores and political identity, was found to have no significance with the p-value of (p=0.123). The data show that participants who held the most extreme political views did not have the highest self-reported EI scores. The highest trait EI scores, 69.73, were for the most moderate participants, those who do not lean Democrat or Republican. Surprisingly however, the next highest scores are from strongly Democrat and Republican participants, with 68.31 and 68.00, respectively.

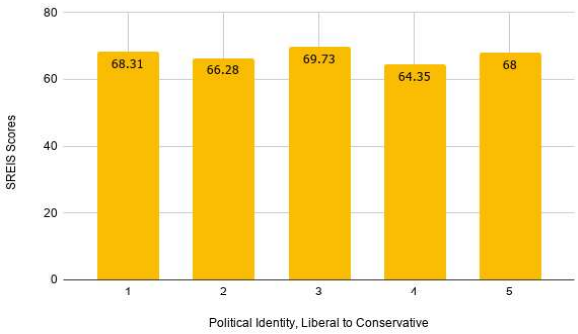

Figure 1. SREIS Total scores by political identity.

A series of one-way ANOVA tests were used to examine the relationship between political identity and the Trait EI surveys administered. The total sum of scores for the audiovisual TASIT were tested to see their relationship to political identity scores (Table 1). A one-way ANOVA was run for Political Identity and TEI test (Table 1). No significance was found in these results (p=0.166). Scores on the TASIT and TEI did not differ across Political Identity (p=0.291, p=0.166).

Table 1. Trait EI scales by political identity.	
Test	P value
TASIT total scores by political identity	p=0.291
TEI scores by political identity.	p=0.166

II. Ability EI

ANOVA tests on the MSCEIT SS total scores were used to determine whether Ability EI was different across the spectrum of political identity. A one-way ANOVA was run for political identity and the SS total scores of the MSCEIT test, evaluating the relationship between the Ability EI test and political identity (Table 2). No significance was found for these results (p=0.407). Scores on the MSCEIT did not differ across Political Identity (p=0.407).

Table 2. Ability EI scales by political identity.	
Test	P value
SS MSCEIT scores by political identity	p=0.407
Univariate analysis of SREIS scores and political identity with sex as the variable.	p=0.526, p =0.247, p=0.702, p=0.927

It was also of interest to examine whether outcomes might differ by sex. Therefore, a univariate analysis with SREIS as the dependent variable while sex and political identity were the fixed factors (Table 2) was used to see if the variable sex was obscuring significant findings. The test showed there to be no significant main effect or interaction present (p=0.526, p =0.247, p=0.702, p=0.927).

DISCUSSION

The study explored the relationship between the two different theoretical models of EI and political preferences. The results found that participants who labeled themselves more conservative on the political identity self-report scale in general had higher Trait EI scores than Ability EI. The opposite was found for those who place themselves on the liberal end of the spectrum, with liberals generally scoring higher on Ability EI compared to Trait EI. This finding supports the idea that there is a difference in EI skills across the political spectrum.

Because of the reported different connections between the two EI constructs and political identities, different types of EI improvement will affect conservatives and liberals differently. Luckily, EI capabilities are not fixed

and can be improved through one-on-one sessions, instructional guides, and online training programs [24].

For Ability EI improvement effects, research points to better leadership and relationships. The scores produced by the performance tasks have predicted leadership capabilities in small group settings [25]. People with higher Ability EI report more positive relationships, even after controlling for personality and IQ [26].

Trait EI has been shown to help predict abilities of transformational leadership, less subjective stress and performance in managers [27]. Higher Trait EI has been correlated to better physical, mental and psychosomatic health, less burnout, and reduced symptoms of psychopathy in mental health nurses [28]; [29].

The study revealed that there is no significant relationship between political identity and EI. With each test examining the relationship between political identity and EI resulting in no significance found, it can be concluded that neither Ability nor Trait EI have a strong correlation to political identity. By looking at the results of the test examining the relationship between the SREIS scores and the self-reported political identity, the analysis suggests that there is no significant difference in SREIS scores across the different political groups. The data fails to reject the null hypothesis, that there is no significant relationship between EI and political identity.

The results of this study are corroborated by recent work in this field. A 2019 study measuring for Ability EI found that those with lower emotional abilities are more likely to be found at the conservative end of the political spectrum, while those who displayed higher emotional abilities are more likely to be found on the left end [30]. This supports the finding that those who identify themselves as conservative have lower Ability EI than Trait EI.

Future research should attempt to use a more extensive political identity scale. The scale from which political identity was evaluated for this study is a five-point scale for ease of identification. Such a complex concept is not easy to minimize into five points when creating the scale. Because of this inherent issue, it is hard to place that much weight on the answer of a single question. Personal political opinions are also equally complex and could benefit from a more thorough identification tool [31].

There is also the issue of the self-report method of determining political identity. Participants could write an answer that is untrue, on purpose or not [32]. This does not detract from the effectiveness of the other self-report tests measuring EI, since those are examining specifically the self-evaluation of those skills [33]. With political identity, this created error variance in the reporting of responses and affects the results. One way to remedy this would be with a much larger sample, with a number in the thousands. Another would be to use surveys inquiring about opinions on specific political issues with the responses revealing political leanings more accurately than conventional political identity polling.

On the other hand, when looking at the adjusted for demographics four branch scores from the MSCEIT, a different pattern emerges for Facilitating and Using emotions to enhance thought. This pattern suggests that extreme Democrats and Republicans relate differently to this factor. From these results, it is implied that extreme Democrats tend to be better skilled to use their emotions to facilitate their thoughts than moderate one's, but for Republicans, the opposite is revealed. In general, subjects with extreme views were shown to be worse at using their emotions to facilitate thought than moderate ones.

Future research should continue to look at how voting patterns are changing across the board and what means for changing emotional patterns of voters. One study that was published in 2019 has found that those on the extreme end of the political spectrum for both liberals and conservatives have more in common with each other than with moderate thinkers in their own parties [34]. This is supported by the results from the SREIS scores, with extreme liberals and conservatives both scoring the second and third highest scores for the scale.

CONCLUSION

This study examined the relationship between politics and emotion. Specifically, the connections between Ability and Trait EI and political identity. The results showed that while there is not a significant correlation between the two theoretical models of EI and political identity, trends revealed how those who lean towards the left tend to excel in managing and utilizing emotions, within the Ability EI scales, while those who lean right score higher on self-report scales, measuring Trait EI.

As the next political cycle rolls in, research needs to continue to be done into the deep emotional split within America. This should be explored through comparison of the social and emotional skills of the two most prominent political ideologies in the country, Democrat and Republican. EI is usually seen in individual and immediate social constructs and situations, for example dealing with a personal issue or a friend’s feelings; however, when EI is considered in the context of political decisions, like voting or protesting, it can be seen to potentially impact society on a larger scale. With that kind of impact, it becomes necessary to dedicate more research into learning about the emotional correlates of political identities.

AKNOWLEDGEMENTS

I would like to thank my mentor for aiding me with my research and for answering my numerous questions over email. I thank my science teachers for helping me develop my research skills and scientific writing abilities.

REFERENCES

[1] Pew Research Center. (2019, May 29). Public Trust in Government: 1958-2019.

[2] Summers, J. (2018, October 25). Poll: Majority of Americans dissatisfied with U.S. politics, doubt divisions will improve soon.

[3] Meisler, G. (2014), "Exploring emotional intelligence, political skill, and job satisfaction", Employee Relations, Vol. 36 No. 3, pp. 280-293.

[4] Clarke, S., Hoggett, P., & Thompson, S. (2006). *Emotion, politics and society*. Basingstoke: Palgrave Macmillan.

[5] Rahn, W. M., Kroeger, B., & Kite, C. M. (1996). A framework for the study of public mood. Political Psychology, 17(1), 29–58.

[6] Vasilopoulos, P. (2019, July 29). Affective Intelligence and Emotional Dynamics in Voters' Decision Making Processes. Oxford Research Encyclopedia of Politics. Retrieved 11 Sep. 2019.

[7] Cooper, S. (2013, March 18). Look For Employees With High EQ Over IQ.

[8] Goleman, D. (1998). Working with emotional intelligence. New York: Bantam Books

[9] Montes-Berges, B., & Augusto, J. (2007). Exploring the relationship between perceived emotional intelligence, coping, social support and mental health in nursing students. Journal of Psychiatric and Mental Health Nursing, 14(2), 163-171.

[10] Martins, A., Ramalho, N., & Morin E. (2010). A comprehensive meta-analysis of the relationship between emotional intelligence and health. Personality and Individual Differences, 49, 554–564.

[11] Ciarrochi, J., Deane, F. P., & Anderson, S. (2002). Emotional intelligence moderates the relationship between stress and mental health. Personality and Individual Differences, 32(2), 197-209.

[12] Davis SK, Humphrey N. The influence of emotional intelligence (EI) on coping and mental health in adolescence: Divergent roles for trait and ability EI. J Adolescence. 2012; 35(5):1369–79.

[13] Hudlicka, Eva. (2005). Modeling interaction between metacognition and emotion in a cognitive architecture. AAAI Spring Symposium - Technical Report. 55-61.

[14] Marcus, G. E. (2013). Political psychology: Neuroscience, genetics, and politics. Oxford, UK: Oxford University Press.

[15] Barbalet, J. (1998). *Emotion, Social Theory, and Social Structure*. Cambridge University Press.

[16] Ganzach, Y. (2016). Cognitive ability and party identity: No important differences between Democrats and Republicans. Intelligence, 58, 18–21. doi: 10.1016/j.intell.2016.05.009

[17] Vasilopoulos, P. (2019, July 29). Affective Intelligence and Emotional Dynamics in Voters' Decision Making Processes. Oxford Research Encyclopedia of Politics. Retrieved 11 Sep. 2019.

[18] Glaser, J., & Salovey, P. (1998). Affect in Electoral Politics. Personality and Social Psychology Review, 2(3), 156–172.

[19] Patterson, M. L., Churchill, M. E., Burger, G. K., & Powell, J. L. (1992). Verbal and nonverbal modality effects on impressions of political candidates: Analysis from the 1984 presidential debates. Communication Monographs, 59, 231- 242.

[20] Levendusky, Matthew. 2009. The Partisan Sort: How Liberals Became Democrats and Conservatives Became Republicans. Chicago: University of Chicago Press.

[21] Mayer, J. D., Salovey, P., & Caruso, D. (2002). The Mayer–Salovey–Caruso Emotional Intelligence Test (MSCEIT), Version 2.0. Toronto, Ontario, Canada: Multi-Health Systems.

[22] Brackett, M. A., Rivers, S. E., Shiffman, S., Lerner, N., & Salovey, P. (2006). Relating emotional abilities to social functioning: A comparison of self-report and performance measures of emotional intelligence. Journal of Personality and Social Psychology, 91(4), 780–795.

[23] Petrides K.V. (2009) Psychometric Properties of the Trait Emotional Intelligence Questionnaire (TEIQue). In: Parker J., Saklofske D., Stough C. (eds) Assessing Emotional Intelligence. The Springer Series on Human Exceptionality. Springer, Boston, MA

[24] Mcdonald, S., Bornhofen, C., Shum, D., Long, E., Saunders, C., & Neulinger, K. (2006). Reliability and validity of The Awareness of Social Inference Test (TASIT): A clinical test of social perception. Disability and Rehabilitation, 28(24), 1529–1542.

[25] Nathanson, L., Rivers, S.E., Flynn, L.M., & Brackett, M.A. (2016). Creating emotionally intelligent schools with RULER. Emotion Review, 8(4), 1-6.

[26] Côté, S., Lopes, P. N., Salovey, P., & Miners, C. T. (2010). Emotional intelligence and leadership emergence in small groups. The Leadership Quarterly, 21(3), 496–508.

[27] Lopes, P. N., Salovey, P., & Straus, R. (2003). Emotional intelligence, personality, and the perceived quality of social relationships. Personality and Individual Differences, 35(3), 641–658.

[28] Barling, J., Slater, F., & Kevin Kelloway, E. (2000). Transformational leadership and emotional intelligence: An exploratory study. Leadership & Organization Development Journal, 21(3), 157–161.

[29] Gerits, L., Derksen, J. J., Verbruggen, A. B., & Taylor, S. J. (2004). Emotional intelligence and adaptive success of nurses caring for people with mental retardation and severe behavior problems. Mental Retardation, 42(2), 106–121.

[30] Schutte, N. S., Malouff, J. M., Thorsteinsson, E. B., Bhullar, N., & Rooke, S. E. (2007). A meta-analytic investigation of the relationship between emotional intelligence and health. Personality and Individual Differences, 42(6), 921–933.

[31] Van Hiel, A., De keersmaecker, J., Onraet, E., Haesevoets, T., Roets, A., & Fontaine, J. R. J. (2019). The relationship between emotional abilities and right-wing and prejudiced attitudes. *Emotion, 19*(5), 917– 922. https://doi.org/10.1037/emo0000497

[32] Theodoridis, A. G. (2013, June 21). Implicit Political Identity: PS: Political Science & Politics.

[33] Robins, R. W., Fraley, R. C., & Krueger, R. F. (2010). Handbook of research methods in personality psychology. New York: Guilford.

[34] O'Connor, P. J., Hill, A., Kaya, M., & Martin, B. (2019). The Measurement of Emotional Intelligence: A Critical Review of the Literature and Recommendations for Researchers and Practitioners. Frontiers in psychology, 10, 1116.

[35] Draca, M. and Schwarz, C., (2019), 'How Polarized are Citizens? Measuring Ideology from the Ground- Up', CAGE working paper no. 432.

Association Between Cerebral Small Vessel Disease and Risk of Recurrent ICH Among U.S. Minority Survivors

Author: Priyanka Senthil
Mentor: Dr. Alessandro Biffi
Davidson Academy; Reno, United States
Email: psenthil@davidsonacademy.unr.edu

Abstract – Compared to White survivors of Intracerebral Hemorrhage (ICH), Black/Hispanic individuals are three times more likely to experience ICH recurrence. Cerebral Small Vessel Disease (CSVD) has long been considered a risk factor for ICH. Our study sought to clarify whether differences in CSVD subtype or severity among minority and White individuals could explain this disparity. We collected data of ICH survivors from the MGH-ICH and ERICH studies. MRI scans were analyzed for CSVD markers as classified by cerebral microbleeds (CMBs). CSVD was identified as either Cerebral Amyloid Angiopathy (CAA) subtype or Arteriolo-Sclerosis (AS) subtype. We analyzed data from the total 2192. When compared to Whites, a higher percentage of minority individuals had markers of CSVD on MRI scans (54% vs. 41%, p<0.001). There was a greater count (higher burden) of AS-associated CMBs in minorities (median: 1, IQR 1-2 vs. median 0, IQR 0-1, p=0.016). Minority ICH survivors are not only more likely to present with CSVD at the time of stroke, but they also have a higher burden of specifically AS-associated CMBs.

Key Words – Arteriolo-Sclerosis; Cerebral Amyloid Angiopathy; Cerebral Small Vessel Disease; Hemorrhage; ICH

INTRODUCTION

Of the different types of stroke, Intracerebral Hemorrhage (ICH) is the most serious and life-threatening due to the limitations of current treatments. To put this in perspective, although only 15% of stroke cases are ICH-related, ICH is responsible for more than half of stroke-related deaths and disability [1-3]. Minority populations are three times more likely than Whites to experience ICH recurrence, which substantially increases the risk of morbidity and mortality. Previous studies have determined that this health disparity may be caused by differences in hypertension control and/or blood pressure (BP) variability [4-6]. However, differences in hypertension alone do not fully explain the magnitude of variation in ICH recurrence risk among the race/ethnic groups [6]. Thus, our study sought to identify differences in other risk factors of ICH recurrence among minority and White individuals that could be attributable to this health disparity.

As determined by MRI-based markers, ICH survivors have a greater presence and burden of Cerebral Small Vessel Disease (CSVD) when compared to the general population. The presence of CSVD not only increases the risk of first-ever ICH, but also the risk of other events, including recurrent ICH, ischemic stroke, cognitive decline, and gait deterioration [7, 8]. The two subtypes of CSVD—cerebral amyloid angiopathy (CAA) and arteriolo-sclerosis (AS)—are similar in many ways though ICH due to CAA occurs in the cortical blood vessels of the brain (lobar), while ICH due to AS occurs in deep and infratentorial regions (basal ganglia, thalamus, and brainstem). The neuroimaging markers of CSVD include cerebral microbleeds (CMBs), lacunar infarcts, enlarged periventricular spaces (EPVS), white matter hyperintensities (WMH), and cortical superficial siderosis (cSS). Understanding the etiological factors of CSVD is needed to develop proper interventions and treatments for ICH. Given that CSVD mainly affects ICH survivors, they are an appropriate group with which to conduct our study.

Findings from previous studies have determined that CSVD increases the risk of first-ever ICH, though no study in the literature to our knowledge has explored potential differences in the presence and burden of CSVD among different racial/ethnic groups. We hope that our study will provide new insights for the biological reasons underlying why recurrent ICH (and its corresponding cognitive effects) disproportionately affects minority individuals. We seek to determine whether 1) differences in baseline CSVD burden and/or severity exist among race/ethnic groups and 2) if increased CSVD burden in minority populations accounts for the increased risk of recurrent ICH in these individuals.

METHODS

I. Participating studies

We analyzed data from two main studies of ICH: (1) the longitudinal MGH-ICH study and (2) the ERICH study. The MGH-ICH study, which took place in Boston, has been recruiting patients since 1994 and is continuing to do so.

The ERICH study, led by the University of Cincinnati, is multi-site, with 42 different sites spanning the United States [9, 10]. The study recruited patients from 2006 to 2010 [9, 10].

II. Study eligibility and patient recruitment

We recruited participants among patients meeting the following eligibility criteria: (1) aged 18 years or older, and (2) diagnosed with acute primary (i.e., spontaneous) ICH as determined by MRI scan (taken within 24 hours of ICH event). Patients who experienced ICH due to trauma, conversion of an ischemic infarct, aneurysm, or brain tumor(s) did not meet our eligibility criteria [9, 11]. Patients were also removed if they had missing data on clinical or demographic variables. Since we sought to investigate racial/ethnic disparities in long-term ICH recurrence rates, we excluded patients who survived less than 3 months after hemorrhage, in agreement with a previously published methodology [9].

III. Baseline data collection

Participants were asked to self-identify their race/ethnicity by selecting from a list recommended by the Office for Management and Budget and the National Institutes of Health that included White (i.e., non-Hispanic White), Black (i.e., non-Hispanic Black), Hispanic (i.e., self-identifying as White-Hispanic or Black-Hispanic), and other (not meeting criteria for inclusion in White, Black, or Hispanic groups). Using established methods of MRI scan analysis, we determined ICH location, CSVD subtype, and hematoma volume [10, 12]. MRI-based markers of CSVD, including cerebral microbleeds (CMBs), lacunar infarcts, enlarged periventricular spaces (EPVS), White matter hyperintensities (WMH), and cortical superficial siderosis (cSS) were also collected and recorded (Figure 1).

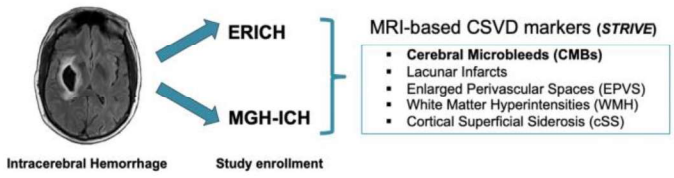

FIGURE 1: Study enrollment and MRI-based markers used to determine CSVD burden and subtype.

IV. Longitudinal follow-up

Following the in-person interview conducted at the time of the ICH event, participants and/or their caregivers (if needed) were interviewed over the phone every 6 months by trained staff using standard protocols and methods [9-11]. Participants and/or their caregivers were asked about new hospitalization events, new hemorrhagic or ischemic stroke events, death, functional status (as determined by the Modified Rankin Score (mRS)), medications, and prescriptions.

V. Univariable and multivariable analyses

All categorical variables were analyzed with the 2-tailed Fisher exact test to identify any non-random relationships between the variables. We used the Mann-Whitney U test to compare continuous variables among the two study samples. Univariate analyses with Kaplan-Meier plots were used to determine the factors most closely related with ICH recurrence among White and Black/Hispanic groups. The Kaplan-Meier results were compared statistically with the log-rank test. We performed multivariable analyses using Cox regression models. MRI scans were analyzed for CSVD markers as classified by cerebral microbleeds (CMBs). CSVD was identified as either Cerebral Amyloid Angiopathy (CAA) subtype or Arteriolo-Sclerosis (AS) subtype and statistical analysis was performed to determine the severity of CMBs. For all eligible patients, we determined whether the presence of cerebral microbleeds ($\geqslant$1) or cortical superficial siderosis increased the risk of ICH recurrence. We initially included in multivariable modeling all factors associated with ICH recurrence in univariable analyses with $p<0.20$. Because of potential associations between ICH recurrence and exposure to antiplatelet agents and/or oral anticoagulants, we pre-specified adjustment for these variables in our multivariable models (regardless of p value). We subsequently used backward elimination procedures to arrive at a minimal model including only variables associated with ICH at $p<0.05$. Multicollinearity in our regression model was assessed by variance inflation factors (VIF) to determine the strength of any correlations between independent variables. The proportional hazard assumption in Cox models was tested via graphical inspection and calculation of Schoenfeld residuals.

VI. Secondary analyses

Our study protocol included prespecified subgroup analyses. First, we sought to conduct secondary analyses stratified by race/ethnicity to compare CSVD markers across White and Black/Hispanic populations. This involved repeating all multivariate analyses for probable CAA- and AS-associated ICH survivors after including interaction terms between race/ethnicity and: (1) presence of cerebral microbleeds ($\geqslant$1) and (2) presence of cortical superficial siderosis. Additionally, in a subset of patients (n=941) with long-term follow-up information, we conducted parallel analyses for Lacunar Infarcts, Enlarged Perivascular Spaces (EPVS), White Matter Hyperintensities (WMH), and Cortical Superficial Siderosis (cSS).

RESULTS

I. Study participants

A total of 2192 ICH survivors fulfilled the initial eligibility criteria. Twenty-eight participants were lost to follow-up or were ineligible due to early case fatality, resulting in the current total sample size of n=2164 (White=1245, Black=460, Hispanic=392, other race/ethnicity=67). Detailed information on characteristics of participants enrolled in the MGH (n=991) and ERICH (n=1201) studies is presented in Table 1.

TABLE 1: Participants' characteristics (overall study).

Variable	**ERICH**	**MGH-ICH**
No. of individuals	**1201 (100)**	**991 (100)**
Demographics		
Age, mean (SD)	60.8 (13.5)	71.4 (12.7)
Sex, Female (%)	510 (42.5)	474 (47.8)
Race / Ethnicity (%)		
White	408 (34.0)	837 (86.9)
Black	401 (33.4)	59 (6.1)
Hispanic	392 (32.6)	0 (0)
Other	0 (0)	67 (7.0)
Education, ≥ 14 years (%)	607 (50.5)	644 (65.0)
***Medical History** (%)*		
Hypertension	915 (77.2)	751 (76.3)
Ischemic heart disease	134 (11.5)	169 (17.2)
Atrial fibrillation	81 (6.7)	171 (17.5)
Diabetes	301 (25.3)	205 (20.9)
Prior stroke	188 (15.8)	181 (18.5)
***Genetic Variables** (%)*		
APOE ε2 (≥1 copy)	177 (14.9)	73 (17.5)
APOE ε4 (≥1 copy)	378 (31.8)	130 (31.8)
***Cerebral Microbleeds** (%)*		
Lobar (≥1 CMB)	399 (31.2)	385 (38.8)
Non-lobar (≥1 CMB)	467 (38.9)	429 (43.3)

II. MRI CSVD markers based on race/ethnicity

Long-term follow up information was collected for 612 ERICH participants and 329 MGH participants. As shown in Table 2, we identified a median of two periventricular and deep white matter hyperintensities (WMHs) in ERICH participants, with interquartile range [IQR] 1-3. We identified a median of two periventricular and deep WMHs in MGH participants, with interquartile range [IQR] 1-2. Thirty-four participants in the ERICH study and 151 participants in the MGH study presented with one or more lacunar infarcts in the lobar region, corresponding to a percentage of 10.6 in the ERICH study and 19.3 in the MGH study. A greater proportion of participants in both studies presented with one or more non-lobar lacunar infarcts, with that number being 70 participants (21.1%) in the ERICH study and 193 in the MGH study (31.5%). The median count for both lobar and non-lobar was one, with an interquartile range of 1-2 for both studies. In ERICH participants, the median basal ganglia enlarged periventricular spaces (EPVS) was two, while in MGH participants, it was one (Interquartile range [IQR] 1-2). There was no difference in median count of centrum semiovale between participants in the ERICH or MGH studies. One hundred and two ERICH participants (35.7%) and 324 MGH participants (31.5%) were identified of having one or more lobar cerebral microbleeds (Median=3, Interquartile range [IQR] 1-9 ERICH, Interquartile range [IQR] 1-8 MGH). One hundred forty ERICH participants (42.5%) and 336 MGH participants (54.9%) were identified of having one or more non-lobar cerebral microbleeds (Median=4, Interquartile range [IQR] 1-5 ERICH, Interquartile range [IQR] 1-4 MGH). When comparing the presence of cortical superficial siderosis (cSS), 44 ERICH participants (13.4%) and 101 MGH participants (16.5%) were identified.

TABLE 2: MRI CSVD markers among study participants with long-term follow-up.

Variable	**ERICH**	**MGH-ICH**
No. of individuals	**329 (100)**	**612 (100)**
White Matter Hyperintensities (WMH)		
Periventricular	2 (1 – 3)	2 (1 – 2)
Deep	2 (1 – 3)	2 (1 – 2)
Lacunar Infarcts		
Lobar		
Presence of ≥1 lacune (%)	34 (10.6)	151 (19.3)
Count, median (IQR)	1 (1 - 2)	1 (1 – 2)
Non-lobar		
Presence of ≥1 lacune (%)	70 (21.1)	193 (31.5)
Count, median (IQR)	1 (1 - 2)	1 (1 – 2)
Enlarged Perivascular Spaces (EPVS)		
Basal Ganglia	2 (1 – 2)	1 (1 – 2)
Centrum Semiovale	2 (1 - 3)	2 (1 – 3)
Cerebral Microbleeds (CMBs)		
Lobar		
Presence of ≥1 CMB (%)	102 (35.7)	324 (31.5)
Count, median (IQR)	3 (1 - 9)	3 (1 - 8)
Non-lobar		
Presence of ≥1 CMB (%)	140 (42.5)	336 (54.9)
Count, median (IQR)	2 (1-5)	2 (1-4)
***Cortical Superficial Siderosis (cSS)** (%)*	44 (13.4)	101 (16.5)

III. Variations in ICH recurrence risk by race/ethnicity

We initially sought to determine whether differences in AS-related CSVD and CAA-related CSVD existed between White and Black/Hispanic ICH survivors as determined by MRI based CSVD markers. We formally compared MRI based CSVD markers, as presented in detail in Tables 3 and 4. Among all identified CSVD markers, the following showed statistically significant ($p<0.05$) preferential association with increased ICH recurrence risk: cerebral microbleeds (overall) ($p=0.039$), non-lobar cerebral microbleeds ($p=0.016$), non-lobar lacunar infarcts (0.023), and basal ganglia EPVS ($p=0.018$). All identified risk factors were significantly greater in Black/Hispanic individuals, suggesting minority ICH survivors presented with higher CSVD burden and severity immediately following the ICH event when compared to their White counterparts (54% vs. 41%, $p<0.001$). Based on aforementioned multivariable analyses, we differentiated between the two CSVD subtypes (CAA- and AS- subtypes). Minority ICH survivors showed a significantly higher burden and severity of AS-associated CMBs (median: 1, Interquartile Range [IQR] 1-2 vs. median 0, IQR 0-1, $p=0.016$). The difference in the burden of CAA-associated CMBs was not statistically significant between the two racial/ethnic groups (median: 0, IQR 0-2 vs. median 0, IQR 0-1, $p=0.12$). Combination of findings from each study revealed consistent associations without evidence of between-study heterogeneity (all $I2<0.05$).

TABLE 3: Comparison of MRI CSVD markers across racial/ethnic study groups among all participants.

ALL PARTICIPANTS (n = 2192)			
MRI Marker	**White**	**Black / Hispanic**	**P-value**
Cerebral Microbleeds (med, IQR)	1 (0 - 4)	1 (1 - 5)	**0.039**
Non-lobar Cerebral Microbleeds (med, IQR)	0 (0 – 1)	1 (1 - 2)	**0.016**
Lobar Cerebral Microbleeds (med, IQR)	0 (0 – 2)	0 (0 - 1)	0.12

TABLE 4: Comparison of MRI CSVD markers across racial/ethnic study groups among participants with long-term follow up information.

LONG-TERM FOLLOW-UP (n = 941)			
MRI Marker	**White**	**Black / Hispanic**	**P-value**
Periventricular WMH (Fazekas med, IQR)	2 (1 - 2)	2 (1 - 2)	0.47
Deep WMH (Fazekas med, IQR)	2 (1 - 2)	2 (1 - 2)	0.21
Lacunar Infarcts (med, IQR)	1 (1 - 3)	1 (1 - 3)	0.32
- *Non-lobar Lacunar Infarcts* (med, IQR)	1 (1 - 2)	1 (1 - 3)	**0.023**
- *Lobar Lacunar Infarcts* (med, IQR)	1 (1 - 2)	1 (1 - 2)	0.22
Basal Ganglia EPVS (med, IQR)	1 (1 - 2)	2 (1 - 2)	**0.018**
Centrum Semiovale EPVS (med, IQR)	2 (1 - 3)	2 (1 - 3)	0.66
Cortical Superficial Siderosis (presence, %)	13.1	12.6	0.39

ICH recurrence risk was calculated based on CVSD markers and race/ethnicity. At time of stroke, Black/Hispanic individuals showed higher CSVD burden and severity than White ICH survivors. High CSVD burden included some or all of the following characteristics: three or more enlarged periventricular spaces, two or more cerebral microbleeds, the presence of cortical superficial siderosis, one or more lacunar infarcts, or White matter hyperintensities. At 5 years after index ICH, Black/Hispanic populations with high CSVD burden were shown to have >22% estimated risk of recurrent ICH while White participants had <15% estimated risk. In correspondence, Black/Hispanic populations with low CSVD burden were shown to have >11% estimated risk of recurrent ICH when compared to their White counterparts (<8%) at 5 years after index ICH. We provide a graphic representation of differences in CSVD burden and ICH recurrence risk by race/ethnicity in Figure 2. Comparison of ICH recurrence risk between Black/Hispanic and White individuals with high CSVD burden provides a p-value of 0.012. Comparison of ICH recurrence risk between Black/Hispanic individuals with high CSVD burden and low CSVD burden provides a p-value of <0.001. Comparison of ICH recurrence risk between Black/Hispanic individuals with high CSVD burden and White individuals with low CSVD burden provides a p-value of <0.001.

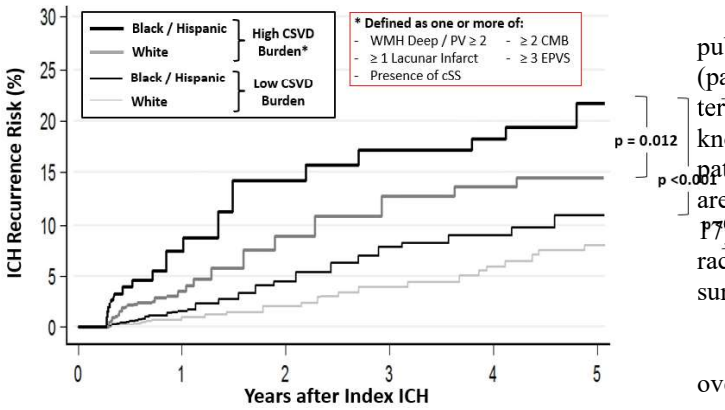

FIGURE 2: ICH recurrence risk based on CSVD markers and race/ethnicity.

DISCUSSION

We present evidence that minority ICH survivors of Black and Hispanic racial/ethnic groups are at a significantly higher risk of recurrent ICH. We utilized data from two large ICH studies to conduct a meta-analysis, identifying for the first time, a strong association between greater CSVD burden in Black/Hispanic populations and increased risk of recurrent ICH.

CSVD is the most potent risk factor for ICH incidence and recurrence, thus warranting specific emphasis from both a clinical management and research standpoint [4, 5, 13]. Black and Hispanic ICH survivors are disproportionately less likely to receive CSVD treatment, with expected consequences of increased ICH recurrence risk. The mechanisms underlying limited success in CSVD treatment among ICH survivors at large remain unclear. However, it is likely that socioeconomic factors, chief availability, and access to health care [14], represent major obstacles toward receiving CSVD treatment for minority ICH survivors. Cultural factors associated with racial/ethnic background are also likely to influence risk of ICH recurrence. For example, cultural beliefs may determine personal behavior towards healing and disease prevention, thus affecting adherence with traditionally prescribed medications [15].

Furthermore, minority ICH survivors presented with higher CSVD burden and severity immediately following the ICH event when compared to their white counterparts, especially in the case of AS-associated CMBs. Given that AS CSVD is exacerbated by hypertension, the racial/ethnic differences pertaining to the AS CSVD subtype may reflect differences in prevention strategies long predating index ICH, such as hypertension and blood pressure control. While CSVD severity has been demonstrated to act as a major risk factor for stroke in general, we provide the first proof of association specific to ICH. As mentioned above, these findings may reflect variations in treatment of CSVD over time.

When compared to ICH survivors in most previously published reports [24], individuals included in our analyses (particularly those enrolled in the ERICH study) differ in terms of earlier age at time of ICH. This discrepancy reflects known disparities in ICH epidemiology among minority patients. Several studies reported that non-white individuals are more likely to present with ICH at a younger age [16, 17]. The pre-specified enrollment targets based on race/ethnicity therefore account for the younger age of ICH survivors in ERICH [12].

Our study has a few limitations. First, despite the overall sample size of our study, there was an unequal sample size among racial groups in the MGH study, with 86.9% of the participants identifying as white and no Hispanic participants. Second, we cannot identify causal relationships between CSVD and ICH recurrence risk, we can only make associations between the two. We also utilized self-reported race/ethnicity to capture the complex network of biological, social, and cultural determinants of the identified health disparity in ICH recurrence. We are unable to further dissect and study these individual aspects of personal racial/ethnic background. However, recent studies in the field of genetic epidemiology identified strong correlations between self-reported race/ethnicity, cultural perception, and genetic ancestry [18]. Our approach also exhibits several strengths. Although participants in the MGH and ERICH studies differed substantially in demographics, medical history, and ICH characteristics, we observed highly consistent associations between race/ethnicity and ICH recurrence risk. Of note, reported associations reached our pre-specified threshold for significance in each study individually and were independently replicated in the other.

CONCLUSION

In summary, we present further evidence that Black and Hispanic survivors of primary ICH are at a significantly higher risk of recurrent ICH than their white counterparts. We found that CSVD severity and burden was greater among Black/Hispanic individuals and partially accounts for the observed racial/ethnic disparities in ICH recurrence risk. Additional studies will be required in order to expand on our findings, as well as to explore novel biological, socioeconomic, and cultural factors accounting for the observed disparities.

AKNOWLEDGEMENTS

I would like to acknowledge the key members of my lab, the Aging and Brain Health Research (ABHR) group at Massachusetts General Hospital, who were involved in this project for their mentorship and guidance. I would also like to acknowledge Juan Pablo Castello PhD for his contributions in the MRI image analyses.

REFERENCES

[1] Feigin VL, Mensah GA, Norrving B, Murray CJ, Roth GA; GBD 2013 Stroke Panel Experts Group. Atlas of the Global Burden of Stroke 1990–2013: the GBD 2013 study. Neuroepidemiology 2015;45:230–236.

[2] Poon MT, Fonville AF, Al-Shahi Salman R. Long-term prognosis after intracerebral haemorrhage: systematic review and meta-analysis. J Neurol Neurosurg Psychiatry 2014;85:660–667.

[3] Krishnamurthi RV, Feigin VL, Forouzanfar MH, et al. Global and regional burden of first-ever ischaemic and haemorrhagic stroke during 1990–2010: findings from the Global Burden of Disease Study 2010. Lancet Glob Health 2013;1:e259–e281.

[4] Hemphill JC III, Greenberg SM ,Anderson CS, et al. Guidelines for the management of spontaneous intracerebral hemorrhage: a guideline for healthcare professionals from the American Heart Association/American Stroke Association. Stroke 2015;46: 2032–2060.

[5] Steiner T, Al-Shahi Salman R, Beer R, et al. European Stroke Organisation (ESO) guidelines for the management of spontaneous intracerebral hemorrhage. Int J Stroke 2014;9:840–855.

[6] Rodriguez-Torres A, Murphy M, Kourkoulis C, et al (2018). Hypertension and intracerebral hemorrhage recurrence among white, black, and Hispanic individuals. Neurology, 91(1), e37–e44. https://doi.org/10.1212/WNL.0000000000005729.

[7] Tsai HH, Kim JS, Jouvent E, Gurol ME. Updates on Prevention of Hemorrhagic and Lacunar Strokes. J Stroke. 2018;20(2):167–179. doi:10.5853/jos.2018.00787.

[8] Mustapha M, Nassir CMNCM, Aminuddin N, Safri AA, Ghazali MM. Cerebral Small Vessel Disease (CSVD) - Lessons From the Animal Models. Front Physiol. 2019;10:1317. Published 2019 Oct 24. doi:10.3389/fphys.2019.01317.

[9] Biffi A, Anderson C, Battey TW, et al. Association between blood pressure control and risk of recurrent intracerebral hemorrhage. JAMA 2015;9:904–912.

[10] Woo D, Rosand J, Kidwell C, et al. The Ethnic/Racial Variations of Intracerebral Hemorrhage (ERICH) study protocol. Stroke 2013;44:e120–e125.

[11] Biffi A, Halpin A, Towfighi A, et al. Aspirin and recurrent intracerebral hemorrhage in cerebral amyloid angiopathy. Neurology 2010;75:693–698.

[12] Biffi A, Bailey D, Anderson CD, et al. Risk factors associated with early vs. delayed dementia after intracerebral hemorrhage. JAMA Neurol 2016;73:969–976.

[13] Walsh KB, Woo D, Sekar P, et al. Untreated hypertension: a powerful risk factor for lobar and nonlobar intracerebral hemorrhage in whites, blacks, and Hispanics. Circulation 2016;134:1444–1452.

[14] Safford MM. Intracerebral hemorrhage, racial disparities, and access to care. Circulation 2016;134:1453–1455.

[15] Brady E. Healing Logics: Culture and Medicine in Modern Health Belief Systems. Logan: Utah State University Press; 2001.

[16] Labovitz DL, Halim A, Boden-Albala B, Hauser WA, Sacco RL. The incidence of deep and lobar intracerebral hemorrhage in whites, blacks, and Hispanics. Neurology 2005; 65:518–522.

[17] Broderick JP, Brott T, Tomsick T, Huster G, Miller R. The risk of subarachnoid and intracerebral hemorrhages in blacks as compared with whites. NewEngl J Med 1992; 326:733–736.

[18] Banda Y, Kvale MN, Hoffmann TJ, et al. Characterizing race/ethnicity and genetic ancestry for 100,000subjects in the Genetic Epidemiology Research on Adult Health and Aging (GERA) cohort. Genetics 2015;200:1285–1295.

Detection of Fake News Using Machine Learning

Shravan Kruthick Sridhar
Global Indian International School, Tokyo, Japan
Email: shravankruthicksridhar@gmail.com

Abstract – Machine learning and artificial intelligence are essential parts of technology today. They help reduce human effort and may also be able to perform certain tasks better than humans. An example of this is the classification of news articles as real or false. Whereas humans would have to do extensive research just to check the validity of a single article, a machine learning algorithm can do that in a much shorter timeframe by recognizing words and patterns that mostly occur in false news articles using techniques such as keyword analysis. Checking the validity of news articles is essential to prevent the spread of misinformation, especially due to the prevalence of fake news nowadays.

Key Words – Machine learning, news classification, keyword analysis, validity of articles

INTRODUCTION

The use of artificial intelligence is extremely common in a wide variety of tasks, from customer service chatbots to helping doctors interpret chest X-rays. In many cases, using machine learning algorithms helps reduce human error and the time required for the completion of an otherwise complex task.

The classification of news articles is a great way to use machine learning. Given a large enough dataset, a suitable algorithm can predict if the information presented in an article is real or not. Using more sophisticated algorithms and larger datasets, we may even be able to compute how much of the article is true.

For this study, I used the Information Security and Object Technology dataset from the University of Victoria, as prescribed by Ahmed et al. in publications from 2017 and 2018. The truthful articles in the dataset were obtained from Reuters.com and the false ones from various sources flagged as unreliable by PolitiFact, a fact-checking organization. This dataset contains over 40,000 entries in total, which is enough to predict with over 95% accuracy using the right algorithm.

I chose this topic to search for a more efficient solution to fact-check articles on the spot, as having people read and validate each article is extremely time-consuming.

Instead of following this long method, I used the fact that false news articles are written in a much different style compared to true articles. False news articles often feature informal, conversational language and words that directly mock or criticize someone. For instance, one of the false articles in the dataset contains the following lines:

"Donald Trump just couldn't wish all Americans a Happy New Year and leave it at that. Instead, he had to give a shout out to his enemies, haters and the very dishonest fake news media. The former reality show star had just one job to do and he couldn't do it. As our Country rapidly grows stronger and smarter, I want to wish all of my friends, supporters, enemies, haters, and even the very dishonest Fake News Media, a Happy and Healthy New Year, President Angry Pants tweeted."

This is a blatant example of a false news article. "President Angry Pants" seems to be a name given by the author and not by formal quotes. It can be assumed that the author is biased against the person in question (President Donald Trump), which resulted in the production of false news.

I. Background

I used four algorithms to classify the news articles: logistic regression, Support Vector Machines (SVM), K Nearest Neighbors (KNN), and decision trees. All of these algorithms operate on different principles. Thus, some may be more accurate than others.

I chose these algorithms because they are computationally simple. They are the ones taught to anyone beginning to learn machine learning. Whereas researchers use sophisticated techniques, such as Hidden Markov Models or Natural Language Processors, for text processing, I was intrigued by the possibility of these simple algorithms yielding accurate results.

Another reason I chose these algorithms is that it only takes a couple of minutes to execute them (except for SVM) and generate output. This can be handy in case an app is developed based on this paper.

Let us take a look at the algorithms I used.

a. Logistic Regression

Logistic regression uses the gradient descent algorithm on a linear model to classify data. This process generates a linear equation with multiple coefficients that determine how much each parameter affects the result, along with a bias that signifies the value of the output when all of the input parameters are 0. Given a list of parameters, this equation outputs a real number. For example, it is possible to predict the price of a house using this equation given the values of parameters, such as the neighborhood crime rate and the number of rooms in the house.

Gradient descent is the algorithm used to produce the line of best fit for data. This is done by calculating the mean deviation of the predicted value for one set of values, scaling it by a factor called the learning rate, and subtracting it from the existing coefficients and bias. The calculated numbers serve as the new coefficients and bias.

Performing this action for each set of values gives us a linear model that we can use to make the predictions. However, in logistic regression, we need a probability that lies between 0 and 1. For this, we need to apply a sigmoid function (Figure 1) to each predicted value.

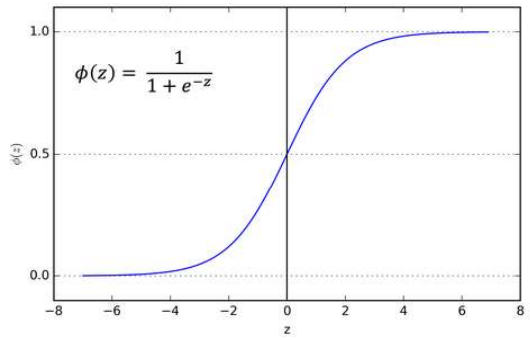

FIGURE 1 [3]: The sigmoid function. It takes in a real number and gives an output between 0 and 1.

b. SVM

In the SVM algorithm, we plot each data point as a point in an n-dimensional space, with n being the number of features. Then, we draw a hyperplane that separates the data point clusters and is as far as possible from the points. The margin is the distance between the hyperplane and the points on either side nearest to it. These points are called support vectors.

In many cases, the data may not be separable using a simple hyperplane. To solve this problem, a method called the kernel trick can be used, which converts a lower-dimensional point into a higher-dimensional one so that it is linearly separable.

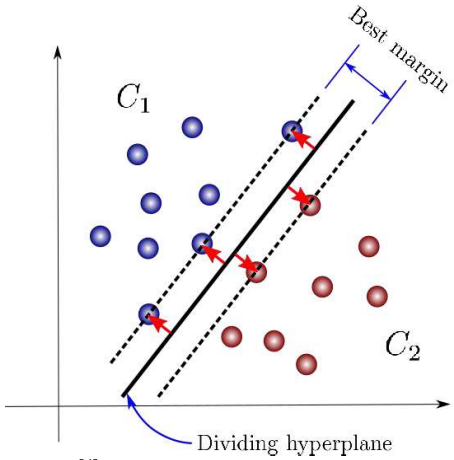

FIGURE 2 [4]: A set of data points separated by a hyperplane.

After this, we only need to see on which side of the hyperplane the given point falls.

c. KNN

The KNN algorithm uses the distance between points to classify data. For each data point's features, we compute the distance to every other data point.

Then, for each new point fed into the algorithm, the distance is computed between it and every other point. After that, the parameter k makes the algorithm consider the k nearest points (points with least distance) from the new point.

Thus, this process becomes a classification by majority. The new point is put into whichever data class occurs the most after the previous step of narrowing down.

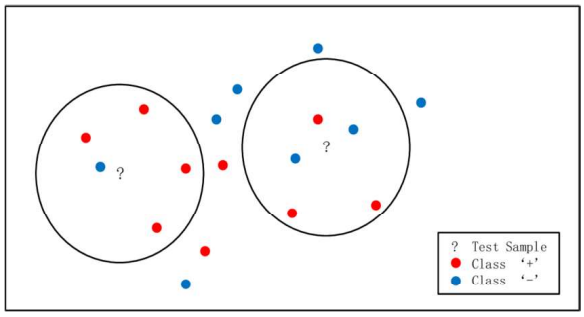

FIGURE 3: A simple example of a KNN algorithm.

If k is very small, the algorithm may overfit the training data, which means that it fits the training data too closely and cannot spot general data trends.

If k is very large, however, the algorithm underfits the data. Underfitting means that the algorithm does not sufficiently model the training data and cannot generalize to new data.

Since this algorithm only groups similarly worded articles, it may fail in case a true and false article contain similar words, despite having completely different meanings and contexts.

d. Decision Trees

The decision tree algorithm uses recursive binary splitting to categorize data [5]. For a decision tree classifier, the algorithm decides which condition to split the data on using a measure called the Gini impurity, which determines how pure a classification is. Specifically, it shows how many data points from multiple classes remain unseparated after one level of classification. The Gini impurity score of a node is the product of the probabilities of each class in the node. The lower this number is, the more accurate the classification.

II. Approach

I used Python to execute the algorithms since it has a machine learning library that helps speed up the process. To perform this task, I first cleaned up the data. After inspecting the data and removing characters such as the newline character \n, I used a TFIDF (Term Frequency Inverse

Document Frequency) [6] vectorizer to transform the strings into numerical data.

A TFIDF vectorizer works as follows: It first computes the number of occurrences of each word in each article; this is its TF value. Then, it computes the number of documents in the entire corpus in which the word occurs; this is its IDF value. The TFIDF is calculated by the following formula:

$$w_{\{i,j\}} = tf_{\{i,j\}} \times \log\left(\frac{N}{df_i}\right)$$

Next, I split the data, designating 20% for testing the model and the rest for training it. Then I was ready to feed the numerical data into the machine learning algorithm.

I used separate instances of TFIDF vectorizers to compute the TFIDF values for both the texts and titles, as I considered that even the article titles may be a good indicator of article validity. I also used two different instances of each algorithm for the same purpose.

One of this method's limitations is that it is not able to detect false statistics in a given article. For example, suppose an article says that 1,000 patients were infected with a disease, but the real number was closer to 400. The algorithms will not be able to detect this error because the method I used generates output based on the combinations of the words used in the articles.

This limitation can be counteracted by adding another layer of fact-checking to the process. This layer may include the checking of statistics. This can be done either by a human or a computer program that utilizes web crawling and parsing information from websites.

EVALUATION

I used multiple metrics to evaluate each of my models [7]:

Accuracy

This is one of the simplest ways by which a model can be judged. A model's accuracy is given by the quotient of the number of correct predictions and the total number of predictions.

However, accuracy alone is not a good measure of a model because of possible class imbalances. For example, if two classification labels are positive and negative, we can make a model that always predicts negative. If the number of true negatives in the data is more than the number of true positives, the accuracy increases, even though we have not built a model that represents the data to the highest possible extent.

Confusion Matrix

As its name suggests, the confusion matrix is a matrix that contains the number of each type of prediction made by the model (true positives, false positives, true negatives, false negatives).

Using the confusion matrix, we can calculate other metrics, such as precision. When used along with accuracy, these metrics can be used to arrive at a good estimate of the classifier's effectiveness.

F1 score

The f1 score of a classification model is given by the following formula:

$$\text{f1} = \frac{(\text{Precision}^{-1} + \text{Recall}^{-1})^{-1}}{2}$$

In this equation, precision is defined as the ratio of the relevant instances and retrieved instances, and recall is the fraction of the total amount of relevant instances retrieved. In other words, precision is the quotient of true positives and the total number of predicted positives. Recall is the quotient of the true positives and total number of actual positives (true positives + false negatives).

Using the harmonic mean instead of the arithmetic mean ensures that the f1 score is low even if one of the two quantities is low.

RESULTS

The results for each model are arranged in tables as follows:

Logistic Regression

Feature	Accuracy	Precision	Recall	F1 score
Title	95.53%	94.52%	96.07%	95.29%
Text	98.70%	98.46%	98.79%	98.62%

SVM

Feature	Accuracy	Precision	Recall	F1 score
Title	96.18%	95.56%	96.52%	96.04%
Text	99.46%	99.32%	99.55%	99.44%

KNN

Feature	Accuracy	Precision	Recall	F1 score
Title	89.95%	86.37%	93.37%	89.73%
Text	69.00%	94.50%	36.22%	52.37%

Decision Trees

Feature	Accuracy	Precision	Recall	F1 score
Title	91.83%	90.72%	92.12%	91.41%
Text	99.52%	99.50%	99.48%	99.49%

CONCLUSION

We can see from the results that the best algorithm for the task of classifying news articles as real or false based on title is SVM, with an accuracy of 96.18% and f1 score of 96.04%. Based on classification by text, however, the decision trees method is marginally better than SVM, with an accuracy of 99.52% and f1 score of 99.49%.

These are not the exact scores that will be obtained if the entire experiment is replicated due to the random separation

of training and testing data, but the results obtained will always be in the same ballpark.

The classifier algorithms could be made more accurate if the title and text data are fed into a single classifier. However, this method is beyond the scope of this paper and was not conducted. Future research could explore this possibility.

REFERENCES

[1] Ahmed, Hadeer, et al. "Detecting Opinion Spams and Fake News Using Text Classification." *Wiley Online Library*, John Wiley & Sons, Ltd, 29 Dec. 2017, onlinelibrary.wiley.com/doi/full/10.1002/spy2.9.

[2] Ahmed, Hadeer, et al. "Detection of Online Fake News Using N-Gram Analysis and Machine Learning Techniques." *Intelligent, Secure, and Dependable Systems in Distributed and Cloud Environments*, edited by L. Traore, I. Woungang, and A. Awad, Springer, 2017, pp. 127-138.

[3] Sharma, Sagar. "Activation Functions in Neural Networks." *Towards Data Science*, 2019, www.towardsdatascience.com/activation-functions-neural-networks-1cbd9f8d91d6.

[4] Carrasco, Oscar Contreras. "Support Vector Machines for Classification." *Towards Data Science*, 2019, www.towardsdatascience.com/support-vector-machines-for-classification-fc7c1565e3. Accessed 16 June 2020.

[5] Starmer, Josh. "StatQuest: Decision Trees." *YouTube*, uploaded by StatQuest with Josh Starmer, 23 January 2018, www.youtube.com/watch?v=7VeUPuFGJHk.

[6] Mamun, Iftekher. "Creating a TF-IDF in Python." *Medium*, 2020, www.medium.com/@imamun/creating-a-tf-idf-in-python-e43f05e4d424. Accessed 18 June 2020.

[7] Yıldırım, Soner. "How to Best Evaluate a Classification Model." *Towards Data Science*, www.towardsdatascience.com/how-to-best-evaluate-a-classification-model-2edb12bcc587. Accessed 23 June 2020.

Mental Health in Adolescents: Analysis of a Nationally Representative Dataset, 2009-2018

Elena Su
Brookline High School; Brookline, Massachusetts, USA
Email: esu2021@gmail.com

Abstract - According to the World Health Organization (WHO), adolescence marks a period of vulnerability for the onset of mental health conditions. Depression is the ninth leading cause of illness and disability in all adolescents. In this paper, data from the National Survey on Drug Use and Heath (NSDUH; N=563,275), a nationally representative survey of U.S. adolescents and adults, were analyzed. Between 2009 and 2018, increases in rates of major depressive episodes (MDE) in the past year (66.5%), serious psychological distress in the last month (82.7%), serious thinking about killing self in the past year (59.5%) were observed among adolescents, with girls having higher rates of MDE than boys (20.89% vs. 8.28% in 2018) and also higher percent change in rates than boys (70.0% vs 62.1%). The same trend was not found for adults ages 26 and over. Black non-Hispanic adolescents had a lower rate of MDE than other race/ethnicity groups in all years (9.83% vs. at least 14.66% in 2018). Results suggest the need for more mental health prevention and treatment programs for adolescents, who are undergoing a critical juncture in their development.

Key Words – mental health, adolescents, depression

INTRODUCTION

Adolescence, defined as when an individual is between 10-19 years of age, is a critical period for later life health and well-being. Supportive family, school, and community environments allow adolescents to maintain their mental health. However, adolescents are particularly vulnerable to the onset of mental health conditions. For U.S. adolescents and young adults, serious psychological distress, major depression, suicidal thoughts, and attempted suicide were more common in the late 2010s than in the mid-2000s [1]. Every year, mental illnesses take a heavy toll on adolescents worldwide. Globally, suicide is the third leading cause of death in teenagers aged 15 to 19, with an estimated 53,000 deaths due to suicide in 2016. Notably, it is the second leading cause of death for girls in this age group. Recognized risks for adolescent mental health problems include, but are not limited to poverty, violence, forced migration, substance use, chronic illness, harsh parenting, bullying, sexual violence, early pregnancy, early and/or forced marriages, and being a member of a minority or discriminated group [2]. According to a report from the WHO and its partners, most adolescent deaths can be prevented with good health services, education, and social support. But in many cases, adolescents who suffer from mental health disorders, substance use, or poor nutrition cannot obtain critical prevention and care services – either because these services do not exist, or because of a lack of awareness of these services. In addition, many behaviors that impact health later in life, such as physical inactivity, poor diet, and risky sexual health behaviors, develop during adolescence.

"Adolescents have been entirely absent from national health plans for decades," says Dr. Flavia Bustreo, the Assistant Director-General of the WHO. "Relatively small investments focused on adolescents now will not only result in healthy and empowered adults who thrive and contribute positively to their communities, but it will also result in healthier future generations, yielding enormous returns." [2]

The present study examines the 10-year trend in the rates of MDE, serious psychological distress, and serious suicidal thoughts for adolescents in the U.S. Knowledge of changing mental health trends provides important insight into potential risks, as well as protective factors, for adolescents. Research results in trends for various mental health problems in adolescents are variable [3]. Twenge and her co-authors analyzed data from the National Survey on Drug Use and Health (NSDUH), which is a nationally representative survey that has tracked drug and alcohol use, mental health, and other health-related issues in individuals age 12 and over in the U.S. [1]. They analyzed survey responses from more than 200,000 adolescents between the ages of 12 and 17 from 2005 to 2017. Additionally, they looked at the results of almost 400,000 adults aged 18 and over from 2008 to 2017. The rate of individuals reporting symptoms consistent with major depression in the last 12 months increased 52 percent in adolescents from 2005 to 2017 (from 8.7 percent to 13.2 percent) and 63 percent in young adults aged 18 to 25 from 2009 to 2017 (from 8.1 percent to 13.2 percent).

In addition, Sourander and co-authors examined the 10-year time trend changes of psychiatric symptoms, smoking and alcohol use in a study of Finnish adolescents [4]. Representative population-based samples with same methods at two time-points, same age range and with 10-year period between the time points were gathered to investigate secular changes in adolescents' emotional and behavioral problems. Seventh and ninth grade students filled in the Strengths and Difficulties Questionnaire (SDQ) and

questions regarding alcohol use and smoking anonymously during a school lesson in 1998 (n = 1458) and 2008 (n = 1569). The self-reports of SDQ showed substantial stability in emotional and behavioral problems from 1998 to 2008. There was no increase between the two timepoints in self-reports of SDQ total, conduct, hyperactivity, emotional or peer problems when using the 90th percentile clinical cut-off points.

This paper focuses on the mental health of adolescents in the U.S., and uses the most recent NSDUH data to compare mental health conditions between adolescents and older adults, girls and boys, and among race/ethnicity groups. The need for mental health treatment is also analyzed over the 10-year period from 2009 to 2018.

METHODS

Data used in this study are from NDSUH, which is an annual survey of participants of 12 years and older, administered by the U.S. Substance Abuse and Mental Health Services Administration since 1971, but the survey underwent significant questionnaire redesign and improvements in 1979 and 2002 [5]. Data are available for public use. A total of 563,275 adolescents and adults participated in the survey during the 10-year study period. The numbers of participants were similar across years, ranging from 55,160 (the lowest count) in 2013 to 58,397 (the highest count) in 2011. Demographic variables included sex (male or female) and race/ethnicity (black, white, Hispanic, or other). The overall response rate was 48.79 percent for people aged 12 or older [5].

Outcome variables included in this study were: MDE in the past year, serious psychological distress in the past month, seriously think about killing self in the past 12 months, and needed mental health treatment but did not get it in the past 12 months. All these data were collected consistently over the study period. However, while MDE was available for all participants of NDSUH, the other 3 variables were available for participants of 18 years and older. All analyses were descriptive in nature and results were not weighted based on the age distribution of the U.S. population. P-values were from Chi-square test for comparing 2-sample proportions. Due to disclosure limitations for respondent confidentiality, a state variable is not included in public-release datasets.

RESULTS

Of the 563,275 participants included in this study, 200,162 (35.5 percent), 121,159 (21.5 percent) and 241,954 (43.0 percent) were 12-19, 20-25 and 26+ years old, respectively. Of the 200,162 adolescents, 98.574 (49.3 percent) were girls, 111,474 (55.7 percent), 27,181 (13.6 percent), 40,334 (20.4 percent), and 21,173 (10.6 percent) were White (non-Hispanic), Black (non-Hispanic), Hispanic, and Other, respectively.

Figure 1 shows that the percent with MDE in the past year increased for the 12-19 and 20-25 age groups, especially after 2011. The 12-19 age group had the highest increase, changing from 8.67 percent in 2009 to 14.43 percent in 2018 (P<0.001), a relative change of 66.5 percent (Table 1). The percent with MDE for the 26+ age group declined slightly from 7.69 percent in 2009 to 7.24 percent in 2018 (P=0.066), a relative decrease of 5.8 percent (Table 1).

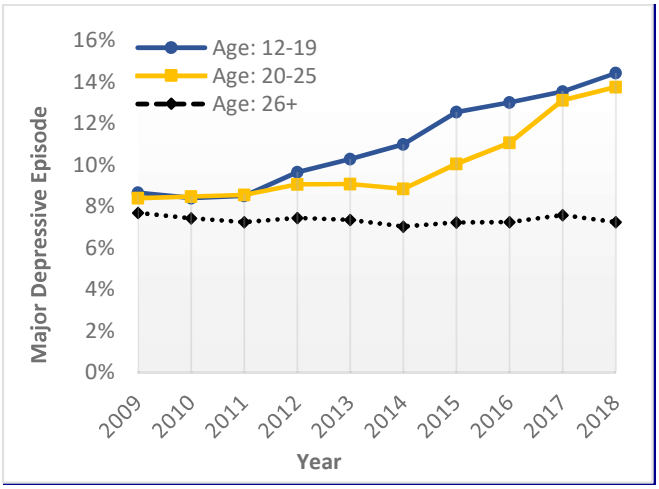

FIGURE 1: Percent with MDE in the past year by age group, 2009-2018.

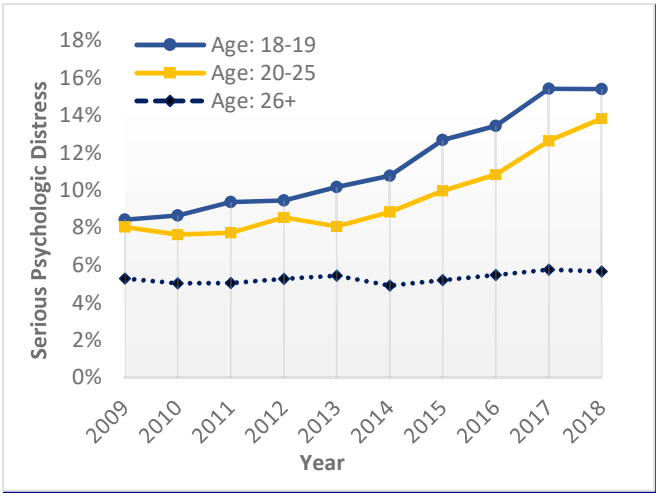

FIGURE 2: Percent with serious psychological distress in the past month by age group, 2009-2018.

Percent with serious psychological distress in the past month and percent with serious thinking about killing self were presented in Figure 2 and Figure 3, respectively, with data included in Table 1. The trends were similar in Figure 2 and Figure 3. The 18-19 age group had the highest percent with these mental health outcomes among the 3 age groups. The relative percent changes over the 10-year period in this study were 82.7 percent and 59.5 percent for serious psychological distress in the past month and serious thinking about killing self in the past 12 months (P<0.001 for both),

respectively, for the 18-19 age group. There were no significant changes in these mental health outcomes for the 26+ age group (P=0.082 and P=0.45, respectively).

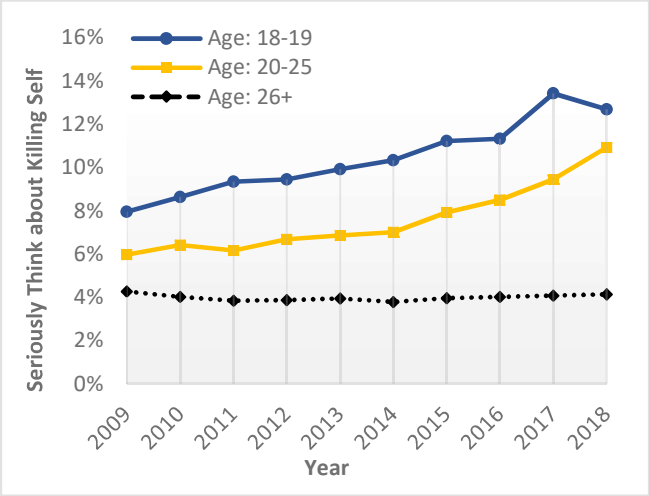

FIGURE 3: Percent with serious thinking about killing self in the past year by age group, 2009-2018.

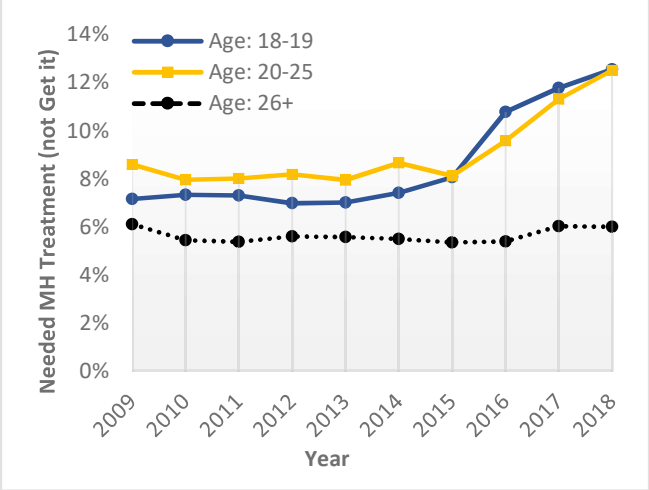

FIGURE 4: Percent needing mental health treatment but did not get it in the past year by age group, 2009-2018.

As shown in Figure 4, the 18-19 and 20-25 age groups had higher percent of participants who needed mental health treatment but did not get it in the past year, as compared to the 26+ age group. Both the 18-19 and 20-25 age groups reported increasing cases of not getting mental health treatment starting 2015, particularly for the 18-19 age group. The 18-19 age group had noticeably lower percent than the 20-25 age group for each year before 2015 but had similar or slightly higher percent after 2015.

There were differences in self-reported MDE in the past year between boys and girls, and among race/ethnicity groups, as shown in Figure 5 and 6, and Table 2. Figure 5 shows that girls had remarkably higher percent of MDE than boys, for each year during the 10-year period (P<0.001), with the difference being larger in more recent years. Since 2009, the percent increased from 12.29 percent to 20.89 percent for girls (a relative percent increase of 70.0 percent, P<0.001), and increased from 5.11 percent to 8.28 percent for boys (a relative percent increase of 62.1 percent, P<0.001).

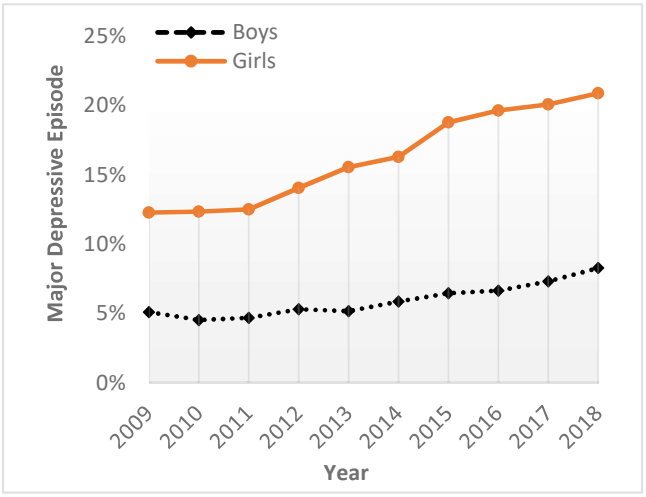

FIGURE 5: Percent with MDE in the past year by sex, 2009-2018.

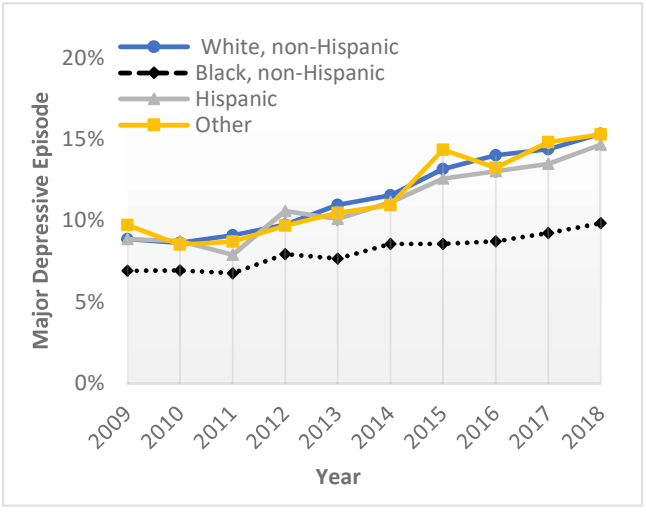

FIGURE 6: Percent with MDE in the past year by race/ethnicity group, 2009-2018.

TABLE 1: Percent of participants with each mental health outcome by age group

Age (years)	Outcomes	2009	2010	2011	2012	2013	2014	2015	2016	2017	2018	Change
12-19	MDE	8.67	8.40	8.51	9.65	10.28	11.00	12.55	13.01	13.54	14.43	66.5%
	SPD	8.42	8.65	9.37	9.44	10.17	10.76	12.67	13.43	15.41	15.38	82.7%
	STK	7.95	8.63	9.33	9.44	9.92	10.32	11.21	11.32	13.41	12.68	59.5%
	NMH	7.15	7.33	7.30	6.98	7.01	7.40	8.06	10.77	11.78	12.55	75.4%
20-25	MDE	8.39	8.48	8.55	9.06	9.07	8.85	10.05	11.07	13.12	13.76	63.9%
	SPD	8.03	7.63	7.72	8.55	8.07	8.83	9.96	10.83	12.63	13.82	72.0%
	STK	5.97	6.41	6.16	6.68	6.85	7.00	7.91	8.49	9.43	10.92	83.0%
	NMH	8.59	7.95	8.01	8.18	7.94	8.66	8.12	9.57	11.30	12.50	45.5%
26+	MDE	7.69	7.42	7.25	7.45	7.36	7.03	7.23	7.24	7.57	7.24	-5.8%
	SPD	5.28	5.02	5.04	5.27	5.44	4.91	5.20	5.47	5.76	5.65	7.1%
	STK	4.27	4.02	3.84	3.87	3.93	3.78	3.95	4.02	4.08	4.13	-3.2%
	NMH	6.11	5.43	5.37	5.60	5.57	5.50	5.35	5.38	6.02	5.99	-1.9%

Abbreviation for outcomes:
MDE: major depressive episode in the past year, SPD: serious psychological distress in the past month, STK: seriously think about killing self in the past 12 months, and NMH: needed mental health treatment but did not get it in the past 12 months.

TABLE 2: Rate of major depressive episode by sex and race/ethnicity for adolescents (12-19 years)

Characteristics	2009	2010	2011	2012	2013	2014	2015	2016	2017	2018	Change
Boys	5.11	4.54	4.68	5.31	5.18	5.86	6.47	6.66	7.31	8.28	62.1%
Girls	12.29	12.36	12.51	14.07	15.58	16.31	18.80	19.65	20.10	20.89	70.0%
White, non-Hispanic	8.86	8.62	9.10	9.73	10.96	11.55	13.16	14.00	14.38	15.32	73.0%
Black, non-Hispanic	6.92	6.94	6.76	7.92	7.65	8.55	8.56	8.72	9.23	9.83	42.2%
Hispanic	8.84	8.74	7.88	10.58	10.08	11.12	12.58	13.03	13.48	14.66	65.8%
Other	9.72	8.52	8.69	9.68	10.46	10.93	14.34	13.23	14.81	15.28	57.2%

The analysis of race/ethnicity groups showed an increasing trend of more cases of self-reported MDE for all groups. The trend was similar among White (non-Hispanic), Hispanic and Other groups (Figure 6), and these groups had higher percent of MDE than the Black (non-Hispanic) group.

DISCUSSIONS

This study included data from a nationally representative datasets contributed by a large number (563,275) of participants over a 10-year period. There was a clear and consistent trend that the mental health condition for adolescents in the U.S. was worsening. This trend was in contrast to the 26+ age group, which showed very little or no change over the study period. Overall, the percent of adolescents with mental health conditions was about twice as high as the adults of 26+ years. Girls, in particular, require additional prevention and treatment programs as the percent with MDE among the girls was more than twice the percent of MDE among the boys of the same age group. These findings are consistent with those in published papers by Twenge, et al. [1] and Park, et al. [2]. With respect to ethnicity, a study showed that White students with symptoms of depression were more than twice as likely as their Black counterparts to have received a prior diagnosis of depression, with mixed results for Hispanic students [6]. Additional research is needed to determine whether ethnic disparities are related to income, insurance status, and previous psychological treatment.

Multiple factors could contribute to the worsening mental health conditions among adolescents in the U.S. One of them is screen media. A study showed that children and adolescents who spent more time using screen media were lower in psychological well-being than low users. High users of screens were significantly more likely to display poor emotion regulation (not staying calm, arguing too much, being difficult to get along with), an inability to finish tasks, lower curiosity, and more difficulty making friends[7]. In Twenge's paper [1], it was noted that cultural trends in the last 10 years may have had a larger effect on mood disorders and suicide-related outcomes among younger generations compared with older generations. The increased use of

electronic communication and digital media may have changed modes of social interaction enough to affect mood disorders. This may have had a bigger impact on adolescents because older adults' social lives are more stable. Older adults might also be less likely to use digital media in a way that interferes with sleep -- for example, they might be better at not staying up late on their phones or using them in the middle of the night. Indeed, additional analysis (data not shown) indicated that 99% of the adolescents who participated in the NSDUH survey in 2018 had access to a cell phone. Individuals who spend more time on social media and less time with others face-to-face reported lower well-being and are more likely to be depressed [8, 9]. Media influence can exacerbate the disparity between an adolescent's lived reality and their perceptions or aspirations for the future, in addition to affecting adolescents' sleep. Studies have shown that sleep duration among U.S. adolescents appears to be declining [10]. Thus, it is important to get enough sleep, and make sure the device use does not interfere with sleep and normal life.

Another factor that poses some adolescents at greater risk of mental health conditions is their living conditions, stigma, discrimination or exclusion, or lack of access to quality support and services. These include adolescents with chronic illness, autism spectrum disorder, an intellectual disability or other neurological condition; pregnant adolescents, adolescent parents, or those in early and/or forced marriages; orphans; and adolescents from minority ethnic or sexual backgrounds or other discriminated groups. In 2017, slightly less than 1 in 5 children lived in families with incomes below the federal poverty line, the lowest level since 2009 [11]. In this study, adolescents and young adults reported higher percent of needing mental health treatment but did not get it in the last year. Adolescents with mental health conditions are in turn particularly vulnerable to social exclusion, discrimination, stigma (affecting readiness to seek help), educational difficulties, risk-taking behaviors, physical ill-health and human rights violations. It is crucial to address the needs of adolescents with defined mental health conditions.

Other important factors affecting adolescents' mental health include the quality of their home life and relationships with peers. Violence (including harsh parenting and bullying) and socioeconomic problems are recognized risks to mental health. Children and adolescents are especially vulnerable to sexual violence, which has a clear association with detrimental mental health [2].

There are limitations to this study. First, the data are based on self-reports of mental health, and their value depends on respondents' willingness to report, truthfulness and memory. Although some experimental studies have established the validity of self-reported data in similar contexts and NSDUH procedures were designed to encourage honesty and recall, some underreporting and overreporting may take place. Second, individuals were interviewed only once and were not followed for additional interviews in subsequent years. Thus, this study did not show changes in mental health for a fixed group of participants. However, major findings in this study are consistent with those in published papers, and the large volume of data over a long period of time are important for studying this important topic. The public access to the NSDUH data made it possible for many researchers to analyze, discuss, publish results and ideas, which will hopefully lead to better understanding of mental health conditions and, ultimately, the breaking down of barriers that inhibit adolescents' mental health.

REFERENCES

[1] Twenge JM, Cooper AB, Joiner TE, Duffy ME, Binau SG, Age, period, and cohort trends in mood disorder indicators and suicide-related outcomes in a nationally representative dataset, 2005–2017. Journal of Abnormal Psychology, 2019, 128 (3), 185–199.

[2] World Health Organization, website https://www.who.int/en/news-room/detail/16-05-2017-more-than-1-2-million-adolescents-die-every-year-nearly-all-preventable.

[3] Park MJ, Scott JT, Adams SH, Brindis CD, and Irwin CE, Adolescent and young adult health in the United States in the past decade: little improvement and young adults remain worse off than adolescents, Journal of Adolescent Health 55 (2014) 3-16.

[4] Sourander A, Koskelainen M, Niemela S, Rihko M, Ristkari T, Lindroos J, Changes in adolescents mental health and use of alcohol and tobacco: a 10-year time-trend study of Finnish adolescents, Eur Child Adolesc Psychiatry (2012) 21:665–671.

[5] Substance Abuse and Mental Health Data Archive (SAMHDA), https://datafiles.samhsa.gov/

[6] Thomas JF, Temple JR, Perez N, and Rupp R, Ethnic and Gender Disparities in Needed Adolescent Mental Health Care, J Health Care Poor Underserved. 2011, 22(1): 101–110

[7] Twenge, JM, Campbell WK, Associations between screen time and lower psychological well-being among children and adolescents: Evidence from a population-based study, Preventive Medicine Reports, 12 (2018), 271-283.

[8] Lin, LY, Sidani, JE, Shensa A, Radovic A, Miller E, Colditz JB et al. (2016), Association between social media use and depression among U.S. young adults. Depression and Anxiety, 33, 323–331. http://dx.doi.org/10.1002/da.22466

[9] Shakya HB, Christakis NA (2017). Association of Facebook use with compromised well-being: A longitudinal study. American Journal of Epidemiology, 185, 203–211. http://dx.doi.org/10.1093/aje/kww189

[10] Twenge JM, Krizan Z, Hisler G (2017). Decreases in self-reported sleep duration among U.S. adolescents 2009–2015 and association with new media screen time. Sleep Medicine, 39, 47–53.

[11] Child Trends Databank. (2019). *Children in poverty*. Available at: https://www.childtrends.org/?indicators=children-in-poverty

Finding Nutritious Alternatives to Ingredients in Recipes Using Machine Learning

Saachi Subramaniam
South Brunswick High School; South Brunswick, United States
Email: saachisubramaniam@gmail.com

Abstract – In the United States, close to 678,000 deaths per year are attributed to nutrition-related causes with obesity and malnutrition as the leading cause of death. By helping users reform their diets, malnutrition in all forms can be combated. This research discusses the factors involved in food nutrition and the integration of nutritious foods into users' lifestyles. Through the utilization of Python, natural language processing and APIs, this work supplements individuals with nutritional alternatives. In this work, Each ingredient is categorized, and analyzed for nutritional value, then a similar product with higher nutritional value is reported to the user. The work also implements a graphical user interface that allows users to easily interact with the database and obtain results quickly.

Key Words – Healthy Eating, Nutrition, Diets, Food Pairings

INTRODUCTION

According to a study done by Pew Research, 72% of American's believe good nutrition is the key to a long and healthy life. However when the same study asked subjects to identify the statement which best describes their eating habits. Only 18% reported their main focus as "health and nutrition." [1] Furthermore, more than 48% of Americans rarely or never seek out information about how their food is produced according to a food literacy study done by Michigan State University. [2] The American perception of food and nutrition is based largely on misinformation and "fad diets." Fad diets refer to specific eating restrictions that become popular for a short time. Often, fad diets are not backed by scientific research but instead, merely promote disordered eating. Many fad diets revolve around cutting out certain food groups and restricting caloric intake. This work proposes an intuitive approach to nutrition rather than a restrictive approach. The work focuses on the nutritional composition of each ingredient whereas fad diet models may focus on certain food groups such as vegetables while excluding food groups like carbohydrates. However, this research was conducted with the intent of incorporating more nutritious foods into users' diets while preserving the taste of dishes, focusing on an intuitive model as opposed to a restrictive model. Some of the benefits of intuitive eating include developing a healthier relationship with food, becoming more attuned to the body's natural hunger and fullness cues, and leading a happier lifestyle. This research's foundations in intuitive eating promotes healthy relationships with food by encouraging users to have awareness for their eating choices. Furthermore, the work gives users the freedom to make their own dietary choices while simultaneously offering nutritious alternatives.

BACKGROUND

This research employed three different tools in order to classify, analyze, and suggest ingredient alternatives. These three tools are Web Scraping, Natural Language Processing and APIs.

I. Web Scraping

This research employed Web Scraping in order to retrieve results from websites such as Google Shopping. Web scraping is the process by which computers extract data from websites. With web scraping, computers send requests to websites, and extract information relevant to the user. Information can then be used for a variety of business and personal related outcomes. The automation of data extraction allows for companies to retrieve competitor's prices, users to receive up-to-date news alerts, and for fantasy sports enthusiasts to calculate the statistics of their favorite fantasy sports leagues. While web scraping is primarily used in price monitoring, market research, and content monitoring, this work utilized web scraping to extract product information from Google Shopping, as well as gather ingredient information from the web.

II. Natural Language Processing (NLP)

Natural Language Processing is a subsection of a larger field of study known as Machine Learning. Machine Learning algorithms identify patterns in training data which allows the algorithms to apply the same patterns to new data. Training data refers to datasets that machine learning algorithms use to learn and identify patterns. When given a new data point, these algorithms are able to use previously identified patterns to draw new conclusions about the data. Machine Learning powers social media feeds, movie recommendation services, and many smart assistants such as Siri or Alexa. Natural Language Processing (NLP) uses the same pattern recognition principle and applies it to oral and written language. NLP is able to

manipulate, analyze, and derive meaning from human language. Natural Language Processing technology has been used in spell-checking devices and spam inbox filtering services. This work implements NLP to categorize ingredients into different food groups based on name.

III. APIs (Spoonacular)

Application Programming Interface (API) is the intermediary connecting two applications together. APIs can perform certain tasks and retrieve information through a user request, and send the information back to the user, or complete the task. Currently, APIs exist for many different fields and topics such as food, music, news and weather. For this work, the specific API used was Spoonacular. The Spoonacular API holds nutrition information for ingredients, recipes, and products. This information was later used in the classification model and in the algorithms for determining nutritional value.

RELATED WORKS

This section discusses similar, pre-existing works related to nutrition, dietetics, and the use of natural language processing in food analysis.

Due to the fact that the concept of a proper diet is rapidly evolving, many researchers have created algorithms for making healthy foods more accessible. Benjamin Share, James Ordner, and Zack Cinquini's "Optimizing meals under dietary constraints" presents the implementation of machine learning algorithms in order to both predict the success of a recipe according to users' dietary restrictions, and make substitution recommendations accordingly. [3] The latter half of the paper discussing methods for food recommendation systems proved most relevant for the purposes of this research. The system analyzed the ingredient to be substituted and the proposed substitution in relation to how often the two ingredients appeared in recipes together. The paper notes that this algorithm worked well for rarer ingredients, however failed to produce accurate recommendations for common ingredients which appear in many recipes. For common ingredients, the work utilized Naive Bayes to construct a more complex approach.

The second related work by Stanley C. Rak, describes a method for determining the nutritional value of a food. [4] Rak used a weighting system to score certain vitamins and nutrients depending on their healthiness. Then, Rak calculated the nutritional value of the food according to the amount of different vitamins, nutrients, and fats present in the food. This approach inspired the conditional algorithm for determining nutritional value.

RESEARCH QUESTION

How can we help Americans make healthier eating choices by providing healthy substitutions for unhealthy food items that may be in their recipes?

APPROACH

This approach contains three different elements within the work. First, an ingredient is classified into a general food group through the classification model. Then, a search term is generated for the ingredient based on the nutrition recommendations for ingredient's classification. Finally, the search term is inputted into Google Shopping where the work scrapes the results and displays them using a graphical interface. Figure 1 above documents the flow of this approach, and briefly outlines each element of the method. *(See Figure 1)*

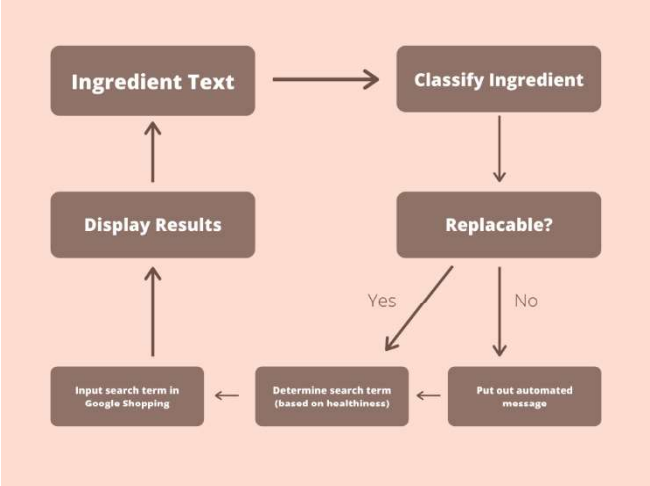

FIGURE 1: Workflow chart for method

I. Classification

This work applied Natural Language Processing and APIs in order to increase the accuracy of the categorization model. The categorization model decomposed ingredients into a general food group by feeding the inputted ingredient through two stages of categorization. Stage one integrated NLP's "Bag of Words" in order to compute a preliminary set of categorizations. The Bag of Words model is a specific approach to Natural Language Processing that converts text into vectors, which computers are better able to comprehend. This model can count the frequency of a set of characters in a given input, and assign a value to the characters accordingly. This allows the model to draw patterns based on the frequency of a set of characters. The "Bag of Words" approach uses sets of training data to teach machine learning algorithms how to interpret new data. The program uses training data to identify key ingredients in each item, and uses this information to sort the food into its respective food group. These food groups are based on the Eurocode Main Food Group Rules. [5] The first stage of classification identified all milks, juices, and common meat products into their respective food categories. For example, when "apple juice" undergoes the first stage of categorization, it is identified as a beverage. The machine learning algorithm uses patterns from the training data to recognize that all juices should be classified as a beverage. All items that are not categorized in the first stage, move to

the second stage. In the second stage, the work utilizes the Spoonacular API to retrieve the grocery store aisle of the inputted ingredient. Each grocery store aisle corresponded with a general food group, therefore each food item's grocery store aisle got converted into a food group. Finally, if an item cannot be classified into a food group, the work notifies the user, and asks for another ingredient.

II. Determining Nutritional Value

This component of the work used the food group from the classification model in order to create search terms for healthier alternatives. Each food group contained different specifications and algorithms for determining nutritional value. These algorithms are as follows: Replacement, Web Scraping, and Conditional. These algorithms take into account the requirements for healthy ingredients, and devise a search term for the ingredient according to the specifications. The replacement algorithm used a list of nutritious and innutritious ingredients to determine the nutritional value of the item. If the item was in the list of innutritious ingredients, the search term for the ingredient used one of the ingredients in the nutritious list. If the item was nutritious, the work notified the user that the proposed ingredient is already healthy. The web scraping algorithm used data from the web to determine the nutritional value of the proposed ingredient. Using the data, the web scraping algorithm produced a search term for the ingredient. The fish category is a notable example of the web scraping algorithm. The web scraping algorithm for the the fish category scraped data from the United States Environmental Protection Agency's mercury levels in fish chart. [6] This chart identified the mercury levels in common seafood products and made recommendations based on the amount of mercury in a fish. The algorithm scraped the website data for the name of the seafood product and the EPA recommendation. Then, a list of safe seafood products was created. If the proposed ingredient had a positive EPA recommendation, the work would notify the user that the proposed ingredient is healthy. If the ingredient had a negative EPA recommendation, the search term for the proposed ingredient would be derived from the list of safe seafood products. The conditional algorithm is the final method used for determining nutritiousness. This algorithm applies conditions to the ingredient, which forms the search term. For example, the grains category included the conditions "whole wheat" because whole wheat grain products are more nutritious than other grain products. "Whole wheat" was then added to the ingredient name in order to create the full search term. Due to the fact that each food category's specifications were of various levels of complexity, some search terms and conditions were harder to identify than others.

III. Web Scraping Google Shopping

After identifying the different categories of foods and the different qualities that made them healthy, the third element of the work transformed the search terms into ingredients that could be substituted into a dish. The process of converting theoretical keywords into real ingredients occurred through Google Shopping. By entering keywords into Google Shopping and web scraping the results, the work was able to bridge the gap between search terms such as "whole wheat pasta" and the names of real ingredients such as "Great Value Whole Wheat Spaghetti." In this component, the work entered keywords into the Google Shopping website, scraped information about the resulting items, and displayed the information in the output. One of the main benefits to using Google Shopping as opposed to other online shopping sites is its accessibility. Google is one of the most universal corporations, with branches across the globe. In order to make results most practical for users, the work uses Google Shopping because it is universal, and contains millions of different ingredients from many different countries. Google Shopping is not limited by geographical location, therefore ingredients are most likely to be very widely accessible. Not only this, but ingredients from countries outside the Unites States are available because Google Shopping is not limited by geographical location.

a. Displaying Products with Regex

In order to make information more legible to users, the work utilized Regular Expressions. Regular Expressions (RegEx) are sequences of characters used as a search pattern. These "capture groups" can be used to delete, replace, and match certain parts of strings. In this work, the web-scraped information contained HTML tags and irrelevant website information. Regular Expressions matched patterns of unneeded characters and deleted them. This converted hard to decipher information into simple and clear ingredients which could then be displayed to users.

IV. Graphical User Interface

This research implemented a graphical user interface which coherently displayed ingredient information to users. The work employed PyGame in order to add functionality to the display. Each page design was imported into PyGame from Figma. Then, buttons and text fields were placed as needed throughout the display. Creating buttons and text fields in PyGame required coordinate locations. Once coordinate locations were provided, users was able to click with the provided coordinates and perform an action. The full graphical user interface features a log in page, sign up page, and home screen where users can enter ingredients and interact with the software. *(See Figure 2)*

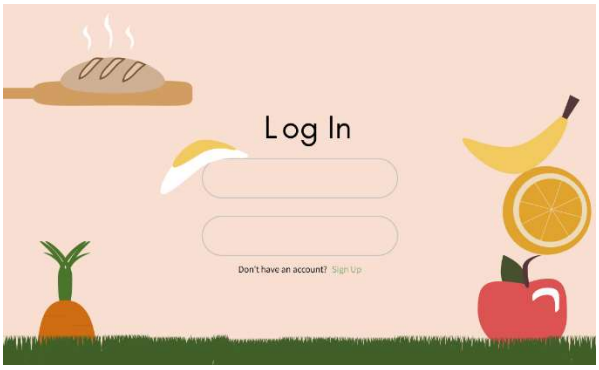

FIGURE 2: Log In page of graphical user interface

FIGURE 3: Homepage of graphical user interface

RESULTS

This research aimed to integrate healthy choices into users' lifestyles by producing nutritious alternative to potentially unhealthy ingredients. The results of this work produced five nutritious alternatives for the ingredient inputted. This model was able to accurately suggest ingredient alternatives for all fruit, vegetable, protein, dairy, and beverage products, including common household ingredients. However, certain name-brand confectionary items were not able undergo the categorization model successfully. In the future, the usage of multiple datasets may improve the categorization model by allowing it to categorize a wider variety of products. The applicability of these results were then tested by feeding different ingredients with commonly known healthier substitutes. The results were compared against the substitute in order to determine efficacy. Examples *(See Figure 4)* of potential user inputs and results are shown below. Furthermore, the usage of a browser interface allowed each result to be verified in real time. The interface, as opposed to a headless browser, displays the work inputting and retrieving the results through the browser. *(See Figure 5)* The main limitation of this model is the incompatibility with newer versions of Google Shopping. Due to the web scraping component of this work relying heavily on the site design of Google Shopping, as Google Shopping is updated, the web crawler is unable to gather data using the newer version.

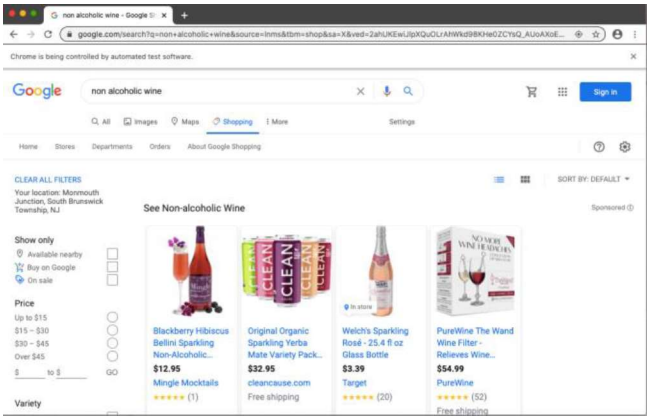

FIGURE 4: Browser interface with sample input non-alcoholic wine

Whole Milk	Silk Soymilk, Original - 64 fl oz Silk Organic Soymilk, Organic, Unsweet - 64 fl oz Silk Original Soy Milk 32 oz Great Value Soy Milk, Original - 0.5 gl (1.89 lt) Silk Soymilk, Very Vanilla - 12 pack, 8 fl oz containers
Venison	Mori-nu Silken Extra Firm Tofu 12.3oz House Foods Tofu Firm, 16.0 oz, Size: 16 fl oz Nasoya Organic Extra Firm Tofu - 14oz Nasoya Tofu, Organic, Extra Firm - 14 oz House Foods Tofu, Premium, Extra Firm - 16 oz
White Bread	Nature's Own 100% Whole Wheat Bread - 20 oz loaf Oroweat 100% Whole Wheat Bread - 24oz 100% Whole Wheat Bread 20oz - Market Pantry Great Value 100% Whole Wheat Bread, Round Top, 20 oz, Size: 12.1, 3.98, 4.21 Arnold Whole Grains Bread, 100% Whole Wheat - 1 lb

FIGURE 5: Sample inputs and their outputs for ingredients with commonly known healthier substitutes

FUTURE WORKS

This work could be improved by implementing Image Recognition Software (IR). As opposed to having users manually enter ingredients, an image recognition feature could scan recipes and report all ingredients with viable substitutions. Furthermore, image recognition software could identify similar recipes and suggest similar ingredient substitutions for them which would improve the speed and efficacy of this model.

In addition, the integration of a cross-checking feature in which the work checks multiple sources for the nutrition information of an ingredient would improve the accuracy of the work altogether. Similarly, allowing users to

check nutrition and allergen information for a product may be a next step. The cross-checking feature may also be useful in conjunction with the "allergen check" component to ensure that users are getting the most accurate allergen information.

ACKNOWLEDGEMENTS

The author wishes to thank Sara Metwalli for her guidance and aid in the research and production of the work, as well as for proofreading the paper.

REFERENCES

[1] *Public views about Americans' eating habits*. (2016, December 1). https://www.pewresearch.org/science/2016/12/01/public-views-about- americans-eating-habits/

[2] *MSU Food Literacy and Engagement Poll: Wave I – Food@MSU*. (n.d.). Retrieved August 28, 2020, from https://www.canr.msu.edu/news/msu-food-literacy-and-engagement-poll

[3] *5240107.pdf*. (n.d.). http://cs229.stanford.edu/proj2017/final-reports/5240107.pdf

[4] Rak, S. C. (2011). U.S. Patent Application No. 12/658,820.

[5] *Eurocode Main Food Groups: classification and policy, version 99/2*. (n.d.). Retrieved August 25, 2020, from http://www.ianunwin.demon.co.uk/eurocode/docmn/ec99/ecmgintr.htm

[6] EPA, U. S., & OW. (2016). *EPA-FDA Fish Advice: Technical Information*. https://www.epa.gov/fish-tech/epa-fda-fish-advice-technical-information

A Review of the Current Education for Children with Attention Deficit and Hyperactivity Disorder and the Effects of COVID-19

Melanie Sun
Mission San Jose High School; Fremont, United States
Email: melaniesuns@gmail.com

Abstract – The education of students with ADHD, one of the most common neurodevelopmental disorders, is a growing concern for many parents and teachers. Affected children often exhibit symptoms of hyperactivity and/or inattentiveness, which make learning in a traditional classroom more difficult. In the United States, there are laws in place to provide them with individualized learning plans that outline any special accommodations or modifications they need. Some parents choose to homeschool their children so that they can receive an even more individualized education. Due to the COVID-19 pandemic and social distancing protocols, these children are unable to receive the level of instruction they need from their teachers. The symptoms of the disorder make the transition to distance learning even more difficult than for the typical student, so parents are becoming more involved in the education of their child despite limited resources. However, as there are limits to what parents can provide, it is crucial that additional alternatives are developed so that families in need can be provided for in the future.

Key Words – ADHD, School-aged children, distance learning, COVID-19, homeschooling

INTRODUCTION

Attention deficit and hyperactivity disorder (ADHD) is one of the most common neurodevelopmental disorders. About 9.4 percent of children aged 3-17 in the United States have ever been diagnosed, and approximately one third of affected individuals will continue to experience symptoms as adults [1, 2]. ADHD cannot be tested for in a lab, and diagnoses usually rely on information from parents and teachers and other medical evaluations [3].

Affected individuals are generally recognized by hyperactivity, difficulty staying focused, and impulsive behavior [4, 5]. Based on the symptoms they exhibit, they are categorized as predominantly inattentive type, predominantly hyperactive-impulsive type, or combined type according to the criteria set by The Diagnostic and Statistical Manual of Mental Disorders (DSM-V) [4, 6]. Children who are predominantly inattentive may have difficulty paying attention to details, following directions, staying organized, and remembering their daily schedule [3]. Predominantly hyperactive-impulsive children often find it challenging to stay seated in class or working quietly and may also excessively interrupt others who are speaking [3]. Combined type children exhibit symptoms of both the predominantly inattentive type and the hyperactive-impulsive type [3]. Individuals with ADHD also lack executive functions, including sustained attention, planning and organization, and working memory, which have been shown to determine a student's academic achievement [7].

Studies show that individuals diagnosed with ADHD have a higher mortality rate, are of greater risk for other mental health conditions, and are more likely to be involved in criminal behavior [8]. At school, affected children show academic underachievement, are more likely to repeat a grade or be expelled/suspended, and are 4 to 5 times more likely to require special education services [9].

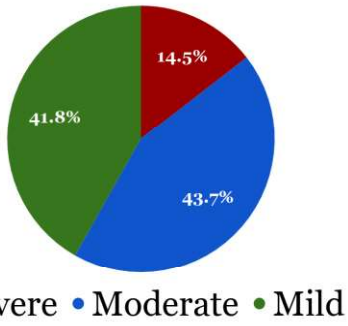

FIGURE 1: Parent-reported Severity of ADHD Symptoms in Children. Data Source: 2016 National Survey of Children's Health

As Figure 1 shows, about 14.5 percent of affected children exhibit severe symptoms, while the majority of children experience mild to moderate symptoms. Although ADHD cannot be cured, the symptoms can be treated with pharmacotherapy and psychotherapeutic interventions [10, 11]. Pharmacotherapy is generally viewed as an essential element for treatment as it is more cost-effective [11]. Some psychotherapeutic interventions include behavioral parent training (BPT), behavioral classroom management (BCM), and organization training [3].

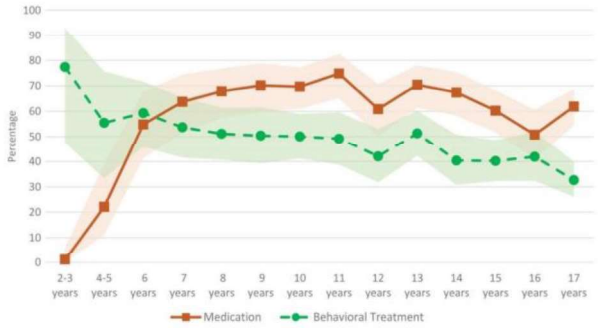

FIGURE 2: Parent-reported treatment types for children and adolescents with ADHD by age. Source: Danielson, Melissa L et al. "Prevalence of Parent-Reported ADHD Diagnosis and Associated Treatment Among U.S. Children and Adolescents, 2016." *Journal of clinical child and adolescent psychology : the official journal for the Society of Clinical Child and Adolescent Psychology, American Psychological Association, Division 53* vol. 47,2 (2018): 199-212.

Figure 2 estimates the types of treatment children with ADHD usually receive at specific ages. As shown by the shaded areas, therapy, rather than medication, is the most common form of treatment for very young children, while school-aged children typically rely on a combination of both medication and behavioral interventions to treat their symptoms.

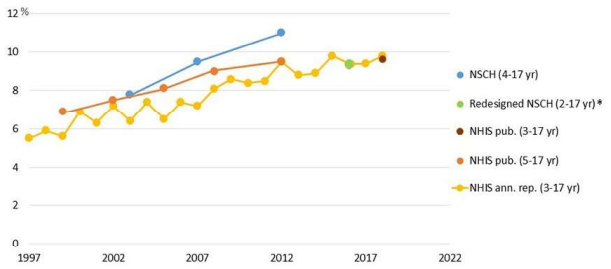

FIGURE 3: Percent of children with a parent-reported ADHD diagnosis Source: CDC. "ADHD Throughout the Years." *Centers for Disease Control and Prevention*, 31 Mar. 2020, www.cdc.gov/ncbddd/adhd/timeline.html.

The increasing prevalence of parent-reported ADHD diagnoses in school-aged children in recent years is depicted in Figure 3. However, it is unknown if this increase is simply due to more children receiving diagnoses or if there is a change in the number of affected children [12]. Furthermore, since the data are parent-reported and is not confirmed by medical professionals, there may be some information bias present [1]. Despite these limitations, it is clear that with this growing trend of diagnosed individuals, it is vital that there are adequate resources available for them. Therefore, the quality of these children's education, which has a large impact on their growth and future, is an increasingly important concern.

CURRENT EDUCATION

Currently, there are two laws in the United States that determine the extent of services and accommodations that children with ADHD receive in traditional schools: the Individuals with Disabilities Education Act (IDEA), and Section 504 under the Rehabilitation Act of 1973 [13]. Alternatively, some parents choose to homeschool their children [7].

I. IDEA and Section 504

Within the 13 categories of disabilities organized by IDEA, children with ADHD are classified as "Other Health Impaired (OHI)" [13]. Before special services can be provided, a group of professionals will observe and assess the child to determine the degree of a child's disability [13]. If a child exhibits symptoms that are severe enough to impair their ability to learn and participate in a traditional classroom environment, they can qualify for an Individualized Education Program (IEP) plan [13]. The document is a personalized plan designed for the student together by teachers, therapists, and parents [13]. It outlines detailed information regarding the student's goals, standardized tests, extracurricular activities, and behavior at school, as well as states any accommodations in the classroom and modifications to the curriculum the student may need to learn [14]. If the child exhibits behavioral issues, professionals can carry out functional behavioral assessment (FBA) to propose interventions included in the IEP plan [15]. The process of FBA generally involves a series of tests in which practitioners gather data relevant to the target behaviors by observing the child and interviewing parents or teachers; then, they analyze the data and create individualized intervention strategies [15]. In addition to special education, the IEP plan also provides services outside of the school setting, such as speech therapy [16].

The 504 plan is similar to an IEP plan, but it provides for individuals who do not exhibit symptoms severe enough to qualify for an IEP plan, and is more common for children diagnosed with ADHD [13]. Under the less formal 504 Plan, children remain in the classroom environment with special accommodations, and special education services outside of school are not provided [13].

Due to the nature of IDEA, a family's economic status has a large effect on the amount of benefits a child can receive [17]. The act is heavily reliant on a parent's ability to advocate for their child and be vocal about the services their child requires, and working, low-income parents often do not have the time or money to do so [17]. Furthermore, schools in underprivileged communities lack adequate resources and are unable to provide their students with the same level of services as those available at wealthy schools [17]. As a result, the teachers at these schools, who are often inexperienced and burdened by heavy workloads, have greater difficulty developing elaborate IEP plans and ensuring that the needs of all of the students are met [17].

II. Common Accommodations and Services

Both IEP and 504 plans can provide children with ADHD with accommodations inside the classroom if it is necessary for a child [13, 14]. Accommodations vary based on the individual student's needs, but common interventions include additional time to take tests, more detailed instructions for assignments, special seating away from distractions, specific cues to increase focus during lessons, and encouraging cooperative behavior [13, 14, 18].

Children with ADHD may also receive behavioral therapy in the classroom [3, 19]. Behavioral classroom management is an evidence-based program that focuses on and supports a child's positive behaviors [19]. By managing the classroom in an orderly manner and setting clear expectations for the child, the process has shown to decrease the frequency of negative behaviors, promote student engagement, and enhance the social and emotional learning of the child [19]. Through organizational skills training, children can learn essential time management and planning skills that can help them enhance their school performance and social ability [20]. Teachers can encourage target behaviors by rewarding a student when they are more organized than usual. They can also utilize checklists and schedules to help the child manage their assignments and allocate their time wisely [20].

III. Homeschooled Students

One of the reasons parents choose to homeschool their children is if they feel that the needs of their children are not adequately addressed at a traditional school [7, 21]. By homeschooling their children, parents can be certain that the needs of their children are met [7, 21]. Each state has its own set of requirements for parents who wish to homeschool their children, which can range from a high school diploma to a teacher's certificate, so any legal issues must first be clarified before homeschooling can begin [21]. The educational setting varies between each family, but it is certain that homeschooled students with ADHD receive an education that is heavily focused on individualized learning and caters to their specific needs [7, 21].

Homeschoolers may decide to hire a teacher who will design a curriculum similar to that of a conventional school, or they may allow their children to follow a student-led curriculum in which they choose what they want to learn and focus on real-world experiences [7]. However, most families decide to employ a balanced curriculum that contains aspects of each of these two more extreme situations [7]. For example, a parent could teach their child the majority of subjects and hire a professional to teach the more advanced courses [21]. In the case of working parents, they usually provide resources such as workbooks or recorded lessons to their child, who is trusted to complete their work with little supervision [21]. Oftentimes, parents keep in contact with the school that their children would regularly be attending and are able to receive access to certain facilities provided by the school [21].

The learning experience for homeschooled students with ADHD is entirely personalized to meet their needs [7, 21]. The lack of restrictions results in an individualized and flexible learning environment [7, 21]. As long as the student is able to focus, teaching can be done almost anywhere: in parks, on a car ride, or even on a trampoline [21]. A 2018 interview conducted by Melissa Felkins at Walden University recorded the experiences of homeschooled students with ADHD [7]. One student ADHD stated that she could learn at her own pace and the flexibility of her schedule allowed her to have time to herself and focus on other activities [7]. Furthermore, several students stated that they had access to resources and tools that are normally prohibited in traditional learning environments [7]. For example, a student shared that she understood material better when she drew her notes rather than writing them down, but this method is not likely to be approved by teachers in conventional schools. [7]. Outside the home setting, the students had social interactions based on their own social needs and could participate in extracurricular activities [7].

Despite the individualized learning that homeschooling provides, it is a concern that parents may not be able to recognize crucial development milestones in their children and fail to realize when their children are behind in their learning [7]. In this case, homeschooled children with ADHD may receive behavioral treatment, which is more effective the earlier it is carried out, later than children who are observed on a daily basis by trained professionals [7].

THE EFFECTS OF COVID-19

As a result of the COVID-19 pandemic, children with ADHD who attend traditional schools need to adapt to distance learning from home with limited support from special education services [16, 22]. Although the special circumstances pose challenges for these families, parents are stepping in to provide for their children to the best of their abilities [23].

I. The Obstacles to Learning

In a questions and answers document released in March 2020 by the United States Department of Education, it was stated that IDEA, Section 504, and other laws "do not address a situation in which elementary and secondary schools are closed for an extended period of time" [24]. The document claims that if schools do not provide instruction to the general student population, they are not required to do so for special education students [24]. Likewise, schools that continue to provide services to the general student population are required to provide for special education students as well [24]. If a school closes, the IEP and Section 504 team are required to determine the services the child requires, but it is not mandatory for them to design distance learning plans [24]. Public schools that continue instruction are required to

determine the method of distance learning they wish to implement for special education students based on the resources that are available to them [24].

As a result of distance learning, children lack contact with their teachers and face-to-face interaction with their peers [7, 16, 22]. Students with hyperactive-type ADHD who already experience difficulties staying on task and organized due to the symptoms of the disorder may find that it is even more challenging to concentrate on their schoolwork and allocate their time accordingly due to distractions in their home environment and a lack of structure in the day [5, 16]. Since it is already difficult for these students to follow directions given by teachers face-to-face, instructions given virtually may be an even more challenging for them to understand [25]. As a result of these changes, children are under increased levels of stress and require additional support from those around them [16, 25]. In addition, there is a concern that special education students, which include children with ADHD, will have regressed in their learning and social ability when they return to an educational setting due to an extended period of time away from their instructors and peers [22].

Several special education teachers overcame some of the difficulties that came with transitioning to online learning, though the process required additional effort and compromise from all of the parties involved [22]. With the help of either the Zoom or the Google Classroom programs, teachers were able to spend time with their students virtually on a daily basis [22]. The instructors also guided parents in ways that they can teach the students and become more involved in their learning [22].

II. Recommendations for Parents

During these difficult times, parents are providing additional support to their children, and their role in their children's education is becoming even more prominent. Parents are encouraged to communicate with teachers and ask questions frequently [25]. At home, a quiet workspace away from toys and other distractions is recommended for children so that they can focus on learning [26]. Since children with ADHD have shorter attention spans, the time period set for learning is to be kept short (45 minutes) and the goals for each period should be clearly set [25]. Experts suggest that ideally, a child's positive performance is reinforced with specific feedback that identifies the correct behaviors [16, 25]. For example, it is more beneficial for a child if their parent says "good job putting your books back in the drawer," rather than "good job today." [25] It is also recommended for parents to encourage physical activity throughout the day, which can help ease a child's symptoms of hyperactivity and reduce stress [16, 25].

FIGURE 4: An example of a visual schedule by the Centers for Disease Control and Prevention Source: *Creating Structure*. 2020, www.cdc.gov/parents/essentials/activities/activities-structure.html.

A visible schedule, as shown in Figure 4, can be created for the child so that each day is well-structured and available time can be allocated in an organized manner [16, 26]. The checkboxes allow the student to keep track of their progress throughout the day and marking completed tasks can give them a sense of fulfillment [26].

III. The Limitations of Parent Involvement

Even if parents are doing their utmost to assist their children and become more involved in their learning, it is difficult for them to be able to provide support on the level of professionals. It is also important to consider that many parents, especially those in low-income families, may not have the time or resources to be able to step into a teacher's role [22]. Parents who work at home are able to assist their child with learning to a greater extent, but others who need to leave for work cannot provide that degree of support. In an interview conducted by Courtney Norris at PBS News in April 2020, parents of children with special needs shared their experiences with distance learning [23]. They expressed their concerns about the quality of education that they are able to provide to their children with the limited resources available to them [23]. Some felt that the schools are not addressing the needs of children with disabilities and were burdened because they believed that stepping into the role of multiple professionals at once is beyond their capabilities [23]. Parent Erin Croyle expressed her frustration, stating: "I try to do a schedule, and I try to get something to happen every day. And, every day, I feel like a failure" [23].

IMPLICATIONS

Regardless of whether children with ADHD attend conventional schools or are homeschooled, it is clear that the adults around them strive to support the children in what they believe to be the best ways possible. Although IEP and 504 plans are created considering the specific needs of each child, they have several limitations. The circumstances of families of lower socioeconomic status are not accounted for, so those children cannot receive the full benefits of the laws that govern special education. Furthermore, homeschooling children provides a level of individualization that traditional schools cannot reach. With homeschooling, students can be provided further and more flexible accommodations that suit their personal way of learning. For example, homeschooled students may choose to start learning later in the day if they feel that they can concentrate better during those times, while children at traditional schools need to follow the schedule set by the school. The personalization of learning and the wide variety of tools available that homeschooling provides is especially beneficial for students with ADHD because of how differently the disorder affects each individual. However, as homeschooling a child requires a lot of work from parents, it is not a realistic option for working parents with young children. Parents may be able to trust that older students finish their work on a daily basis, but it is unreasonable to expect a young child to do the same. As mentioned earlier, homeschoolers may not be able to identify if their children are learning at the same pace as other children of the same age, and for a working parent who spends even less time with their child, it may be even harder to notice these subtle differences.

As many parents develop their own strategies to support their children during the COVID-19 pandemic despite limited guidance from schools, it is possible that homeschooling children with ADHD could become a more popular option for families who have the capability to do so and are confident in their abilities. Students who were previously homeschooled before the pandemic may not need to cope with as many changes as those attending traditional schools, and may find that their learning is not as negatively impacted. Still, for many parents, homeschooling their children may have simply be a last resort due to current circumstances because they feel that they are not experienced enough to be solely responsible for the education of their children.

As social distancing protocols are lifted in certain parts of the United States and children return to schools, some teachers are able to continue instructing students in traditional classroom environments. Nonetheless, it is critical that special education organizations are ready to provide concerned families with solutions and essential resources to ensure that children with special needs can have the quality of education that they deserve during this pandemic and other emergencies that could possibly occur in the future.

CONCLUSION

With the increasing number of ADHD diagnoses, it is crucial that affected children are able to receive an education that addresses their needs. Although the symptoms of the disorder pose many challenges for them as they learn and build skills essential for their well-being, the individualization of their education, whether it is in the form of accommodations at traditional schools or homeschooling, gives them the opportunity to grow alongside their peers. However, students in less fortunate communities often encounter a lack of resources, which shows how much educational opportunities can vary between special education children protected under the same laws. Distance learning during the COVID-19 pandemic further reveals the challenges that children with ADHD face as they struggle to adapt to unfamiliar schedules and different learning environments. Even as parents and teachers seek to provide students with support and resources to the best of their abilities, it is evident from the concerns of parents that there is a lack of guidance for families of affected students.

There are several limitations to the information presented in this paper. As mentioned before, the majority of statistical data relies on parent-reports and therefore may be subject to information bias. Additionally, this paper generally focuses on the positive aspects of homeschooling and fails to consider students who may not have found the homeschooling experience to be as enjoyable. The included interviews of homeschooled ADHD students and parents of special education students are not accurate representations of those populations as a whole because of the small number of individuals being interviewed and the fact that the interviewees had the option to not participate. Furthermore, the recommendations for parents presented in this paper, despite being suggested by professionals, may not be applicable to every single child with ADHD due to how much the symptoms can vary between individuals.

Regardless of the limitations, it is clear that without an increase in the resources and alternatives available for these families, these difficulties will continue to persist and will arise again during another crisis. There is a necessity for widely-accessible special education services that will adequately support these students through any obstacles they may face now as well as in the future, and for this, the united efforts of educators, special education providers, and parents is key.

ACKNOWLEDGEMENTS

I would like to thank Ms. Kuei for introducing this opportunity to me and for providing guidance throughout the writing process.

REFERENCES

[1] Danielson, Melissa L et al. "Prevalence of Parent-Reported ADHD Diagnosis and Associated Treatment Among U.S. Children and Adolescents, 2016." *Journal of clinical child and adolescent psychology : the official journal for the Society of Clinical Child and Adolescent Psychology, American Psychological Association, Division 53* vol. 47,2 (2018): 199-212.

[2] "Attention Deficit and Hyperactivity Disorder (ADHD) | Boston Children's Hospital." *Childrenshospital.Org*, 2017, www.childrenshospital.org/conditions-and-treatments/conditions/a/attention-deficit-and-hyperactivity-disorder-adhd.

[3] "Inattention & Hyperactivity (ADHD) - Effective Child Therapy." Effective Child Therapy, 2017. effectivechildtherapy.org/concerns-symptoms-disorders/disorders/inattention-and-hyperactivity-adhd/.

[4] "NIMH » Attention-Deficit/Hyperactivity Disorder (ADHD)." *Nih.Gov*, Nov. 2017, www.nimh.nih.gov/health/statistics/attention-deficit-hyperactivity-disorder-adhd.shtml.

[5] "What Is ADHD?" *Psychiatry.Org*, 2017, www.psychiatry.org/patients-families/adhd/what-is-adhd.

[6] Singh, Ajay, et al. "Overview of Attention Deficit Hyperactivity Disorder in Young Children." *Health Psychology Research*, vol. 3, no. 2, 30 Sept. 2015, www.ncbi.nlm.nih.gov/pmc/articles/PMC4768532/, 10.4081/hpr.2015.2115.

[7] Felkins, Melissa. *ScholarWorks Experiences of Current or Former Homeschool Students Who Report ADHD Symptoms*.

[8] Barbaresi, W. J., et al. "Mortality, ADHD, and Psychosocial Adversity in Adults With Childhood ADHD: A Prospective Study." *PEDIATRICS*, vol. 131, no. 4, 4 Mar. 2013, pp. 637–644, www.ncbi.nlm.nih.gov/pmc/articles/PMC3821174/, 10.1542/peds.2012-2354.

[9] Loe, I. M., and H. M. Feldman. "Academic and Educational Outcomes of Children With ADHD." *Journal of Pediatric Psychology*, vol. 32, no. 6, 28 May 2007, pp. 643–654, academic.oup.com/jpepsy/article/32/6/643/1021192, 10.1093/jpepsy/jsl054.

[10] Hoseini, Bibi, et al. "Attention Deficit Hyperactivity Disorder (ADHD) in Children: A Short Review and Literature." *ADHD in Children International Journal of Pediatrics*, vol. 2, no. 12, 2014, p. 446, ijp.mums.ac.ir/article_3749_9acfec461035c63b00d431b2b03f5b85.pdf.

[11] Vaughan, Brigette S, and Christopher J Kratochvil. "Pharmacotherapy of ADHD in Young Children." *Psychiatry (Edgmont (Pa. : Township))*, vol. 3, no. 8, 2006, pp. 36–45, www.ncbi.nlm.nih.gov/pmc/articles/PMC2957280/.

[12] CDC. "ADHD Throughout the Years." *Centers for Disease Control and Prevention*, 31 Mar. 2020, www.cdc.gov/ncbddd/adhd/timeline.html.

[13] "Is an IEP or 504 Plan Best for Your Child? How to Decide." *ADDitude*, 11 July 2014, www.additudemag.com/iep-step-5-evaluate-your-options/.

[14] Gardner, Amanda. "IEP for Kids With Disabilities." *WebMD*, WebMD, 29 Apr. 2017, www.webmd.com/add-adhd/childhood-adhd/adhd-iep-for-adhd#1-3.

[15] *WWC Intervention Report Children Identified With or At Risk for an Emotional Disturbance Functional Behavioral Assessment-Based Interventions.* 2016.

[16] "ADHD & Learning During COVID-19." *HealthyChildren.Org*, 2020, www.healthychildren.org/English/health-issues/conditions/COVID-19/Pages/ADHD-and-Learning-During-COVID-19.aspx.

[17] Koseki, M. "Meeting the Needs of All Students: Amending the Idea to Support Special Education Students from Low-Income Households Recommended Citation." *Fordham Urban Law Journal*, vol. 44, 2017, p. 793, ir.lawnet.fordham.edu/cgi/viewcontent.cgi?article=2698&context=ulj.

[18] "20 Classroom Accommodations That Target Common ADHD Challenges." *ADDitude*, 9 June 2009, www.additudemag.com/20-adhd-accommodations-that-work/.

[19] Classroom management module. "Classroom Management Module." *Https://Www.Apa.Org*, 2010, www.apa.org/education/k12/modules-classroom-management.

[20] Langberg, Joshua M, et al. "Organizational-Skills Interventions in the Treatment of ADHD." *ResearchGate*, Expert Reviews, Nov. 2008, www.researchgate.net/publication/23392043_Organizational-skills_interventions_in_the_treatment_of_ADHD?enrichId=rgreq-839c63f490e7e221e56540534c5e2bbe-XXX&enrichSource=Y292ZXJQYWdlOzIzMzkyMDQzO0FTOjE4ODA0OTc2MTc3NTYxOUAxNDIxODQ1OTY1Mjgx&el=1_x_3&_esc=publicationCoverPdf.

[21] "Homeschooling LD/ADD Children: Great Idea or Big Mistake? | LD Topics | LD OnLine." *Ldonline.Org*, 2020, www.ldonline.org/article/5917/.

[22] Hill, Faith. "Special Education Goes Remote in the COVID-19 Pandemic." *The Atlantic*, The Atlantic, 18 Apr. 2020, www.theatlantic.com/education/archive/2020/04/special-education-goes-remote-covid-19-pandemic/610231/.

[23] "The Challenge of Distance Learning for Parents of Children with Special Needs." *PBS NewsHour*, PBS NewsHour, 29 Apr. 2020, www.pbs.org/newshour/show/the-challenge-of-distance-learning-for-parents-of-children-with-special-needs.

[24] *QUESTIONS AND ANSWERS ON PROVIDING SERVICES TO CHILDREN WITH DISABILITIES DURING THE CORONAVIRUS DISEASE 2019 OUTBREAK*. 2020.

[25] "Support for Kids With ADHD During the Coronavirus Crisis | Child Mind Institute." *Child Mind Institute*, 7 May 2020, childmind.org/article/giving-kids-with-adhd-support-and-structure-during-the-coronavirus-crisis/.

[26] "Cook Children's Health Care System." *Cook Children's Health Care System*, 2019, cookchildrens.org/coronavirus/resources/special-needs/Pages/homeschooling-adhd.aspx.

The Effects of Demographics on Political Party Affiliation in American High School Students

Daniela Tejada and Katie Stewart
Pine Crest School; Fort Lauderdale, United States
Email: katie.stewart@pinecrest.edu and daniela.tejada@pinecrest.edu

Abstract - This study analyzes the relationship between demographic factors and political party affiliation in America, and how the addition of American youth to the voting population could possibly change political trends. This study administered an anonymous electronic survey to American high school students in grades nine through twelve, with a qualifier question of never having voted before. Participants were asked demographic identifier questions, including age, race/ethnicity, region, and religion. Participants were asked which political party they aligned with. The survey contained twenty-four questions to identify the participants' alignment with the goals and beliefs of either the Democrat or Republican parties to account for error in the participants' responses to the political affiliation question. The survey questions used a Likert scale, where participants were assigned a score based on their responses. The independent variable of this study was demographics, with the goal being to find its possible connection to political party affiliation, the dependent variable. The results of the survey demonstrated that most minority individuals identified with Democrat or Democrat-leaning ideals. Based on the results, it was concluded that the next political trend will have more Democrat/Democrat-leaning citizens, influenced by the rise in minorities and more liberal mindsets in American youth.

Key Words - Demographics, Politics, High School, Ethnicity

INTRODUCTION

Due to controversy and quickly changing demographics, the political environment in America has been transformed in recent years. America's youth has exhibited a more liberal mindset than older generations, while immigration has also been rising at an exponential rate, adding to the rapidly developing changes in America's political environment (Itkowitz, 2019). This study analyzes how these factors correlate with political party affiliation in America and how the addition of American youth to the voting population could possibly impact political trends in the country.

I. Demographics in the United States

An article by the Harvard Kennedy School Institute of Politics, "Race and Ethnicity Still Play a Role in Political Attitudes," notes that there is a young voter disparity between racial groups for the past 30 years, specifically whites and African Americans (Harvard Kennedy School Institute of Politics, n.d). In an analysis of President Obama's approval ratings, no demographic factor, such as gender, age, religion, or education, was as strong in determining support as race, with his highest support coming from African Americans (Harvard Kennedy School Institute of Politics, n.d). However, Gallup published an article by Frank Newport, a senior scientist with a doctorate in sociology, showing that non-Hispanic whites have generally controlled the political sphere, with the largest percentage in every party (Newport, 2012). When taking population numbers into account, the largest percentage of whites affiliate themselves with the Republican party, while minorities tend to align with the Democratic Party, except for Hispanics, who identify with the Independent Party (Newport, 2012). This demonstrates that although minorities almost all vote for non-Republican parties, whites still have a larger impact on politics in the country. This analysis calls into question how the support for political parties might change, as according to senior demographers Kevin M. Pollard and William O'Hare,"by the middle of the 21st century, non-Hispanic whites will make up a slim and fading majority of Americans" (Pollard & O'Hare, 1999, para. 1).

II. Influences on the Political Behaviors of Minorities

"A Deep Dive Into Party Affiliation: Sharp Differences by Race, Gender, Generation, Education," a Pew Research study, shows the political alignment trends of various groups, by analyzing religion, race, and age as factors (Pew Research Center, 2015). This article further solidified the concept that race and ethnicity have a large impact on political party affiliation, with minorities staunchly supporting both the Democratic and Independent Party instead of the Republican Party, which continues to be mainly supported by the non-Hispanic white majority. Additionally, it notes that younger generations typically tend to lean more Democratic than their predecessors, such as the Silent Generation, consisting of individuals born between 1925 and 1945 (Pew Research Center, 2015).

Aida Just, an associate professor of political science at Bilkent University in Turkey, highlights the various factors contributing to the political behavior of individuals belonging to a minority group in the United States (U.S.). Just notes how ethnic groups tend to stick together and support their group's goals, especially in times when information is short or they perceive a lack of equal opportunity (Just, 2017). Additionally, Just writes that some minority individuals vote for a party with more ethnic officials, simply because they feel represented. If this is the case, it can be assumed that an influx of minority groups into the country may affect the results of votes, with some officials getting elected simply because minority groups feel represented by them (Just, 2017), a concept relating to social interest, defined as "the more you can relate to the sameness you share with someone else, the more belongingness you can feel" (MacMahon, 1997, p. 4). Finally, in a study by Pippa Norris and Robert Mattes on how ethnicity affects political party alignment, it was concluded that ethnicity did affect party affiliation in 12 African nations (Mattes & Norris, 2003), which this study hypothesizes will also be the case in America.

III. Possible Future Effects of Demographics on Political Behavior

It was hypothesized that support for the Democratic Party will increase once the current American youth reaches voting age, due to demographic factors. It is believed that the new wave of liberalism in American youth and the rising diversity in the country due to immigration will further boost the party's support. African Americans are predicted to continue on the current trend of voting for the Democratic party, regardless of socioeconomic standing or education, since the party has traditionally supported the ethnic group's values. Additionally, the majority of whites in high socioeconomic brackets or low education will continue voting for the Republican party. However, it is hypothesized that LatinX/Hispanic groups will move their support towards the Democratic Party in light of anti-immigrant/anti-Hispanic sentiments rising from the Republican Party and incumbent President.

America's political environment has been predominantly controlled by the white population. With the demographic makeup in America rapidly changing, the question of how politics will evolve as more minorities join the voting pool is of interest. Newport states that "the independent and Democratic segments of the U.S. population are now less white than they were in 2008, reflecting the uptick in the U.S. nonwhite population over these five years" (Newport, 2018, para. 12). Data from the U.S. Census Bureau shows that the proportion of U.S. children who are immigrants has grown, with the majority of this increase coming from second-generation immigrants, which have risen nine percent from 1994 to 2017 (Child Trends, 2018). In her analysis, Just states that " [by] being born in [the] host country, second-generation immigrants feel more entitled to equal treatment than their foreign-born parents, and therefore become more involved in politics than either foreign-born individuals or subsequent immigration generations" (Just, 2017, para. 40).

A graph by Pew Research Center illustrates that African Americans overwhelmingly align with the Democratic Party, with 64% supporting the party. The graph indicates that many minority groups tend to support the Democratic party, regardless of socioeconomic status or education. This trend, however, is not reflected in the white population, with the majority tilting Republican, especially those of lower socioeconomic status and education (Pew Research Center, 2015). Taking these factors into account, it is only logical to assume that political trends in America will shift as the demographic groups who are voting undergo a drastic change.

METHODS

This study was conducted by administering an anonymous electronic survey to American high school students in grades nine through twelve under the age of 18. Prior to beginning the survey, all participants were required to sign a consent form explaining possible risks and removing their obligation to participate at any time if they so desired. The first questions were about voting status and age. If the participant was under the age of 18 and had never voted before, then they qualified to partake in the study.

Following the qualifiers, there were five questions about religion, ethnicity, and inhabited region with the purpose of identifying the demographic information of the participants, while also identifying any potential extraneous variables that could influence political party affiliation. Using the example of two Pew Research Center Political Typology Quizzes, a list of 24 questions were created to identify an individual's political affiliation.

In this study, the independent variable was demographics, with the goal being finding its connection to political party affiliation, the dependent variable. Besides explicitly asking for a participant's political affiliation near the beginning of the survey, the questions were geared towards identifying whether participants aligned with the goals of certain parties, aiding to eliminate possible bias, misconception, or conformity.

The majority of the questions used a Likert scale comprising of *strongly agree*, *agree*, *disagree*, and *strongly disagree* with no opportunity to stay neutral. Respondents were sorted into Democratic, Democratic Leaning, Republican-leaning, and Republican groups. The participant's group was decided using the scale where a strongly agree on a Democrat identifier question earned a score of four points, three points for agree, two for disagree, and one for strongly disagree. In terms of Republican identifier questions, a strongly agree earned one point, agree earned two points, disagree earned three, and finally strongly disagree earned four. The range of possible points was from 24 to 96. A response score between 24 to 42 points classified as Republican, 43 to 60 classified as Republican-leaning, 61 to 78 classified as Democrat-leaning, and 79 to 96 classified

as Democrat. These groups were then cross checked with the demographics of the participants to identify whether a correlation existed. Following the political party affiliation questions, there were also two questions asking participants whether they were planning to vote in the 2020 Election, and if so, for which candidate, trying to further identify the next possible voting trend in America's youth.

RESULTS

After evaluating participant data, the participants were grouped into two categories, Republican/Republican-leaning and Democrat/Democrat-leaning. Figures five, six, and seven show questions from the survey corresponding with liberal social views.

Besides being sorted into groups based on political affiliation, the participants were also grouped based on ethnicity, religion, and region to analyze possible trends. In terms of religion, all unaffiliated/none, Atheist, Hindu, Protestant, and Muslim/Islamic participants identified as fully Democrat or Democrat-Leaning. The other religions were more mixed. However, almost all groups identified as mostly Democrat, with the Jewish participants having only seven Republican/Republican-leaning members out of a group of 40. The Christian and Catholic groups showed similar results, with only seven out of 24 participants identifying as Republican or Republican-leaning. Finally, the Eastern Orthodox and Buddhist groups were predominantly Republican/Republican-leaning, with the only Buddhist participant being Republican-leaning and two out of three Eastern Orthodox participants being Republican-leaning.

As seen in figure four, the researchers also accounted for the four regions in the United States, however, the majority of the participants came from the South. All of the seven participants from the Midwest identified as Democrat or Democrat-leaning, all but one out of eight participants in the Northeast identified as Democrat or Democrat-leaning, and the two participants from the West were one Democrat-leaning and one Republican-leaning. Finally, the results from the South were mixed, but the majority identified as Democrat or Democrat-leaning, and only 16 out of 70 participants identified as Republican or Republican-leaning.

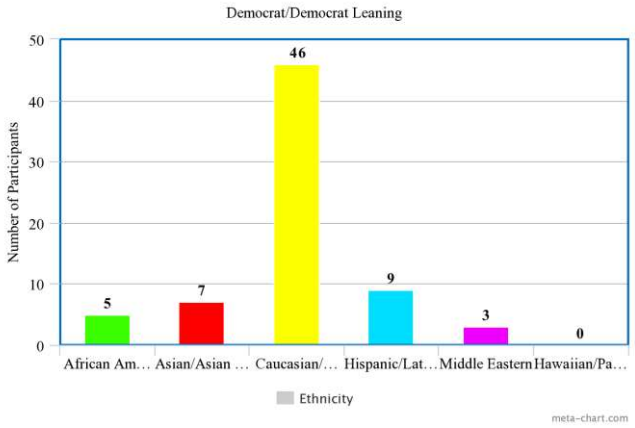

FIGURE 1: The number of participants who aligned Democrat or Democrat-Leaning alongside ethnicity.

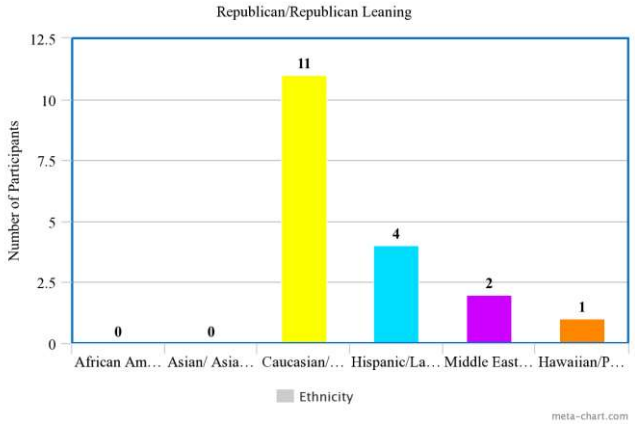

FIGURE 2: The number of participants who aligned Republican or Republican-Leaning alongside ethnicity.

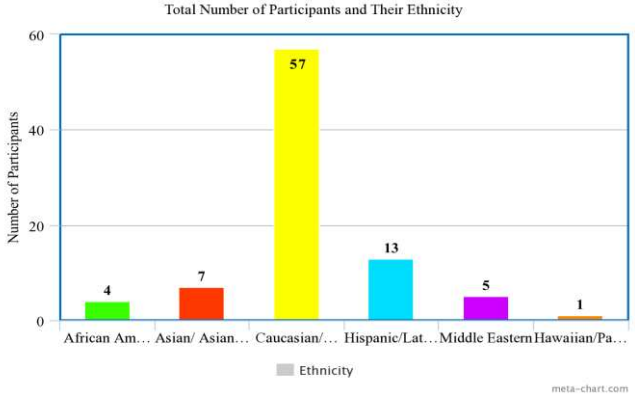

FIGURE 3: Total amount of participants per ethnicity.

Region	Democrat/Democrat-leaning	Republican/Republican-leaning
Midwest	7	0
Northeast	7	1
South	54	16
West	1	1

FIGURE 4: Number of Democrat/Democrat-leaning versus Republican/Republican-leaning participants based on region.

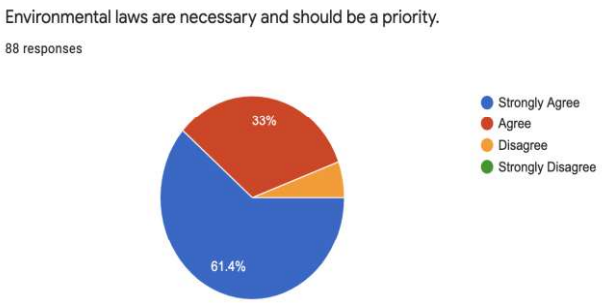

FIGURE 5: A question from the survey that shows liberal social views concerning environmental regulations.

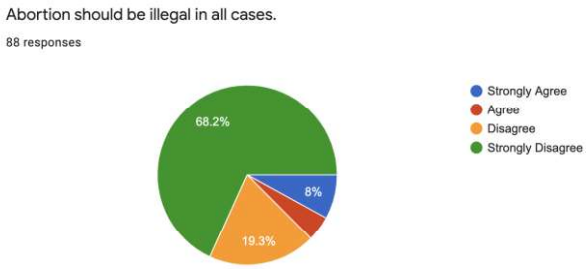

FIGURE 6: A question from the survey that shows liberal social views concerning abortion.

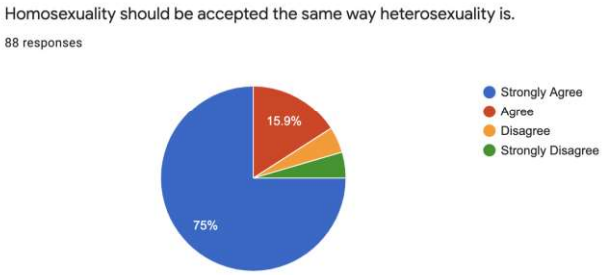

FIGURE 7: A question from the survey that shows liberal social views concerning acceptance of homosexuality.

CONCLUSION

Based on the results, it was implied that the next political trend will have more Democrat/Democrat-leaning citizens due to the rise in minorities and more liberal mindsets in American youth. In terms of region or religion, the data showed that it did not have a major effect on political affiliation, as the results varied widely for both categories. When it comes to region, due to the anonymous nature of the study, the precise location of the participants was unknown, with their broader region being the only identifier for location.

The ethnicity grouping, however, showed much more correlation to political affiliation, with the data showing minorities such as African-Americans and Asian-Americans all aligned with Democrat or Democrat-leaning ideals. According to Pew Research study, "A Deep Dive Into Party Affiliation: Sharp Differences by Race, Gender, Generation, Education," eighty percent of African-Americans lean Democratically, which is reflected in the data collected by this study and further illustrates the tendency for African-Americans to align with the Democratic Party. Additionally, many participants who marked themselves as Republican in the preliminary identifier questions actually aligned with many liberal social views, causing their score from the survey to push them into the Democrat-leaning group. Overall, even regardless of ethnicity, the majority of the participants identified as Democrat or Democrat-leaning, showing that there is a possibility of a new political trend in America.

As seen in Figure one, all four of the African-American participants were either Democrat or Democrat-leaning, with none affiliating with the Republican party. These findings from the study correlate with previous research, as both a graph from Pew Research and an article by Frank Newport, published on Gallup, showed that minority groups, especially African-Americans, tend to align with Democratic ideals. This idea that minorities generally identify with the Democratic Party is further reinforced by data from figures one and two, which show that in each minority group, the majority of participants are Democratically aligned, with all seven Asian/Asian-American participants, nine out of thirteen Hispanic/LatinX participants, and three out of five Middle Eastern participants aligning with the party. The only minority group opposing the norm was the Hawaiian/Pacific Islander group, where the only participant aligned with the Republican party. This result, however, was attributed to a lack of sample size, as there was only one participant identifying with the Hawaiian/Pacific Islander ethnicity group.

In figures five, six, and seven, it is observed that liberal social views are shared between the majority of participants, regardless of political affiliation. These liberal social views, such as an emphasis on environmental regulations, acceptance of homosexuality, and pro-choice sentiment, although generally held by the Democratic party, appeared in the study's result to be shared amongst the majority of participants. Figure five demonstrates that 94.4 percent of participants either strongly agree or agree that environmental laws should be a priority. Figure six further reinforces this concept of growing liberal views, with 87.5 percent of participants believing that abortion should be legal in all cases. Finally, figure seven shows that 90.9 percent of participants believe that homosexuality should be accepted the same way as heterosexuality, once again driving home the point that American high school students are shying away from more conservative views held by Republicans and older individuals. Overall, eighteen out of eighty-seven participants aligned as either Republican or Republican-leaning, an approximate 20.7 percent. However, a large amount of these participants agreed with typically Democratic ideals, illustrating that the American youth appears to share more liberal social views, regardless of political affiliation.

The findings of this study showed that there is a movement towards more liberal social views by American high school students. This movement could mean a large change in future voting trends, as it appears that the American youth who are soon to be eligible to vote hold much more liberal social views and tend to lean more Democratically than their predecessors. With this in mind, the Democratic Party may be receiving more votes from American youth, overthrowing the relative balance that currently exists between the Republican and Democratic parties. With an election coming up soon, this potential new voting trend may present an advantage to the Democratic Party, as even Republican-aligned youth tend to hold typically Democratic ideals that may sway them to vote for a candidate of the opposing party.

FUTURE APPLICATIONS

Due to the nature of the course in which this study was conducted, there were a variety of time constraints that limited the timeframe in which data could be collected. Additionally, this study had no funding, as it was conducted in a high school classroom setting. The constraints of the course made the dissemination of the survey to a wider sample size difficult, however, the researchers were able to account for the four regions of the United States and a wide variety of ethnic groups.

Future researchers should consider methods to expand the sample size of such a study, including the possible addition of a financial motive for participants. Furthermore, in order to collect a larger array of data, the researchers encourage keeping the survey open for responses for a longer period of time.

Regardless of the limitations of this study, the researchers believe that the sample size of nearly 100 participants from across the United States was sufficient to make a conclusion about the possible future trends in American political party affiliation.

REFERENCES

[1] Abadi, M. (2018, May 10). Even the US government can't agree on how to divide up the states into regions. Retrieved from https://www.businessinsider.com/regions-of-united-states-2018-5#but-thats-not-the-only-way-to-divide-up-the-country-several-federal-agencies-use-this-map-of-the-10-standard-federal-regions-drawn-up-by-the-office-of-management-and-budget-5.

[2] Child Trends. (2018). *Immigrant Children* [Article]. Retrieved from https://www.childtrends.org/indicators/immigrant-children

[3] Gerber, A. S., Huber, G. A., & Washington, E. (2010). Party Affiliation, Partisanship, and Political Beliefs: A Field Experiment. Retrieved from https://www.jstor.org/stable/40982894?seq=3#metadata_info_tab_contents

[4] Harvard Kennedy School Institute of Politics. (2019). *Race and Ethnicity Still Play a Role In Political Attitudes* [Article]. Retrieved from https://iop.harvard.edu/race-and-ethnicity-still-play-role-political-attitudes

[5] Itkowitz, C. (2019, January 17). The next generation of voters is more liberal, more inclusive and believes in government. Retrieved from https://www.washingtonpost.com/politics/2019/01/17/next-generation-voters-are-more-liberal-more-inclusive-believe-government/.

[6] Just, A. (2017, May 16). Race, Ethnicity, and Political Behavior. Retrieved from https://oxfordre.com/politics/view/10.1093/acrefore/9780190228637.001.0001/acrefore-9780190228637-e-238

[7] MacMahon, S. (1997). *The Portable Therapist*. Istanbul: Ilhan yayinevi. Mcl

[8] Mcleod, S. (1970, January 1). Likert Scale Definition, Examples and Analysis. Retrieved from https://www.simplypsychology.org/likert-scale.html

[9] Newport, F. (2013, February 8). Democrats Racially Diverse; Republicans Mostly White. Retrieved from https://news.gallup.com/poll/160373/democrats-racially-diverse-republicans-mostly-white.aspx-mostly-white.aspx

[10] Norris, P., & Mattes, R. (2003). Does Ethnicity Determine Support for the Governing Party? The Structural and Attitudinal Basis of Partisan Identification in 12 African Nations. *SSRN Electronic Journal*. doi: 10.2139/ssrn.385209

[11]Pew Research Center. (2015). *A Deep Dive Into Party Affiliation*: *Sharp Differences by Race, Gender, Generation, Education* [Article]. Retrieved from https://www.people-press.org/2015/04/07/a-deep-dive-into-party-affiliation/

[12]Pew Research Center. (2016). *Political Party Quiz* Quiz]. Retrieved from https://www.people-press.org/quiz/political-party-quiz/

[13] Pew Research Center. (2017). *Political Typology Quiz* [Quiz]. Retrieved from https://www.people-press.org/quiz/political-typology/

[14]Pew Research Center. (2019). *Religion & Public Life*. Retrieved from https://www.pewforum.org/religious-landscape-study/

[15] Pollard, K. M., & O'Hare, W. P. (1999, September 1). America's Racial and Ethnic Minorities. Retrieved from https://www.prb.org/americasracialandethnicminorities/

[16] Price, P. C., Jhangiani, R. S., Chiang, I.-C. A., Leighton, D. C., & Cuttler, C. (2017, August 21). Overview of Survey Research. Retrieved from https://opentext.wsu.edu/carriecuttler/chapter/7-1-overview-of-survey-research/

PyITA: A Taylor Expansion-Based Data Augmentation Program for ANN Potentials Applied to TiO_2

Zhengbo Xiang
American School in Japan; Tokyo, Japan
Email: 21xiangz@asij.ac.jp

Abstract – The efficiency of Artificial Neural Network (ANN) potentials enables the modeling of materials at scales that are too computationally expensive for conventional first-principles approaches. However, the force and energy-prediction accuracy of ANNs are generally limited by the availability of training data and training hours. The enlistment of more efficient training methods can partially mitigate this limitation. In this paper, I demonstrate the capabilities of my new Python program, PyITA, which executes a recently demonstrated Taylor expansion-based data augmentation technique[11]. Using my program, I was able to evaluate the powerful methodology by constructing and comparing ANN potentials for the chemical species titania (TiO_2). I compared the error distributions of the augmented potentials with that of the non-augmented potentials. Potentials were trained on both a large (7815 structures) and a small (500 structures) dataset. I ultimately found insufficient evidence to confirm that the data augmentation method is effective for increasing the accuracy of either force predictions or energy predictions on either dataset.

Key Words – Materials Informatics, Artificial Neural Networks, Machine Learning

INTRODUCTION

I. Background

Atomistic simulations are crucial to an informatics approach to materials science. Thanks to their extraordinary accuracy, *first principles*-based quantum mechanical modelling is often used to yield potentials that are crucial to the study of material characteristics[1,2]. For instance, Density Functional Theory (DFT) calculations rely on a very accurate approximation of the many-body Schrodinger equations[3]. DFT has been applied to the study of superconductivity[4], magnetism[5], and phase-change materials[6]. Owing to its flexibility and accuracy, it is a powerful tool.

However, even DFT can be too computationally expensive and impractical for the study of certain complex materials and interfaces[7]. Increasingly, ANNs trained on reliable data (such as DFT calculations) are used to predict material properties instead[7,8,9,10]. Critically, the difficulty of ANN potential training scales linearly with the number of atoms in the training set. In contrast, the difficulty of DFT calculations often scales cubically, quartically, or even quintically with structure size. As such, ANN potentials can be applied to systems that are too large to be practically modelled by DFT calculations.

Despite their advantages over first principles-based methods, the training of sufficiently accurate ANN potentials is often hampered by the limited availability of sufficiently large datasets. Data augmentation allows us to enhance limited training datasets, improving the data-efficiency/effectiveness of ANN training models. Advances in data augmentation techniques will reduce the research cost of future studies in computational materials science.

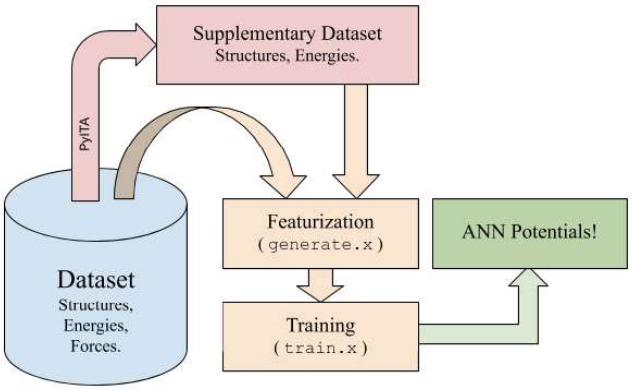

FIGURE 1: This flowchart demonstrates how ANN potentials are constructed with *PyITA*. *PyITA* neither modifies nor replaces preexisting featurization and training methods. Instead, it creates additional input data from the original dataset by modifying copies of pre-existing structures. The supplementary dataset contains all data generated by *PyITA*. In this paper, any reference to an "enhanced", "extended", or "augmented" dataset refers to the set of all structures in the relevant parent and supplementary datasets (ie. the original dataset combined with the supplementary dataset).

II. PyITA & Aenet

Aenet[7] is an open source software package developed by Dr. Artrith and Dr. Urban. In this paper, Aenet was used to perform dataset featurization, conduct neural network training, and produce energy/force predictions.

Aenet contains three notable configuration files, conventionally named `generate.in` (for featurization), `train.in` (for training), and `predict.in` (for prediction). `generate.in` contains the locations (/path/to/file) of every structure file in the training dataset. The training dataset is a collection of XCrySDen-format (`.xsf`) structure files that state the atomic symbols and Cartesian positional coordinates of constituent atoms, the forces acting on each constituent atom (in the +x, +y, and +z directions respectively), and the total structural energies.

Cooper *et al.* demonstrated the incorporation of force information in training via a Taylor expansion as an incredibly new and promising method for increasing the effectiveness of ANN training[11]. The Taylor expansion itself allows us to computationally-efficiently estimate approximate energies of new structures. I independently implemented this method in a now open-source Python program: *PyITA* (Python Implementation of Taylor-expansion for Aenet)[12]. *PyITA* functions as a pre-featurization external data augmentation program (Figure 1).

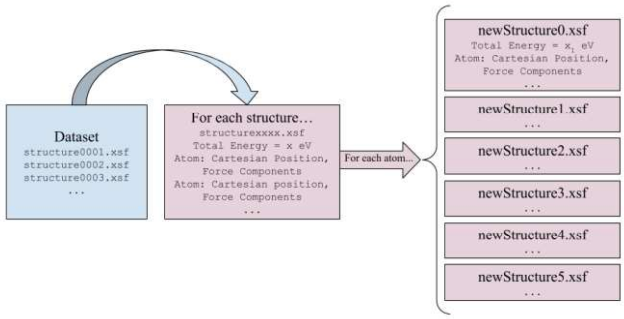

FIGURE 2: Flowchart demonstrating *PyITA*'s creation of additional structures. Six additional structures are created for each atom in each structure in the original dataset until the supplementary dataset reaches a sufficient size (based on user-configured *a*-value).

Force information from structures in the original dataset are used to generate additional approximate structure data (coordinates and energies) near the positions of existing structures. For each atom in any parent structure, *PyITA* can create six additional approximate structures (Figure 2).

After prompting the user for an augmentation-factor *a* (also referred to as the *a*-value in this paper) and a user-configurable displacement constant δ, *PyITA* reads every existing structure (`.xsf`) file in the provided training (parent) dataset into a list. A new structure is created by displacing any atom in any parent structure by δ in one of six directions (+x, +y, +z, -x, -y, -z). *PyITA* does so iteratively, starting from the first atom of the first existing structure and stopping when the number of created structures is equal to the product of *a* and the number of structures in the original dataset. The new structures are written as `.xsf` files in a user-designated directory, effectively forming the supplementary dataset. The file locations of all structures in the supplementary dataset are written to a new `generate.in` file. The original `generate.in` file remains untouched so that additional *PyITA* structures based on the same parent configuration file can be easily created.

Crucially, based on the first-order Taylor expansion demonstrated in Equations 10 and 11 of the *Cooper et al.* paper[11], we approximate the energy of each new structure as the energy of its parent structure subtracted by the product of δ and the component force experienced by the original structure in the direction of the displacement. Algorithmically, atomic displacement in any negative direction is treated as a displacement of equal magnitude in the corresponding positive direction such that $\delta = -\delta_0$.

As this method is essentially a form of data augmentation, I refer to datasets enhanced by *PyITA* as "augmented" in my paper.

III. Approach & Promise

Using *PyITA*, I test the feasibility of the Taylor expansion approach for the efficient training of ANN potentials on TiO_2. The study of TiO_2 is especially valuable because it is a powerful model material with applications in optics, nanotubes research, and photocatalysis. Recently, Xiang *et al.*[12] utilized TiO_2 to demonstrate the application of ANN potentials to the study of the flexoelectric effect.[13] In this paper, I utilize a training dataset containing 7815 TiO_2 structures. Dr. Artrith and Dr. Urban graciously provided this dataset to the public[7].

I hope to aid future research in the field of materials informatics by evaluating a new and potentially more effective method for the training of TiO_2 potentials.

METHODS

Initially, I trained five ANN potentials on a dataset consisting of 500 structures randomly chosen from a 7815-structure dataset. I also trained five additional ANN potentials on a *PyITA*-augmented version of the same 500-structure dataset (δ=0.03 and *a*=6). I assigned Trial Numbers (one through five) to the ANN potentials in each category. I trained each ANN potential to 15 iterations, randomly choosing 10% of each dataset as an independent test set. I configured the ANN architecture to include two hidden layers per atomic species, each with 15 nodes. I used the Limited-Memory Broyden-Fletcher-Goldfarb-Shanno (LM-BFGS)[14] training method, as implemented in Aenet.

I then created two additional potentials. I trained one potential on the entirety of the 7815-structure TiO_2 dataset and another potential on a *PyITA*-augmented version of the full 7815-structure dataset (δ=0.03 and *a*=4). This time, I selected an augmentation factor lower than the earlier *a*=6

value due to computational constraints. However, I preserved the neural network architecture and training configurations of the previously constructed 500-structure potentials.

Finally, the most crucial outcome of the Cooper *et al.* Taylor expansion method is an improvement in the accuracy of force predictions. To test this, I created ten additional ANN potentials: Five trained on the previously discussed 500-structure dataset, and another five trained on an augmented version of said 500-structure dataset. Again, I held the neural network architecture constant.

RESULTS AND DISCUSSION

I computed the relative energy errors for each of the original 500-structure potentials based on data from the independent test sets. I calculated the median relative energy error for the five non-augmented ANN potentials to be approximately 3.27 meV, while the median relative energy error for the five augmented ANN potentials was approximately 4.22 meV. Further, the range of errors on the augmented potential was greater than the range of errors on the non-augmented potential (Figure 3). It appears that the augmentation technique as performed using the current approach failed to improve energy predictions based on the 500-structure datasets.

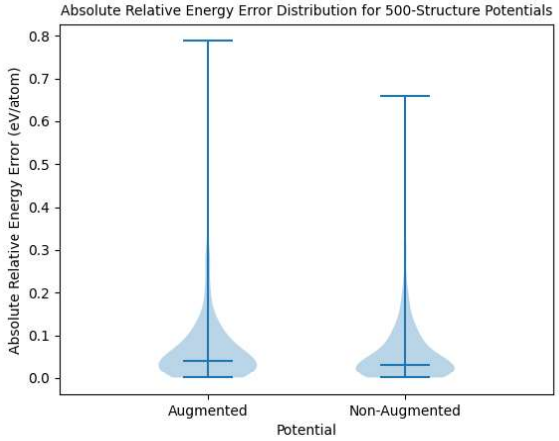

FIGURE 3: The violin plot represents a combination of all five respective potentials of the augmented and non-augmented datasets, as the distributions were computed with the combined validation data (across trials) for each dataset (*e.g.* The "augmented" distribution is constructed from the absolute relative energy errors of predictions by all five potentials based on the augmented dataset). The absolute errors in relative energy were computed with the independent test set. They are defined as the absolute values of the differences between the relative (per-atom) energies of the reference structure (computed by DFT) and the ANN-computed relative energies.

I initially hypothesized that since 500-structure datasets are unusually small for ANN potentials characterizing materials as complex as TiO_2, there may simply not have been a sufficiently diverse set of training data for the potential to yield consistently accurate predictions, regardless of the application of data augmentation techniques. If the structures represented in the training dataset are very similar, the neural network may overfit.

However, augmentation remains apparently ineffective in the 7815-structure potentials. The enhanced 7815-structure potential had a higher median and mean absolute relative energy error than its non-augmented counterpart. However, in contrast with our findings for the 500-structure potentials, the augmented 7815-structure potential yielded absolute relative energy errors with a much smaller range than the non-augmented 7815-structure potential (Figure 4). If future research identifies a decrease in the range of relative energy errors as a consistent feature of our data augmentation technique, *PyITA* could help achieve more robust extrapolation than what is possible with energy-only training.

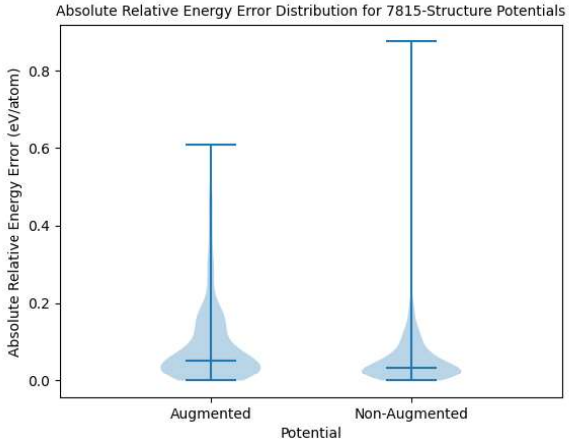

FIGURE 4: This plot demonstrates the distributions of absolute errors in relative energy for the respective augmented and non-augmented potentials trained on the full 7815-structure dataset (Left: Augmented, Right: Non-Augmented). The median absolute error in relative energy for the augmented potential was 5.4 meV, which is noticeably higher than the non-augmented potential's median absolute error of 3.5 meV. However, the augmented potential's error distribution has a noticeably smaller range.

I observed that distribution-features across trials varied greatly for both augmented and non-augmented 500-structure potentials. This variability may also exist in 7815-structure potentials. More trials (potentially with a larger iteration count and a larger independent test set) must be performed to concretely determine the impact of our augmentation technique on the distribution of absolute relative energy errors.

Finally, I calculated the frequency of errors in absolute force for each atom in each structure of the independent test set by subtracting the predicted interatomic forces from the reference (DFT-calculated) interatomic forces in each Cartesian direction. The distribution of absolute errors in force predictions are compared in Figure 5.

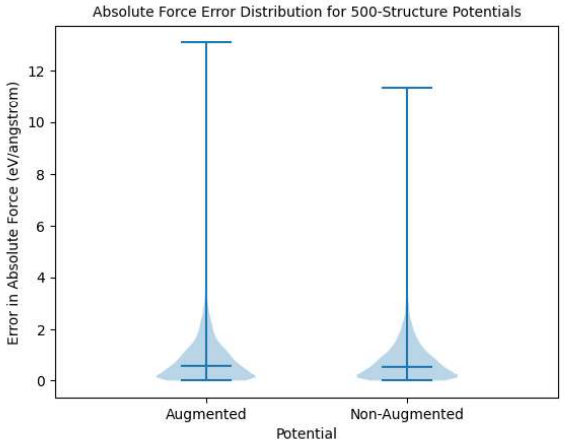

FIGURE 5: This plot demonstrates the distributions of absolute errors in force predictions for the augmented and non-augmented 7815-structure potentials. The median absolute error in force predictions for the augmented potential was marginally higher than that of the non-augmented potential (0.597 eV/Angstrom vs. 0.574 eV/Angstrom). The range of the errors in the augmented potential was also noticeably larger.

CONCLUSION AND FUTURE STUDIES

I have not found sufficient evidence to demonstrate that the Taylor expansion-based data augmentation technique is effective in increasing the accuracy of either force prediction or energy prediction in TiO_2. This does not, however, mean that the technique is not suitable for the study of TiO_2.

After I thoroughly tested my error calculation methodology and closely reviewed the outputs of my error calculation software, I suspect that the problem could be explained by the large variations in accuracy I observed across trials. In other words, due to the constraints presented by my limited access to computational resources, the per-trial variations in the distributions of both energy and force errors were large enough to make it difficult to draw meaningful conclusions.

I strongly suspect that the specific neural network architecture used in my study—especially due to the relatively low number of iterations/epochs—prevented the augmentation technique from being effective. Training to a greater number of iterations leads to better-fitting models, which could result in changes to the size of the training dataset being much more impactful.

It is also possible that the relatively low *a*-values used in my calculations have played a factor. With more time and computational resources, I would be able to determine an attainable "sweet spot": a computationally achievable configuration which noticeably improves my potentials' predictive capabilities.

Finally, my findings may hint to a limitation in the Cooper *et al.* methodology. That is, the first order Taylor expansion-based data augmentation strategy might consistently fail for LM-BFGS ANN potentials that are not trained to a sufficient number of iterations. It is possible that preserving the Cooper *et al.* Taylor expansion to a greater order would be appropriate when training resources are limited, as it would reduce the signal-to-noise ratio of the supplementary dataset. However, this modification might also greatly increase the computational intensiveness of the data augmentation process. Further study would be necessary to confirm this hypothesis.

Materials informatics is a field in its infancy. I eagerly anticipate exciting future research on data augmentation for the development of ANN-potentials.

AKNOWLEDGEMENTS

I would like to extend special thanks to my mentor Dr. Hieu Nguyen for providing me with guidance and affirmation throughout the duration of my research. Further, I wish to especially acknowledge my friend Kylie for helping me debug *PyITA* and its accompanying back-end scripts through many sleepless nights. I express my deepest gratitude to the Aenet team for providing the public with excellent, well-documented, and free software which will continue to greatly accelerate the development of the field of materials informatics. Finally, I appreciate the help I received from Dr. Nongnuch Artrith and the Aenet community through the Aenet mailing list.

REFERENCES

[1] Ward, L., & Wolverton, C. (2017). Atomistic calculations and materials informatics: A review. Current Opinion in Solid State and Materials Science, 21(3), 167–176.

[2] Pokluda, J., Černý, M., Šob, M., & Umeno, Y. (2015). Ab initio calculations of mechanical properties: Methods and applications. Progress in Materials Science, 73, 127–158.

[3] Kryachko, E. S., & Ludeña, E. V. (2014). Density functional theory: Foundations reviewed. Physics Reports, 544(2), 123–239.

[4] Uzunok, H. Y., Zafer, T., Tütüncü, H. M., Karaca, E., Bağcı, S., & Srivastava, G. P. (2020). Probing physical properties and superconductivity of noncentrosymmetric superconductors LaPtGe and LaPtGe3: A first-principles study. Computational Materials Science, 185, 109949.

[5] Pandey, S., Demaske, B., Ejegbavwo, O. A., Berseneva, A. A., Setyawan, W., Shustova, N., & Phillpot, S. R. (2020). Electronic structures and magnetism of Zr-, Th-, and U-based metal-organic frameworks (MOFs) by density functional theory. Computational Materials Science, 184, 109903.

[6] Zhang, W., Deringer, V. L., Dronskowski, R., Mazzarello, R., Ma, E., & Wuttig, M. (2015). Density-functional theory guided advances in phase-change materials and memories. MRS Bulletin / Materials Research Society, 40(10), 856–869.

[7] Artrith, N., & Urban, A. (2016). An implementation of artificial neural-network potentials for atomistic materials simulations: Performance for TiO2. Computational Materials Science, 114, 135–150.

[8] Artrith, N., & Kolpak, A. M. (2014). Understanding the composition and activity of electrocatalytic nanoalloys in aqueous solvents: a combination of DFT and accurate neural network potentials. Nano Letters, 14(5), 2670–2676.

[9] Lacivita, V., Artrith, N., & Ceder, G. (2018). Structural and Compositional Factors That Control the Li-Ion Conductivity in LiPON Electrolytes. Chemistry of Materials: A Publication of the American Chemical Society, 30(20), 7077–7090.

[10] Sosso, G. C., Miceli, G., Caravati, S., Behler, J., & Bernasconi, M. (2012). Neural network interatomic potential for the phase change material GeTe. Physical Review. B, Condensed Matter, 85(17), 174103.

[11] Cooper, A. M., Kästner, J., Urban, A., & Artrith, N. (2020). Efficient training of ANN potentials by including atomic forces via Taylor expansion and application to water and a transition-metal oxide. Npj Computational Materials, 6(1), 54.

[12] Xiang, Z. (2020). pyITA (Version 0.1) [Computer software]. Github. https://github.com/alanatransrights/pyITA

[13] Xiang, L., Zeng, X., Huang, X., & Li, G. (2020). The application of artificial neural-network potentials for flexoelectricity: Performance for anatase-type TiO2. Physics Letters. A, 384(10), 126217.

[14] Byrd, R. H., Lu, P., Nocedal, J., & Zhu, C. (1995). A Limited Memory Algorithm for Bound Constrained Optimization. *SIAM Journal of Scientific Computing*, *16*(5), 1190–1208.

Estimation of Post Milling Particle Size Distribution Using Linear Transformation in Parameter Space

Jesang Yim
Kimball Union Academy; NH, United States of America
Email: yimejsang@gmail.com

Abstract - The research attempts to predict the change in the size distribution of the particles after the milling process. The data for the research was sourced from https://www.innocentive.com/. It consisted of pre and post-milling data of the size distributions of the particles. This research made two assumptions: the distribution of particle sizes can be described by combining several individual normal distribution graphs with different parameters. Curve fitting was used to find out the best fitting parameters of the component normal distribution functions. We also assumed that the formula for predicting post-milling distribution from pre-milling distribution is linear, i.e., a matrix operation on the pre-milling parameters will predict the post-milling one. A single matrix should be able to convert all 26 *datasets*. However, only 25 of the datasets were used in order to test the remaining one for cross-validation. Four normal distributions were determined to be optimal for describing the particle size distribution in the data. The prediction had a sum of squared errors ratio ranging from 4.95% to 31.2%, with the average value of 18.7%, which shows the potential of this approach. With more data, or with an ability to conduct the experiment, higher and more consistent particle size predictions should be within reach.

Key Words - Milling, Linear Transformation, Parameter Space, Particle Size Distribution

INTRODUCTION

The research is about predicting the distribution of sizes of the particles after the milling process using normal distribution functions and linear transformation.

I. Hypothesis

The hypothesis of this research is that the particle size distribution in post-milling data can be predicted using normal distribution functions of particle sizes of pre-milling data. And that there exists a single matrix which can be used to convert all 26 parametrized datasets from pre-milling data to post-milling data.

II. Background Research

a) Milling Process and Different Types of Milling

Milling is a process of making particles into smaller pieces. There are various types of milling, such as ball mill, rod mill, pebble mill, burrstone mill, or tower mill. Slurry milling is a type of milling where particles are mixed with liquid. Typically, metal particles such as zinc, lead, silver, aluminum, and nickel are milled for industrial processes, and grains are milled in milling machines through various types of mills. [1]

b) Normal Distribution and Different Types of Distribution functions

The normal (Gaussian) distribution is a function that shows how the probability of variables is distributed [2]. The normal distribution is also called a bell curve, and it can be applied to various random processes. The bell curve is one of the most commonly used forms of distributions. The density is higher in the middle and lower at both ends of the graph. The middle part of the graph has values closer to the mean of the values. The bell curve is symmetric, and the center of the curve indicates the mean. [3]

Even non-normal distribution functions can be shown as a sum of multiple normal distribution functions with different parameters. In normal distribution, the mode, mean, and the median are identical and at the center, and the graph is symmetric with respect to the center. [4] Besides normal distribution, there are several different types of distributions such as Cauchy distribution, power distribution, and Poisson distribution.

Perhaps it is possible that this research can be repeated with other probability distributions. Normal distribution was chosen because of its familiarity, and its ubiquitous implementations in all computer languages.

III. Existing Literature Related to this Research

Existing literature consists of research on the effect of ball and feed particle size distribution and the effect of slurry density on ball milling. [5] This research is different from those previous studies, as the particle size distributions after the milling process will be predicted by a mathematical analysis.

This idea of modeling an arbitrary distribution as a combination of multiple normal distributions is an idea of this author's mentor, and was not published anywhere to the best of our knowledge. Thus it is uncited.

IV. Materials for Research

a) Mathematica was used in this research as a programming language [6].
b) There were 26 datasets provided by Innocentive that show the size and number of particles before and after the milling process. The policy of Innocentive does not disclose who the SEEKERS are. All that the company provided was the data without any mention of the materials or machines used. Therefore, this research was all based on pure mathematical work.

EXPERIMENTAL PROCEDURE

This research consists of four parts:

a) Deciding the number of normal distributions based on the sum of squared estimates of errors (SSE) to describe the particle distribution.
b) Finding the parameters, i.e., the heights, means, and the standard deviations of the component normal distributions.
c) Determining the matrix to transform pre-milling distribution data to post-milling distribution data while minimizing error.
d) Measurement of performance by measuring errors in the predictions.

The graphs of 26 datasets do *not* look like normal distributions. However, we assume that this non-normal distribution looking graph is composed of several normal distributions. In order to increase the prediction accuracy, we find out the number of normal distributions consisting of the data graph.

I. Importing the Dataset

In the first part of the research, we import pre-milling and post-milling data of particles' sizes in a .CSV file. The file contains 26 datasets, and each of the dataset contains particle size and the number of particles underneath each size. The particle numbers are normalized to add up to 100. Since the exponential scale was used to measure the particle sizes, we took the log of each particle number to make it linear.

II. Fitting the Parameters and Solving the Equation by Using FindFit Function

The default normal distribution function is defined as (a exp(-((x-b)/c)^2)), where {a, b, c} are the parameters: a is the amplitude, b is the mean, and c is the standard deviation of the normal distribution. The equations change according to the number of normal distributions. In the normal distribution graph, a is the height of the graph, b is the center of the graph, and c indicates the spread of the graph. Equation 1 and 2 below show how the function looks like in different numbers of normal distributions.

$$\left(a_1\, exp\left(-\left(\frac{x-b_1}{c_1}\right)^2\right)\right)+\left(a_2\, exp\left(-\left(\frac{x-b_2}{c_2}\right)^2\right)\right)+\left(a_3\, exp\left(-\left(\frac{x-b_3}{c_3}\right)^2\right)\right)\#(1)$$

$$\left(a_1\, exp\left(-\left(\frac{x-b_1}{c_1}\right)^2\right)\right)+\left(a_2\, exp\left(-\left(\frac{x-b_2}{c_2}\right)^2\right)\right)+\left(a_3\, exp\left(-\left(\frac{x-b_3}{c_3}\right)^2\right)\right)+\left(a_4\, exp\left(-\left(\frac{x-b_4}{c_4}\right)^2\right)\right)\#(2)$$

We use the FindFit function, which calculates and finds out the predicted parameters according to the given equation and variables, to find the values of parameters of the distribution. FindFit function takes the data, {equation, constraint}, {parameter, starting value} and the variable used in the equation, and returns the parameters. Constraints limit the range of parameters in the equation, and the starting value sets the starting point of the parameters. Without the constraints, the fit value can be wildly off the mark. Some constraints were trivial such as the heights, means and standard deviations being positive numbers. Others were determined by trial and error. A single set of constraints was used for all data.

```
FindFit[sdPreMillingDataPaired[[i]], {sfexponential,
 sfConstraint}, sfparameter, x, Method → "NMinimize"]
```

Figureure. 1. FindFit Function

```
sfConstraint4 = {6 ≤ a1 ≤ 8, 0 < a2 < 0.5, 0.5 < a3 < 1.7,
   0.1 < a4 < 2.5, 4 < b1 < 5, -1.5 < b2 < 1, 5 < b3 < 6.5, 3 < b4 < 3.9,
   0.8 < c1 < 1, 0.6 < c2 < 1.65, 0.5 < c3 < 0.65, 0.7 < c4 < 2.5};
```

Figure. 2. Example of Constraints

```
sfparameter4 = {{a1, 6}, {b1, 4.5}, c1, a2, {b2, 0.5}, c2, a3,
   {b3, 6}, c3, a4, {b4, 3}, c4};
```

Figure. 3. Parameters and their starting points

Figure. 1, Figure. 2, and Figure. 3 above show how FindFit function, constraints, and starting values work. Figure. 4 below is the result of using FindFit function.

$$\{a1 \to 0.623848,\ b1 \to 3.49757,\ c1 \to 2.49512,\ a2 \to 2.27611 \times 10^{-19},\ b2 \to 1.27016,\ c2 \to 0.143678,\ a3 \to 6.59942,\ b3 \to 4.47633,\ c3 \to 0.943641,\ a4 \to 0.14814,\ b4 \to -0.0905873,\ c4 \to 0.355804\}$$

Figure. 4. Resulting Parameters After Using FindFit Function

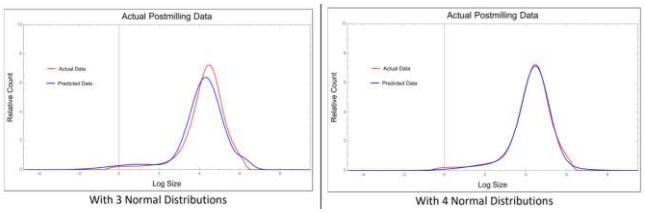

Figure. 5. Addition of Components

Figure. 5 above shows the addition of 4 different components. The 4 different normal distribution graphs add up to each other and form one non-distribution function, which looks like a distribution function.

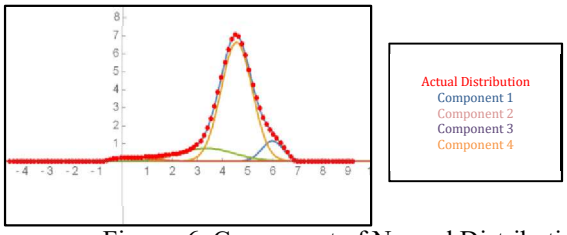

Figure. 6. Component of Normal Distributions

Figure. 6 above shows the components of the normal distributions inside the particle distribution graphs. It clearly indicates that the particle distribution graph actually consists of several components. As the graph shows, three components are not enough to cover the full distribution graph.

Figure. 7 below shows how the actual and predicted post-milling data look like when using 3 and 4 normal distributions. This was typical.

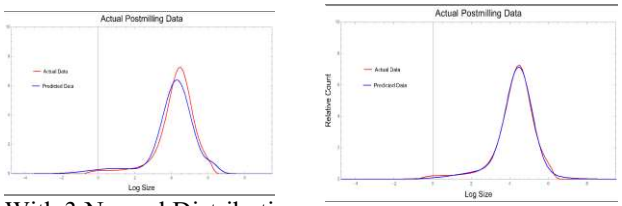

Figure. 7. Actual Data with Predicted Data using 3 and 4 Normal Distributions

III. Calculating Errors and Deciding the Number of Distributions

The number of normal distributions we tried ranges from one to five. The equations for each normal distribution function are used to plot a graph. The graph includes both predicted and real values of particles' sizes and their numbers. Errors are defined by calculating the sum of error squared between the predicted value and the actual value of each dataset. $(actual - predicted)^2$ was used as the equation for calculating errors. The number of graphs with minimum error is chosen as the number of the normal distribution function. Figure. 8 and Figure. 9 below show the predicted and actual data with errors, respectively using 3 and 4 normal distributions.

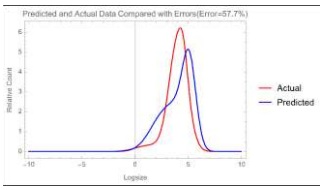

Figure. 8. Predicted and Actual Data Compared with Errors using 3 Normal Distributions

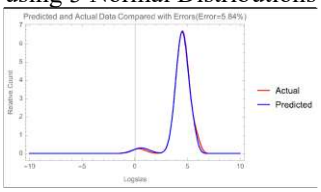

Figure. 9. Predicted and Actual Data Compared using 4 Normal Distributions

IV. Creating Matrix with Optimized Parameters from FindFit

In the second part, we use a matrix to predict the formula that shows the relationship between the pre-milling data and the post-milling data. Parameters of the pre-milling and post-milling normal distributions are expressed in a 12×1 matrix. There are 3 parameters per normal distribution and 4 normal distributions. Therefore, the matrix of parameters will have 12×1 matrix.

A key to deriving the matrix for the post-milling data is by multiplying the key with the pre-milling data. Matrix of

size 12×12 is composed of parameters that are fitted in the previous step. 12×1 pre-milling data parameters will be multiplied to 12×12 matrix, and the result should be the 12×1 matrix composed of parameters from post-milling data. Figure. 10 below shows the relationship of the matrix and parameters of pre-milling and post-milling distributions.

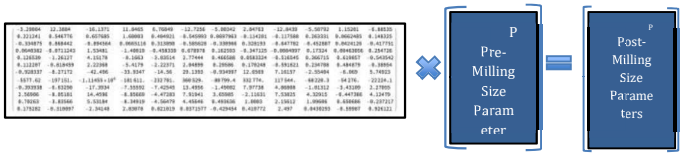

Figure. 10. Matrix and Parameters

V. Calculating Errors and testing the matrix

In the third part, we review the errors from the previous parts. For the cross-validation, since we only have 26 datasets, we use 25 of the datasets to test our predicted post-milling dataset against the remaining single data set. Cross validation is needed to prevent the overfitting and to test if the predicted matrix fits well to the actual data. We repeat this for all 26 datasets by excluding 1 different dataset on each iteration.

```
eq01 = matrix01.sfparameter;
data02 = Table[Flatten[{preParamsTable[[i]], postParamsTable[[i, rowNumber]]}],
  {i, 1, useTheseData}];
matrix = Values@FindFit[data02, eq01, matrix01, sfparameter]
```

Figure. 11. How Matrix Can Be Found using FindFit Function

DATA ANALYSIS AND DISCUSSION

The data chart shows the name of particle samples and their numbers according to each size. Using those 26 datasets about the particles' sizes and their counts, we created the normal distributions.

I. Compare the Graphs with Different Numbers of Normal Distribution Functions

The distribution graphs are composed of several individual normal distribution graphs. These individual graphs cumulate to create the predicted distribution graph. Referring to the Figureure below, four individual normal distributions in the color [blue, green, orange, and brown] accumulate to the distribution graph in red dots.

In this procedure, as shown above in Figure. 7, we combined different numbers of individual normal distributions ranging from 1 to 4. The cumulative distribution graph with 4 individual graphs had the smallest error compared to the others.

II. Set the Constraints and Starting Values for Each Parameter

Figure. 13 below shows how parameters and the starting values for the parameters are set.

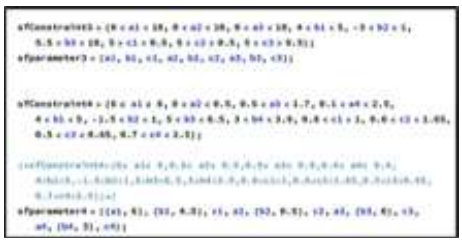

Figure. 13. Constraints and Starting Values for Each Parameters

III. Calculate the Errors from Each Graph and Decide What Number of Distributions to Use

We found that a cumulative distribution graph consisting of 4 individual normal distribution graphs generates the smallest error. As mentioned in the previous section, we use $(a\ exp(-\left(\frac{x-b}{c}\right)^2))$ to compute the error. The error generated from a graph consisting of 4 individual normal distribution graphs is 1.49% (3 significant Figureures). Figure. 14 below shows the comparison of predicted and actual data of 4 different normal distribution graphs.

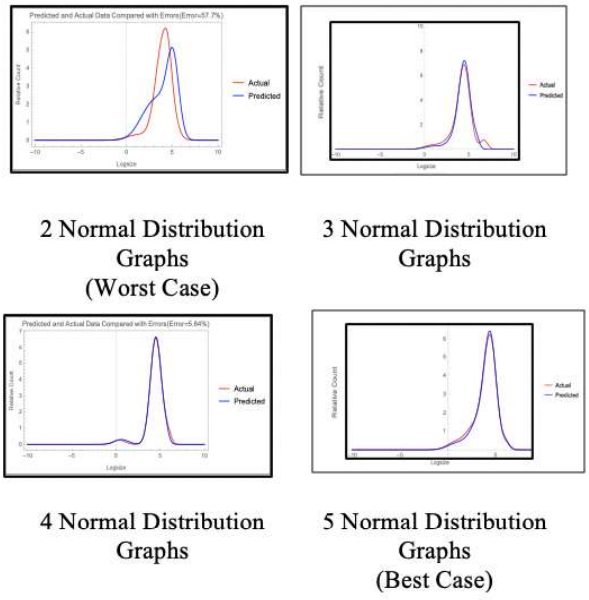

Figure. 14. Predicted and Actual Data Compared with Errors

IV. Find the Matrix that Can Be Used to Predict the Post Milling Data from Pre-milling Data

As the error from 4 normal distribution graphs is minimal with the error of 18.7 percent, we can deduce that we can predict an accurate enough post-milling distribution from pre-milling distribution. We can do this by multiplying the key matrix with the pre-milling data parameters and predicting the parameters for post-milling data. Therefore, the hypothesis that we can predict the distribution of post-milling data from pre-milling data is true.

```
eq01 = matrix01.sfparameter;
data02 = Table[Flatten[{preParamsTable[[i]], postParamsTable[[i, rowNumber]]}],
  {i, 1, useTheseData}];
matrix = Values@FindFit[data02, eq01, matrix01, sfparameter]
```

Figure. 15. How Matrix Can Be Found Using FindFit Function

-3.29084	12.3884	-16.1371	11.8465	6.76849	-12.7256	-5.80342	2.84763	-12.8439	-5.58792	1.15201	-6.88535
0.221241	0.546776	0.657685	1.60803	0.484921	-0.545993	0.8697963	-0.114281	-0.117588	0.263331	0.8662485	0.148325
-0.334875	0.868442	-0.894564	0.8665116	0.313898	-0.585628	-0.338966	0.328193	-0.647782	-0.452887	0.8424126	-0.417751
0.8648382	-0.8711243	1.53481	-1.48019	-0.458339	0.678978	0.162593	-0.347125	-0.8884997	0.17324	0.89463056	0.254726
0.126539	-1.26127	4.15178	-8.1663	-3.83514	2.77444	0.466588	0.0583324	-0.516545	0.366715	0.619857	-0.543542
0.112287	-0.818459	2.22368	-5.4179	-2.22371	2.04899	0.29586	0.170248	-0.591621	0.234788	0.484879	-0.38954
-0.928337	-8.27172	-42.496	-33.9347	-14.56	29.1393	-0.934997	12.6569	7.16157	-2.55404	-6.069	5.74923
-5577.62	-197151.	-1.11455×10^{6}	-181611.	-23270l.	360529.	-88799.4	332774.	117544.	-68220.3	-54276.	-22224.1
-0.393938	-6.63298	-17.3934	-7.55592	-7.42545	13.4956	-1.49002	7.97738	4.86888	-1.81312	-3.43109	2.27855
2.56906	-8.05181	14.4596	-8.85669	-4.47283	7.91941	3.65985	-2.11631	7.53825	4.32915	-0.447386	4.12479
0.70263	-3.83566	5.53184	-8.34919	-4.56479	4.45646	0.493636	1.0003	2.15612	1.89686	0.658686	-8.237217
0.175282	-0.310897	-2.34148	2.83078	0.821819	0.0371577	-0.429454	0.410772	2.497	0.8430293	-0.59987	0.926121

Figure. 16. 12 X 12 Matrix Answer

CONCLUSION

I. Results

From this research, we can conclude that the hypothesis is true: it is possible to find a matrix that can transform the pre-milling particle size distribution to the post-milling particle size milling distribution. We found that 4 normal distributions fit the original normal distribution with minimum error, and provided the most accurate matrix formula that can be used for a precise prediction of sizes of post-milling data. Multiplying the matrix with the parameters of pre-milling data from 4 different normal distributions gave the parameters of predicted post-milling data with 18.7% accuracy.

The significance of this 18.7% accuracy is unusually difficult to evaluate due to the circumstances in which the data was obtained. The data was posted on the innocentive.com site by an anonymous company that was referred only as SEEKER. The SEEKER didn't specify what the error rate they were currently getting, nor what accuracy they were looking for.

Thus, this research has to settle with the success in demonstrating the feasibility of using multiple normal distributions to model and compute transformations in distribution. It is not possible to claim any benefit without knowing the current base rate and the cost of error.

II. Challenges in the Research

The challenges in this research were mainly from the fitting part. The values from the function were different although the codes were exactly the same. The hardest part of the research was debugging the code. Since the codes were repeated several times to compare different values, the entire result came out to be wrong if the initial code was not correct. One of the errors was in the code generating the code. Each parameter needed different constraints each time, but the parameters were only given once. Once the debugging was complete, the code worked all together.

The other challenge in the research was using the FindFit function. Without the specified initial conditions, it would find the fit in the wrong places. The constraints were needed in a known situation of the graph so that the most numerous particle sizes would go to each of the parameters and form different normal distribution graphs that fit into the total distribution. Without the constraint, the parameters found using the function changed every time the code was run. Taming the constraints to find out the intuitive result took many trials and errors.

IDEAS FOR FUTURE RESEARCH

I. Improving Accuracy by Using a Larger Set of Data on the Specific Research

There could be two types of future research. One could be building further on this specific research with a larger set of data to improve the accuracy. With a larger dataset, we could increase the number of normal distribution graphs that form the cumulative distribution graph. We could check if increasing the number of individuals beyond 4 would reduce errors. A larger dataset will also enable us to increase the size of the matrix, which can be tested to see if it has a higher accuracy and precision compared to 4 individual normal distribution functions.

Another research could be done using multiple normal distribution fitting techniques to represent non-normal distribution looking patterns and predict the post-event dataset from the given pre-event dataset. Any strange looking non-normal distributed dataset can be turned and analyzed into multiple normal distributions, resulting in the prediction of post-event distributions.

II. Application of the Method to Predict Post-event Patterns in the Real World

This method can be also used to predict post-event patterns in the real world. For example, an online shopping mall can analyze how well their new advertisement worked by comparing the clicking rates of customers before and after the advertisement. Real world events that have changes in-pre-event data and post-event data can use this method to predict the pattern.

The methodology in this research can be used to find ways to predict the change in the distribution of other pre-events and post-events as well. This research shows that events that display complex distribution functions that do not fit any known distribution functions can still be represented using different weighted sums of known distributions and their parameters, extending this method to areas that deal with unusual distributions. For example, the effect of a certain farming method to the crops' sizes can be tested before and after the use of the method by examining the distribution of crop sizes. This future research is expected to be less

challenging after this research dealing with a number of size categories. This future research would have its own challenges as it takes a long time to produce the crops after using the farming method. After predicting the size distributions, farmers can produce bigger crops and leverage the economic profit using the results of this research. Although confronted with unknown distribution models, this research enables to solve it by making weighted sums of known distributions.

REFERENCES

[1] M.Baron, A.Chamayou, L.Marchioro, J.Raffib, "Radicalar probes to measure the action of energy on granular materials," *Advanced Powder Technology,* vol. 16, no. 3, pp. 199-211, 2005.

[2] G. Casella and R. L. Berger, Statistical Inference, Duxbury: Thomson Learning, 2002.

[3] A. Lyon, "Why are Normal Distributions Normal?," vol. 65, pp. 621-649, 2014.

[4] Casella, George; Berger, Roger.L, Statistical Inference, Duxbury, 2001.

[5] D. S. M. ,. S. S. N. ,. E. A. Augustine B. Makokha, "Effect of Slurry Solids Concentration and Ball Loading on Mill Residence Time Distribution," *International Journal of Mining Engineering and Mineral Processing,* vol. 3, no. 2, pp. 21-27, 2014.

[6] "Wolfram Mathematica," [Online]. Available: http://www.wolfram.com/mathematica/.